MECHANISMS OF OSTEOBLAST REPROGRAMMING AND DIFFERENTIATION DURING ZEBRAFISH CAUDAL FIN REGENERATION

ANA SOFIA DA SILVA PEREIRA BRANDÃO

Tese para obtenção do grau de Doutor em Biomedicina

Doutoramento em associação entre:

Universidade NOVA de Lisboa (Faculdade de Ciências Médicas | NOVA Medical School)

Universidade de Aveiro

julho, 2019

MECHANISMS OF OSTEOBLAST REPROGRAMMING AND DIFFERENTIATION DURING ZEBRAFISH CAUDAL FIN REGENERATION

Ana Sofia da Silva Pereira Brandão

António Jacinto, Investigador Principal e Prof. Associado, NMS-FCM

Anabela Bensimon-Brito, PhD, Max Planck Institute for Heart and Lung Research

Duarte Mesquita, PhD, Centro de Estudos de Doenças Crónicas (CEDOC)

Tese para obtenção do grau de Doutor em Biomedicina

Doutoramento em associação entre:

Universidade NOVA de Lisboa (Faculdade de Ciências Médicas | NOVA Medical School)

Universidade de Aveiro

julho, 2019

The research described here was performed at the Chronic Diseases Research Center (CEDOC), NOVA Medical School - Faculdade de Ciências Médicas, between 2013 and 2018. Its execution was supported by a PhD fellowship from the Portuguese Foundation for Science and Technology (SFRH/BD/51990/2012). This work was accomplished under the supervision of Dr António Jacinto, Dr Anabela Bensimon Brito and Dr Duarte Mesquita.

Este trabalho de investigação foi realizado no Centro de Estudos de Doenças Crónicas (CEDOC) da NOVA Medical School - Faculdade de Ciências Médicas, entre 2013 e 2018, ao abrigo de uma bolsa de Doutoramento, financiada pela Fundação para a Ciência e a Tecnologia (SFRH/BD/51990/2012). Esta tese de doutoramento foi supervisionada pelo Dr. António Jacinto, Dra. Anabela Bensimon Brito e pelo Dr. Duarte Mesquita.

Table of contents

Acknowledgements

First of all, I would like to thank my supervisor António Jacinto for giving me the opportunity to be a part of his amazing lab and supervising my PhD work. I would like to especially thank you for allowing me to express myself scientifically and for trusting in my capacities, since fly hemoteam days! Thank for your positivism in times of need.

I would like to thank my co-superiors Anabela Bensimon Brito and Duarte Mesquita for introducing me to this fishy fish world. I have learned and laughed a lot with both of you!

A very special thanks to Anabela "Bels" for all the advice, availability, support and friendship throughout the years and specially for trusting in my work. I cannot thank you enough!

I would like to give a special acknowledgement to those who helped me in this herculean task of correcting and assembling this thesis (you know who you are) and to the following people:

To Lara Carvalho and Telmo Pereira. We have been together since the very beginning of this and other journeys. You always helped me and encouraged me to accomplish my goals. I am most fortunate to have you in my life! You are the *best of the best of the best*!

To Jorge Borbinha, my first illegitimate student and partner in crime. Thank you for helping me throughout this work, for all your enthusiasm (excessive sometimes), support and importantly, for making me laugh...*may the force be with you*!

To Raquel Lourenço, my fish postdoc advisor. Thank you for your help and for always checking on me. It is a pleasure to see your qPCR yields (not being ironic). Also, I think we should create a Hippo/Yap pathway support group entitled "*vamos acabar com o Yap antes que ele acabe connosco*".

To Susana Ponte (a minha Susie-Q), one of the pillars of this lab and my oldest PhD companion: companion of peculiar PhD constraints (no mínimo!). Thank you for always being available to help and for the support since good old fly days.

To Ana Farinho, the most talented histology professional that I know. The reason why I have such nice images to show is also due to your magnificent work. Thank you for caring about my work and for caring about me.

To Inês Cristo, for always pushing me further and for being a friend…*No fish dies on my watch*!

I would like to thank the most amazing Lab ever, the Tissue Morphogenesis and Repair lab, old and present lab members. It's been 8 years of amazing parties, retreats and, most importantly, of amazing people. I would like to give a special thanks to: Guadalupe Cabral, for the advice, trust and encouragement; *la belissima* (needed this opportunity to add some Italian to this thesis) Carolina Crespo (*che parla come le campane*) for conversations, laughter and drinks; to my woman from the North Diana Saraiva; to Ana Teresa Matias; to the WestSide Bros, Diogo Paramos and José Marques, for sharing their special place; à "incríbel" Mafalda Pinho; Rita Gorgulho; Ana Teresa Tavares; Nídia de Sousa; and Valdir Semedo. Um grande bámos equipa para vocês todos, vocês são um espetáculo!

A special thanks to Ana *El mariachi* Roberto, for all the valuable help throughout this PhD. It would have been much harder if it wasn't for you. Thanks for caring.

Corporate Cláudia Queiroga, thanks for all the funny moments and for having such good advice to give.

Ana Soares and Cláudia Pereira, for all the goofy things we say and for being (along with Susana Ponte) the best company to have in a PhD retreat.

To Rita Teodoro, for all the useful comments (during our joint labmeetings) and advice.

My zebra comrades from the Cilia Regulation and Disease Lab.

To Petra Pintado and Fábio Valério for taking care of our fishy friends and for all the help.

To Cláudia Andrade, for always being in a good mood, even when sorting few cells.

To Leonor Saúde and to the members of the Embryonic Development and Regeneration Lab for advice and reagent sharing. A big thanks to Lara Carvalho and Aida Barros from the Instituto de Medicina Molecular fish facility, for always being available to help with such enthusiasm.

To the members of the Instituto Gulbenkian de Ciência fish facility. Thank you for receiving and maintaining our fish lines.

A big and special acknowledgement to all living beings that contributed for the experiments performed in this thesis! Aos zebrinhas que estão sempre comigo!!!

The members of the coordination of the Biomedicina PhD Program for accepting me and to FCT for funding this PhD thesis.

To my amazing friends: Inês Lagoas (my fierce palaeontologist…sorry Archaeologist); Inês Marques (a Neura mais Zen que conheço) and Ana Moreno (my strong independent almost British woman). Thank you for your support and company. I am free at last… agora sim podemos ir celebrar!

To my four-legged friend, Dexter, for providing me with the fluffiness required to do this thesis and for being a source of cuteness …and pain at the same time.

Quero agradecer a toda a minha família, mas principalmente:

Ao Manecas e à Adelaide que sempre tomaram conta de mim e que até hoje me fazem rir sempre que os vou visitar. Vocês são os melhores avós do mundo!

Aos meus pais, Paula e Carlos, que me fazem sentir a pessoa mais extraordinária deste planeta e que sempre me apoiaram de forma incondicional em tudo. Do coração, um grande obrigado.

E porque deixo sempre o melhor para o fim, queria agradecer ao João Costa, porque sem ele nada disto teria sido possível. Muito obrigado por tudo Johnny boy!

Abstract

Regeneration is an impressive biological process that allows the replacement of lost body parts due to damage or injury, restoring both tissue architecture and function. It is well documented that while mammals have a limited capacity to regenerate lost tissues, other vertebrates, such as amphibians and teleost fish, exhibit a remarkable capacity to regenerate organs, like the heart and the retina, and large sections of the body, such as the limb and the fin.

Zebrafish has become an important model system to study vertebrate regeneration and the adult caudal fin is one of the most used tissues to comprehend how tissues are restored. This structure is easily accessible to surgery, amenable to live imaging, its amputation does not compromise survival and regeneration is particularly fast, occurring over the course of two weeks. Fin regeneration is an epimorphic process since it relies on a specialized structure called blastema, which is composed of a proliferative heterogeneous population of dedifferentiated cells with restrictive lineage potential. After caudal fin amputation, a regenerative program is activated and occurs in three sequential phases: wound healing, blastema formation, and regenerative outgrowth. These events comprise a tight coordination between proliferation, patterning and differentiation to reconstitute the architecture and the size of the original tissue. The adult caudal fin is composed of multiple tissues, including blood vessels, nerves, mesenchyme and the structural support, the bony-rays (skeletal elements). Each bony-ray is surrounded and maintained by an outer and inner monolayer of bone secreting cells, the osteoblasts. Many studies have focused on bone regeneration since the zebrafish caudal fin provides a unique model to understand bone formation and osteoblast dynamics upon tissue damage and regeneration.

After caudal fin amputation, formation of the new bone elements depends greatly on tissue plasticity (changes in cellular identity). This is achieved through the activation of two complementary processes that enable the assembly of an osteoblast progenitor pool during blastema formation: dedifferentiation of resident mature osteoblasts and commitment of joint-associated osteoblast progenitors. Complex regulatory mechanisms subsequently maintain and expand the osteoblast progenitor pool and promote their redifferentiation into mature osteoblasts to restore the skeletal tissue. Therefore, both osteoblast progenitor assembly and redifferentiation are critical aspects of caudal fin bony-ray regeneration. Interestingly, ablation of mature osteoblasts prior to caudal fin amputation does not affect normal bone regeneration, suggesting that *de novo* bone formation can rely solely on the commitment of joint-associated osteoblast precursors or on new osteoblast progenitors arising from alternative sources.

In this PhD thesis, I aimed to unravel key aspects of caudal fin bone regeneration, focusing on new regulators of osteoblast dedifferentiation and redifferentiation and alternative sources for *de novo* osteoblast formation in osteoblast-depleted fins.

To investigate novel regulators of osteoblast dedifferentiation, we performed a genome-wide gene expression analysis of osteoblasts undergoing dedifferentiation. With this analysis, we concluded that this process occurs much earlier in the regenerative process than what was previously thought. Furthermore, we characterized the molecular basis of osteoblast dedifferentiation regarding epigenetic modulation, signal transduction, cell adhesion reorganization, epithelial to mesenchymal transition and acquisition of migratory behaviour and proliferation. Particularly, we observed that osteoblasts change their metabolic signature upon injury. This was predicted based on the upregulation of several glycolytic and lactate producing enzymes, which is followed by an increase in the expression of oxidative phosphorylation electron transport chain components. We hypothesize that osteoblast dedifferentiation relies on a bivalent metabolism that uses both glycolysis and oxidative phosphorylation, which may reflect an adaption to the energetic demands of regeneration. Since the link between metabolic adaptation and regeneration remains poorly understood, we decided to address it by inhibiting the glycolytic influx. We observed major defects in the regenerative process, including impaired assembly of the wound epidermis, a major signalling centre during regeneration, and fewer cells re-entering the cell cycle. In addition, we showed that several osteoblast markers were downregulated and that osteoblast populations became disorganized. This suggests that metabolic adaptation plays an important role in regeneration, in particular during osteoblast dedifferentiation.

In addition to the transcriptional analysis, we followed a targeted approach. We examined the role of the Hippo signalling pathway as a potential regulator of osteoblast dedifferentiation, by inhibiting Yap (Hippo pathway effector). This prevented mature osteoblasts to migrate, re-enter the cell cycle and to assemble the osteoblast progenitor pool. In parallel, we evaluated the role of this pathway in mediating osteoblast redifferentiation during regenerative outgrowth. We noticed that Yap inhibition leads to a decrease in the number of differentiating osteoblasts and to the misregulation of key signalling pathways, such as Bmp and Wnt signalling. We provide evidence that Yap not only promotes osteoblast differentiation through activation of Bmp signalling via *bmp2a* expression but also restricts the osteoblast progenitor pool by inhibiting Wnt signalling to the differentiation front by regulating *dkk1a*. Altogether, these results lead us to propose that the Hippo/Yap signalling pathway regulates osteoblast dedifferentiation as well as redifferentiation. This reveals a previously unknown duality if the Hippo/Yap pathway in controlling two different aspects of osteoblast biology during caudal fin regeneration.

Lastly, we provide evidence into the cellular and molecular mechanisms that regulate *de novo* osteoblast formation in osteoblast-depleted caudal fins. We identified an additional osteoblast progenitor population that arises at the outer and inner bone surfaces adjacent to

the epidermal and mesenchymal compartments, respectively. These cells are not part of a uniform population but seem to form two distinct osteoblast progenitor populations with different origins or expression profiles. Lineage tracing experiments revealed that mesenchymal cells within the intraray compartment, but not epidermal cells, contribute to generate new osteoblasts in osteoblast-depleted caudal fins. This provides new evidence of an additional source of osteoblasts for regeneration. Moreover, we showed that both Retinoic Acid and Bmp signalling pathways are activated in this osteoblast progenitor population and are important to induce their commitment and recruitment during caudal fin regeneration. Thus, we elucidate potentially dormant regenerative mechanisms that emerge to ensure correct bone formation in caudal fins lacking mature osteoblasts.

Taken together, this PhD thesis provides novel insights into new regulators of bone formation and alternative cells that can contribute to correct bone regeneration upon injury. We expect that defining the mechanisms regulating tissue plasticity, reprogramming and fate specification during bone reconstitution have major implications not only to understand the basic mechanisms that regulate tissue regeneration but also to the field of regenerative medicine and bone cancer biology.

Resumo

A regeneração é um processo biológico notável que permite a restituição de tecidos após lesão ou amputação, que incluí a recuperação da função, forma e tamanho do tecido original. Enquanto que os mamíferos possuem uma capacidade limitada de regenerar tecidos, outros vertebrados, como anfíbios e alguns peixes teleósteos, são dotados de uma capacidade extraordinária de regenerar órgãos, como o coração e a retina, e grandes superfícies corporais, como membros e barbatanas.

O peixe-zebra (*Danio rerio*) é utilizado como modelo para o estudo de processos regenerativos em vertebrados. A barbatana caudal do peixe-zebra surgiu como uma das estruturas mais utilizadas para estudar regeneração. Esta estrutura é de fácil acesso à cirurgia de amputação, passível ao uso de técnicas de microscopia, não comprometendo a sobrevivência do animal, sendo que o seu processo regenerativo é consideravelmente rápido. A regeneração da cauda é um processo epimórfico, uma vez que depende da formação de uma estrutura especializada designada blastema. Esta estrutura é composta por uma população heterogénea de células com capacidade proliferativa. Após amputação da cauda, o programa regenerativo é caracterizado por três fases sequenciais: fecho da ferida, formação do blastema e, por fim, crescimento e diferenciação. Durante o processo regenerativo, a coordenação entre proliferação e diferenciação é de grande importância para assegurar e alcançar a estrutura e tamanho iniciais. A barbatana caudal é constituída por vários tecidos, incluindo vasos sanguíneos, nervos, tecido mesenquimal e tecido ósseo, este último sendo constituído por raios ósseos que providenciam estabilidade à cauda. Cada um destes raios ósseos é revestido externa e internamente por uma monocamada de células produtoras de osso, os osteoblastos.

Muitos estudos têm-se focado na regeneração destes elementos ósseos presentes na barbatana caudal, uma vez que este sistema possibilita a compreensão do processo regenerativo do osso e a dinâmica dos osteoblastos neste contexto.

Após amputação da cauda, a formação do novo tecido ósseo depende consideravelmente da plasticidade celular (alterações na identidade celular). Isto é alcançado durante a formação do blastema, através da ativação de dois processos complementares que permitem a formação de um conjunto de progenitores de osteoblastos: desdiferenciação de osteoblastos maduros presentes no tecido não danificado e diferenciação de progenitores presentes na zona da articulação. Posteriormente, mecanismos regulatórios mantêm e expandem o grupo de progenitores e promovem a sua diferenciação em osteoblastos completamente diferenciados, capazes de produzir matriz óssea e de reconstituir o tecido ósseo. Desta forma, a formação dos progenitores de osteoblastos assim como a sua correta diferenciação são essenciais para promover a regeneração dos raios ósseos da barbatana caudal. Curiosamente, a ablação de osteoblastos maduros antes do início do processo regenerativo não afeta a regeneração dos elementos ósseos, o que sugere que, neste contexto, que a sua formação depende

unicamente de progenitores associados à articulação ou de fontes celulares alternativas ainda por descobrir.

Durante esta tese de doutoramento, procurei elucidar aspetos chave da regeneração do osso da barbatana caudal do peixe-zebra, nomeadamente os processos regulatórios que controlam o programa de desdiferenciação dos osteoblastos maduros bem como a sua posterior diferenciação, e as fontes alternativas de progenitores de osteoblastos em caudas desprovidas de osteoblastos maduros. Com o intuito de investigar novos mecanismos regulatórios do processo de desdiferenciação, recorremos a uma análise global do transcriptoma dos osteoblastos nesta fase da regeneração. Esta análise revelou que o processo de desdiferenciação ocorre muito cedo durante o processo regenerativo. Para além disso, caracterizámos a base molecular do programa de desdiferenciação, no que diz respeito a mecanismos epigenéticos, metabolismo, vias de transdução de sinal, adesão celular, transição epitélio-mesênquima, migração e proliferação. Em particular, observámos que várias enzimas glicolíticas e produtoras de lactato exibem a sua expressão aumentada no início da desdiferenciação, seguidas de um aumento na expressão de componentes da cadeia transportadora de eletrões. Estes resultados demonstram que os osteoblastos alteram significativamente o seu metabolismo em resposta à amputação. Desta forma, propomos a hipótese de que a desdiferenciação dos osteoblastos depende da aquisição de um metabolismo bivalente no qual as vias glicolíticas e de fosforilação oxidativa são usadas para melhor adaptar os osteoblastos aos novos requisitos do processo regenerativo. Uma vez que a ligação entre adaptação metabólica e regeneração ainda está pouco explorada, decidimos investigar como é que o processo regenerativo é influenciado pela glicólise. Ao inibirmos o fluxo glicolítico, verificámos que o crescimento do tecido regenerativo é significativamente reduzido. Neste contexto, vários fenótipos foram observados: inibição da proliferação; desorganização da população de osteoblastos dentro do blastema; alterações na expressão de vários marcadores de osteoblastos; e deformação da epiderme especializada que se forma durante a regeneração, cuja função secretora de moléculas sinalizadoras é essencial para a desdiferenciação. Estes resultados sugerem que esta adaptação metabólica tem um papel importante durante a regeneração, em particular no processo de desdiferenciação.

Para além da análise de transcriptoma, estudámos também uma via de sinalização em particular, a via Hippo, através da manipulação genética do seu efetor Yap. Descobrimos que a inibição de Yap durante a fase de desdiferenciação impede a migração e proliferação de osteoblastos maduros e a formação de novos progenitores. Para além disso, a inibição desta via durante a fase de rediferenciação leva a uma diminuição substancial dos osteoblastos em diferenciação e a uma alteração na expressão de componentes de vias de sinalização cruciais, *bmp2* (via BMP) e *dkk1* (via Wnt). Estes dados evidenciam que Yap promove a diferenciação dos osteoblastos através da ativação da via BMP e restringe o grupo de progenitores através da inibição da via Wnt. Estes resultados permitem-nos propor que a via de sinalização Hippo/Yap regula quer a desdiferenciação dos osteoblastos quer a sua subsequente

rediferenciação, o que revela a dualidade do mecanismo de ação desta via em fases diferentes do processo regenerativo da barbatana caudal.

Por último, revelamos a existência de mecanismos celulares e moleculares que regulam a formação de novos progenitores de osteoblastos em caudas desprovidas de osteoblastos maduros. Identificámos assim uma fonte adicional de progenitores que emerge na interface da matriz óssea com os tecidos adjacentes, nomeadamente a epiderme e o mesênquima. Estes progenitores não parecem formar uma população homogénea, mas sim duas populações distintas com diferentes origens ou com diferentes padrões de expressão. Recorrendo a técnicas de seguimento de linhagem, conseguimos identificar o mesênquima, mas não a epiderme, como uma fonte de novos osteoblastos em caudas desprovidas de osteoblastos maduros. Estes resultados põem em evidência uma origem adicional de osteoblastos que contribui para o processo regenerativo. Para além disso, demonstramos que as vias de sinalização do Ácido retinóico e Bmp estão ativas nesta população de progenitores e têm um papel crucial na formação e recrutamento desta fonte adicional de osteoblastos durante o processo regenerativo. Assim, este trabalho permite revelar que, em barbatanas caudais desprovidas de osteoblastos maduros, mecanismos regenerativos que se encontram normalmente inativos, são estimulados e asseguram a formação correta dos elementos ósseos neste contexto.

De uma forma geral, esta tese de doutoramento identifica novos mecanismos de regulação da formação do tecido ósseo e fontes celulares alternativas que contribuem e garantem a correta regeneração do osso após lesão. Antevemos que o conhecimento dos mecanismos que regulam a plasticidade celular, reprogramação e especificação de linhagem durante a regeneração do osso possam ter implicações fulcrais não só para o conhecimento dos processos básicos que promovem regeneração, mas também no campo da medicina regenerativa e neoplasias.

Thesis contributions

All Chapters and figures integrating this thesis were written and assembled by the author. Experimental procedures and analysis included in Chapters III, IV and V were performed by the author and by the following collaborators:

Chapter III

Microarray chip assay was performed by OakLabs GmbH (Henningsdorf, Germany). Microarray data analysis was done by OakLabs GmbH (Henningsdorf, Germany) and by Patrícia Brito (researcher at CEDOC). Jorge Borbinha (PhD student from António Jacinto's Lab) performed q-PCR experiments displayed in Figure 7. Telmo Pereira (CEDOC, former lab member from António Jacinto's Lab) contributed with technical support in image acquisition and quantification of osteoblast motility shown in Figure 24.

Chapter IV

Rita Mateus (former PhD student from António Jacinto's Lab) provided preliminary insights which allowed the follow-up of the project. Telmo Pereira (CEDOC, former PhD student from António Jacinto's Lab) assisted with technical support in the quantifications depicted in Figure 33. André Macedo (CEDOC, PhD student from Alisson Gontijo's Lab) aided in q-PCR technical support and quantifications.

Chapter V

Anabela Bensimon Brito (former postdoc at António Jacinto's Lab) contributed in the assembly of the basic tools to implement the project. Jorge Borbinha (PhD student from António Jacinto's Lab) contributed with technical performance of experiments shown in Figure 41 (EdU labelling), Figure 44 (lineage tracing epidermis) and Figure 46 (lineage tracing mesenchyme).

Thesis publications

The work presented in in Chapter III of this thesis is currently in preparation for submission for publication in the near future:

> Ana S. Brandão, Jorge Borbinha, Anabela Bensimon-Brito, Raquel Lourenço and António Jacinto. ***Metabolic reprogramming triggers and controls the zebrafish caudal fin regenerative response****.*

The work presented in Chapter IV of this thesis has been submitted and is currently under revision in *Journal of Cell Science.*

> Ana S. Brandão, Anabela Bensimon-Brito, Raquel Lourenço, Jorge Borbinha and António Jacinto. ***Yap induces osteoblast differentiation by modulating Bmp signalling during zebrafish caudal fin regeneration****.* Short Report, 2019. JOCES/2019/231993.

During the course of my PhD, I have also participated in other study from the lab that is under preparation for submission for publication in the near future:

> Raquel Lourenço, Ana S. Brandão, Jorge Borbinha and António Jacinto. ***Yap regulates Müller glia development and reprogramming in damaged zebrafish retinas.***

List of abbreviations

Abbreviation	Full form
ΔCt	Cycling threshold
µM	microMolar
µL	microLiter
3PO	(2E)-3-(3-Pyridinyl)-1-(4-pyridinyl)-2-propen-1-one
4-OHT	4-Hydroxytamoxifen
AEC	Apical Epithelial Cap
AER	Apical Ectodermal Ridge
AJ	Adherens Juctions
alf	*another longfin*
ALM	Accessory limb model
Amp	Ampicillin
BEL	Basal Epidermal Layer
BLC	Bone-lining cell
Bmp	Bone morphogenetic protein
Bmpr	Bone morphogenetic protein receptor
Bmpri	Bone morphogenetic protein receptor inhibitor
bp	basepairs
°C	Degree Celsius
Ca^{2+}	Calcium
CA	Constitutively active
cDNA	Complementary DNA
Col10a1	Collagen 10a1
CRISPR	Clustered regularly interspaced short sequences
Ctgf	Connective tissue growth factor
Cx43	Connexin 43
DAPI	4',6-Diamidino-2-Phenylindole
DAMPs	Damage-associated molecular patterns

Abbreviation	Full form
DB	Distal Blastema
DMSO	Dimethyl sulfoxide
DN	Dominant negative
DNA	Deoxyribonucleic Acid
Dod	Devoid of blastema
Dpa	Days-post amputation
Dpf	Days-post fertilization
E3	Embryo medium
ECM	Extracellular Matrix
EGFP	Enhanced Green Fluorescent Protein
EMT	Epithelial to Mesenchymal Transition
ESC	Embryonic Stem Cell
ESTs	Expressed sequence tags
EtOH	Ethanol
FACS	Fluorescent Activated Cell Sorting
FDR	False discovery rate
Fgf	Fibroblast growth factor
Fgfr	Fibroblast growth factor receptors
FP	Fluorescent protein
GAGE	Generally Applicable Gene-set Enrichment
GFP	Green Fluorescent Protein
GO	Gene Ontology
GSA	Gene set analysis
h	Hour(s)
HAT	Histone acetyltransferase
HCA	Hierarchical clustering analysis
HDAC	Histone deacetylase
HDM	Histone demethylase
HMT	Histone methyltransferase

Abbreviation	Full form
Hpa	Hours-post amputation
Hpf	Hours-post fertilization
HS	Heat-shock
HSC	Hematopoietic Stem Cells
Igf	Insulin growth factor
IP	Intraperitoneal
iPSC	Induced Pluripotent Stem Cells
Jak/Stat	Janus kinase/Signal transducers and activators of transcription
JNK	c-Jun N-terminal kinase
Kan	Kanamycin
Kb	Kilobase
KEGG	Kyoto Encyclopedia of Genes and Genomes
Krtt1c19e/ Krt19	Keratin type 1 c19e
LB	Luria Broth
Lef1	Lymphocyte enhancer binding factor 1
MSC	Mesenchymal Stem Cell
MeOH	Methanol
mg	milligram(s)
miRNA	microRNA
min	minute(s)
mL	milliLitre(s)
mM	miliMolar
MMPs	Matrix metalloproteinases
mRNA	messengerRNA
Msxb (a,b,c,d)	Muscle segment homeobox
Mtz	Metronidazole
nAG	Newt Anterior Gradient protein
nL	Nanoliter(s)
nm	Nanometer

Abbreviation	Full form
NTR	Nitroreductase
ON	Overnight
Osc/Bglap	Osteocalcin / Bone gamma-carboxyglutamate protein
Osx/Sp7	Osterix
OxPhos	Oxidative phosphorylation
PB	Proximal Blastema
PBS	Phosphate Buffered Saline
PBT	Phosphate Buffered Saline with Triton X-100
PC	Principal component
PCA	Principal component analysis
PCNA	Proliferating cell nuclear antigen
PCR	Polymerase Chain Reaction
PD	Proximo-distal
PFA	Paraformaldehyde
Pfkfb3	Phosphofructokinase-2/fructose-2,6-bisphosphatase 3
pg	Picogram(s)
PZ	Patterning Zone
q-PCR	Quantitative-PCR
RA	Retinoic Acid
RE	Restriction enzymes
RIN	RNA integrity number
RNA	Ribonucleic Acid
ROS	Reactive oxygen species
RPM	Revolutions per minute
RT	Room temperature
Runx2	Runt-related transcription factor 2
SASP	Senescence- associated secretory phenotype
SD	Standard deviation
Sdf1	Stromal cell-derived factor 1

Abbreviation	Full form
sec	Second(s)
Shh	Sonic hedgehog
sof	*shortfin*
Sox9	SRY-Box 9
SSR	Site-specific recombination
TAE	Tris-Acetate-EDTA
TALEN	Transcription activator-like effector nuclease
Taz	Transcriptional co-Activator with PDZ binding motif
TenC	Tenascin C
Tg	Transgenic
Tgfβ	Transforming Growth Factor beta
TJ	Tight Junctions
TM	Melting temperature
TREEs	Tissue regeneration enhancer elements
Treg	Regulatory T cell
TSP	Tissue specific promoter
U	Units
WE	Wound Epidermis
Wnt	Wingless-type MMTV integration site family
WT	Wild type
Yap	Yes-Associated Protein

List of tables

List of figures

Chapter 1

INTRODUCTION

1 REGENERATION

1.1 Defining regeneration

Regeneration is undoubtedly one of the most impressive and inspiring biological processes and endures as one of the more mysterious fields of developmental biology. This process is defined as the capacity to fully restore lost or damaged body parts after damage or injury (Tsonis 2002; Bely and Nyberg 2010; Poss 2010) and was first reported in 1740 by Abraham Trembley, who discovered the regenerating properties of the Hydra head. Later, in 1766, Peter S. Pallas reported the singular regenerative properties of the planarians capable of restoring entire animals from a single body piece. In 1768, Lazzaro Spallanzani demonstrated that, after amputation or tissue damage, amphibian tadpoles and salamanders were capable of reproducing reliable copies of the existing tissues (Spallanzani 1769; Sánchez Alvarado 2000; Rink 2011).

The terms regeneration and repair have been used indiscriminately to describe a wide range of phenomena and they often refer to the same thing. However, these terms should not be confused with wound healing or wound repair, often referred to non-regenerative healing as it results in the replacement of a once functional tissue by a collagenous and fibrotic scar. Conversely, regeneration culminates in the replacement of the missing cell, tissue, organ or structure, by a quite faithful copy, recreating both tissue architecture and function without scarring (Tsonis 2002; Gurtner et al. 2008; Atala et al. 2010; Jaźwińska and Sallin 2016). Regeneration can be triggered by a variety of insults, occur at different levels of biological organization (cellular, tissue, organ, structure and whole-body level) (Figure 1) and at different phases of an organism life cycle, encompassing a vast spectrum of mechanisms that restore normal tissue structure (Bely and Nyberg 2010; Slack 2017). The latter can be divided in 5 main phenomena: (1) *Physiological or homeostatic regeneration*, which defines the natural renewal of cells that maintains the tissue in equilibrium (e.g. renewal of blood cells and epidermal cells, epithelial cells in the gut and deer antlers); (2) *Morphallaxis*, which concerns the complete reorganization and remodelling of the organism body to restore the lost parts without recurring to cell division (e.g. invertebrates such as hydra and some annelids); (3) *Hypertrophy*, which includes: *compensatory*, if it leads to an increase in size of a paired organ after its pair is lost (e.g. kidney and lungs); or *regenerative*, if it involves the restoration of the mass of damaged internal organs (e.g. liver and pancreas); (4) *Epimorphic regeneration*, when regeneration is achieved through the formation of a blastema, a mass of less differentiated proliferative cells with intrinsic morphogenic potential to restore the damaged structure (e.g. limb and tail regeneration in urodeles and fin regeneration in teleost fish) (Agata et al. 2007; Carlson 2007; Stoick-Cooper et al. 2007; Kawakami 2009; Iismaa et al. 2018) and (5) *Tissue or cellular regeneration*, which refers to the repair of local and limited damage to an organ via reconstitution of only one cell type without the formation of a blastema (e.g. skeletal muscle).

It is important to clarify that there is no correlation between a particular regenerative mechanism and particular species, i. e. one or more regenerative mechanisms can occur in the same animal depending on the tissue, extent of the damage and on the animal life stage (Bely and Nyberg 2010; Slack 2017). Central questions in the regeneration field that remain for more than a century inconclusive, include: (1) What defines and regulates the capacity to regenerate? (2) What are the cellular sources that contribute to regeneration? (3) What are the factors that trigger and initiate regeneration in the injured area? (4) How is the balance between proliferation and differentiation/patterning achieved during regeneration? (Poss 2010).

In this chapter, I will summarize the general concepts of regenerative biology setting the basis for the central aims of this thesis.

1.2 Diversity of the regenerative abilities across species and animal models

The ability to regenerate is widely distributed throughout the Metazoa. Although the extent of the regenerative capacity varies considerably across the animal kingdom, nearly every phylum has one or several species capable of regenerating missing parts. To explain why some animals regenerate and others do not, several theories have been postulated and subject to extensive debate. Regeneration could result either from a homologous trait, with a single evolutionary origin that arose early in Metazoans, or from convergent evolution that evolved in a variety of independent contexts (Sánchez Alvarado 2000; Brockes et al. 2001; Brockes and Kumar 2008; Bely and Nyberg 2010; Garza-Garcia et al. 2010). Over the course of evolution, there is a striking hierarchy of regenerative capacity among organisms, with a few exceptions. At the top of the hierarchy stand the invertebrates, such as Cnidarians (*Hydra* genus), Platyhelminthes (flatworm planarians) and Echinoderms (starfish), as they are capable of renewing whole animals from small fragments of tissue. Vertebrates also possess remarkable examples of high regenerative ability that go far beyond physiological regeneration. These include the amphibian Urodeles (salamanders, e.g. newt and axolotl) and Anurans (frogs, e.g. *Xenopus* and toads), and the teleost fish (e.g. zebrafish). Both amphibians and teleost fish can regenerate a vast array of organs and tissues that include the spinal cord, jaws, retina and lenses, limbs, tails and fins. In contrast, at the lower end of the hierarchy, with a poor regenerative capacity, stand taxonomic groups such as Aves (birds) and Mammalia (mammals). It is well described that mammals, including humans, have a very limited capacity to regenerate lost tissues nevertheless, they are capable of performing homeostatic regeneration to replace cells that are lost during daily activities, like epithelial or blood cells (Bely and Nyberg 2010; Galliot and Ghila 2010; Poss 2010; Li et al. 2015; Yun 2015; Grillo et al. 2016; Zhao et al. 2016) (Figure 1). However, severe damage to the heart, limbs and spinal cord, for instance, culminates in a non-regenerative response, and rather leads to fibrotic scarring and loss of normal tissue function. An exception to this is the mammalian liver, which can regenerate to some extent. In homeostasis, the liver has a low cell turnover rate, but upon

injury, it can recover through a combination of cellular hypertrophy and proliferation (Stanger 2015).

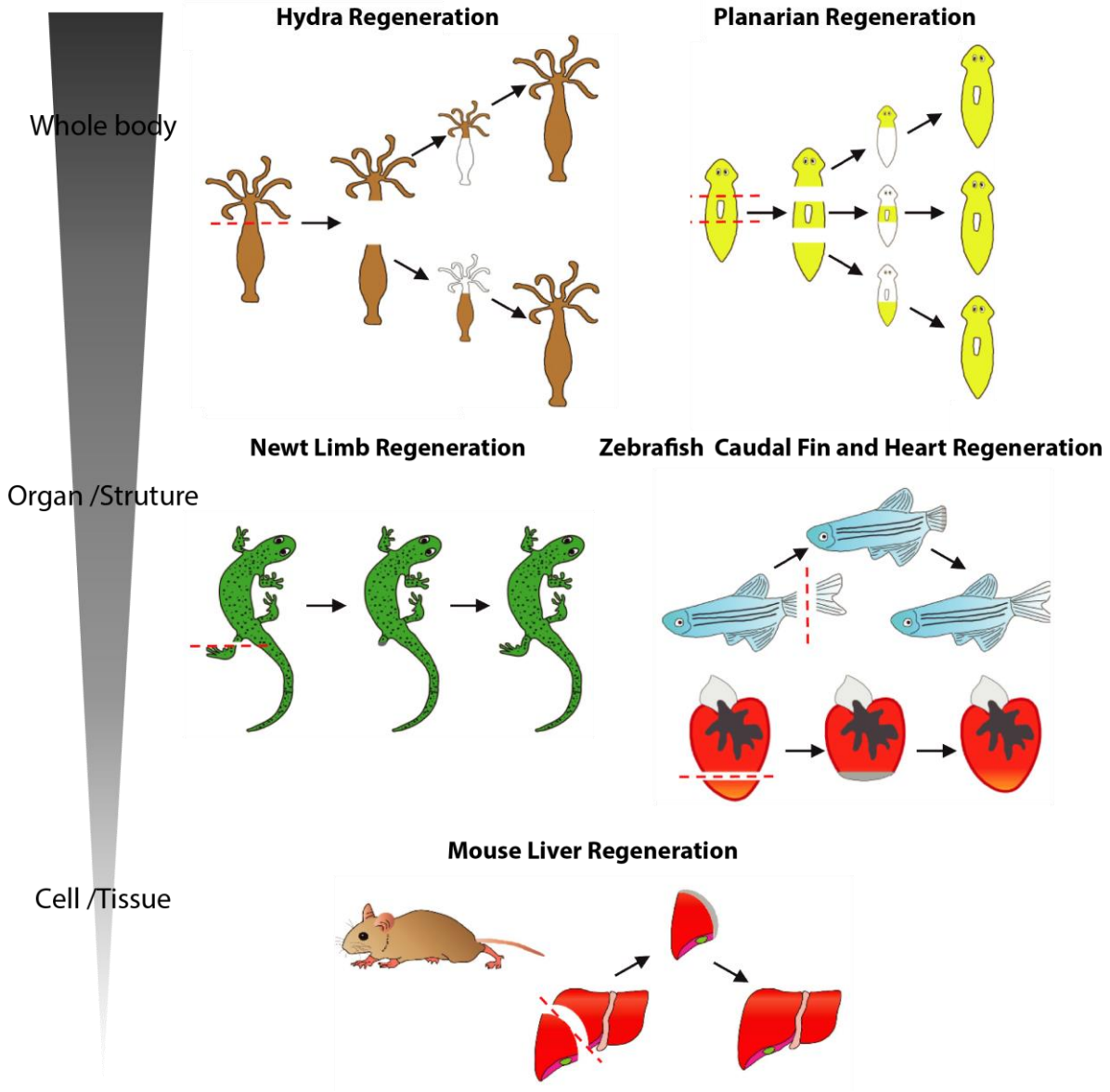

Figure 1: Animal models of regeneration and their regenerative capacity. At the top of the hierarchy with the highest regenerative capacity are Planarians and Hydra, capable of regenerating the whole body. These are followed by lower vertebrates, such as the newt and zebrafish that can regrow lost parts, like the limb, tail, fin, and organs like the heart. At the bottom, there are animals such as mammals that have lower regenerative capacity mainly at the cell/tissue level. The liver is an exception, being a highly regenerative organ. The red dashed line indicates amputation/resection. Adapted from (Bely and Nyberg 2010; Zhao et al. 2016).

Moreover, some species show a decline in regenerative capacity with age. Examples of these are the progressive loss of limb regeneration from the larval phase to adult stage in Anuran amphibians and the ability of the mouse heart to fully regenerate in neonates but not later (Zhao et al. 2016; Iismaa et al. 2018). In addition, differences in the regenerative capacity between sexes have also been observed, with zebrafish female being able to regenerate the pectoral fins, while males do not possess this capacity (Nachtrab et al. 2011). It is not clear,

however, the basis for these regenerative differences between organisms. Some hypotheses have arisen in this context: (1) one possibility is that certain genes are present only in highly regenerative species and not in species with lower regenerative capacity; (2) or organisms with high regenerative ability certain phylogenetically conserved genes activated only during regeneration, maybe through specific regeneration regulatory elements (Poss 2010; Kang et al. 2016; Pfefferli and Jaźwińska 2017); (3) a third hypothesis, which is related to the previous, concerns the epigenetic control during regeneration, supporting a model in which an organism with high regenerative capacity may possess specific chromatin profiling with reversible histone modifications in contrast to animals with lower regenerative abilities (Maki et al. 2010; Katsuyama and Paro 2011; Goldman et al. 2017).

This highlights the huge variability in the regenerative capacity and the necessity to uncover the origin of such abilities among animals. Since no animal comprises all the strategies that permit regeneration in all biological contexts, it is fundamental to combine and integrate information from several model systems of regeneration in biomedical research (Sánchez Alvarado 2008). The most common invertebrate models include hydra and planarians, which are useful to understand how a single cell can generate an entire animal composed of a multitude of tissues and organs. The most used vertebrates models encompass amphibians (Urodels and Anurans), zebrafish (*Danio rerio*) and mice (Figure 1) (Grillo et al. 2016). Amphibians and zebrafish are useful models to uncover the mechanism that regulate regeneration of specific organs (e.g. heart, retina, spinal cord, pancreas) and whole-body sections (e.g. limbs and fins) that include coordination between several tissues. Mice models are usually used to study homeostatic regeneration or regeneration of specific organs with exceptional regenerative potential (e.g. liver and bone). Studying these animal models allows to elucidate the cellular and molecular phenomena underlying the several means by which regeneration is attained in different biological contexts.

1.3 Cellular mechanisms of regeneration

When the equilibrium of a tissue is perturbed by injury, cellular mechanisms are invoked to promote efficient regeneration of the missing tissue. Thus, to understand any regenerative system, it is crucial to find the cellular origins of the renewed tissues. It has been thought that this equilibrium was mainly recovered by tissue resident stem cells that replicate and differentiate into the missing cells. This may be true under physiological conditions, but thanks to the increasing number of genetic tracing tools and live-imaging techniques, other cellular contributions have been observed, challenging the notion that differentiated cells in adult animals were irreversibly committed to a specific cell fate (Zhou and Melton 2008; Jopling et al. 2011; Jessen et al. 2015; Tata and Rajagopal 2016). In fact, mature cell plasticity and the ability to reprogram have become a major point of interest in regenerative biology. Cell plasticity is defined as the intrinsic capacity of cells that makes them amenable to be reprogramed (process of reverting mature, specialized cells into less differentiated cells) and

adopt the biological properties of other cell types that may belong to the same or different lineages (Galliot and Ghila 2010; Jopling et al. 2011; Tanaka and Reddien 2011; King and Newmark 2012; Sánchez Alvarado and Yamanaka 2014; Jessen 2015; Tata and Rajagopal 2016). This characteristic should not be mistaken by "artificial" reprogramming that leads to the conversion of differentiated somatic cells to pluripotent cells (induced pluripotent stem cells, iPSCs) *in vitro* (Takahashi and Yamanaka 2006; Eguizabal et al. 2013).
Overall, several mechanisms can contribute to the formation of new cells that will compose the regenerated tissue after damage (Figure 2):

(1) tissue resident *stem cells* or *progenitor cells*, which are capable of self-renewing and provide a source of differentiated cells. For example: planarian regeneration is exclusively dependent on a population of pluripotent stem cells, called neoblasts, which can give rise to all adult cells (Tanaka and Reddien 2011; King and Newmark 2012; Elliott and Sánchez Alvarado 2013); axolotl limb, zebrafish and mammalian skeletal muscle regeneration relies on the proliferation of satellite cells (Poss 2010; Tanaka and Reddien 2011; Perathoner et al. 2014; Sandoval-Guzmán et al. 2014; Li et al. 2015; Ratnayake and Currie 2017); and spinal cord regeneration in zebrafish is achieved through the activation of ependymal precursors (Ribeiro et al. 2017) (Figure 2);

(2) *dedifferentiation (or transient reprogramming)* of fully differentiated cells, which allows cells to revert to a less differentiated progenitor-like state within its own lineage, with the acquisition of proliferative capacity, some examples include: Newt skeletal muscle regeneration, which depends on the fragmentation of multinucleated muscle fibres that re-enter the cell cycle and proliferate (Eguizabal et al. 2013; Sandoval-Guzmán et al. 2014; Li et al. 2015; Wang and Simon 2016); and zebrafish heart regeneration, during which cardiomyocytes dedifferentiate and proliferate (Ramachandran et al. 2010; Goldman 2014; Lenkowski and Raymond 2014)) (Figure 2);

(3) *transdifferentiation* of specific cell types, which consists on the conversion of an existing differentiated cell into another cell type, either through direct conversion without cell division or encompassing a transient dedifferentiation step (e.g. after newt lens removal, pigmented epithelial cells dedifferentiate and transdifferentiate into lens cells (Li et al. 2015; Tata and Rajagopal 2016; Zhao et al. 2016); transdifferentiation can also occur during regeneration of pancreatic β-cells in the zebrafish and the mouse, in which α-cell or acinar cells dedifferentiate and convert into β-cell (Ye et al. 2015; Iismaa et al. 2018)) (Figure 2).

Although many of the cellular sources required for regeneration have already been determined, the specific cellular mechanisms that regulate the regeneration of many tissues and organs are still far from being fully understood. For the purpose of this thesis, the next section will focus on studies and current understanding of epimorphic regeneration.

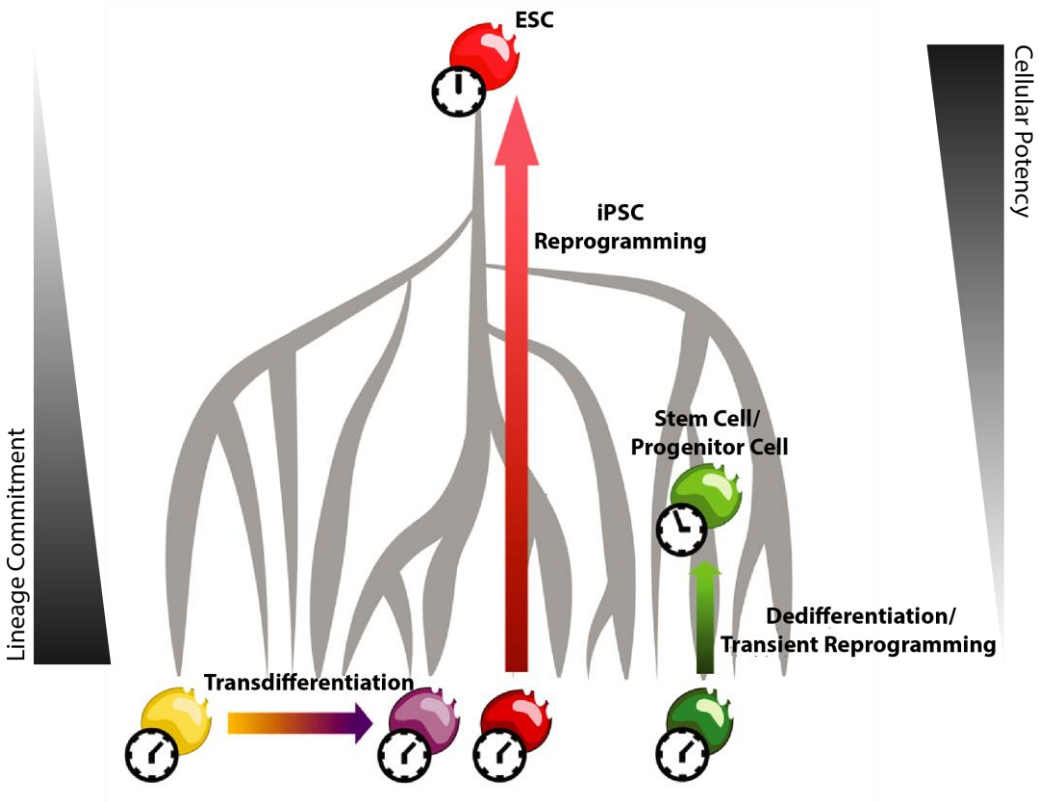

Figure 2: Cellular mechanisms that contribute to regeneration. During development, a pluripotent cell (light red ball), such as an embryonic stem cell (ESC), follows different developmental paths (grey paths) and gradually commits to differentiate into mature cells from different lineages (yellow, purple, dark red and dark green balls). It is nowadays possible to revert the entire developmental process through induced pluripotent reprogramming and transform a lineage committed cell (e. g. dark red ball) to a pluripotent cell (light red ball). Animals with high regenerative capacity have developed cellular mechanisms to completely recover damaged organs or even appendages amputation. These cellular mechanisms include: activation of resident stem cells or progenitors (light green ball); dedifferentiation of mature cells (dark green ball) to lineage restricted progenitors (light green ball); and transdifferentiation, where a cell (yellow ball) switches identity and converts directly to another mature cell (purple ball). Adapted from (Beyret et al. 2018).

2 GENERAL TRAITS OF EPIMORPHIC REGENERATION – INSIGHTS FROM ADULT APPENDAGE REGENERATION

I propose to call those cases of regeneration in which a proliferation of material precedes the development of the new part "epimorphosis".

Thomas H. Morgan, 1901

The concept of *epimorphosis* (from the Greek: epi, upon; morphosis, form) was originally noted and termed by Thomas H. Morgan to describe a regenerative process in which there is a complete reconstitution of damaged tissue or region via the formation of a specialized structure known as blastema (Morgan 1901, 1902; Sánchez Alvarado 2000). The blastema is considered to be the ultimate hallmark and the driving force of epimorphic regeneration and an important trait of amphibian and teleost fish regeneration. This structure is defined as a transient proliferative mass of less differentiated cells that originates from the uninjured tissue and accumulates near the stump region. It is covered by a specialized epithelium and

ultimately differentiates into the multitude of cell types that integrate the appendage (Brockes and Kumar 2005; Iismaa et al. 2018; Seifert and Muneoka 2018). One fascinating trait of the blastema is its self-organizing properties: once it is fully assembled, it can regenerate an entire limb autonomously even when grafted to different locations of the body (Yokoyama 2008). The blastema, especially that of the amphibian limb, shares many similarities both in form and in organization with the early embryonic limb buds assembled during vertebrate embryogenesis (Sánchez Alvarado 2000). In fact, limb development and limb regeneration research have largely advanced in parallel without a consensual view on the differences and similarities between both processes. A remarkable and classic example of epimorphic regeneration is the regeneration of appendages in adult vertebrates, such as the limbs and tails of Urodele amphibians (newt and axolotl) and the fins of Teleost fish (zebrafish). Despite structurally distinct it is clear that, upon injury, these structures go through similar regeneration phases, regenerating complex structures composed by different tissues such as skeletal muscle, bone, connective tissue, vasculature, nerves and epidermis (Tornini and Poss 2014). Epimorphic regeneration occurs in tight and sequential manner in three main phases: (1) *Wound healing*, occurs right after appendage amputation and involves migration of epidermal cells at the edge of the cut skin to cover the wound, forming the wound epidermis (WE). (2) *Blastema formation*, which comprises the activation, migration and aggregation of cells at the stump region, where they proliferate to reconstitute the missing appendage. (3) *Redifferentiation and outgrowth*, where the blastema continues to proliferate distally while proximal cells differentiate to form the new tissues. This later phase appears to mimic and be governed by the same lineage specification rules as vertebrate embryonic development. (Stoick-Cooper et al. 2007; Yokoyama 2008; Kawakami 2009; Galliot and Ghila 2010; Poss 2010; Nacu and Tanaka 2011; Tanaka 2016; Zielins et al. 2016; Stocum 2017). However, how regeneration and development differ is still under debate. It has been suggested that the main differences between appendage epimorphic regeneration and development rely on the initiation of the regenerative program, namely in the initial triggers of the process during wound healing and in the mechanisms that control blastema formation (Poss 2010; Nacu and Tanaka 2011).

Here, I will summarize relevant features of epimorphic regeneration, considering studies in the amphibian and teleost fish appendages, giving special emphasis to the mechanisms of cell plasticity and reprogramming.

2.1 Initial triggers of the regenerative response

Soon after amputation of a limb or fin many transcription-independent signals are released to the tissue, leading to the wound detection and establishment of early responses (Niethammer 2016). These signals, which are not only specific to regenerating tissues, but also occur during wound healing (Owlarn et al. 2017), include: calcium release from internal storages (Yoo et al. 2012; Cordeiro and Jacinto 2013); production of reactive oxygen species (ROS) at the wound

edge (Gauron et al. 2013; Love et al. 2013; Tauzin et al. 2014; Meda et al. 2017); cell breakage and necrosis, which leads to the release of damage-associated molecular patterns (DAMPs) (Enyedi et al. 2013; Niethammer 2016; Sandoval-Guzmán and Currie 2018); emergence of apoptotic cells that are capable of modulating the proliferation and survival of surrounding cells, a phenomenon known by "apoptosis-induced compensatory proliferation" (Géraudie and Ferretti 1997; Fan and Bergmann 2008; Boulevard 2010; Vriz et al. 2014; Perez-Garijo and Steller 2015); and collapse of the trans-epithelial electrostatic potential, which leads to differences in tissue osmolarity due to damage of the epidermal tissue barrier (Enyedi et al. 2013; Gault et al. 2014). It was also demonstrated that vascular dynamics and hemostasis serve as a foundation for the healing process, with vasoconstriction and platelets activating the intrinsic clotting cascade and leading to the release of cytokines and growth factors that initiate the inflammatory response (Yokoyama 2008). Importantly, these factors can function as chemoattractants for resident and more peripheral cells, which become activated and contribute to the regenerative process (Niethammer 2016), in some cases by directly activating signalling pathways and mitogenic signals that promote cell reprogramming and proliferation (Gauron et al. 2013; Love et al. 2013; Tauzin et al. 2014; Perez-Garijo and Steller 2015; Galliot et al. 2017; Sandoval-Guzmán and Currie 2018).

2.2 Pro-regenerative environment modulation: role of the immune system and senescent cells

Senescent cells and immune response are known to be crucial in promoting a regeneration permissive microenvironment by stimulating surrounding cells (Karin and Clevers 2016; Ritschka et al. 2017). However, they are described to function as double-edged swords, since the imbalance of these responses can easily lead to detrimental effects in tissue regeneration.

Senescence acts as a response to prevent the proliferation of cells exposed to deleterious stress, thus acting as an anti-tumorigenic mechanism (Yun 2015). The emergence of these cells can be triggered upon stress stimuli and are, for instance, accumulated after amputation of the axolotl limb (Yun et al. 2015; Stocum 2017). Recent studies have demonstrated that senescent cells are not passive players during repair, as previously anticipated, and can actually have beneficial outcomes. During mouse wound healing, removal of accumulated senescent cells at the wound margin lead to inefficient wound healing, by eliciting a pro-regenerative response (Demaria et al. 2014; Serrano 2014). This is mainly achieved by secretion of extracellular matrix proteases, growth factors, chemokines and cytokines (collectively known as senescence-associated secretory phenotype, or SASP). The SASP can activate the recruitment of immune cells and the proliferation of surrounding resident cells (including stem and progenitor cells), thereby influencing cell reprogramming and fate determination (Mosteiro et al. 2016). To avoid prolonged SASP activation, senescent cells must be cleared by macrophages and this was also shown to be obligatory for blastema formation and regeneration (Yun et al. 2015; Stocum 2017).

Immune cells have been shown to be essential for regeneration of the salamander limb and the zebrafish caudal fin (Godwin et al. 2013; Petrie et al. 2015). The first immune response leads to a pro-inflammatory phase, with recruitment of neutrophils and macrophages (Sandoval-Guzmán and Currie 2018). These cells are required to restore the barrier function, to remove pathogens, cell debris and apoptotic cells, and produce pro-inflammatory cytokines. After this acute pro-inflammatory phase, macrophages switch from a pro- to an anti-inflammatory phase, characterized by clearance of the pro-inflammatory neutrophils and secretion of paracrine factors and anti-inflammatory cytokines known to stimulate angiogenesis and proliferation of resident cells (Kizil et al. 2015; Mescher 2017; Mescher et al. 2017). An unresolved pro-inflammatory phase may lead to chronic inflammation that is often associated with fibrotic scar formation (Galliot et al. 2017; Sandoval-Guzmán and Currie 2018). It is hypothesized that one of the differences between species with low, such as mammalians, and high regenerative capacities comes from the fact that the latter possess more efficient self-resolving inflammatory mechanisms that aid in tissue formation and remodelling (Karin and Clevers 2016; Lai et al. 2017). Interestingly, recent work demonstrated that in zebrafish regulatory T cells (T_{reg}) are required for proper tissue regeneration in an organ-specific manner by promoting precursor cell proliferation (Hui et al. 2017; Jahn and Weidinger 2017).

2.3 Establishment of the apical epidermal cap (AEC) and epidermis-mesenchyme interactions

After appendage resection, epidermal cells migrate to cover the wound edge forming the WE. Initially, this epidermis serves solely as a barrier from the extracellular environment. Then, it progressively thickens atop of the blastema cells and becomes a specialized secretory epithelium, the apical epidermal cap (AEC), that is considered to be analogous to the apical epidermal ridge (AER) found in developing avian and mammalian limb buds. Both the AEC and AER are indispensable for regeneration and limb development, respectively, sharing many morphological traits and expressing similar genes. In contrast to the AER, the formation of the AEC is triggered via signalling events that happen following injury, and its maintenance is regulated by regeneration-promoting signals (Nacu and Tanaka 2011; Murawala et al. 2012; Seifert and Muneoka 2018). Indeed, studies in urodeles and zebrafish show that the AEC functions as a signalling centre, secreting extracellular factors and mitogens that promote blastema cell proliferation, outgrowth and patterning (Christensen and Tassava 2000; Lee et al. 2009; Campbell et al. 2011; Zielins et al. 2016).

2.4 Nerve dependency and interplay between nerves and AEC

Salamanders and zebrafish have been used to address the requirement of nerves for regeneration and together, they have demonstrated that denervation leads to inhibition of regeneration (Kumar and Brockes 2012; Simões et al. 2014; Pirotte et al. 2016; Meda et al. 2017) with innervation being required for proliferation in the blastema (Maden 1978). Indeed,

although the formation of WE is independent of nerves, the maintenance and activity of the AEC as a signalling centre depends on its innervation by the regenerating axons, necessary for proper blastema formation and proliferation (Kumar and Brockes 2012; Zielins et al. 2016). In the newt, nerves specifically contribute to this process by inducing a mitogenic factor, newt anterior gradient protein (nAG), which is downregulated in aneurogenic/denervated limbs (Kumar et al. 2009; Zielins et al. 2016). In fact, overexpression of nAG can substitute nerves and is sufficient to promote the regeneration of a denervated appendage (Kumar et al. 2009; Tanaka 2016; Meda et al. 2017).

2.5 Histolysis of extracellular matrix: promoting cell migration for blastema assembly

The extracellular matrix (ECM) is a 3D network that provides both structural and functional information to cells in a tissue. The properties of the ECM provide mechanical and biochemical cues that regulate cell behaviours, such as migration, adhesion, polarity, survival, proliferation and differentiation. Consistent with this, ECM remodelling and degradation, or histolysis, plays important roles during appendage epimorphic regeneration both in zebrafish and in urodele amphibians (Santamaría and Becerra 1991; Yang et al. 1999b; Godwin et al. 2014; Govindan and Iovine 2015; LeBert et al. 2015; Iismaa et al. 2018). Histolysis occurs through the action of matrix metalloproteinases (MMPs) synthesized by different types of cells/tissues, including immune cells, WE and AEC (Bellayr et al. 2009; Stocum 2017). MMPs seem to have two main roles during regeneration: to promote the breakdown of ECM collagenous and laminin components, which improves epithelial cell migration; and to degrade the ECM that surrounds the wounded area thereby stimulating the activation and migration of resident cells from the site of injury to the stump to contribute to blastema formation (Bellayr et al. 2009; Stocum 2017). In parallel, a more pro-regenerative ECM is assembled, enriched in tenascin and fibronectins, which is also thought to stimulate cell growth, proliferation and migration (Godwin et al. 2014).

2.6 Cell plasticity and reprogramming of differentiated cells: a case of dedifferentiation and lineage-specific memory

Throughout the years, many important questions have been raised, most notably on the origin, plasticity and potency of the cells that compose the blastema. It has been speculated that the blastema is composed by a homogeneous group of cells that gives rise to all cell types of the regenerated tissue. This would imply that the cells that originate the blastema have the capacity to become multipotent or even pluripotent (Echeverri and Tanaka 2002). However, recent findings show that the blastema is composed of a heterogeneous cell population with lineage-restricted potential (King and Newmark 2012; Zielins et al. 2016). This was shown using transgene-based lineage tracing in amphibian limb and zebrafish caudal fin regeneration to follow the progeny of cells from multiple tissues, such as skeletal muscle, bone, connective tissue, epidermis, dermis and vasculature. These studies showed that blastema cells are

generated from mature cells close to the amputation region that proliferate while remaining lineage restricted and redifferentiate to the same cell type that they derived from (Figure 3) (Kragl et al. 2009; Tanaka and Reddien 2011; Tu and Johnson 2011; King and Newmark 2012; Stocum 2017). Thus, the current established view is that the cellular plasticity found in appendage regeneration relies mainly in the dedifferentiation of mature cells (Echeverri et al. 2001; Odelberg 2005; Straube and Tanaka 2006; Satoh et al. 2008; Knopf et al. 2011; Sandoval-Guzmán et al. 2014; Wang and Simon 2016; Iismaa et al. 2018). Exceptions to this are the contribution of resident stem cells, such as satellite cells in the salamander limb, which contribute to new skeletal muscle, and melanocyte stem cells in zebrafish caudal fin regeneration that differentiate to distinct pigment cell populations (Morrison et al. 2006; Tu and Johnson 2010). Overall, this suggests that blastema cells do not show the pluripotency of embryonic stem cells (ESCs) and instead they rely on a partial dedifferentiation process that guarantees the plasticity required to proliferate and rebuild the missing tissue.

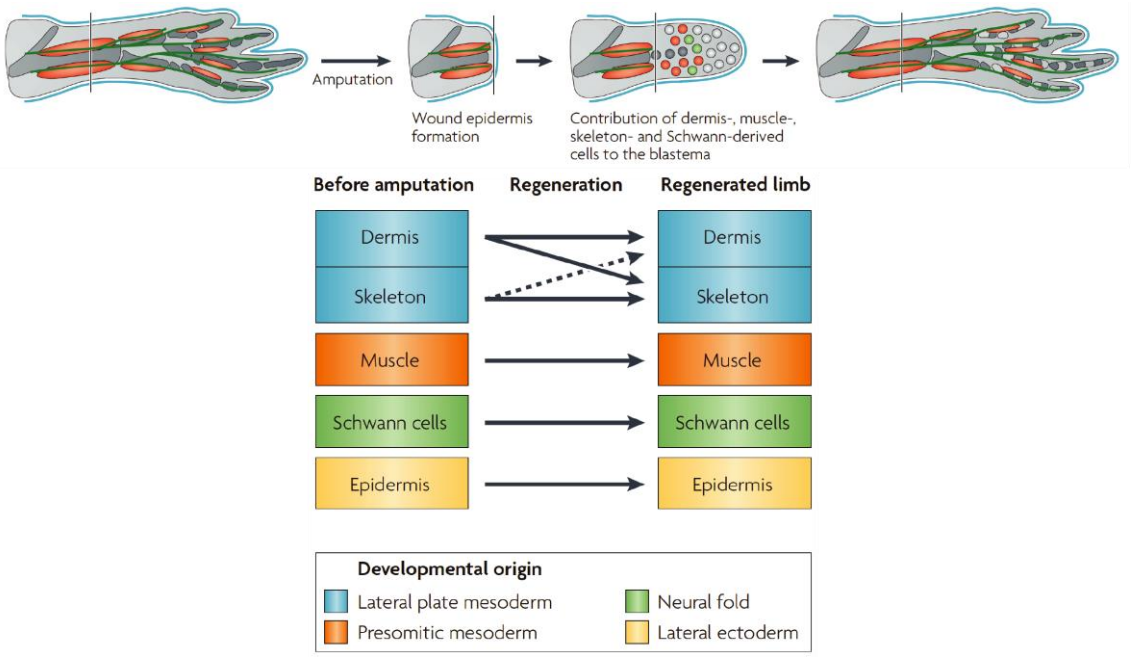

Figure 3: Cellular memory and lineage restriction during axolotl limb regeneration. Tissue-grafting experiments by Kragl and colleagues (Kragl et al. 2009) revealed the contributions of different resident cells for blastema formation during limb regeneration. They demonstrated that the most relevant tissue lineages like muscle, cartilage, Schwann cells and epidermis remain restricted to their developmental origin and do not transdifferentiate to other lineages during regeneration. Blastemal cells arise from different tissue types but remain compartmentalized in the blastema, occurring little lineage switching when forming the new limb structures. Adapted from (Poss 2010).

2.7 Activation of cell cycle re-entry and controlled growth

Regulation of cell cycle re-entry and proliferation is one of the most important requirements for regeneration. Many of the mechanisms and signalling pathways that regulate proliferation during regeneration have been described, however, the key molecules that trigger cell cycle re-entry still remain unclear (Poleo et al. 2001; Santos-Ruiz et al. 2002; Stoick-Cooper et al.

2007). Several researchers have hypothesized that cancer-related pathways are involved in regeneration since the proliferation of a mass of dedifferentiated cells in adult tissue resembles tumorigenesis. Nevertheless, during regeneration other factors must also play a part given that, in contrast to cancer development, blastemal cells undergo coordinated and controlled growth (Seifert and Muneoka 2018). In fact, two sources of evidence support this hypothesis: cell cycle progression is tightly controlled in the blastema with most blastema cells entering S-phase but becoming arrested in the G2 phase of the cell cycle, only entering mitosis when there are enough cells to form a blastema (Stocum 2017); in addition, in contrast to what occurs in cancer, the activity of p53, a tumour suppressor typically inhibited in cancer cells, is required for the regeneration in the axolotl limb (Yun et al. 2013; Seifert and Muneoka 2018).

2.8 Deployment of major signalling pathways and positional identity during outgrowth

After blastema assembly, lineage restricted progenitor cells and/or tissue resident stem cells subsequently undergo redifferentiation, maturation and patterning to replace the lost tissues. During outgrowth, expression pattern is similar to that of development, implying that in this phase regeneration recapitulates ontogeny, however, at a higher growth rate (Iovine 2007). Major signalling pathways were demonstrated to be essential for this process, regulating the coordination between cell proliferation and differentiation, such as: Fibroblast growth factors (Fgf), Bone Morphogenetic Proteins (Bmp), Hedgehog family proteins, Notch, Retinoic acid (RA) and Wingless-type MMTV integration site family (Wnt) (Stoick-Cooper et al. 2007; Poss 2010; Antos et al. 2016). Moreover, the ability of cells to specify their position in three dimensions is critical for proper patterning in a regenerating tissue. One of the most important epimorphic regeneration properties is the existence of a positional memory, defined as positional information that instructs cells on how to pattern the new appendage during regeneration (Wolpert 1969; Poss 2010). During development, cells respond to graded concentrations of specific signalling cues or morphogens from which they withdraw “positional values” specific spatial patterns of gene expression (Turing 1952; Wolpert 2011). In contrast to embryonic limb bud development, positional memory in appendage regeneration appears to be controlled by a combination of cell autonomous and non-autonomous graded factors. Importantly, during salamander limb regeneration, the site of injury can occur at any level along the proximo-distal (PD) axis of the limb with the blastema cells faithfully replacing the missing parts (Mariani 2010). Amputation at the level of the upper arm results in a blastema harbouring cells that convert to form lower arm and hand. In contrast, amputation at the hand level generates hand blastema cells that are not able to become upper arm cells, as revealed by grafting experiments (Pescitelli and Stocum 1980; Echeverri and Tanaka 2005; Nacu and Tanaka 2011; Tanaka 2016). This positional identity was also shown to be an important feature in zebrafish caudal fin regeneration, where cells show a distinct transcriptional profile depending on their PD identity (Rabinowitz et al. 2017).

2.9 Transcriptional regulation: role of epigenetics and microRNAs

Regeneration is characterized by major changes at the level of gene expression. Therefore, to comprehend the regenerative process, it is of major importance to consider how regenerative programs are regulated transcriptionally by early injury signals (Chen and Poss 2017). Epigenetic regulation is likely to play a major role in cell plasticity, reprogramming and lineage specification events occurring during appendage regeneration. (Katsuyama and Paro 2011; Beyret et al. 2018). Epigenetic gene regulation involves the alteration of chromatin structure through histone modifications (Hawkins et al. 2011; Orkin and Hochedlinger 2011; Chen and Dent 2014; Guo and Morris 2017). It was demonstrated that the elimination of repressive histone methylation signatures (Stewart et al. 2009), nucleosome remodelling and deacetylase complex (NuRD) (Pfefferli et al. 2014) is required for transcriptional activation of genes during zebrafish caudal fin regeneration. Nevertheless, the maintenance of some histone modifications also seems to be required to promote heritable cellular memory to maintain limb cell properties during *Xenopus* limb bud regeneration (Hayashi et al. 2015). Another related question is whether the chromatin state at homeostasis determines the regeneration ability. This remains largely unclear, but it has been demonstrated that zebrafish contains "dormant" or bivalent chromatin with both active and suppressive histone modifications, considered to be in a more flexible state than mammalian chromatin (Stewart et al. 2009; Katsuyama and Paro 2011). Interestingly, recent reports identified enhancer elements that preferentially and/or specifically activate gene expression in damage and regeneration contexts. These are designated by tissue regeneration enhancer elements (TREEs) and have a widespread distribution in the vicinity of genes with induced expression during zebrafish heart regeneration (Chen and Poss 2017; Goldman et al. 2017).

In addition to chromatin regulation, microRNAs (miRNAs) also provide a potential means to rapidly silence gene expression during regeneration by targeting complementary mRNA. Several microRNAs have been shown to have important roles during zebrafish caudal fin and axolotl limbs regeneration, namely miR-133 and miR-21 respectively (Thatcher et al. 2008; Yin et al. 2008; Holman et al. 2012; King and Yin 2016).

Further characterization of the transcription factors, epigenetic changes and microRNA networks will be extremely important to understand the mechanism of dedifferentiation during regeneration.

Overall, the blastema is a highly proliferative and transient structure, whose assembly is regulated by many factors secreted by nerves and by the AEC. Notably, this structure has two main intrinsic characteristics fundamental for regeneration: (1) cellular memory, whereby cells that form the blastema arise mainly from dedifferentiation of mature cells that are lineage restricted; and (2) positional memory, whereby cells know which missing structures

they have to give rise to. Ultimately, orderly differentiation and patterning originate the multitude of cell types that make up the missing tissues.

3 ZEBRAFISH AS A MODEL SYSTEM TO STUDY REGENERATION

Zebrafish (*Danio rerio,* Cyprinidae, Teleostei) is a tropical, freshwater teleost fish native to river basins in and surrounding East India. It was first established as a laboratory model system by Streisinger and colleagues during the 1970s with the purpose of generating genetic manipulation tools to study vertebrate biology (Streisinger et al. 1981; Gemberling et al. 2013).

3.1 General features of zebrafish as a model system

Over the last 70 years, zebrafish has become a valuable tool to dissect the principles of early vertebrate development and organogenesis, behaviour, metabolism and human pathologies (Lieschke and Currie 2007; Goldsmith and Jobin 2012; Tavares and Lopes 2013; Santoro 2014; Fazio and Zon 2017). A vast array of technical and practical advantages make zebrafish one of the most powerful model systems, which include: low cost and easy maintenance; large number of offspring (over 100 embryos per clutch, useful for high-throughput chemical and genetic screens); transparent embryos with rapid external development (suitable for high resolution live imaging); short generation time (reaching adulthood in 3-4 months); a fully mapped genome with significant homology with the human genome (approximately 70%), including noncoding regions; amenability to molecular manipulation in early stage embryos (such as gene knockdowns via morpholino technology); genome editing technology, with the possibility of transgenesis (*tol2*- or Meganuclease-mediated) and mutagenesis (CRISPR/Cas9 and TALEN) to understand gene function (Grunwald and Eisen 2002; Brittijn et al. 2009; Lieschke et al. 2009; Soroldoni et al. 2009; Goldsmith and Jobin 2012; Gemberling et al. 2013; Howe et al. 2013; Zhang et al. 2013; Varshney and Burgess 2014; Kawakami et al. 2016). Importantly, many human disease-related genes have orthologues in zebrafish and their study has already contributed to gain insight into their pathophysiology (Lieschke and Currie 2007; Brittijn et al. 2009). Thus, zebrafish offers several advantages that make it a more advantageous model system or, at least, an important complement to the more established vertebrate genetic model, the mouse. Furthermore, the zebrafish community has available a high-quality genome resource (https://www.sanger.ac.uk/science/data/zebrafish-genome-project) with genetic maps that have greatly facilitated the identification and characterization of disease-causing mutations. In addition, a zebrafish histological atlas (http://bio-atlas.psu.edu/zf/) has also been developed, covering all developmental stages of zebrafish lifespan from embryo to adult in order to visualize and better comprehend the anatomical structures that can be distinguished at any particular stage. Finally, the community also benefits from a centralized database (https://zfin.org/) with up to date information regarding

available techniques, mutant and transgenic strains, genetic maps, expressed sequence tags (ESTs) and publications (Goldsmith and Jobin 2012).

Despite being widely used throughout the years for the study of vertebrate embryonic development, the first use of fish as a scientific model organism was in the regeneration field by Thomas Hunt Morgan, who studied regeneration of amputated fish fins (Morgan 1901, 1902). Over the past decade, zebrafish have become a primary model system for the study of vertebrate regeneration (Gemberling et al. 2013; Goessling and North 2014; Shi et al. 2015), possessing a remarkable capacity to regenerate damaged organs and entire structures after amputation/resection and other mechanical or chemical injuries. Currently, studies have covered nearly all major organs and tissues in the adult system, like the heart (Kikuchi and Poss 2012; Kikuchi 2014), fins (Akimenko et al. 2003; Poss et al. 2003; Kawakami 2009), retina (Wan and Goldman 2016; Ail and Perron 2017), brain (Kizil et al. 2012), spinal cord (Ghosh and Hui 2016; Noorimotlagh et al. 2017), bone (e.g. jaw and scales) (Spoorendonk et al. 2010; Wang et al. 2012; Witten et al. 2017; Iwasaki et al. 2018), pancreas (Curado et al. 2007; Beer et al. 2016), liver (Wang et al. 2017), skeletal muscle (Ratnayake and Currie 2017), intestine (Schall et al. 2015), kidney (Sander and Davidson 2014; Cirio et al. 2015), hair cells (Lush and Piotrowski 2014) and barbels (LeClair and Topczewski 2010). These studies have allowed the elucidation of the cellular and molecular mechanisms underlying regeneration, holding promising contributions to the field of regenerative medicine.

3.2 Zebrafish caudal fin regeneration

Fish fins are known to be the analogous structures to the terrestrial vertebrate limb (Yano and Tamura 2013) thus exhibiting many similarities regarding regenerative features. The first known report about fin regeneration was described by Broussonet in 1786 based on experiments with the goldfish (Broussonet 1786). Since then, fish caudal fins, in particular from the zebrafish, have become an excellent and popular model for studying the principles underlying appendage epimorphic regeneration (Poss et al. 2000b; Kawakami 2009; Pfefferli and Jaźwińska 2015).

3.2.1 Models to study tissue repair and regeneration using the caudal fin

Several types of injury to the adult zebrafish caudal fin can trigger a regenerative/repair program and, depending on the type of question to be analysed, three main models can be employed: amputation (Figure 4A), cryoinjury (Figure 4B) or bone crush/fracture injury (Figure 4C). The oldest and most popular method is the caudal fin amputation model, where amputations are made by surgically removing the fin with a sterile razor blade (Poss et al. 2000a). These studies allowed to shed light into many cellular and molecular mechanism that control regeneration and gave useful insights about the most important questions in the field, such as: what triggers cells to acquire a regenerative program?; what is the source of the cells

that compose the blastema?; what are the signalling pathways that coordinately regulate growth and patterning during regeneration? (Kawakami 2009; Antos et al. 2016). The other two methods recently established were the cryoinjury and the crush injury. The cryoinjury method (Figure 4B) is performed by transection of the caudal fin using a frozen blade, which disrupts tissue integrity and leads to the loss of the dead fin tissue after two days post-cryoinjury. This type of procedure is used to study the detrimental effects of prolonged tissue damage, inflammation and ischemia on the execution of the regenerative programme. These effects also occur in the amputation/resection model but to a lesser extent (Chassot et al. 2016). Lastly, the bone crush injury model (Figure 4C) consists on the breakage of the bony-rays by applying mechanical force without tissue removal. This leads to transverse fractures in single segments of the bony-rays and triggers a remodelling process with the formation of a "hard callus". This process takes longer than bone regeneration after amputation and resembles mammalian bone fracture healing, thus being more suitable to study bone fracture repair processes (Sousa et al. 2012; Geurtzen et al. 2014).

Besides the adult caudal fin, some studies have also used fin fold (caudal fin primordium) amputation to study tissue regeneration during zebrafish larval stages (Figure 4D). This system is permissive to single cell live imaging which, coupled with molecular biosensors (e.g. for ROS or Ca^{2+}), allow the analyses of very early responses to amputation. Although the adult caudal fin has a more complex architecture than the fin fold, the overall early regenerative mechanisms seem to be conserved (Kawakami et al. 2004; Niethammer et al. 2009; Mateus et al. 2012; Yoo et al. 2012).

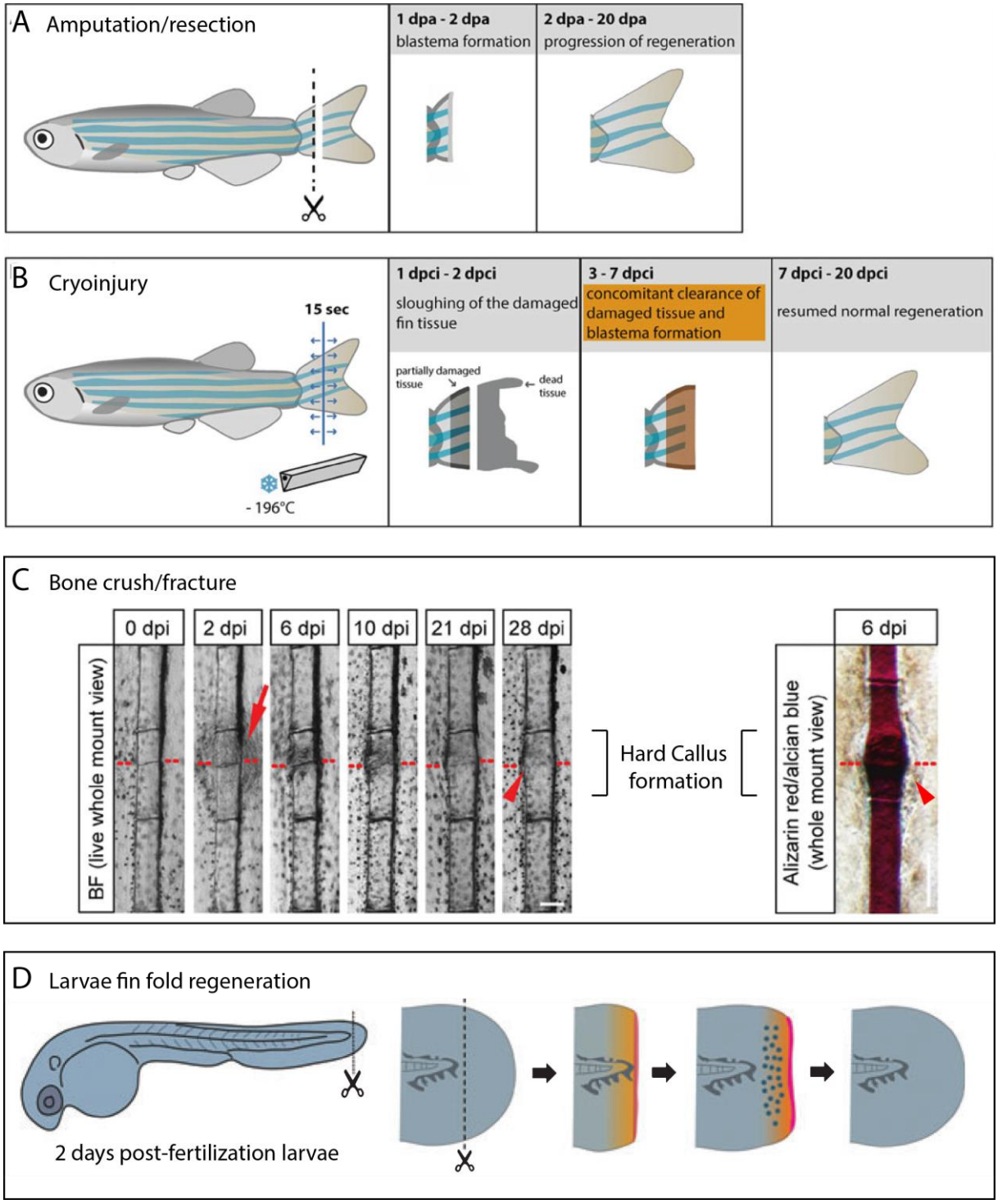

Figure 4: Models of injury to the zebrafish caudal fin. (A) In the adult caudal fin amputation model, half of the fin is removed surgically with a razor blade (black dashed line marks the amputation plane). (B) Adult caudal fin cryoinjury model is based on the destruction of the fin using a cold blade for 15 seconds along the plane of injury (blue line). (C) Adult caudal fin fracture model is based on the application of mechanical force on a single bony-ray (dashed red lines); whole mount images of bright field and alizarin red/alcian blue (bone labelling) show epidermal thickening (red arrow) and callus formation (red arrow-head). (D) Zebrafish larva fin fold regeneration is achieved by amputation as early as 2 days post-fertilization. Dpi: days post-injury. Dpci: Days post-cryo-injury. Dpa: Days post amputation. BF: brightfield. Adapted from (Kawakami 2009; Geurtzen et al. 2014; Chassot et al. 2016).

3.2.2 Zebrafish caudal fin structure: emphasis on skeletal elements

The zebrafish caudal fin derives mostly from the ventral side of the larval fin primordium, the fin fold, and is a non-muscularised structure, displaying a symmetrical and bi-lobed morphology (Figure 5A and B) (Pfefferli and Jaźwińska 2015). It is composed and supported by a dermal skeleton (similar to intramembranous bone, with no cartilaginous scaffold) that encompasses features similar to bone and to cartilage and is composed of a bone matrix with a very particular composition not found in other skeletal structures (Marí-Beffa et al. 2007). The fin skeleton consists of 16-18 segmented bony-rays, also called lepidotrichia, that extend along the whole length of the fin and bifurcate, with the exception of the most lateral rays (Figure 5A, B and C). The bony-ray segments are intercalated by soft intersegment joints (Figure 5A'and B') and each ray is separated by soft interray tissue (Figure 5A' and B) (Borday et al. 2001; Akimenko et al. 2003; Pfefferli and Jaźwińska 2015).

Since zebrafish continuously grow during adulthood, fins also extend in length by addition of new segments to the distal-most regions of the bony-rays (Akimenko et al. 2003), a process called homeostatic regeneration (Wills et al. 2008; Marí-Beffa and Murciano 2010). Both bony-ray and interray regions are coated by a multilayered pigmented epidermis, composed by several keratinocyte layers and a basal layer containing stem/progenitor cells (Becerra et al. 1983; Hong et al. 2011). Each bony-ray consists of a pair of concave juxtaposed hemirays, resembling a pair of parenthesis, that enclose an inner intraray compartment composed mainly of mesenchymal or connective tissue with fibroblast-like cells (Figure 5B', D'' and D''') but also arterial capillaries, nerve fibers, pigment cells and resident blood cells (macrophages, plasma cells and neutrophils) (Figure 5D'''). In addition to these cell types, a monolayer of osteoblasts, also designated as scleroblasts, covers the bone matrix on the inner (facing the mesenchymal compartment) and outer (facing the epidermis) side of the hemirays (Figure 5D'''). The bony-ray matrix is mainly composed of collagens and glycosaminoglycans, which are synthesized and secreted by the osteoblasts (Santamaría et al. 1992; Marí-Beffa et al. 1996; Marí-Beffa and Murciano 2010). These osteoblasts are flattened and elongated cells derived from paraxial mesoderm (Lee et al. 2013) that are attached to the lepidotrichia surface (Becerra et al. 1983; Marí-Beffa et al. 1996; Bruneel and Witten 2015). The predominant portion of the bony-ray is composed of calcified bone matrix, while the distal-most 3-4 segments are thinner and remain non-mineralized. The distal tips of each bony-rays encase a bundle of fusiform spicules, named actinotrichia, which are composed of unmineralized fibrils of collagens associated with non-collagen components, providing a flexible support to the fin edge (Figure 5C) (Akimenko et al. 2003; Durán et al. 2011; Pfefferli and Jaźwińska 2015). In the interray space, mesenchymal components are also found, with the exception of arteries, which are substituted by venous capillaries (Marí-Beffa et al. 1996; Akimenko et al. 2003; Kawakami 2009; Tal et al. 2010; Tu and Johnson 2011). During regeneration, this multitude of tissues and cell types is fully restored and interactions between cells are re-established and coordinated to ensure proper growth and patterning to pre-injured levels.

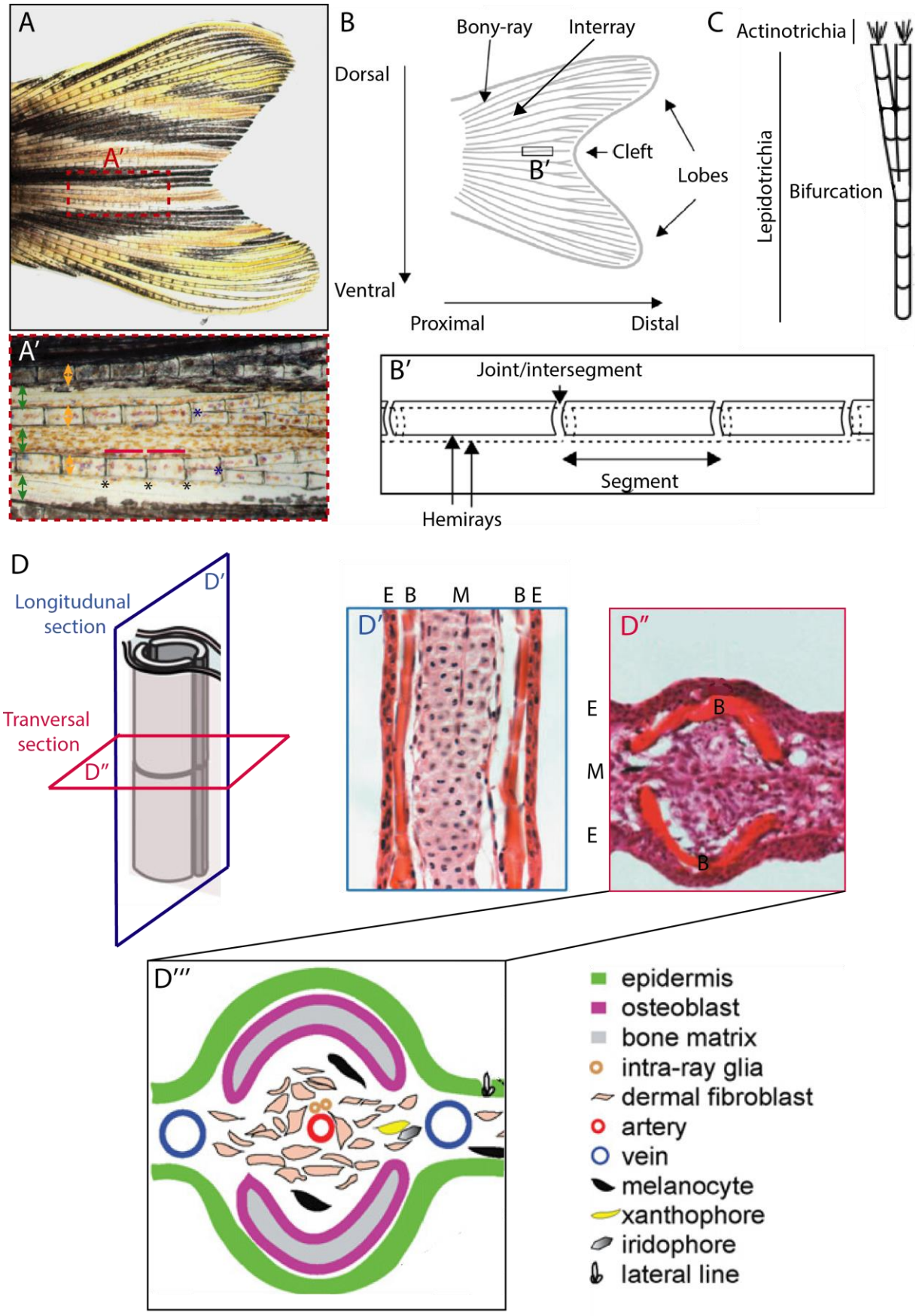

Figure 5: Organization, structure and histology of the adult zebrafish caudal fin. (A-A') Representative example of a zebrafish caudal fin with magnified panel (red dashed box) showing the bony-rays (orange double arrow-heads), which are composed of segment (red lines) and intersegment/joint (black asterisks), intercalated by

interray regions (green double arrow-heads). Bony-rays bifurcate (blue asterisks) at the distal regions of the fin. (B-B') Schematic representation of the caudal fin bilobed structure where the cleft refers to the caudal fin region between two lobes. Black box represents magnified panel showing in more detail the bony-bony ray structure. (C) Scheme representing a dermal skeleton of a bony-ray, which is composed of flexible actinotrichia spicules and lepidotrichia (the bony-ray per se), that splits at a bifurcation point into two sister rays. (D-D'') Cartoon showing the bony-ray structure with longitudinal (D') and transversal (D'') planes of sectioning and the respective representative images of caudal fin hematoxylin and eosin staining. (D''') Illustration depicts the organization of the different cell types found in a transversal section of a bony-ray, including: epidermis, osteoblasts, fibroblast-like cells, pigmented cells (melanocytes, iridophores and xanthophores), endothelium (artery and veins), intraray glia and lateral line cells. (E) epidermis; (M) mesenchymal compartment (or intraray compartment) and (B) bone matrix. Adapted from (Akimenko et al. 2003; Tu and Johnson 2011; Rolland-Lagan et al. 2012; Pfefferli and Jaźwińska 2015; Puri et al. 2017).

3.2.3 General features of adult caudal fin regeneration

Zebrafish caudal fin regeneration relies on the formation of a blastema and therefore it is a classic model of epimorphic regeneration, comprising all characteristic traits of this regenerative program. However, it also endues its own particular properties that make it quite advantageous in comparison with the traditional amphibian limb models. The caudal fin comprises a simpler anatomical organization, with fewer cell types involved in regeneration and quicker regeneration times, taking only about 2-3 weeks in contrast to 1 month in amphibians (Poss et al. 2003; Yokoyama 2008). Complete reconstitution of the missing fin is highly dependent on the temperature since at 33°C regeneration occurs nearly twice as quickly than at 25°C. In addition, the caudal fin is easily accessible to surgery and its analysis does not require to sacrifice the animal. The external location and its transparency makes it also suitable for live imaging (Poss et al. 2000a, 2003; Pfefferli and Jaźwińska 2015). This structure has an almost unlimited ability to regenerate, allowing repetitive amputations without compromising its regenerative capacity (Azevedo et al. 2011). The initial stages of regeneration do not seem to be affected by age, but mild differences were observed during the late outgrowth phase between young and old animals (Shao et al. 2011; Itou et al. 2012). Caudal fin regeneration leads to the formation of an almost flawless replica of the original structure with the exception of initiation of the bony-ray bifurcation. An amputation near the bifurcation plane induces a distalization of the regenerated bifurcation, suggesting that the positional memory for bony-ray bifurcations depends on the PD level of the amputation (Azevedo et al. 2012).

Another important feature is that the caudal fin bony-rays regenerate independently of one another. Each bony-ray gives rise to an individual blastema, which functions as autonomous regenerative units and thus as experimental replicates in the same animal (Pfefferli and Jaźwińska 2015). Also, bony-ray regeneration is a unidirectional process, since ablation of only some ray segments, which creates a discontinuity in the ray, leads to regeneration of the damaged ray from the proximal region toward the distal edge. It is proposed that this unidirectionality is correlated with the nerve supply since this type of ablation deprives the distal part of the ray of its normal innervation (Akimenko et al. 2003). Moreover, bony-ray growth control is achieved along the PD axis (Lee 2005), as shown by experiments using the

staircase-like amputations: a more proximal amputation induces the formation of a larger blastema that regenerates faster than the one formed via a more distal amputation (Figure 6A). This is mainly attained through a higher proliferation rate in more proximal regenerates than in distal regenerates (Akimenko et al. 1995, 2003; Lee 2005). In addition, the caudal fin bi-lobed architecture has allowed researchers to demonstrate that growth rates vary between medial (cleft region) and lateral regions (lobe regions). These findings were observed by amputating the lateral rays of both fin lobes at the same level but with different slopes, resembling the shape of two teeth of a saw (Figure 6B). When the adjacent stump tissue is more distal than the border (lobe region) stump growth is favoured, whereas the opposite delays regeneration. This feature was designated by Morgan as "regulative influence" (Morgan 1902; Akimenko et al. 2003) and later shown to depend on the interaction between ray and interray blastemas that allow for bifurcation formation. Most bony-rays form bifurcations since they are surrounded by interray tissue, with the exception of most lateral rays, which possess only one neighbour interray tissue.

Strikingly, and in contrast to amphibians, where blastema cells possess the same positional memory even when transplanted to other locations, the caudal fin blastema memory appears to have the potential to be reset. For instance, when a fragment of a lateral ray (lobe) is transplanted into a medial region (cleft), it is able to acquire features of medial rays such as bifurcation formation, suggesting that bony-rays have morphogenetic plasticity dependent on the surrounding environment (Murciano et al. 2002; Akimenko et al. 2003; Tamura et al. 2010).

Finally, all these features render the caudal fin an excellent model for understanding epimorphic regeneration and can even be more advantageous over more traditional models, like amphibian limb regeneration.

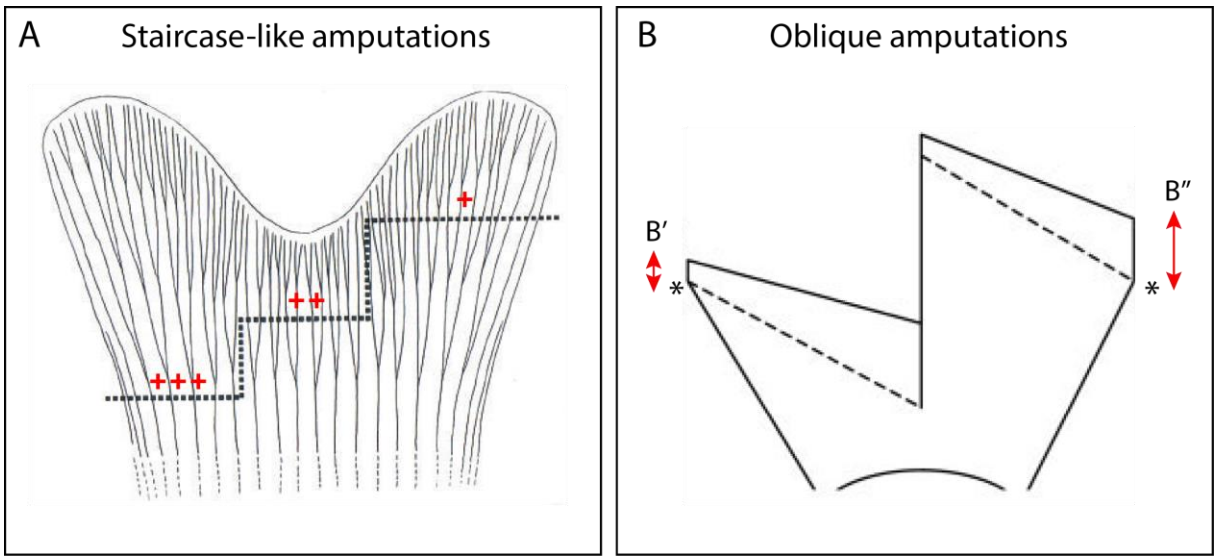

Figure 6: Different caudal fin amputations reveal general traits of the regenerative process. (A) Staircase-like amputations in a single zebrafish caudal fin at three different levels along the PD axis demonstrated that proximal amputations have higher growth rates in comparison to more distal amputations (+ show the degree of growth).

(B) Oblique amputations show that growth regulation also occurs along the medial-lateral axis. When the neighbour stump is more distal than the border (situation B'') the growth rate is increased when compared with the opposite situation (when the stump is more proximal than the border) (B'), even when the more lateral rays are amputated at the same level (asterisks). Adapter from (Akimenko et al. 1995, 2003).

3.2.4 Phases of caudal fin regeneration

A huge amount of research has been done to understand the caudal fin regenerative process, including unbiased approaches like transcriptomic (Padhi et al. 2004; Schebesta et al. 2006; Thatcher et al. 2008; Nachtrab et al. 2013; Kang et al. 2016; Nauroy et al. 2018) and proteomic analyses (Nolte et al. 2014; Rabinowitz et al. 2017), drug screening assays (Mathew et al. 2007; Oppedal and Goldsmith 2010) and mutagenic screens (Johnson and Weston 1995; van Eeden et al. 1996). According to these data, the regeneration program can be divided into several successive but overlapping steps (Figure 7A): (1) Wound healing and wound epidermis formation (from 0 to 18 hours-post amputation (hpa)); (2) Blastema formation (from 12 to 48 hpa); and (3) Regenerative outgrowth (from 48 hpa to 20 days-post amputation (dpa)) (Poss et al. 2000b). Each one of these phases will be described in further detail in the next sections of this chapter.

3.2.4.1 Wound healing phase

This phase occurs as soon as the damage is inflicted, resulting in almost no bleeding or inflammation. As early as 1-3 hpa, a thin layer of epidermal cells migrate to seal the wound, leading to wound closure (Figure 7A) (Poss et al. 2003). It is thought that this process requires primarily F-actin-mediated contraction at the wound margin and collective cell migration, as observed in simple epithelia of Drosophila and vertebrates (Wood et al. 2002; Kawakami 2009). This collective cell migration process involves not only the epidermal cells near the wound site but also cells located several segments away from the amputation plane (Poleo et al. 2001; Santos-Ruiz et al. 2005). Recently, it was demonstrated through Cre/loxP cell tracing and clonal analysis that the bony-ray stump is covered by the mobilization of the epidermal cells from the interray compartment. During this process, the stump is covered within 1 hpa by basal and suprabasal cells that are closely followed by superficial epidermal cells, many of which undergo extrusion during the process (Chen et al. 2016a; Shibata et al. 2018). The new epidermal cell layer develops into a multi-layered wound epidermis with three distinct cell layers: an outer superficial layer composed of flat condensed cells; an intermediate layer with loose cells that contain mucous cells; and a basal layer that consists on a well-organized sheet of cuboidal cells with protrusions that produce the extracellular basement membrane (Santamaría and Becerra 1991; Santos-Ruiz et al. 2002). During this phase, the basal epidermal layer (BEL) produces Laminin β 1a, promoting the polarization of this cell layer (Chen et al. 2015). Surprisingly, this process is independent of cell proliferation and does not require a blood supply, depending exclusively on cell migration and rearrangements (Poleo et al. 2001; Nechiporuk and Keating 2002). In the following 12 to 18 hpa, the epidermis accumulates

additional layers by the proliferation of basal and suprabasal epidermal cells. By 18 to 24 hpa, concomitant with blastema formation, the wound epidermis maturates into a specialized structure, which starts a transcription program distinct from the uninjured epidermis, designated AEC (Poss et al. 2003). This structure acts not only as a physical barrier but also as an organizer. In particular, the BEL functions as a signalling centre for the underlying intraray mesenchymal compartment by communicating growth and patterning signals throughout regeneration (Lee et al. 2009). A well-established marker of the BEL is the *lymphoid enhancer binding factor 1* (*lef1*), which is required for epithelial-mesenchymal communication (Poss et al. 2000a). Various signalling pathways were demonstrated to be important for the maintenance and function of this regeneration epidermis. Fgf signalling regulates epidermal expression domains by controlling the expression of *lef1* and *sonic hedgehog* (*shh*), in proximal lateral regions next to the amputation plane, and the non-canonical Wnt ligand *wnt5b*, in the distal region of the epidermis (Lee et al. 2009) (Figure 8B). Recent work has also demonstrated Bmp signalling as an important player during wound epidermis formation, namely as an organizer of the BEL by regulating *wnt5b* expression (Thorimbert et al. 2015).

While wound healing is happening, immune cells, neutrophils and macrophages, sense tissue damage and are recruited to the injury area scavenging apoptotic bodies and small cell debris (Li et al. 2012; Petrie et al. 2015; Niethammer 2016). Tissue damage is detected by differences in interstitial osmotic pressure, calcium signalling, ROS production and apoptosis of damaged cells (Niethammer et al. 2009; Yoo et al. 2012; Gault et al. 2014; Niethammer 2016; Chen and Poss 2017). These studies have shown that ROS mediates immune cell chemotaxis, by activation of the redox sensor Lyn, a Src family kinase (Niethammer et al. 2009; Yoo et al. 2012; LeBert et al. 2018). In addition, during adult caudal fin regeneration, ROS production is not only observed at early stages (0-2hpa) but also sustained until later time-points (for at least 24 hpa), suggesting additional roles during regeneration. In this context, ROS triggers two distinct responses: apoptosis and c-Jun N-terminal kinase (JNK) activation, with the last being necessary to activate other target signalling pathways and both being required to activate compensatory proliferation and thus regeneration (Gauron et al. 2013; Vriz et al. 2014). In the mesenchymal compartment other signalling pathways are activated during wound healing, such as: canonical Wnt (Stoick-Cooper et al. 2006) and Activin-βA (in the interray) (Jaźwińska et al. 2007), as early as 3 hpa, and Fgf20a, (Whitehead et al. 2005), Insulin growth factor (Igf) (Hirose et al. 2014) and RA (Blum and Begemann 2012) signalling at 6hpa. These pathways (and others) are crucial for the establishment of epithelial-mesenchymal interactions that are fundamental to ensure epidermal maintenance but also the establishment of a blastema.

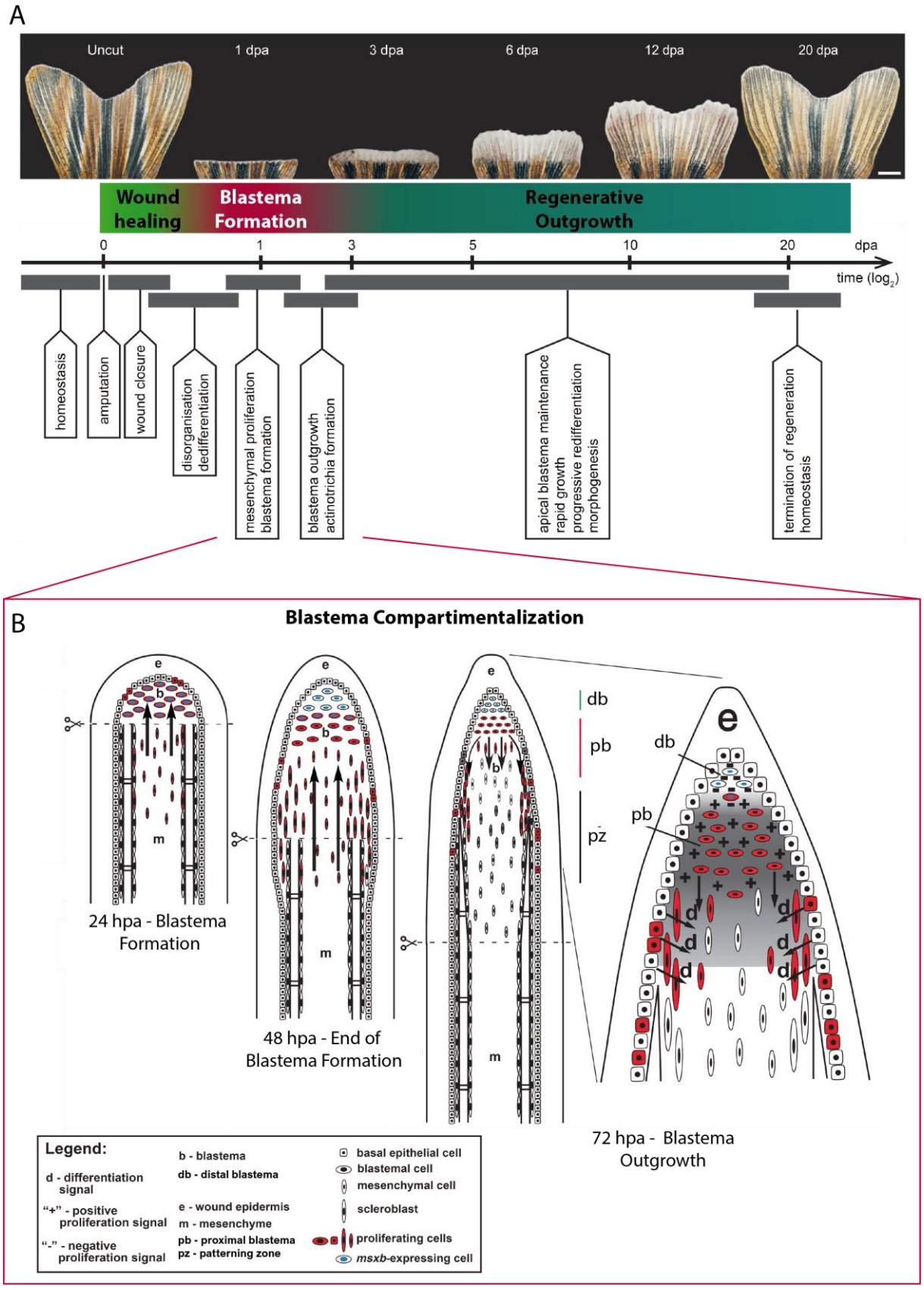

Figure 7: Adult zebrafish caudal fin regeneration. (A) Time-lapse imaging of the same fin during the regeneration process at 27 °C. Prior to amputation, the caudal fin presents a bilobed morphology. Upon amputation, the regenerative process is activated and can be divided in three sequential and overlapping phases: Wound healing (0-12 hpa), that culminates in the formation of a wound epidermis; Blastema formation (12-48 hpa); and

Regenerative Outgrowth (48hpa-20 dpa). (B) Schematic representation (longitudinal plane) of blastema compartmentalization and proliferation during regeneration. At 72 hpa, already in the outgrowth phase, three different compartments can be defined: distal blastema (db) with non-proliferative cells; proximal blastema (pb) composed of highly proliferative cells; and the patterning zone (pz) where cells proliferate moderately and start receiving differentiation signals from the epidermis that control their redifferentiation. Hpa: hours post-amputation; Dpa: Days post-amputation. Dashed lines represent the amputation plane. Adapted from (Nechiporuk and Keating 2002; Pfefferli and Jaźwińska 2015).

3.2.4.2 Blastema formation phase

The blastema, as mentioned previously, is the hallmark and a prerequisite of epimorphic regeneration. In caudal fin regeneration, this structure accumulates atop of each bony-ray and provides an adequate number of cells to build the lost tissue (Figure 7A). The blastema formation phase can be subdivided in two main events (Figure 7A). From 12 to 24 hpa, overlapping with the maturation of the wound epidermis, the intraray cells (e.g. fibroblasts and osteoblasts) located around 1 segment below the amputation plane (within a distance of approximately 150 µm) become disorganized, polarize and migrate towards the wound epidermis to integrate the blastema (Figure 7A) (Poleo et al. 2001; Nechiporuk and Keating 2002). Data from lineage-tracing experiments show that mature cells from different lineages will give rise to the blastema and will ultimately redifferentiate to their own lineage. Therefore, the blastema is composed of a heterogeneous population of cells that arise from dedifferentiation of mature cells (for most lineages composing the caudal fin) or by commitment of resident stem cells (e. g. pigment population) that remain lineage restricted and do not transdifferentiate into other cell types (Knopf et al. 2011; Sousa et al. 2011; Tu and Johnson 2011; Stewart and Stankunas 2012; Tornini et al. 2017). Another recent report has shown, through clonal analysis, the relative contribution of the blastema connective tissue (mesenchymal fibroblasts) to the regenerative process. They demonstrated that while some clones give rise to very few cells, others originate entire cell populations within the regenerated connective tissue. This provides evidence for another level of heterogenicity within blastema cells, meaning that not all cells contribute the same during blastema assembly and during outgrowth and this is determined during blastema formation. The emergence of a pre-pattern in which blastemal cells acquire preferences along the PD axis, argues against a former model in which cells within specific lineage compartment of the blastema have identical PD fates (Tornini et al. 2016).

Subsequently, in the time-window between 24-48 hpa, dedifferentiated cells at the stump start to proliferate and reorganize (Figure 7A) (Poss et al. 2000b). Within 48 hpa, the blastema is fully assembled and can be subdivided into a distal and a proximal compartment with distinct features that are further enhanced during regenerative outgrowth (Figure 7B) (Nechiporuk and Keating 2002). During this phase, the wound epidermis provides architectural cues, functioning as a source of growth factors that stimulate blastema formation and proliferation, such as Shh, Bmp2, Wnt5b (Stoick-Cooper et al. 2006), Fgf20a and other Fgfs (Laforest et al. 1998; Whitehead et al. 2005; Stoick-Cooper et al. 2006; Lee et

al. 2009; Shibata et al. 2016). In this system, RA signalling in the intraray mesenchymal compartment induces the expression of both *igf2b* and *wnt10a*, which then induce Fgf20a mainly in the wound epidermis (Stoick-Cooper et al. 2006; Chablais and Jazwinska 2010; Blum and Begemann 2012; Gemberling et al. 2013; Shibata et al. 2016). It is important to emphasise that inhibition of any of these signalling pathways precludes both blastema formation and wound epithelium organization. Importantly, mutants for *fgf20a*, also designated devoid of blastema (dob), fail to undergo intraray disorganization, show defective wound epidermis formation and do not initiate proliferation. Accordingly, inhibition of the Fgf receptor FgfR1 leads to a similar phenotype (Poss et al. 2000b) while blocking Fgf signalling did not impair cell dedifferentiation (Knopf et al. 2011), suggesting that its primary role is to control blastema cell proliferation. In fact, Fgf signalling inhibits the expression of miRNA-133, whose downregulation is required for proliferation to occur (Yin et al. 2008). This places Fgf20a as a major molecule regulating several and critical aspects for blastema formation and proliferation.

Despite being subject of fewer research studies, regeneration of the interray region is also important for the adequate restoration of caudal fin architecture. In this context, Activin-βA and RA seem to take leading roles in maintaining and regulating, also at later time-points, the identity of the interray compartment (Jaźwińska et al. 2007; Blum and Begemann 2015a).

Overall, this shows that a reciprocal communication between the wound epithelium and the mesenchyme is one of the prerequisites for blastema formation, where several signalling pathways, specially Fgf signalling, play key roles. Impairment in blastema formation consequently culminates in the abrogation of the subsequent regenerative outgrowth phase.

3.2.4.3 Regenerative outgrowth phase

Regenerative outgrowth is characterized by redifferentiation and patterning events, where previously dedifferentiated cells differentiate again to reconstitute the missing tissues (Figure 7A). These events occur concomitantly with growth control mechanisms that ensure the establishment of proper fin dimension and signals when the structure has reached its pre-injury size. Importantly, to achieve the correct tissue architecture and size, a tight coordination between differentiation and patterning with proliferation and growth mechanism has to be met. The switch between blastema formation to regenerative outgrowth is accomplished through morphological and molecular changes. During outgrowth, the cell cycle accelerates from a median G2 phase length of approximately 6 hours to 1 hour, when comparing to the blastema formation phase. At the onset of outgrowth (72 hpa), the blastema is a highly organized structure with two different domains (Figure 7B): the distal (DB) and the proximal blastema (PB). The DB is composed of slow-cycling cells and high expression of the blastema marker *msxB* (Akimenko et al. 1995; Nechiporuk and Keating 2002). The PB, which is segregated from the DB region, has a higher proliferation rate and is defined as being negative for *msxB* and positive for *msxC* and *mps1* (Akimenko et al. 1995; Nechiporuk and Keating 2002;

Poss et al. 2002). In addition, a third region is also established immediately proximal to the PB, called the patterning zone (PZ or differentiation zone), where some cells redifferentiate and maturate to form the new structures of the fin. Importantly, these three compartments are characterized by having specific gene expression and proliferative profiles, maintaining their identity until regeneration is completed (Poss et al. 2003). These gene expression profiles are similar to those that occur during development and include pathways, such as: Fgf, Wnt/β-catenin, BMP, Activin, RA, Shh, Igf, Notch, Hippo/Yap, mTOR, Sdf1 and Calcineurin signalling (Wehner and Weidinger 2015; Antos et al. 2016; Sehring et al. 2016). It is important to note that many of these pathways are not restricted to one function but play several roles during outgrowth and regulate directly or indirectly other pathways. I will briefly summarize some of the most relevant signalling pathways maintaining epidermal compartment, DB, PB and PZ during outgrowth (Figure 8A).

To maintain the epidermis as a potent signalling centre that regulates the underlying blastema compartment, the same signalling pathways that lead to the establishment of the AEC during wound healing are maintained, such as: Shh, Bmp2 and Lef1 in the proximal-lateral epidermal region (just adjacent to the PB and PZ), which signal to the underlying blastema cells, and Fgf and Wnt5b in the more distal epidermal region (just adjacent to the DB) (Figure 8B) (Laforest et al. 1998; Lee et al. 2009; Wehner and Weidinger 2015). Furthermore, canonical Wnt signalling indirectly regulates *lef1* and *shh* expression to maintain the identity of the epidermis (Figure 8B). The proliferation and survival of the epidermis are regulated by Sdf-1/Cxcr4 and Igf2b/Igf1R signalling, respectively. While the ligands *sdf-1* and *igf2b* are produced by blastema cells, the receptors *cxcr4* and *igf1R*, respectively, are expressed by the wound epidermis, leading to Sdf1 and IGF signalling activation in the epidermis (Figure 8B) (Dufourcq and Vriz 2006; Chablais and Jazwinska 2010). The DB compartment expresses Wnt/β-catenin, RA and Fgf signalling that maintain the non-proliferative and stem cell-like characteristics of this small group of cells (Figure 8C) (Lee 2005; Smith et al. 2006; Blum and Begemann 2012; Wehner et al. 2014). In the PB, many signalling pathways have been shown to be active and required to sustain blastema proliferation, including: Notch, mTORC1, Yap and BMP (*bmp6*) (Figure 8C) (Smith et al. 2006; Grotek et al. 2013; Munch et al. 2013; Hirose et al. 2014; Mateus et al. 2015). RA and Wnt/β-catenin signalling are also essential for blastema proliferation but via a non-cell autonomous manner (Blum and Begemann 2012)(Figure 8C) (Wehner et al. 2014). Finally, the PZ region is under the control of Bmp2 and Shh coming from the epidermal compartment, which is essential for bone differentiation and will be discussed in further detail in the next section of this Chapter.

Moreover, in order to form a fin with the proper size and structure, there must be a positional component that defines the differential rates of outgrowth between distal and proximal regions. This has been associated with the levels of Fgf signalling provided by the epidermis: higher levels of Fgf signalling in proximal regions lead to a higher mitotic index in adjacent blastema cells, whereas low Fgf levels in distal regions are associated with lower mitotic rates

in the adjacent blastema (Lee 2005). However, some questions remain: which factors coordinate the growth factor levels so that structures regenerate to determined sizes and proportions? In this context, Calcineurin, a protein phosphatase, has been proposed to inhibit regenerative outgrowth, by switching from high (allometric growth) to low outgrowth rates (isometric growth) once the correct caudal fin size is reached (Kujawski et al. 2014; Antos et al. 2016). Accordingly, another longfin (*alf*) and shortfin (*sof*) mutants (van Eeden et al. 1996; Iovine et al. 2005; Perathoner et al. 2014; Rabinowitz et al. 2017), which code for the Calcineurin targets Potassium channel Kcnk5b and Connexin43 (Cx43), respectively, display altered fin outgrowth proportions (Antos et al. 2016). Also, it was demonstrated that inhibition of proton pumping activity of the V-ATPase, which leads to decreased proton efflux, compromises regenerative outgrowth (Monteiro et al. 2014). All these evidences suggest that proportional growth is regulated by intercellular ion signalling and membrane potential.

Taken together, these studies highlight the complexity of regenerative outgrowth during caudal fin regeneration.

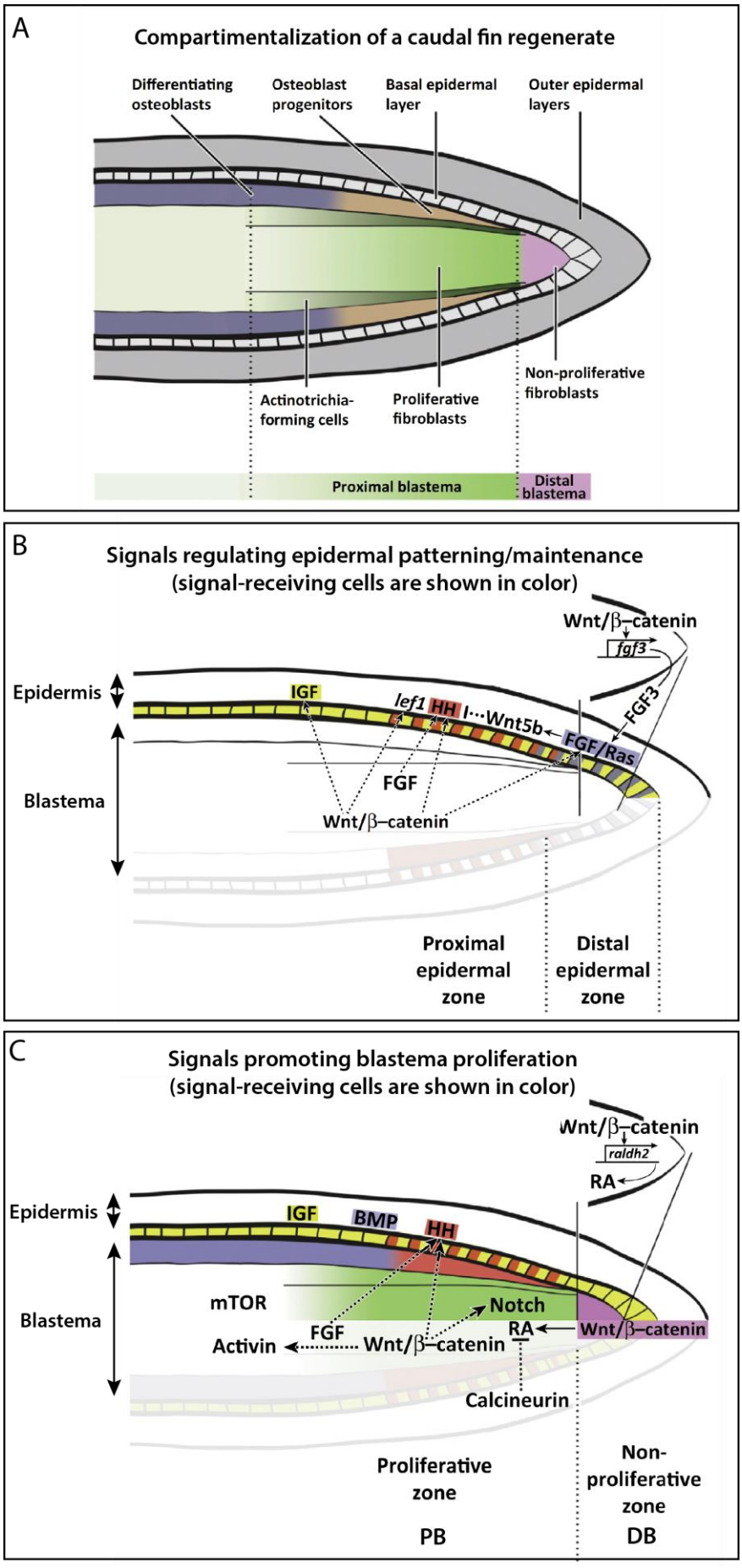
A
Compartimentalization of a caudal fin regenerate
Differentiating osteoblasts
Osteoblast progenitors
Basal epidermal layer
Outer epidermal layers
Actinotrichia-forming cells
Proliferative fibroblasts
Non-proliferative fibroblasts
Proximal blastema
Distal blastema
B
Signals regulating epidermal patterning/maintenance
(signal-receiving cells are shown in color)
Wnt/β–catenin
fgf3
FGF3
Epidermis
IGF
lef1
HH
Wnt5b
FGF/Ras
FGF
Blastema
Wnt/β–catenin
Proximal epidermal zone
Distal epidermal zone
C
Signals promoting blastema proliferation
(signal-receiving cells are shown in color)
Wnt/β–catenin
raldh2
RA
Epidermis
IGF
BMP
HH
mTOR
Notch
Blastema
FGF
RA
Wnt/β–catenin
Activin
Wnt/β–catenin
Calcineurin
Proliferative zone
PB
Non-proliferative zone
DB

Figure 8: Signalling pathways that govern caudal fin regenerative outgrowth. (A) Schematic representation of a longitudinal view of a 3 day-post-amputation caudal fin bony-ray blastema, where various tissue compartments can be distinguished. (B) Scheme representing a bony-ray blastema and depicting the most important signalling pathways that regulate epidermal patterning and maintenance. (C) Scheme representing a possible model for the regulation of blastemal cell proliferation. Coloured regions indicate domains that respond to the signalling factors depicted in the same colour. Signals whose source is unknown are on a white background. Dashed arrows indicate positive or negative interactions that are indirect or not shown to be direct. Adapted from (Wehner et al. 2014; Wehner and Weidinger 2015)

4 ADULT CAUDAL FIN BONE REGENERATION

The most abundant and important components of the adult zebrafish caudal fin are the dermal skeletal elements or bony-rays. These components give structure to the fin but also flexibility, providing the optimal architecture for its hydrodynamic function. Bone regeneration and bone producing cell (osteoblast) formation have been the subject of many research studies. These have uncovered many of the cellular and molecular mechanisms that allow proper bony-ray formation during caudal fin regeneration, although much remains to be elucidated. It is important to emphasise that key regulators of bone formation are highly conserved between mammals and zebrafish. Thus, the study of bone regeneration in zebrafish can provide new insights into the fundamental processes of osteoblast reprogramming and differentiation that could eventually be applied in the context of bone regenerative medicine. From now on I will focus on the current understanding of the mechanisms of bone regeneration triggered after caudal fin amputation, which is the main theme addressed in this thesis.

4.1 Bone development and the osteoblast lineage

In this section, I will highlight the key regulators that control the commitment and maturation of osteoblasts, which allow for proper bone development and repair in mammals, and how zebrafish could be used as a model system to study bone development and regeneration.

4.1.1 Osteoblast lineage: insights from mammalian systems

For many years, classical bone research has been done mostly using mice, chicken and cell culture systems. These model systems enabled the understanding of the basic mechanisms by which bones develop, how they are maintained and how they repair in case of damage/fracture. Bones can form through two main processes: endochondral ossification, characteristic of long bones, which requires a cartilaginous scaffold; and intramembranous ossification, characteristic of flat bones, which does not require a cartilage-based scaffold (Deng et al. 2008; Long 2012). In both types of ossification, bone is built through osteogenesis (deposition of bone matrix), modelling and remodelling events. Bone formation and maintenance are mediated by two cell types: osteoblasts, the bone-forming unit that produces the bone matrix; and osteoclasts, the bone-resorbing unit that degrades bone matrix

(Berendsen and Olsen 2015; Rutkovskiy et al. 2016). Given the aims of this thesis, I will focus on the description of the osteoblast lineage.

Osteoblasts from different bone types arise from two distinctive embryonic germ layers: one originates from neural crest cells (derived from the neural ectoderm), a mesenchymal cell type unique to vertebrates, and builds mainly intramembranous bones; the other derives from the paraxial mesoderm (somites) or from the lateral plate mesoderm and requires a cartilage-based model. Independently of their origin and type of ossification, the common ancestor of osteoblasts are Mesenchymal stem cells (MSCs), multipotent stem cells capable of giving rise to different cell lineages (myoblast, osteoblast, chondrocyte, or adipocytes), that originate preosteoblasts (Long 2012; Berendsen and Olsen 2015; Rutkovskiy et al. 2016). The osteoblast lineage is often divided into stages corresponding to their differentiation status: mesenchymal progenitors, preosteoblasts (also referred to as osteoprogenitors/osteoblast precursors), immature/intermediate osteoblasts, mature osteoblasts and osteocytes (Figure 9). Each stage of differentiation is characterized by the expression of certain molecular markers. The primary commitment towards the osteoblast lineage is governed by the so-called "master transcriptional regulator" Runt-related transcription factor 2, *Runx2* (also called *Cbfα1*) (Figure 9). RUNX2 triggers the commitment of SOX9 mesenchymal progenitors in osteoprogenitors (Akiyama et al. 2005; Ono and Kronenberg 2016), which possess proliferative ability (Figure 9) (Ducy et al. 1997; Rutkovskiy et al. 2016). Corroborating this, neonatal mutant mice for *Runx2* have a complete lack of ossification (Komori et al. 2017). Moreover, RUNX2 is also required throughout the differentiation stages, since it is crucial for the activation of other genes that are decisive for the maintenance of the osteoblast lineage and maturation. Subsequently, another transcription factor, *Osterix* (*Osx*, also named *Sp7*), is required to stimulate differentiation and the transition from osteoprogenitors to immature osteoblasts, also considered to be an intermediate state between osteoprogenitors and mature osteoblasts (Figure 9) (Nakashima et al. 2002). Similarly, *Osx*-deficient mice do not form bone due to a failure of osteoblast differentiation (Nakashima et al. 2002). OSX was shown to be required downstream of RUNX2, as *Runx2*-deficient mice fail to express *Osx*, whereas *Osx*-null mice retain *Runx2* expression (Nakashima et al. 2002). At this stage, immature osteoblasts start expressing *Alkaline phosphatase* (*Alp*), *Osteopontin* and *Collagen type 1*, which will compose the bone extracellular matrix. Gradually these osteoblasts become mature and start expressing bone matrix proteins, such as *Osteonectin* (*Osn*, also named *Sparc*) and *Osteocalcin* (*Osc*, also referred as *Bgla*). In fact, the expression of key osteoblast intermediate and mature markers, such as *Osx* and *Osc*, is directly regulated by RUNX2 (Karsenty 2008; Long 2012; Rutkovskiy et al. 2016) further emphasising the role of *Runx2* in maintaining the osteoblast lineage. OSN and OSC are both required for calcium ion homeostasis and deposition of mineral, crucial for proper bone matrix mineralization (Figure 9). At this phase, mature osteoblasts possess a cuboidal morphology and are in direct contact with the bone surface. In some cases, a subset of matures osteoblasts can be embedded and trapped in the bone

matrix, becoming an osteocyte, which translates mechanical cues to bone remodelling (Figure 9). After bone remodelling, remaining osteoblast have two options, they can either undergo apoptosis or remain attached to the bone surface, becoming inert post-mitotic bone-lining cells (BLCs) (Long 2012; Rutkovskiy et al. 2016).

The transcriptional control of osteoblast differentiation is much more complex and many signalling pathways have been currently implicated in this process (Wu et al. 2016). For example, the transcription factor TWIST-1, TGF-b and NOTCH signalling are known to inhibit RUNX2 activity and maintain the mesenchymal progenitor niche. On the other hand, signalling pathways such as BMP, WNT/ β-catenin, RA, Parathyroid hormone, MSX2, HH and FGF are known to have diverse roles and to be required in various steps of osteoblast differentiation and maturation (Phimphilai et al. 2006; Marie 2008; Ling et al. 2009; Witkowska-Zimny et al. 2010; Long 2012; Beederman et al. 2013; Rutkovskiy et al. 2016). In this context, RA and BMP signalling pathways possess important pro-osteogenic activities. The current understanding on the effects of RA signalling during osteoblast lineage specification is controversial and highly variable. RA can exert various biological outputs by binding to nuclear receptors, retinoic acid receptors (RARs) and retinoid X receptors (RXRs), which bind to the DNA and mediate target gene activation (Das et al. 2014). During osteoblast lineage determination, some studies show that RA is able to modulate *Runx2* activation and promote osteoblast formation (Dingwall et al. 2011) and matrix deposition (Li et al. 2010), while others have shown that RA restricts osteoblast differentiation (Herschel Conaway et al. 2013). Thus, additional data is required to clarify the role of RA signalling during osteoblast formation. The BMP signalling pathway members belong to the TGF-b superfamily. In this pathway, BMP ligands signal through heteromeric receptor complex, composed of type I and type II receptors at the cell surface. Activated BMP receptors signal phosphorylate cytoplasmic downstream targets SMAD1/5/8 proteins, which then complex with SMAD4 and translocate into the nucleus, where they regulate gene transcription (Kamiya and Mishina 2011; Rahman et al. 2015). BMPs are important regulators of several differentiation stages of the osteoblast lineage and function. They were demonstrated to either commit mesenchymal stem cells towards the osteoblast fate, by regulating directly *Runx2* expression (Phimphilai et al. 2006; Beederman et al. 2013; Rahman et al. 2015; Wu et al. 2016) and to direct osteoblast differentiation from osteoprogenitors to immature osteoblast (Long 2012). Additionally, many BMP ligands were shown to have a strong osteogenic capacity by increasing bone matrix deposition (Chen et al. 2012). Importantly, based on these findings, clinical trials have been initiated using BMP2 and BMP7 to improve fracture repair and craniofacial deformities (Wu et al. 2016). Therefore, BMP signalling is considered to be fundamental to the osteoblast lineage, regulating several aspects of bone homeostasis and repair.

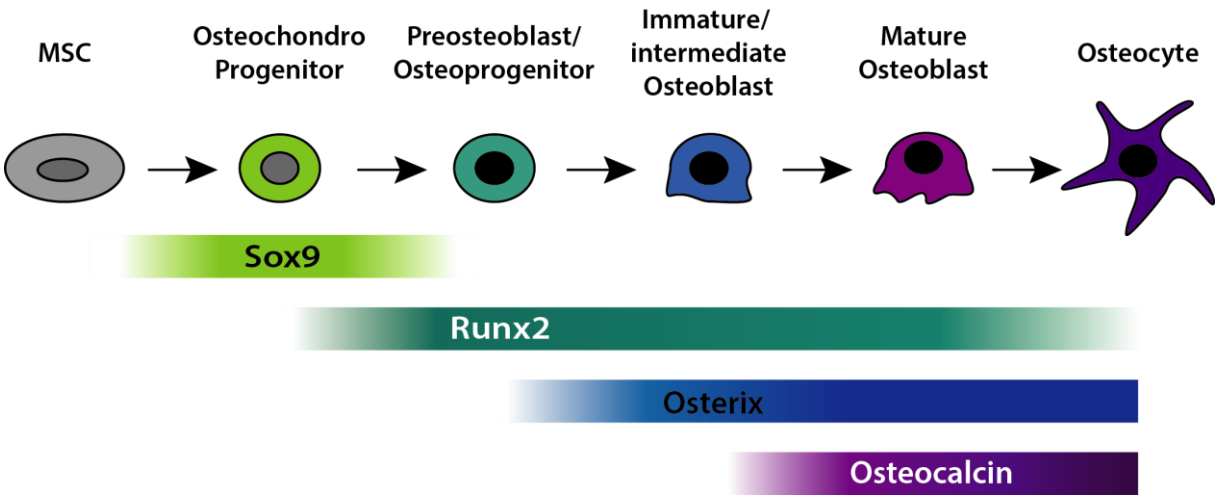

Figure 9: The different stages of osteoblast lineage differentiation. Mesenchymal progenitors, derived from mesenchymal stem cells (MSC), can give rise to osteoblasts and chondrocytes and are initially characterized by the transcription factor *Sox9*. When these cells start to express the transcription factor *Runx2* they become committed to the osteoblast lineage. These preosteoblasts further maturate into immature osteoblast through the activity of another transcription factor *Osterix*. By the time they reach full maturation, they start expressing extracellular bone matrix proteins, such as *Osteocalcin*, important for mineralization of the bone matrix. The mature osteoblast, after secreting the bone matrix, can become trapped in it and become osteocytes.

4.1.2 Bone pathologies and repair in mammals

Bone replacement or remodelling occurs throughout adulthood, to ensure skeletal size, shape and integrity. However, upon fracture or injury, the events that trigger bone remodelling are quite different and require complex mechanisms. The fracture repair process can be considered as part of an intrinsic capacity for regeneration, since bone can heal, in most cases, without forming a fibrotic scar. Fracture repair is typically characterized by four overlapping stages: an initial inflammatory phase, followed by a cartilaginous soft callus assembly, hard callus formation with mineralized bone matrix deposition and culminating with initial bone union and remodelling (Schindeler et al. 2008; Marsell and Einhorn 2011). In this process, endogenous MSC, and not mature osteoblasts, present in the stromal tissue of the bone marrow are thought to be the primary source of osteoprogenitors responsible for new osteoblast formation (Bielby et al. 2007; Sacchetti et al. 2007; Colnot 2009; Raggatt and Partridge 2010; Park et al. 2012; Sims and Martin 2014; Ono and Kronenberg 2016; Liu et al. 2018b). Importantly, this population of MSC grows scarce throughout adulthood and new lines of evidence suggest other potential sources. In fact, a study has demonstrated that a population of recruited osteoblast precursors from surrounding tissues have the capacity to enter into the bone marrow stroma of developing and fractured bones, along with invading blood vessels and promote the remodelling process. They seem to be intimately associated with the endothelium in a pericyte-like fashion (pericytes are cells that surround endothelial cells, giving support and structure) (Maes et al. 2010; Mohamed and Franceschi 2017). In the same line of thought, pericytes were shown to have osteogenic potential *in vivo*, giving rise to MSC (Doherty et al. 1998; Sims and Martin 2014). Conversely, reports showed that, depending

on the type of bone, osteoblasts can arise via transdifferentiation of hypertrophic chondrocytes not only during development but also during post-natal remodelling and repair (Zhou et al. 2014; Aghajanian and Mohan 2018). Finally, upon trauma, the periosteum, a thin membrane of fibrous connective tissue that surrounds bone, can also be a source of osteoblasts (Colnot 2009). All these data suggest that the source of new osteoprogenitors can be quite heterogeneous and more studies are required to understand this variability (Ono and Kronenberg 2016).

In addition to questioning the origin of osteoblasts during bone remodelling, researchers have also debated questions related to bone pathological conditions. When bone repair fails and fracture healing is delayed, the structure can show adverse anatomical positions, or even progress into pseudo-arthrosis or non-unions (Marsell and Einhorn 2011). Under certain pathological conditions the imbalance between the rate of bone resorption and bone formation can also leads to metabolic, genetic and oncogenic bone disorders that lead to defective skeletal integrity, such as: osteoporosis (the most prevalent bone remodelling disorder), Paget's disease, osteopetrosis, cleidocranial dysplasia and osteosarcoma (Feng and McDonald 2011; Luu et al. 2011; Marie 2015). Disorders that are characterized either by an increase or reduction of bone formation are directly correlated with osteoblast dysfunctions (Marie 2015). Consequently, the knowledge of the cellular sources that can be differentiated into new osteoblasts, as well as the molecular mechanism that triggers correct osteoblast formation and potentiate bone regeneration and maintenance, are of major importance. In this sense, model systems that encompass with mammals a functional conservation of pathways required to regulate skeletal homeostasis and development, while privileged with an enhance regeneration ability, are model systems of excellence to be used in this context.

4.1.3 The zebrafish as a model system to study bone development and regeneration

Zebrafish has become a powerful model system to understand the basic mechanisms of bone formation during development and regeneration. Inclusively, many human skeletal pathologies have their counterpart in zebrafish, which consequently, has been used for the study of several human skeletal diseases, such as osteoporosis and osteogenesis imperfecta (Spoorendonk et al. 2010; Laizé et al. 2014; Witten et al. 2017). Despite of this, there are many differences between the formation and composition of the zebrafish and the mammalian skeletons, that may result from adaptations to different habitats. Other important differences include: zebrafish hematopoiesis takes place in the head kidney and not inside the bone marrow; and zebrafish is continuously growing throughout adult life, thus the growth of skeletal tissue is considered to be different from mammalian skeletal remodelling (Bruneel and Witten 2015). However, key features are maintained between the two systems, such as: presence of the major skeletal tissues (including cartilage, bone and dentine); same bone formation processes (endochondral and intramembranous); conservation of the major cell types (chondroblast, osteoclast and osteoblast lineages) (Spoorendonk et al. 2010; Apschner

et al. 2011; Bruneel and Witten 2015; Witten et al. 2017). An important common trait that is worth emphasizing, which is a consequence of the characteristics mentioned above, is the preservation of key transcription factors that regulate osteoblast lineage determination as well as the signalling molecules that ensure their differentiation during development (Li et al. 2009) (Figure 9). Upon caudal fin regeneration, osteoblasts undergo a succession of proliferative, differentiation and maturation events that ensure proper bone formation (Durán et al. 2011; Antos et al. 2016; König et al. 2018). Currently, there is a considerable amount of stable transgenic reporters that adequately reflect the differentiation status of bone-forming cells at the different stages of osteogenic commitment, allowing to monitor skeletal phenotypes *in vivo* during a regenerative context (Watson and Kwon 2015; Bensimon-Brito et al. 2016; Cardeira et al. 2016). Therefore, the caudal fin can be used as a particularly suitable system to reveal new insights into fundamental processes of skeletal development and osteoblast lineage specification events (Marí-Beffa et al. 2007; Witten et al. 2017), since it gives the unique opportunity to study bone formation in a regenerative context.

In the following section, I will describe the current understanding on the mechanism that trigger and control osteoblast reprogramming, plasticity and redifferentiation during zebrafish caudal fin regeneration.

4.2 Mechanisms of osteoblast formation during zebrafish caudal fin regeneration

One of the most well-established regenerative processes in the zebrafish adult caudal fin is the bone formation process, which is mediated by osteoblasts. Upon caudal fin amputation, osteoprogenitors must be recruited to the amputation site, proliferate and subsequently undergo differentiation into mature bone cells. All these processes have to be tightly regulated and coordinated to ensure correct regeneration of the caudal fin skeletal elements.

4.2.1 Osteoblast sources during caudal fin regeneration: a role for reprogramming and plasticity

Our lab and others have demonstrated in the past, through genetic lineage tracing, that upon caudal fin amputation mature osteoblasts undergo a reprogramming event and dedifferentiate, acquiring the cellular properties of less differentiated cells (Figure 10A) (Knopf et al. 2011; Sousa et al. 2011; Stewart and Stankunas 2012). In general terms, dedifferentiation is defined as the reverse of a developmental program by which a fully differentiated post-mitotic cell, with its specialized genetic program and function, can re-enter the cell cycle and act as a progenitor cell. This phenomenon is characterized by differences at the level of gene transcription and protein regulation that consequently are followed by differences in morphology and function. The dedifferentiation program implies cease of the development-related gene activity and activation of genes that keep the progenitor cell phenotype (Cai et al. 2007; Grafi 2009; Maden 2013; Eguizabal et al. 2013). In fact, dedifferentiation is not a

unique feature of bone regeneration being fairly conserved and prevalent among many adult zebrafish organs and structures with capacity to regenerate (Qin et al. 2009; Liu et al. 2018a), including: heart regeneration, which relies on the dedifferentiation and proliferation of remaining cardiomyocytes (Jopling et al. 2010; Kikuchi et al. 2010); photoreceptor regeneration, during which Müller glia cells dedifferentiate to re-establish the photoreceptor population (Ramachandran et al. 2010; Gorsuch et al. 2017); and after muscle resection, with myocytes dedifferentiating and proliferating to restore the lost muscle (Saera-Vila et al. 2016; Louie et al. 2017). During bony-ray regeneration, resident mature osteoblasts are activated by injury signals, start dedifferentiating, detach from the bone surface and migrate distally towards the stump to incorporate the blastema at around 24 hpa (Figure 10A). Regarding the transcriptional profile, the osteoblast dedifferentiation process is characterized by a downregulation of mature and intermediate osteoblast markers, such as *osteocalcin* and *osterix*, and upregulation of the progenitor marker *runx2* (Knopf et al. 2011; Sousa et al. 2011). Strikingly, the dedifferentiation process is also accompanied by behaviour and morphology changes. Mature osteoblasts that reside in the segment closest to the amputation plane seem to undergo a Wnt/β-catenin dependent epithelial-to-mesenchymal transition (EMT) before migrating to integrate the blastema (Knopf et al. 2011; Sousa et al. 2011; Stewart et al. 2014). Once in the blastema, they increase proliferation to amplify and establish a pool of osteoprogenitors (Figure 10A). Furthermore, it has been demonstrated that after incorporation in the blastema, dedifferentiated osteoblasts are restricted to give rise only to new osteoblasts in the new regenerated tissue (Figure 10A). This indicates that despite their dedifferentiated status, osteoblasts remain lineage restricted and do not undergo transdifferentiation into other cell types during regeneration (Tu and Johnson 2011; Stewart and Stankunas 2012). A further evidence of this limited dedifferentiation capacity is the upregulation of *Runx2*, a feature typical of osteoprogenitors. Importantly, this was the first *in vivo* demonstration that, upon caudal fin amputation, the ability of the bony-ray elements to regenerate depends on the plasticity of mature osteoblasts. In addition, mature osteoblast dedifferentiation is not solely observed in the caudal fin, but seems to contribute to other bone repair models, such as during caudal fin bone crush/fracture and injury to the zebrafish skull cranial vault (Sousa et al. 2012; Geurtzen et al. 2014). Therefore, a fundamental question is what triggers and regulates osteoblast dedifferentiation during regeneration? It has been shown in plants that stress signals are enough to trigger cell dedifferentiation and cell fate decisions (Grafi and Barak 2015). To date, the signals that control osteoblast dedifferentiation during regeneration remain poorly enlightened and many questions remain unanswered: Can stress induced by amputation also trigger osteoblasts to reprogram and is it enough to promote their dedifferentiation? Since differentiated and progenitor cells have specific chromatin signatures might epigenetic regulation also be part and required for the osteoblast dedifferentiation program? Are there any transcription factors capable of converting cell fate and required to regulate dedifferentiation of osteoblasts?

The only pathway described to have a role in regulating osteoblast dedifferentiation is the Retinoic acid signalling pathway (Figure 10B). A research study demonstrated that during homeostasis, a population of intraray fibroblasts continuously secretes RA to adjacent mature osteoblasts to potentiate bone matrix deposition. After amputation, differentiated osteoblasts have to inactivate RA signalling, by upregulating the RA degrading enzyme *cyp26b1*, to cease matrix deposition and to undergo dedifferentiation (Figure 10B) (Blum and Begemann 2015b). Despite being a source of newly formed bone during regeneration, osteoblast dedifferentiation seems to be a rather unclear and poorly characterized process. Hence, further studies are necessary to comprehend and bring into light the fundamental mechanism that regulate osteoblast reprograming and plasticity during regeneration.

Although the major source of regenerating osteoblasts seems to derive from mature osteoblasts, a study revealed that after their genetic ablation, bone regeneration occurs normally and indistinguishable from fins harbouring a resident osteoblast population. This implies that in this challenging condition, osteoblast dedifferentiation is dispensable for correct bone formation and that alternative osteoblast sources, yet to be identified, are recruited and contribute to *de novo* osteoblast formation (Singh et al. 2012). It is possible that upon osteoblast depletion, dormant cellular mechanisms, which generally do not contribute to fin regeneration, are activated to give rise to new osteoblasts, thus ensuring correct bone formation after amputation. This data further highlights the remarkable cellular plasticity during bone formation in regenerating caudal fins. In mammals, bone remodelling relies on new osteoprogenitors derived from MSC (Sims and Martin 2014; Ono and Kronenberg 2016; Liu et al. 2018b). However, zebrafish has no *bona fide* MSC and fibroblasts that compose the mesenchyme seem to be the possible source of new osteoprogenitors. Alternatively, a population of perivascular cells, which are known to give rise to MSC in humans (Doherty et al. 1998; Bergers 2005; Crisan et al. 2008), was detected along the blood vessels of the caudal fin (Lund et al. 2014). However, their osteogenic capacity and requirement for *de novo* osteoblast formation during regeneration remains to be clarified, particularly in osteoblast-depleted fins. More recently, a reservoir of osteoprogenitors, derived from embryonic somites, was identified in the caudal fin. These precursor cells, present in the bony-ray intersegment joints, also called joint-associated osteoprogenitors, were shown to give rise to new osteoblasts under normal homeostatic maintenance (Ando et al. 2017) and function as a complementary source of osteoblasts for regeneration, together with dedifferentiating mature osteoblast (Ando et al. 2017). However, it remains to be investigated whether these progenitors could compensate for the lack of mature osteoblasts and explain the normal bone regeneration observed in osteoblast-depleted fins. Moreover, osteoblast ablation in mice also provided evidence for the activation of alternative osteogenic sources. In adult mice, inert post-mitotic bone-lining cells were identified as a major contributor of osteoblasts and preosteoblasts during bone remodelling (Matic et al. 2016). Importantly, several questions arise from these research data: What are the alternative sources capable of *de novo* osteoblast

formation when the mature population is absent, and dedifferentiation compromised? Are joint-associated osteoprogenitors enough to replenish the osteoblast progenitor pool and compensate for mature osteoblasts loss? What are the signalling pathways required and the molecular mechanism behind *de novo* osteoblast formation in osteoblast depleted fins? Thus, it is of major importance to decipher not only the cellular sources, identifying the cell types with osteogenic potential, but also the molecular mechanism behind *de novo* osteoblast formation during regeneration when dedifferentiation of the resident osteoblast population is compromised.

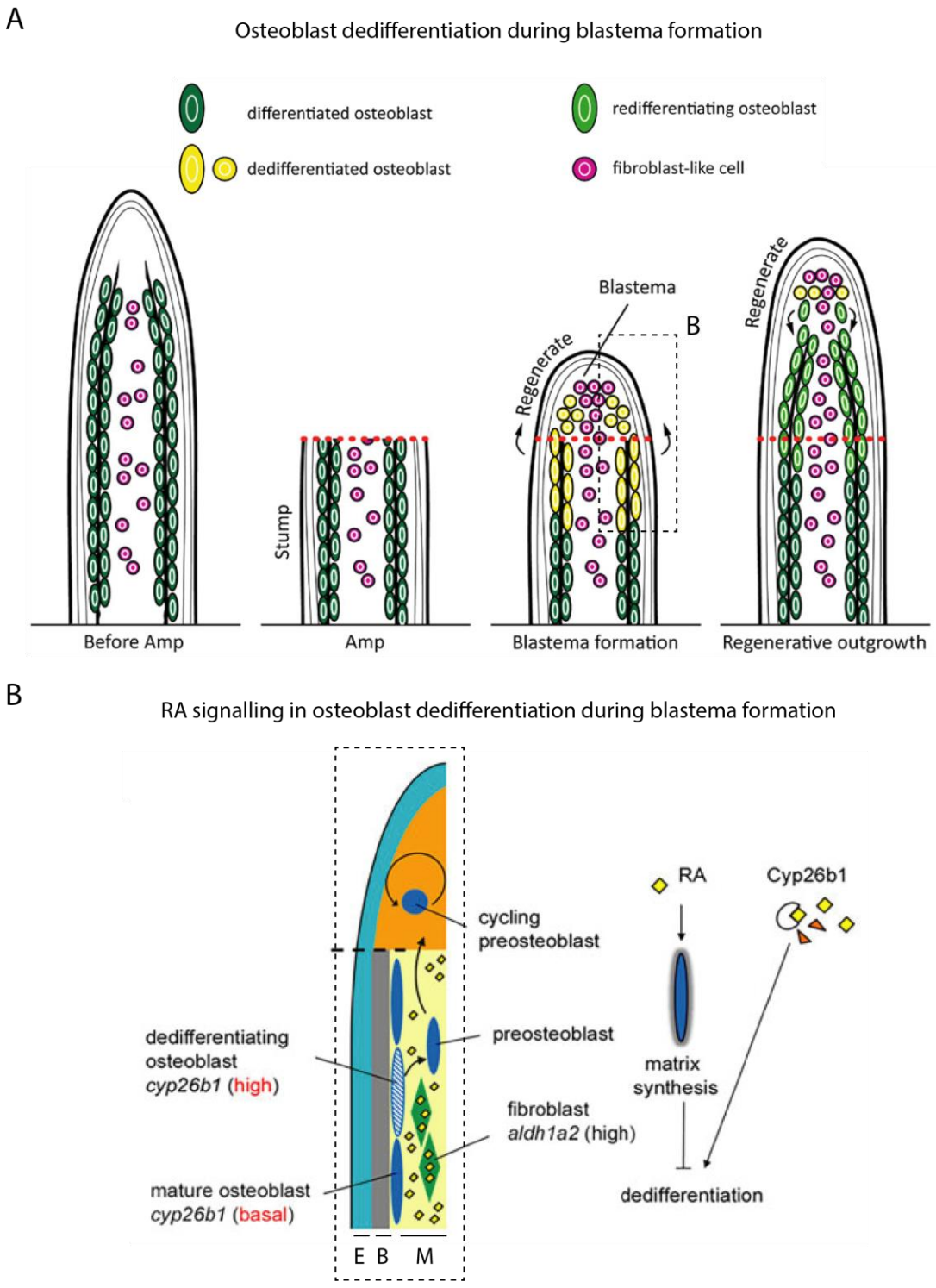

Figure 10: Osteoblasts dedifferentiation during caudal fin regeneration. (A) Scheme representing a longitudinal view of a bony-ray prior (before amp) and during regeneration depicting the mechanism underlying de novo osteoblast formation during caudal fin regeneration. Within the first 24 hours after amputation, distally located stump osteoblasts dedifferentiate and start to proliferate. Upon dedifferentiation, osteoblasts migrate distally and populate the lateral regions of the blastema, where they will redifferentiate and maturate. Thus, bone is *de novo* regenerated from differentiated, mature osteoblasts that undergone a reprogramming event. (B) RA signalling is the only pathway that has been directly implicated to regulate osteoblast dedifferentiation. To dedifferentiate, osteoblasts need to upregulate the expression of the RA degrading enzyme, Cyp26a1, so that they degrade RA coming from adjacent fibroblasts. Dashed lines represent the amputation plane. Amp: amputation; E: epidermis; B: bone; M: mesenchyme. Adapted from (Knopf et al. 2011; Blum and Begemann 2015b).

4.2.2 Osteoblast redifferentiation and bone patterning

Bone regeneration in zebrafish caudal fin requires tight coordination between progenitor cell proliferation and differentiation. After mature osteoblast dedifferentiation, these cells proliferate within the blastema but, at the onset of regenerative outgrowth, they must redifferentiate to produce the new skeletal tissue. During outgrowth, there is a re-activation of molecules that were once important for development. In fact, ontogeny and the outgrowth phase of regeneration share similar expression patterns, suggesting comparable molecular mechanisms governing both processes (Iovine 2007; Poss 2010). However, it is still unclear the molecular machinery that regulates osteoblast redifferentiation during regeneration. During the outgrowth phase, when blastema is fully maturated and compartmentalized, osteoblasts start to redifferentiate, exhibiting a proximo-distal hierarchical organization that comprehends overlapping compartments, reflecting their maturation status. This organization can be demonstrated by the temporal and spatial patterns of early (Runx2), immature/intermediate (Osx) and mature (Osc) osteoblast markers. In close contact with the blastema distal compartment, self-renewing $Runx2^+$ osteoblasts subtype maintains the osteoprogenitor pool (Figure 11). As these progenitors populate the proximal blastema, they start to differentiate into immature/intermediate $Runx2^+Osx^+$ proliferating osteoblasts. This last osteoblast subtype will give rise to slow-cycling, ECM producing Osx^+Osc^+ population, localized in the patterning zone of the regenerate (Figure 11) (Brown et al. 2009; Sousa et al. 2011; Stewart et al. 2014). Therefore, these three partially overlapping domains portray different stages of osteoblast maturation in which more distal cells represent the most progenitor-like osteoblasts and conversely the more proximal the most mature. Reports have shown that Wnt/β-catenin signalling is active in distally located $Runx2^+$ osteoprogenitors, while Bmp signalling is active proximally, where osteoblasts differentiate and mature (Figure 11) (Quint et al. 2002; Wehner et al. 2014). Based on these findings the proposed model for osteoblast maturation is the following: continuously secreted Wnt in the distal blastema region, activates canonical Wnt signalling in $Runx2^+$ osteoprogenitors to support and maintain, directly or indirectly, their self-renewal; in contrast, autocrine Bmp signalling regulates and directs their differentiation into Osx^+ osteoblasts. Additionally, Bmp signalling restricts Wnt/β-catenin signalling to the progenitor zone by secreting Wnt antagonists, including *dkk1b* (Figure 11) (Stewart et al. 2014; Wehner et al. 2014; Wehner and Weidinger 2015). Moreover, RA signalling was also found to be a key player in this model via a non-cell autonomous manner, by which osteoprogenitor differentiation is attained by differences in RA concentrations along the PD axis. Similar to Wnt/β-catenin signalling activity, RA production is high in the distal blastema cells, but rapidly decreases in more proximal cells. In contrast, *cyp26b1* (RA degrading enzyme) expression is high in proximal blastema cells, extends far proximally but is absent in more distal cells. High RA levels in the distal blastema promote proliferation and prevent premature osteoblast differentiation along the skeletogenic lineage, while reduction of RA levels in more proximal blastema regions, through activation of Cyp26b1, result in

osteoblast differentiation. Strikingly, overexpression of RA is sufficient to downregulate *dkk1b* and *bmp2b*, which may imply that RA signalling might inhibit osteoprogenitor differentiation by inhibiting Bmp and promoting Wnt/β-catenin signalling (Figure 11) (Blum and Begemann 2015b). Along the same line of thought, Notch signalling, which activation is restricted to the proliferative blastema region, was also shown to be necessary to maintain and support progenitor cells in a proliferative state and to prevent their differentiation into mature osteoblasts (Grotek et al. 2013; Munch et al. 2013). Shh was also shown to be important for osteoblast distribution and maturation. While *shh* expression is restricted to a subset of cells in the proximo-lateral domains of the basal layer of the epidermis, just immediately adjacent to the site of amputation, its receptor *patched1/2* is expressed not only in the same location as *shh* but also in the adjacent differentiated osteoblasts (Laforest et al. 1998), where it activates *bmp2b* expression. Furthermore, over-expression of both Shh and BMP in blastema cells induce ectopic bone formation during regeneration (Quint et al. 2002). Effects of Shh ectopic expression were able to be rescued via inhibition of Bmp signalling, suggesting that indeed during osteogenic maturation Bmp is required and acts as a downstream target of Shh (Quint et al. 2002). Overall, this signalling network leads to the establishment of a temporally and spatially organized osteogenic lineage hierarchy that balances a simultaneous need for osteoblast proliferation and differentiation, until fin regeneration is complete (Figure 11).

Besides correct osteoblast differentiation during regeneration, proper bone patterning is also necessary. Interestingly, besides its role in osteoblast maturation, shh was also found to be required for bony-ray bifurcation. Prior to the establishment of the bifurcation, *shh* domain of expression in the basal epidermis splits into two clusters on each side of the bony-ray, directing the osteoprogenitor position (Laforest et al. 1998; Zhang et al. 2012; Armstrong et al. 2017). This mechanism depends on the direct contact of *shh* expressing epidermal cells via cellular protrusions and *patched 1/2* expressing osteoprogenitors. These two pools of osteoprogenitors continue to regenerate independently to form a bifurcated ray (Armstrong et al. 2017). Importantly, laser ablation of *shh* expressing cells in the wound epidermis culminates in delayed ray bifurcation (Zhang et al. 2012). In addition to the bifurcation, bony-rays are segmented by joints, which convey flexibility to the caudal fin skeleton. This joint region is established by an oscillatory expression of the homeobox gene *even-skipped related 1* (*evx1*) (Borday et al. 2001; Rolland-Lagan et al. 2012; Ton and Iovine 2013) which is inhibited by the gap junction protein Connexin-43 during segment elongation (Piccirillo et al. 2013). Mutant zebrafish for *evx1* completely lacks joints (Schulte et al. 2011). Another study has addressed the role of the inflammatory response cellular components during caudal fin regeneration. They show that macrophage accumulation at the damaged site was relatively slow when compared to neutrophils, and that ablation of the macrophage population lead to a reduction in the average number of segments and bifurcations in the regenerated bony-ray, and also exhibited a decreased bone mineralization profile. This further indicates additional

roles for macrophages during regeneration, with their depletion impairing bony-ray patterning and the quality of bone formation (Petrie et al. 2015).

These studies emphasize the complexity of osteoblast maintenance, maturation and bone patterning during regenerative outgrowth. Overall, there must be a tight coordination between osteoblast proliferation and differentiation along the PD axis to ensure correct bone formation. Furthermore, bone patterning is essential to provide the correct tissue architecture and function so that the missing tissue is replaced by a replica that mimics the original caudal fin.

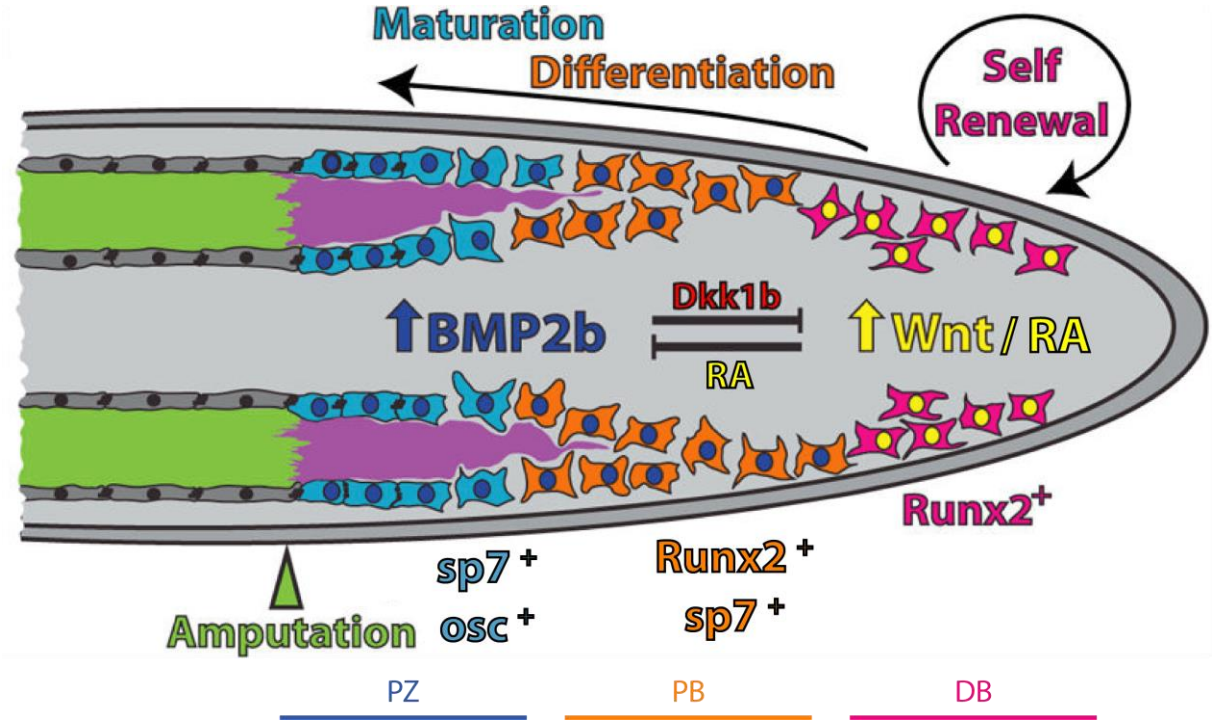

Figure 11: Hierarchical organization of the osteoblast lineage during regenerative outgrowth and its regulation. Scheme depicting the longitudinal organization of osteoblast differentiation along the PD axis of the regenerating caudal fin. Wnt and RA signalling act in the distal blastema region to maintain the pool of Runx2^{+} osteoprogenitor cells. In the proximal blastema and patterning zone, Bmp signalling in osteoprogenitors promotes both Osx (Sp7)-associated differentiation, maturation into Osc producing osteoblasts and constrains Wnt activity through *dkk1b* expression. Conversely, RA restricts activation of Bmp signalling and *dkk1b* expression towards the progenitor compartment. PZ: Patterning zone; PB: Proximal blastema; DB: Distal blastema. Adapted from (Stewart et al. 2014).

4.3 The Hippo/Yap signalling pathway: potential regulator of osteoblast lineage during caudal fin regeneration

The Hippo signalling pathway emerged as an evolutionarily conserved signal transduction pathway that plays an important function in tissue growth and organ size control during development, tissue homeostasis and regeneration. This pathway acts predominantly via regulation of proliferation, cell survival and cell fate determination often in a context-dependent fashion (Halder and Johnson 2011; Cherrett et al. 2012; Fu et al. 2017). The Hippo pathway was initially identified in *Drosophila melanogaster* through genetic screens for

suppressors of tissue overgrowth that when mutated lead to overgrowth phenotypes. For instance, mutations of the *hippo* (*hpo*) gene culminate in an overgrown head (resembled a hippopotamus) caused by an abnormal proliferation (Udan et al. 2003; Halder and Johnson 2011). Remarkably, later studies identified that the general components and functions of the pathway are highly conserved throughout the eukaryotic kingdom (Yao et al. 2013; Varelas 2014; Irvine and Harvey 2015). The Hippo signal transduction pathway comprises a kinase core cascade that like many other pathways conveys signals perceived at the plasma membrane to a transcriptional response within the nucleus. In vertebrates, the core module of this signalling cascade encompasses two protein kinases: Mst1/2 (Hippo in *Drosophila*) and Lats1/2 (Warts (Wts), in *Drosophila*). Upon pathway activation, Mst1/2 kinase phosphorylates and activates the Lats1/2 kinase that in its turn phosphorylates and repress the activity of the key transcriptional co-activators of the pathway: Yes-associated protein 1 (Yap) and transcriptional co-activator with a PDZ-binding motif (Taz) (homologs of Yorkie (Yki) in *Drosophila*). Yap/Taz phosphorylation promotes their cytoplasmic retention and exclusion from the nucleus through 14-3-3 binding. When the Hippo pathway is inactivated, and the core kinase cassette is not phosphorylated, Yap and Taz can translocate to the nucleus where they associate with multiple transcription factors inclusively of other signalling pathways (such as Tgfβ/ Bmp and Wnt signalling) and behave as co-activators of target gene transcription in a context and tissue specific manner. Yet, the *bona fide* DNA binding partner for Yap and Taz is the Tead/Tef family of transcription factors (homolog of Scalloped (Sd) in *Drosophila*), generally activating proliferation and growth and inhibiting apoptosis (Figure 12). (Huang et al. 2005; Wu et al. 2008; Cherrett et al. 2012; Irvine 2012; Attisano and Wrana 2013; Yu and Guan 2013; Hiemer and Varelas 2013; Piccolo et al. 2014; Varelas 2014; Hansen et al. 2015; Irvine and Harvey 2015). In terms of structure, both Yap and Taz possess WW domains that confer signalling specificity and recognize specific motifs in other proteins. They share a C-terminal PDZ-binding motif, which promotes interaction with various proteins and includes a transcriptional activation domain that regulates the transcriptional roles of Yap/Taz. The N-terminal domain encloses a Tead binding domain that mediates the interaction between Yap/Taz and Tead. Finally, but equally importantly, to promote Yap and Taz subcellular localization and prevent their translocation to the nucleus, Lats1/2 phosphorylates Yap at five serine/threonine residues and Taz in four of these sites. Mutation in these serine residues jeopardizes the ability of the Hippo pathway to inhibit Yap/Taz translocation to the nucleus (Cherrett et al. 2012; Piccolo et al. 2014; Varelas 2014; Santucci et al. 2015). These structural components emphasise the notion that the Hippo pathway can be regulated by a multitude of upstream inputs, such as: cell polarity and adhesion, cellular stress, signals received through G protein-coupled receptors and mechanical cues. Given that the Hippo pathway regulates cell proliferation and apoptosis, growth, survival and stem cell maintenance and/or differentiation depending on the cellular context, they became important regulators of

regeneration and tissue repair in a wide range of biological contexts (Piccolo et al. 2014; Moya and Halder 2016; Fu et al. 2017).

In *Drosophila* intestine, Yki is activated upon damage to promote intestinal stem cell and enterocyte proliferation to replace the damaged cells (Staley and Irvine 2010). This was also found to be true for mouse models of intestinal repair, where Yap is required for intestine repair but not during physiological homeostasis (Cai et al. 2010). On the other hand, in adult mouse heart, Hippo pathway is active and blocks cardiomyocyte proliferation to restrict regeneration (Heallen et al. 2012). In the context of animals with greater regenerative capacity, the role of this pathway remains poorly investigated. Nonetheless, during *Xenopus* limb bud regeneration, overexpression of a dominant negative form of Yap reduced cell proliferation, induced apoptosis and impaired limb patterning genes (Hayashi et al. 2014). Importantly, our lab has demonstrated that Yap is required for proper caudal fin regeneration by controlling cell proliferation and regulating regenerative outgrowth key signalling pathways. This regulation is correlated with differences in cell density, morphology, cytoskeleton and cell-cell contacts along the blastema PD axis in a gradient-like manner: in more proximal regions of the regenerate, were cells are more spread, Yap is nuclear and therefore active, in contrast, in the more distal blastema, where cell density is higher, Yap is mainly inactive (Mateus et al. 2015).

Several lines of evidence have drawn attention to the potential role of the Hippo pathway in regulating cell differentiation and establishing cell fate. Various studies have shown that ectopic expression of Yap during development maintains stem cell or progenitor states at the expense of terminal differentiation in several tissues, such as the intestine, epidermis, neural tube and brain (Hiemer and Varelas 2013; Piccolo et al. 2014; Zhao 2014; Moya and Halder 2016; Fu et al. 2017). Yap was also found to be important for maintenance of mouse embryonic stem cells and reprogramming of mouse embryonic fibroblasts to an iPSC state (Hiemer and Varelas 2013; Piccolo et al. 2014). Since the capacity to dedifferentiate is the underlying mechanism behind new osteoblast formation, it would be interesting to evaluate the requirement of the Hippo/Yap pathway for osteoblast dedifferentiation during caudal fin regeneration. In fact, this pathway has been shown to regulate cell dedifferentiation in several systems. Combined inactivation of the Hippo pathway core components *hpo* or *wts* together with Retinoblastoma (tumour suppressor) lead to widespread dedifferentiation of photoreceptor cells in the *Drosophila* eye. Double mutants fail to maintains neuronal identity and became uncommitted eye specific cells (Nicolay et al. 2010). Other report shows that Hippo pathway activation is necessary to maintain the adult mouse hepatocytes in a differentiated state and that Yap induced expression triggers their dedifferentiation through Notch signalling (Yimlamai et al. 2014). More interestingly, in planarians, cell dedifferentiation does not normally occur since regeneration depends on neoblast cells. Strikingly, *hippo* inhibition in non-regenerating conditions triggers spontaneous dedifferentiation of mature cells leading to the formation of undifferentiated overgrowths. Therefore, in planarians, the

main role of Hippo in normal physiological conditions is to maintain the differentiated cell state (de Sousa et al. 2018).

Only more recently the role of the Hippo pathway has been addressed in the context of osteogenesis and during osteoblast lineage specification and maturation. In this context, Yap and Taz roles are controversial since both have been shown to promote or inhibit osteoblast differentiation and bone formation. Yap and Taz were shown to regulate MSC towards osteoblast lineage fate, by interacting with Runx2 and potentiating the osteoblast transcriptional program *in vivo* and *in vitro* (Figure 12) (Hong et al. 2005; Hiemer and Varelas 2013). *In vitro* studies suggest that this process seems to be dependent on the stiffness of the ECM in which MSC are cultured. Increased stiffness leads to Yap/Taz nuclear translocation and renders cells to commit towards osteoblast differentiation, whereas softer matrix leads to disabled Yap/Taz signalling and differentiation into adipocytes (Dupont et al. 2011a; Piccolo et al. 2014). This model was correlated with phenotypes of mice mutants for the secreted metalloprotease MT1-MMP that induces ECM remodelling. In the mutants, MSC are trapped into the ECM network, unable to spread and contained in a small adhesive area. In this situation, Yap/Taz are retained in the cytoplasm and targeted to degradation and development of osteopenia (characterized by bone loss and defective bone formation) (Tang et al. 2013; Piccolo et al. 2014). In the same line of thought, another report suggested that during mouse development, transcription factors Snail and Slug, known to direct EMT programs, regulate Yap/Taz to promote MSC differentiation into osteoblasts (Tang and Weiss 2017). More recent reports tried to further clarify this question by using conditional depletion of Yap/Taz from osteoblast lineage, which lead to reduced osteoblast activity and bone formation, and reduced bone matrix maturation, leading to spontaneous fractures in the neonatal mouse (Kegelman et al. 2018). This was also found to be similar during adult mouse bone remodelling, in which conditional knockout for Yap in osteoblasts reduces their proliferation and differentiation and increases adipocyte formation (Pan et al. 2018). Finally, other reports state that Yap/Taz have opposing roles in the regulation of the osteoblast fate, depending on their differentiation status: Yap/Taz in osteoprogenitors maintains the progenitor state and oppose differentiation towards osteoblast commitment, while Yap/Taz in mature osteoblasts promotes bone formation (Seo et al. 2013; Xiong et al. 2018). All data described, points to a clear regulation of bone formation mediated by the Hippo pathway and its co-effectors Yap/Taz. However, many of these studies were done *in vitro* or lead to mouse neonate lethality, making impossible to evaluate the existence of distinct features Yap/Taz regulation during development or adulthood, and importantly do not allow to evaluate the role of this pathway in the context of bone repair and regeneration. It would be important to elucidate if the Hippo pathway could be implicated and required for osteoblast lineage commitment during regenerative outgrowth, to further clarify the controversial roles of this pathway in osteoblast fate determination.

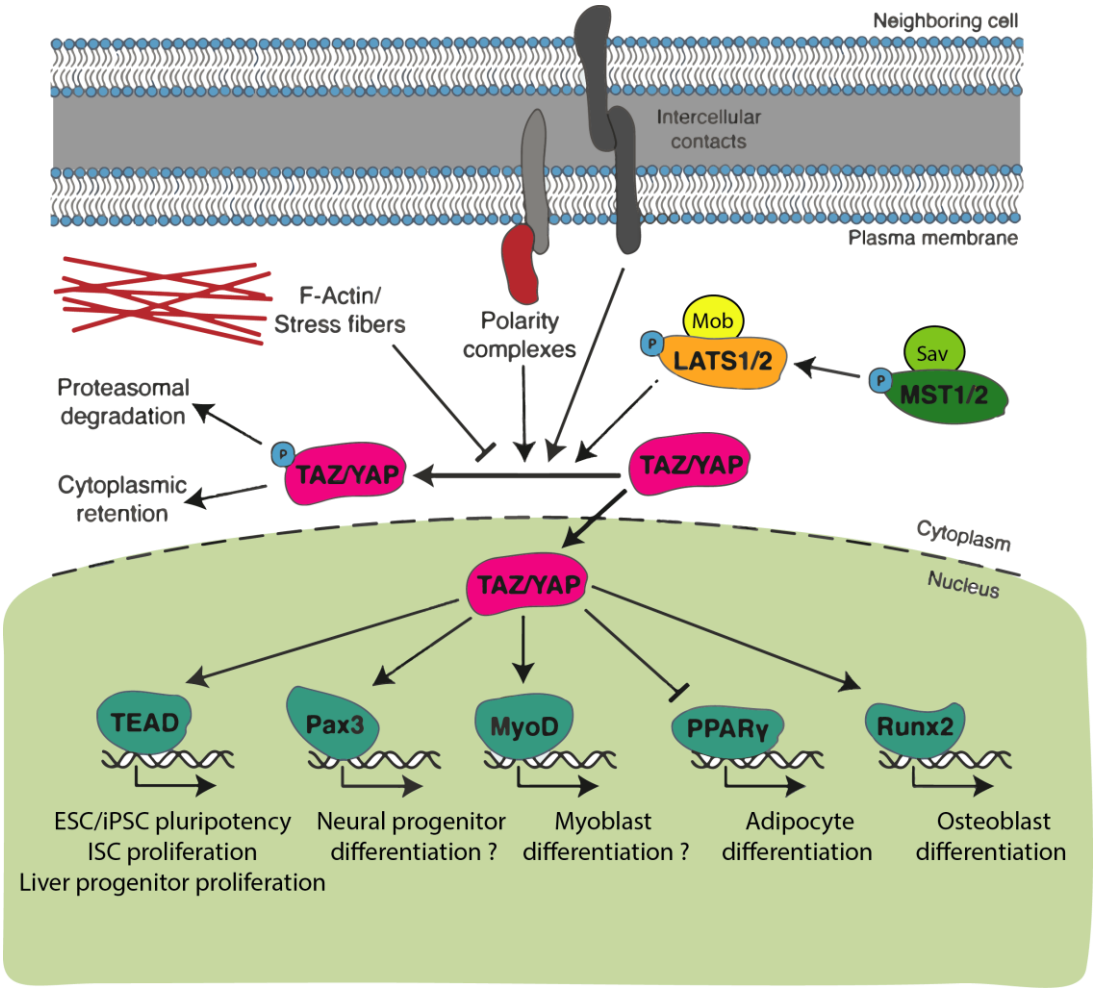

Figure 12: The Hippo pathway regulators and regulations during cell fate determination. Scheme depicting the regulation of the Hippo pathway activity. The Hippo pathway effectors Yap and Taz can be regulated by a multitude of upstream inputs/cues and leads to multiple transcriptional outputs, which depend largely on context. This pathway is composed by a core kinase cascade (Mst1/2 and Lasts1/2) that is highly conserved throughout the eukaryotic kingdom. If signalling cues lead to activation of the pathway, the kinase core cascade is activated and culminates in Yap/Taz phosphorylation and sequestration in the cytoplasm and subsequent degradation. When the pathway is inactive, Yap/Taz are not phosphorylated and are able to be translocated to the nucleus and activate target gene expression, depending on the tissue and context. Other cues can regulate Yap/Taz activity independently of the Kinases, such as mechanical stimuli generated by the elasticity of the extracellular matrix. In the nucleus, Yap/Taz interact in most cases with Tead transcription factors and regulate pluripotency and stem cell proliferation. On the other hand, they can also mediate stem cell differentiation into other lineages by interacting with other transcription factors, such as Runx2, to mediate stem cell commitment towards the osteoblast lineage. Adapted from (Hiemer and Varelas 2013).

5 SPECIFIC AIMS

This PhD thesis aims at understanding the central questions regarding the cellular and molecular mechanisms that regulate bone formation during regeneration using the zebrafish caudal fin as a model system. During the course of this work, I investigate three main topics:

1) In Chapter III, I investigate new regulators of osteoblast reprogramming and dedifferentiation during zebrafish caudal fin regeneration using two approaches:
    a. By performing a genome-wide gene expression analysis of osteoblasts undergoing dedifferentiation;
    b. By addressing the role of the Hippo pathway in regulating osteoblast dedifferentiation during regeneration, by manipulating the pathway effector Yap;
2) In Chapter IV, I determine the role of the Hippo pathway effector Yap in mediating osteoblast fate specification and maturation during caudal fin regeneration by performing loss-of-function studies;
3) In Chapter V, I shed light into the mechanisms underlying *de novo* osteoblast formation in mature osteoblast-depleted caudal fins by determining:
    a. The cellular sources capable of generating new osteoblasts using lineage tracing tools and specific cell ablation methods;
    b. The molecular mechanisms required for new osteoblast formation through loss-of-function studies on major pro-osteogenic pathways.

.

Chapter II

MATERIAL AND METHODS

1 ETHICS STATEMENT

All handling and experiments involving animals were approved by the Animal User and Ethical Committees at Centro de Estudos de Doenças Crónicas (CEDOC) and accredited by the Direcção Geral de Alimentação e Veterinária (DGAV) according to the directives from the EU (Directive 2010/63/UE) and National legislation (Directive 113/2013) for animal experimentation and welfare.

2 ZEBRAFISH MAINTENANCE, HANDLING AND TRANSGENIC LINES

2.1 Embryo raising

For zebrafish line maintenance, mating pairs were set up. Eggs were collected, maintained in a Petri dish containing E3 medium (5 mM NaCl, 0.17 mM KCl, 0.33 mM $MgSO_4$, 0.01% Methylene Blue) and kept in a 28 °C incubator, until reaching the desired developmental stage for screening. After reaching 6 days post-fertilization (dpf), larvae were transferred to the circulating system to grow until adulthood (Westerfield 2000).

2.2 Adult zebrafish manipulation and amputation

All adult wild-type (WT) AB strain and transgenic zebrafish lines were maintained in a circulating system with 14 hour/day and 10 hour/night cycle periods at 28 °C. All experiments were performed in 3-12 months old adult fish (Westerfield 2000) and all transgenic animals used as heterozygotes.

Caudal fin amputations were performed in fish anaesthetized in 160 mg/mL MS-222 (Sigma-Aldrich) using a sterile scalpel (Poss et al. 2000a). Regeneration was allowed to proceed until defined time-points in an incubator at 33 °C ± 1 °C, except for heat-shock experiments (see section 5), and the water was renewed daily. Amputations were made 1 or 2 segments below the first bone-segment bifurcation, removing approximately one half of the fin. Regenerated fins from anaesthetized animals were collected at predefined time-points post-amputation as previously described (Poss et al. 2000a).

2.3 Zebrafish transgenic lines used in this study

Several zebrafish transgenic lines were obligingly provided by other laboratories and proved to be extremely useful in the context of this study. These lines were: Tg(*ola.Bglap:*EGFP)^{hu4008} and Tg(*Hsa.RUNX2-Mmu.Fos:*EGFP)^{zf259}, kindly provided by Gilbert Weidinger (Knopf et al. 2011); Tg(*osterix:*mCherry-NTRo)^{pd46}, Tg(*hsp70l:*RFP-dnyap1) and Tg(*hsp70l:*RFP-*cayap1*) kindly provided by Kenneth Poss (Singh et al. 2012; Mateus et al. 2015); TgBAC(*aldh1a2:aldh1a2*-GFP)^{kn2} and Tg(*hsp70l:cyp26a1*)^{kn1}, kindly provided by Gerrit Begemann (Blum and Begemann 2012; Pittlik and Begemann 2012); Tg(*careg*:*Cre-ERT2^{Mercury}),*

kindly provided by Anna Jazwinska (Pfefferli and Jaźwińska 2017); Tg(*krtt1c19e:Cre-ERT2*)^{fr35}, kindly provided by Matthias Hammerschmidt (Fischer et al. 2014); and Tg*(-9.8actb2:LOXP-*DsRed-*LOXP*-EGFP*)*, kindly provided by Didier Stainier (Kikuchi et al. 2010); and Tg(*Tcf/Lef-miniP:*d2GFP)^{isi01} (Shimizu et al. 2012). The line Tg(*ctgfa:*EGFP) was already available in our lab, generated in the context of a previous project (Mateus et al. 2015). Table I describes each line and its purpose within the project.

Table I: List of zebrafish transgenic lines used in the project.

Zebrafish transgenic lines	Abbreviation	Line type	Description
Tg(*ola.Bglap:*EGFP)^{hu4008}	*osc:*EGFP	Reporter	EGFP expression exclusively in mature osteoblasts
Tg(*osterix:*mCherry-NTRo)^{pd46}	*osx:NTRo*	Reporter/ Ablation	mCherry expression in immature and mature osteoblasts; used to induce specific osteoblast ablation and to monitor *osx* expression
*Tg(Has.RUNX2-Mmu.Fos:*EGFP)^{zf259}	*runx2:*EGFP	Reporter	EGFP expression in all osteoblast differentiation stages; highly expressed in osteoprogenitors
TgBAC(*aldh1a2:aldh1a2-*GFP)^{kn2}	aldh1a2:GFP	Reporter	EGFP labelling in cells expressing *aldh1a2*; used to visualize cells synthesizing RA
Tg(*ctgfa:*EGFP)	*ctgfa:*EGFP	Reporter	EGFP labelling in cells expressing *ctgfa*, here used as a mesenchymal marker
Tg(*Tcf/Lef-miniP:*d2GFP)^{isi01}	*6xTCF:*d2GFP	Reporter	D2GFP labelling in cells with activated β-catenin-dependent transcription; shows the spatio-temporal pattern of

Zebrafish transgenic lines	Abbreviation	Line type	Description
			Wnt/β-catenin pathway activation
Tg(*hsp70l:cyp26a1*)^{kn1}	*hsp70:cyp26a1*	Heat-shock inducible loss of function	Induces *cyp26a1* expression upon heat-shock; it degrades RA, leading to inhibition of the signalling pathway
Tg(*hsp70l:*RFP-*dnyap1*)	*DN-yap*	Heat-shock inducible loss of function	Activates the expression of a dominant negative form of *yap1* upon heat-shock; leads to inhibition of *yap1* target gene transcription
Tg(*hsp70l:*RFP-*cayap1*)	*CA-yap*	Heat-shock inducible gain of function	Activates the expression of a constitutively active form of *yap1* upon heat-shock; leads to constant activation of *yap1* target gene transcription
Tg(*careg*:*Cre-ERT2)*	*careg:creERt2*	Lineage tracing	Allows lineage tracing of mesenchymal cells in the caudal fin when combined with *β-act2: RSG*
Tg(*krtt1c19e:*Cre-ERT2)	*krt19:creERt2*	Lineage tracing	Allows lineage tracing of basal epidermal cells when combined with *β-act2: RSG*
*Tg(-9.8actb2:LOXP-*DsRed-*LOXP*-EGFP*)*	*β-act2:RSG*	Lineage tracing, switch line	Switch cassette to be combined with the Cre-ERT2 lines for permanent cell labelling

3 MOLECULAR BIOLOGY AND CLONING TECHNIQUES

During the course of this study, several plasmid DNA constructs were generated in order to develop zebrafish transgenic lines for specific cell ablation based on the NTR/MTZ system. The final constructs to be injected in zebrafish embryos will be described in detail below.

3.1 Target fragment amplification by Polymerase Chain Reaction (PCR)

For desired DNA fragment amplification, namely the GFP-NTRo coding sequence and the *krtt1c19e promoter*, standard PCR protocols were performed according to the manufacturer's instructions using either Tap Polymerase (Fermentas) for PCR products smaller than 2 kilobases (Kb) or Titanium Taq Polymerase (Clontech), for longer amplicons. In-Fusion primers sets were designed specifically to hybridise with the target sequence (for further primer details see Table II and section 3.4). Thermal cycling conditions were as follows: initial denaturation step at 95 °C for 3 minutes (min); followed by 35 cycles of a 3-step temperature cycle (denaturation: 95 °C for 30 seconds (sec); primer annealing: 65 °C for 30 sec; and polymerase extension: 72 °C, duration depending on the size of the fragment (generally 1 minute elongation per Kb)); and a final extension step at 72 °C for 10 min.

Table II: List containing the primer sequences used for In-Fusion cloning methodology.

Amplified sequence	Forward Primer (5'>3')	Reverse Primer (5'>3')	Annealing Temperature	Product length	Objective
GFP-NTRo coding sequences	GCGGATCCC GCCACCATG GTGAGCAAG GGCGAG	TCACTATAGT TCTAGAGAAT TCTCACACCT CGGTC	65 °C	1428 bp	Insert the GFP-NTRo coding sequence into the *col10a1* promoter backbone
krtt1c19e promoter	TATAGGGGC GAATTGGGT ACCAATTCGC CCTTTACACC ATGG	CATGGTGGC GGGATCCGT GGATGGTGG TTGGTGTCTT	65 °C	3939 bp	Substitute the *col10a1* promoter by the *krtt1c19e promoter* sequence into the *col10a1:* GFP-NTRo backbone

3.2 Restriction Enzyme digestion

To insert amplified target sequences onto specific destination plasmids, the latter had to be linearized through restriction enzymes single or double digestion protocols. For that, digestions were performed for approximately 2 hours (h) at 37 °C using 5-10 Units (U) of commercially available restriction enzymes and corresponding buffers. Reactions were subsequently inactivated according to manufacturer's protocol (for further details see Table III). Digestion protocols were also established to confirm proper insertion between plasmid and target sequence.

Table III: List of restriction enzymes used for cloning.

Restriction Enzymes	Digested Plasmid	Length (bp) of target sequence	Objective
XbaI and NcoI (Fermentas)	*col10a1:*nlGFP	9020	Substitution the nlGFP sequence from *col10a1:*nlGFP *with the* GFP-NTRo *sequence*
BamHI and KpnI (Fermentas)	*col10a1:*GFP-NTRo	4598	Substitution of the *col10a1* promoter by the *krtt1c19e promoter sequence in the col10a1:*GFP-NTRo *backbone*
EcoRI (Promega)	*col10a1:*GFP-NTRo	6500; 3297bp; 670	Confirm correct insertion of the amplified insert
EcoRI (Promega)	*krtt1c19e:* GFP-NTRo	4748; 2118; 896; 676; 125	Confirm correct insertion of the amplified insert

3.3 Analysis and isolation of desired DNA fragments by agarose gel electrophoresis

To separate and purify digested plasmid DNA fragments and amplified PCR products, agarose gel electrophoresis was performed. Agarose (Agarose electrophoresis grade, Invitrogen) was dissolved in commercially available 1x Tris-Acetate-EDTA (TAE) buffer (Fisher Scientific) at a final concentration of 1%, which allows the resolution of DNA fragments between 500 base pairs (bp) and 10 Kb in size. Further, DNA was visualised by adding Gel Red (Biotium) to a final concentration of 0.4 µg/mL. For gel loading, DNA samples were mixed with Orange DNA loading dye (ThermoFisher Scientific) in a 6:1 proportion and electrophoresis carried out in 1x TAE buffer at 100-120 V, until proper separation of the DNA fragments. Subsequently, DNA was visualised under ultraviolet light at 365 nm and fragment size was estimated by comparison to a DNA ladder composed of linear DNA strands of known molecular weight (Gene ruler 1 Kb DNA ladder, Thermo Scientific). For subsequent cloning steps, plasmid DNA

and PCR fragments of the desired size were excised using a sterile scalpel and purified using the Wizard® SV Gel and PCR Clean-Up System (Promega), according to manufacturer's instructions.

3.4 In-fusion methodology for cloning DNA inserts into desired vectors

The In-Fusion HD cloning technology (Clontech Laboratories) allows a fast and directional cloning of one or more fragments of DNA into any destination plasmid (Figure 13). Ligation between the insert and the plasmid is only possible if both share 15 bp of homology at each end. This is achieved by engineering specific primers with 15-bp overlaps homologous to the destination plasmid ends. For this, cloning plasmids were linearized by restriction enzymes double digestions and target inserts amplified by PCR. Both linearized vectors and PCR products were purified, as mentioned in section 3.3, and In-Fusion ligation reaction was set up: 50 ng of linearized vector and 200 ng of the insert, regardless of their lengths, were incubated with the In-Fusion Enzyme premix, according to the manufacturer's protocol. This allows the In-Fusion Enzyme to fuse specific DNA fragments efficiently and precisely by homology between the 15-bp overlaps. The reaction mix with the final construct was transformed into commercial competent E. coli.

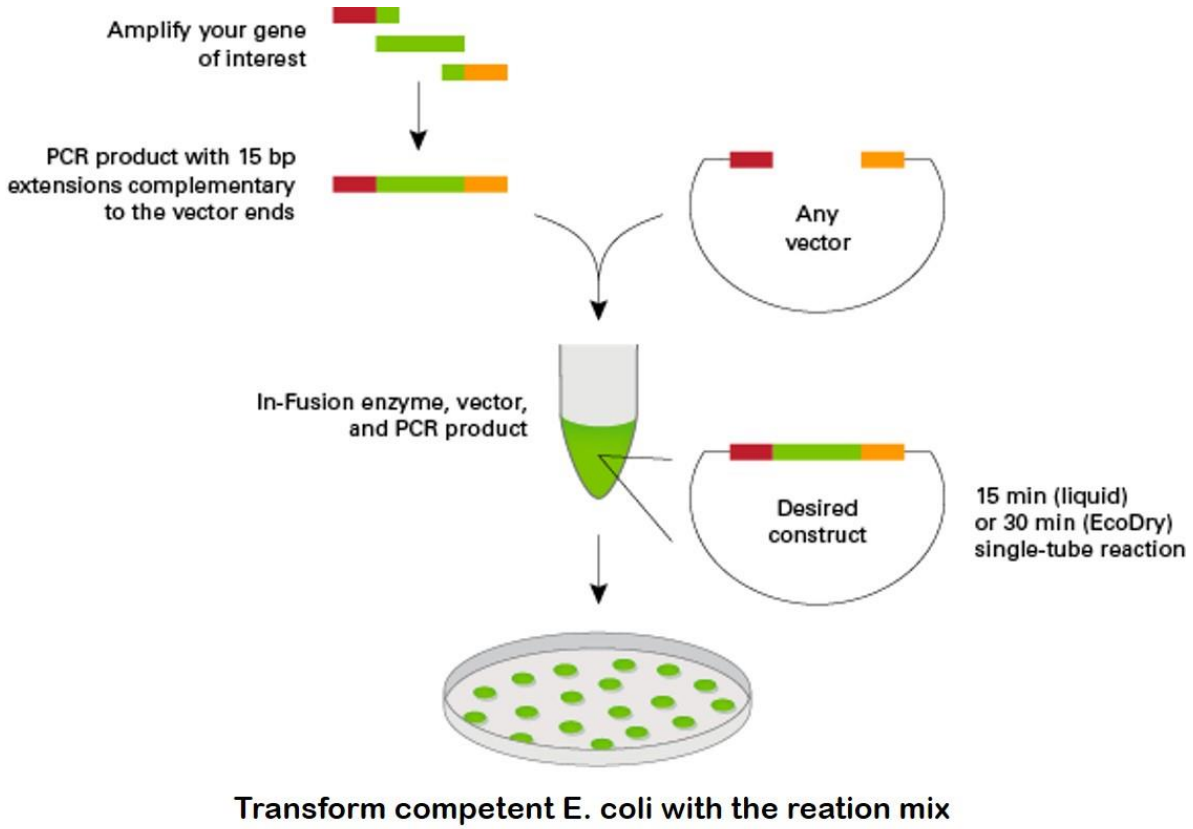

Figure 13: Schematic representation of the In-Fusion cloning strategy. Linearized destination vector and amplified sequence of interest, with primers containing a 15 bp extension homology to the destination vector ends, were assembled in the In-Fusion reaction mix. This allows recombination between the homologous

sequences of the linearized plasmid with the PCR product. Adapted from In-Fusion® HD Cloning Kit User Manual (Clontech Laboratories).

3.5 Plasmid transformation of competent E. coli bacteria

For plasmid DNA transformation E. cloni® 10G chemically competent cells (Lucigen) were used. Frozen aliquots of competent cells were thawed on ice, incubated with the plasmid DNA for 30 min on ice, followed by a 42 °C heat-shock for 45 sec and returned to ice. 300 µL of cold Luria Broth medium (LB) were added to the mix, which was then incubated at 37 °C with shaking (150 rotations per minute (rpm)) for 1 h. 200 µL of the transformed bacteria were plated in LB medium with agar (35 g/L; Sigma-Aldrich) and ampicillin (Amp) (100 µg/mL; Sigma-Aldrich) or kanamycin (Kan) (50 µg/mL), depending on the plasmid selection marker, and incubated overnight (ON) at 37 °C. On the following day, selected colonies were grown in liquid LB with Amp or Kan, ON at 37 °C at 250 rpm.

3.6 Plasmid DNA purification and quantification

For small scale purification of plasmid DNA, 4 mL of ON bacterial culture of transformed competent cells were processed using the Wizard® Plus SV Minipreps DNA Purification System (PROMEGA), according to the manufacturer's protocol.

For large scale purification of plasmid DNA, 100 mL of selective LB medium was inoculated with 5 µL of the plasmid bacterial culture, shaken ON at 250 rpm at 37 °C and processed using the HiSpeed Plasmid Midi Kit (Qiagen), according to the manufacturer's instructions. DNA concentration was determined using a Nanodrop 2000 spectrophotometer (Thermo Scientific).

3.7 Plasmid constructs generated

*3.7.1 Col10a1:*GFP-NTRo *construct*

To produce the *col10a1:*GFP-NTRo construct, the Meganuclease plasmid *col10a1:*nlGFP and *pGNTNo*, kindly provided by Christoph Winkler and Maik Grohmann, respectively, were used. The *col10a1:*nlGFP plasmid contains a 5.865-kb upstream regulatory region of the *Oryzias latipes col10a1* locus, driving the expression of a nuclear-targeted Green Fluorescence Protein (GFP) (Renn et al. 2013). The *pGNTRo* contains the coding sequences of GFP and the codon optimized sequence of the Nitroreductase (NTRo) fusion construct (Grohmann et al. 2009). To generate the *col10a1:*GFP-NTRo construct, the cloning consisted on replacing the nlGFP from the *col10a1:*nlGFP plasmid backbone by the GFP-NTRo fusion sequence. In the final construct, the *col10a1* promoter drives the expression of the GFP-NTRo fusion coding sequence and is flanked by I-SceI sites, allowing genomic recombination with Meganuclease (Figure 14). For this, the *col10a1:*nlGFP plasmid was digested with the NcoI and XbaI restriction enzymes (Fermentas), to excise the nlGFP sequence, and the GFP-NTRo sequence was amplified from

the *pGNTRo* by PCR using Taq Polymerase (Fermentas) and a specific In-Fusion primer pair (for RE and primer details see Table III and Table IV, respectively). Plasmid digestion and PCR product purification, ligation mix and transformation were performed as described above. After transformation, selected colonies were grown, plasmid DNA purified and digested with EcoRI (Promega) to confirm proper insertion of the fragment. The best clones were sequenced with appropriate primers (see Table IV), using the Stab Vida Sanger Sequencing services, and the construct with fewer errors was used for zebrafish embryo microinjection.

*3.7.2 Krtt1c19e:*GFP-NTRo *construct*

To produce the *krtt1c19e:*GFP-NTRo final construct, the Meganuclease vector *col10a1:*GFP-NTRo*,* generated above, and the *p5E- krtt1c19e*, kindly provided by Matthias Hammerschmidt were used (Fischer et al. 2014). The *p5E-krtt1c19e* plasmid contains a 3939-Kb promoter region of the *krtt1c19e* gene (Lee et al. 2014). To generate the *krtt1c19e:*GFP-NTRo construct, cloning consisted in replacing the *col10a1* regulatory region from the *col10a1:*GFP-NTRo plasmid backbone by the *krtt1c19e* promoter sequence. In this final construct, the *krtt1c19e* promoter drives the expression of GFP-NTRo fusion coding sequence and is flanked by I-SceI sites, allowing recombination with Meganuclease (Figure 15). For this, the *col10a1:GFP-NTRo* plasmid was digested with the KpnI and BamHI restriction enzymes (Fermentas) to substitute the *col10a1* regulatory region by the *krtt1c19e* promoter sequence, which was amplified from the *p5E-krtt1c19e* by PCR using the Titanium Taq Polymerase and a specific set of In-Fusion primers (for RE and primer details see Table III and Table IV, respectively). Plasmid digestion and PCR product purification, ligation mix and transformation were performed as described above. After transformation, selected colonies were grown, plasmid DNA purified and digested with EcoRI (Promega) to confirm proper integration of the fragment. The best clones were sequenced with appropriate primers (see Table IV), using the Stab Vida Sanger Sequencing services, and the best construct with fewer errors was used for microinjection.

Table IV: List containing the primers used for sequencing.

Primer Name	Primer Sequence (5'>3')	Objective
NTRo Forward	GATGCTGTGCCCATCGAA	Sequence the correct insertion of the GFP-NTRo coding sequence at the 3' end of the *col10a1* promoter backbone
GFP Reverse	AAGTCGTGCTGCTTCATGTG	Sequence the correct insertion of the GFP-NTRo coding sequence at the 5' end of the *col10a1* promoter backbone. Confirm the correct substitution of the *col10a1* promoter by the *krtt1c19e*

Primer Name	Primer Sequence (5'>3')	Objective
		promoter at the 3' end of the *col10a1:*GFP-NTRo backbone
I-SceI Forward	TAGGGATAACAGGGTAAT	Sequence the correct substitution of the *col10a1* promoter by the *krtt1c19e promoter* at the 5' end of the *col10a1:*GFP-NTRo backbone

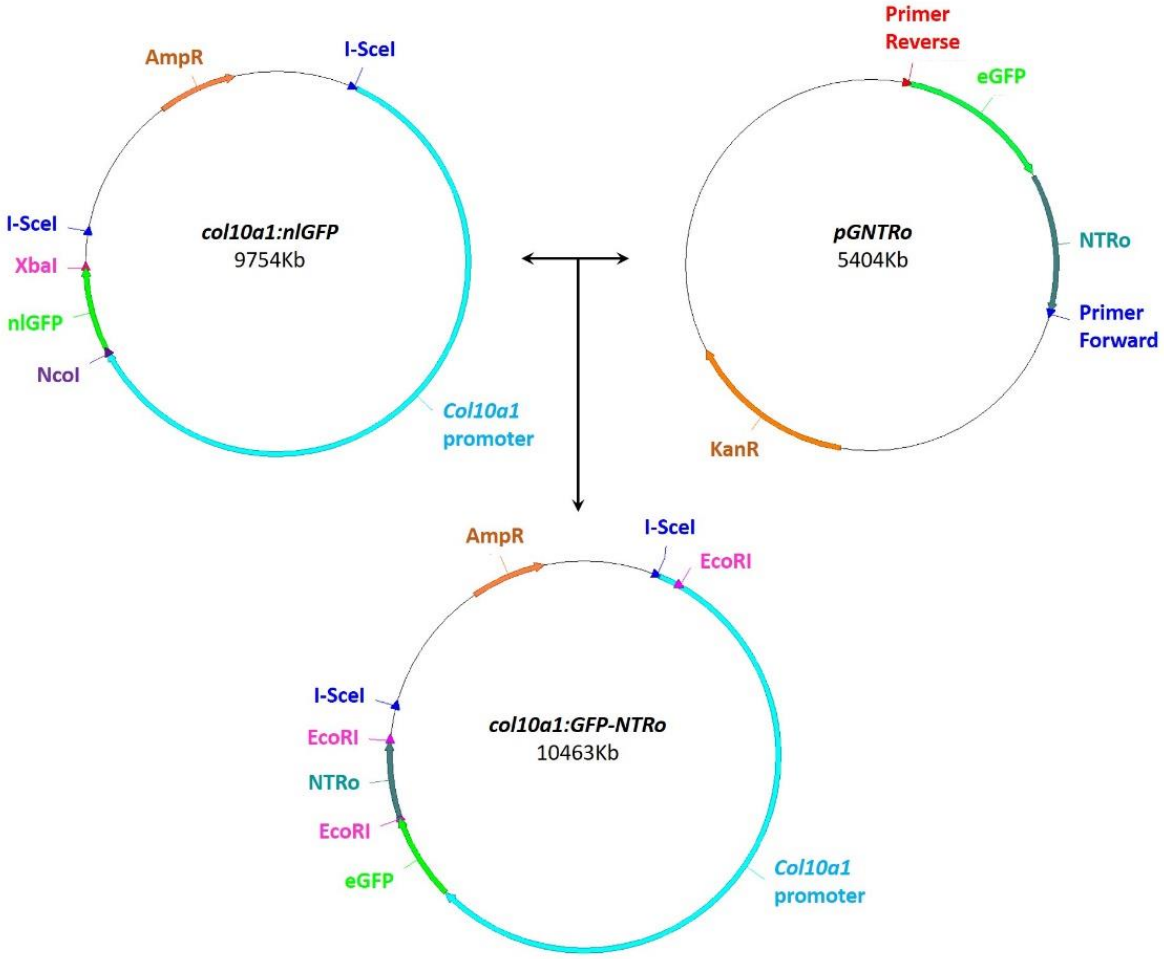

Figure 14: Generation of *col10a1*:GFP-NTRo construct. The *col10a1*:nlGFP plasmid is digested with XbaI and NcoI. The GFP-NTRo fusion sequence is amplified from the pGNTRo and inserted in the destination vector generating the *col10a1*: GFP-NTRo construct. Correct insertion was confirmed by digesting selected clones with EcoRI. Clones with the correct insertion were sent for sequencing.

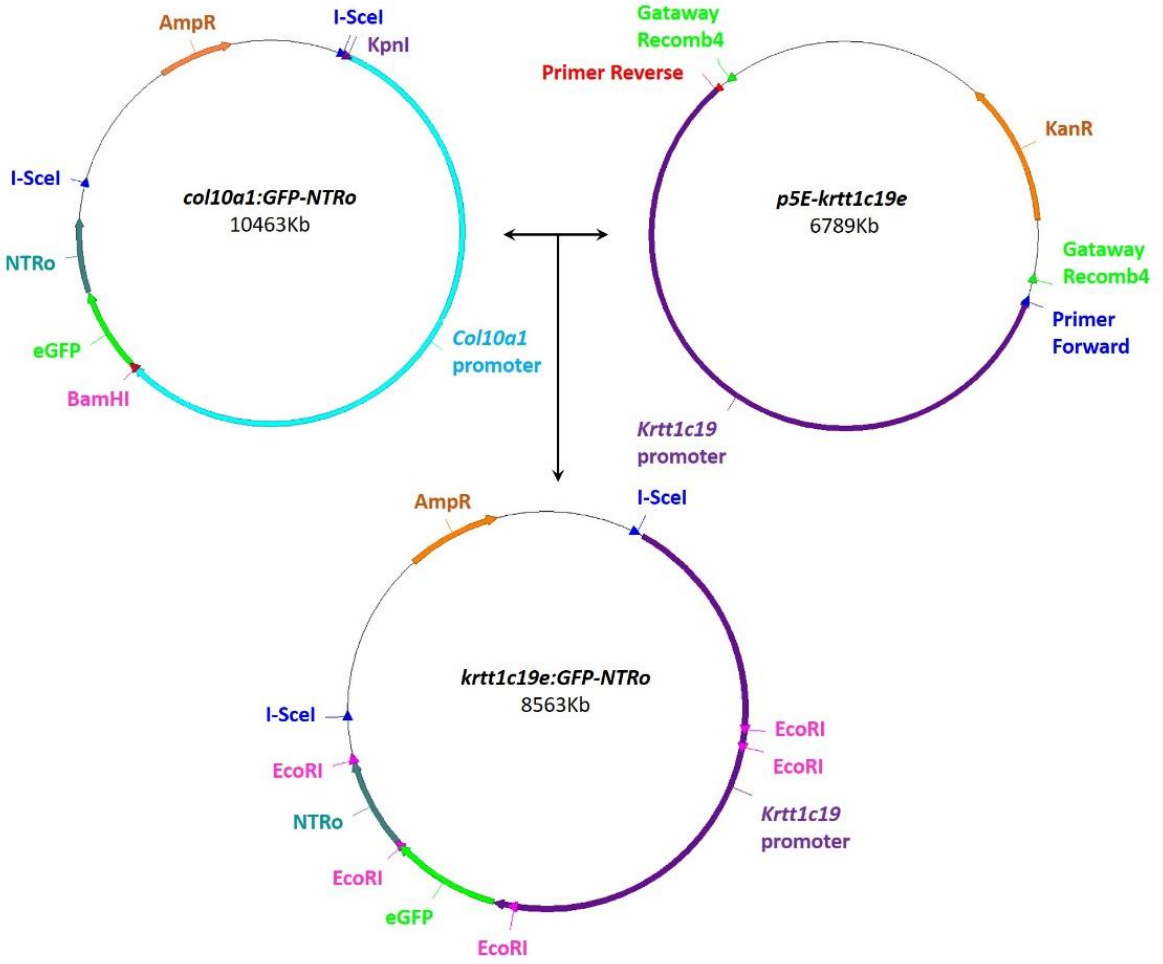

Figure 15: Generation of *krtt1c19e*:GFP-NTRo construct. The *col10a1*:GFP-NTRo plasmid is digested with KpnI and BamHI to excise the *col10a1* promoter sequence. The *krtt1c19e* promoter sequence is amplified from the p5E- *krtt1c19e* and inserted in the destination vector in order to generate the plasmid *krtt1c19e*:GFP-NTRo. Correct insertion was confirmed by digesting selected clones with EcoRI and the clones with correct insertion were sent for sequencing.

4 GENERATION OF TRANSGENIC LINES

4.1 Microinjection of DNA constructs into zebrafish embryos

WT AB strain zebrafish embryos were placed on an agar plate containing E3 medium and injected at one-cell stage using a pressure injector (PV820 Pneumatic PicoPump) (hold pressure = 3 psi; eject pressure = 20 psi), DNA borosilicate glass capillaries (World precision instruments) and a Nikon SMZ745 stereoscope. Since all injected constructs, namely *col10a1:*nlGFP, *col10a1:*GFP-NTRo and *krtt1c19e:*GFP-NTRo, were flanked by I-SceI sites, they were co-injected with the I-SceI Meganuclease enzyme. For that, capillaries were filled with the injection mix (50 ng/µL DNA; 1x Taq Buffer with KCl (Fermentas); 5 mM $MgCl_2$ (Fermentas); 1 U/mL Meganuclease I-SceI (Roche); or, 50 ng/µL DNA; 1X Buffer CutSmart (NEB); 1 U/mL Meganuclease I-SceI (NEB) and calibration was performed in a calibration graticule

(PyserSGLimited), adjusting the pressure to inject 100 pg of plasmid DNA per embryo (Soroldoni et al. 2009)

4.2 Embryo screening

Injected embryos were screened and imaged under a fluorescence stereoscope at 24 hours-post fertilization (hpf) for *krtt1c19e:*GFP-NTRo injected embryos, and at 72 hpf for *col10a1:*nlGFP and *col10a1:*GFP-NTRo injected embryos. GFP-positive embryos that mimicked the expression patterns of *krtt1c19e* (epidermis basal keratinocyte layers) and *col10a1* (head developing bones, such as ceratobranchial, maxilla, cleithrum, and opercle) (Li et al. 2009) were selected and raised until sexual maturity (3-6 months). After reaching adulthood, they were outcrossed to WT AB fish to identify founders (germline carriers) for stable transgenic line generation. Table V describes each line generated in the context of this work and its purpose.

Table V: List of zebrafish transgenic lines generated in the context of this study.

Line Name	Abbreviation	Line Type	Description
Tg(*col10a1:*nlGFP)	*col10a1:*nlGFP	Reporter	nlGFP expression in osteoblasts; also labels joint associated osteoprogenitors in the adult caudal fin
Tg(*col10a1:*GFP-NTRo)	*col10a1:*GFP-NTR	Ablation	Ablation of specific cell types and tissues that express *col10a1,* namely joint associated osteoprogenitors in the adult caudal fin
Tg(*krtt1c19e:*GFP-NTRo)	*krtt1c19:*GFP-NTR	Ablation	Ablation specific cell types and tissues that express *krtt1c19e,* namely the basal epidermal layer keratinocytes

5 HEAT-SHOCK AND CHEMICAL TREATMENTS

Heat-shock (HS) inducible transgenic strains, namely dominant-negative and constitutively active forms of Yap, *hsp70l:*RFP-dnyap1 and *hsp70l:*RFP-*cayap1*, respectively, used to manipulate the Hippo/Yap signalling pathway, and *hsp70l:cyp26a1*, used to inhibit the Retinoic acid (RA) signalling pathway, were analysed as heterozygotes with wild-type siblings

serving as controls. Importantly, these transgenics lines enable the temporal control of the pathway at specific time-points during regeneration. Transgenic animals and siblings were maintained at 28 °C and heat-shocked once a day at 38 °C for 1 h, by incubation in pre-heated water. For Yap manipulation during dedifferentiation (Chapter III), animals were subjected to one HS prior to amputation. To manipulate Yap function during regenerative outgrowth phase (Chapter IV) animals are left to regenerate normally during the blastema formation phase (0-48 hpa), and heat-shocked daily during the 3 following days. After heat-shock, caudal fin regeneration assays were performed at 28 °C, fins from anaesthetized animals were collected at predefined time-points post-amputation (Blum and Begemann 2012; Mateus et al. 2015) and then processed for cryosectioning or pooled for RNA extraction.

For experiments involving chemical treatments, the following drugs were used: the Pfkfb3 inhibitor 3-(3-pyridinyl)-1-(4-pyridinyl)-2-propen-1-one) (525330, Sigma-Aldrich), referred as 3PO (Schoors et al. 2014), was used to inhibit glycolytic influx and the glucose metabolism (Schools et al, 2014); and the Bmpr inhibitor, (LDN193189, StemRD), referred as Bmpri, was used to inhibit the BMP signalling pathway (Stewart et al. 2014). For both 3PO and BMPRi, stock solutions were dissolved in Dimethyl sulfoxide (DMSO, Sigma-Aldrich) at 40 mM and 10 mM, respectively. 3PO and Bmpri were added to the fish water to obtain the final concentration of 15 µM and 5 µM, respectively. For controls, the equivalent volume of drug vehicle (DMSO) was added to the water. For these experiments, caudal fin regeneration assays were performed at 33 °C and drugs were replaced daily. At the desired time-points, fish were anaesthetized, fins imaged under a Zeiss Lumar V-12 fluorescence stereoscope and collected at predefined time-points after fin amputation for subsequent cryosection processing.

6 NTR/MTZ ABLATION ASSAYS

The NTR/MTZ system is one of the most widely used methods in the zebrafish community to selectively deplete multiple cell types in zebrafish, allowing for temporal and spatial control of the ablation. (Curado et al. 2007, 2009; White and Mumm 2013). This system is based on the ability of the Nitroreductase (NTR) enzyme to convert an innocuous pro-drug, metronidazole (Mtz), that is added to the fish water, into a cytotoxic agent that causes the death of the NTR-expressing cells without affecting the neighbouring cells. The NTR is usually under the control of a tissue-specific promoter (expressed in the cell population of interest). Additionally, NTR is generally fused to a fluorescent protein (FP), allowing for cell visualization and providing an easy and accessible way to confirm the success of the ablation (Figure 16).
Transgenic zebrafish expressing the NTR enzyme and a fluorescent reporter under the control of a tissue specific promoter were incubated with the pro-drug solution, Metronidazole (Mtz) (Sigma-Aldrich, M1547) dissolved in fish water with 0.2% of DMSO. Control animals were incubated in fish water with 0.2 % DMSO. Animals were maintained for 24 h in the dark at 28 °C in these solutions, as previously described (Curado et al. 2009). To recover from treatment, both Mtz and vehicle-treated zebrafish were rinsed and returned to the circulating system's

water for 48 hours at 28 °C. Afterwards, controls and Mtz-treated fish displaying a reduced fluorescence intensity (readout for ablation efficiency), were subjected to caudal fin amputation. Fish were then allowed to regenerate in an incubator at 33 °C, or at 28 °C when the in combination with heat-shock inducible transgenic lines. Regenerated fins were collected from anaesthetized fish at desired time-points post-amputation and then processed for cryosectioning. This ablation protocol relies on critical variables such as Mtz time of exposure and concentration. Since the efficiency of the ablation depends greatly on the tissue to be ablated, several concentrations of Mtz were tested for each ablation line independently and when in combination with other ablation lines (see Table VI for Mtz final concentration details). In this context, the *osx:*mCherry-NTRo is used to evaluate new sources of osteoprogenitor when the mature osteoblast population is not available. The *col10a1:*GFP-NTRo fish are used to ablate joint-associated osteoprogenitors and the *krtt1c19e:*GFP-NTRo fish are used to ablate basal epidermal cells. The later transgenic lines were combined with the *osx:*mCherry-NTRo line to evaluate if ablation of joint-associated osteoprogenitor and basal epidermal cells are potential sources for *de novo* osteoblasts when the mature osteoblast population is compromised. The *osx:*mCherry-NTRo line was also combined with lineage tracing transgenic lines for the epidermis and for the mesenchyme to address whether in osteoblast ablation context they can provide a source of newly formed osteoblasts during regeneration. In addition, the osteoblast ablation line was combined with available reporter lines and with loss of function transgenics to manipulate a given signalling pathway and test its requirement for *de novo* osteoblast formation during regeneration (for further details see Table VI).

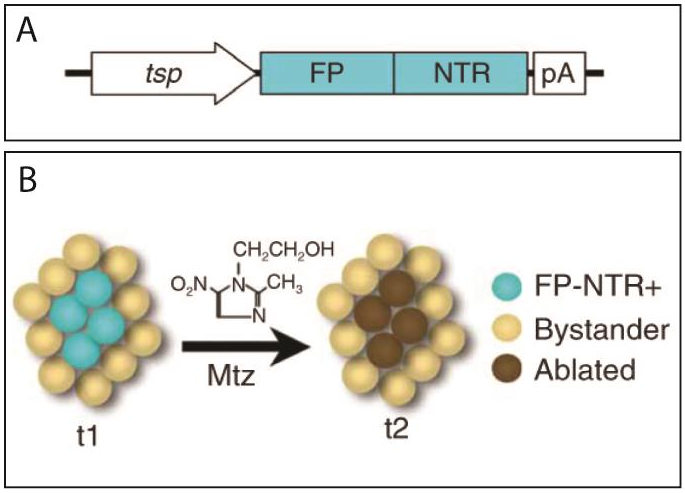

Figure 16: Experimental set up for Mtz/NTR tissue-specific ablation. (A) A tissue-specific promoter (tsp) drives the expression of NTR coupled with a fluorescent protein (FP). (B) After adding Mtz, FP-NTR expressing cells (blue balls) undergo apoptosis and die (brown balls), while leaving the surrounding cells unharmed (beige balls). Adapted from (Curado et al. 2009).

7 LINEAGE TRACING ASSAYS

One of the most classical questions in the regeneration field is the origin of the cells that compose the regenerated tissue. To address this, lineage tracing or fate mapping can be used. This technique involves the permanent labelling of a specific cell or tissue so that its descendants are easily traceable, thus providing information about the progeny, location and differentiation status of a single cell in its natural habitat during regeneration (Kretzschmar and Watt 2012). One of the most used systems to track cells is the site-specific recombination (SSR) system Cre/loxP (Hans et al. 2009). This system usually combines the two following transgenes: (1) a tamoxifen-inducible Cre recombinase fused to the tamoxifen receptor ERT2, which is under the control of a tissue specific promoter, so that it is produced only in the cells/tissue of interest; (2) and a recombination-competent fluorescent responder (or "switch"). Upon Cre induction by tamoxifen, it promotes the excision of loxP sites, present in the switch line, in the cells/tissue of interest that become permanently labelled with a fluorescent reporter (Figure 17A and B) (Chen and Poss 2017; Carney and Mosimann 2018).
We took advantage of this system to address the contribution of specific cell types to bone repair in caudal fins virtually devoided of mature osteoblasts. We used transgenic lines containing a tissue specific promoter regulating the expression of a ligand-inducible CreER(T2) that allows temporal control of recombination upon administration of the tamoxifen active metabolite, 4-hydroxy-tamoxifen (4-OHT). These lines were combined with a red-to-green fluorescence reporter line (switch line) to detect Cre activity. In the absence of Cre activity the reporter line expresses DsRed under the control of the *β-actin2* promoter, which as previously used to for lineage tracing in the caudal fin (Singh et al. 2012); when a recombination event occurs, EGFP is expressed instead, enabling the tracing of the progeny of the cells of interest (Hans et al. 2009; Mosimann et al. 2011). To understand the contribution of specific cell types in osteoblast depleted fins, we generated triple transgenic lines containing the promoter of interest driving CreER(T2), the switch line and the osteoblast ablation line (for further details see Table VI). For 4-OHT (Sigma-Aldrich, H7904) pharmacological treatments, 10 mM stock solutions were dissolved in 100% ethanol in the dark and stored at −80 °C for three months. Fish were incubated in the dark with 4-OHT or with the corresponding dilution of ethanol (Felker et al. 2016). When combining the lineage tracing procedures with osteoblast ablation, Mtz treatments were performed as described in the previous section.

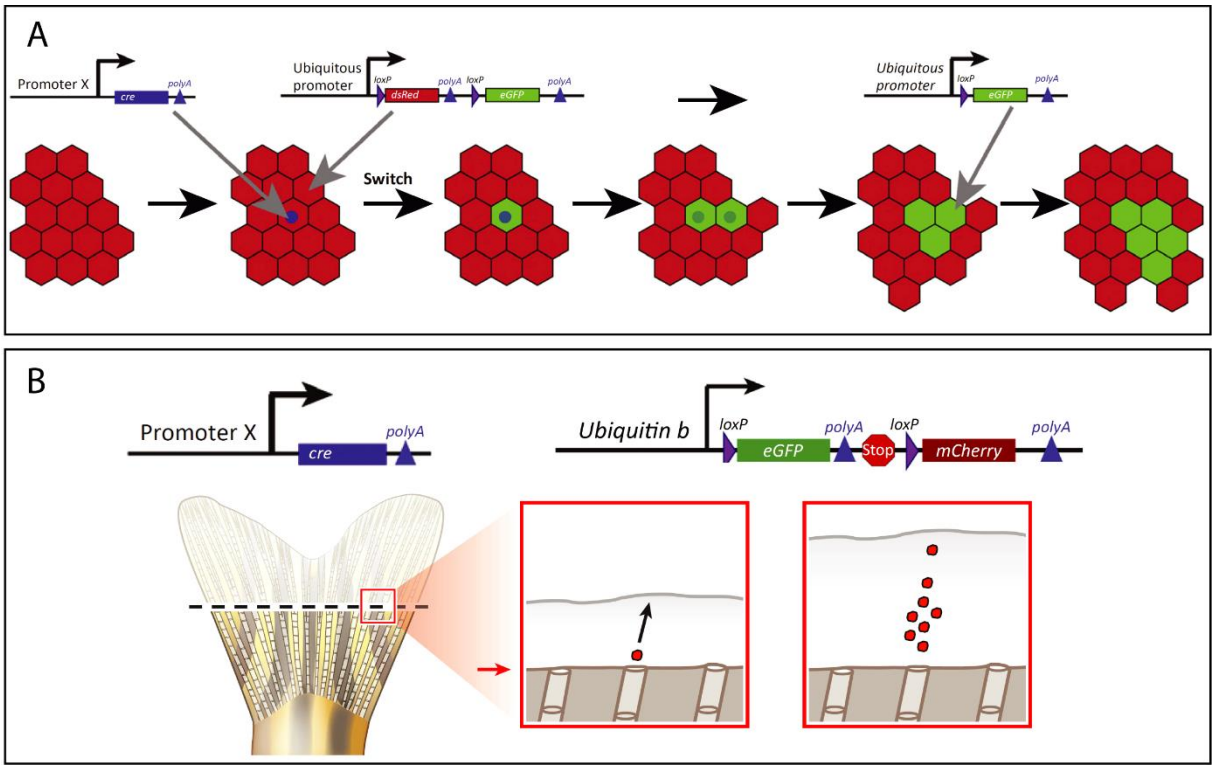

Figure 17: Lineage tracing through Cre/loxP mediated recombination. (A) Schematic representation of a possible lineage tracing approach. Promoter X drives the expression of a tamoxifen-inducible Cre recombinase in a specific cell type. After tamoxifen mediated Cre induction, Cre promotes the switch from recombination-competent responder (or "switch"). The latter is composed of two cassettes: one driven by a ubiquitous cis-regulatory element, which cages a red fluorescent reporter downstream of a transcriptional stop sequence flanked by loxP recognition sites for Cre. Downstream of this first cassette there is another cassette that harbours a second green fluorescent reporter. Upon Cre induction by tamoxifen it promotes the excision of the loxP flanked cassette only in the cells/tissue of interest, switching the fluorophore colour from red to green (independently of the activity of the ubiquitous promoter), that become permanently labelled. Thus, enabling to trace all promoter X-activating cells and descendants (Chen and Poss 2017; Carney and Mosimann 2018). (B) Schematic representation of lineage tracing of a single blastemal cell and its contribution over time in regenerating fin tissue. Dashed line represents the amputation plane. Adapted from (Chen and Poss 2017; Carney and Mosimann 2018).

7.1 Mesenchymal cell fate mapping

For mesenchymal cell fate tracing, we used the *careg:*creERt2*; β-act2:*RSG*; osx:*mCherry-NTR triple transgenics. To permanently label the mesenchymal cells that contribute to the regenerative process, fish were subjected to osteoblast ablation, caudal fin amputation and then incubated in 5 µM 4-OHT in circulating system water during the first 24 hpa. Sibling controls were incubated with the equivalent amount of ethanol (Pfefferli and Jaźwińska 2017). Fins were allowed to regenerate until desired time-points post-amputation and were collected for subsequent cryosectioning.

7.2 Epidermal cell fate mapping

For epidermal cell fate tracing, we used the *krt19:*creERt2*; β-act2:*RSG*; osx:*mCherry-NTR triple transgenics. 4-OHT treatments were performed during zebrafish developmental

stages to allow for a complete labelling of the adult epidermis. For this, 24 to 96 hpf embryos were treated with 5 µM 4-OHT in embryo medium in the dark at 28 °C, and the solution was replaced daily. Sibling controls were treated with the corresponding amount of ethanol. Embryos were then returned to normal circulating system conditions and left to grow until adulthood (Fischer et al. 2014). Adult fish were subjected to the osteoblast ablation protocol, as described in section 6. Caudal fins of fish showing an efficient ablation were amputated, allowed to regenerate until predefined time-points post-amputation and were collected for subsequent tissue processing and cryosectioning.

Table VI: Transgenic lines used for NTR/Mtz cell ablation and Cre/loxP lineage tracing assays.

Double and triple transgenic lines	Abbreviation	Mtz concentration	Objective
Tg(*osterix:*mCherry-NTRo)^{pd46}; Tg(*ola.Bglap:*EGFP)^{hu4008}	*osx:*NTRo*; osc:*EGFP	8.5 mM	Osteoblast ablation and mature osteoblast labelling
Tg(*osterix:*mCherry-NTRo)^{pd46} ; Tg(*Hsa.RUNX2-Mmu.Fos:*EGFP)^{zf259}	*osx:* NTRo*; runx2:*EGFP	8.5 mM	Osteoblast ablation and labelling of all osteoblast differentiation stages, including osteoprogenitors
Tg(*osterix:*mCherry-NTRo)^{pd46} ; Tg(*ctgfa:*EGFP)	*osx:* NTRo*; ctgfa:*EGFP	8.5 mM	Osteoblast ablation and mesenchymal cell labelling
Tg(*osterix:*mCherry-NTRo)^{pd46} ; Tg(*col10a1:*nlGFP)	*osx:* NTRo*; col10a1:*nlGFP	8.5 mM	Osteoblast ablation and mesenchymal cell and joint associated osteoprogenitor labelling
Tg(*osterix:*mCherry-NTRo)^{pd46} ; TgBAC(*aldh1a2:*aldh1a2-GFP)^{kn2}	*osx:* NTRo*; aldh1a2:*GFP	8.5 mM	Osteoblast ablation and visualization of endogenous sources of RA synthesis
Tg(*krtt1c19e:GFP-NTRo*)	*krt19:*GFP-NTRo	7.5 mM	Basal epidermal layer ablation
Tg(*osterix:*mCherry-NTRo)^{pd46} ; Tg(*hsp70l:cyp26a1*)^{kn1}	*osx:* NTRo*; hsp70l:cyp26a1*	8.5 mM	Osteoblast ablation and RA signalling manipulation

Double and triple transgenic lines	Abbreviation	Mtz concentration	Objective
Tg(*careg*:*Cre-ERT2); Tg(-9.8actb2: LOXP*-DsRed-*LOXP*-EGFP); Tg(*osterix:*mCherry-NTRo)^{pd46}	*careg:*creERt2*;* *β-act2:*RSG*;* *osx:* NTRo	8.5 mM	Labelling/tracing mesenchymal cell progeny in osteoblast depleted fins
Tg(*krtt1c19e:*Cre-ERT2); *Tg(-9.8actb2: LOXP*-DsRed-*LOXP*-EGFP); Tg(*osterix:*mCherry-NTRo)^{pd46}	*krt19:*creERt2*;* *β-act2:*RSG*;* *osx:* NTRo	8.5 mM	Labelling/tracing epidermal progeny in osteoblast depleted fins

8 FLOW CYTOMETRY

For flow cytometry analysis, adult zebrafish caudal fins were amputated and dissociated into single cell suspensions. For that, fins were incubated for 20 min at 28 °C with vigorous shaking in a solution of Liberase DH Research Grade (0,05mg/ml, Roche) reconstituted in 1x Phosphate Buffered Saline (PBS). After complete tissue disaggregation, cell suspensions were passed through a 30 µm filter (CellTricks, Sysmex) and centrifuged at 300g for 5 min at 4 °C. Cell pellets were then resuspended in 1x PBS with 10% fetal bovine serum (Biowest) and cell cycle analysis or Fluorescence Activated Cell Sorting (FACS) was performed.

8.1 Cell cycle analysis

Cell cycle analysis was performed in caudal fins collected from *DN-yap* transgenic animals and the corresponding sibling controls subjected to heat-shock and caudal fin amputation. Caudal fins were dissociated into a single cell suspension as mentioned above. Cells were incubated with Vybrant DyeCycle Green (Invitrogen) diluted in 1x PBS at a final concentration of 10 µM for 20 min at 28 °C. Samples were acquired in a CyAn ADPTM flow cytometer (Beckman Coulter) equipped with a 25 mW solid state 488 nm laser using low flow rate acquisition. Vybrant DyeCycle is excited at 488 nm with fluorescence measured in the FITC channel (520/20 bandpass filter). Cell debris and cell aggregates were excluded from the sample analysis. Exclusion of cell debris was done by side scatter (SSC log) and forward scatter (FSC linear) and exclusion of aggregates and doublets by monitoring forward scatter width (FSC-W) and height (FSC-H). To separate cells according to fluorescence intensity, WT AB strain was used as an unstained/negative control. This allowed us to identify the negative population and determine the level of background fluorescence, and thus to properly gate the positive population. DNA content was measured using the fluorescence intensity that should be

proportional to DNA mass. Around 15 000 events were plotted and the distribution of cells in G0/G1, S, and G2/M phases was determined using the Watson pragmatic fitting algorithm of FlowJo software (Version 10, Williamson Way, Ashland, USA).

8.2 Fluorescence activated cell sorting (FACS)

To specifically isolate the mature osteoblast population that contributes to the regenerative process and perform a transcriptome analysis by microarray chip assay, we took advantage of the *osc:*EGFP transgenic like and isolated *osc*-positive cells through FACS. FACS was carried out on a MoFlo high-speed cell sorter (Beckman Coulter, Fort Collins, USA) using a 488 nm laser (200 mW air-cooled Sapphire, Coherent) at 140 mW for scatter and a 530/40 nm bandpass filter for GFP measurements. Primarily, cell debris and aggregates were removed from the analysis as described in the previous section. The fluorescence scatter (Comp-FL Log::GFP) was used to separate cells according to their GFP fluorescence intensity with a maximum of stringency to avoid cross-contamination of the desired cell population. Zebrafish WT AB strain was used as a negative control to set the GFP-positive population. The instrument was run at a constant pressure of 207 kPa (30 psi) with a 100 µm nozzle and frequency of drop formation of approximately 40 kHz. Three independent biological replicates were performed for each condition. As control samples, we isolated osteoblasts from the middle region of the uncut fin (corresponding to our osteoblast population in homeostasis from non-regenerating fins). In amputated samples, we isolated osteoblasts from the first bone segment below the amputation plan, at several time-points during dedifferentiation, 3 hpa, 6 hpa and at 9 hpa. For each, 300 GFP-positive cells were collected into lysis and RNA stabilization buffer (provided by OakLabs GmbH) and vigorously shaken for 1 min. To verify the quality of the samples, cell death and purity were measured. Cell death was measured by incubating the samples with propidium iodide (PI, Sigma-Aldrich) to a concentration of 1 µg/ml and using the 488 nm laser for PI excitation. PI fluorescence was measured on the PI channel (613/20 BP). Only samples with cell death below 10-20% and purity above 90% were used for subsequent analysis. Samples were maintained at -80 °C until sent to OakLabs GmbH (Henningsdorf, Germany) for cDNA generation, microarray chip set up and data analysis.

9 MICROARRAY CHIP ASSAY

To compare the transcriptome profiles of mature osteoblasts in homeostasis to osteoblasts during dedifferentiation a genome-wide gene expression profiling was set up by using the 8x60K ArrayXS Zebrafish platform by Agilent and performed by OakLabs GmbH (Henningsdorf, Germany). A microarray consists of a membrane containing multiple oligonucleotides (probes) that represent the different regions of the genome. Each gene can be represented by more than one probe, increasing the robustness of the analysis. The 8x60K ArrayXS Zebrafish represents approximately a total of around 60000 zebrafish transcripts, which includes 48000 coding genes, 8075 non-coding genes and 19140 predicted genes annotated in the Zv9 release

75. Given that, from each sample analysed, RNA was retrieved from only 300 osteoblasts, an adaptation from a single cell protocol was established and performed by OakLabs GmbH. Primarily, RNA samples were processed by Oaklabs and underwent a quality control to determine the quality and quantity of the total RNA, using the 2100 Bioanalyzer (Agilent Technologies), the RNA 6000 Pico Kit and a photometrical measurement with the Nanodrop 2000 spectrophotometer (Thermo Scientific). Sample quality was evaluated based on the Bioanalyzer's RNA integrity number (RIN) and the two distinct peaks representing the 18S and 28S rRNA, as well as the overall electropherogram. Only samples with RIN ≥ 8 were used. Subsequently, 2 µL of the lysis and RNA stabilization buffer, from three biological replicates of each condition (uncut, 3 hpa, 6hpa and 9hpa isolated osteoblasts), was used for cDNA synthesis and pre-amplification using the Ovation One Direct system (NuGEN). The generated cDNA was labelled with Cy3--dCTP using the SureTag DNA Labelling Kit (Agilent) prior to microarray hybridisation. Microarray blocking, hybridisation and wash were performed using Agilent's Oligo aCGH/ChIP-on-Chip Hybridisation Kit following the manufacturer's protocol. Ultimately, fluorescence signals were detected by the SureScan Microarray Scanner (Agilent Technologies) at a resolution of 3 µm for SurePrint G3 Gene Expression Microarrays, and 5 µm for HD Microarray formats. This resulted in a raw data output of 1-colour hybridisation using the Agilent's Feature Extraction software version 11. Raw data was then subjected to processing and analysis (see section 14 of materials and methods). The retrieved data was used to compare the expression profiles of osteoblasts in homeostasis with the other time-points during regeneration, thus delivering 3 different comparison data sets: 3 hpa versus uncut, 6 hpa versus uncut and 9 hpa versus uncut

10 TOTAL RNA ISOLATION AND QUANTITATIVE -PCR (q-PCR)

For gene expression analysis, including microarray validation, regenerates from 4-5 caudal fins, including one bony-ray segment proximal to the amputation plane, were harvested per experiment and per time-point analysed. Samples were homogenized in Trizol reagent (Invitrogen) for cell disruption and RNA extraction. Chloroform was added, and the homogenate allowed to separate into a clear upper aqueous layer (containing RNA). RNA was precipitated from the aqueous layer by adding an equal amount of 100% ethanol and loaded into RNeasy Micro Spin columns (Qiagen). The rest of the protocol was followed according to the RNeasy Micro kit (Qiagen) manufacturer's protocol for total RNA purification. RNA purity/quality parameters were measured using the Nanodrop 2000 spectrophotometer (Thermo Fisher Scientific). cDNA was synthesized from 1 µg total RNA with the Transcriptor High Fidelity cDNA Synthesis Kit (Roche), using a mixture of oligo dT and random primers. All q-PCR primers were subjected to a standard calibration curve using 10-fold dilutions of cDNA to verify the efficiency of each primer pair. Primers were designed to amplify regions at exon to exon boundaries and 150-200 amplicons (primer sequences are listed in Table VII). q-PCR was performed using a FastStart Essential DNA Green Master Mix and a Roche LightCycler 480.

Cycle conditions were: 15 min pre-incubation at 95°C and 3 step amplification cycles (50x), each cycle for 30 sec at 95°C, 15 sec at 65°C or 68°C (depending on primer melting temperature (TM)) and for 30 sec at 72°C, followed by melting curve analysis, to confirm specific product amplification. q-PCR analysis is described in section 14 of this chapter.

Table VII: Primer sequences for q-PCR experiments.

Gene Symbol	Forward Primer (5'>3')	TM (°C)	Reverse Primer (5'>3')	TM (°C)
ef1α ENSDARG00000039502	ACGCCCTCCTGGCTTTCAC	68.8	TGGGACGAAGGCAACACTG	67.5
ef1α ENSDARG00000039502	CCTGGGAGTGAAACAGCTG	63.6	GCCTCCAGCATGTTGTCAC	64.6
osc1/bglap ENSDARG00000058414	TGACGTGGCCTCTATCATCA	64.4	TTTATAGGCGGCGATGATTC	63.6
osc2/bglapl ENSDARG00000104467	AACTCTGCCAGTGCTGAAGG	64.6	GGTCTCAGCCATGTGTTCAC	63.3
osn ENSDARG00000019353	GGTCGTGGAGGATGTTATTGC	65.4	GGGGCAGGTCAAAGGGTC	66.7
osx/sp7 ENSDARG00000019516	TCCAGACCTCCAGTGTTTCC	64.2	ATGGACATCCCACCAAGAAG	63.8
runx2a ENSDARG00000040261	ACGGTAATGGCTGGAAATGA	64.1	GTCCGTCCACTGTGACCTTT	64.1
runx2b ENSDARG00000059233	AGCTTCACCCTGACGATTACA	63.5	CCAGTTCACTGAGACGGTCA	64.1
col10a1a ENSDARG00000054753	GCATTCTTCTTCTCCTGGTG	61.4	CCTGAACCCCAACCCCC	67.7
wls/wnt 1	TAAGCCAGGTGAGTGAGGGTCA	68	TCAGCGCTTGACTGCTCATCTC	69.2

Gene Symbol	Forward Primer (5'>3')	TM (°C)	Reverse Primer (5'>3')	TM (°C)
ENSDARG00000009534				
wnt10a ENSDARG00000017155	CTCTCACGACATCAGTTGGCAC	67.1	CATGCTGCTGCTGCTCTTCTG	68.7
wnt3a ENSDARG00000058822	GATGCCCGCTCTGCTATGAATC	68.9	CCGATGTTTCTCAACCACCATTTC	69.2
dkk1a ENSDARG00000014103	ACATCCCAGGAGAACCACAG	64	AAACTTGTCCCTCTGTCAGCA	63.8
dkk1b ENSDARG00000045219	TCCTAAAAGAGGGCCAGGTC	64.3	TCCCTCGACTCAAGTCTGCT	64.2
bmp2a ENSDARG00000013409	ATCAGGAGCTTCCACCATGA	64.7	TGAACGTTAATGCGGTGAAA	63.9
bmp2b ENSDARG00000041430	CTGAAAACGATGACCCGAAC	64.4	AACTGCTGCGTTGTTTTTCC	64
bmp4 ENSDARG00000019995	AGCAGTGCCTTCAAAGGTTG	64.3	CATGGGGAAACAGTCCATGT	64.7
aldh1a2 ENSDARG00000053493	GAAACCTGCTGAGCAAACCCC	69	TGCTCTTTCCTGCTGCTTCTTG	67.9
cyp26a1 ENSDARG00000033999	AGCCGGAGAGATTCATGAGCAA	69.2	GGGTCCGTTTGAGAGAATCCAA	68.2
cyp26b1 ENSDARG00000077121	CTCCAATCCTGACCCCATCAA	68.2	GCAGGTCGATGGGAAGACTGA	68.8
Pfkpa ENSDARG00000028000	CAGAAGACTCGGCCTGTTTG	64.9	GCAACTTCAGCCACCACTG	64.7
Aldoaa ENSDARG00000011665	CTCAATGCCATGAACCAGTG	64.2	GGCCTGGCTGTTGTTAAGAG	63.7
pgam1a	TGAGAGGCATTGTGAAGCAC	64.1	CTTTGCGAACGGTTTCCTC	64.6

Gene Symbol	Forward Primer (5'>3')	TM (°C)	Reverse Primer (5'>3')	TM (°C)
ENSDARG00000005423				
pgam1b ENSDARG00000014068	GCAGATCAAGGAGGGAAAGAG	64.1	GGCTTCAGGTTCTTGTCCAG	63.8
eno1a ENSDARG00000022456	TCACCGTTCTGGAGAGACG	64.3	GAAGCGAGCCTTGTCTCCT	63.7
ldha ENSDARG00000101251	GTCAAGGGAATGCATGGTG	64.1	CTGAACACCCCACAAGGTC	63.2
gapdhs ENSDARG00000039914	CCAATGAAGGGAATTCTGGG	65.3	CAGGTCAGCAACACGATGG	65.6
mtfr1 ENSDARG00000045304	TGAACCCACAGATGCAGC	63.8	CAAACAGCGGTGTTTCCAC	64.2
ndufv2 ENSDARG00000013044	CGATGGTCCAAATCAACG	62.6	CAGGTCAGCTCTCACACCA	62.9
sdhdb ENSDARG00000030139	TCTTCTGAGCCTGGCACC	64.4	GACAGAACAAACAGGCCTGC	64.8
dlat ENSDARG00000015918	GGCATGTATGGCATCAAGC	64.1	GATCGCAGCTCAGAGTCACA	64.6
mdh2 ENSDARG00000043371	GAGCCAGGTTCACATTCTCC	63.7	CCCAAGGCCAAGGTTCTTT	65.1
cox6c ENSDARG00000038577	TGCGTTTGCTCTTTCCCTC	65.4	GGCCTGGCACTTTCAAAGAT	65.3

11 EdU INCORPORATION

To evaluate cell proliferation after osteoblast ablation, cells were labelled during S-phase by 5-ethynyl-2´-deoxyuridine (EdU, Thermo Scientific C10337) incorporation assays. *osx:*NTRo transgenic animals were subjected to Mtz treatment and caudal fin amputation, as described above, and allowed to regenerate until the desired time-points. Animals were anesthetised 3 h prior to caudal fin collection, placed ventral side up on a slit in a sponge and 20 µL of 10 mM EdU solution (2.5 mg/ml diluted in 1x PBS) were administered via intraperitoneal (IP) injection. IP injections were performed with an insulin syringe U-100 G 0,3 mL and a 30G needle (BD Micro-fine) inserted at a low angle with the tip pointing cranially close to the pelvic girdle (Blum and Begemann 2015b). Upon collection, caudal fins were processed for cryosectioning and subjected to EdU labelling protocols (as described in section 12.3).

12 HISTOLOGY

12.1 Skeletal colourations

12.1.1 Calcein staining

To specifically label calcified structures, in particular, the newly regenerated bony-rays during Yap and glycolysis manipulation experiments, we used the fluorescent chromophore calcein. For that, *DN-yap* and sibling controls, previously subjected to HS, and *osx:*mCherry-NTRo animals, exposed to 3PO and vehicle (DMSO, controls), were subjected to caudal fin amputation. Specimens were allowed to regenerate until predefined time-points post-amputation, fins were collected and immersed into a 0.2% calcein solution (2 g of calcein powder (Sigma-Aldrich, C0875-56) in 1 L of 1x PBS, pH 7.4) for 15 min. Afterwards, fins were rinsed in 1x PBS several times and left for 10 min in PBS 1x to allow the excess, unbound calcein, to diffuse out of the tissues (Jun Du et al. 2001). Fins were imaged using a Zeiss Lumar V-12 fluorescence stereoscope and collected for subsequent tissue processing and cryosection.

12.1.2 Alizarin red S staining

To follow the migration of mature osteoblast along the bony-ray segments, we performed live-imaging analysis using the transgenic line *osc:*EGFP and an Alizarin red S (ARS, Sigma-Aldrich) staining, which allows *in vivo* monitoring of bone mineralized structures. ARS *in vivo* staining protocol was performed prior to caudal fin amputation and consisted on incubating the animals in a 0.01 % ARS solution for 15 min in the dark. ARS solution was prepared using water from the circulating system and pH adjusted to 7.4 with a KOH solution, as previously described (Bensimon-Brito et al. 2016). Animals were rinsed at least 3 times for 5 min in system water and then transferred to new containers. *osc:*EGFP transgenics were subjected

to caudal fin amputation and imaged using a confocal microscope Zeiss LSM 710 at the desired time-points post-amputation.

12.2 Tissue processing for cryosections

Fins were collected and fixed overnight in 4% Paraformaldehyde dissolved in 1x PBS. After fixation, fins were stored in 100% methanol (except for the EdU incorporation assay) at -20 °C until required for subsequent analysis. They were then gradually rehydrated in a series of methanol/1x PBS (75%, 50% and 25%) and incubated ON in a 30% sucrose (Sigma-Aldrich) solution diluted in 1x PBS for cryoprotection. The following day fins were embedded in 7.5% gelatin (Sigma-Aldrich)/ 15% sucrose in 1x PBS and subsequently frozen in isopentane at -70°C. The frozen samples were stored at -80 °C until sectioning. Longitudinal caudal fins sections were sectioned in 12 µm-thick slices using a Microm cryostat (Cryostat Leica CM3050 S), collected on Superfrost slides and maintained at -20 °C until further use.

12.3 Immunofluorescence on cryosections

For immunofluorescence assays on frozen caudal fin cryostat sections, the following protocol was performed. Sections were thawed for 15 min at room temperature (RT), washed twice in 1x PBS at 37°C for 10 min for gelatin removal, followed by a 0.1 M glycine (Sigma-Aldrich, in PBS 1x) incubation for 10 min. Sections were then permeabilized in acetone for 7 min at -20°C and incubated for 20 min in 0.2% PBST (1x PBS with 0.2% Triton X-100). Afterwards, they were incubated in a blocking solution of 10% non-fat dry milk in PBST for 2-4 h at RT. Samples were then incubated with primary antibodies, diluted in blocking solution, ON at 4°C (for further antibody details see Table VIII). On the following day, samples were washed with PBST at least 6 x 10 minutes and then incubated with secondary antibodies, diluted in blocking solution, for 2 h at RT and protected from light (for further antibody details see Table IX). Subsequently, slides were washed 3 times, 10 min each, in PBST and then counterstained with 4',6-diamidino-2-phenylindole (DAPI; 0.001 mg/mL in 1x PBS, Sigma-Aldrich) for 5 min the dark for nuclei staining. Slides were washed 3 times with PBST, 10 min each, and mounted in fluorescent Mounting Medium (DAKO). Slides were then stored at 4°C protected from light until image acquisition.

Exceptions to the above immunofluorescence protocol were the following.

For anti-Runx2 and anti-PCNA staining, slides were subjected to an antigen retrieval step after gelatin removal, which consisted of a 15-min incubation at 95 °C with Sodium Citrate Buffer (10mM Tri-sodium citrate with 0.05% Tween20, pH 6).

For anti-pSmad 1/5/8 staining, slides were incubated in a blocking solution of 10% non-fat dry milk in PBST, containing 650 mM NaCl, and subsequently washed with PBST, containing 650 mM NaCl.

For anti-Yap staining, slides were washed in PBDX (1% BSA, 1% DMSO, 0,2% Triton-100, 50% PBS 1x in Milli-Q water) instead of 0.2% PBST and blocked in PBDX containing 1.5% Goat Serum. Incubation with anti-YAP was done ON at RT.

For EdU detection assay the manufacturer's protocol from Click-iT® Plus EdU Alexa Plus 488 Imaging Kit (Life Technologies) was followed. Briefly, samples were permeabilized with acetone and washed with PBST and then incubated with the Click-iT® reaction cocktail (Click-iT® reaction buffer; $CuSO_4$; Alexa Fluor 488 azide; reaction buffer additive) for 30 min in the dark. Afterwards, they were washed with PBST and the protocol followed as described above.

Table VIII: List of primary antibodies used for immunofluorescence assays.

Antibody	Host	Dilution	Retrieval	Wash	Block	Localization Cell type	Company
Anti-Runx2 (27-K)	Mouse	1:50	Sodium Citrate Buffer, pH 6	PBST	10% non-fat dry milk/PBST	Nucleus; all osteoblast stages, specially osteoprogenitors	Sta Cruz Biotechnology, 101145
Anti-Osx/Sp7 (A-13)	Rabbit	1:100	-	PBST	10% non-fat dry milk/PBST	Nucleus; immature to mature osteoblast	Sta Cruz Biotechnology, 22536-R
Anti-ZNS5	Mouse	1:200	-	PBST	10% non-fat dry milk/PBST	Membrane; osteoblast marker	Zebrafish International Resource Centre, 011604
Anti-TenascinC	Rabbit	1:100	-	PBST	10% non-fat dry milk/PBST	Extracellular matrix; secreted by osteoprogenitors	US Biological, 137.T2550-23
Anti-Laminin	Rabbit	1:100	-	PBST	10% non-fat dry milk/PBST	Extracellular matrix protein; enriched at the basal lamina	Thermo Scientific

Antibody	Host	Dilution	Retrieval	Wash	Block	Localization Cell type	Company
Anti-p63	Rabbit	1:100	-	PBST	10% non-fat dry milk/ PBST	Nucleus of epidermal cells	Gene Tex, GTX124660
anti-phospho Smad 1/5/8	Rabbit	1:100	-	650mM NaCl in PBST	10% non-fat dry milk/650 mM NaCl /PBST	Reporter for active BMP signalling	Cell Signaling, 9511
Anti-Yap FL (63.07)	Mouse,	1:100	-	PBDX	1,5% Goat Serum/ PBDX	Nuclear or cytoplasmic; to monitor Hippo pathway activity	Sta Cruz Biotechnology, 101199
Anti-PCNA	Rabbit	1:100	Sodium Citrate Buffer, pH 6	PBST	10% non-fat dry milk/PBST	Nucleus; proliferating cells (G1, S, G2, M)	Sta Cruz Biotechnology, F2007
Anti-GFP	Rabbit	1:100	-	PBST	10% non-fat dry milk/PBST	GFP	Invitrogen
Anti-GFP	Mouse	1:100	-	PBST	10% non-fat dry milk/PBST	GFP	Invitrogen
Anti-Ds-Red/mCherry	Rabbit	1:200	-	PBST	10% non-fat dry milk/PBST	mCherry	Enzifarma

Table IX: List of secondary antibodies used for immunofluorescence assays.

Fluorophore	Host	Specificity	Dilution	Company
Alexa Fluor 488	Goat	Mouse	1:500	Invitrogen, A11001
Alexa Fluor 488	Goat	Rabbit	1:500	Invitrogen, A11070
Alexa Fluor 568	Goat	Mouse	1:500	Invitrogen, A11031
Alexa Fluor 568	Goat	Rabbit	1:500	Invitrogen, A11036
Cy5	Goat	Mouse	1:250	Invitrogen, A10524

13 IMAGE ACQUISITION AND PROCESSING

13.1 Embryo, adult zebrafish and adult caudal fin imaging

Images of live anesthetised transgenic embryos, adult fish and adult caudal fins were acquired in a Zeiss Lumar V-12 fluorescence stereoscope equipped with a Zeiss digital colour camera using a 0.8X air objective and the Zen 2 PRO blue software. For ablation, heat-shock and 3PO experiments, both controls and manipulated animals were imaged using identical settings (magnification, contrast, gain and exposure time). Images were acquired using transmitted light and the GFP and/or TexasRed filters, according to the fluorescent reporter expressed or labelling. For image analysis and processing, composite maximum intensity images were assembled using the Fiji software (Schindelin et al. 2012). For whole adult specimen image acquisition, concatenation of several images along the proximal-distal axis was performed using the Fiji plugin 3D Pairwise Stitching (Schindelin et al. 2012). All Images were then processed using the Adobe Photoshop CS5 and Adobe Illustrator CC.

13.2 Live-imaging

For live-imaging analysis of osteoblast migratory dynamics *in vivo* during regeneration, we used *osc:*EGFP transgenic animals counterstained with ARS. To accommodate adult zebrafish for live-imaging, animals were anesthetised and maintained in glass-bottom Petri dishes. Imaging was performed in a confocal microscope Zeiss LSM 710 using the software ZEN 2010B SP1. *osc:*EGFP fish were imaged with a 10x air objective using the 488 nm and 568 nm, since ARS signals fluorescent light when excited with 530-560 nm wavelength excitation light wavelengths. Additionally, the transmitted light channel was used for the 488 nm excitation

light (Bensimon-Brito et al. 2016). Time-lapse images were acquired always in the same region of the fin, capturing the first 2 segments below the amputation plane and the blastema region. Images were taken every 5 h following amputation, during the first 25 hpa, and imaged using identical settings (magnification, contrast, gain and exposure time). For image processing, composite maximum intensity z-stack projections were made using the Fiji software (Schindelin et al. 2012). Time-lapses of the same bony-ray region, corresponding to the first and second segments below the amputation plane, were assembled and computationally registered with the Fiji StackReg and MultiStackReg plugins. All Images were then processed using the Adobe Photoshop CS5 and Adobe Illustrator CC.

13.3 Fixed samples imaging

All immuno-labelled cryosections were analysed in a confocal microscope Zeiss LSM 710 using the software ZEN 2010B SP1. Caudal fin sections images were acquired using a 40x water objective with 0.6x or 0.8x zoom, and 405, 488, 568, and 633 nm excitation wavelengths, coupled with transmitted light. Sequential images were acquired to capture the first segment below the amputation plane and the entire regenerated region. For all experiments and corresponding controls, images were acquired employing identical settings (magnification, contrast, gain and exposure time) and in identical/comparable regions. For image analysis and processing, composite maximum intensity z-stack projections were made using the Fiji software (Schindelin et al. 2012). When required, concatenation of several images along the proximal-distal axis of the same longitudinal section was performed using the Fiji plugin 3D Pairwise Stitching (Schindelin et al. 2012). All Images were then processed using the Adobe Photoshop CS5 and Adobe Illustrator CC.

14 QUANTIFICATIONS AND STATISTICAL ANALYSIS

14.1 Microarray chip analysis

Microarray chip detection was performed by OakLabs GmbH (Henningsdorf, Germany) and microarrays data quality assurance, data analysis and statistics were done by OakLabs GmbH and by a collaborator at Centro de Estudos de Doenças Crónicas (CEDOC-FCM), Patrícia Brito. For microarray chip detection, scanned arrays were first detected by the SureScan Microarray Scanner (Agilent Technologies), as mentioned in the Microarray chip assay section 9, in a raw data output of 1-colour hybridisation to obtain absent/present calls and to assure that all quality parameters were in the recommended range. Data generated was used to perform a transcriptomic comparison between the osteoblast control population (homeostasis/uncut) and osteoblast populations retrieved at 3 hpa (beginning of dedifferentiation) and at 6 hpa and 9 hpa (time-points during dedifferentiation).

14.1.1 Data Normalization

Background signals were subtracted and then normalized prior to the statistical analysis. For that, the arrays were quantile normalised using the ranked mean quantiles (Bolstad et al. 2003). Briefly, the mean signal of each target was ranked relative to all other targets and the ranked signal value replaced with the mean quantile value of the same rank.

14.1.2 Quality Assurance

For data quality control and to identify potential outlier samples hierarchical clustering and a principal component analysis were performed.
Hierarchical clustering can be evaluated by clustering samples using a correlation metric, resulting in a dendrogram. The clustering is based on normalised expression values. Samples that have the most similar expression profiles are clustered together. Therefore, hierarchical clustering is useful for identifying outlying samples. Technical replicates are expected to be the most similar followed by biological replicates from the same origin. Samples with similar expression patterns are located close to each other.
Principal component analysis (PCA) was developed to explain the intrinsic variability of the data. The data is visualised in a two-dimensional coordinate system, where both axes represent the two highest variabilities (principal components) of the data. The labels on the axes show the relative weights (in percentage) for the first component (x-axis) and the second component (y-axis). Similar to the hierarchical clustering algorithm, we can observe in this plot whether or not the distance of samples within one group is bigger than the distance between samples of different groups. Usually, the first two principal components give a good impression of how the differentially expressed probe sets clusters according to their variance.

14.1.3 Statistical Analysis

Fold change was determined based on the normalised data set and expression ratios obtained. In this data set a logarithmic base 2 transformation was performed (i.e. log2 (expression ratio)), to make the mapping space symmetric and the up-regulation and down-regulation comparable, prior to the significance test. For example, if the expression ratio is 1, then log2 (1:0) = 0 represents no change in expression; if the expression ratio is 4, then log2 (4:0) = 2:0 and for expression ratio of log2 (0,25) = -2:0. The mean and standard deviations of the four sets of isolated osteoblast samples (control/uncut, 3 hpa, 6 hpa and 9 hpa) were then compared with each other (3 hpa versus uncut; 6hpa versus uncut and 9hpa versus uncut) using a Welch's t-test (or unequal variances t-test) and generating 3 data sets with the differential expressed genes between both conditions. Furthermore, all log2 values that lie between -1 and 1 were ignored. Additionally, to conclude statistical significance of differential expression for each gene between the conditions analysed, only p-values less than 0,05 were considered/accepted.

14.1.4 Data Visualization

To aid in the visualization of the data sets we used volcano plots.
The volcano plot arranges genes along dimensions: fold change and statistical significance. The horizontal axis represents the log2 fold change for each gene between two groups of samples, namely between 3 hpa versus uncut, 6hpa versus uncut and 9hpa versus isolated osteoblasts, and the vertical axis represents the p-value (on a negative log 10 scale: the smaller the p-values the larger the -log10 p-value).

14.1.5 Gene enrichment analysis

A gene enrichment analysis was performed based on the significant differentially expressed genes. These genes were assigned to corresponding biological process categories according to the Gene Ontology (GO) framework (http://www.geneontology.org/). Afterwards, data were summarised using the PANTHER classification system (http://www.pantherdb.org/) that showed which biological pathways were more representative in our gene expression data sets using *Danio rerio* as the reference genome.

14.1.6 Pathway map analysis

The parameters used for the pathway analysis were set according to the method referred to as Generally Applicable Gene-set Enrichment (GAGE), a new Gene set analysis (GSA) method (Luo et al. 2009). GAGE is used to infer functional and mechanistic changes using all available gene expression data (cutoff-free) since small but coordinated gene expression in a pathway can have great biological relevance even when the changes are not statistically different. For this, gene IDs were translated from Ensembl to Entrez based on Assembly GRCz11 (Genome Reference Consortium Zebrafish Build 11). After the GSA analysis, these Entrez IDs were used and analysed through KEGG pathway database resource for pathways related to canonical signalling and metabolic pathways (https://www.genome.jp/kegg/pathway.html), that illustrates, the more representative pathways in our microarray analysis. Only pathways with p-values less than 0,05 and FDR (q-value) less than 0.1 were considered significantly different.

14.2 q-PCR analysis

All samples were analysed in 4-6 biological pools. For each biological pool, q-PCR was performed for each target gene in 3 technical replicates. Gene expression values were normalized using the *elongation factor 1α* (*ef1α*, NM_131263) housekeeping gene and relative expression was calculated using the 2(-ΔΔC(T)) method (Livak and Schmittgen 2001). To determine differentially expressed genes, results were plotted using GraphPad Prism software and two-tailed Student's t-test with Welch's correction was used. Only p-values<0.05 were considered statistically significant.

14.3 Imaging analysis and quantification

14.3.1 Adult caudal fin regenerate measurements

To measure the area of regenerated tissue in the caudal fin, images of live, anaesthetized fish were used. The regenerated fin was delineated from the amputation plane to the distal end of the regenerate, using the Area tool on Fiji software (Schindelin et al. 2012), thus resulting in one measurement value per animal.

The percentage of bony-ray formation in calcein stained animals and the percentage of specific osteoblast populations in anesthetised live animals positive for *osx:*mCherryNTRo and *runx2:*EGFP, were determined using Fiji (Schindelin et al. 2012). The percentage of bone formation and of the specific osteoblast populations is defined by the area occupied by calcein or osteoblast labelling in relation to the total fin regenerated area. Briefly, the area of fluorescence intensity for each image was determined by empirically establishing a threshold to separate the signal fluorescence intensity from the background. The average fluorescence area was then normalized to the total tissue regenerate area, performed as described above. Each measurement gave rise to one value per animal. The individual data were processed using Microsoft *Excel™*.

Determination of bony-ray width (width at the basis of each regenerated bony-ray) calcein staining experiments were performed using Fiji (Schindelin et al. 2012). Fluorescence signal was thresholded using the Otsu algorithm. Subsequently, the width at the basis of each newly formed bony-ray region was measured using the line tool on Fiji (Schindelin et al. 2012). These widths were averaged which resulted in one value per animal.

For all the analysis performed above, the detailed number of animals used is discriminated in the corresponding figures in the results section, while the means and standard deviations (SD) are displayed in the graphs.

14.3.2 Quantification of osteoblast migration

Live-imaging time-lapses were used to measure osteoblast motile behaviour in *osc:*EGFP transgenic animals counterstained with ARS. The osteoblast mature population from the first and second segments below the amputation plane were imaged overtime during the first 25 hpa. The area of fluorescence intensity was determined by establishing a threshold background and the GFP centre of intensity was determined for each sequential time-lapse, by using the tool centre of mass on Fiji ImageJ (Schindelin et al. 2012) for both first and second segments below the amputation plane. To determine cell displacement in a specific time-interval for each two sequential time lapses, the GFP centre of intensity of the earlier time-lapse was subtracted from the following time-lapse and so on until the last time-lapse, as illustrated in the examples below:

GFP centre of intensity 5 hpa - GFP centre of intensity 0 hpa = Relative cell displacement from 0-5 hpa time-interval
GFP centre of intensity 10 hpa - GFP centre of intensity 5 hpa = Relative cell displacement from 5-10 hpa time-interval

For all the analysis performed above, 3 different bony-rays per animal, from a total of 3 animals were analysed. Data were expressed as the relative cell displacement between specific time-intervals and means ± SD were plotted in graphs.

14.3.3 Quantifications performed on cryosections

Cell populations in longitudinal cryosections of individual regenerating bony-rays were quantified by analysing the first segment proximal to the amputation plane and the regenerated area. For that, cells were counted, including EdU positive cells, PCNA positive cells, osteoblast subtypes and osteoprogenitors, using the Cell-counter plugin on Fiji and normalizing to total fin area.

To measure the relative contributions of each osteoblast subtype ($Runx2^{+}Osx^{-}$ and $Runx2^{+}Osx^{+}$) in the regenerated tissue, a cell ratio profile was established by dividing the average number of one osteoblast subtype by the other in control and in experimental conditions, ratios = 1 mean that both populations are equally represented in the regenerated tissue. To measure the relative occupancy of each tissue type (epidermis, mesenchyme and osteoblasts) in the regenerated tissue, a tissue ratio profile was established by dividing the average area of each tissue by the others in control and in experimental conditions. These ratios were averaged to give one value per animal.

For each quantification 3-6 animals per condition were used and cryosections corresponding at least to 3 bony-rays per animal were analysed. The exact number of animals used is discriminated in the corresponding figure in the results section. Data are expressed as the number of cells per 100 μm^2 and means ± SD are displayed in the graphs.

14.3.4 Statistical Analysis

For all adult caudal fin regenerate measurements, quantifications of osteoblast migration and quantifications performed on cryosections, statistical significance between controls and manipulated animals or between different time-points post-amputation or time-intervals was determined by non-paired, non-parametric comparison, using the Mann-Whitney U test in the Prism Graphpad software, version 6. Only p-values less than 0,05 were considered statistically significant.

Chapter III

OSTEOBLAST REPROGRAMMING AND DEDIFFERENTIATION DURING CAUDAL FIN REGENERATION

“It's a poor sort of memory that only works backwards,' says the White Queen to Alice.”

Lewis Carroll, Alice's Adventures in Wonderland & Through the Looking-Glass

1 CHARACTERIZATION OF OSTEOBLAST DEDIFFERENTIATION TIME-WINDOW DURING CAUDAL FIN REGENERATION

Two of the key steps during the caudal fin regenerative process are the dedifferentiation and recruitment of the cells that contribute to the formation of the blastema (Galliot and Ghila 2010; Jopling et al. 2011; Tanaka and Reddien 2011). We and others have previously demonstrated that after zebrafish caudal fin amputation, skeletal tissue regeneration occurs through mature osteoblast dedifferentiation (Knopf et al. 2011; Sousa et al. 2011; Tu and Johnson 2011; Stewart and Stankunas 2012). Mature osteoblasts lose their differentiated character, by loss of expression of mature markers, undergo an EMT-like event and migrate distally to incorporate the blastema where they subsequently increase their proliferation rate (Knopf et al. 2011; Sousa et al. 2011; Stewart et al. 2014). However, the exact time-window of osteoblast dedifferentiation, as well as the factors that trigger and regulate the process during regeneration remain poorly enlightened. Cellular dedifferentiation is characterized by several events (Figure 18A): cell shape-changes, re-acquisition of proliferative capacity/ cell cycle re-entry, downregulation of mature markers, and upregulation of progenitor-like markers (Jopling et al. 2011; Tanaka and Reddien 2011; King and Newmark 2012). Therefore, the first part of this project consisted in characterizing the initial hours of the dedifferentiation process to clarify the specific time-window of osteoblast dedifferentiation.

In order to visualize the mature osteoblast population undergoing the first stages of dedifferentiation, we used the promoter reporter line for *osteocalcin2* (*osc/bglal*), *Tg1(Ola.Bglap:*EGFP*)*^{hu4008} (referred as *osc*:EGFP), a mature osteoblast marker (Li et al. 2009; Knopf et al. 2011; Rutkovskiy et al. 2016). This line has a stable GFP signal and, although it is not ideal to observe immediate changes in gene expression, it allows us to follow osteoblasts during dedifferentiation even upon *osteocalcin* downregulation. Taking advantage of this line, a thorough characterization of the osteoblast migratory behaviour, acquisition of proliferative capacity and expression of specific markers, was performed (Figure 18).

To detect when mature osteoblasts start to alter the transcription levels of mature and early osteoblast markers we monitored the expression of *osc* and *runx2a*, respectively (Li et al. 2009; Rutkovskiy et al. 2016). By q-PCR analysis, we observed that mature osteoblasts start to downregulate *osc*, as early as 3 hours post-amputation (hpa), although no changes in the expression of the earliest osteoblast progenitor marker *runx2a* were observed (Figure 18F). Suggesting that mature osteoblasts start to undergo transcriptional changes very early during regeneration. Although at this stage we did not notice upregulation of *runx2*, indicative of a progenitor state (Figure 18F), we were able to observe expression of Tenascin C (TenC), an extracellular matrix (ECM) glycoprotein normally secreted by osteoblast precursors (Mackie and Tucker 1992; Alford and Hankenson 2006) and is considered to be a trait of pro-regenerative ECM (Godwin et al. 2014). TenC was already shown to be upregulated in the mesenchymal compartment at later time-points during regeneration (Jaźwińska et al. 2007;

Knopf et al. 2011). We observed through immunofluorescence that TenC starts to be produced by mature osteoblasts close to the amputation plane at 6 hpa in contrast to the uncut situation (Figure 18E). At this time-point, only mature osteoblasts seem to be the source of TenC in the regenerating fin (Figure 18E).

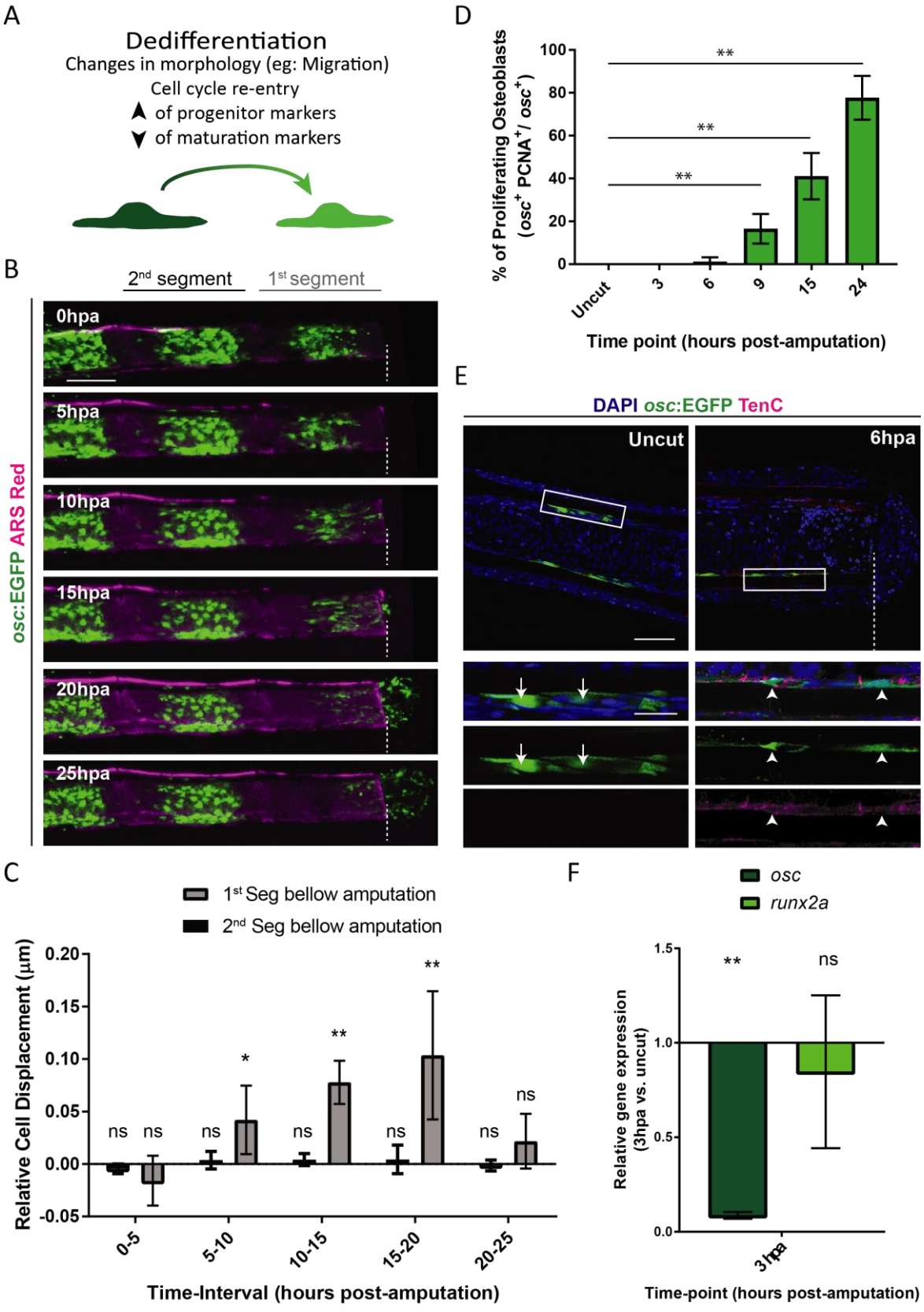

Figure 18: Osteoblast dedifferentiation time-window during caudal fin regeneration. (A) Biological features of the dedifferentiation process. (B) Live imaging analysis of the osteoblast migratory behaviour in the 1st and 2nd segments below the amputation region, during 1 day after amputation using a promoter reporter line that labels mature osteoblasts (*osc*:EGFP). The bone is labelled with Alizarin red (magenta). Osteoblasts in the 1st segment are recruited towards the stump in contrast to osteoblasts in the 2nd segment. (C) Quantification of the relative osteoblast displacement over time in the 1st and 2nd segments below the amputation plane of the same animal; statistical analysis displayed on graph corresponds to Mann-Whitney test with Mean ± SD (n=9 bony-rays compiled from 3 different fish). (D) Quantification of osteoblast cell cycle re-entry through immunofluorescence against PCNA (proliferation marker) in *osc*:EGFP animals reveal that these cells start acquiring proliferative capacity at 9 hpa; statistical analysis displayed on graph corresponds to Mann-Whitney test with Mean ± SD (n= 3 fish, 12 sections analysed). (E) Representative images of TenC (magenta) immunofluorescence in longitudinal fin cryosections of *osc*:EGFP (mature osteoblasts, green) animals; arrows indicate osteoblasts in uncut caudal fins, which do not produce TenC, and arrowheads indicate osteoblasts at 6 hpa expressing Tenascin C. (F) Quantitative RT-PCR showing the expression of *osc* and *runx2a* at 3 hpa relative to uncut condition; statistical analysis displayed on the graph corresponds to Unpaired t test with Welch's correction (3 biological replicates corresponding to pools of 4-5 fins were used for each condition). Dashed lines represent the amputation plane and white boxes the magnified panels. Scale bars represent 100 µm in B, 50 µm in E and 20 µm in magnified panels in E. hpa (hours post-amputation); ns: non-significant; * p< 0.05; **p< 0.01.

Afterwards, we analysed when these cells become motile. It is known that only the osteoblasts that reside in the first segment below the amputation plane migrate and contribute to the blastema, which can be seen at 24 hpa (Knopf et al. 2011; Pfefferli and Jaźwińska 2015). We used the *osc*:EGFP transgenic line and imaged the same bony-rays every 5 hours during the first 25 hpa to follow osteoblasts and measure their relative displacement during regeneration. This analysis revealed that osteoblasts become motile at the 5-10 hpa time-interval and reach the amputation plane around 24 hpa, in contrast to the osteoblasts that reside in the second segment below the amputation plane, which stay immotile, therefore serving as a negative control for migration (Figure 18B and C).

To address when these cells acquire proliferative capacity, we performed PCNA (marker for late G1 cell cycle phase) immunostainings and observed that osteoblasts enter progressively in the cell cycle. Around 20% of osteoblasts are PCNA-positive at around 9 hpa and at 24 hpa almost all osteoblasts in the first segment below amputation have entered the G1 phase (Figure 18D).

Taken together, these data reveal that opposed to what has been previously described (Knopf et al. 2011; Sousa et al. 2011), mature osteoblasts that respond to the injury and contribute to blastema formation show dedifferentiation signs very early during regeneration, in a time-window between 3-6 hpa, still during the wound healing phase. Knowing the precise time-window of dedifferentiation gives us the opportunity to study the transcriptomic changes that occur specifically during dedifferentiation.

2 MATURE OSTEOBLAST ISOLATION, MICROARRAY SET UP AND DATA OVERVIEW

Osteoblast dedifferentiation during regeneration remains a poorly characterized process. Thus, after identifying the time-window at which osteoblast dedifferentiation is triggered, we carried out an unbiased approach to screen and identify new factors involved in this process. For that, we have isolated osteoblasts and analysed the transcriptomic changes that occur during dedifferentiation.

2.1 Mature osteoblast isolation from homeostasis and regenerating fins and microarray experimental design

To obtain the gene expression profile of osteoblast undergoing dedifferentiation, our strategy consisted in a genome-wide transcriptomic analysis, using microarray technology, of isolated *osc*:EGFP-positive osteoblasts from uncut fins and at 3, 6 and 9 hpa, the time-points at which the first osteoblast dedifferentiation features were detected. We choose to analyse these time-points because they reflect a progression in the osteoblast dedifferentiation program that is related to the successive acquisition of dedifferentiation traits. We used osteoblasts from uncut/non-regenerating conditions as our control population as they are the closest to what we may consider to a homeostatic state (Figure 19). The 3 hpa time-point was defined as the early beginning of the dedifferentiation process because it is the earliest time-point that we were able to detect differences at the transcriptional level between osteoblast in homeostasis and during regeneration (Figure 18F) but the other dedifferentiation features are not visible yet (Figure 19B, a). The 6 hpa time-point reflects differences at the level of osteoblast morphology and behaviour (Figure 18B, C and E), so we considered this time-point represents the full launch of the dedifferentiation programme (Figure 19B, b). At 9 hpa additional phenotypic changes in osteoblast are observed, including cell cycle re-entry (Figure 18D)(Figure 19B, c). We opted to analyse all three time-points during dedifferentiation to make sure that no important regulators were left aside. The purpose was to compare the expression profiles of osteoblasts in homeostasis with the other time-points during regeneration (Figure 20A), thus delivering 3 different comparison data sets: 3 hpa versus uncut (Figure 19B, a), 6 hpa versus uncut (Figure 19B, b) and 9 hpa versus uncut (Figure 19B, c). We established a protocol to specifically and accurately isolate these osteoblast populations by Fluorescence-activated cell sorting (FACS) (Figure 20A), which enabled the collection of osteoblast from *osc*:EGFP animals due to the stable and specific EGFP expression. In a first analysis, we determined that the isolated osteoblasts represent 1-3% of the total caudal fin sample (Figure 20A, examples of uncut and 6hpa conditions are shown). Optimization of the tissue digestion and cell dissociation protocol gave us a good purity percentage of *osc*:EGFP positive cells (around 90%) and a low number of dead cells (around 10%) (Figure 20B). After osteoblast isolation, the analysis of their gene expression profile was performed at OakLabs GmbH (Henningsdorf, Germany) using the Agilent zebrafish 8x60K ArrayXS.

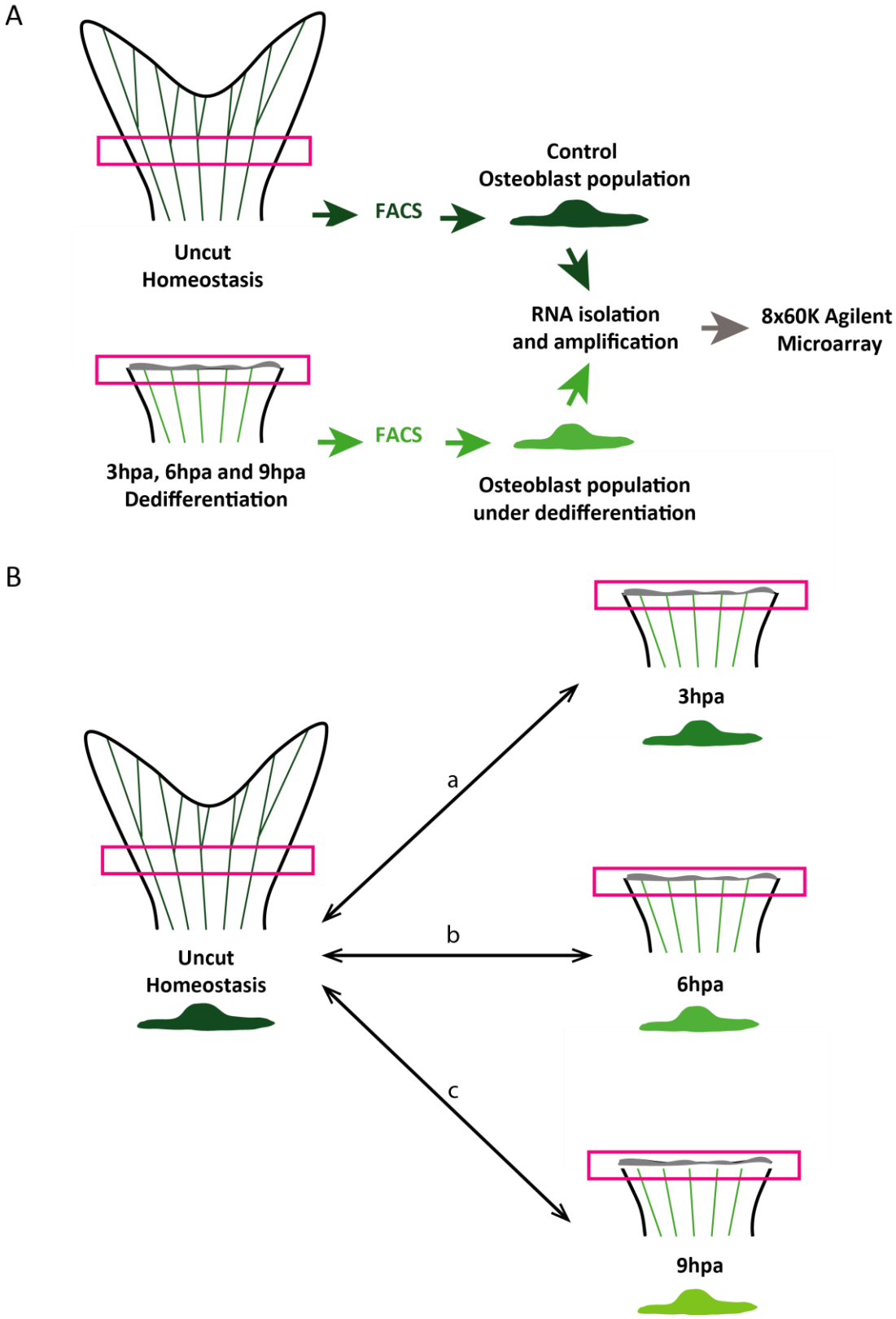

Figure 19: Microarray experimental design and data analysis rationale. (A) Schematic representation of the experimental design used to obtain the transcriptional profile of dedifferentiating osteoblasts using *osc*:EGFP transgenic animals. Osteoblasts from caudal fin tissue corresponding approximately to one bony-ray segment in length (pink boxes), from uncut, 3, 6 and 9 hpa were collected, dissociated into a single cell suspension and isolated by FACS and sent to OakLabs for RNA extraction and microarray chip assay. (B) In order to identify potential triggers and regulators of osteoblast dedifferentiation during regeneration, the transcriptome profile

of osteoblast at the beginning of dedifferentiation (3 hpa) and during dedifferentiation (6 hpa, and 9 hpa) were independently compared to the uncut/homeostasis controls transcriptome. After comparing the different data sets, three different groups of differentially expressed genes were obtained: 3 hpa versus Uncut (a); 6 hpa versus Uncut (b); and 9 hpa versus Uncut (c). Pink boxes correspond to the regions used to isolate osteoblasts for each condition. hpa: hours post-amputation.

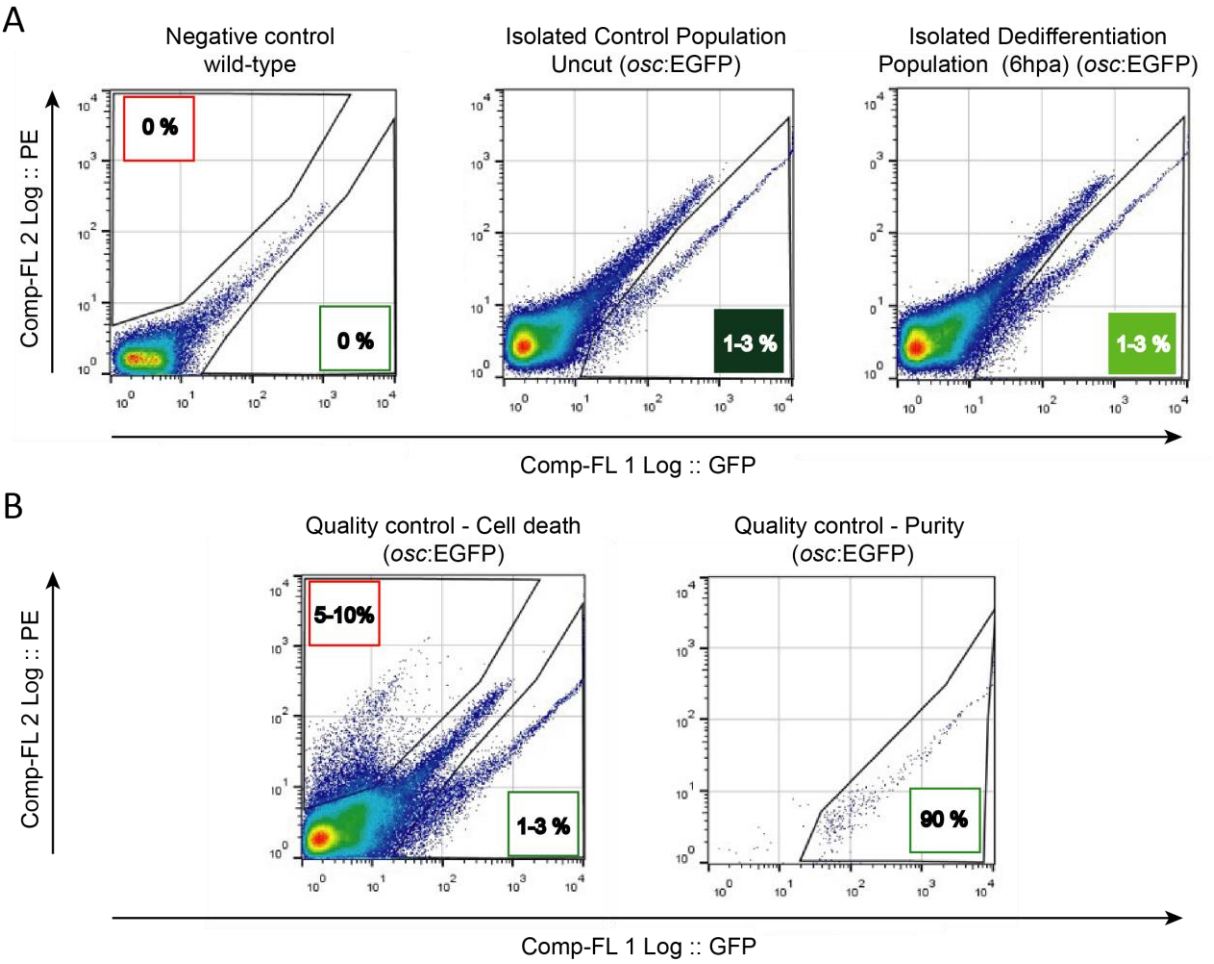

Figure 20: Isolation of mature osteoblasts by Fluorescence Activated Cell Sorting (FACS). (A) Representative flow cytometry plots of caudal fin cells from wild-type (negative control) and *osc*:EGFP transgenic animals from uncut and an example of the 6 hpa time-point is displayed. In *osc*:EGFP transgenic animals it is possible to observe the presence of GFP^+ osteoblasts. (B) Sample quality assessment through the evaluation of cell death, by propidium iodide (PI) staining, and purity (representative examples are displayed). In flow cytometry plots, GFP fluorescence intensity is given by the x axis (Comp-FL 1 Log ::GFP) and PE fluorescence intensity (used to identify PI-positive cells), is given by the y axis (Comp-FL2 Log::PE). Numbers in the lower right boxes indicate relative percentages of GFP^+ cells and numbers in the upper left boxes indicate the relative percentage of PI^+ cells. hpa: hours post-amputation.

2.2 Genome-wide expression profile of osteoblasts in homeostasis and in regenerating caudal fins

The transcription profiles obtained went through a quality control analysis performed by OakLabs and by a collaborator, Patrícia Brito (CEDOC). The intent of this evaluation was to identify possible outlier samples that should be removed from the data set. In order to identify possible outliers among the biological replicates, a hierarchical clustering analysis (HCA) and a principal component analysis (PCA) were performed. In the latter, samples were grouped in a 2-dimensional space by a two-component model (principal component 1 (PC1) and principal component 2 (PC2)) to explain the intrinsic variability of the data. Through these two analyses, biological replicates from the same condition should cluster together (Figure 21A). Both HCA and PCA found a biological replicate from the control samples (Uncut B1) that did not cluster with any of the other ones (Figure 21A, red cluster and red arrow), including with the other control biological replicates. Thus, it was considered as an outlier sample and removed from the transcriptome profile comparisons. The other biological replicates, with exception of the control, which formed its own cluster (samples 2 and 3), the replicates from different time-points often clustered together (see example of sample 6 (3 hpa B3) and sample 10 (9 hpa B1)) (Figure 21A). This means that the transcriptomic profile of the osteoblast samples collected from the different regenerating conditions was very similar. After removing the outlier sample, the PCA was repeated (Figure 21B, C and D) for each time-point during regeneration together with control samples. We observed that there was a big overlap between the 3 hpa and the uncut samples, which were not possible to segregate using both the first and second principal components (PC1 and PC2, respectively) (Figure 21B). Nevertheless, the PC1 was able to explain 30% of the data variability and discriminate the uncut from the 6 hpa samples, and both PC1 and PC2 were able to fully separate the uncut samples from the 9 hpa (Figure 21C) explaining approximately 55% of the data variability (Figure 21D). This indicates that from the three regenerating conditions analysed, the 3 hpa time-point isolated osteoblasts have a more similar gene expression profile to the osteoblasts from the uncut condition.

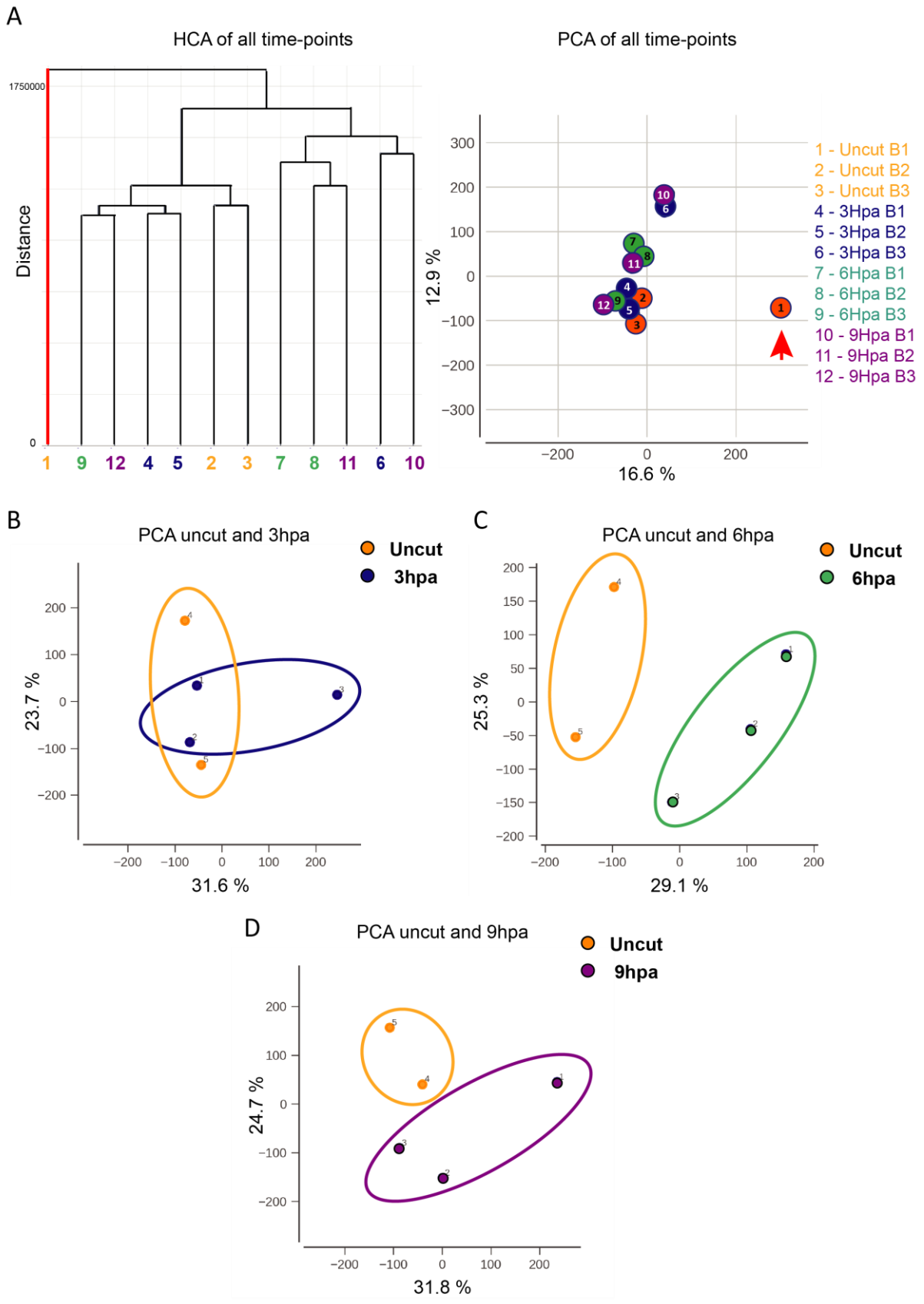

Figure 21: Microarray sample analysis using hierarchical clustering and principal component analysis of transcript profiles. (A) Hierarchical clustering analysis (HCA) and Principal component analysis (PCA) of the data,

including all time-points and all corresponding three biological replicates (B1, B2 and B3) were performed. Colour-coded spheres define the different samples and corresponding biological replicates from uncut (orange) and the different time-points analysed during regeneration: 3 hpa (blue), 6 hpa (green) and 9 hpa (purple). Samples that have the most similar expression profiles are clustered together or appear in close proximity. Sample number 1 (Red cluster and red arrow, Uncut B1) has the least similar expression profile when compared to the other samples and was considered to be an outlier and removed from the transcriptome profile comparisons. (B) PCA after removing the outlier sample from the uncut/control group. A two-component model was then used to explain the variability and correlation between the uncut samples (orange dots, orange ellipse) and each one of the time-points analysed after amputation: 3 hpa (blue dots, blue ellipse), 6 hpa (green dots, green ellipse) and 9 hpa (purple dots, purple ellipse). By removing the outlier sample, we were able to better segregate the homeostasis condition (uncut) from the time-points collected during dedifferentiation. hpa: hours post-amputation

After comparing the transcriptome profile of osteoblasts in homeostasis with the osteoblast populations retrieved during regeneration three sets of differentially expressed genes were obtained: 3 hpa versus uncut (Figure 22A), 6 hpa versus uncut (Figure 22B) and 9 hpa versus uncut (Figure 22C). In particular, we found that between 3 hpa and uncut, between 6 hpa and uncut, and between 9 hpa and uncut there were around 1622 (846 downregulated and 776 upregulated), 2170 (1040 downregulated and 1130 upregulated) and 1693 (868 downregulated and 825 upregulated) genes differentially expressed, respectively (Figure 22A-C). We then analysed the general behaviour of the data using a Chord Diagram, which allows to display the inter-relationships between the different data sets. This analysis revealed that the three transcriptome comparisons showed that there were genes specifically regulated at each time-point (Figure 22D, white square), genes common between time-points (Figure 22D, green squares) and common to all 3 time-points analysed (Figure 22D, blue square). This transcriptomic analysis showed significant changes in gene expression, suggesting that mature osteoblasts start changing their transcriptome very early during regeneration (Figure 22).

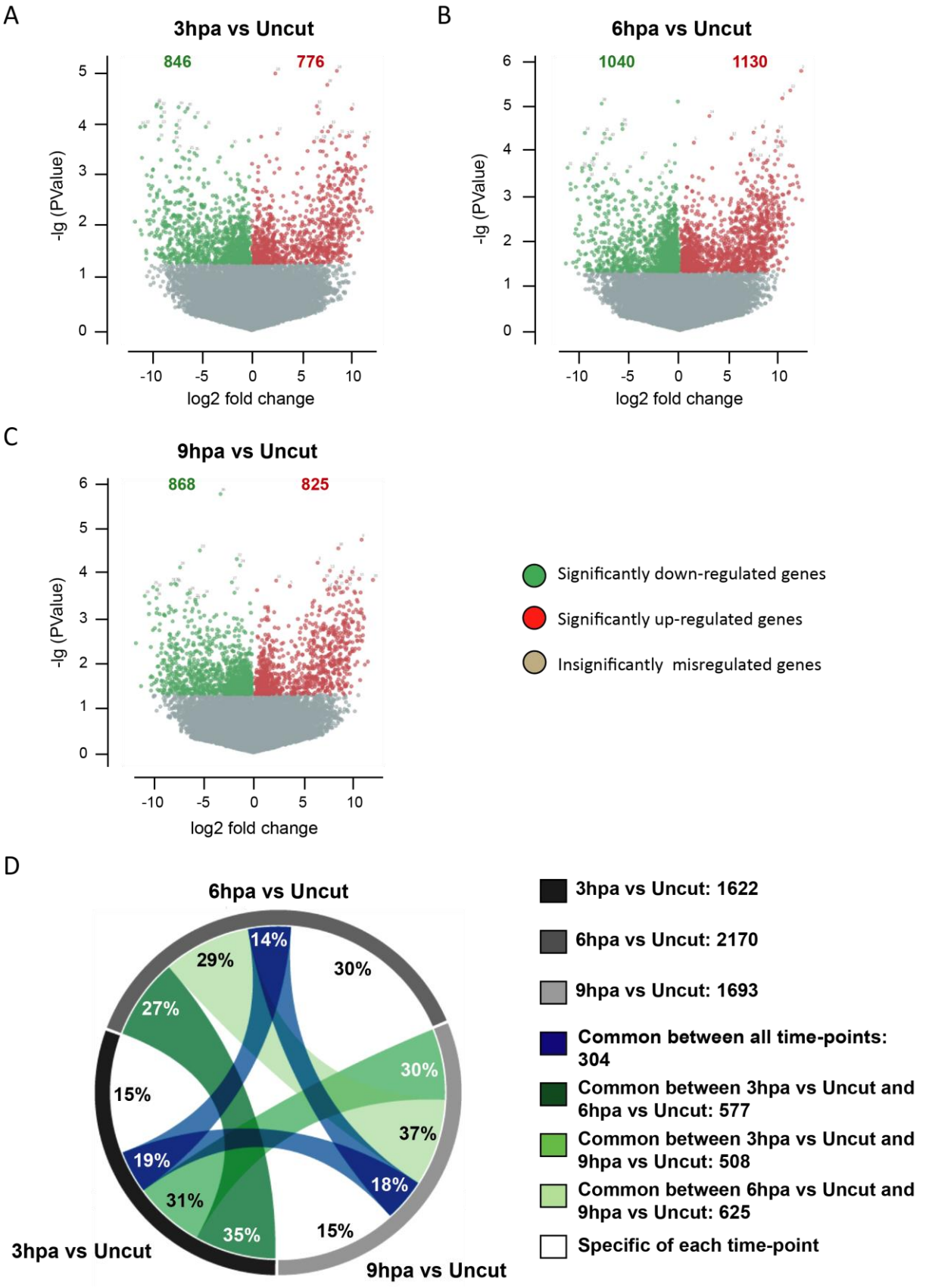

Figure 22: General overview of the differentially expressed transcripts between homeostatic and dedifferentiating osteoblasts. (A-C) Number of transcripts altered in the microarray analysis. Volcano plot showing differentially expressed genes at 3 hpa (A), 6hpa (B) and 9 hpa (C). In volcano plots, the horizontal axis represents the log2 fold-change between each two groups of samples represented and the vertical axis

represents the p-value (on a negative log10 scale: the smaller the p-values the larger the -log10 p-value). Upregulated genes are shown in red and downregulated genes are shown in green. Significant changes were considered for a log2 FC>1 or <-1 for a p-value> 0.05. (D) Overall data visualization in a Chord Diagram. This graphical method allows to display the inter-relationships between data. The data is arranged radially around a circle with the relationships between the 3 time-points analysed drawn as arcs connecting the data (the % occupied by each arc is displayed). Dark grey group represents the data from the differentially expressed genes between the 3 hpa versus uncut; middle grey group represents the data from the from differentially expressed genes between 6 hpa versus uncut; light grey group represents the data from the from differentially expressed genes between 9 hpa versus uncut; Blue data represents the common set of genes between all the groups; dark green represents the common set of genes between 3 hpa versus uncut and 6 hpa versus uncut; middle green represents the common set of genes between 3 hpa versus uncut and 9 hpa versus uncut; light green represents the common set of genes between 6hpa versus uncut and 9hpa versus uncut; and white represents the specific differentially expressed genes for each group. hpa: hours post-amputation.

3 MICROARRAY DATA ANALYSIS: NEW REGULATORS OF OSTEOBLAST DEDIFFERENTIATION DURING ZEBRAFISH CAUDAL FIN REGENERATION

To facilitate the interpretation of our gene expression data, we started by performing a gene enrichment analysis. This analysis is useful to evaluate whether our differentially expressed genes are associated with specific biological processes and to gene expression signatures, particularly relevant for osteoblast dedifferentiation. For that, genes were assigned to different biological categories according to the Gene Ontology (GO) framework and analysed using the PANTHER classification system. Here we show the most enriched biological processes at 3hpa versus uncut condition (Figure 23). Serving as an example, the Cellular component organization or biogenesis (GO:0071840) category represents around 10% of the zebrafish genome and is enriched to 15% in our 3 hpa data set and so on for the other categories (Figure 23). For the other time-points, the enriched gene categories were very similar to the 3 hpa time-point.

We also performed a cutoff-free pathway analysis, since small but coordinated gene expression in a pathway can have great biological relevance even when the changes are not statistically different. For this, we used a new Gene Set Analysis (GSA) together with the KEGG pathway database. We focused this analysis on pathways related to canonical signalling and metabolic pathways which seem to be relevant given the previous gene enrichment results. This analysis showed specific signalling and metabolic pathways that were significantly represented in our transcriptome data sets, for data visualization see Supplementary Table 1.

Considering the more representative GO categories in the gene enrichment analysis, we decided to focus in categories known to be important to regulate cell fate decisions in other contexts and associated with some of the dedifferentiation traits analysed previously during regeneration (Figure 18). These categories were: metabolic regulation (GO:0008152 and GO:0044238); cell cycle control (GO:0007049); cytoskeletal dynamics, migration regulation and ECM remodelling and cellular junction assembly (which are all part of the GO:0016043 and GO:0071840 category); signal transduction pathways (within GO:0009987 category); and chromatin organization and remodelling (GO:0006325).

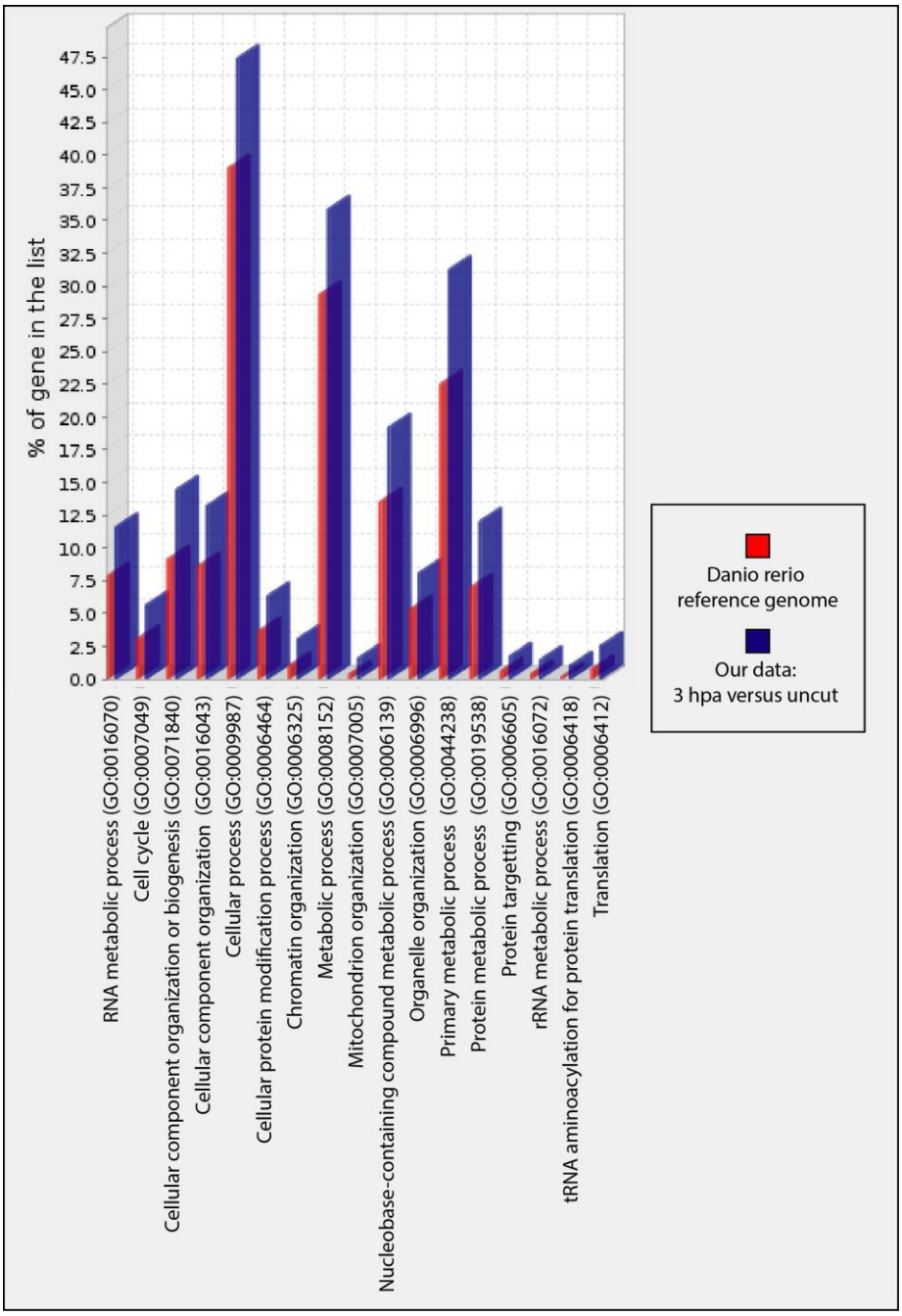

Figure 23: Gene enrichment analysis of 3 hpa versus uncut conditions. Graph shows the most enriched biological process categories found in at 3 hpa (of the differentially expressed genes). Red columns represent the % of each category in the zebrafish genome and blue columns the % of each category in our data set.

Overall, the gene enrichment analysis revealed new genes and general processes that could be important to trigger and regulate osteoblast dedifferentiation. In the sections below, we will take a closer look at the most relevant gene categories and their potential implication in regeneration, in particular in osteoblast dedifferentiation.

3.1 Genes related to metabolic adaptation and cell cycle regulation

The microarray analysis revealed that one feature of osteoblast dedifferentiation seems to be related to its metabolic requirements (Table X and Table XI). In particular, several important glycolytic enzymes, such as *pfkpa*, *aldoaa*, *pgam1a*, *hk1* and *pdhb* were highly and consistently upregulated in osteoblasts as early as 3 and 6 hpa, when compared to uncut controls, and some were also upregulated until 9 hpa (Table X). This suggests that osteoblasts during dedifferentiation may change their metabolic profile to better adapt to new energetic demands of the regenerative process (see Supplementary Figure 1 for an overview of the differentially expressed genes within the glycolytic pathway). It is known that, in homeostatic conditions, differentiated, non-dividing somatic cells use oxidative phosphorylation (OxPhos) as their primary source of energy. In contrast, highly proliferative progenitor cells, which exhibit different metabolic requirements, rely mainly on glycolysis to increase cell biomass and divide (Heiden et al. 2009; Lunt and Vander Heiden 2011; Moussaieff et al. 2015; Prigione et al. 2015; Mathieu and Ruohola-Baker 2017). Therefore, we speculate that osteoblasts in a regeneration context may suffer a metabolic adaptation, also designated as metabolic reprogramming, in the form of a glycolytic switch triggered very early during this process. Many stem/progenitor cell populations use primarily glycolysis, resulting in lactate production instead of pyruvate oxidation in mitochondria (Lunt and Vander Heiden 2011). In agreement with this notion, we identified an increase in the expression of the enzyme *lactate dehydrogenease A4, ldha*, responsible for the interconversion of pyruvate and lactate (Table X).

Table X: Genes involved in cell metabolism, namely in the glycolytic pathway, differentially expressed at 3, 6 and 9 hpa in comparison to uncut controls. Upregulated genes are shown in red and downregulated genes in green.

TargetName	Log2FC 3hpa	PValue	Log2FC 6hpa	PValue	Log2FC 9hpa	PValue	GeneSymbol	Description	Pathway
ENSDART00000033394	11.180	0.0012	11.676	0.0046	8.2212	0.0673	***pfkpa***	*phosphofructokinase, platelet a*	Glycolysis
ENSDART00000156258			3.5999	0.0213			***pfkpb***	*phosphofructokinase, platelet b*	
ENSDART00000146867	9.4329	0.0072	9.1218	0.0118	8.9584	0.0105	***aldoaa***	*aldolase a, fructose-bisphosphate, a*	
ENSDART00000075744	-3.0575	0.0492	-4.1173	0.0268			***aldob***	*aldolase b, fructose-bisphosphate*	
NSDART00000008287	8.615	0.0005	9.4851	0.0002	8.7456	0.0002	***pgam1a***	*phosphoglycerate mutase 1a*	
ENSDART00000057638	9.5359	0.0027	7.9664	0.0153			***hk1***	*hexokinase 1*	
ENSDART00000056523			8.9514	0.0088	2.3894	0.0340	***hkdc1***	*hexokinase domain containing 1*	
ENSDART00000038465	7.8971	0.0015	7.4729	0.0160			***pgam1b***	*phosphoglycerate mutase 1b*	
ENSDART00000006513			6.6016	0.0192	3.3803	0.0188	***pdhb***	*pyruvate dehydrogenase (lipoamide) beta*	
ENSDART00000016502	7.3794	0.0087	7.1912	0.0186			***dlat***	*dihydrolipoamide S-acetyltransferase*	
ENSDART00000133322			5.7441	0.0135			***eno1a***	*enolase 1a, (alpha)*	
ENSDART00000059886	4.1016	0.0139	3.9901	0.0329	4.4268	0.0362	***ldha***	*lactate dehydrogenase A4*	
ENSDART00000076974	9.5914	0.0093	10.319	0.0045	9.7589	0.0028	***gfpt2***	*glutamine-fructose-6-phosphate transaminase 2*	**Glutamate Biogenesis**
ENSDART00000018228	8.5210	0.0087	9.1934	0.0688	3.6074	0.3326	***gsk3b***	*glycogen synthase kinase 3 beta*	**Glicogen synthesis**
ENSDART00000145262	-9.6881	0.0328			-9.3029	0.0112	***acadm***	*acyl-Coenzyme A dehydrogenase*	**Fatty acid β-oxidation**

We also detected the upregulation of genes that control mitochondria dynamics and function, particularly mitochondrial fission, such as *mtfr1* and *fis1* at 3 and 6 hpa, respectively (Table XI). This may represent another form of metabolic adaptation since mitochondria fusion and fission cycles are known to have a great impact in cellular metabolism and cell identity (van der Bliek et al. 2013; Xu et al. 2013; Khacho et al. 2016). Since OxPhos occurs inside mitochondria, its efficiency is maximized by fusion and diminished by fission events (van der Bliek et al. 2013). Curiously, this peak in the expression of mitochondrial fission-related genes seems to happen during 3-6 hpa, whereas at 9 hpa they are downregulated (Table XI).

Table XI: Genes involved in mitochondrial function, namely in mitochondrial dynamics and in the oxidative phosphorylation pathway, differentially expressed at 3, 6 and 9 hpa in comparison to uncut controls. Upregulated genes are shown in red and downregulated genes in green.

TargetName	Log2FC 3hpa	PValue	Log2FC 6hpa	PValue	Log2FC 9hpa	PValue	GeneSymbol	Description	Pathway
ENSDART00000130077	8.2106	0.0401			-9.3029	0.0112	***mtfr1***	*mitochondrial fission regulator 1*	**Mitochondrial dyamics**
ENSDART00000135509			10.794	0.0442			***fis1***	*fission 1 (mitochondrial outer membrane) homolog*	
ENSDART00000047471			8.1584	0.0329	10.681	0.0021	***cluha***	*clustered mitochondria (cluA/CLU1)*	
ENSDART00000108699			7.8518	0.0374	7.0614	0.0258	***coa3***	*cytochrome C oxidase assembly factor 3*	**Mitochondria Electron Transport Chain**
ENSDART00000146609			8.8856	0.0153			***coa5***	*cytochrome C oxidase assembly factor 5*	
ENSDART00000147926	-7.1652	0.0419					***cox5b***	*cytochrome c oxidase subunit Vb*	
ENSDART00000056319					3.2397	0.0403	***cox6a1***	*cytochrome c oxidase subunit Vla polypeptide 1*	
ENSDART00000056319	10.732	0.0178	10.811	0.0335			***cox6c***	*cytochrome c oxidase subunit Vlc*	
ENSDART00000048927					11.692	0.0025	***cox10***	*cytochrome c oxidase assembly homolog 10 (yeast)*	
ENSDART00000036927					7.9253	0.0167	***ndufs1***	*NADH dehydrogenase (ubiquinone) Fe-S protein 1*	
ENSDART00000112112	-7.4993	0.0003					***ndufb3***	*NADH dehydrogenase (ubiquinone) 1 beta subcomplex, 3*	
ENSDART00000104298	-5.4247	0.0352					***ndufb5***	*NADH dehydrogenase (ubiquinone) 1 beta subcomplex 5*	
ENSDART00000056712	9.0361	0.0013					***etfdh***	*electron-transferring-flavoprotein dehydrogenase*	
ENSDART00000039865					6.4854	0.0133	***sdhdb***	*succinate dehydrogenase complex, integral membrane protein b*	

We also observed differences in genes related to the electron transport chain in the three time-points analysed. At 3 hpa, several components of the electron transport chain, such as *cox5b*, *ndufb3* and *ndufb5* were downregulated, suggesting a decrease in OxPhos (Table XI). In contrast, several other genes related to OxPhos, such as cytochrome c subunits or assembly factors, NADH and succinate dehydrogenase components, were highly upregulated in osteoblasts at 6 hpa (three genes) and at 9 hpa (five genes; Table XI) (see Supplementary Figure 2 for overview of the differentially expressed genes within the oxidative phosphorylation pathway).

Overall, these data suggest a clear and tight regulation of osteoblast metabolism, where both glycolysis and OxPhos could be playing important roles at different time-windows during regeneration when compared to homeostatic osteoblasts: glycolysis seems to be activated throughout the time-points analysed whereas Oxphos appears to become more relevant later, between 6-9 hpa.

One of the most important requirements during regeneration is the acquisition of proliferative capacity, which could be correlated with the metabolic changes described above (Lunt and Vander Heiden 2011). In fact, this transcriptomic analysis showed that various cell cycle components are differentially regulated during the analysed time-points (Table XII). Interestingly, we observed what might be considered two different responses triggered by amputation: an anti-proliferative response, in which osteoblasts seem to have activated mechanisms of cell cycle arrest and possibly repair, with high upregulation of *tp53* and *tp53 regulating kinase* in all time-points; and a pro-proliferative response, with upregulation of *cyclinD1*, which drives the G1/S transition and other cyclin-dependent kinases, starting at 6 hpa. This suggests the presence of two different osteoblast populations: one that was possibly deleteriously affected as a consequence of the amputation and another that has initiated a proliferative response. The second population was already identified in our previous analysis, with localization of PCNA between 6 and 9 hpa (Figure 18D), further validating our microarray. In addition, we observed a general decrease in the genes related to mitotic regulation, *anapc4*, *esco1* and *cyclin B3* (Table XII). This suggests that the cell cycle is tightly regulated during regeneration: cells re-enter the cell cycle during dedifferentiation but may only divide later in the regenerative process.

Taken together these data imply that both metabolism and cell cycle processes comprise a very dynamic set of genes that were differentially expressed during this early regenerative time-points, suggesting their potential requirement during osteoblast dedifferentiation during regeneration.

Table XII: Genes involved in cell cycle regulation, differentially expressed at 3, 6 and 9 hpa in comparison to uncut controls. Upregulated genes are shown in red and downregulated genes in green.

TargetName	Log2FC 3hpa	PValue	Log2FC 6hpa	PValue	Log2FC 9hpa	PValue	GeneSymbol	Description	Pathway
ENSDART00000051549	9.8801	0.00569	12.0558	0.00059	11.1213	0.01103	***tp53***	*tumor protein p53*	**Cell Cycle and DNA repair**
ENSDART00000129854			6.7821	0.02105	6.6425	0.02475	***tp53rk***	*TP53 regulating kinase*	
ENSDART00000046678			10.8998	0.00259			***pak2b***	*p21 (CDKN1A)-activated kinase 2b*	
ENSDART00000151687	7.5792	0.03102					***cdkn2aip***	*CDKN2A interacting protein*	
ENSDART00000130326	5.8042	0.00767	5.8383	0.02404			***rbb4***	*retinoblastoma binding protein 4*	**Cell cycle Regulation**
ENSDART00000008144			8.0202	0.00149	9.1503	0.02404	***rbb4l***	*retinoblastoma binding protein 4, like*	
ENSDART00000149828			6.5949	0.00383	5.8750	0.00520	***ccnd1***	*cyclin D1*	
ENSDART00000134116			-2.7299	0.04824			***ccnb3***	*cyclin B3*	
ENSDART00000157148			7.1842	0.02673			***cinp***	*cyclin-dependent kinase 2 interacting protein*	
ENSDART00000049061	-8.2423	0.01950					***cdkn1ba***	*cyclin-dependent kinase inhibitor 1Ba*	
ENSDART00000133836			8.1611	0.04952			***cdk2ap2***	*cyclin-dependent kinase 2 associated protein 2*	
ENSDART00000065859			3.9275	0.04409			***cdk9***	*cyclin-dependent kinase 9 (CDC2-related kinase)*	
ENSDART00000020576	9.4757	0.00072	4.3054	0.02412	5.6076	0.01178	***cdc25***	*cell division cycle 25 homolog*	
ENSDART00000143948	-8.3366	0.00468	-8.7391	0.03547	-9.2935	0.01858	***rfc1***	*replication factor C (activator 1) 1*	
ENSDART00000146203	-6.6570	0.04358			-7.8814	0.01252	***anapc4***	*anaphase promoting complex subunit 4*	
ENSDART00000026592	6.3132	0.02342					***anapc5***	*anaphase promoting complex subunit 5*	
ENSDART00000111891	-6.7975	0.00781			-8.2417	0.04901	***esco1***	*establishment of sister chromatid cohesion N-acetyltransferase 1*	

3.2 Acquisition of migratory behaviour and ECM remodelling

During regeneration, the cells that contribute to form the blastema must reach the amputated region in order to proliferate. To do so, cells have to sense the signals released from the wound edge, become activated and migrate towards the damaged area. During caudal fin regeneration, osteoblasts undergo a process that resembles epithelia-to-mesenchymal transition (EMT) as they populate the blastema (Stewart et al. 2014). In addition, as our previous analysis demonstrated, osteoblasts become motile as early as 5 hpa (Figure 18B and 1C). It is known that EMT and directed cell migration are both complex events that comprehend the sequential regulation of several processes, namely cytoskeletal reorganization, modulation of cell-cell adhesion, ECM remodelling and focal adhesion regulation (Quaranta 2000; Devreotes and Horwitz 2015). Accordingly, we observed a high number of differentially expressed genes related to these categories in all three time-points analysed (Table XIII and Table XIV).

Actin regulation and myosin-mediated contraction are essential for cell migration (Lee and Dominguez 2010; Murrell et al. 2015). We observed an upregulation of the Arp2/3 complex, *arpc4*, and the *Drosophila* slingshot homolog, *ssh2a*, which are essential for actin polymerization and depolymerization, respectively (Table XIII). An upregulation of myosin motors was also observed, such as *myo1ea* (Table XIII). The microtubule network is also known to be an important regulator of cell migration (Kaverina and Straube 2011; Etienne-Manneville 2013). In agreement with this, genes of known modulators of microtubule dynamics were differentially expressed, suggesting they might also be important during the initial regenerative process (Table XIII). Members of the Rho GTPase family, which have been shown to regulate actin and myosin dynamics (Raftopoulou and Hall 2004) were also upregulated in this context (see cytoskeleton regulation, Table XIII).

We also observed the downregulation of typical epithelial genes such as Adherens Junctions (AJs) components (*α-catenin*, *β-catenin, cadherin 1* and *cadherin 2*) at 6 and 9 hpa, and a Tight Junctions (TJ) component (*tjp2a*/*zo2)* at 3 hpa (Table XIV). In homeostasis, osteoblasts display an epithelial-like organization, with their membranes connected to each other by AJs (Stewart et al, 2014), so these junctional components should be downregulated during osteoblast EMT and migration, in agreement to what we observe.

The assembly of focal adhesion complexes that link the actin cytoskeleton to the ECM has been shown to be involved in cell migration (Wozniak et al. 2004; Levy et al. 2010). Some of the most important components of these complexes are integrins (Huttenlocher and Horwitz 2011). The microarray data demonstrated a clear peak of expression of several integrin subunits, specifically at 6 hpa (Table XIV). Adaptor proteins that link the integrins to the actin cytoskeleton, *talin1* and *talin2*, were also upregulated at 6 and 9 hpa (Table XIV).

In parallel, we also noticed that several components of the ECM were differentially regulated, including collagens, laminins and tenascins (Table XIV). Depending on the ECM composition, it may promote a more pro-regenerative microenvironment and potentiate cell migration behaviours (Alford et al. 2015; Govindan and Iovine 2015). The main function of osteoblasts is to produce collagen fibres, which are the most abundant component of the bone matrix, and interestingly several collagens were downregulated during the dedifferentiation time-window. Another important ECM glycoprotein, Tenascin C, which is known to be produced by osteoblast progenitors (Knopf et al, 2011) and to aid cell motility, was upregulated in our gene expression data set at 6 and 9 hpa. In accordance, we have demonstrated, during the characterization of the dedifferentiation time-window, that this protein is produced by mature osteoblast at 6 hpa (Figure 18E). Additionally, during the dedifferentiation time-window, several transcripts related to ECM remodelling (Table XIV) were differentially expressed in some time-points when compared to the uncut condition. One of these transcripts, *adam8b* (*a disintegrin and metalloproteinase domain 8b*), is greatly upregulated in all three time-points (Table XIV). This gene encodes for a protein that is associated with

increased invasive activity (Sriraman et al. 2008). Therefore, this gene may further support the pro-migratory behaviour of osteoblasts at this point.

Overall these results show that cytoskeletal rearrangements, ECM remodelling, focal adhesion assembly and junction disassembly are important to promote osteoblast EMT and migration. Importantly, this transcriptome analysis aid to identify new regulators of osteoblasts EMT and migration that may be required as part of their dedifferentiation program.

Table XIII: Genes involved in cytoskeletal dynamics, differentially expressed at 3, 6 and 9 hpa in comparison to uncut controls. Upregulated genes are shown in red and downregulated genes in green.

TargetName	Log2FC 3hpa	PValue	Log2FC 6hpa	PValue	Log2FC 9hpa	PValue	GeneSymbol	Description	Pathway
ENSDART00000099803	-9.3541	0.02633					***arpc2***	*actin related protein 2/3 complex, subunit 2*	**Actin cytoskeleton Regulation**
ENSDART00000146470	9.1801	0.01744	9.5216	0.00892	9.3492	0.03100	***arpc4***	*actin related protein 2/3 complex, subunit 4*	
ENSDART00000017053			5.1687	0.01701			***cttn***	*cortactin*	
ENSDART00000127845	7.6313	0.02782	9.6589	0.04507	9.4935	0.01808	***ssh2a***	*slingshot homolog 2a (Drosophila)*	
ENSDART00000081196					-9.1218	0.01842	***scinlb***	*scinderin like b*	
ENSDART00000009545	8.8044	0.03985					***pak4***	*p21 protein (Cdc42/Rac)-activated kinase 4*	
ENSDART00000052539	7.7117	0.00387	10.8640	0.00463	9.6297	0.00839	***myo1ea***	*myosin IE, a*	**Myosin cytoskeleton**
ENSDART00000149823					7.5907	0.01296	***myh9a***	*myosin, heavy polypeptide 9a, non-muscle*	
ENSDART00000124862			-3.8204	0.00955	-3.8498	0.01206	***smyhc2***	*slow myosin heavy chain 2*	
ENSDART00000066177	-3.8913	0.01935			-3.7348	0.03532	***tuba2***	*tubulin, alpha 2*	**Microtubule dynamics**
ENSDART00000108950			9.5984	0.00016			***ttll4***	*tubulin tyrosine ligase-like family, member 4*	
ENSDART00000154778			9.1515	0.00985			***map1ab***	*microtubule-associated protein 1Ab*	
ENSDART00000054274	4.9792	0.00170	5.6223	0.00118	5.8492	0.00085	***macf1***	*microtubule-actin crosslinking factor 1*	
ENSDART00000151342					7.0247	0.01118	***arhgap42a***	*Rho GTPase activating protein 42a*	**Cytoskeleton regulation**
ENSDART00000152951					6.3055	0.00973	***cdc42ep4b***	*CDC42 effector protein (Rho GTPase binding) 4b*	
ENSDART00000014024	5.1679	0.03686					***plecb***	*plectin b*	**Mechanical integrity**

Table XIV: Genes involved in cell migration and motility, differentially expressed at 3, 6 and 9 hpa in comparison to uncut controls. Upregulated genes are shown in red and downregulated genes in green.

TargetName	Log2FC 3hpa	PValue	Log2FC 6hpa	PValue	Log2FC 9hpa	PValue	GeneSymbol	Description	Pathway
ENSDART00000013609			6.5990	0.00542	7.8474	0.00736	***tln1***	*talin 1*	**Focal Adhesion**
ENSDART00000023584			4.8597	0.01179	5.9123	0.02673	***tln2***	*talin 2*	
ENSDART00000133531	11.0903	0.01297	8.8776	0.01825			***cib1***	*calcium and integrin binding 1 (calmyrin)*	
ENSDART00000005784	-2.8529	0.04691					***itgb1bp1***	*integrin beta 1 binding protein 1*	
ENSDART00000148454			3.6389	0.01060			***itgb1b.1***	*integrin, beta 1b.1*	
ENSDART00000075261			3.4850	0.01435			***itgb1b***	*integrin, beta 1b*	
ENSDART00000142522			9.2226	0.01824			***itfg2***	*integrin alpha FG-GAP repeat containing 3*	
ENSDART00000143056	-3.6363	0.04490	-4.0468	0.04414			***zyx***	*zyxin*	
ENSDART00000112445	-2.7466	0.04942					***tenc1a***	*tensin like C1 domain containing phosphatase a*	
ENSDART00000130442	-4.9620	0.03350					***col4a1***	*collagen, type IV, alpha 1*	**Extracellular Matrix**
ENSDART00000135769	-5.8043	0.02279			-7.4828	0.00065	***col6a3***	*collagen, type VI, alpha 3*	
ENSDART00000033844	-6.5333	0.03481			-7.0435	0.03951	***col7a1***	*collagen, type VII, alpha 1*	
ENSDART00000033363	-5.3380	0.00820			-6.4422	0.03261	***col11a2***	*collagen type XI alpha-2*	
ENSDART00000098706			2.6965	0.00266			***lamc2***	*laminin, gamma 2*	
ENSDART00000026107			8.8917	0.00919	9.3254	0.00350	***tnc***	*tenascin C*	
ENSDART00000123700					-9.2311	0.00073	***tnw***	*tenascin W*	
ENSDART00000111772	-4.0635	0.02391			-3.3047	0.02192	***thbs2b***	*thrombospondin 2b*	
ENSDART00000144217			8.6765	0.00603	9.5352	0.00341	***ctsba***	*cathepsin B, a*	**Extracellular Matrix Remodelling**
ENSDART00000020456	-4.6618	0.01606	-4.3608	0.00163			***mmp15***	*matrix metallopeptidase 15*	
ENSDART00000067447	-4.9883	0.04811					***mmp30***	*matrix metallopeptidase 30*	
ENSDART00000066471	8.0247	0.00022	8.9237	0.00260	8.2259	0.00178	***adam8b***	*a disintegrin and metalloproteinase domain 8b*	
ENSDART00000149378	4.9281	0.03256					***mxra8b***	*matrix-remodelling associated 8b*	
ENSDART00000140050	-8.2354	0.00944	-6.7096	0.02955	-6.0020	0.02169	***ctnna1***	*catenin (cadherin-associated protein), alpha 1*	**Adherens Junctions**
ENSDART00000081675			-5.2578	0.02397	-4.0746	0.01689	***ctnnb2***	*catenin, beta 2*	
ENSDART00000147057			-7.7335	0.03425	-7.8503	0.03814	***cdh1***	*cadherin 1*	
ENSDART00000024627	-7.1713	0.01397					***cdh2***	*cadherin 2*	
ENSDART00000092343	-6.3689	0.0133					***tjp2a***	*tight junction protein 2a (zona occludens 2)*	**Tight Junctions**

3.3 Regulation of gene transcription by signal transduction networks and chromatin activation state

In the beginning of this project, we hypothesized that signal transduction and chromatin remodelling could be one of the most relevant gene categories to regulate osteoblast dedifferentiation *in vivo* during regeneration. They were the best candidates likely to play a role in cell fate plasticity and cell fate decisions, as they can modulate directly gene expression by regulating specific transcription factors or promoting their recruitment to gene regulatory regions that specify cell identity (Guo and Morris 2017).

Our transcriptome analysis detected several signal transduction pathways that were differentially expressed throughout the time-points analysed (see Table XV and Table XVI), namely: Wnt, Igf, Jak/Stat, Tgf-β and Map/Erk signalling pathways. Most of them were already demonstrated to play a role in caudal fin regeneration, but at later stages in the regenerative process (Jaźwińska et al. 2007; Chablais and Jazwinska 2010; Gauron et al. 2013; Hirose et al. 2014; Stewart et al. 2014; Wehner and Weidinger 2015), and some have already been shown to regulate cell dedifferentiation in other contexts (Cai et al, 2007). Nevertheless, the link between these pathways and osteoblast dedifferentiation during caudal fin regeneration is still unclear.

We can hypothesize that Wnt signalling is activated during osteoblast dedifferentiation, as *wnt10a* and *dvl2* are upregulated at 6hpa (Table XV). Corroborating our analysis, it has already been demonstrated that *wnt10a* is upregulated at this time-point, but only in whole caudal fins (Stoick-Cooper et al. 2006), and not specifically in osteoblasts.

Our analysis also showed a clear regulation of the insulin signalling pathway, with some of the components being up and downregulated (Table XV). Although we found variability in the time-points analysed, there is a general tendency for osteoblasts to increase the expression of insulin signalling ligands and to decrease the expression of the receptors. This may indicate that osteoblasts act as a source of insulin ligands but do not activate the signalling pathway during dedifferentiation. Another interesting observation was the upregulation of *leptin b* in all three time-points (Table XV). Leptin b is a hormone that activates the leptin signalling pathway, already shown to be upregulated during caudal fin regeneration at later time-points (Kang et al. 2016). Leptins are conserved secreted hormones that control energy homeostasis and glucose metabolism (Dalman et al. 2013; Park and Ahima 2014; Michel et al. 2016). Leptin signalling can act in parallel and/or interact with the insulin signalling pathway in other contexts and regulate energy consumption and glucose metabolism (Amitani et al. 2013; Thon et al. 2016), suggesting that both pathways may cooperate and play a role during the metabolic changes (Table X and Table XI) that might occur during regeneration, and in particular during osteoblast dedifferentiation.

Interestingly, some components of the Jak/Stat signalling pathway, known to regulate proliferation, cell fate and cell migration (Rawlings 2004; Murray 2007), were also found to be

differentially regulated in our microarray (Table XVI). Some of the components of this pathway, such as *jak1*, *jak2a* and *stat1a*, had a clear tendency to be upregulated in all time-points, suggesting its activation and a possible role in osteoblast dedifferentiation during caudal fin regeneration.

Table XV: Genes from signal transduction pathways, differentially expressed at 3, 6 and 9 hpa in comparison to uncut controls. Upregulated genes are shown in red and downregulated genes in green.

TargetName	Log2FC 3hpa	PValue	Log2FC 6hpa	PValue	Log2FC 9hpa	PValue	GeneSymbol	Description	Pathway
ENSDART00000016369	-5.6371	0.03837					***wls***	*wntless homolog (Drosophila)*	**Wnt signalling**
ENSDART00000147714	-4.2903	0.03570					***wisp1a***	*WNT1 inducible signaling pathway protein 1a*	
ENSDART00000007308			10.5239	0.00997			***wnt10a***	*wingless-type MMTV integration site family, member 10a*	
ENSDART00000051491					-10.047	0.00456	***sfrp1a***	*secreted frizzled-related protein 1a*	
ENSDART00000102498	-7.4724	0.04357			-9.4158	0.02178	***sfrp2***	*secreted frizzled-related protein 2*	
ENSDART00000098520			6.2899	0.01665			***fzd10***	*frizzled homolog 10*	
ENSDART00000135316			7.8791	0.04700			***dvl2***	*dishevelled, dsh homolog 2 (Drosophila)*	
ENSDART00000130507			-2.0807	0.00914	-2.0440	0.00188	***aida***	*axin interaction partner and dorsalization antagonist*	
ENSDART00000018228	8.5210	0.00872					***gsk3b***	*glycogen synthase kinase 3 beta*	
ENSDART00000011506	5.7291	0.00879					***nkd2a***	*naked cuticle homolog 2a*	
ENSDART00000080076					-2.5493	0.00996	***rxfp3***	*relaxin/insulin-like family peptide receptor 3*	**Insulin signalling**
ENSDART00000026576	6.5730	0.04750	8.3774	0.03420			***igfbp1a***	*insulin-like growth factor binding protein 1a*	
ENSDART00000128607			6.4693	0.02500			***igfbp5b***	*insulin-like growth factor binding protein 5b*	
ENSDART00000009642	-5.6632	0.01127			-9.1512	0.00232	***igf2a***	*insulin-like growth factor 2a*	
ENSDART00000053924	-8.2067	0.01306					***irs2***	*insulin receptor substrate 2*	
ENSDART00000105823			-10.669	0.00029			***insrb***	*insulin receptor b*	
ENSDART00000133203	4.2934	0.00946	6.6085	0.00662	8.5219	0.03225	***lepb***	*leptin b*	**Leptin signalling**

The transcriptome analysis also demonstrated three other signalling pathways that seem to be important during the early time-points of regeneration: Toll, Tgf-β and Map/Erk signalling pathways (Table XVI). However, in contrast to the above-mentioned pathways, we found no evident direction in their regulation, with some components being up and others downregulated. These pathways are known to be involved in immunity, response to stress, proliferation, apoptosis and cell fate decisions and all of these biological features are important during the regenerative context (Pearson G et al. 2001; Shaul and Seger 2007; Massagué 2012; Anthoney et al. 2018).

Table XVI: Genes from signal transduction pathways, differentially expressed at 3, 6 and 9 hpa in comparison to uncut controls (continuation). Upregulated genes are shown in red and downregulated genes in green.

TargetName	Log2FC 3hpa	PValue	Log2FC 6hpa	PValue	Log2FC 9hpa	PValue	GeneSymbol	Description	Pathway
ENSDART00000038990	7.2002	0.01720	6.3875	0.04644	6.8206	0.00126	***jak1***	*Janus kinase 1*	**Jak/Stat signalling**
ENSDART00000127639	5.1187	0.00071	2.6842	0.04328			***jak2a***	*Janus kinase 2a*	
ENSDART00000002000	4.5619	0.03426	4.2713	0.03497	4.8201	0.02507	***stat1a***	*signal transduction and activation of transcription 1a*	
ENSDART00000146467			-7.8342	0.01747			***stat6***	*signal transducer and activator of transcription 6*	
ENSDART00000150030	4.5887	0.04157	6.4787	0.04421			***tlr5b***	*toll-like receptor 5b*	**Toll signalling**
ENSDART00000130393	-10.538	0.00490	-10.371	0.00004	-10.003	0.00373	***tlr7***	*toll-like receptor 7*	
ENSDART00000139243	-3.0410	0.01906	-3.8548	0.00864	-3.6589	0.02695	***tlr19***	*toll-like receptor 19*	
ENSDART00000075568	-8.0552	0.00660	-6.8989	0.03603			***nog***	*noggin*	**TGF-β siganlling**
ENSDART00000085388					-8.1987	0.00209	***bmp3***	*bone morphogenetic protein 3*	
ENSDART00000043462			10.3910	0.00915			***acvrl1***	*activin A receptor type II-like 1*	
ENSDART00000144402			-8.1201	0.04691			***fstl3***	*follistatin-like 3 (secreted glycoprotein)*	
ENSDART00000089274					-9.1596	0.02773	***tab3***	*TGF-beta activated kinase 1/MAP3K7 binding protein 3*	
ENSDART00000125371	3.9699	0.01764					***mknk1***	*MAP kinase interacting serine/threonine kinase 1*	**MAP/Erk signalling**
ENSDART00000027782			3.5276	0.02791	3.9348	0.01978	***mknk2a***	*MAP kinase-interacting serine/threonine kinase 2a*	
ENSDART00000122053					-4.8988	0.03108	***map2k6***	*mitogen-activated protein kinase kinase 6*	

Last but not less important, another class of genes crucial to regulate cell-fate changes includes genes that promote chromatin remodelling (Orkin and Hochedlinger 2011; Guo and Morris 2017). Our gene expression profile demonstrated that there were several differentially expressed chromatin modifying enzymes mainly at 3 hpa and 6 hpa when compared to the homeostasis situation (see Table XVII). These enzymes regulate chromatin structure and activate or suppress gene expression by modifying nucleosome histones or by mobilizing the DNA-histone structure. Chromatin modifying enzymes can be divided into the following groups: histone acetyltransferases (HATs); histone methyltransferases (HTMs); histone deacetylase (HDACs); and histone demethylase (HDMs) (Kouzarides 2007; Onder et al. 2012; Zhang et al. 2016). In general, HATs such as *kat5*, *mrgbp* and *crebbpb* were upregulated with a peak of expression at 6 hpa, while HDMs like *kdm2aa* and *kdm5bb* were also upregulated but at 3 and 6 hpa (Table XVII). Both HDMs and HDMs upregulation may be associated with increased transcriptional activation. In contrast, the HDAC proteins *hadac4* and *hadac8* were upregulated and *kmt2bb*, an HTM, was downregulated at 3 and 6 hpa (Table XVII), which may potentiate gene silencing. Additionally, we observed downregulation of histones *h1f0* and

h2afy2, components of the nucleosomes, at 3 and 6 hpa, respectively, that can also regulate the general state of chromatin compression leading to modification of chromatin landscape (Zhang et al. 2016). In accordance with our results, a few studies have demonstrated that histone modifying enzymes are important for fin regeneration (Stewart et al. 2009; Pfefferli et al. 2014). Overall, we observed a dynamic transcriptional response during the early hours of regeneration that peaked at a specific time-window between 3-6 hpa. We observed a response of chromatin modifying enzymes and nucleosome components (histones), both responsible for the packaging state of the DNA and, consequently, chromatin reorganization and availability to transcription factors, which may regulate gene expression and, thus, cell identity (Cavalli 2006; Onder et al. 2012; Harikumar and Meshorer 2015; Zhang et al. 2016). Therefore, it is possible that chromatin remodelling may play a substantial role during osteoblast dedifferentiation.

Taken together, data from our genome-wide gene expression profiling of osteoblast during dedifferentiation reflects major phenotypic changes observed in osteoblast that allowed to further characterize the process. Importantly, it also revealed potential new regulators of the dedifferentiation program, which included metabolic changes, signal transduction pathways and chromatin remodelling events.

Table XVII: Genes involved in the regulation of chromatin remodelling, differentially expressed at 3, 6 and 9 hpa in comparison to uncut controls. Upregulated genes are shown in red and downregulated genes in green.

TargetName	Log2FC 3hpa	PValue	Log2FC 6hpa	PValue	Log2FC 9hpa	PValue	GeneSymbol	Description	Pathway
ENSDART00000142420			6.7953	0.0063			***kat5***	*K(lysine) acetyltransferase 5*	**Chromatin modifying enzymes**
ENSDART00000042469			8.8183	0.0088	8.8129	0.0106	***mrgbp***	*MRG/MORF4L binding protein, H4/H2A histone acetyltransferase complex*	
ENSDART00000091873	8.8116	0.0079	7.7814	0.0092			***crebbpb***	*CREB binding protein b* (histone acetyltransferase acti vity)	
ENSDART00000036277	7.8362	0.0239					***hdac4***	*histone deacetylase 4*	
ENSDART00000083190			6.8113	0.0014			***hdac8***	*histone deacetylase 8*	
ENSDART00000148870	-6.4622	0.0140					***kmt2bb***	*lysine (K)-specific methyltransferase 2Bb*	
ENSDART00000135067	7.4125	0.0293					***kdm2aa***	*lysine (K)-specific demethylase 2Aa*	
ENSDART00000149173	3.2072	0.0443	5.7026	0.0024			***kdm5bb***	*lysine (K)-specific demethylase 5Bb*	
ENSDART00000056286			-11.4139	0.0070			***h1f0***	*H1 histone family, member 0*	**Histones**
ENSDART00000058162	-9.2863	0.0371					***h2afy2***	*H2A histone family, member Y2*	

4 THE ROLE OF METABOLIC REPROGRAMMING DURING DEDIFFERENTIATION AFTER CAUDAL FIN AMPUTATION – FOCUS ON BONE REGENERATION

Since our microarray data suggested an important role of cellular metabolism in osteoblasts at early stages of caudal fin regeneration, we decided to further examine a possible correlation between metabolism and cell dedifferentiation. Given the role of metabolism in regulating cell reprogramming, we hypothesize that osteoblasts undergo a glycolytic shift preceding dedifferentiation. This metabolic adaptation could be required to reprogram osteoblasts to a less differentiated state so that they can proliferate and potentiate bone regeneration. Despite the considerable amount of information on the role of metabolism in health and disease, the link between metabolic adaptation, regeneration and repair remains poorly understood.

4.1 Metabolic reprogramming as a general regeneration feature

Given the dramatic increase in the expression of glycolytic enzymes and complexes from the electron transport chain, we primarily set out to evaluate and validate through q-PCR analyses the expression of some of these components. We perform this analysis using the whole regenerating tissue (corresponding to the first bony-ray segment below the amputation) to evaluate if this changes in gene expression were specific to osteoblast during dedifferentiation or if they were also observed as a general behaviour during regeneration. (Figure 24). For this analysis, we compare the 6 hpa to the uncut condition, since it is the first time-point after amputation when both glycolysis and OxPhos enzymes are upregulated during osteoblast dedifferentiation.

We observed that most glycolytic enzymes, including *pfkpa*, *aldoaa*, *gapdhs* and *pgam1A*, are upregulated (Figure 24) in the whole regenerating caudal fin. The *lactate dehydrogenase a* (*ldha*) expression was also significantly upregulated, inclusively at higher levels when compared to our microarray data (Figure 24). This enzyme is crucial for the glycolic switch, since can it convert the pyruvate generated through glycolysis into lactate, reducing the pyruvate oxidation in mitochondria, shifting the source of energy from OxPhos to glycolysis. Some components of the electron transport chain, such as *dlat*, *sdhdb* and *cox6c* (Figure 24), were also upregulated, however, this upregulation was not as dramatic as observed in the microarray data (Table X and Table XI) or as the increase in the expression of the glycolytic pathway genes. Increasing the number of biological replicates would be important to complete this analysis and give a more robust expression profile. Nevertheless, this indicates that similarly to osteoblasts undergoing dedifferentiation during regeneration, the whole regenerating tissue responds to amputation by increasing the glycolytic influx and possibly Oxphos. This suggests that the metabolic adaptation seen in osteoblasts may be part of a general program to induce caudal fin regeneration.

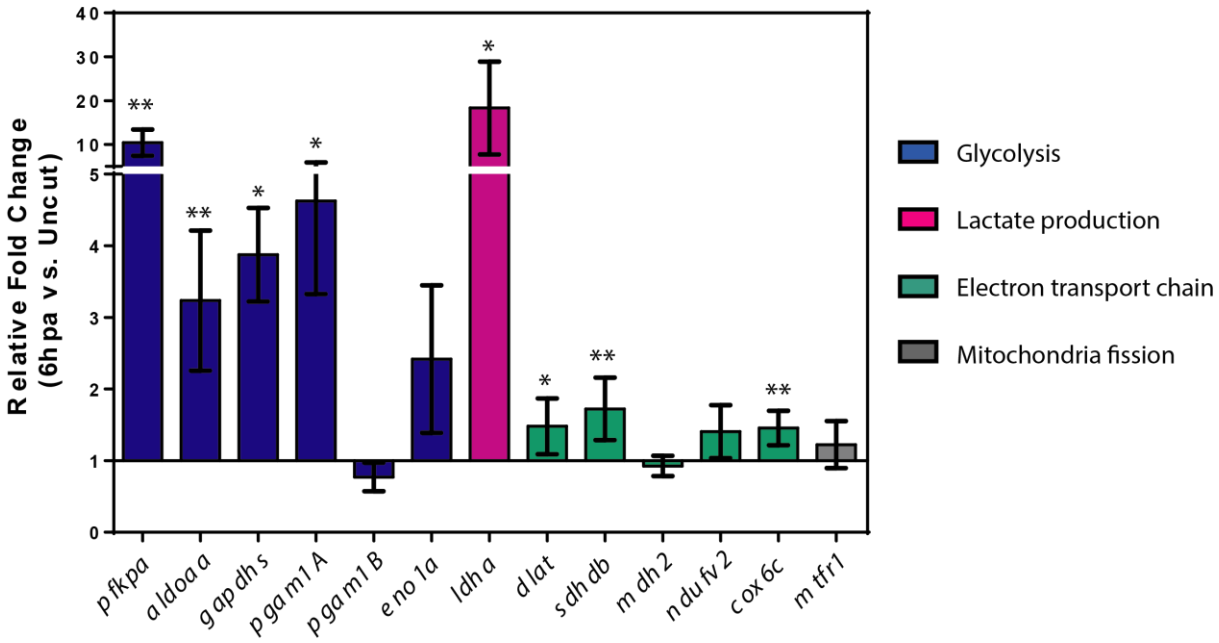

Figure 24: Evidence for metabolic adaptation in whole regenerating caudal fins. Quantitative q-PCR showing the expression of several glycolytic enzymes and components of OxPhos: *pfkpa*, *aldoaa*, *gapdhs*, *pgam1A* *pgam1B* and *eno1a* for glycolytic pathway; *ldha* for lactate production; *dlat*, *sdhdb*, *mdh2*, *ndufv2* and *cox6* for the electron transport chain; and *mtfr1* that is required for mitochondria fission. Graph shows the relative gene expression for each transcript at 6 hpa in relation to uncut/homeostasis situation caudal fins; transcript levels are plotted on a $\log_2$ scale with uncut control samples averaged to $\log_2 0 = 1$; statistical analysis displayed on the graph corresponds to Unpaired t test with Welch's correction (6 biological replicates are shown, and each replicate corresponds to a pool of 4-5 fins). Hpa: hours post-amputation; *: $p < 0.05$, **: $p < 0.01$.

4.2 Inhibition of glycolysis impairs osteoblast formation

Both the microarray and the q-PCR data indicate that the glycolytic enzymes are upregulated after caudal fin amputation, in the time-window of osteoblast dedifferentiation. Thus, we hypothesize that a glycolytic switch is required for osteoblast dedifferentiation and bone regeneration. To test our hypothesis, we used a specific inhibitor of the glycolytic influx, the small molecule 3-(3-pyridinyl)-1-(4-pyridinyl)-2-propen-1-one (3PO), which partially inhibits the glycolytic activator Phosphofructokinase-2/fructose-2,6-bisphosphatase 3 (Pfkfb3) (Schoors et al. 2014). 3PO was administered from 0 to 48 hpa, corresponding to the blastema formation phase, which is a direct consequence of the dedifferentiation process. During this period, we can easily monitor and evaluate if the impairment of glycolysis leads to major defects or phenotypes during bone regeneration (Figure 25A). We noticed that animals treated with the glycolytic inhibitor 3PO exhibited a general impairment of the regenerative process at 48 hpa, seen by the reduced regenerated area when compared to vehicle-treated controls (Figure 25B and 6D). The 3PO-treated animals also showed a decrease in expression of osteoblast markers, such as *osx* (immature/intermediate osteoblast marker), visualised with the transgenic line Tg(*osterix:*mCherry-NTRo)^{pd46} (referred to as *osx*:mCherry, Figure 25B) and E), and *runx2* (early/osteoprogenitor marker), visualised with the transgenic *line Tg(Has.RUNX2:*EGFP*)*^{zf259} (referred to as *runx2*:EGFP; Figure 25C and F)), when compared to control animals at 48 hpa. This was measured by the percentage of regenerated area occupied

by each of the markers mentioned above. We also observed that, when we stopped administering 3PO (at 48 hpa), caudal fins recovered and were similar to control fins at 120 hpa, both in terms of regenerate size and bone formation (Figure 25B, 120 hpa). Nevertheless, bone patterning defects were often noticed (in approximately 50% of the fins) at this time-point (Figure 25B, 120 hpa, arrow).

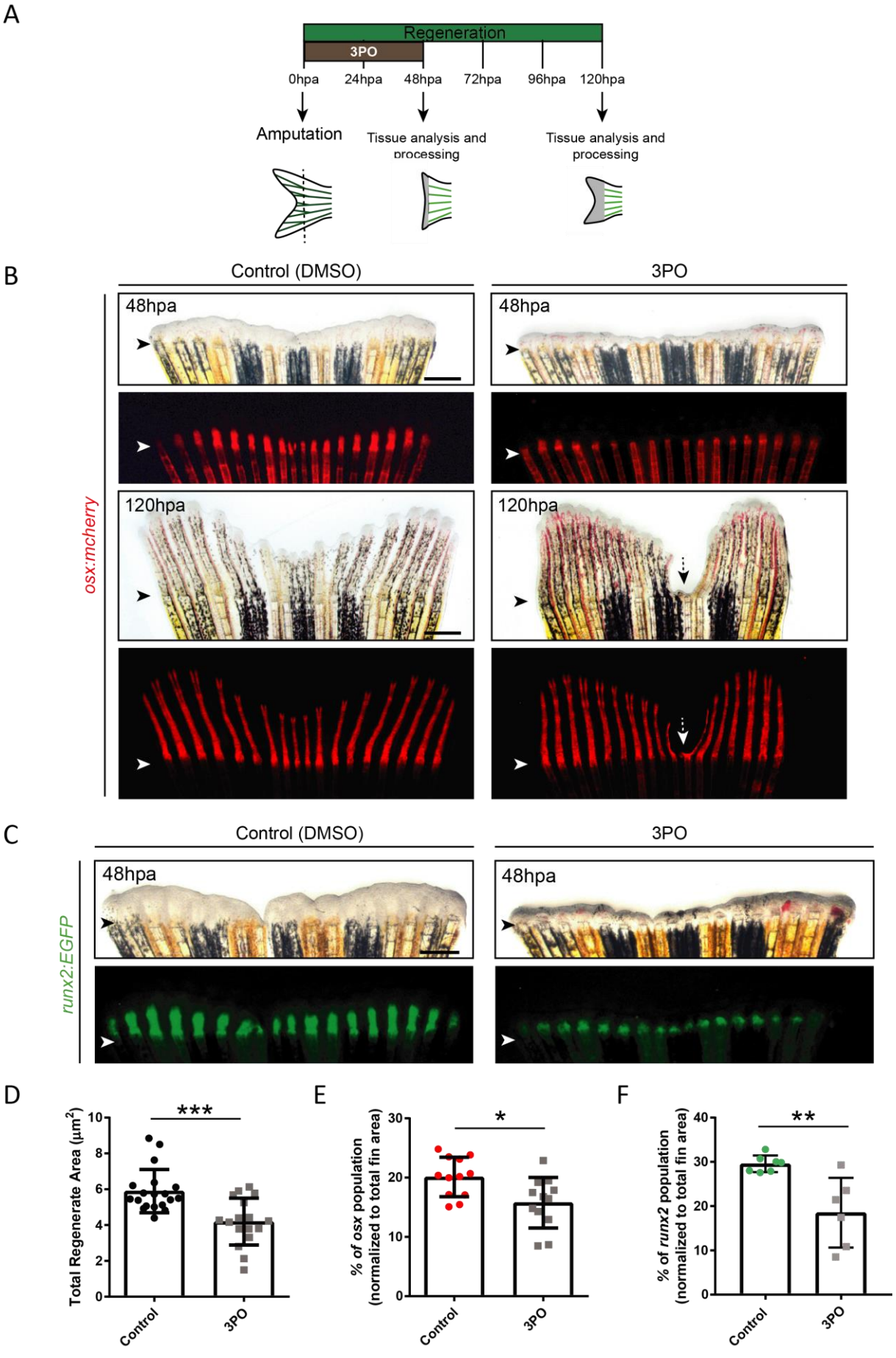
A
Regeneration
3PO
0hpa
24hpa
48hpa
72hpa
96hpa
120hpa
Amputation
Tissue analysis and processing
Tissue analysis and processing
B
Control (DMSO)
3PO
48hpa
120hpa
osx:mcherry
C
Control (DMSO)
3PO
48hpa
runx2:EGFP
D
Total Regenerate Area (µm²)
***
Control
3PO
E
% of osx population (normalized to total fin area)
*
Control
3PO
F
% of runx2 population (normalized to total fin area)
**
Control
3PO

Figure 25: Inhibition of glycolysis impairs fin regeneration and emergence of bone markers. (A) Schematic representation of the strategy used to manipulate the glycolytic influx during the blastema formation phase of the regenerative process. The glycolytic inhibitor 3PO is administered daily until 48 hpa, after which caudal fins are imaged and either collected for tissue processing or left to regenerate until 120 hpa. (B) Representative images of *osx*:mCherry (immature/intermediate osteoblast marker, red) transgenic caudal fins treated with the vehicle DMSO (control) or with 15 µM 3PO and imaged at 48 hpa at 120 hpa. (C) Caudal fin representative images of *runx2*:EGFP (preosteoblast /early osteoblast marker, green) transgenic fins treated with the vehicle DMSO (control) or with 15 µM 3PO and imaged at 48 hpa. (D) Quantification of the total regenerate area at the end of the blastema formation phase, 48 hpa; statistical analysis displayed on the graph corresponds to Mann-Whitney test with Mean ± SD (n= 19 fish for controls; n= 12 fish for 3PO treated animals). (E) Quantification of the percentage of *osx*:mCherry fluorescence normalized to the total regenerate area at 48 hpa; statistical analysis displayed on the graph corresponds to Mann-Whitney test with Mean ± SD (n= 12 fish for the control condition; n= 12 fish for 3PO treated condition). (F) Quantification of the percentage of *runx2*:EGFP fluorescence normalized to the total regenerate area at 48 hpa; statistical analysis displayed on graph corresponds to Mann-Whitney test with Mean ± SD (n= 7 fish for controls; n= 6 fish for 3PO treated condition). hpa: hours post-amputation; arrow heads define the amputation plane; arrow indicates bone patterning defect; scale bars represent 1mm; * p< 0.05, **p< 0.01, ***p< 0.001.

Following this, we characterized in more detail the observed phenotype and how different osteoblast populations behave in this context (Figure 26A). It is known that normal regenerating fins present different osteoblast subtypes according to their maturation state. Within the blastema at 48 hpa, bone maturation occurs in a hierarchical organization of overlapping proximal-distal compartments: the more distal blastema includes a self-renewing $Runx2^{+}Osx^{-}$ progenitor subtype (example in Figure 26B control region 1), while the proximal blastema region, next to the amputation plane, is populated by a proliferative $Runx2^{+}Osx^{+}$ osteoblast subtype that is already committed to differentiate (example in Figure 26B control region 2) (Brown et al. 2009; Stewart et al. 2014). As expected, in control *osx*:mCherry cryosections co-labelled with a Runx2 antibody, we observed this hierarchical organization, with both populations having approximately the same number of cells (Figure 26B, C and D). In contrast, 3PO treated animals showed an accentuated decrease in the numbers of proliferating $Runx2^{+}Osx^{+}$ immature osteoblasts, while the osteoprogenitor $Runx2^{+}Osx^{-}$ subtype remains unchanged within the blastema (Figure 26B and C). Additionally, the remaining $Runx2^{+}Osx^{+}$ subtype appears to be more dispersed in the blastema instead of occupying a more proximal position near the stump (Figure 26B). As a consequence of the decrease in the number of the $Runx2^{+}Osx^{+}$ subtype, the ratio between the two populations, which was close to 1 in controls, is altered in the 3PO treated animals (Figure 26D). Overall, these data show that glycolysis is required during tissue regeneration, in particular for bone repair.

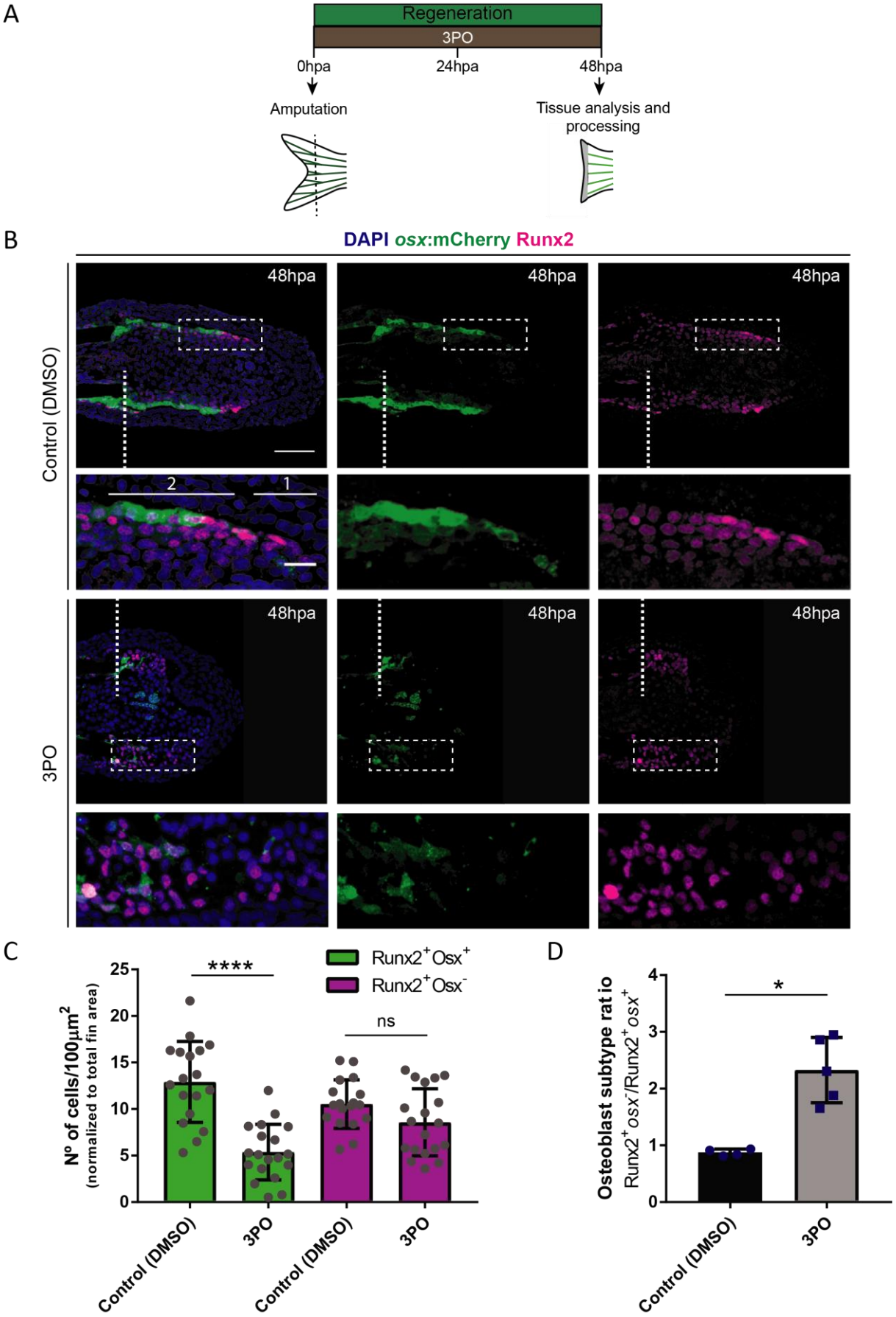
A
Regeneration
3PO
0hpa
24hpa
48hpa
Amputation
Tissue analysis and processing
B
DAPI osx:mCherry Runx2
Control (DMSO)
3PO
48hpa
2
1
C
Nº of cells/100µm2 (normalized to total fin area)
Runx2+Osx+
Runx2+Osx-
****
ns
Control (DMSO)
3PO
Control (DMSO)
3PO
D
Osteoblast subtype ratio
Runx2+osx-/Runx2+osx+
*
Control (DMSO)
3PO

Figure 26: Inhibition of glycolysis impairs the formation of the Runx2^{+}Osx^{+} osteoblast subtype. (A) Schematic representation of the strategy used to manipulate the glycolytic influx during the blastema formation phase of the regenerative process and address new osteoblast subpopulation formation. (B) Representative images of 48 hpa *osx*:mCherry (immature/intermediate osteoblast marker, green) caudal fins cryosectioned longitudinally and immunostained for Runx2 (preosteoblast/osteoprogenitor marker, magenta) and counterstained with DAPI (nuclei, blue) in specimens treated with vehicle DMSO (control) or with 15 µM 3PO. (C) Quantification of Runx2^{+}Osx^{-} and Runx2^{+}Osx^{+} osteoblasts subtypes on comparable 48 hpa caudal fin cryosections; bars on graph correspond to total number of each osteoblast subtype normalized to total fin area and statistical analysis corresponds to Mann-Whitney test with Mean ± SD displayed (n= 18 bony-rays compiled from 4 fish for the vehicle DMSO (control) condition; n= 19 bony-rays compiled from 5 fish for the 3PO treated condition). (D) Quantification of the ratio between the Runx2^{+}Osx^{-} osteoblast subtype in relation to the Runx2^{+}Osx^{+} osteoblast subtypes at 48 hpa; bars on graph correspond to the average ratios between osteoblasts subtypes, giving one value per animal; statistical analysis corresponds to Mann-Whitney test with Mean ± SD displayed (n= 4 fish for the vehicle DMSO (control) condition; n= 5 fish for the 3PO treated condition). hpa: hours post-amputation; dashed lines define the amputation plane; scale bars represent 200 µm and 50 µm in magnified panels; * p< 0.05, **** p< 0.05, ns: non-significant.

4.3 Glycolysis regulates cell proliferation and wound epidermis assembly

Thereafter we decided to deepen our understanding on the reason why this phenotype was occurring. We can propose three hypotheses to explain the phenotypes induced by 3PO treatment: first, proliferation could be reduced leading to a decrease in the Runx2^{+}Osx^{+} subtype, the signalling pathways that regulate osteoblast differentiation could be impaired or Runx2^{+}Osx^{+} could be undergoing cell death.

We started by analysing the ability of the cells to re-enter cell cycle upon amputation, which is often related to the dedifferentiation process (Cai et al. 2007; Maden 2013; Eguizabal et al. 2013). Since we have previously observed a considerable number of PCNA^{+} cells at 24 hpa (Figure 18D), we decided to inhibit the glycolytic influx in the first 24 hpa in *osc*:EGFP transgenic animals, that specifically label mature osteoblasts (Figure 27A). We observed that, in contrast to the control animals, 3PO-treated animals have a clear decrease in PCNA (late G1 marker) staining, suggesting that indeed the partial inhibition of glycolysis can lead to the impairment of cell proliferation. In fact, this decrease in proliferation markers was observed not only in *osc*-positive osteoblasts but also in epidermal and mesenchymal cells, the other major cell types that compose the caudal fin (Figure 27B and C). This is in accordance with our hypothesis that the glycolytic switch may be important as a general mechanism to promote regeneration. In the future, other proliferation markers will have to be used and other time-points explored to further confirm and characterize this result. The other two hypotheses still need to be tested. Both cell death and correct expression of the pathways known to regulate the differentiating population could influence the number of Runx2^{+}Osx^{+} osteoblast subtype in the glycolysis inhibition context. Nonetheless, this indicates that reduced cell proliferation could be one of the reasons for defective Runx2^{+}Osx^{+} osteoblast subtype formation.

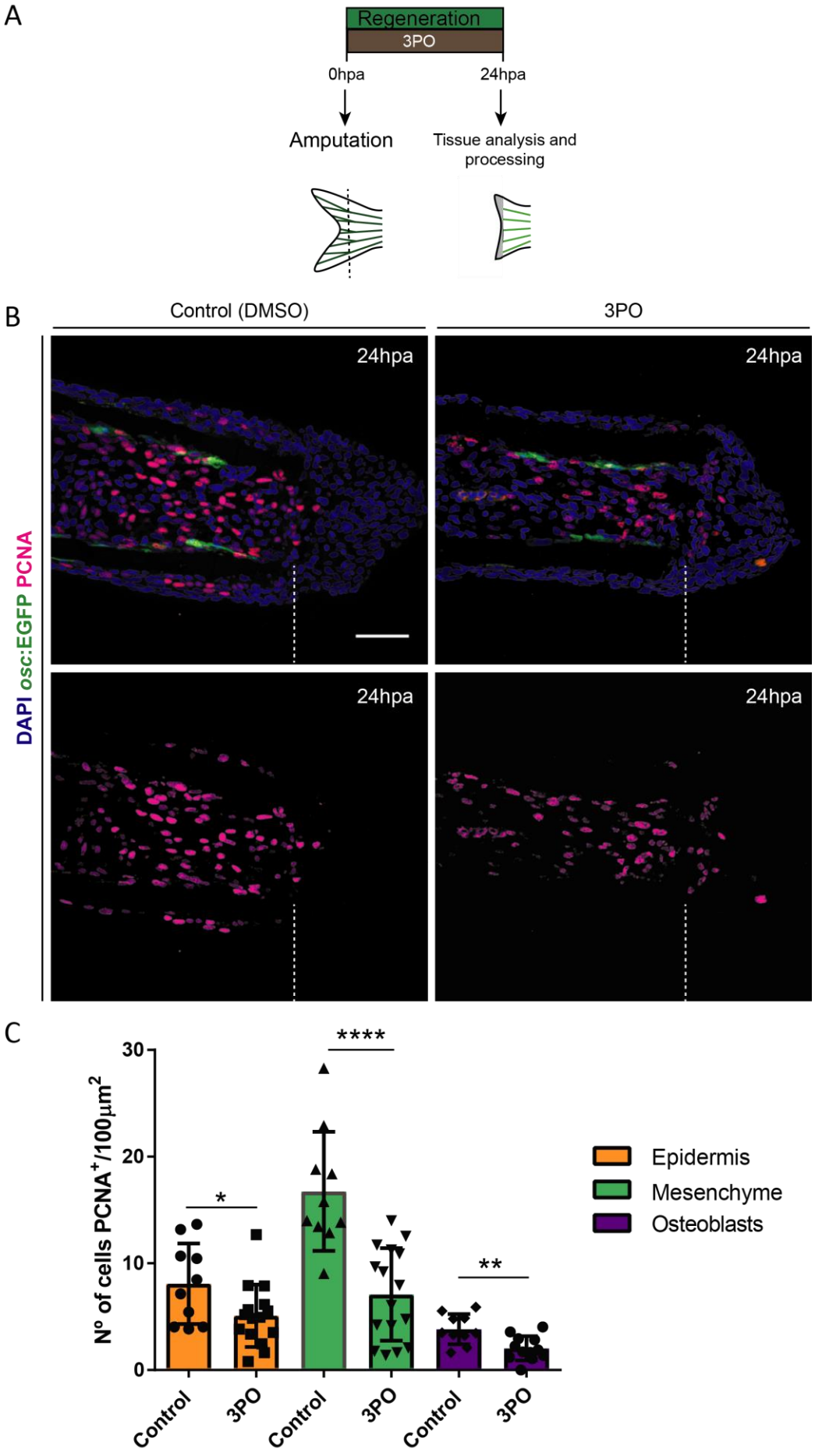
A
Regeneration
3PO
0hpa
24hpa
Amputation
Tissue analysis and processing
B
Control (DMSO)
3PO
24hpa
24hpa
24hpa
24hpa
DAPI osc:EGFP PCNA
C
Nº of cells PCNA+/100µm2
30
20
10
0
*
****
**
Control
3PO
Control
3PO
Control
3PO
Epidermis
Mesenchyme
Osteoblasts

Figure 27: Inhibition of glycolytic influx impairs cell cycle re-entry during blastema formation. (A) Schematic representation of the glycolysis inhibition protocol using 3PO to address cell cycle re-entry during blastema formation. 3PO is administered at 0 hpa and caudal fins collected at 24 hpa and processed for cryosectioning. (B) Representative images of immunostaining for PCNA (late G1 proliferating cells, red) in *osc*:EGFP (osteoblasts, green) caudal fin longitudinal cryosections counterstained with DAPI (nuclei, blue) at 24 hpa, in controls and 3PO treated animals. (C) Quantification of $PCNA^+$ cells in comparable fin cryosections at 24 hpa; bars correspond to total number of $PCNA^+$ cells in the different major caudal fin compartments and cell types (epidermis, mesenchyme and osteoblasts) normalized to total tissue area, in vehicle (controls, n= 10 bony-rays compiled from 3 different fish) and 3PO treated animals (n= 15 bony-rays compiled from 4 different fish); statistical analysis displayed on graph corresponds to Mann-Whitney test with Mean ± SD. hpa: hours post-amputation; dashed lines define the amputation plane; scale bars represent 50 µm; * p< 0.05, **p< 0.01, ****p< 0.0001.

Another interesting observation during glycolytic inhibition was that the regenerated epidermis or wound epidermis showed major defects in terms of organization (Figure 28A). The WE is a well-organized stratified epithelium with a hierarchical organization composed of: a superficial layer, several suprabasal keratinocyte layers and a pool of keratinocyte stem cells in the basal epidermal layer (BEL). The presence of this specialised regeneration epithelium is critical for its success (Le Guellec et al. 2004; Chen et al. 2016a). To address whether wound epidermis defects could be involved in the regeneration phenotypes observed in 3PO treated animals (Figure 25, Figure 26 and Figure 27), we analysed in more detail the organization of the wound epidermis at 48 hpa, after glycolysis inhibition during blastema formation. We noticed that, in contrast to *osx*:mCherry controls, the animals treated with 3PO had a thicker wound epidermis with more differentiated keratinocyte layers (Figure 28A, double arrowheads), observed through immunofluorescence against p63 (an epidermal marker). The percentage of each cell type that composes regenerating fins differs between controls and treated animals. Whereas controls contain roughly the same percentage of epidermal and mesenchymal cells (46% and 40%, respectively) and 14% of osteoblasts, 3PO-treated animals showed an increase in the percentage of the epidermal population to 61% and a decrease in both the mesenchymal and osteoblast populations to 29% and 10%, respectively (Figure 28A and C). Consequently, the ratios between the epidermal cells and other cell types were also disturbed during regeneration (Figure 28D and E). An important characteristic of the wound epidermis is the formation of the BEL. The BEL is characterized by a high secretory activity, serving as a potent signalling centre, directing growth and patterning signals, during regeneration (Poss et al. 2000a, 2003; Bouzaffour et al. 2009; Chen et al. 2015, 2016a; Thorimbert et al. 2015; Shibata et al. 2016). This basal layer expresses a specialised component of the ECM, *laminin beta 1a (lamb1a),* during regeneration (Chen et al. 2015). Laminin function is required, not only to establish polarity in basal epithelial cells and regulate the localization of receptors for signalling but also to promote alignment and hierarchical organization of regenerating osteoblasts (Armstrong et al. 2017). Given this, we analysed the dynamics and localization of Laminin in regenerating fin cryosections as a readout of effective wound epidermis formation. Interestingly, while Laminin was strongly localized to the extracellular basement membrane of the BEL in control fins along the regenerated epidermis, in 3PO-treated animals Laminin staining was decreased, mislocalized and discontinuous along the

blastema (Figure 28B, arrows). This led us to conclude that 3PO administration compromised significantly the WE formation and organisation, which might explain, at least partially, the general impairment in caudal fin growth and specification of osteoblast subtypes during regeneration.

Taken together these results point to an important role of metabolism during bone regeneration either autonomously, by impairing osteoblast cell cycle re-entry, thereby affecting their dedifferentiation process, and/or non-autonomously by inhibiting wound epidermis formation. Impairment of both processes can lead to the major defects observed in bone repair during caudal fin regeneration.

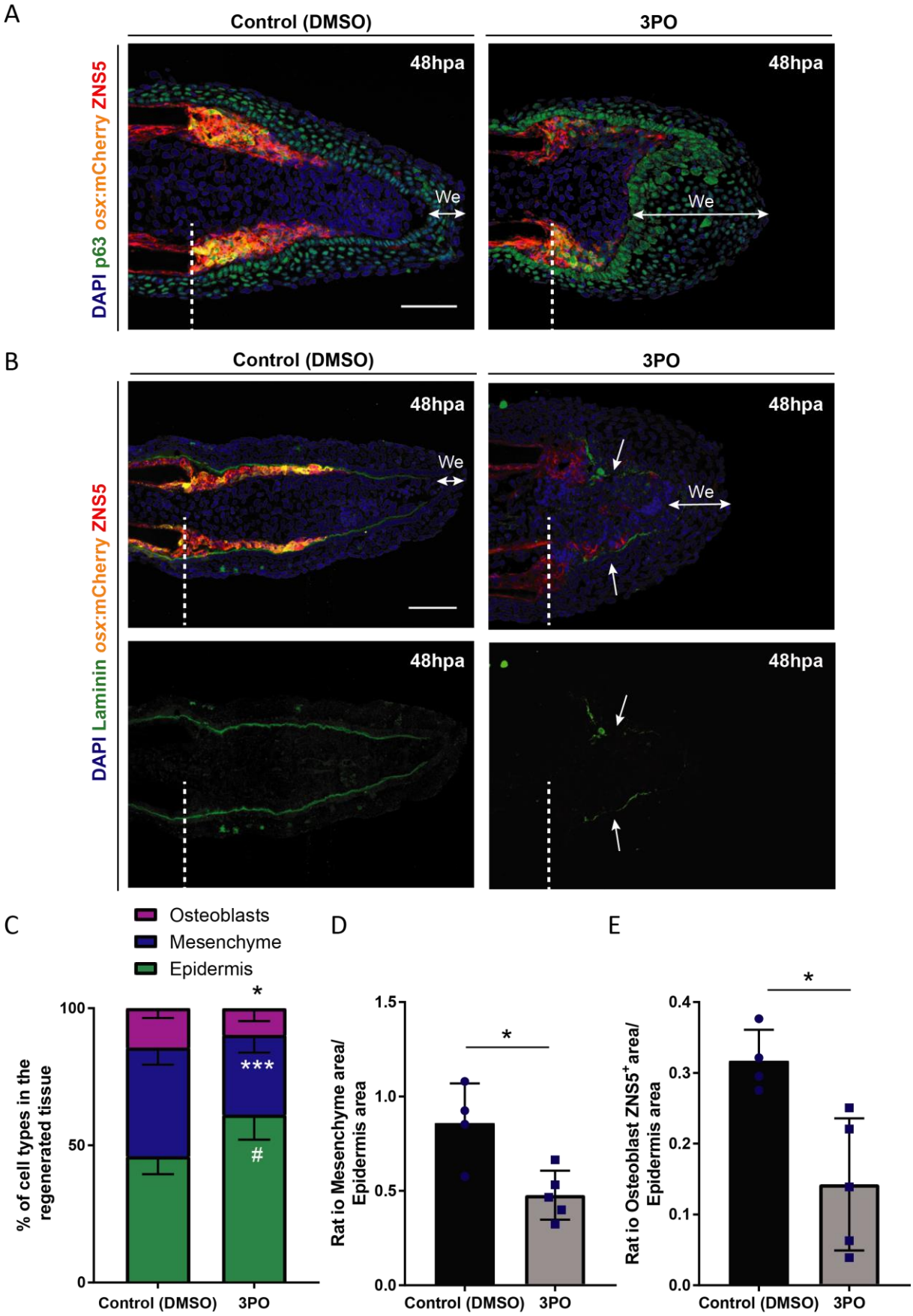

Figure 28: Inhibition of glycolysis leads to major wound epidermis defects during regeneration. (A) Representative images of immunostaining for p63 (epidermal marker, green) and ZNS5 (pan osteoblast marker,

red) in *osx*:Cherry (osteoblasts, orange) caudal fin longitudinal cryosections counterstained with DAPI (nuclei, blue) at 48 hpa. The wound epidermis is thicker in 3PO treated animals (double arrowheads). (B) Representative images of immunostaining for laminin (basal lamina/ BEL marker, green) and ZNS5 (pan osteoblast marker, red) in *osx*:mCherry (osteoblasts, orange) caudal fin longitudinal cryosections counterstained with DAPI (nuclei, blue) at 48 hpa. While in control fins laminin localizes continuously below the BEL, in 3PO treated animals laminin has several discontinuities, leading to a misshapen wound epidermis. (C) Quantification of the percentage of different cells types that compose the regenerating fin, in comparable caudal fin cryosections; bars correspond to percentage of different major cell types in the fin (epidermis, mesenchyme and osteoblasts) calculated through the area occupied by each cell type in relation to the total regenerated area in vehicle DMSO (controls, n= 16 bony-rays compiled from 4 different animals) and 3PO treated animals (n= 15 bony-rays compiled from 5 different animals). (D) Quantification of the ratio between the area occupied by the mesenchymal compartment in relation to the area occupied by the epidermal cells in the regenerate; bars on graph correspond to the average area ratios, giving one value per animal (n= 4 fish for the vehicle DMSO (control) condition; n= 5 fish for the 3PO treated condition). (E) Quantification of the ratio between area occupied by $ZNS5^{+}$ osteoblasts in relation to the area occupied by the epidermal cells in the regenerate; bars on graph correspond to the average area ratios, giving one value per animal (n= 4 fish for the vehicle DMSO (control) condition; n= 5 fish for the 3PO treated condition). Statistical analysis displayed on graphs corresponds to Mann-Whitney test with Mean ± SD hpa: hours post-amputation; We: wound epidermis; dashed lines define the amputation plane; double arrowheads correspond to the width of the wound epidermis; scale bars represent 200 µm; * p< 0.05, ***p< 0.001, # p< 0.0001.

5 DECIPHERING THE POTENTIAL ROLE OF THE HIPPO/YAP SIGNALLING PATHWAY DURING OSTEOBLAST DEDIFFERENTIATION

After our transcriptomic wide approach, we performed a target gene approach. With this strategy, we sought to characterize the signalling pathways that regulate cell dedifferentiation. The Hippo/YAP signalling pathway represents a potential candidate for such a role, as it has been involved in regulating cell fate decisions and cell dedifferentiation in other contexts (Nicolay et al. 2010; Zhao 2014; de Sousa et al. 2018). Our lab has previously shown that this pathway regulates cell proliferation during the caudal fin regenerative outgrowth phase (Mateus et al, 2015). However, the contribution of the Hippo pathway for osteoblast dedifferentiation has been largely unaddressed. Therefore, we explored a possible involvement of the Hippo effector, Yap, during this process.

5.1 The Hippo pathway effector Yap translocates to the nucleus of mature osteoblasts during dedifferentiation

We started by investigating Yap activation or inactivation in specific osteoblast populations after amputation. Since this pathway is regulated at the protein level we looked at the intracellular dynamics of this transcriptional co-activator upon amputation. When Yap cytoplasmic, is considered to be in an inactive form that culminates in degradation. In contrast, Yap nuclear translocation is a read out of is activation and regulation of target gene transcription (Irvine 2012; Piccolo et al. 2014). Thus, we observed Yap subcellular location in mature osteoblasts and in osteoprogenitors by performing immunofluorescence studies using a Yap antibody on *osc*:EGFP and *runx2*:EGFP transgenic animals, respectively.

In uncut *osc*:EGFP animals, Yap expression looks fuzzy and weak in the whole fin, including in osteoblasts (Figure 29A-A’’’). As early as 3 hpa, at the beginning of dedifferentiation, Yap is translocated from the cytoplasm to the nucleus (suggesting its activation) in some mesenchymal cells (Figure 29B-B’’’, arrowheads) and it becomes stronger in some mature osteoblasts attached to the bone surface (Figure 29B-B’’’, arrows). At 6 hpa, almost all mesenchymal cells (Figure 29C-C’’’, arrowheads) and some mature osteoblasts have accumulated Yap in the nucleus (Figure 29C-C’’’, arrows). This translocation of Yap to the nucleus in mesenchymal cells and in mature osteoblasts persisted until later time-points (24 hpa) (Figure 29D-D’’’). This suggests that Yap is active in several cell types in the caudal fin during the dedifferentiation time-window. Thus, indicating Yap as a possible candidate to regulate the dedifferentiation process.

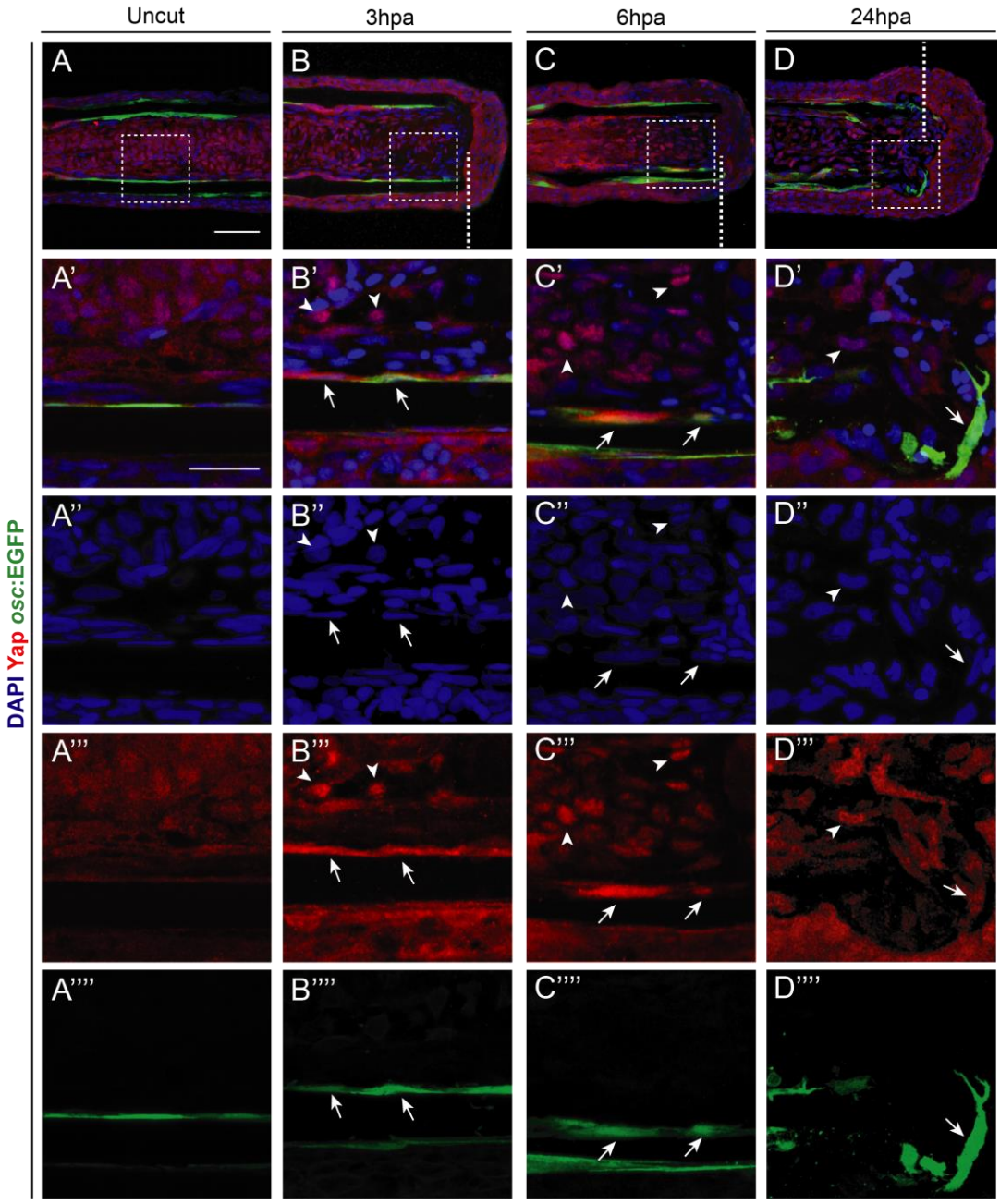

Figure 29: The Hippo pathway effector Yap translocates to the nucleus of osteoblast and inner mesenchyme during the dedifferentiation time-window. Representative images of *osc*:EGFP (mature osteoblasts, green) longitudinal caudal fin cryosections immunostained for Yap (red) and counterstained with DAPI (nuclei, blue). (A-A'''') In uncut fins, Yap has a fuzzy localization either in the cytoplasm and/or in the nucleus of osteoblast and in the mesenchymal compartment. (B-B'''') At 3 hpa, Yap translocates to the nucleus in the mesenchymal compartment and becomes more intensely accumulated in osteoblasts. (C-C'''') At 6 hpa, during the dedifferentiation time-window, Yap is localized in the nucleus, and therefore active, in mesenchymal cells and in some *osc*$^{+}$ osteoblasts. (D-D'''') Yap remains nuclear in mesenchymal cells and in some *osc*$^{+}$ osteoblasts from 6 until 24 hpa. Arrow heads indicate examples of mesenchymal cells with nuclear Yap and arrows indicate examples of *osc*$^{+}$ osteoblasts with nuclear Yap. hpa: hours post-amputation; dashed lines define the amputation plane; dashed boxes represent magnified panels; scale bars represent 50 µm in A, B C and D and 20 µm in magnified panels (A'-D'''').

Next, we investigated the subcellular localization of YAP in osteoprogenitors (*runx2*:EGFP positive cells), that are thought to derive partially from mature osteoblasts. We observed that,

at 24 hpa, *runx2* was highly upregulated in comparison to control uncut fins (Figure 30A-A'', B-B''). Several of this emerging Runx2^{+} cells had nuclear localized Yap (Figure 30Bi-Biv, arrows), suggesting that Yap is active and possibly regulating osteoprogenitor formation, which is an important feature of the dedifferentiation process.

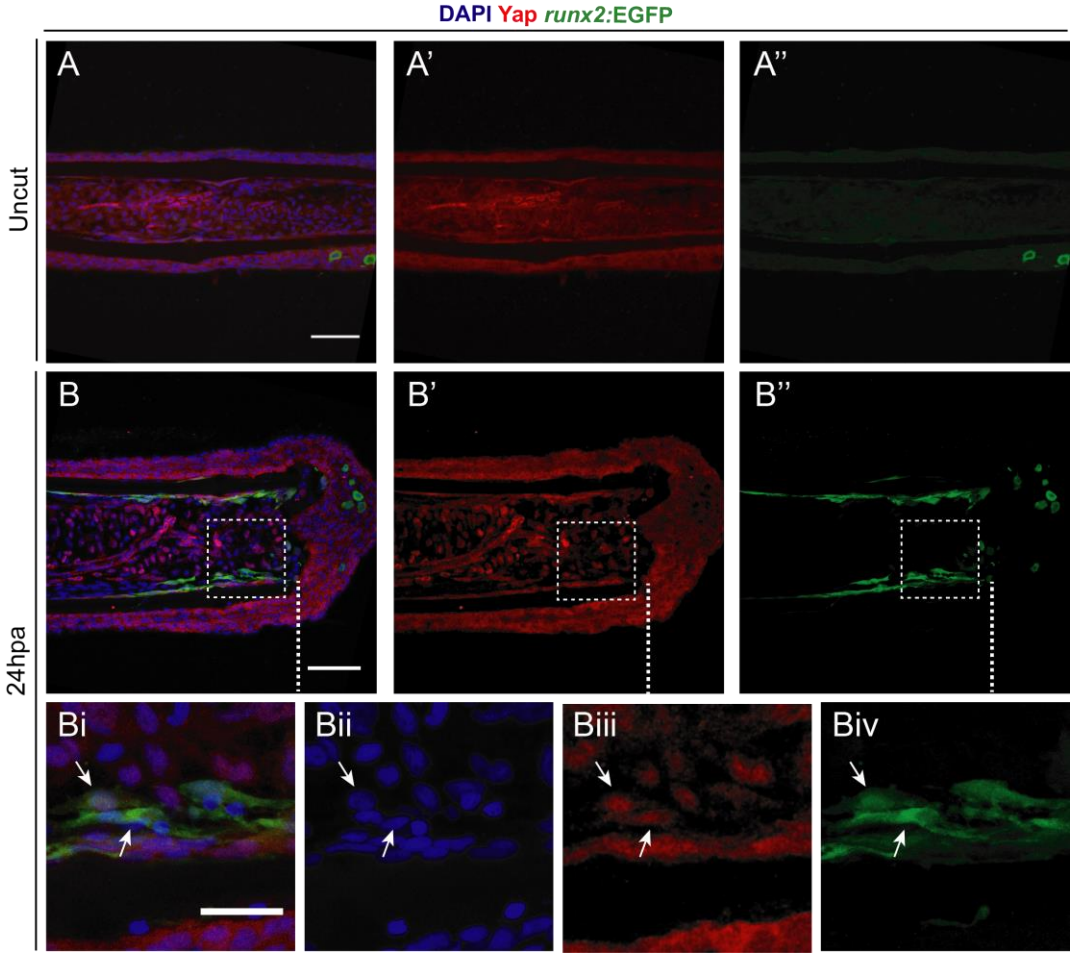

Figure 30: The Hippo pathway effector Yap is nuclear localized in osteoprogenitors during blastema formation. Representative images of *runx2*:EGFP (osteoprogenitors, green) longitudinal caudal fin cryosections immunostained for Yap (red) and counterstained with DAPI (nuclei, blue). (A-A'') In a non-regenerative condition (uncut) no osteoprogenitors are observed in the *runx2*:EGFP transgenic animals and Yap has a fuzzy localization, being all over the cells that compose the inner mesenchymal compartment. (B-Biv) At 24 hpa, osteoprogenitors derived from the dedifferentiation of mature osteoblasts can be seen with the *runx2*:EGFP transgenic line. At this time-point, some *runx2*$^{+}$ progenitors can be seen with Yap accumulation in the nucleus. Arrows indicate examples of *runx2*$^{+}$ osteoblasts with nuclear Yap. hpa: hours post-amputation; dashed lines define the amputation plane; dashed boxes represent magnified panels; scale bars represent 50 µm in A-A'' and in B-B'' and 20 µm in magnified panels (Bi-Biv).

5.2 Genetic manipulation of the Hippo effector Yap culminates in severe osteoblast dedifferentiation defects

To evaluate the requirement of the transcription co-activator Yap during osteoblast dedifferentiation *in vivo*, we performed functional assays and analysed dedifferentiation features. For such purpose, we used a genetic tool, namely a heat-shock (HS) inducible transgenic line expressing a Dominant Negative (DN) of Yap, referred to has DN-Yap

(Tg*(hsp70l:RFP-dnyap1)*^{zf621}) (Figure 31A) (Mateus et al. 2015). In this line, the serine residues, which are phosphorylated by Lats1/2 and retain Yap in the cytoplasm, as well as the transcription activation domain are mutated. This means that upon HS, DN-Yap is always able to translocate to the nucleus, competing with the endogenous Yap for Tead binding sites. However, due to a mutation in the activation domain, it does not activate target gene expression. We gave a single HS to these transgenic fish just prior to amputation, to ensure that dedifferentiation was affected, and assessed whether blocking the activity of Yap would have an effect in osteoblast cell cycle re-entry and motility, and in osteoprogenitor formation at 24 hpa. At this time-point, when the blastema is still being formed, the DN-Yap construct is still expressed (data not shown) and regeneration defects should be more obvious to detect (Figure 31A). In all assays, we compared DN-Yap animals subjected to HS, defined as DN-Yap^{+} HS^{+} to the corresponding heat-shocked sibling controls, DN-Yap^{-} HS^{+}.

We started by analysing the acquisition of migratory performance by osteoblasts that reside in the first segment below amputation, from 0 to 24 hpa in DN-Yap^{-} HS^{+} and in DN-Yap^{+} HS^{+} animals. For that, we combined our DN-Yap transgenic line with the mature osteoblast reporter line, *osc*:EGFP. Contrasting to heat-shocked sibling controls (*osc*:EGFP; DN-Yap^{-} HS^{+}), in which osteoblasts have reached the amputation plane around 24 hpa (Figure 31B), in animals expressing the DN-Yap construct (*osc*:EGFP; DN-Yap^{+} HS^{+}), osteoblasts showed defective migration, with fewer cells reaching the amputation plane (Figure 31B and C).

Another process, which is a consequence of osteoblast dedifferentiation is the emergence of osteoprogenitors (Runx2^{+}) that are essential in the regenerative outgrowth phase. To investigate the requirement of Yap for proper osteoprogenitor formation, we used the DN-Yap transgenics and performed immunostainings for Runx2 (osteoprogenitor marker) in caudal fin cryosections. When we inhibited Yap function we noticed a decrease in the number of Runx2^{+} cells which, in sibling controls, are normally accumulated near the amputation at 24 hpa (Figure 31D and E). Alternatively, we tried to confirm the role of Yap in osteoprogenitor formation by over-activating the pathway. For this, we used a genetic tool expressing a Constitutively Active (CA) form of Yap, referred as CA-Yap (*Tg(hsp70l:RFP:cayap1)*^{zf622}) (Mateus et al. 2015) through heat-shock (Figure 31A). We noticed that, in contrast to the DN-YAP animals, animals expressing CA-Yap (CA-Yap^{+} HS^{+}) had an increased number of Runx2^{+} cells when compared to sibling controls (CA-Yap^{-} HS^{+}) (Figure 31D and E).

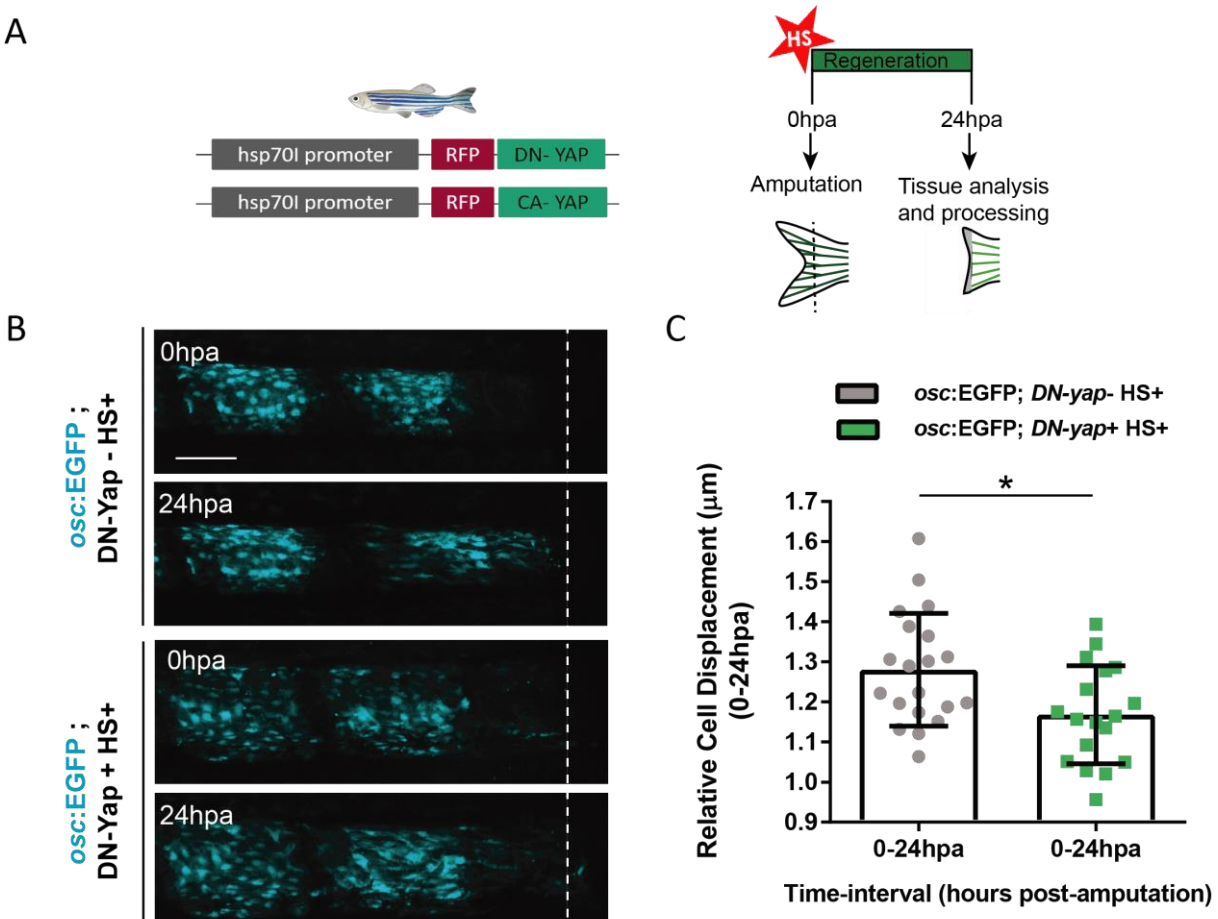
A
hsp70l promoter
RFP
DN- YAP
hsp70l promoter
RFP
CA- YAP
HS
Regeneration
0hpa
24hpa
Amputation
Tissue analysis
and processing
B
osc:EGFP ;
DN-Yap - HS+
0hpa
24hpa
osc:EGFP ;
DN-Yap + HS+
0hpa
24hpa
C
osc:EGFP; DN-yap- HS+
osc:EGFP; DN-yap+ HS+
Relative Cell Displacement (µm)
(0-24hpa)
1.7
1.6
1.5
1.4
1.3
1.2
1.1
1.0
0.9
*
0-24hpa
0-24hpa
Time-interval (hours post-amputation)

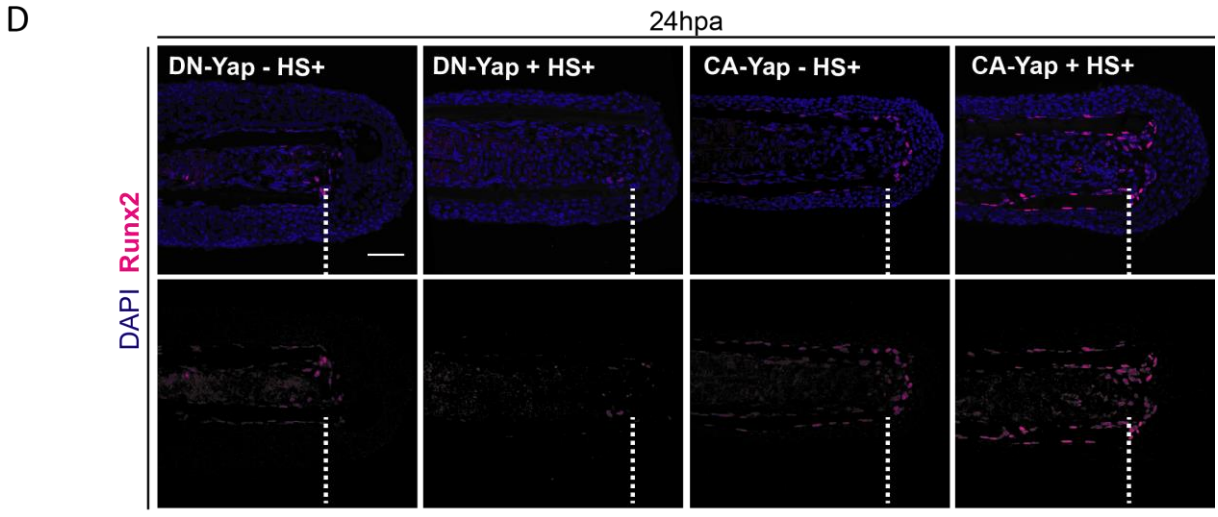
D
24hpa
DN-Yap - HS+
DN-Yap + HS+
CA-Yap - HS+
CA-Yap + HS+
DAPI Runx2

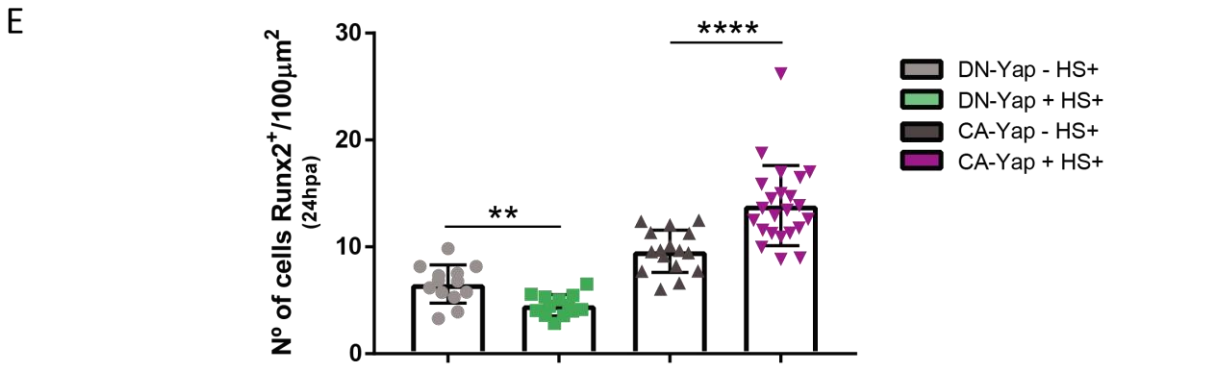
E
Nº of cells Runx2+/100µm2
(24hpa)
30
20
10
0
**
****
DN-Yap - HS+
DN-Yap + HS+
CA-Yap - HS+
CA-Yap + HS+

Figure 31: Genetic manipulation of the Hippo pathway effector Yap leads to impairment of several dedifferentiation features in osteoblasts. (A) Schematic representation of the transgenic lines used to address Yap function during regeneration and the corresponding manipulation protocol used. We used heat-shock (HS) induced transgenic lines that express either a Dominant Negative (DN-Yap+) or a Constitutively Active (CA-Yap$^+$) form of Yap upon temperature induction. HS are given prior to amputation and caudal fins are either imaged or collected for tissue processing. (B) Representative live imaging images of double transgenic specimens *osc*:EGFP; DN-Yap$^+$ the and corresponding sibling controls, *osc*:EGFP; DN-Yap$^-$, used to follow mature osteoblasts during regeneration and to manipulate Yap function at the same time. Animals were heat-shocked and imaged at 0 h and 24 h to quantify the ability of osteoblast to migrate upon expressing the DN-Yap construct. (C) Quantification of the relative osteoblast displacement from 0-24hpa in *osc*:EGFP; DN-Yap$^+$ and corresponding controls, *osc*:EGFP; DN-Yap$^-$, both heat-shocked at 0 hpa (HS+); statistical analysis displayed on graph corresponds to Mann-Whitney test with Mean ± SD (n= 18 bony-rays compiled from 4 different fish in *osc*:EGFP; DN-Yap$^-$ HS$^+$, n=20 bony-rays compiled from 5 different fish in *osc*:EGFP; DN-Yap$^+$ HS$^+$). (D) Representative immunofluorescence images of longitudinal cryosections of DN-Yap$^+$, CA-Yap$^+$ and the corresponding sibling controls. These animals were subjected to HS just before amputation and caudal fins immunostained for Runx2 (preosteoblast /osteoprogenitor marker, magenta) and counterstained for DAPI (nuclei, blue) at 24 hpa. (E) Quantification of osteoprogenitors, Runx2$^+$ cells, formed after amputation upon Yap manipulation in comparable caudal fin cryosections normalized to total fin area; statistical analysis displayed on graph corresponds to Mann-Whitney test with Mean ± SD (n= 13 bony-rays compiled from 4 different fish in DN-Yap- HS$^+$ siblings and in DN-Yap$^+$ HS$^+$ contexts, n=16 bony-rays compiled from 5 different fish in CA-Yap$^-$ HS$^+$ siblings and n=23 bony-rays compiled from 6 different fish in CA-Yap$^+$ HS$^+$ context). hpa: hours post-amputation; dashed lines define the amputation plane; scale bars represent 100 µm in B and 50 µm in D; * p< 0.05, **p< 0.01, ****p< 0.0001.

Lastly, we addressed the ability of osteoblasts to initiate proliferation. We performed PCNA (late G1 marker) immunofluorescence assays in transgenic DN-Yap$^+$ animals and in the corresponding DN-Yap$^-$ controls, both subjected to heat-shock just before amputation. In DN-Yap$^-$ HS$^+$ sibling controls the great majority of the different cell types that compose the caudal fin (epidermis, mesenchyme and osteoblasts) were PCNA positive (Figure 32A and B), suggesting that they have entered the cell cycle. Conversely, the DN-Yap$^+$ HS$^+$ fish showed an accentuated decrease in the number of PCNA-positive cells in the osteoblast and mesenchymal populations, but not in the epidermal compartment (Figure 32A and B). This was further confirmed through a flow cytometry cell cycle profile, which analysed in detail the total percentage of cells in G1, S and G2/M phases at 24 hpa in DN-Yap$^+$ HS$^+$ fish and sibling controls. In accordance, the cell cycle profile showed that DN-Yap$^+$ HS$^+$ animals have fewer cells in S phase and more cells in G1 than DN-Yap$^-$ HS$^+$ controls (Figure 32C).

Taken together these data point to an important role of the Hippo/Yap signalling pathway in regulating osteoblast dedifferentiation. Here we show that the Hippo pathway effector Yap regulates some of the most important dedifferentiation features, such as osteoblast migration and cell cycle re-entry, thereby ensuring correct osteoprogenitor formation.

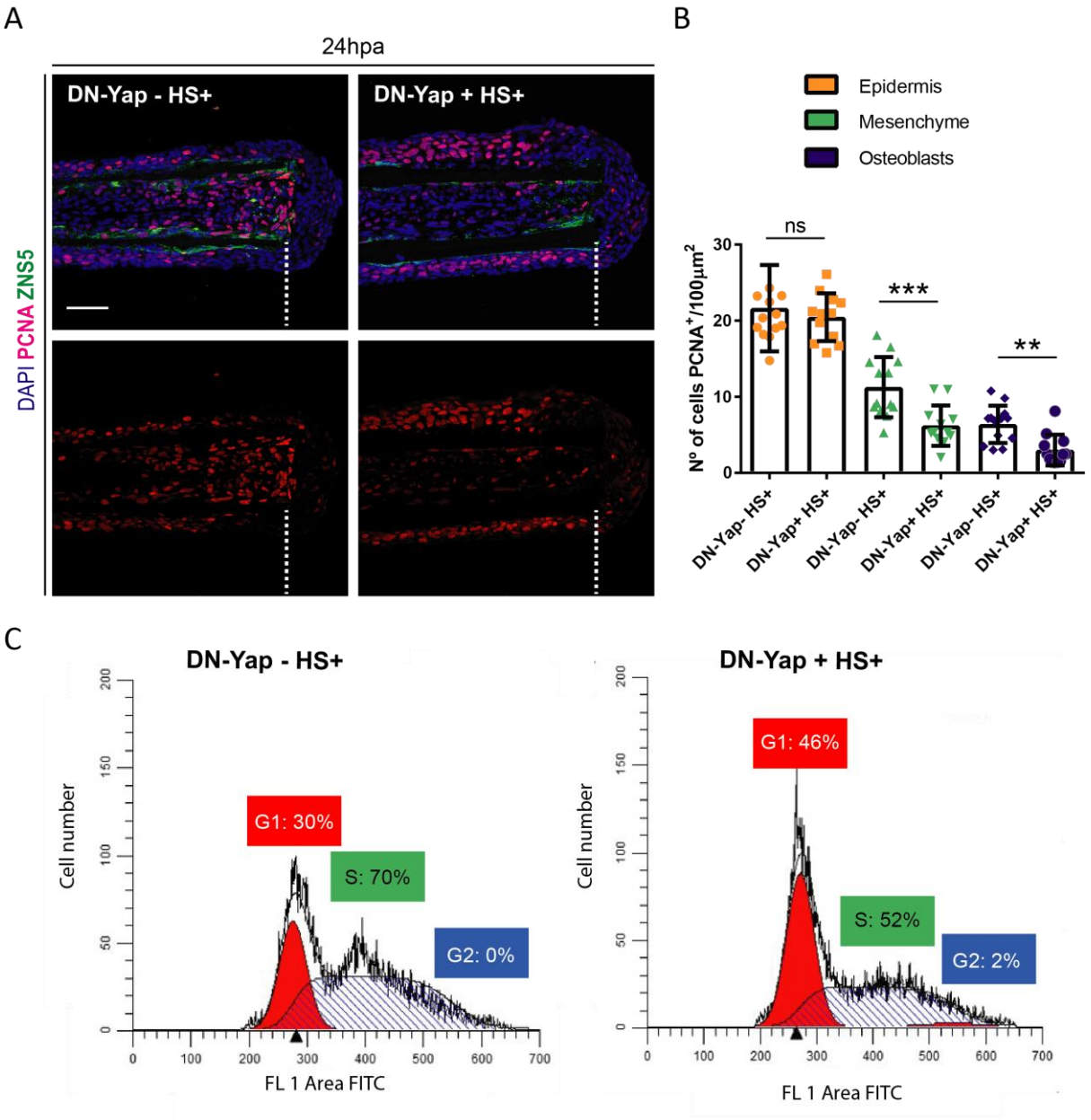

Figure 32: Genetic manipulation of the Hippo pathway effector Yap leads to impairment of cell cycle re-entry. (A) Representative immunofluorescence images of longitudinal cryosections of DN-Yap$^+$ and corresponding sibling control fish. These animals were subjected to heat-shock just before amputation, caudal fins collected at 24 hpa and immunostained for PCNA (late G1 proliferation marker, magenta), ZNS5 (a pan osteoblast marker, green) and counterstained for DAPI (nuclei, blue). (B) Quantification of PCNA$^+$ cells in comparable fin cryosections at 24 hpa; bars correspond to total number of PCNA$^+$ cells in the different major caudal fin compartments and cell types (epidermis, mesenchyme and osteoblasts) normalized to total tissue area in DN-Yap$^-$ HS$^+$ (sibling controls, n= 13 bony-rays compiled from 4 different fish) and in DN-Yap$^+$ HS$^+$ animals (n= 12 bony-rays compiled from 4 different fish); statistical analysis displayed on graph corresponds to Mann-Whitney test with Mean ± SD. (C) Flow cytometry analysis of the cell cycle profile of a pool of DN-Yap$^-$ HS$^+$ (sibling controls) and of DN-Yap$^+$ HS$^+$ caudal fins at 24 hpa (subjected to heat-shock before amputation); in the graph the percentage of the total number of cells in G1, S and G2/M phases of the cell cycle is shown for each condition. hpa: hours post-amputation; dashed lines define the amputation plane; scale bars represent 50 µm; **p< 0.01, ***p< 0.001; ns: non-significant.

Chapter IV

YAP REGULATES THE SIGNALLING CENTRES THAT GOVERN OSTEOBLAST REDIFFERENTIATION DURING REGENERATION

“Begin at the beginning,” the King said, very gravely,

“and go on till you come to the end: then stop”

Lewis Carroll, Alice's Adventures in Wonderland & Through the Looking-Glass

1 HIPPO/YAP SIGNALLING REGULATES BONE FORMATION DURING OUTGROWTH BY CONTROLLING OSTEOBLAST DIFFERENTIATION

Bone is one of the most abundant tissues that compose the zebrafish caudal fin, thus it is essential that, after damage, the fin skeletal tissue is fully recovered. After caudal fin amputation, bone regenerates through a very complex process that requires several regulatory mechanisms. Primarily, dedifferentiation of mature osteoblasts provides an osteoprogenitor source ($Runx2^+$ cells) that expands during blastema formation. This first process was already addressed in the previous chapter. Afterwards, during regenerative outgrowth, which starts after blastema formation (around 48 hpa), two distinct processes take place: maintenance and expansion of the progenitor pool ($Runx2^+$ cells) until regeneration is completed; and sequential and controlled redifferentiation of the progenitors into $Runx2^+Osx^+$, which have proliferative capacity. The latter population will further differentiate into fully mature osteoblasts to replace the lost skeletal tissue (Brown et al. 2009; Stewart et al. 2014). These events are intrinsically correlated with the different blastema compartments: the distal blastema (DB) region is populated by the progenitor pool ($Runx2^+$); the proximal blastema (PB) is composed of the already differentiating but proliferative $Runx2^+Osx^+$ osteoblast subtype; fully mature osteoblasts, capable of secreting extracellular bone matrix reside in the patterning zone (PZ) closer to the amputation region (Figure 7B and Figure 11A Chapter I) (Nechiporuk and Keating 2002; Brown et al. 2009; Stewart et al. 2014; Wehner and Weidinger 2015). Progenitor maintenance and expansion and controlled redifferentiation are regulated by antagonist activities and special segregation of specific signalling networks, as described in the introduction Chapter (Stewart et al. 2014; Wehner et al. 2014; Blum and Begemann 2015b).

1.1 Yap signalling downregulation leads to major defects in bone formation during caudal fin regeneration

Although our understanding of the regenerative outgrowth process has increased significantly in the last years, the precise mechanisms by which different signalling pathways interact to ensure correct bone formation are still unknown and potential regulators are missing from this context. Recently, the Hippo/Yap signalling pathway has been implicated in cell fate commitment of mesenchymal stem cells into the osteoblast lineage and directing proper osteoblast differentiation (Hong et al. 2005; Dupont et al. 2011a; Hiemer and Varelas 2013; Piccolo et al. 2014; Varelas 2014; Pan et al. 2018; Xiong et al. 2018). The role of this pathway in mediating osteoblast commitment relies mostly on cell culture and mammalian studies. However, this regulation was found to be highly context dependent and, in some cases, lead to incoherent or contradictory results. Therefore, other animal models with advantageous genetic tools would aid to clarify the role of this pathway in osteoblast lineage specification, particularly in a regenerative context. In the preceding Chapter III, we have demonstrated a

potential role for the Hippo/Yap signalling pathway in controlling osteoblast dedifferentiation during regeneration. In this Chapter, we evaluate whether the Hippo/Yap pathway is playing a part on the complex network that governs osteoblast differentiation during the regenerative outgrowth.

To address this question, we took advantage of the transgenic line expressing a dominant negative form of Yap, DN-Yap, upon heat-shock (Mateus et al. 2015), used in the previous Chapter. We performed caudal fin amputations to DN-Yap^{+} and DN-Yap^{-} siblings and allowed them to regenerate until 48 hpa, when the blastema is fully formed, making sure not to interfere with the dedifferentiation process and with progenitor cell assembly. From 48 hpa until 96 hpa we heat-shocked the fish daily and either imaged and collected the fins at 120 hpa (5 days post-amputation (dpa)) for cryosectioning or for q-PCR experiments (Figure 33A). In contrast to DN-Yap^{-} HS^{+} control animals, the DN-Yap^{+} HS^{+} animals had a significant impairment in the formation of new bone, as visualised by the decrease in calcein staining (Figure 33B and C), which labels calcified structures, when normalized to the total regenerated fin area. In addition, we observed that the DN-Yap^{+} HS^{+} fish formed thinner (Figure 33B and D) bony-rays, which presented some fractures (data not shown). This indicates that, indeed, Yap seems to play an important role in mediating bone formation specifically during the regenerative outgrowth phase.

1.2 Diminished Yap activity correlates with impairment in the formation of the differentiating osteoblast subtype

To understand the mechanism by which Yap controls bone repair during fin regeneration, we characterized the bone formation phenotype more thoroughly. Previous data from our lab has demonstrated that Yap intracellular localization in the mesenchymal compartment varies according to blastema compartmentalization and cell density: Yap is more cytoplasmic in distal regions, where cells are more compacted, and progressively becomes nuclear towards proximal regions, where cells are more spread. Importantly, Yap was shown to be required for mesenchymal proliferation and necessary for regeneration to proceed (Mateus et al. 2015).

To understand Yap requirement during bone formation, we evaluated how the different osteoblast subtypes, namely the progenitor pool (Runx2^{+}Osx^{-}) and the differentiating osteoblasts (Runx2^{+}Osx^{+}) were behaving in this context by monitoring osteoblast subtype numbers and expression of specific bone markers. We started by analysing cryosections of 120 hpa caudal fins subjected to the protocol mentioned above (Figure 33A), immunostained for Runx2 (osteoprogenitor marker) and for Osx (immature/intermediate osteoblast marker) and counterstained for calcein and DAPI. By evaluating the overall regenerated structure in both siblings and in DN-Yap expressing animals, we observed that while in controls (DN-Yap^{-} HS^{+}) the regenerated tissue was correctly compartmentalized along the PD-axis, comprising the PZ, PB and DB regions, in DN-Yap^{+} HS^{+} animals this did not occur (Figure 33A).

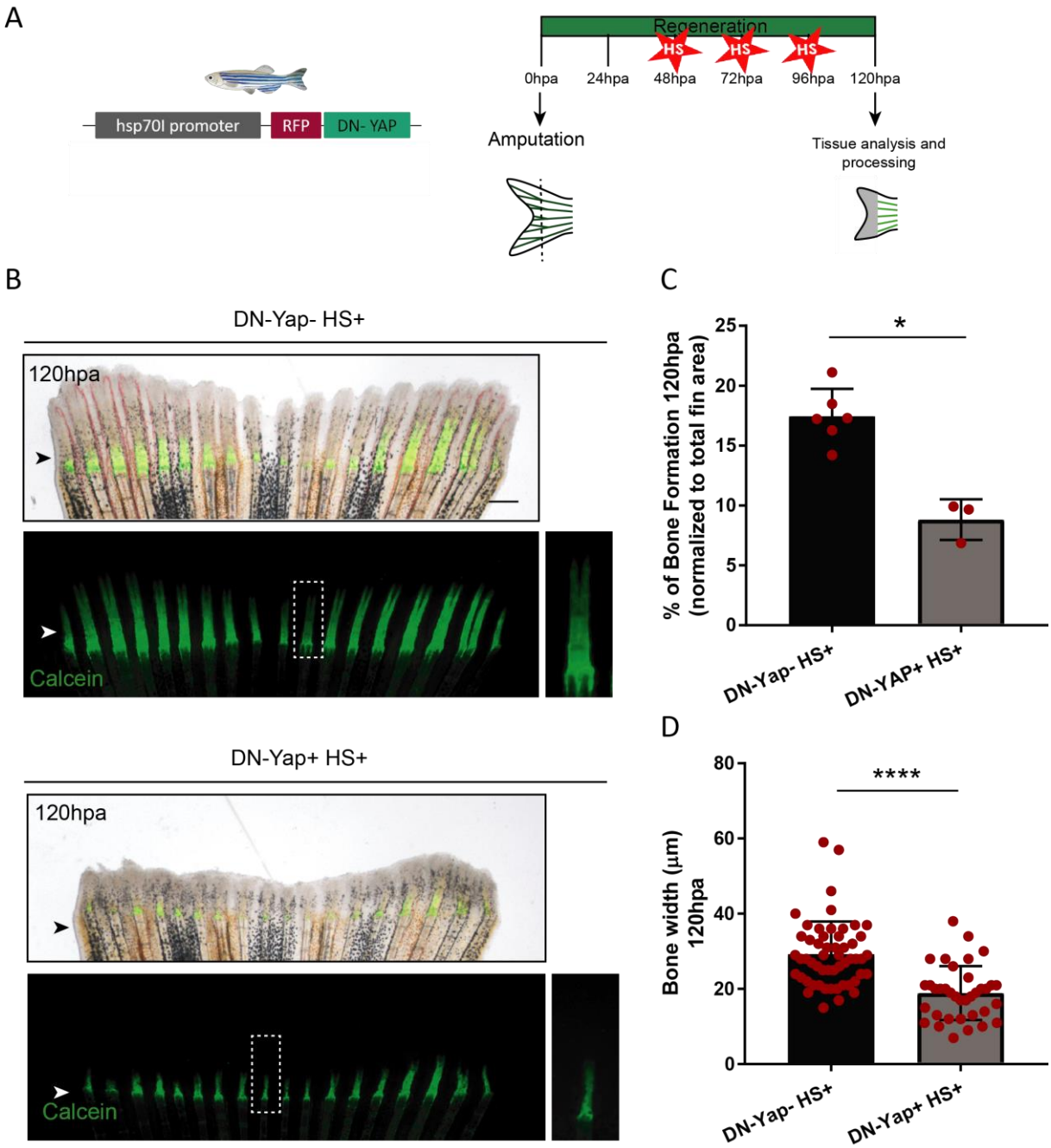

Figure 33: Manipulation of Yap during the regenerative outgrowth phase leads to bone regeneration defects. (A) Schematic representation of the experimental setup and transgenic line used to manipulate Yap function. After blastema formation (48 hpa), DN-Yap$^-$ siblings and DN-Yap$^+$ are subjected to daily heat-shocks during the 3 subsequent days. (B) Representative images of whole caudal fins stained for calcein (labels more strongly the newly formed bone, green) at 120 hpa used to monitor and quantify the percentage of bone formation and thickness. When compared to sibling control DN-Yap$^-$ HS$^+$ animals, DN-Yap$^+$ HS$^+$ have impairment in bone formation and the bony-rays that are formed are thinner. (C) Quantification of the percentage of calcein fluorescence in relation to the total regenerate area at 120 hpa; statistical analysis displayed on graph corresponds to Mann-Whitney test with Mean ± SD (n = 6 fish for the control condition DN-Yap$^-$ HS$^+$; n = 3 fish for the DN-Yap$^+$ HS$^+$). (D) Quantification of the bony-ray width; bars on graph correspond to single measurements of each bony-ray of each fish; statistical analysis displayed on graph corresponds to Mann-Whitney test with Mean ± SD (n = 54 bony-rays from 4 animals for the control condition DN-Yap$^-$ HS$^+$; n = 36 bony-rays compiled from 3 animals for the DN-Yap$^+$ HS$^+$). hpa: hours post-amputation; arrowheads define the amputation plane; scale bar: 1 mm; dashed rectangles correspond to magnified panels of calcein stained bony-ray segments for DN-Yap$^-$ HS$^+$ and DN-Yap$^+$ HS$^+$; *: $p < 0.05$, ****: $p < 0.0001$.

We noticed that, conversely to DN-Yap^{-} HS^{+} sibling controls, DN-Yap^{+} HS^{+} animals had a significant decrease in the number of the differentiating Runx2^{+}Osx^{+} osteoblast subtype that populates the patterning zone and proximal blastema region, whereas the Runx2^{+}Osx^{-} progenitor subtype that populates the distal blastema remains unaltered (Figure 34A and B). Consequently, the ratios between both populations were also affected (Figure 34C). A closer look at these markers and to their corresponding location within the blastema (Figure 34A', A'' and Ai), demonstrates that in sibling controls, as expected, proximal regions were populated by the Runx2^{+}Osx^{+} subtype (co-localization of Runx2 and Osx Figure 34A'), whereas the distal blastema is mainly composed of the Runx2^{+}Osx^{-} subtype (poor co-localization of Runx2 and Osx Figure 34A''). In contrast, in DN-Yap^{+} HS^{+} animals, proximal regions, close to the amputation plane, were characterized by the Runx^{+}Osx^{-} subtype (poor co-localization of Runx2 and Osx Figure 34Ai), resembling the pattern of Runx2^{+}Osx^{-} progenitor subtype in distal regions of the blastema of control animals (compare Ai with A'', Figure 34).

For a more detailed analysis, we performed gene expression quantification by q-PCR of DN-Yap^{+} HS^{+} caudal fins at 120 hpa in comparison to sibling controls (Figure 35A). We examined several osteoblast markers that define their maturation state: early progenitor markers, such as *runx2a* and *runx2b*; intermediate markers (immature but committed osteoblasts), such as *osterix* (*osx*) and *collagen 10a1* (*col10a1*); and late/mature markers (bone-forming osteoblasts), like *osteocalcin* (also known as *bone gamma-carboxyglutamate protein*, *bglap*), *osteocalcin2* (also known as *bone gamma-carboxyglutamate protein-like, bglapl*), and *osteonectin* (*osn* or *sparc*) (Li et al. 2009; Knopf et al. 2011; Sousa et al. 2011; Blum and Begemann 2015b; Rutkovskiy et al. 2016). When compared to sibling controls, DN-Yap^{+} HS^{+} animals showed a significant downregulation of the intermediate marker *col10a1* and of mature markers, such as *bglap*, *bglapl* and *osn*, while the expression of early markers was unchanged (Figure 35A). This is in accordance with our previous observation that the number of the differentiating osteoblast population (Runx2^{+}Osx^{+}) is decreased whereas the progenitors (Runx2^{+}Osx^{-}) remain unchanged (Figure 34A and B). From the transcripts analysed, the *col10a1* transcript was the most downregulated. To further validate the q-PCR results, we used a reporter line for *col10a1*, *col10a1*:nlGFP (for further information about the generation of this line see Chapter V of the results section), generated in the context of this PhD thesis. We subjected *col10a1*:nlGFP; DN-Yap^{+} double transgenic animals and *col10a1*:nlGFP; DN-Yap^{-}, sibling controls to the same Yap activity inhibition protocol (Figure 33A). As expected, we observed a significant decrease in *col10a1* fluorescence in *col10a1*:nlGFP; DN-Yap^{+} HS^{+} when compared to *col10a1*:nlGFP; DN-Yap^{-} HS^{+} animals (Figure 35B and C) after normalizing to the total regenerated area.

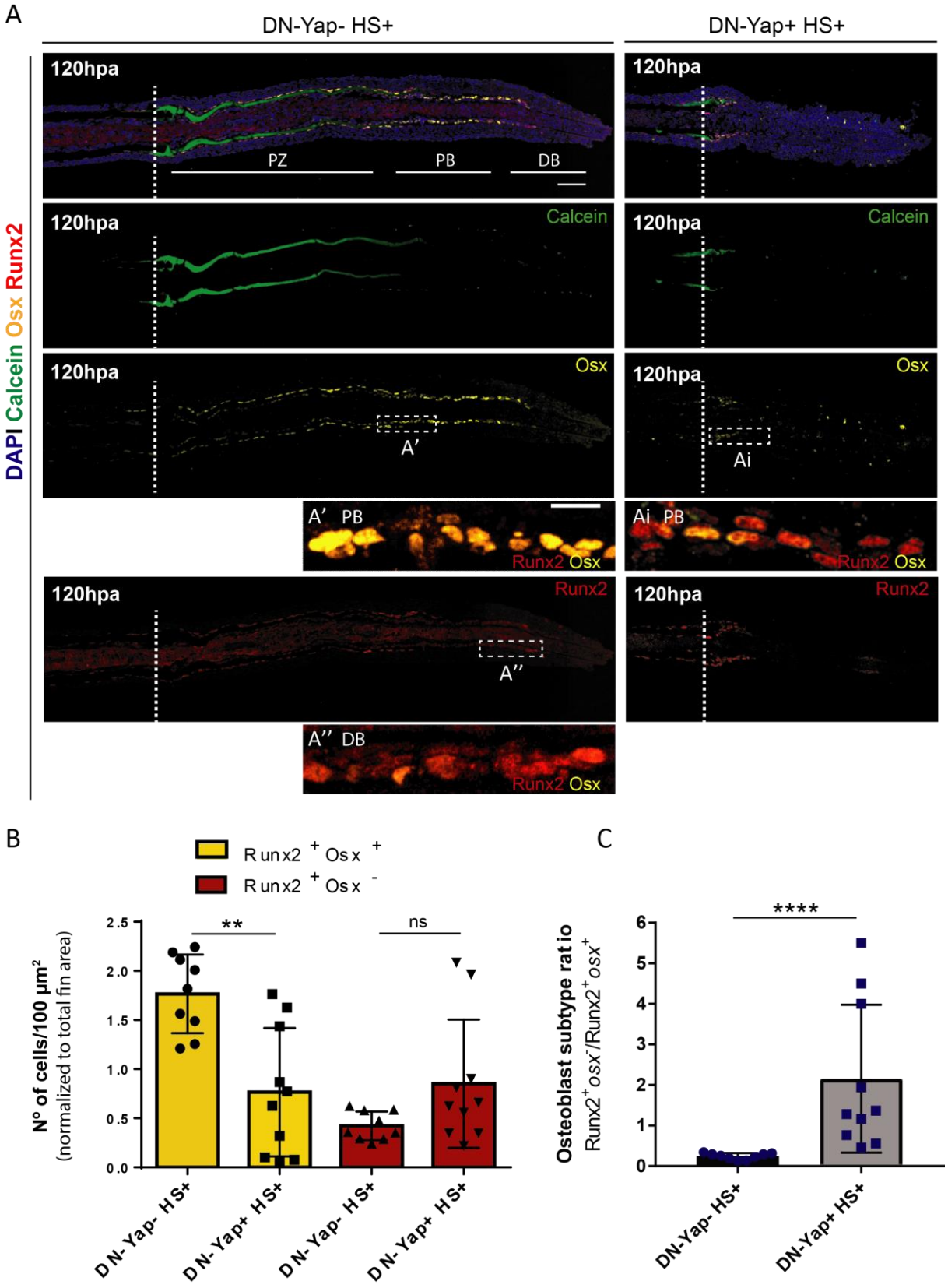

Figure 34: Inhibition of Yap activation leads to a defect in the formation of the differentiating osteoblast subtype during regenerative outgrowth. (A) Representative immunofluorescence images of 120 hpa caudal fins longitudinal cryosections from DN-Yap- HS+ and DN-Yap+ HS+ animals subjected to the protocol illustrated in Figure 33A. Cryosections were immunostained for Osx (immature/intermediate osteoblast marker, yellow) and Runx2 (osteoprogenitor/preosteoblast marker, red) and counterstained for calcein (newly formed bone matrix,

green) and DAPI (nucleus, blue). In contrast to the DN-Yap- HS+ sibling controls, DN-Yap+ HS+ form less bone. (B) Quantification of Runx2+Osx- and Runx2+Osx+ osteoblast subtypes on comparable 120 hpa caudal fin cryosections of DN-Yap- HS+ and DN-Yap+ HS+; bars on graph correspond to total number of cells from each osteoblast subtype normalized to total fin area; statistical analysis corresponds to Mann-Whitney test with Mean ± SD (n = 9 bony-rays from 3 fish for the DN-Yap- HS+ (sibling controls) condition; n = 10 bony-rays from 3 fish for the DN-Yap+ HS+ condition). Activation of the DN form of Yap leads to a decrease in the number of the proliferative Runx2+Osx+- differentiating osteoblast subtype, but not in the Runx2+Osx-. (C) Quantification of the ratio between the Runx2+Osx- and the Runx2+Osx+ osteoblast subtypes at 120 hpa; statistical analysis corresponds to Mann-Whitney test with Mean ± SD (n = 9 bony-rays from 3 fish for the DN-Yap- HS+ (sibling controls) condition; n = 10 bony-rays from 3 fish for the DN-Yap+ HS+ condition). hpa: hours post-amputation; PZ: Patterning zone; PB: Proximal blastema; DB: Distal blastema; dashed lines define the amputation plane; scale bars represent 200 µm and 20 µm in magnified panels; ** p< 0.01, **** p< 0.0001, ns: non-significant.

Taken together, these results suggest that the Hippo/Yap signalling pathway has a clear and important role in bone repair during regenerative outgrowth, which may not solely rely on a general effect on cell proliferation, as described by our lab (Mateus et al. 2015), but also by regulating osteoblast differentiation. Reduction of Yap-mediated signalling led to an impairment in the formation of the Runx2^{+}Osx^{+} differentiating osteoblast subtype, which populates the patterning and proximal blastema regions, and to a decrease in several key intermediate and late osteoblast markers. This reinforces the hypothesis that Yap may be required to induce osteogenic differentiation during regeneration.

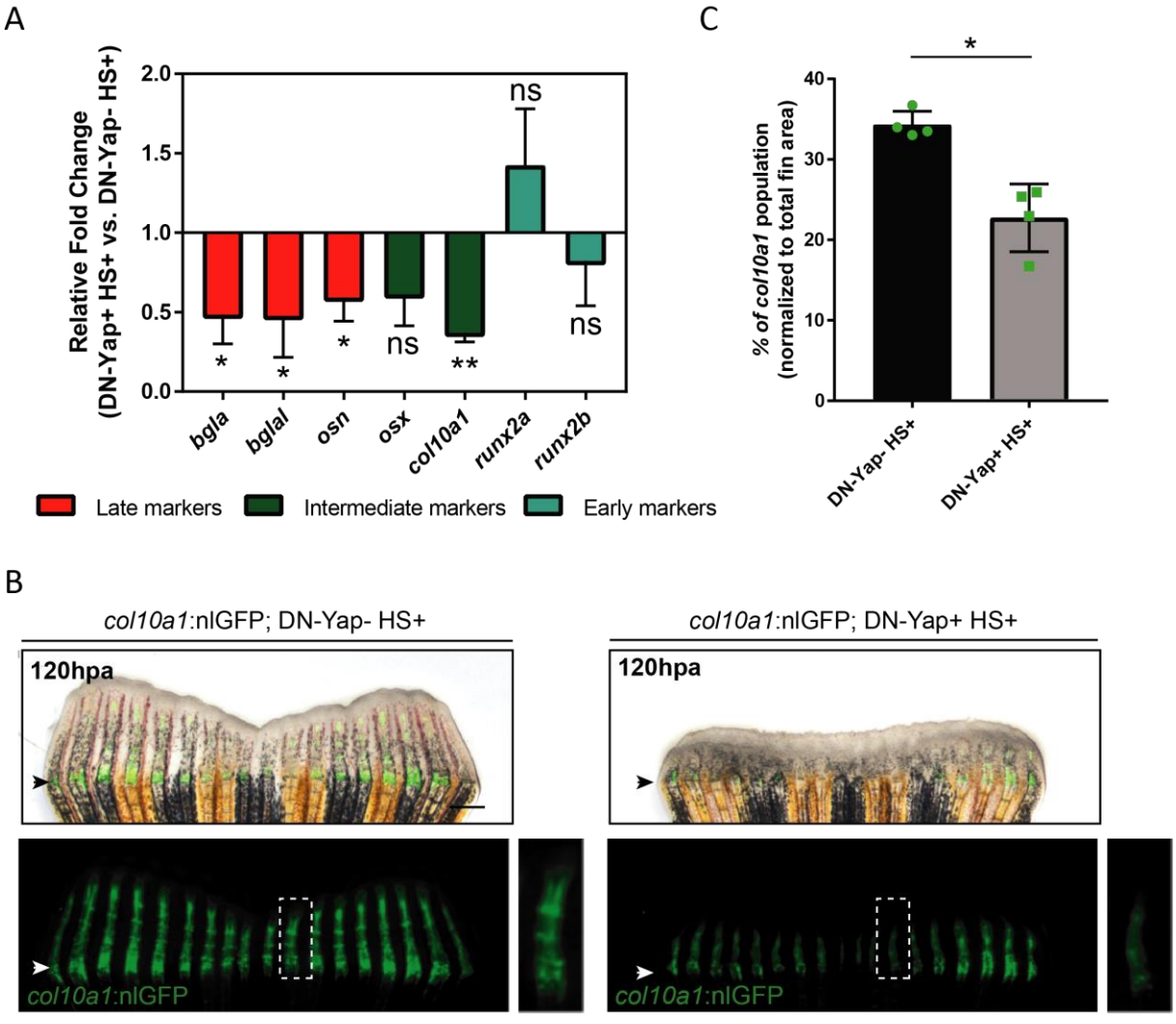

Figure 35: Inhibition of Yap signalling during regenerative outgrowth leads to the downregulation of mature and intermediate bone markers, but not of early markers. (A) Quantitative RT-PCR showing the expression of late/mature, intermediate/immature and early/progenitor osteoblast markers at 120 hpa in DN-Yap^{+}HS^{+} in relation to the DN-Yap^{-} HS^{+} regenerated caudal fins. Transcript levels are plotted on a $\log_2$ scale with DN-Yap^{-} HS^{+} sibling control samples averaged to $\log_2 0 = 1$; statistical analysis displayed on the graph corresponds to Unpaired t test with Welch's correction (4 biological replicates were used, each corresponding to a pool of 4-5 fins). This analysis demonstrates that both late and intermediate markers are downregulated in DN-Yap^{+} HS^{+} caudal fins compared to controls, while early markers remain unchanged. (B) Representative images of 120 hpa whole caudal fins from double transgenic specimens: *col10a1*:nlGFP; DN-Yap^{+} and *col10a1*:nlGFP; DN-Yap^{-} sibling controls. This further confirms that the *col10a1* transcript is diminished in *col10a1*:nlGFP; DN-Yap^{+} animals, in comparison to sibling controls. (C) Quantification of the percentage of *col10a1*:nlGFP fluorescence in *col10a1*:nlGFP; DN-Yap^{+} and *col10a1*:nlGFP; DN-Yap^{-} sibling controls relative to the total regenerate area at 120 hpa; statistical analysis displayed on graph corresponds to Mann-Whitney test with Mean ± SD (n= 4 fish for the control condition *col10a1*:nlGFP; DN-Yap^{-} HS^{+}; n= 4 fish for the *col10a1*:nlGFP; DN-Yap^{+} HS^{+}). Hpa: hours post-amputation; arrowheads define the amputation plane; scale bar represent 1 mm; dashed rectangles correspond to magnified panels of a *col10a1*:nlGFP bony-ray segment in DN-Yap^{-} HS^{+} and DN-Yap^{+} HS^{+}; *: $p < 0.05$, **: $p < 0.01$, ns: non-significant.

2 YAP IS REQUIRED TO REGULATE BONE REPAIR THROUGH A PARACRINE SIGNALLING, CONTROLLING MAJOR SIGNALLING CENTRES DURING FIN REGENERATION

Due to the bone regeneration defects observed after compromising Yap activity, we decided to decipher the molecular mechanism through which Yap regulates the differentiating osteoblast population. We started by addressing the dynamics of Yap subcellular localization in the different osteoblast subtypes. When the Hippo pathway is activated, Yap is phosphorylated and considered to be in an inactive form that culminates in its sequestration in the cytoplasm and degradation. On the other hand, when the Hippo pathway is inactive, Yap is not phosphorylated can be translocated to the nucleus and activate target gene expression (Irvine 2012; Piccolo et al. 2014). Previous work published by our lab showed that Yap is nuclear (mostly active) in proximal regions of the regenerate and more cytoplasmic (mostly inactive) in distal regions (Mateus et al. 2015). However, the intracellular Yap dynamics has only been evaluated at the level of the mesenchymal compartment, and not specifically in the different osteoblast populations (Mateus et al. 2015).

2.1 Yap activation correlates with activated Bmp signalling in the proximal mesenchymal region, adjacent to the differentiating osteoblasts

To fill this gap, we used reporter lines to label different osteoblast populations, *osx*:mCherry (labels immature/intermediate osteoblasts) and *runx2*:GFP (labels the more distal osteoprogenitor pool), and monitored Yap intracellular localization by immunofluorescence in 72 hpa caudal fin cryosections (Figure 36 and Figure 37, respectively). We choose the 72 hpa time-point because the blastema is already fully established and it is the first day of the regenerative outgrowth phase, when the main signalling networks that modulate this phase have been established (Poss et al. 2003; Wehner and Weidinger 2015).

Surprisingly, we found that Yap was excluded from the nucleus (and consequently inactive) of the differentiating osteoblast population, visualised through *osx*:mCherry, either in the patterning zone and in the proximal blastema region (Figure 36A'-Aiii and B'-Biii, arrows in Ai-Aiii and Bi-iii point to examples of Osx^{+} osteoblasts with no nuclear accumulated Yap).

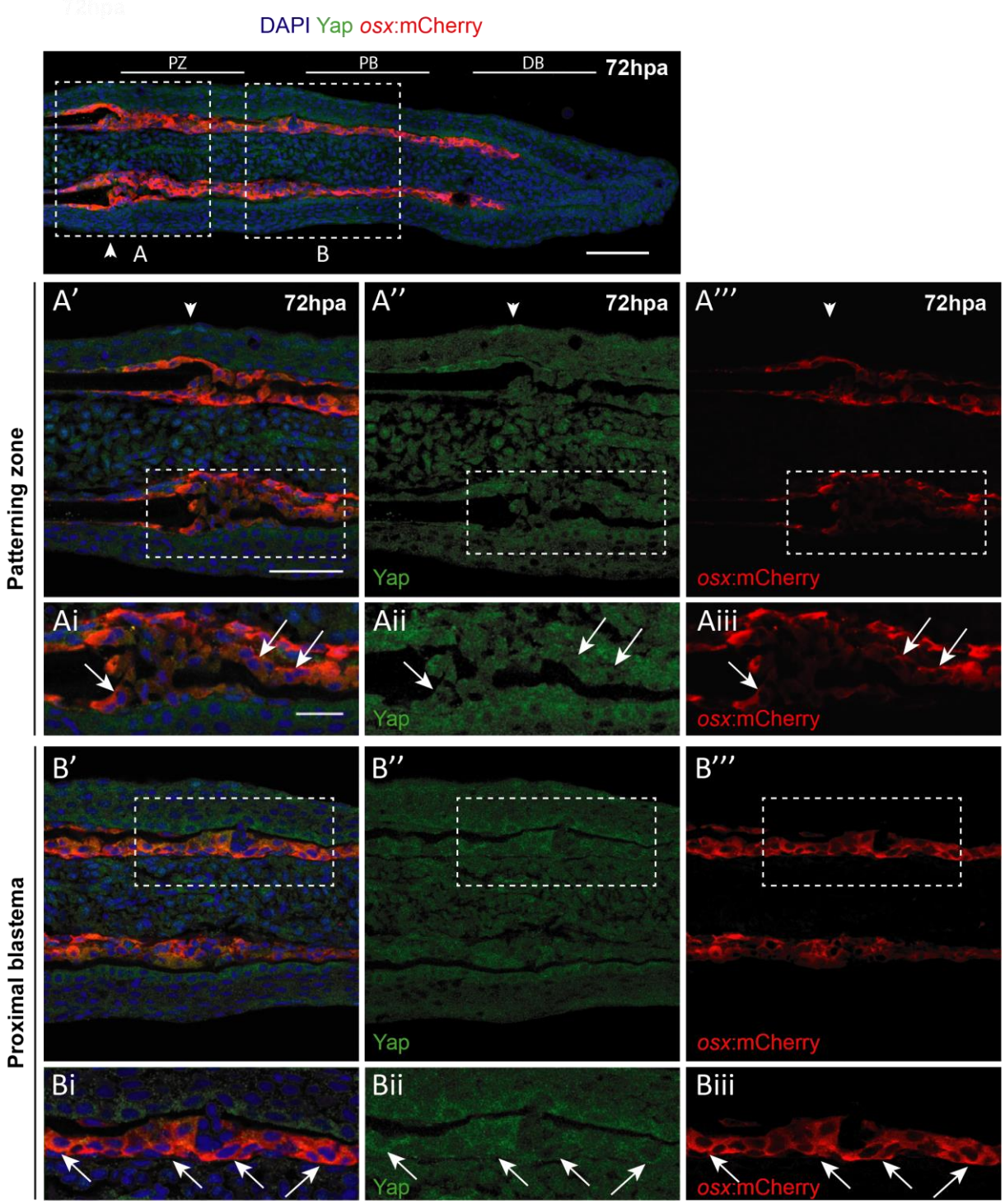

Figure 36: Nuclear Yap (active) does not co-localize with redifferentiating osteoblasts in the patterning zone and in the proximal blastema during regenerative outgrowth. Representative images of 72 hpa longitudinal cryosections of *osx*:mCherry (immature/intermediate osteoblast marker, red) transgenic animals immunostained for Yap (green) and counterstained for DAPI (nucleus, blue). (A'-A''') Magnified panels of the region in A bounded by a dashed white box representing the patterning zone(PZ) of the regenerate. (Ai-Aiii)

Correspondent magnified panels of the regions in A'-A''' bounded by dashed white boxes. Arrows point to examples of *osx*:mCherry-positive osteoblasts in the PZ with Yap excluded from the nucleus. (B'-B''') Magnified panels of the region in B bounded by a dashed white box corresponding to the proximal blastema (PB) region of the regenerate. (Bi-Biii) Corresponding magnified panels of the regions in B'-B''' bounded by dashed white boxes. Overall, these results suggest that Yap is not active in the more proximal osteoblast populations Arrows point to examples of *osx*:mCherry-positive osteoblasts without nuclear Yap. hpa: hours post-amputation; arrowheads define the amputation plane; scale bars in A and B correspond to 200 µm, in A'-A'' and B'-B''' correspond to 50 µm and in Ai-Aiii and Bi-Biii represent 20 µm.

Similarly, when we checked the most distal osteoprogenitor pool, labelled with *runx2*:EGFP, no co-localization between the distal Runx2^{+} progenitors and activated Yap (nuclear) was observed (Figure 37A'-Aiii, arrows in Ai-Aiii point to examples of Runx2^{+} osteoblasts with Yap excluded from the nucleus). This indicates that Yap is not active in both differentiating and progenitor osteoblast populations and therefore suggests that it does not induce directly the differentiation of the osteoblasts during outgrowth.

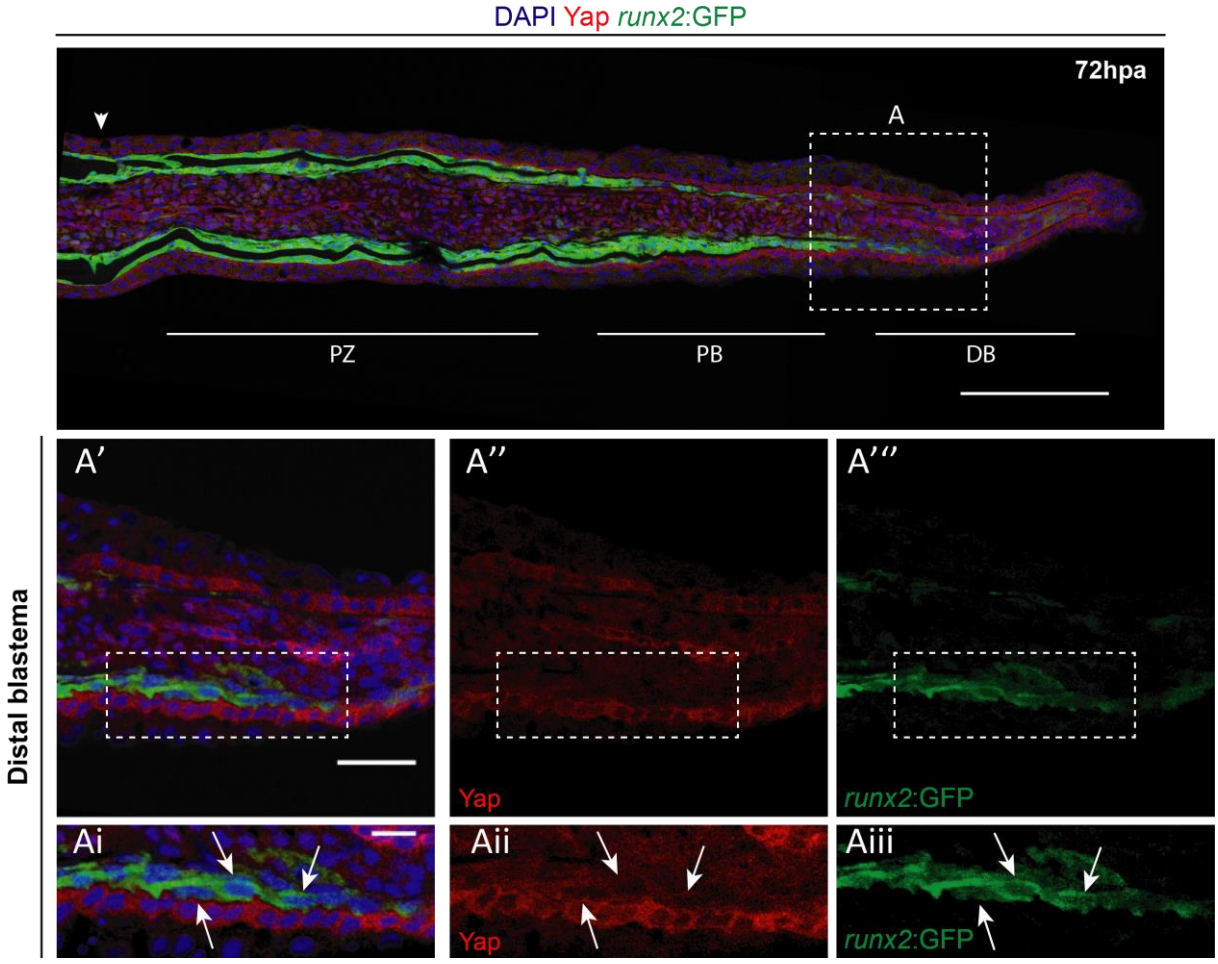

Figure 37: Nuclear Yap (active) does not co-localize with progenitor osteoblast in the distal blastema during regenerative outgrowth. Representative images of 72 hpa longitudinal cryosections of *runx2*:EGFP (osteoprogenitor/preosteoblast marker, green) transgenic animals immunostained for Yap (red) and counterstained for DAPI (nucleus, blue). (A'-A''') Magnified panels of the region in A bounded by a dashed white box representing the distal blastema (DB). (Ai-Aiii) Correspondent magnified panels of the regions in A'-A''' bounded by dashed white boxes. Arrows show *runx2*:EGFP positive osteoblasts in the distal blastema region with Yap excluded from the nucleus. hpa: hours post-amputation; arrowheads define the amputation plane; scale bars in A correspond to 200 µm, in A'-A''' correspond to 50 µm and in Ai-Aiii represent 20 µm.

Thus, this raises the possibility that Yap may regulate the differentiating osteoblast population via a non-cell autonomous manner. To investigate this hypothesis, we examined whether active (nuclear) Yap co-localizes and influences other signalling pathways that are important to maintain and coordinate the balance between osteoprogenitor formation and the rate of differentiation during regenerative outgrowth. As described in the introduction Chapter, osteoprogenitor pool maintenance and osteoblast differentiation along the PD-axis occurs via the establishment of signalling centres with antagonist activities. Briefly, Wnt signalling is active in the more distal blastema and maintains the osteoprogenitor pool, whereas Bmp signalling is active in differentiating osteoblasts, therefore controlling differentiation (Stewart et al. 2014). As regeneration proceeds some $Runx2^{+}$ osteoprogenitors become distant from the influence of Wnt activity and start to redifferentiate in the proximal blastema due to Bmp activity, becoming $Runx2^{+}Osx^{+}$ osteoblasts. In proximal regions Bmp is also responsible to block the propagation of Wnt signalling, restricting its activity to the distal compartment (Stewart et al. 2014; Wehner et al. 2014).

We began by analysing whether Bmp signalling activation correlates with active (nuclear) Yap at the cellular level. Secreted Bmp ligands activate specific Bmp serine/threonine kinase receptors (Bmpr) that in turn phosphorylate Smad1, 5, and 8 (pSmad1/5/8) transcription factors, promoting their nuclear translocation and activation of downstream genes (Wang et al. 2014). We monitored the localization of both Yap and pSmad1/5/8 (pSmad1/5/8), by immunostaining in longitudinal cryosections of wild-type animals at 72 hpa (Figure 38A). In the proximal blastema region, we observed a clear co-localization between Yap and pSmad1/5/8 (both nuclear, active) in the mesenchymal compartment in close contact with differentiating osteoblasts, identified by their epithelial-like organization (Figure 38A, grey dashed box and corresponding magnified panels, arrows point to examples of mesenchymal fibroblasts with both nuclear Yap and pSmad1/5/8 in the proximal blastema region). Conversely, in the distal blastema mesenchyme, both markers show a more diffuse pattern and no nuclear accumulation, except for the nuclear pSmad1/5/8 present in the epidermal compartment (Figure 38A, blue dashed box and corresponding magnified panels of the distal blastema region, arrow points to an epidermal cell with nuclear pSmad1/5/8).

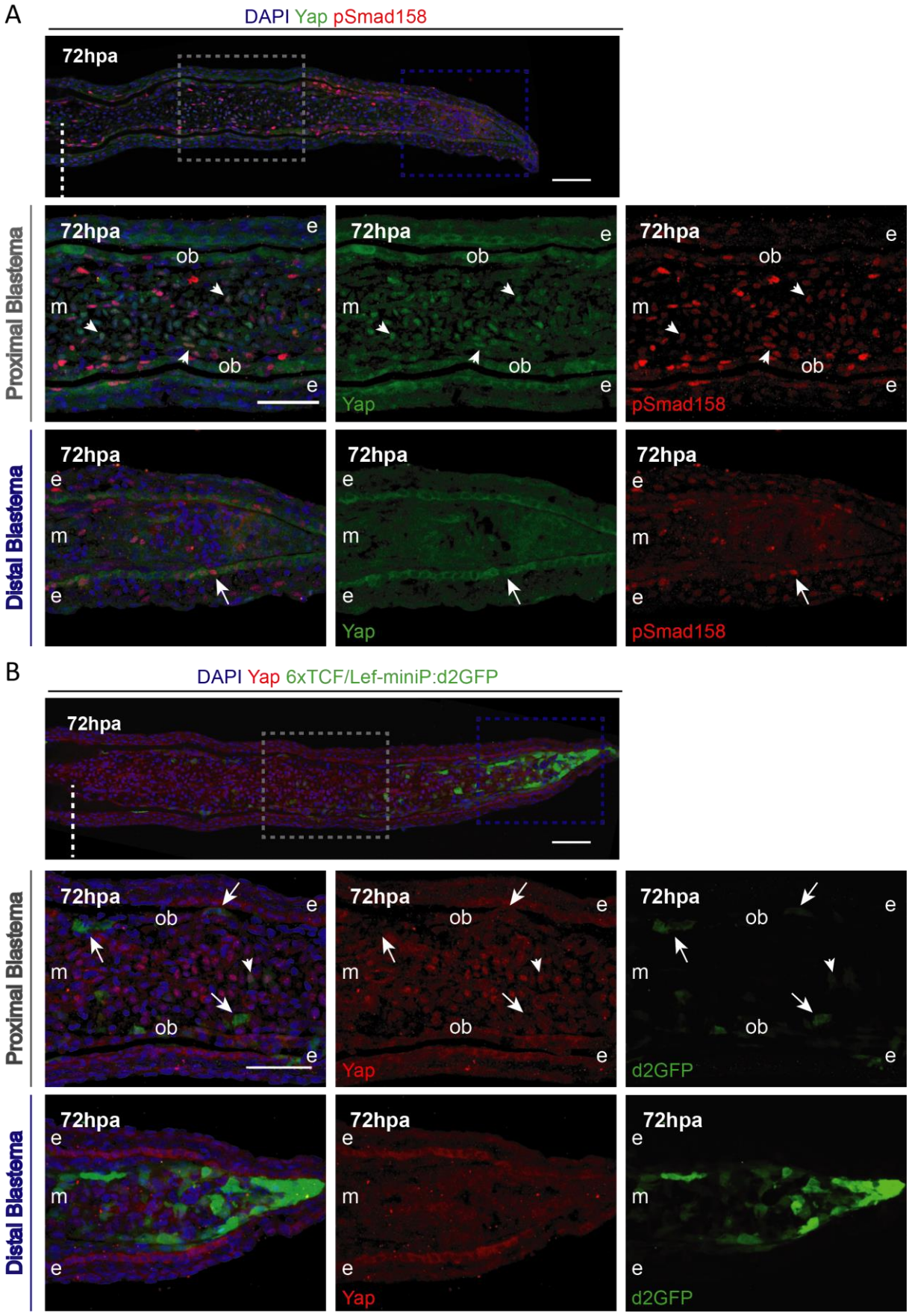

Figure 38: Nuclear Yap co-localizes with active Bmp signalling in the mesenchyme of the proximal blastema region, but not with active Wnt signalling in the distal blastema. (A) Representative images of 72 hpa

longitudinal cryosections of wild-type animals immunostained for Yap (green) and pSmad1/5/8 (active Bmp signalling, red) and counterstained for DAPI (nucleus, blue). Regions bounded by dashed grey and blue boxes are magnifications of the proximal and distal blastema regions, respectively. In the proximal blastema, nuclear Yap and nuclear pSmad1/5/8 co-localize in the mesenchymal compartment, suggesting that both pathways are active. Arrowheads indicate examples of mesenchymal cells with both nuclear Yap and pSmad1/5/8. In the distal blastema, both Yap and pSmad1/5/8 appear to have a fuzzier expression in the mesenchymal compartment, with the exception of pSmad1/5/8 in the epidermis (arrowhead), suggesting that both signalling pathways are less active in that region. (B) Representative images of 72 hpa longitudinal cryosections of *6*xTCF*/Lef-mini*:*d2*GFP (reports Wnt signalling activation, green) specimens immunostained for Yap (red) and counterstained for DAPI (nucleus, blue). Regions bounded by dashed grey and blue boxes are magnifications of the proximal and distal blastema regions, respectively. In the proximal blastema, we observed many mesenchymal cells with nuclear Yap and few cells with activated Wnt signalling, suggesting that both pathways have a poor co-localization index. Arrows point to examples of mesenchymal cells with active Wnt signalling but with Yap excluded from the nucleus; Arrowhead shows an example of a mesenchymal cell with both pathways activated. In the distal blastema, Wnt signalling was activated in many mesenchymal cells but Yap has a fuzzy expression, with no clear nuclear accumulation, suggesting that these pathways play contrasting roles. Hpa: hours post-amputation, m: mesenchyme, e: epidermis, ob: differentiating osteoblasts; dashed lines define the amputation plane; scale bars correspond to 200 μm and 50 μm in magnified images.

Similarly, we examined the activity of canonical Wnt signalling pathway, which is mediated through β-catenin transcription activation (MacDonald et al. 2010), and its dynamics in relation to Yap subcellular localization along the blastema PD axis. For that, we used a transgenic line expressing a Wnt signalling reporter of β-catenin-dependent transcription, the *6xTCF/Lef-miniP:*2dGFP, referred to as *6xTCF:*d2GFP (Shimizu et al. 2012; Wehner et al. 2014). 72 hpa cryosections of *6xTCF:*dGFP animals immunostained for Yap showed that, in the proximal blastema region, where the majority of the mesenchymal cells present nuclear Yap, Wnt signalling was mainly inactive. Wnt activation was only observed in very few scattered cells, either osteoblast (mainly) or mesenchymal cells (Figure 38B, grey dashed box and corresponding magnified panels of the proximal blastema region, arrows). Thus, demonstrating a poor correlation between cells with activated Wnt signalling and cells with nuclear Yap within the proximal blastema region (Figure 38B, grey dashed box and corresponding magnified panels, arrowhead). In contrast, in the most distal blastema compartment, Wnt signalling was active in a high number of cells, whereas Yap was mostly cytoplasmic, thus mainly inactive (Figure 38B, blue dashed box and corresponding magnified panels of the distal blastema region).

Overall, these findings highlight an important role for the transcriptional co-activator Yap during bone repair, specifically during osteogenic differentiation. Although we did not observe any co-localization between activated Yap and osteoblast markers, Yap accumulates in the nucleus of mesenchymal cells in the proximal blastema region just adjacent to the osteoblast differentiation zone, suggesting that Yap regulation of osteoblast differentiation might be via a non-cell autonomous mechanism. Importantly, in this region, Yap nuclear accumulation correlates with activated Bmp signalling, which may imply that these pathways work together in mediating proper osteoblast differentiation but not in maintaining the osteoprogenitor pool. In accordance with this last idea, we observed a very poor correlation between active

Yap and Wnt signalling, suggesting that these pathways may have opposing activities during regenerative outgrowth and thus during bone repair.

2.2 Hippo/Yap signalling pathway may regulate both Bmp and Wnt signalling centres via paracrine signalling during caudal fin regeneration

After proposing that Yap regulation of osteoblast differentiation during regenerative outgrowth is via a non-cell autonomous mechanism, we set out to investigate in more depth how Yap may regulate this process. We performed a gene expression analysis by q-PCR of DN-Yap$^+$ HS$^+$ caudal fins at 120 hpa in comparison to caudal fins from sibling controls, subjected to the Yap manipulation protocol (Figure 33A). In this context, we examined the expression of signalling pathways known to conduct osteoblast lineage specification during caudal fin regeneration (Laforest et al. 1998; Stewart et al. 2014; Wehner et al. 2014; Blum and Begemann 2015b), such as Wnt, Bmp, Shh and RA. The main aim of this experiment was to ascertain whether the expression of any of these pathways is Yap-dependent. We examined several key components that belong to the Wnt (*dkk1a*, *wls*, *wnt10a* and *wnt3a*), Bmp (*bmp2a*, *bmp2b* and *bmp4*), RA (*aldh1a1* and *cyp26a1*) and Shh (*shha*) signalling pathways, known to control bone regeneration dynamics directly or via secondary signals. Indeed, we observed that in caudal fins subjected to downregulation of Yap transcriptional activity (DN-Yap$^+$ HS$^+$) there is a significant reduction in the expression levels of *dkk1a* and *bmp2a* transcripts in comparison to sibling controls (Figure 39). Both Dkk1a and Bmp2a are secreted proteins: Dkk1a is a negative regulator of Wnt-mediated signalling and Bmp2 is a ligand that activates Bmp signalling upon receptor binding (Rosen 2009; MacDonald et al. 2010; Wang et al. 2014). Therefore, these data suggest that Yap can regulate the expression *dkk1a* and *bmp2a* and consequently modulate the activity of both Wnt and Bmp signalling during regenerative outgrowth, respectively. In addition, we noticed a tendency for Wnt ligands, such as *wnt10a* and *wnt3a*, to be upregulated. *aldh1a2* (which encodes for the enzyme that catalyses the synthesis of RA) and *cyp26a1* (that encodes for the enzyme that degrades RA), also showed a tendency to be up and downregulated, respectively, whereas *shha* expression remains unaltered between both conditions. Although more numbers are required to strengthen these results, they suggest that both Wnt and RA signalling may be more activated in the DN-Yap$^+$ HS$^+$ context (Figure 39).

Taken together these results point to a dual role of the Hippo/Yap signalling pathway on the redifferentiation of osteoblasts. On one hand, and similar to what has been shown for Bmp signalling (Stewart et al, 2014), Yap may inhibit Wnt signalling expansion to the proximal blastema region by regulating the expression of *dkk1a* in the proximal blastema, consequently restricting Wnt activation and Runx2$^+$ osteoblasts to the distal blastema. On the other hand, Yap promotes the secretion of Bmp2a by the mesenchymal cells in the proximal blastema region. Secreted Bmp2 ligands then act on adjacent osteoblasts to activate Bmp signalling, and thus, regulating/inducing their differentiation via paracrine signalling.

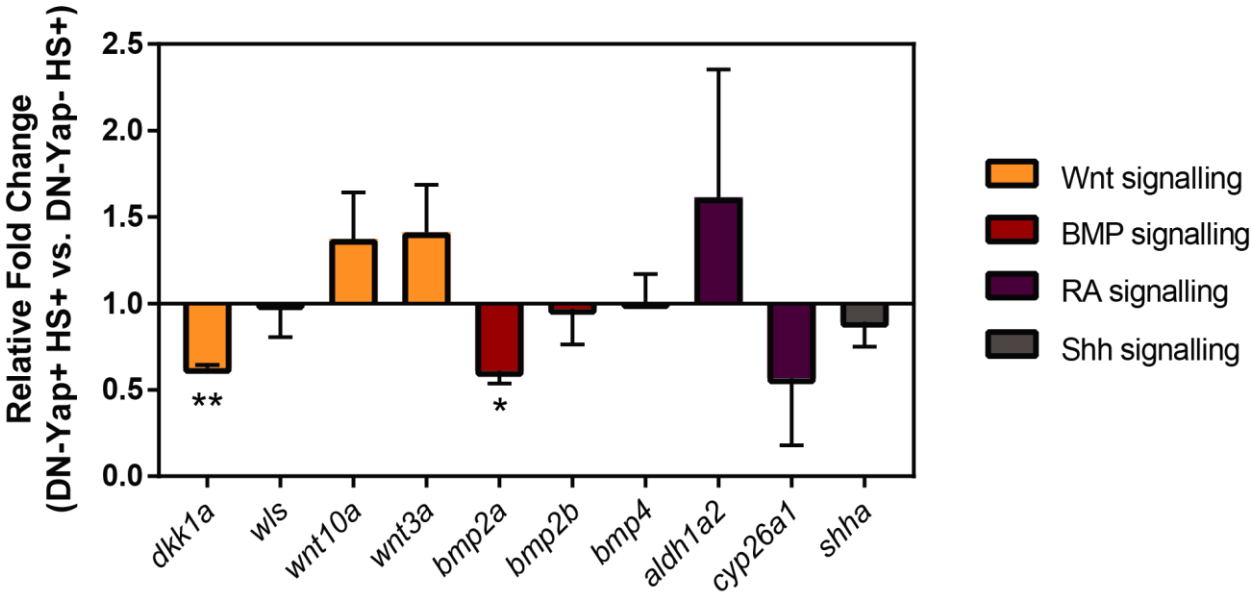

Figure 39: Manipulation of Yap signalling may lead to destabilization of major signalling centres during regenerative outgrowth. Quantitative q-PCR showing the expression of several signalling pathways known to regulate osteoblast populations and growth during regeneration: Wnt signalling (*dkk1a*, *wls*, *wnt10a1* and *wnt3a*), Bmp signalling (*bmp2a*, *bmp2b* and *bmp4*), retinoic acid (RA) signalling (*aldh1a2* and *cyp26a1*) and Sonic hedgehog signalling (*shha*) in DN-Yap^{-} HS^{+} and DN-Yap^{+} HS^{+} regenerated caudal fins, subjected to the protocol illustrated in Figure 33A, at 120 hpa. Graph shows the relative gene expression for each transcript in DN-Yap^{+} HS^{+} in relation to DN-Yap^{-} HS^{+} sibling controls, transcript levels are plotted on a $\log_2$ scale with DN-Yap^{-} HS^{+} sibling controls samples averaged to $\log_2 0 = 1$; statistical analysis displayed on the graph corresponds to Unpaired t test with Welch's correction (4 biological replicates are shown and each replicate corresponds to a pool of 4-5 fins). This analysis demonstrated that in relation to DN-Yap^{-} HS^{+} sibling controls, caudal fins expressing the DN form of Yap, DN-Yap^{+} HS^{+} show a downregulation of *dkka1* (Wnt signalling inhibitor) and *bmp2a* (Bmp receptor ligand), which can disrupt signalling during regeneration and affect bone repair.

Chapter V

OSTEOGENIC PLASTICITY CHALLENGED: UNRAVELING *DE NOVO* OSTEOBLAST SOURCES DURING FIN REGENERATION

“Where should I go?" -Alice.

"That depends on where you want to end up." - The Cheshire Cat.

Lewis Carroll, Alice's Adventures in Wonderland & Through the Looking-Glass

1 BONE SURROUNDING TISSUES MAY PRESENT ALTERNATIVE SOURCES FOR *DE NOVO* OSTEOBLAST FORMATION DURING REGENERATION OF OSTEOBLAST DEPLETED FINS

A key question in the regeneration field focuses on the origin of cells that contribute to the regenerative process. Significant progress has been made in clarifying the source of new cells during regeneration in multiple different regenerative contexts (Tanaka 2003; Kragl et al. 2009; Knopf et al. 2011; Sousa et al. 2011; Tu and Johnson 2011; Sandoval-Guzmán et al. 2014; Tornini et al. 2016; Weidinger 2017). As mentioned in the introduction Chapter, there are several means or routes by which injured tissues can provide new cells to form the regenerated tissue: from resident stem cells and from mature cells dedifferentiation or transdifferentiation (Galliot and Ghila 2010; Poss 2010; Tanaka and Reddien 2011; Eguizabal et al. 2013). Bony-rays, one of the main components of the caudal fin, have been the subject of many research studies, focused in identifying which cells contribute to bone regeneration upon amputation and which cells have the intrinsic or developmental capacity to do so when stimulated or under challenging conditions. Formation of new bone during regeneration has been shown, by us and others, to be dependent on dedifferentiation of mature osteoblasts that remain close to the lesion site (Knopf et al. 2011; Sousa et al. 2011; Tu and Johnson 2011; Stewart and Stankunas 2012). In Chapter III we have also shown in more detail the transcriptional changes associated with this process and dissected some pathways that could be important to regulated dedifferentiation. Surprisingly, another lab has demonstrated, through genetically induced cell death, that after mature osteoblast ablation bone regeneration is not delayed or compromised (Singh et al. 2012). This suggests that dedifferentiation may be dispensable for proper bone regeneration and that in the absence of mature osteoblasts other alternative sources, yet to be identified, may be recruited to form new osteoblasts. In addition, it has been recently identified a reservoir of osteoprogenitors associated with the intersegment/joint regions of the caudal fin that contribute to bone formation, as a complement to mature osteoblast dedifferentiation (Ando et al. 2017). The authors hypothesized that these cells provide an alternative source for *de novo* osteoblast formation in osteoblast depleted fins, however, this is yet to be proven (Ando et al. 2017). Overall, this may indicate that, during regeneration, formation of new osteoblast may depend greatly on different forms of tissue plasticity. Therefore, the main aims of this Chapter are to identify potential cellular sources with the ability to generate new osteoblast, in the absence of mature osteoblast, and the molecular mechanism behind *de novo* osteoblast formation.

1.1 In response to mature osteoblast ablation, tissues adjacent to the bone matrix, epidermis and mesenchyme, initiate a proliferative response during regeneration

In order to address the previous questions, we took advantage of the NTR/Mtz system used to genetically ablate specific cell types in a temporal controlled manner (Curado et al. 2007, 2009). We used the *osx*:mCherry-NTRo transgenic line, referred to as *osx:*NTRo, in which the promoter of *osx* (immature/intermediate specific osteoblast marker) drives the expression of the NTR enzyme thus allowing specific ablation of differentiated and mature osteoblasts (Singh et al. 2012). To reproduce efficient mature osteoblast ablation, we performed a similar protocol to the one previously described (Singh et al. 2012). We combined the osteoblast ablation line with a mature osteoblast reporter line, *osc*:EGFP, and observed that the *osx:*NTRo successfully induced the efficient ablation of *osc*-expressing cells(Singh et al. 2012). Double transgenic animals, *osx:*NTRo; *osc*:EGFP, were incubated for one day either with the drug vehicle DMSO (control) or with Mtz solution and left to recover for two days. Caudal fins were imaged prior to the treatment and after the recovery period, to monitor proper osteoblast ablation (Figure 40A). In contrast to control animals, which show intense and demarcated *osx* or *osc* expression along the bony-rays surface prior to the treatment and after recovery, Mtz treated animals show a strong decrease in both markers (Figure 40B). In accordance with what had been demonstrated, this strategy effectively promotes mature osteoblast ablation and can be used to investigate the origin of cells capable of generating new osteoblasts in the absence of the mature osteoblast population.

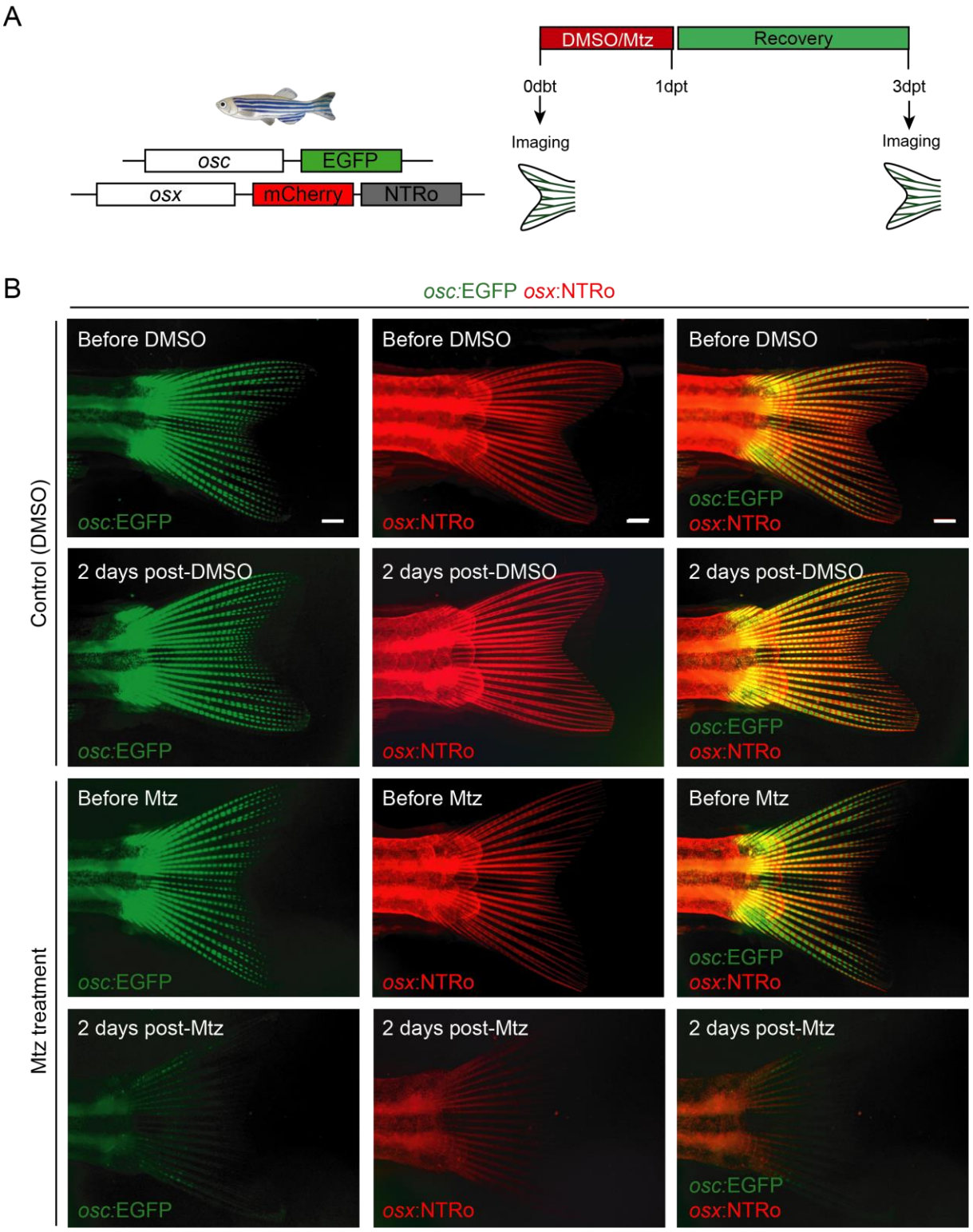

Figure 40: Osteoblasts ablation assay. (A) Schematic representation of the experimental outline used to induce osteoblasts ablation. This procedure is based on the NTR/MTZ system and relies on a transgenic line that expresses the coding regions of the fluorescent reporter mCherry and the Nitroreductase (NTR) enzyme under the control of *osterix* (*osx*, specific osteoblast marker) regulatory regions, *osx*:mCherry-NTRo (*osx:*NTRo). In this protocol we combined the osteoblast ablation line with a reporter line that labels mature osteoblast, *osc*:EGFP, to confirm proper mature osteoblast ablation. The *osc*:EGFP; *osx:*NTRo double transgenics were either exposed to a pro-drug Metronidazole (Mtz) or to the vehicle (DMSO) for one day and left to recover for two days. (B) Representative images of caudal fins from control and Mtz treated animals before manipulation and after the recovery period. We can observe that while in control animals *osx* and *osx* expression remains unchanged during

the procedure, in Mtz treated animals there is a strong decrease in both markers, confirming correct mature osteoblast ablation. Green: *osc*:EGFP; Red: *osx:*NTRo. dbt: days before treatment; dpt: days post-treatment Scale bar represents 1mm.

For subsequent experiments, animals with efficient osteoblast ablation were subjected to caudal fin amputation. We started by analysing which cells and/or tissues responded to osteoblast ablation by initiating a proliferative response. For that, we determined EdU incorporation (S-phase marker) upon osteoblast ablation. Following the recovery period, both control (DMSO) and Mtz treated animals were subjected to caudal fin amputation and allowed to regenerate until desired time-points (Figure 41A). Uncut (0 hpa), 15 hpa and 24 hpa caudal fins from both experimental conditions were collected, cryosectioned and immunostained for mCherry (to visualize *osx* expression and validate osteoblast ablation) and EdU (to label S-phase proliferating cells). Already before amputation (uncut), we observed significantly more proliferating cells, EdU^+, in the epidermis of Mtz treated caudal fins, contrasting to controls (Figure 41B', C' and D). At 15 hpa this discrepancy becomes more evident, with a significant increase in the number of EdU^+ cells in the epidermis and mesenchyme (already detected at 6 hpa, Figure 41D) of Mtz treated animals (Figure 41B'', C'' and D). We could also notice that at 15 hpa these EdU^+ cells seem to appear more frequently at the interphase of the bone with the surrounding tissues, epidermis and mesenchyme. At 24 hpa control and Mtz-treated fish no longer show significant differences in the number of EdU-positive cells (Figure 41B'', C''' and D). The initial differences regarding the number and location of proliferating cells, between controls and Mtz, treated animals, could be due to a response of the surrounding tissues to the osteoblast induced cell death. In fact, dying cells can release a vast range of molecules and particles that can influence and trigger a proliferative response by the neighbouring cells (Boland et al. 2013; Vriz et al. 2014; Perez-Garijo and Steller 2015). Nevertheless, it may also mean that the bone adjacent tissue could contribute to bone formation, by replacing the bone surrounding osteoblasts that were lost after ablation.

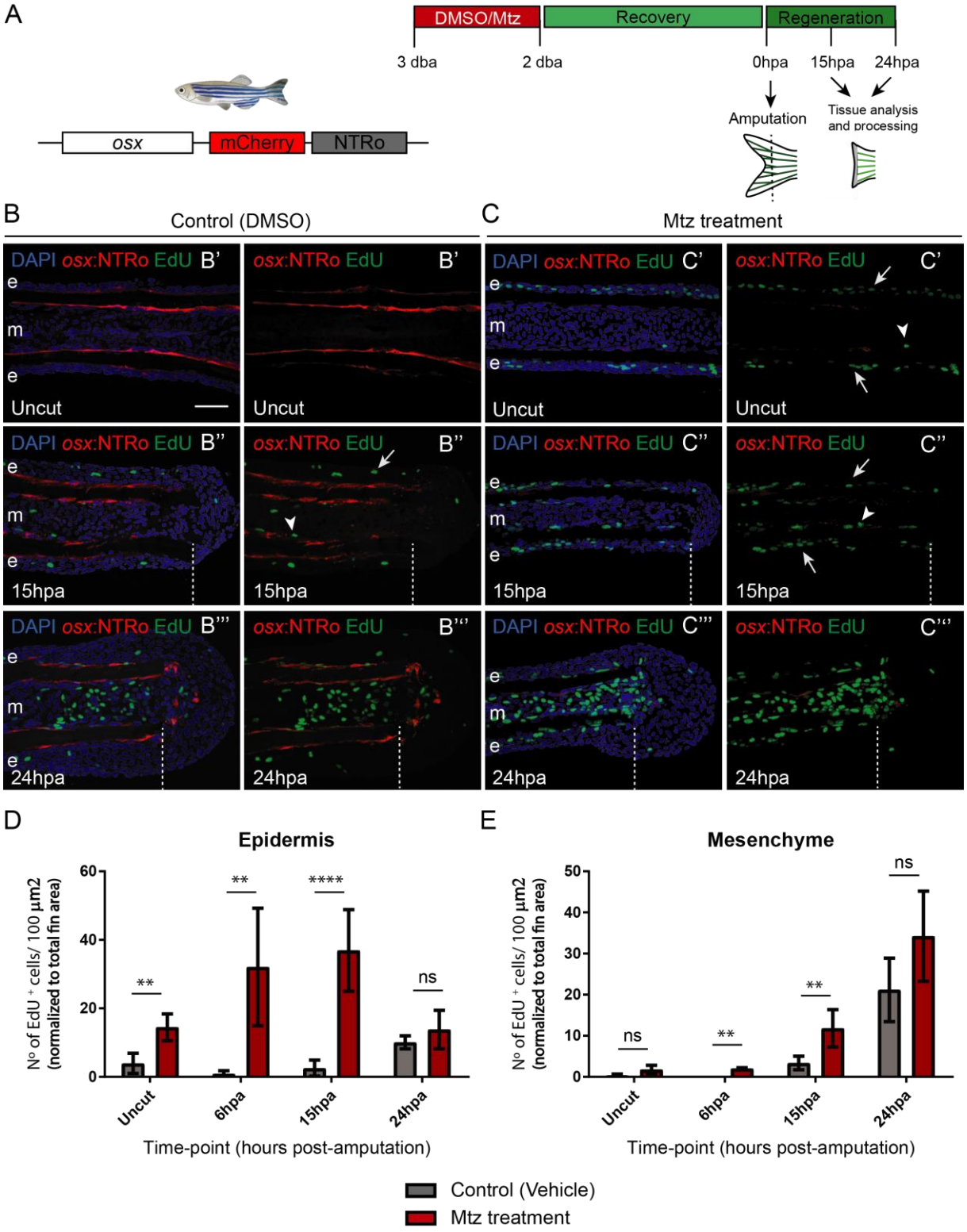

Figure 41: Mesenchymal and epidermal tissues adjacent to the bone matrix respond to osteoblast ablation by initiating a proliferative response during regeneration. (A) Schematic representation of the strategy used to induce osteoblasts genetic ablation. The *osx*:mCherry-NTRo (*osx:*NTRo) transgenic animals were either exposed to the vehicle (DMSO) (B) or to the pro-drug Metronidazole (Mtz) (C) for one day and left to recover for two days. Caudal fins were then amputated, and tissue imaged or collected for subsequent processing. (B and C) Assessment of cell proliferation in osteoblast depleted fins. Representative images of uncut (B' and C'), 15 hpa (B'' and C'') and 24 hpa (B''' and C''') caudal fin longitudinal cryosections of *osx:*NTRo animals subjected to DMSO (controls) (B) or Mtz (C) incubations. Cryosections were immunostained for mCherry (to visualize *osx* expression

and confirm correct osteoblast ablation, red), EdU (S-phase marker, green) and counterstained for DAPI (nucleus, blue). We can observe that already before amputation (uncut) there are more cells proliferating in the epidermis of Mtz treated caudal fins, contrasting to controls (C' and B', respectively). At 15 hpa this discrepancy becomes more evident also in the mesenchymal compartment (B'' and C''). At 24 hpa many cells have entered the S-phase in both conditions (B''' and C'''). Arrows indicate examples of proliferating cells adjacent to the epidermis and arrowheads point to examples of proliferating cells in the mesenchyme. (D and E) Proliferation dynamics in the caudal fin epidermis (D) and mesenchyme (E). Graphs show the quantification of EdU-positive cells in uncut, 6 hpa, 15 hpa and 24 hpa time-points in controls and osteoblast depleted fins (Mtz treatment); bars on graph correspond to total number of EdU^+ cells normalized to total fin area; statistical analysis corresponds to Mann-Whitney test with Mean ± SD displayed (n= 9 bony-rays compiled from 3 fish for each time-point and for each condition (control and Mtz treatment)). This shows that, accordingly to the images represented in B and C, there is an increase of epidermal cell proliferation in the uncut and in the first time-points analyzed after amputation in the Mtz treated condition, when compared to controls. There is also a peak of proliferation at 6 hpa and 15 hpa in the mesenchymal compartment, just adjacent to the bone matrix when compared to controls. dba: days before amputation, hpa: hours post-amputation, e: epidermis, m: mesenchyme; dashed lines define the amputation plane; scale bars represent 50 μm; ** p< 0.01, **** p< 0.0001, ns: non-significant.

1.2 New osteoprogenitors arise at the outer and inner interphase between the bone matrix and the surrounding tissues in osteoblast depleted fins during regeneration

We then examined from where new osteoprogenitors may arise in osteoblast depleted fins during regeneration. Runx2 is the first transcription factor required for determination of the osteoblast lineage, being first detected in preosteoblasts/osteoprogenitors and consequently directing their commitment (Komori 2006; Long 2012; Rutkovskiy et al. 2016). This factor is expressed throughout the osteoblast developmental stages, from early to mature, and co-localizes with both *osx* and *osc* in the mature osteoblast population surrounding the bony-ray surface (see Supplementary Figure 3). Thus, to facilitate the interpretation of the results, we will define the differentiated and mature osteoblast population, ablated using the NTR/Mtz system, as $Runx2^+Osx^+$ and the osteoprogenitors as $Runx2^+Osx^-$. For that, we performed immunostainings for Runx2 in cryosections of control and Mtz treated *osx:*NTRo animals at uncut (0 hpa), 15 hpa and 24 hpa time-points. We can observe that, while in control uncut fins only mature osteoblast ($Runx2^+Osx^+$) surround the bone tissue (Figure 42A' and C), in Mtz uncut fins these cells were efficiently ablated (Figure 42B' and C). Interestingly, some osteoprogenitors $Runx2^+Osx^-$ start to emerge at the interphase between the bone matrix and the epidermis in Mtz treated fins (Figure 42B' arrows and D). At 15 hpa, Mtz conditions present a significant increase in the number of newly formed $Runx2^+Osx^-$ osteoprogenitors, which appear mostly next to the epidermis and mesenchymal compartment at the interphase with the bone surface (Figure 42B'' arrows and arrowheads, respectively, and D). In controls, although they were not subjected to osteoblast ablation, some $Runx2^+$ single positive cells were also observed in the mesenchymal compartment (Figure 42A''arrows and D). At 24 hpa in the control condition both mature $Runx2^+Osx^+$ and osteoprogenitor $Runx2^+Osx^-$ cells seem to contribute to the blastema formation process (Figure 42A''' arrows and arrowheads, C and D), while in the Mtz condition only newly formed $Runx2^+Osx^-$ contribute to the process (Figure 42B''' arrows and arrowheads, D). These $Runx2^+Osx^-$ osteoprogenitors that arise in the ablation context were sufficient to compensate for the lack of mature osteoblast, since in the

regenerating caudal fin the total osteoblast number ($Runx2^{+}Osx^{+}$ together with $Runx2^{+}Osx^{-}$) remained the same or even higher (depending on the time-point) in the ablation context (Figure 42C and D). We also confirmed the specificity of the Runx2 labelling with the commercially available antibody, through co-localization with a reporter line for *runx2*, *runx2*:EGFP, in the ablation context. Thus, confirming that these cells are indeed osteoprogenitors (see Supplementary Figure 4). Given the fact that $Runx2^{+}Osx^{-}$ osteoprogenitors appear not only in osteoblast ablation conditions but also in a normal regenerative situation, this may suggest that alternative progenitor sources are also recruited during normal regeneration and not only upon osteoblast ablation. We have to consider the possibility that, during normal regenerating conditions, these $Runx2^{+}Osx^{-}$ osteoprogenitors may derive from the dedifferentiation of the mature osteoblast or even from the pool of osteogenic precursors recently found in the joint region (Ando et al. 2017).

Overall, this suggests that bone neighbouring cells could contribute as a source of *de novo* osteoblast formation when the mature osteoblast population is compromised. The epidermis and the mesenchyme in close contact with the bone matrix may be stimulated to proliferate and produce new osteoprogenitors that will replenish the outer (facing the epidermis) and the inner (facing the mesenchyme) bone surface with new osteoblast, thus contributing to the bone regenerative process.

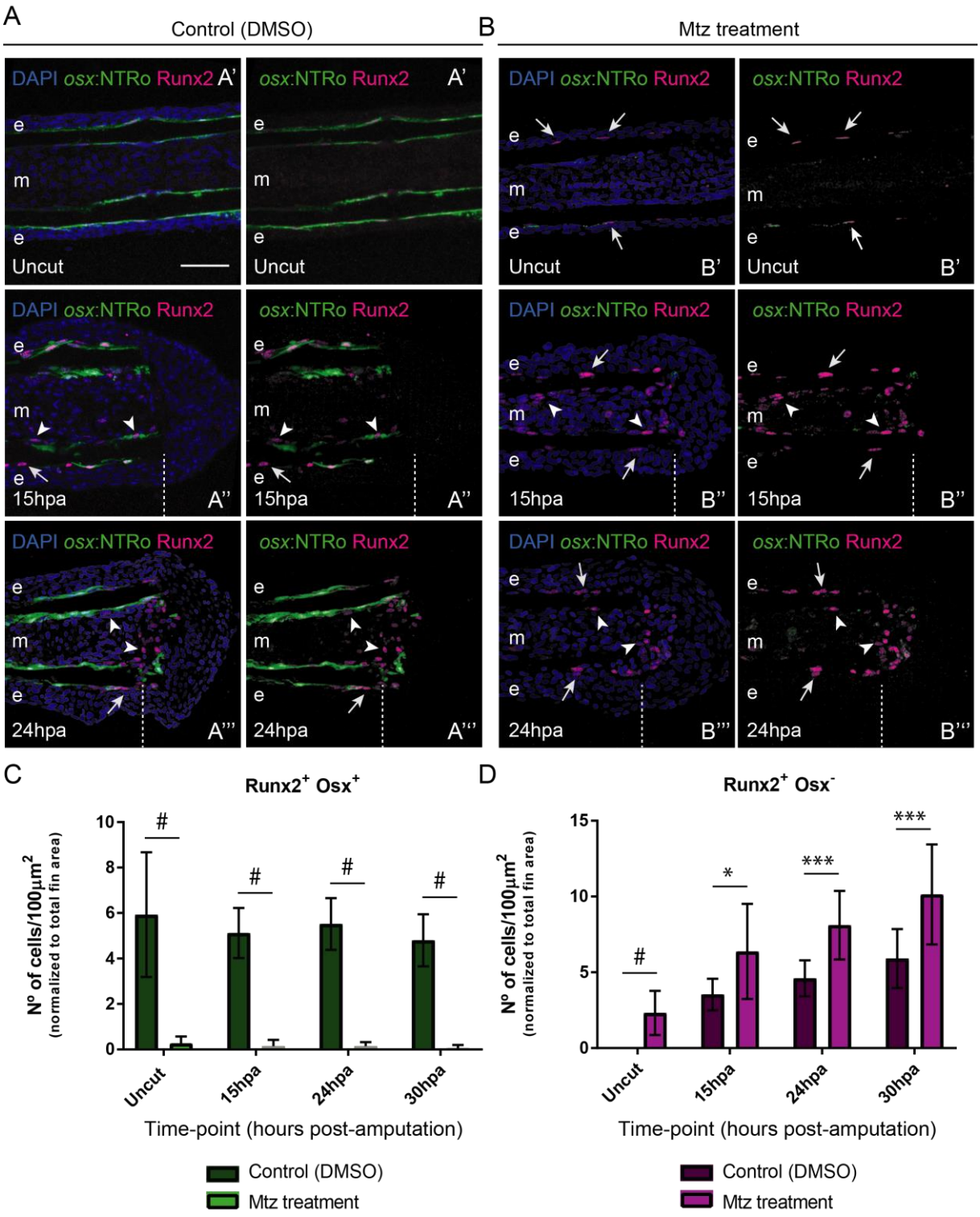

Figure 42: Osteoblast ablation reveals that osteoprogenitors emerge *de novo* at the interphase between the bone matrix and the adjacent tissues during regeneration. (A and B) Assessment of osteoprogenitors appearance in controls (A) and in osteoblast depleted fins (B). Representative images of uncut (A' and B'), 15 hpa (A'' and B'') and 24 hpa (A''' and B''') caudal fin longitudinal cryosections of *osx:*NTRo animals subjected to DMSO (controls) (A) or Mtz incubations (B). Cryosections were immunostained for mCherry (to visualize *osx* expression, green), Runx2 (preosteoblast/osteoprogenitor marker, magenta) and counterstained for DAPI (nucleus, blue). While in control uncut fins only mature osteoblasts ($Runx2^{+}Osx^{+}$) surround the bone tissue, in Mtz treated animals these cells are efficiently ablated and osteoprogenitor $Runx2^{+}Osx^{-}$ cells start to emerge at the interphase between the bone matrix and the epidermis. At 15 hpa, in Mtz treated animals, there is a huge increase in the number of newly formed $Runx2^{+}$ single osteoprogenitors that appear mostly in close contact with the outer

(facing the epidermis) and inner (facing the mesenchyme) bone surface. In controls, some Runx2$^+$ single positive cells are also observed. At 24 hpa in the control situation both Runx2$^+$Osx$^+$ (mature osteoblasts) and Runx2$^+$Osx$^-$ (osteoprogenitors) can be identified close to the stump, while in the Mtz condition only newly formed Runx2$^+$Osx$^-$ seem to contribute to blastema formation. Arrows indicate examples of Runx2$^+$ single osteoprogenitors facing the epidermis and arrowheads point to examples of Runx2$^+$ single osteoprogenitors in the mesenchymal compartment. (C and D) Quantification of mature osteoblasts (Runx2$^+$Osx$^+$) (C) and osteoprogenitors (Runx2$^+$Osx$^-$) (D) in uncut, 15 hpa, 24 hpa and 30 hpa in controls (DMSO) and in osteoblast depleted fins (Mtz treatment); bars on graph correspond to total number of osteoblasts quantified and normalized to total fin area; statistical analysis corresponds to Mann-Whitney test with Mean ± SD displayed (n= 14 bony-rays compiled from 4 fish for each time-point and for each condition). In agreement with the images represented in A, there is a clear decrease of mature osteoblast (Runx2+Osx+) when using the ablation protocol shown in Figure 40A. Additionally, there is a considerable increase in the number of newly formed osteoprogenitors in all time-points examined in the Mtz treatment condition when comparing to control animals. hpa: hours post-amputation, e: epidermis, m: mesenchyme; dashed lines define the amputation plane; scale bars represent 50 µm; *p<0.05, ** p< 0.01, ***p<0.001, # p< 0.0001, ns: non-significant.

2 IDENTIFYING THE CELLULAR SOURCES FOR *DE NOVO* OSTEOBLAST FORMATION DURING FIN REGENERATION: CONTRIBUTION OF THE EPIDERMIS AND MESENCHYME

After identifying bone surrounding tissues, epidermis and mesenchyme, as potential sources for newly formed osteoblasts in fins lacking mature osteoblast during caudal fin regeneration, a more thorough analysis was required. We proposed to access the importance and contribution of both populations using a combination of co-localization analysis and, more importantly, lineage tracing technology based on the binary tamoxifen-inducible Cre/LoxP-system. Lineage tracing enables to irreversibly label these specific cell populations in a given time-window, allowing to fate map their progeny over time during regeneration (Carney and Mosimann 2018), thus being a crucial tool for the purpose of this work.

2.1 Caudal fin stratified epidermis does not seem to contribute for *de novo* osteoblast formation during regeneration

Following the previous results, we aimed to determine whether Runx2$^+$ cells that arise at the outer bone surface, facing the caudal fin epidermis, after osteoblast ablation during regeneration, are derived from the epidermal tissue. We were particularly interested in the basal epidermal cell layer which is known to encompass basal keratinocytes with stem cell-like properties (Lee et al. 2014; Chen et al. 2016a), thus being more easily prone to change cell fate and commit to the osteoblast lineage. We started by performing co-localization studies with an epidermal marker, p63, a key regulator of epidermal stratification and keratinocyte proliferation and differentiation (Mills et al. 1999; Yang et al. 1999a). osx:NTRo animals were incubated with DMSO (controls) or Mtz, and 24 hpa caudal fin longitudinal cryosections were immunostained for Runx2 and p63. This experiment revealed that either in a normal regenerating condition (Figure 43A and Ai) or in osteoblast depleted fins (Figure 43B and Bi), there is no co-localization between Runx2$^+$Osx$^+$ osteoblasts or Runx2$^+$Osx$^-$ osteoprogenitors with p63, suggesting that the epidermis does not contribute to *de novo* osteoblast formation.

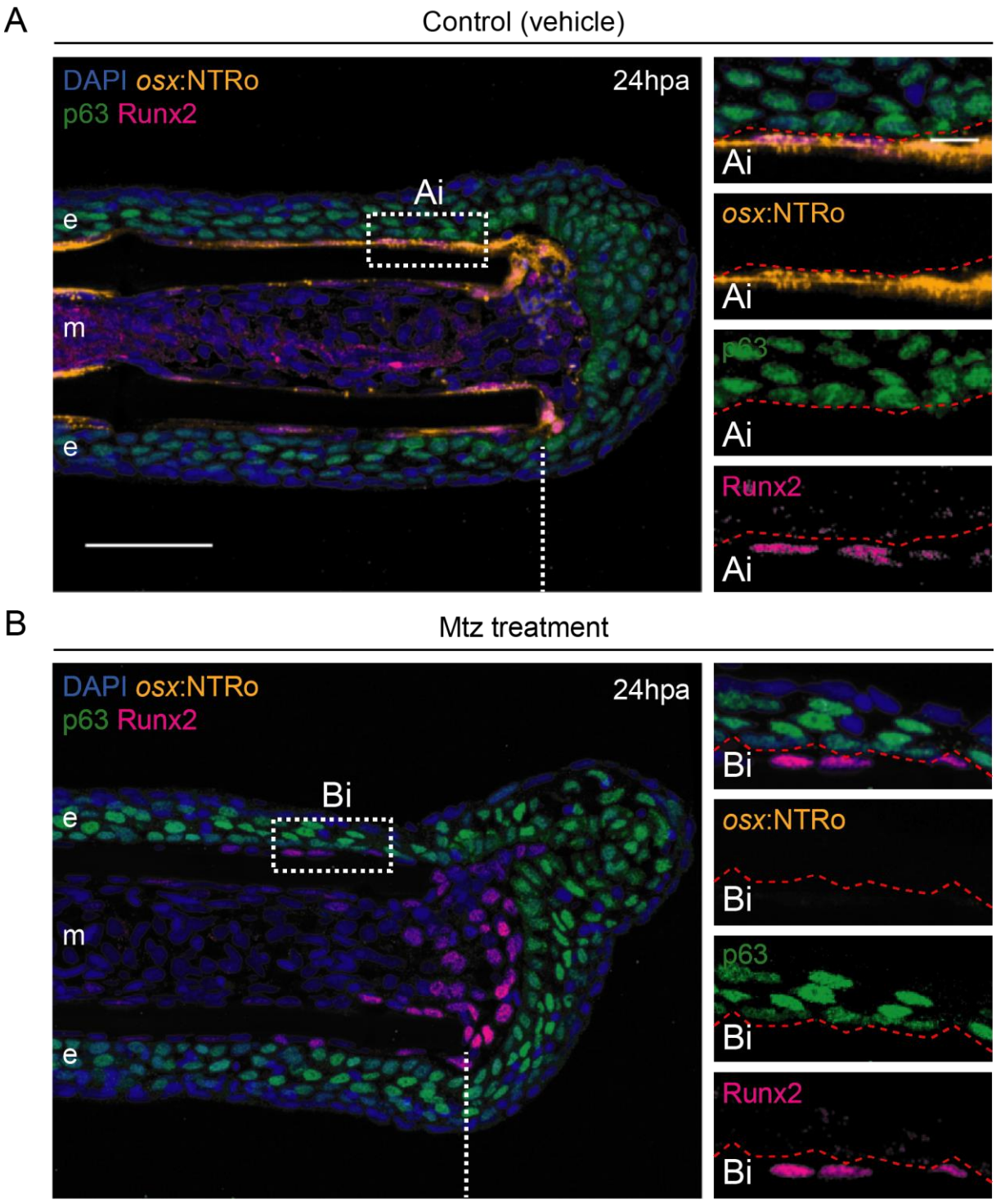

Figure 43: Newly formed osteoprogenitors at the interphase with the epidermal compartment do not have epidermal properties. Representative images of 24 hpa caudal fin longitudinal cryosections of *osx:*NTRo from (A) control animals and (B) animals subjected to Mtz treatment. Sections were immunostained for mCherry (to visualize *osx* expression, orange), p63 (a *bona fide* epidermal marker, green), Runx2 (preosteoblast/ osteoprogenitor marker, magenta) and counterstained for DAPI (nucleus, blue). In control caudal fins, the mature osteoblast population, $Runx2^{+}Osx^{+}$, that surround the bone surface adjacent to the epidermis, present no co-localization with p63 (magnified panels in Ai). In caudal fins with ablated mature osteoblast, the osteoprogenitors $Runx2^{+}Osx^{-}$, that emerge near the bone surface next to the epidermal compartment, are not positive for the epidermal marker p63 (magnified panels in Bi). This suggests that newly formed osteoprogenitors that emerge at the epidermal site and epidermal cells have different cellular identities. hpa: hours post-amputation; dashed

white lines define the amputation plane; dashed boxes delimitate magnified panels Ai and Bi; dashed red lines delimitate the epidermal compartment; scale bars represent 50 µm or 10 µm in magnified panels in Ai and Bi.

To further address a possible contribution of the caudal fin stratified epidermis, specifically the basal keratinocytes, to osteoblast formation in osteoblast depleted fins, we carried out transgenic lineage tracing experiments based on Cre/LoxP-system (Hans et al. 2009; Mosimann et al. 2011; Carney and Mosimann 2018). For that, we used a transgenic line that expresses the tamoxifen-inducible Cre recombinase under the control of a basal keratinocyte specific gene promoter, *krtt1c19e,* referred as *krt19* (Fischer et al. 2014; Lee et al. 2014). We combine the *krt19*:CreERT2 line with a red-to-green switch line, the *β-actin2*:loxP-dsRed-STOP-loxP>EGFP, referred to as *β-actin2*:RSG. If the inducible Cre is not activated by tamoxifen, this line expresses dsRed under the control of the *β-actin2* promoter, but the expression changes to EGFP upon a successful recombination event mediated by tamoxifen administration. We started by testing the lineage tracing protocol for the basal keratinocytes fate mapping as previously described (Fischer et al. 2014). For that, we treated krt19:CreERT2; β-actin2:RSG embryos with tamoxifen (4-OHT) or its vehicle control (EtOH) from 24 to 96 hpf (Supplementary Figure 5A). After the incubation period, it is possible to observe that at 96 hpf *krt19*: CreERT2; *β-actin2*: RSG larvae incubated with 4-OHT, some basal layer cells from the embryonic epidermis were EGFP-positive, while in control larvae no EGFP was observed (Supplementary Figure 5B). These larvae were grown in the circulating system until adulthood and, at three to four months post fertilization animals previously treated with 4-OHT showed $EGFP^+$ epidermal cluster/clones throughout the body axis, including the caudal fin. The appearance of clones rather than whole epidermis labelling can be explained by inefficient tamoxifen-mediated recombination, meaning that not all basal keratinocytes have undergone the switch (Supplementary Figure 5C and Cii). These clones have derived from the embryonic basal epidermal cells that were labelled after 4-OHT treatment, like previously described (Lee et al, 2014). Importantly, after performing caudal fin amputation in a region positive for these clones, we observed EGFP expression all over the regenerated area (Supplementary Figure 5D). With this, we have shown that the protocol is suitable to analyse the contribution of the epidermis to the regenerative process.

We then combined the lineage tracing procedure with the osteoblast ablation protocol (Figure 44A), to evaluate the contribution of the epidermis for new osteoblast formation during regeneration, in an osteoblast ablation context. For that, we combined *krt19*: CreERT2; *β-actin2*: RSG double transgenic with the osteoblast ablation line, generating *krt19*: CreERT2; *β-actin2*: RSG; *osx:*NTRo triple transgenics. These animals were treated at larval stages with 4-OHT and left to grow until adult stage. At this point, they were subject to the ablation protocol (Figure 41A) and incubated with either DMSO (control) or with Mtz. After the recovery period, caudal fins were amputated and left to regenerate until 72 hpa, stage of the regenerative outgrowth when many osteoblasts have already been formed and differentiated to create the new fin bony-rays (Figure 44A). We then performed cryosections of 72 hpa caudal fins from

control animals subjected to the epidermal fate-mapping but not to osteoblast ablation (krt19:CreERT2; β-actin2:RSG; osx:NTRo +4-OHT +DMSO) and animals subjected to both fate-mapping and osteoblast ablation protocols (krt19:CreERT2; β-actin2:RSG; osx:NTRo +4-OHT +Mtz). These cryosections were immunostained for Runx2 (labels osteoblasts at several stages at this time-point), mCherry (labels osx expression) and EGFP (switched cells/clones) (Figure 44B). This histological analysis confirmed that the labelling protocol enables to follow the progeny of single basal keratinocytes that generates permanent labelling, at full extent, of all stratified epidermis inside the clone region. Most importantly, independently of osteoblast ablation, no co-localization between the $EGFP^+$ cell/clones and Runx2 or osx is observed, nor with other cell types within the regenerated fin (Figure 44B and magnified panels in B' and B''). This is in accordance with what has been demonstrated in previous lineage tracing experiments showing lineage restriction in the regenerating caudal fin (Tu and Johnson 2011). Our experiments have shown that the adult epidermis does not transdifferentiate into other cell types of the caudal fin upon amputation, and importantly, it does not seem to contribute to new osteoblast formation even in osteoblast depleted caudal fins, which had not been addressed yet.

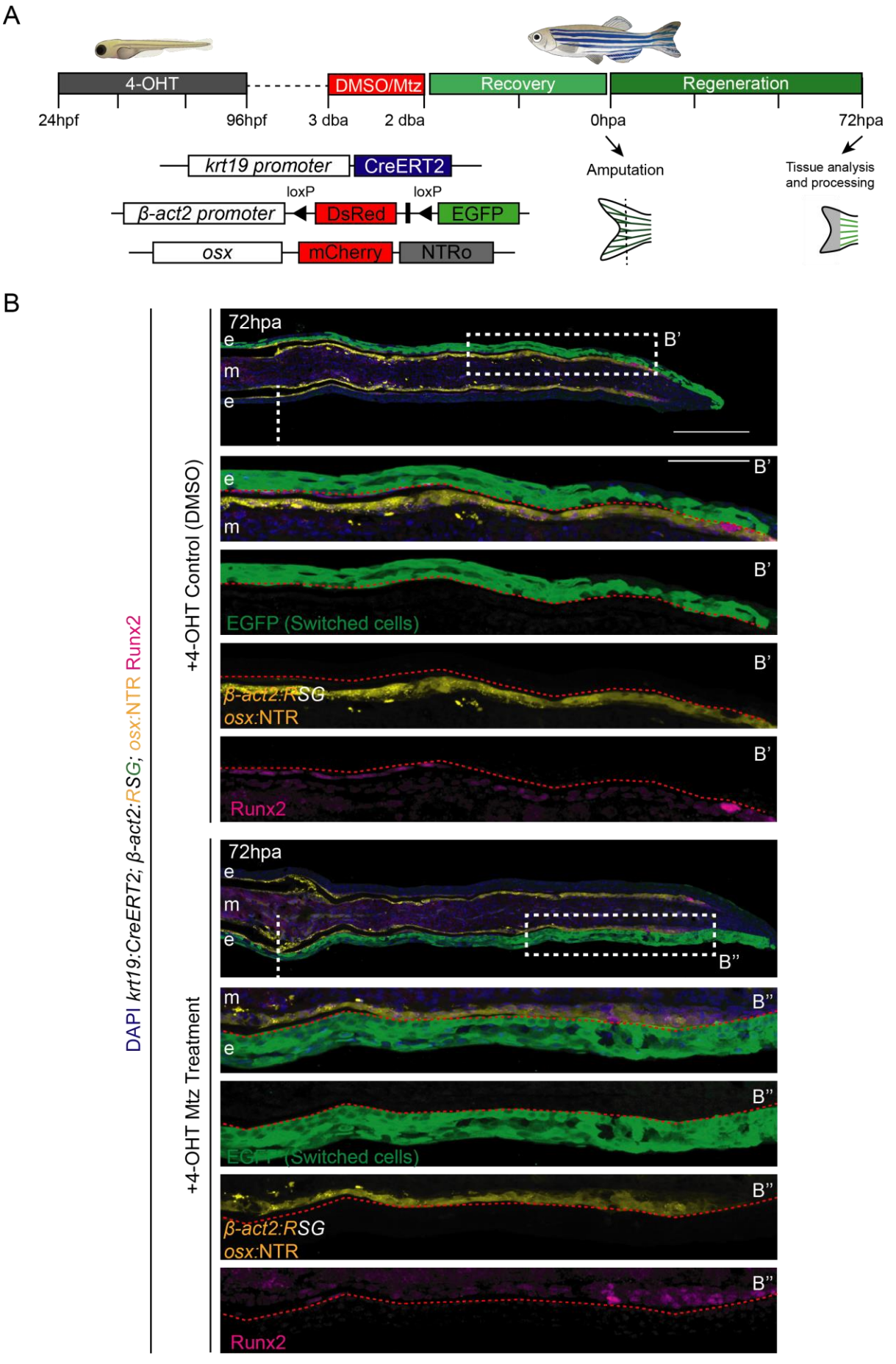
A
4-OHT
DMSO/Mtz
Recovery
Regeneration
24hpf
96hpf
3 dba
2 dba
0hpa
72hpa
Amputation
Tissue analysis and processing
krt19 promoter
CreERT2
loxP
loxP
β-act2 promoter
DsRed
EGFP
osx
mCherry
NTRo
B
DAPI krt19:CreERT2; β-act2:RSG; osx:NTR Runx2
+4-OHT Control (DMSO)
+4-OHT Mtz Treatment
72hpa
e
m
e
B'
B''
EGFP (Switched cells)
β-act2:RSG
osx:NTR
Runx2

Figure 44: Assessing the contribution of the epidermis as a potential source of *de novo* osteoblast formation after mature osteoblast ablation during regeneration. (A) Schematic representation of the experimental setup used to perform genetic fate mapping of the caudal fin epidermal tissue. For that, triple transgenic animals that allow both epidermal specific lineage tracing, using the CreERT2/loxP system, and specific osteoblast ablation, using the NTR/Mtz system, were obtained: *krt19*:CreERT2; *β-actin2*:dsRed>EGFP; *osx:*NTRo, referred as *krt19*:CreERT2; *β-actin2*:RSG; *osx:*NTRo. Embryos with 24 hpf were incubated with 4-OHT for 3 consecutive days, to promote basal epidermal cells permanent labelling (from red to green). Afterwards, larvae were allowed to grow in the circulating system until reaching adulthood. Animals with the strongest fin clones were then subjected to the osteoblast ablation protocol, represented in Figure 41A, and caudal fins subsequently amputated. 72 hpa caudal fins were collected for imaging or for cryosectioning. (B) Representative images of 72 hpa caudal fin longitudinal cryosections of *krt19*:CreERT2; *β-actin2*:RSG; *osx:*NTRo triple transgenic animals previously subjected to basal epidermal cell labelling during larval stages and incubated with vehicle DMSO (4-OHT, +DMSO) or with Mtz (4-OHT, +Mtz treatment). Cryosections were immunostained for mCherry (labelling both *osx* expressing cells and the switch line (which is labelling all cells, *β-actin2*: RSG, yellow)), for GFP (labels the progeny of the basal epidermal cells that have undergone the genetic switch, green), Runx2 (preosteoblast/ osteoprogenitor marker, magenta) and counterstained for DAPI (nucleus, blue). Non-ablated +4-OHT (magnified panels in B') and ablated +4-OHT (magnified panels in B'') animals do not present co-labelling between EGFP positive cells and *osx* or Runx2. This indicates that epidermal cells do not seem to contribute to the osteoblast lineage, in both normal and osteoblast ablation regenerative conditions. dba: days before amputation, hpa: hours post-amputation, hpf: hours post-fertilization; e: epidermis, m: mesenchyme; dashed white lines define the amputation plane; dashed boxes delimitate magnified panels B' and B''; dashed red lines delimitate the epidermal compartment; scale bars represent 200 µm or 10 µm in magnified panels in B' and B''.

2.2 Caudal fin mesenchymal tissue may contribute for *de novo* osteoblast formation during regeneration

It is known that in mammalian systems osteoprogenitors arise from mesenchymal stem cells (MSC) (Bielby et al. 2007; Chen et al. 2016b). Since there are no *bona fide* MSC in the caudal fin, the most similar cell type is the intraray fibroblasts. Given this, we decided to determine whether Runx2^{+} osteoprogenitors, that emerge adjacent to the bone matrix in the inner mesenchymal compartment after osteoblast ablation, are derived from the intraray mesenchymal fibroblasts. We began by performing co-localization studies using a reporter line generated in our lab (Mateus et al. 2015) that allows to visualize the expression of *connective tissue growth factor a* (*ctgfa*), *ctgfa:*EGFP, a reporter for the mesenchymal cells that respond and contribute to the regenerative process (Pfefferli and Jaźwińska 2017). In fact, recent data demonstrated that the *ctgfa:*EGFP reporter does not match *ctgfa* endogenous expression, but contains a *ctgfa* regulatory upstream element that is regulated and activated in an unique manner in the peri-injury mesenchymal cells of the caudal fin, being designated as careg (*ctgfa* reporter in *reg*eneration) (Pfefferli and Jaźwińska 2017). We combined the osteoblast ablation line with *ctgfa*:EGFP, generating *ctgfa*:EGFP; *osx:*NTRo double transgenics, and subjected them to the osteoblast ablation protocol shown in Figure 41A. These animals were incubated with DMSO (controls) or with Mtz, left to recover and caudal fins amputated and collected at 24 hpa, time-point at which osteoprogenitors are already formed and accumulated near the amputation region. 24 hpa caudal fin longitudinal cryosections were immunostained with

Runx2 (osteoprogenitor marker), mCherry (visualize *osx* expression and confirm osteoblast presence) and EGFP (visualize *ctgfa* expression). In both controls (DMSO) and in Mtz treated caudal fins, it is possible to notice that the *ctgfa* is upregulated in the mesenchymal compartment just below the amputation plane (Figure 45A and B, respectively). Additionally, in the control situation, we observe a clear co-localization between the differentiated/mature osteoblast population, $Runx2^{+}Osx^{+}$, with *ctgfa*:EGFP in both the outer (Figure 45A, magnified panel of region e) and inner (Figure 45A, magnified panel of region m) osteoblast layer surrounding the bone surface, demonstrating that mature osteoblasts express *ctgfa* during regeneration. Since *ctgfa* is triggered in mesenchymal cells that respond and contribute to the regenerative process (Pfefferli and Jaźwińska 2017), this may indicate that osteoblasts retain mesenchymal properties, which is in accordance with their ontogeny (mesenchymal origin) (Lee et al. 2013). In contrast to the control condition, in Mtz treated animals, only the new osteoprogenitors, $Runx2^{+}Osx^{-}$, that arise near the inner bone surface in the mesenchyme are positive for *ctgfa*:EGFP (Figure 45B magnified panels of the m region), while the $Runx2^{+}Osx^{-}$ osteoprogenitors that arise at the outer bone surface facing the epidermis are not (Figure 45B magnified panels of the e region). This may indicate that these early outer and inner osteoprogenitors have different origins or that they have different properties and/or functions during bone regeneration, possibly comprising two distinct osteoblast populations that emerge in osteoblast depleted fins during the regenerative process.

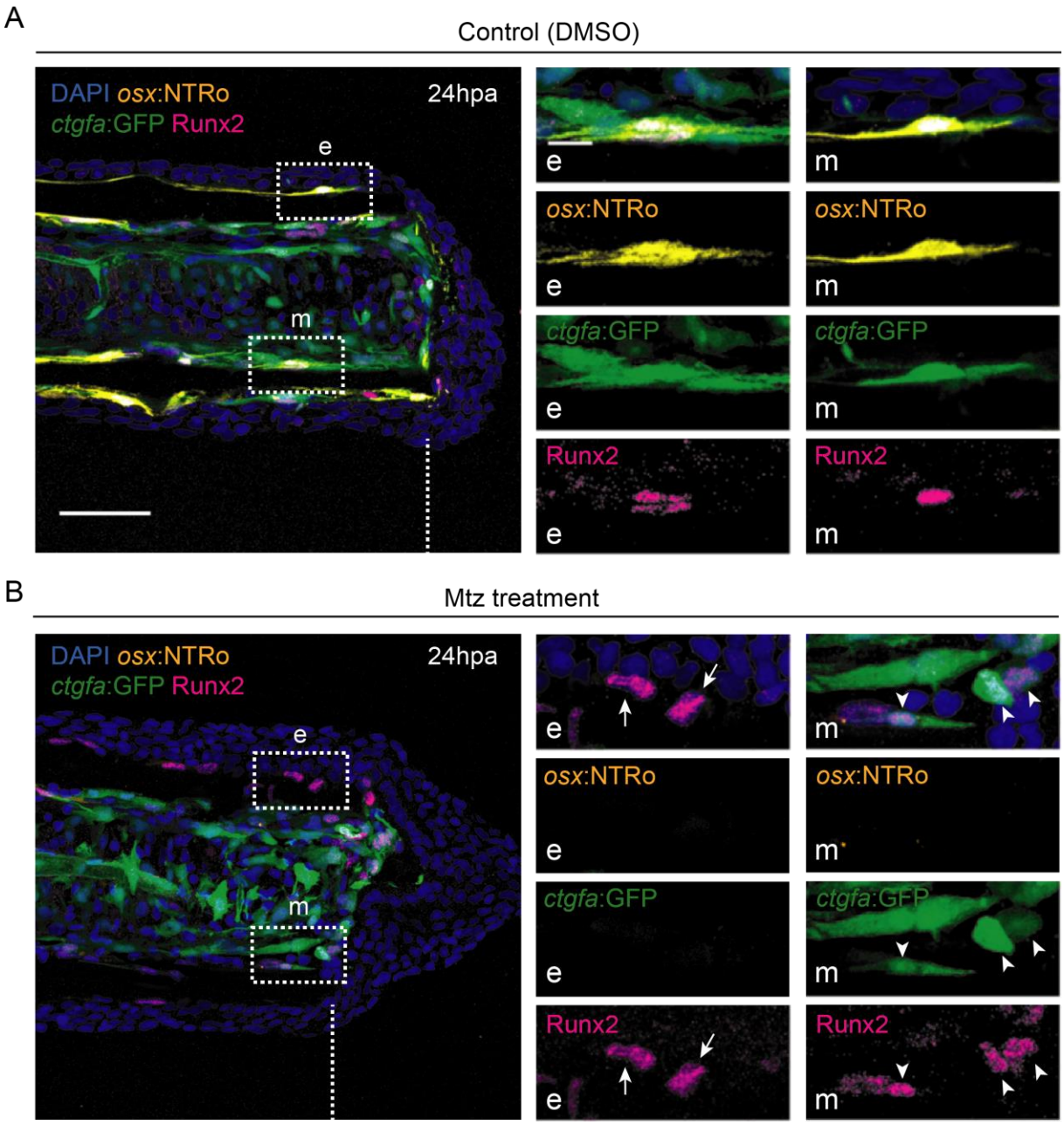

Figure 45: Newly formed osteoprogenitors seem to have different mesenchymal properties in osteoblast depleted caudal fins. Representative images of 24 hpa caudal fin longitudinal cryosections of *osx:*NTRo; *ctgfa*:EGFP double transgenics subjected to vehicle DMSO (controls) (A) and to Mtz treatment (B). Cryosections were immunostained for mCherry (to visualize *osx* expression and confirm osteoblast presence, yellow), GFP (to visualize *ctgfa* expression, which is labelling caudal fin mesenchymal cells, green), Runx2 (preosteoblast/ osteoprogenitor marker, magenta) and counterstained for DAPI (nucleus, blue). (A) We can observe that in control caudal fins, both mature osteoblasts populations that surround the bone, adjacent to the epidermis (magnified panels in e) or in the mesenchymal side (magnified panels in m), there is a co-localization between *osx* and Runx2 with *ctgfa*. (B) In caudal fins subjected to the osteoblast ablation protocol shown in Figure 40A, only the osteoprogenitors (Runx2^{+}) that emerge near the bone surface in the inner mesenchymal compartment (magnified panels in m) are positive for the mesenchymal marker *ctgfa*. In contrast, the Runx2^{+} progenitors that appear next to the epidermal side are negative for this marker (magnified panels in e). Arrows point to Runx2^{+}Ctgfa^{-} osteoprogenitors that emerge at the bone interphase with the epidermis; Arrowheads point to double positive Runx2^{+}Ctgfa^{+} osteoprogenitors that emerge at the bone interphase with the mesenchyme. hpa: hours post-amputation; dashed lines define the amputation plane; dashed boxes delimitate magnified panels e and m; scale bars represent 50 µm or 10 µm in magnified panels in the epidermis (e) and in the mesenchyme (m).

To confirm that the caudal fin intraray mesenchymal tissue contributes to osteoblast formation in osteoblast depleted fins, we carried out lineage tracing of these cells using the inducible Cre /LoxP-system (Hans et al. 2009; Mosimann et al. 2011; Carney and Mosimann 2018). For that, we used a transgenic line with a tamoxifen-dependent Cre recombinase driven by the *careg* regulatory sequence, *careg:*CreERT2, together with *the β-actin2*:RSG line. We started by addressing whether the previously reported protocol for permanent fin mesenchyme labelling (Pfefferli and Jaźwińska 2017) was working in our experimental setup, given that we had to perform this experiment using a different switch line. Since the *careg* regulatory elements are only activated upon damage/injury, we amputated the *careg:*CreERT2*; β-actin2*:RSG transgenic fish in order to induce expression of Cre. Then, we gave a one-day pulse of 4-OHT or EtOH (control) from 0 to 24 hpa and monitored EGFP expression during regeneration (Supplementary Figure 6A). Live-imaging analysis of 48 hpa caudal fins from controls did not reveal any labelling (Supplementary Figure 6B and magnified panels from B'-B'''). On the contrary, animals incubated with 4-OHT showed multiple scattered EGFP-positive cells (Supplementary Figure 6B and magnified panels from Bi-Biii). However, we were never able to obtain the highly efficient and strong labelling throughout the regenerated area shown in the previously reported study (Pfefferli and Jaźwińska 2017). The defective labelling could be explained by differences in the loxP reporter transgenic used to detect Cre-mediated recombination in *ctgfa* expressing cells. Due to technical incompatibilities, we were not able to use the *ubiquitin:*loxP-EGFP-STOP-loxP-mCherry (*ubi*:switch) employed in the mentioned study (Pfefferli and Jaźwińska 2017). Alternatively, we had to resort to the *β-actin2*: RSG that may account for the lower efficiency in reporting Cre recombination events. Despite the low labelling efficiency, we decided to continue with our experiments using this setup.

After validating the experimental setup, we then combined the mesenchyme lineage tracing procedure with the osteoblast ablation protocol and evaluated the contribution of the mesenchymal fibroblasts for new osteoblast formation upon caudal fin amputation, in the osteoblast ablation context. For that, we combined the *careg*: CreERT2; *β-actin2*: RSG double transgenic with the osteoblast ablation line, generating *careg*:CreERT2; *β-actin2*:RSG; *osx:*NTRo triple transgenics. We began by inducing osteoblasts ablation, incubating the animals with DMSO (controls) or with Mtz for one day. After the recovery period, fish were subjected to caudal fin amputation and exposed to 4-OHT during the first day following amputation. Caudal fins were imaged at 72 hpa, when we already have an extensive newly formed osteoblast population, following immunofluorescence analysis in longitudinal cryosections of these fins (Figure 46A). We can observe that in both triple transgenics from control (DMSO) +4-OHT and Mtz treated +4-OHT 72 hpa caudal fins the presence of scattered EGFP-positive cells throughout the regenerated area (Figure 46B). These EGFP-positive cells derive from the pre-existing mesenchymal cells of the stump region, which were labelled in the first day post-amputation. Cryosections of these fins immunostained for EGFP (to visualize

the cells/clones that undergone the switch, green), mCherry (labels *osx* expression, orange) and Runx2 (labels osteoblasts at several stages at this time-point, magenta), show that in both control (DMSO) +4-OHT and Mtz +4-OHT treated animals there are mesenchymal cells (white arrowheads) and blood vessels (white arrow) positive for EGFP (Figure 46C and magnified panels in C' and Ci). However, only in the osteoblast ablation context we were able to observe some epidermal cells presenting EGFP labelling (Figure 46C and magnified panels in Ci, blue arrowheads) and osteoblasts from the regenerate, $Runx2^{+}Osx^{+}$, co-labelling with EGFP (Figure 46C and magnified panels in Ci, magenta arrowheads). Nonetheless, more experiments are required to further confirm these results, given the low efficiency of the labelling. So far, our results suggest that in normal regenerating conditions the mesenchymal cells give rise to the mesenchymal cells of the regenerate, like what was previously described (Tu and Johnson 2011; Pfefferli and Jaźwińska 2017), and that in the osteoblast depleted fins the stump mesenchyme could also be responsible for *de novo* osteoblast formation and compensate for the lack of mature osteoblasts.

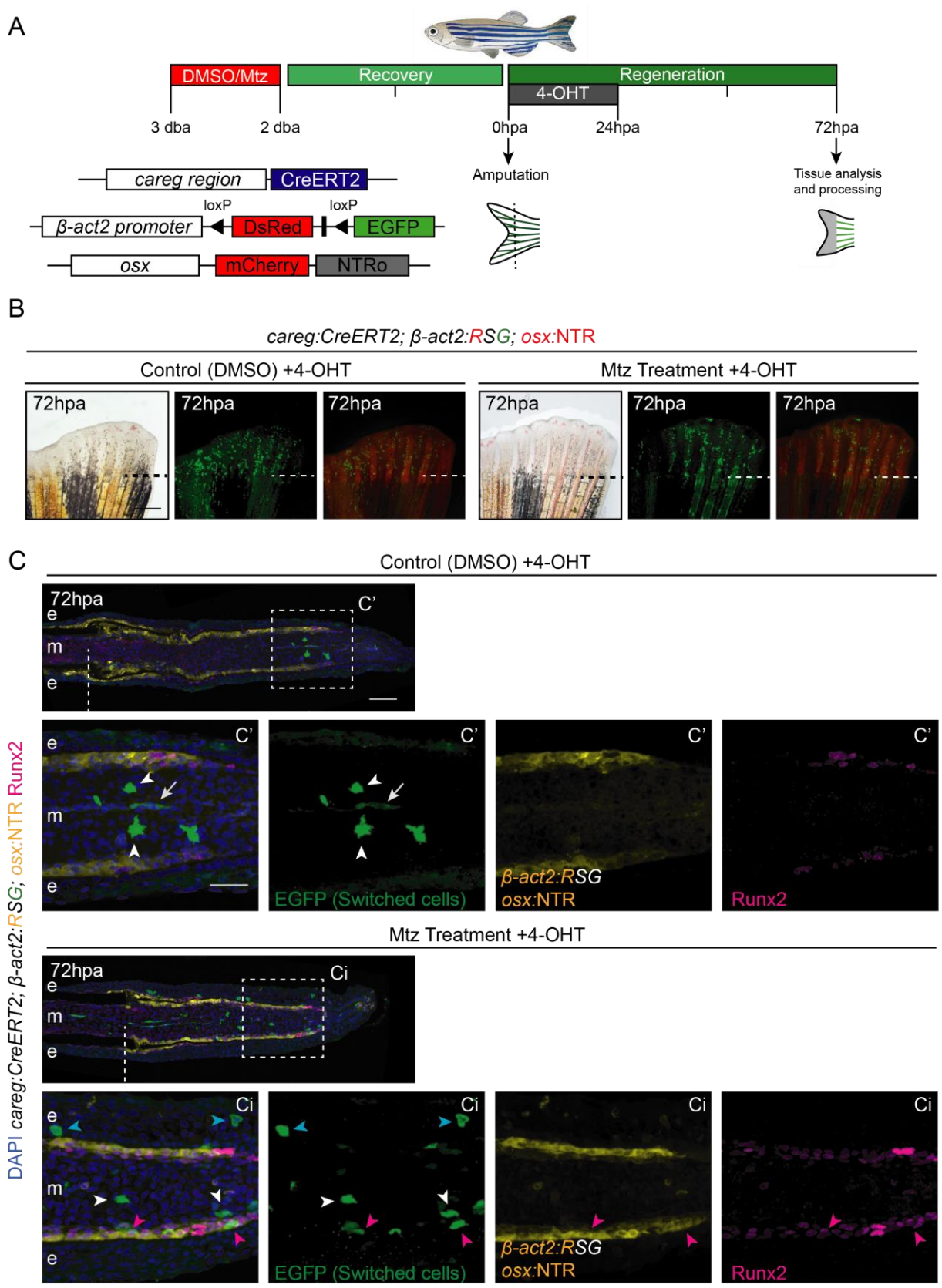

Figure 46: Assessing the contribution of the mesenchyme as a potential source of *de novo* osteoblast formation after mature osteoblast ablation during regeneration. (A) Schematic representation of the experimental setup used to perform genetic fate mapping of the caudal fin mesenchymal tissue. Triple transgenic animals that allow caudal fin mesenchymal specific lineage tracing, using the CreERT2/loxP system, and specific osteoblast ablation, using the NTR/Mtz system, were obtained: *careg*:CreERT2; *β-actin2*:dsRed>EGFP; *osx*:NTRo, referred as

careg:CreERT2; *β-actin2*:RSG; *osx*:NTRo. Animals were exposed to control (DMSO) or Mtz treatment for osteoblast ablation, as represented in Figure 41A. After recovery, animals were subjected to caudal fin amputation and incubated with 4-OHT from 0 to 24 hpa. Fins were collected at the desired time-point after amputation for imaging or later processing. (B) Representative images of triple transgenics subjected either to DMSO (control) or Mtz and both to 4-OHT. It is possible to observe that in both conditions some mesenchymal cells were permanently labelled during the first day after amputation and contributed to the regenerative process. (C) Representative images of 72 hpa caudal fin longitudinal cryosections shown in panel B immunostained for GFP (labels the progeny of the mesenchymal cells that have undergone the genetic switch post-amputation, green), mCherry (labels both *osx* expressing cells and the switch line (which is labelling all cells, *β-actin2*: RSG), yellow), Runx2 (preosteoblast/ osteoprogenitor marker, magenta) and counterstained for DAPI (nucleus, blue). In animals from both conditions, control (DMSO) +4-OHT (magnified panels in C') or Mtz treatment +4-OHT (magnified panels in Ci) groups, it was possible to observe that most of the EGFP-positive cells were mesenchymal fibroblasts, given their location and more spread shape (arrowheads in magnified panels in C' and Ci), including $EGFP^+$ in blood vessels (arrow in magnified panel in C'). In the osteoblast ablation condition, it was also possible to observe few $EGFP^+$ cells in the epidermal compartment (blue arrowheads in magnified panel in Ci) and $EGFP^+$ co-localizing with $Runx2^+Osx^+$ differentiating osteoblasts (magenta arrowheads in magnified panel in Ci). This indicates that caudal fin mesenchymal cells can contribute to *de novo* osteoblast formation in osteoblasts depleted fins. Dba: days before amputation, Hpa: hours post-amputation, e: epidermis, m: mesenchyme; dashed white lines define the amputation plane; dashed boxes delimitate magnified panels C' and Ci; scale bars represent 500 μm in B panels and 200 μm in C or 10 μm in magnified panels in C' and Ci.

2.3 *Col10a1* may define a pool of osteogenic precursors located in the fin intersegment/joint regions of the caudal fin

One of the main aims of this project was to identify alternative sources of osteoblasts that may emerge during regeneration of fins lacking osteoblasts. So far, we have identified osteoprogenitors that arise at the interphase between the bone surface and the surrounding tissues, through the presence of Runx2. In addition, we have also found that at least some of these cells derived from mesenchymal fibroblasts. The next step would be to perform targeted ablation of these progenitors and further defy the intrinsic plasticity of the system, evaluating the relative contribution and significance of this osteoprogenitor population. Therefore, we searched for other markers that could specifically label these osteoprogenitors prior to Runx2 appearance. We found that in medaka the *col10a1*:nlGFP reporter line labels putative osteoblast precursors (Renn et al. 2013). We hypothesised that in zebrafish this could also be the case and generated a transgenic zebrafish reporter line using the same *col10a1*:nlGFP construct which we called *Tg*(*Ola.col10a1*:nlGFP), referred to as *col10a1*:nlGFP (Supplementary Figure 7A). This transgenic line mimics the expression pattern of *col10a1* at larval stages (Li et al, 2009; Yong-Il et al 2013), with several craniofacial skeletal structures positive for GFP at 72 hpf (Supplementary Figure 7B and magnified panels in Bii). In the *col10a1*: nlGFP adult caudal fin, expression can be observed in the intersegment/joint regions (Supplementary Figure 7C and arrowheads in magnified panels in Cii) and also delineating the bone segment (Supplementary Figure 7C and asterisks in magnified panels in Cii). Next, we evaluated in more detail the exact pattern of expression of this reporter line in non-manipulated caudal fins and in fins subjected to the osteoblast ablation protocol. For that, we combined our *col10a1*:nlGFP line with the osteoblast ablation line, generating *col10a1*:nlGFP; *osx:*NTRo double transgenics. Double transgenics were either incubated with DMSO (control)

or with Mtz. After the recovery period we collected uncut (non-regenerating) fins and monitored the behaviour of the reporter line right after the ablation procedure, through the analysis of longitudinal cryosections by immunofluorescence against mCherry (to visualize *osx* expression and confirm correct osteoblast ablation), GFP (to visualize *col10a1* expression) and Runx2 (to label osteoprogenitors) (Figure 47). In control uncut caudal fin cryosections, it is possible to observe that indeed *col10a1* is expressed in a subset of cells that populate the intersegment/joint region (Figure 47A and regions delimitated with dashed orange lines in magnified panels of Ai). In addition, *col10a1* is also expressed by the osteoblasts that surround the outer bone surface, facing the epidermis (Figure 47A and white arrowheads in magnified panels of Ai), but not by the inner osteoblasts layer facing the mesenchymal compartment (Figure 47A and red arrowheads in magnified panels of Ai). Although the *col10a1*:nlGFP transgenic was supposed to have nuclear GFP, fluorescence is also visible in the cytoplasm due to inefficient targeting to the nucleus, a problem that was also observed in the medaka transgenic line since the construct is the same (Renn et al. 2013). In the ablation context we can notice that, in the uncut condition, the group of cells that reside in the intersegment/joint region seems to have expanded in size, suggesting a response triggered by osteoblast ablation (Figure 47B and regions delimitated with dashed orange lines in magnified panels of Ai and Bi). Additionally, and in contrast to controls, *col10a1* is also upregulated in the basal epidermal cells, which have a more cuboidal appearance (Figure 47B and arrows in magnified panels of Bi), and in some Runx2^{+} osteoprogenitors (more flattened cells) that emerge between the bone matrix and the basal epidermal layer (Figure 47B and magnified panel B'). Interestingly, more recently, a study demonstrated the presence of a pool of cells that reside in the intersegment/joint regions of the caudal fin, referred as being resident osteoprogenitor cells. These cells are identified by the expression of the *matrix metalloproteinase 9* (*mmp9*) gene and by the absence of intermediate/immature osteoblast markers, such as *osx*. Joint-associated osteoprogenitors have been demonstrated to be a complementary source of osteoblasts in regenerating fins after amputation since their ablation leads to a reduction in the number of newly formed osteoblasts in the regenerate (Ando et al. 2017). However, in this study, the contribution of these cells in an osteoblast ablation condition was not addressed. Given that our *col10a1*:nlGFP transgenic line is expressed in a restricted subset of cells at the intersegment/joint region that also does not express *osx* (Figure 47A and B), this indicates that our *col10a1*:nlGFP line is potentially labelling this pool of resident osteoprogenitors. Overall, this suggests that *col10a1* is expressed in osteoprogenitors in the intersegment region and that the *col10a1* reporter could be a good tool to study the dynamics of these cells during regeneration. This transgenic line also revealed a very interesting response by other tissues after osteoblast ablation, in a non-regenerating condition. In this context, basal keratinocytes and some Runx2+ osteoprogenitors that emerge in the outer bone surface upregulate *col10a1*.

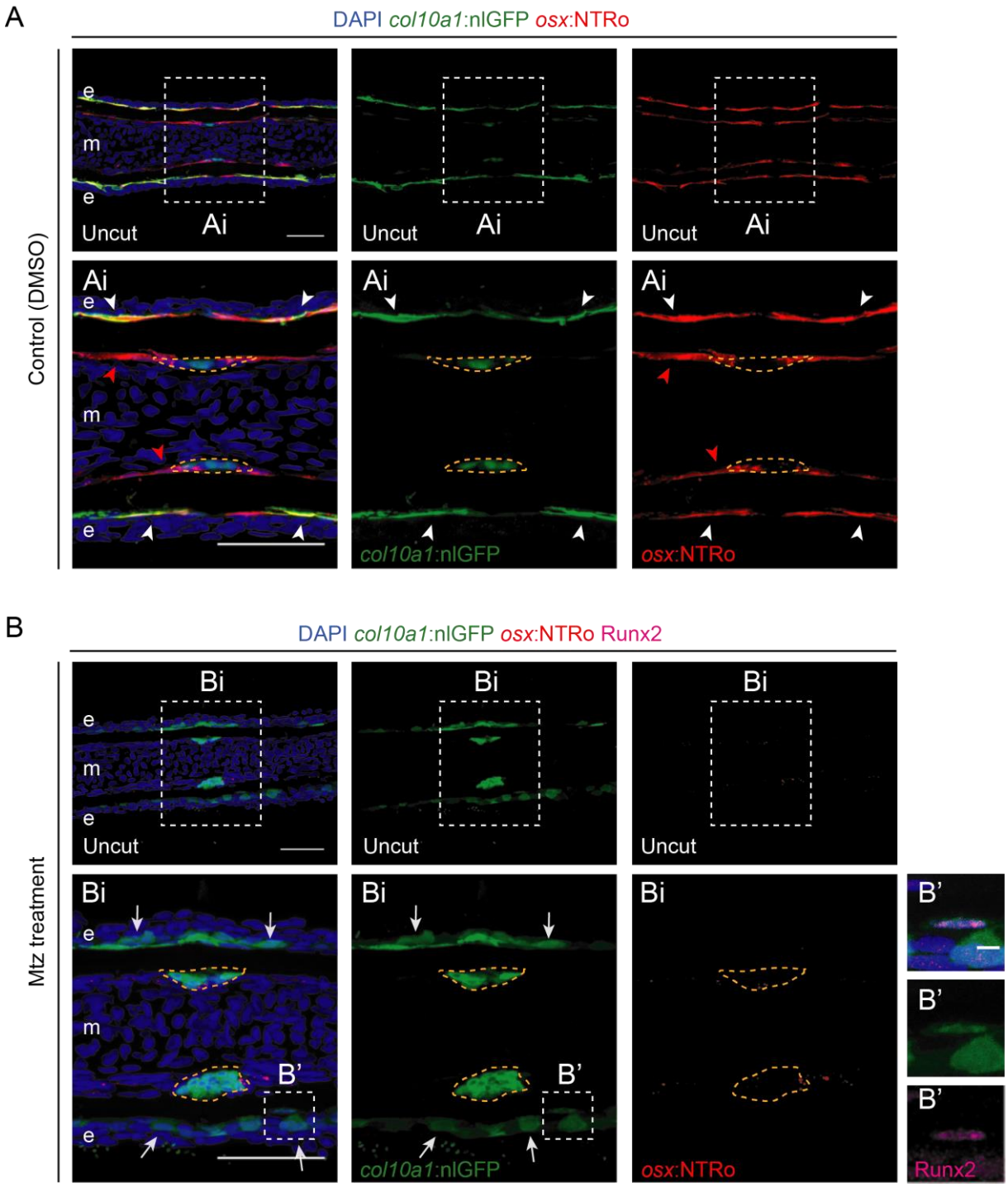

Figure 47: *col10a1*:nlGFP labels possible osteoblast precursors localised in the intersegment/joint region of the caudal fin. (A and B) Representative images of uncut caudal fin longitudinal cryosections of *col10a1*:nlGFP; *osx*:NTRo double transgenic animals subjected to vehicle DMSO (control) (A) or to Mtz incubation (B). Cryosections were immunostained for GFP (to visualize putative osteoprogenitors or other osteoblast precursors, green), mCherry (to visualize osx expression and confirm correct osteoblast ablation, red), Runx2 (preosteoblast/ osteoprogenitor marker, magenta, only shown in B') and counterstained for DAPI (nucleus, blue). (A) In the control condition, *col10a1* is expressed in the osteoblast population (Osx^{+}) at the bone surface facing the epidermis (white arrowheads in magnified panels of Ai), but not in the inner osteoblast layer facing the mesenchyme (red arrowheads in magnified panels of Ai) and in the niche of potential osteoblast precursors localized in the joint region (regions delimitated with dashed orange lines in magnified panels of Ai). (B) In Mtz treated animals, Osx^{+} osteoblasts were ablated and *col10a1* expression is now observed in the basal epidermal cells (cuboid cells, examples are shown in magnified panels of Bi with arrows), in the putative osteoblast

precursor niche, that seems to expand upon ablation (regions delimitated with dashed orange lines in magnified panels of Bi) and also in a few osteoprogenitors, Runx2^{+}, that have emerged after ablation (magnified panels of B'). This indicates that *col10a1* could be used as a potential tool to study sources for de novo osteoblast formation when the mature population is compromised. hpa: hours post-amputation, e: epidermis, m: mesenchyme; dashed white lines define the amputation plane; dashed boxes delimitate magnified panels; scale bars represent 50 µm and 40 µm in magnified panels in Ai and Bi and 5 µm in magnified panels in B'.

3 UNRAVELLING THE MOLECULAR MECHANISM BEHIND *DE NOVO* OSTEOBLAST FORMATION DURING CAUDAL FIN REGENERATION: THE ROLE OF RA AND BMP SIGNALLING

Another important point that we have investigated during the course of this work, was to understand the molecular mechanism that regulates osteoblast formation during regeneration when the mature population is absent. Until now, we have focused our work in unravelling the cellular mechanisms that are put together to ensure proper osteoblast formation when the mature population is compromised. Nevertheless, the molecular mechanisms that trigger and regulate the commitment of other cell sources towards the osteoblast lineage are of equal importance, specifically when the system cannot rely on the dedifferentiation of lineage committed osteoblast and these cells have to be formed *de novo*. In fact, the osteoblast ablation context is a good system to further understand the molecular cascade that governs osteoblastogenesis *in vivo*. Thus, we aimed to investigate which signalling pathways could be important to regulate *de novo* osteoblast formation during regeneration in the context of mature osteoblast ablation. Several signalling pathways have been implicated in regulating the commitment of MSC to the osteoblast lineage in mammalian systems. Bmp, Wnt, RA, Notch and Hedgehog signalling pathways are known important players in this process (Deng et al, 2008; Long, 2012; Beederman et al, 2013; Hu et al, 2018). In the next two sections, we report the potential role of RA and Bmp signalling in regulating *de novo* osteoblast formation during caudal fin regeneration.

3.1 RA signalling is active in osteoprogenitors and seems to be required for their formation in osteoblast depleted fins during fin regeneration

RA signalling has been shown to be a key player in directly regulating osteoblast formation and commitment in mammals and other teleost fish (Renn and Winkler 2012; Green et al. 2017). Most importantly, this signalling pathway also mediates several aspects of blastema formation during zebrafish caudal fin regeneration (Blum and Begemann 2012) and osteoblast dedifferentiation and redifferentiation (Blum and Begemann 2015b). To address whether RA signalling could have a role in *de novo* osteoblast formation during regeneration of osteoblast depleted fins, we began by performing co-localization studies with the transgenic line TgBAC(*aldh1a2:aldh1a2*-GFP)^{kn2}, referred as *aldh1a2*:GFP, that reports the expression of the RA synthesizing-enzyme *aldh1a2* (Pittlik and Begemann 2012). The *aldh1a2* gene encodes a retinaldehyde dehydrogenase that provides the major source of cellular RA. Therefore, we

combined the *aldh1a2*:GFP with the osteoblast ablation line and incubated the double transgenic animals with DMSO (controls) or with Mtz. Following the ablation protocol, animals were subjected to caudal fin amputation, left to regenerate for one day (24 hpa) and the tissue was subsequently collected for analyses by immunofluorescence in longitudinal cryosections. We choose to analyse this time-point because there is already a considerable amount of osteoprogenitors accumulated in the stump region that can be easily monitored. At 24 hpa in both control and Mtz treated animals, *aldh1a2* is expressed throughout the intraray compartment in blood vessels, nerves and in fibroblast-like cells (Figure 48A and B). Given the wide range of cell types expressing *aldh1a2,* it is difficult to clearly observe if it is being expressed in mature osteoblasts or in osteoprogenitors that reside or emerge in the intraray compartment. Therefore, we focused this analysis on the outer osteoblast layer surrounding the bone matrix (dashed boxes in Figure 48A and B). In control fins, we noticed that the mature osteoblast ($Runx2^{+}Osx^{+}$) population, at the interphase with the bone matrix and the epidermis, has a poor co-localization with GFP-expressing cells and, when co-localization is observed, EGFP expression is very low (Figure 48A and arrows pointing to examples in magnified panels in Ai and A'). This result was somewhat expected since RA signalling has been shown to be downregulated in mature osteoblasts that are undergoing dedifferentiation (Blum and Begemann 2015b). In contrast, in Mtz treated animals, newly formed $Runx2^{+}Osx^{-}$ progenitors that emerged at the outer bone surface show intense *aldh1a2* expression (Figure 48B, arrowheads point to examples in magnified panels in Bi and B' of $Runx2^{+}$ cells co-localizing with GFP) and thus potentially increasing RA signalling.

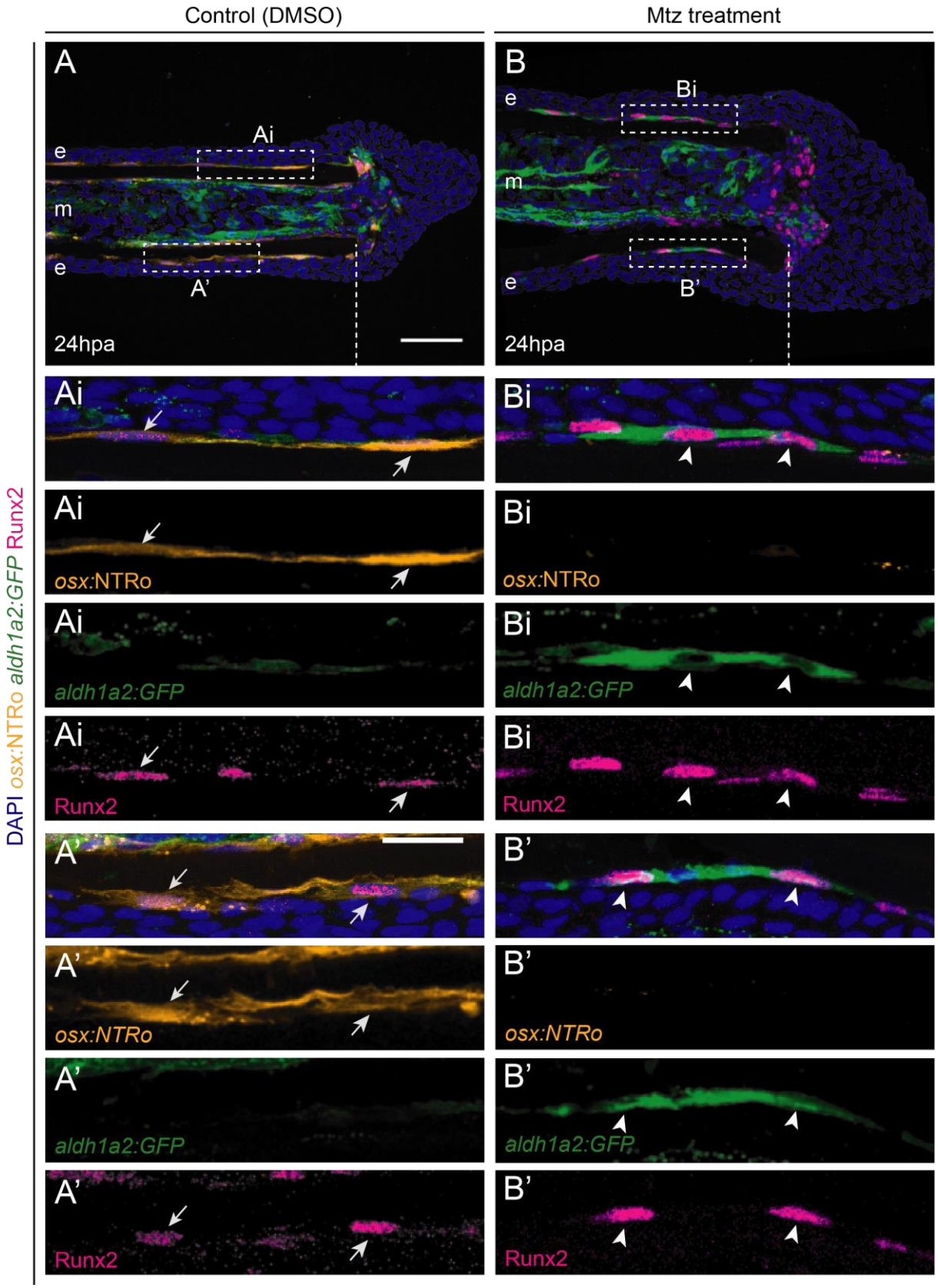

Figure 48: Retinoic acid signalling is active in newly formed osteoprogenitors in osteoblast depleted caudal fins after amputation. (A and B) Representative images of 24 hpa caudal fin longitudinal cryosections of *aldh1a2*: GFP; *osx:*NTRo double transgenic animals subjected to vehicle DMSO (control) (A, Ai and A') or Mtz treatment (B, Bi and B'). Cryosections were immunostained for mCherry (to visualize *osx* expression and confirm correct

osteoblast ablation, orange), GFP (to monitor activated RA signalling, green), Runx2 (preosteoblast/ osteoprogenitor marker, magenta) and counterstained for DAPI (nucleus, blue). In the control condition (A, Ai and A'), *aldh1a2* is expressed mainly in the mesenchymal compartment, associated with the blood vessels, nerves and mesenchymal cells (A). At this time-point, *aldh1a2* is also excluded from Runx2^{+}Osx^{+} osteoblasts that are at the bone surface facing the epidermis (arrows in magnified panels of Ai and A'). In animals subjected to osteoblast ablation (B, Bi and B'), *aldh1a2* is also expressed in the mesenchymal compartment in the blood vessels, nerves and fibroblast-like cells (B). In addition, *aldh1a2* becomes clearly upregulated in the Runx2^{+} osteoprogenitors that are formed *de novo* upon amputation (arrowheads in magnified panels of Bi and B'). This reveals that RA signalling could be an important pathway necessary to generate new osteoprogenitors in osteoblast depleted caudal fins during regeneration. hpa: hours post-amputation, e: epidermis, m: mesenchyme; dashed white lines define the amputation plane; dashed boxes delimitate magnified panels; scale bars represent 50 µm and 10 µm in magnified panels in A', Ai, B' and Bi.

To evaluate whether RA signalling is required for proper osteoprogenitor formation in osteoblast ablated caudal fins during regeneration, we set out to reduce RA levels via overexpression of the RA-degrading enzyme *cyp26a1*, using the heat-shock inducible transgenic line Tg(*hsp70l:cyp26a1*)^{kn1}, referred as *hsp70l:cyp26a1* (Blum and Begemann 2012). We crossed the *hsp70l:cyp26a1* with the osx:NTRo ablation line and performed the ablation protocol. Fish were allowed to recover and subsequently subjected to RA manipulation protocol by giving a 1 h single heat-shock just prior to amputation (Figure 49A). The *hsp70l:cyp26a1; osx:*NTRo double transgenics were thus divided into four main groups according to the procedures that they were exposed to: without Mtz treatment and without HS (Mtz- HS-); without Mtz treatment and with HS (Mtz- HS+), to check the effect of impaired RA signalling in the mature osteoblast population; treated with Mtz and without HS (Mtz+ HS-); and treated with Mtz and with HS (Mtz+ HS+), to address the role of RA signalling during *de novo* osteoprogenitor formation in fins lacking mature osteoblasts. These animals were allowed to regenerate for 24 hpa when osteoprogenitor formation can be monitored, and fins were collected and cryosectioned for immunofluorescence assays to label the different osteoblast populations, mature osteoblasts (Runx2^{+}Osx^{+}) and osteoprogenitors (Runx2^{+}Osx^{-}). When comparing Mtz-HS- with Mtz-HS+, to address the effect of RA signalling impairment in a non-ablation situation, we observed no differences either in the number of mature osteoblasts (Runx2^{+}Osx^{+}) (Figure 49B and C) or in the number of Runx2^{+}Osx^{-} progenitors that emerge in the non-ablation context (Figure 49B and D). Conversely, when we compare Mtz+HS- with Mtz+HS+ group, to address the effect of impairing RA signalling in osteoblast depleted situation, we observed that RA inhibition leads to a clear reduction in the number of osteoprogenitors Runx2^{+}Osx^{-} formed (Figure 49B and D).

The evidences described above, the upregulation of *aldh1a2* in Runx2^{+} osteoprogenitors as well as the decrease in the number of this population when RA signalling is decreased, supports the hypothesis that indeed RA signalling may have a role in the formation and commitment of newly formed osteoblasts after mature osteoblast ablation in regenerating caudal fins.

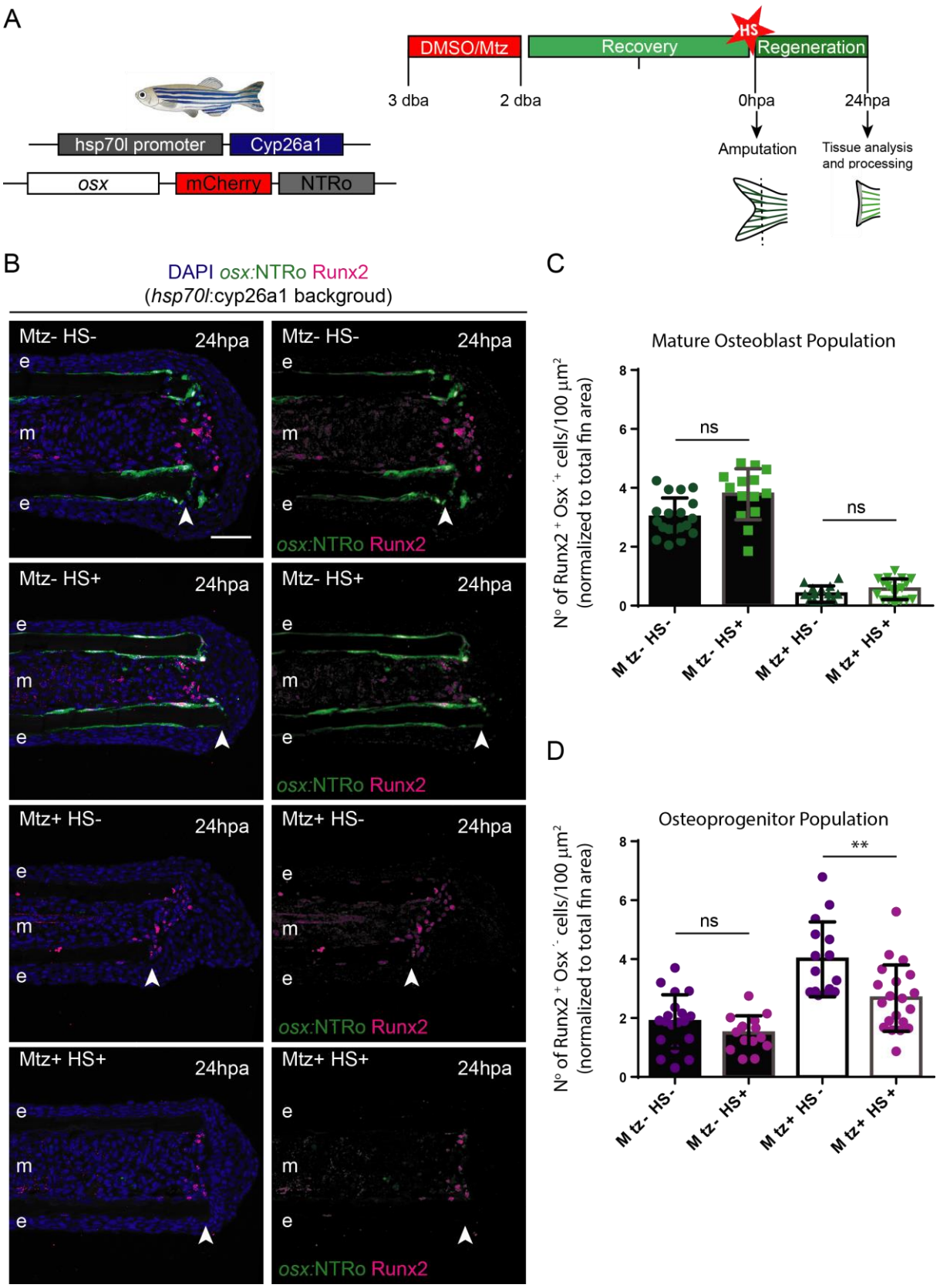

Figure 49: Requirement of retinoic acid signalling for *de novo* osteoblast formation in osteoblast depleted fins during caudal fin regeneration. (A) Schematic representation of the experimental setup used to perform functional manipulation of RA signalling and address the function of this pathway for *de novo* osteoblast formation. We combined the osteoblast ablation line, *osx:*NTRo, with a heat-shock (HS) inducible transgenic line that expresses *cyp26a1* (RA degrading enzyme) upon HS, *osx:*NTRo; *hsp70l:cyp26a1*. Double transgenic animals

were either incubated with Mtz or control DMSO (vehicle), following the ablation protocol shown in Figure 41A. After recovery fish were either subject or not to HS, HS+ and HS-, respectively, and divided in four main groups: controls without Mtz and without HS (Mtz- HS-); controls without Mtz and with HS (Mtz- HS+); treated with Mtz and without HS (Mtz+ HS-); and treated with Mtz and with HS (Mtz+ HS+). Fish were then immediately subjected to caudal fin amputation and fins collected at 24 hpa for tissue imaging and subsequent processing. (B) Representative images of 24 hpa caudal fin longitudinal cryosections of *osx:*NTRo; *hsp70l:cyp26a1* double transgenic animals from the groups described above. Cryosections were immunostained for mCherry (to visualize *osx* expression and confirm correct osteoblast ablation, green), Runx2 (preosteoblast/ osteoprogenitor marker, magenta) and counterstained for DAPI (nucleus, blue). This shows that RA signalling manipulation does not affect the mature osteoblast population nor the $Runx2^+$ osteoprogenitors that are formed in normal regenerating fins, but it might be required for proper *de novo* osteoblast formation after osteoblast ablation. (C) Graph showing the quantification of mature osteoblast ($Runx2^+Osx^+$) at 24 hpa for all experimental groups; bars on graph correspond to total number of $Runx2^+Osx^+$ cells normalized to total fin area and statistical analysis corresponds to Mann-Whitney test with Mean ± SD displayed (Mtz- HS- : n= 19 bony-rays compiled from 4 fish; Mtz- HS+ : n= 15 bony-rays compiled from 4 fish; Mtz+ HS- : n= 15 bony-rays compiled from 4 fish; Mtz+ HS+ : n= 20 bony-rays compiled from 5 fish). (D) Graph showing the quantification of osteoprogenitors ($Runx2^+Osx^-$) at 24 hpa for all experimental groups; bars on graph correspond to total number of $Runx2^+Osx^+$ cells normalized to total fin area and statistical analysis corresponds to Mann-Whitney test with Mean ± SD displayed (Mtz- HS- : n= 19 bony-rays compiled from 4 fish; Mtz- HS+ : n= 15 bony-rays compiled from 4 fish; Mtz+ HS- : n= 15 bony-rays compiled from 4 fish; Mtz+ HS+ : n= 20 bony-rays compiled from 5 fish). dba: days before amputation; hpa: hours post-amputation, e: epidermis, m: mesenchyme; arrowheads define the amputation plane; scale bars represent 50 µm; ** $p< 0.01$, ns: non-significant.

3.2 Bmp signalling is activated in newly formed osteoprogenitors and seems to be required for their formation in normal and in osteoblast depleted fins during regeneration

Bmp signalling is one of the most important regulators of osteoblast formation during development, bone remodelling and repair during fracture healing in mammalian systems (Valcourt and Moustakas 2005; Kamiya and Mishina 2011; Beederman et al. 2013; Wu et al. 2016). Additionally, there are also many studies implicating Bmp signalling during the outgrowth and patterning phase of caudal fin regeneration (Quint et al. 2002; Smith et al. 2006; Stewart et al. 2014; Thorimbert et al. 2015; Wehner and Weidinger 2015). However, its role and requirement for *de novo* osteoblast formation during caudal fin regeneration, after mature osteoblast ablation, has never been tested.

Therefore, to address Bmp signalling activation, we began by performing co-localization studies with a previously tested antibody (Stewart et al. 2014) for active Smad1, 5, and 8 (pSmad1/5/8) (Stewart et al. 2014), also used in the previous Chapter IV. For that, we analysed *osx:*NTRo fins at 24 hpa , time-point at which we can easily evaluate osteoprogenitor formation, exposed to either DMSO (control) or to Mtz, with antibodies against pSmad1/5/8 (to monitor activated Bmp signalling), Runx2 (to label osteoprogenitors) and mCherry (to visualize *osx* expression and proper osteoblast ablation). We observed that in a control situation (Figure 50A and A'), nuclear pSmad1/5/8 is present in mature osteoblasts $Runx2^+Osx^+$ (Figure 50A and white arrowheads in magnified panels of A'), osteoprogenitors $Runx2^+Osx^-$ (Figure 50A and arrows in magnified panels of A') and in basal epidermal cells (Figure 50A and green arrowheads in magnified panels of A'). In the Mtz treated animals (Figure 50B and B'), nuclear pSmad1/5/8 is only observed in some of the newly formed

osteoprogenitors, Runx2^{+}Osx^{-} (Figure 50B and arrows in magnified panels in B'), and in the basal epidermal cells (Figure 50B and green arrowheads in magnified panels in B').

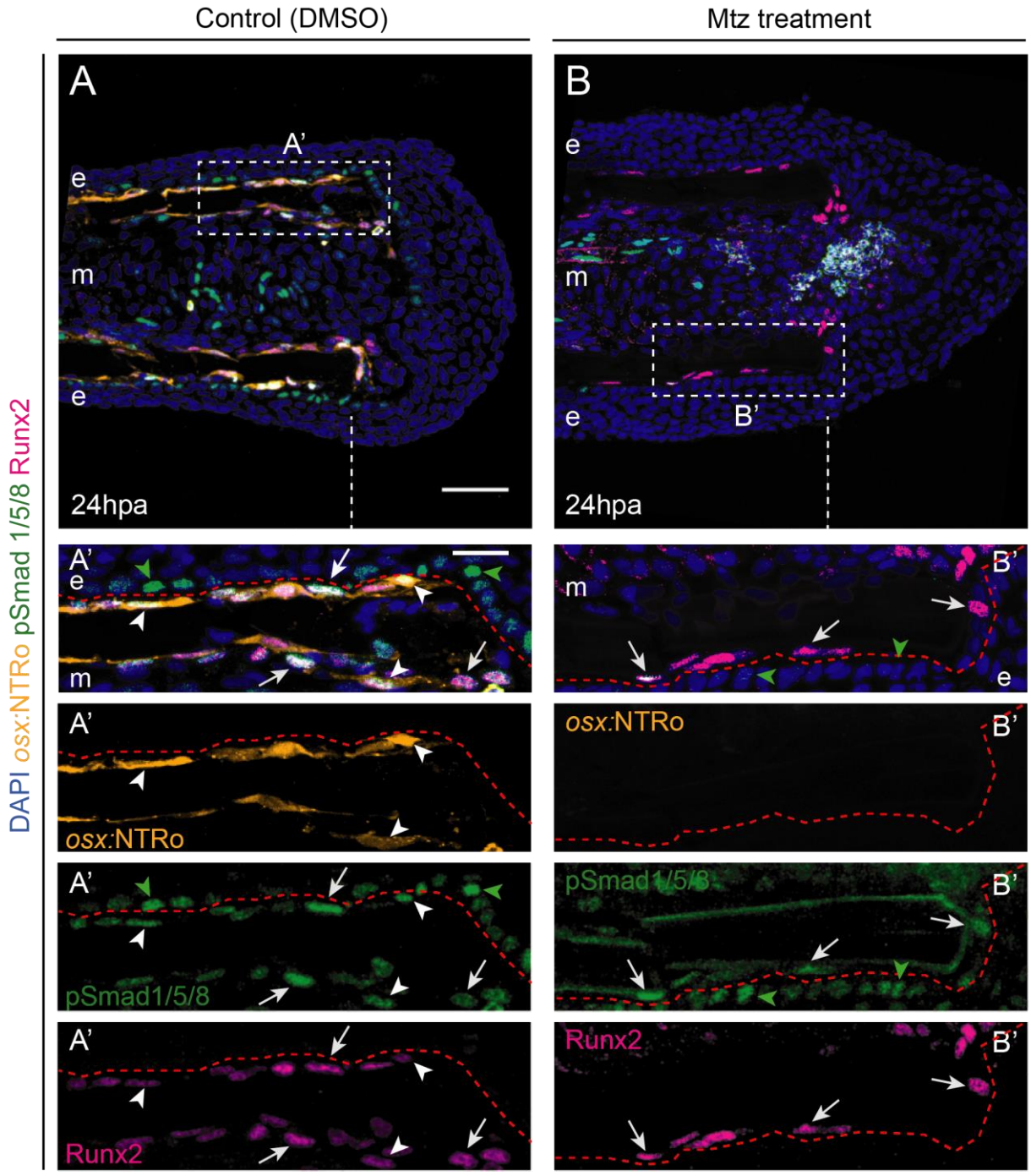

Figure 50: Bmp signalling is active in newly formed osteoprogenitors in normal regenerating condition and during regeneration in osteoblast depleted caudal fins. (A and B) Representative images of 24 hpa caudal fin longitudinal cryosections of *osx:*NTRo transgenic animals subjected to DMSO vehicle (control) (A and A') or to Mtz incubation (B and B'). Cryosections were immunostained for mCherry (to visualize *osx* expression and confirm correct osteoblast ablation, orange), pSmad1/5/8 (to monitor activated Bmp signalling, green), Runx2 (preosteoblast/ osteoprogenitor marker, magenta) and counterstained for DAPI (nucleus, blue). In the control condition (A and A'), active Bmp signalling, visualised through nuclear localized pSmad1/5/8, is mainly observed in the basal epidermal layer (green arrowheads in A'), in Runx2^{+}Osx^{+} osteoblasts (white arrowheads in A') and in Runx2^{+}Osx^{-} osteoprogenitors (white arrows in A'). In osteoblast ablation condition (B and B'), active Bmp

signalling is also seen in the basal epidermal cells (green arrowheads in B') and in some $Runx2^{+}Osx^{-}$ osteoprogenitors (white arrows in B'). This reveals that Bmp signalling could be an important pathway necessary to generate new osteoprogenitors during regeneration, particularly in the context of osteoblast depleted caudal fins. hpa: hours post-amputation, e: epidermis, m: mesenchyme; dashed white lines define the amputation plane; dashed boxes delimitate magnified panels A' and B'; scale bars represent 50 μm and 20 μm in magnified panels in A' and B'.

Consequently, we carried out assays to address the significance of active Bmp signalling in osteoblast depleted caudal fins during regeneration. We blocked Bmp signalling in *osx:*NTRo transgenic animals, subjected to the osteoblast ablation protocol, using a Bmp receptor inhibitor (Bmpri). After the recovery period, *osx:*NTRo transgenic animals were subjected to caudal fin amputation and exposed to the Bmpr inhibitor (BMPRi+) or to the vehicle (DMSO, BMPRi-) during one-day (Figure 51A). Fish were divided into four major groups according to the experimental setup and to the treatments that they were exposed to: without Mtz and without BMPRi (Mtz- BMPRi-); without Mtz and with BMPRi (Mtz- BMPRi+) to address the role of BMP signalling without compromising the mature osteoblast population; with Mtz and without BMPRi (Mtz+ BMPRi-); and with Mtz and with BMPRi (Mtz+ BMPRi+), to address the role of BMP signalling during *de novo* osteoblast formation in osteoblast depleted fins. Fins were allowed to regenerate and collected at 24 hpa for histological analysis (Figure 51A). When we compared Mtz-BMPRi- with Mtz-BMPRi+, to address the effect of inhibiting Bmp signalling in a control situation during regeneration, we observed no differences in the number of mature osteoblasts ($Runx2^{+}Osx^{+}$) (Figure 51B and C) however, there is a significant decrease in the number of $Runx2^{+}Osx^{-}$ progenitors that emerge in the non-ablation context in the Mtz-BMPRi+ group (Figure 51B and D). Moreover, when we compare Mtz+BMPRi- with Mtz+BMPRi+, to address the effect of blocking Bmp signalling in an osteoblast depleted situation during regeneration, we observed a strong osteoblast ablation, meaning that BMP signalling impairment does not affect the efficiency of the ablation protocol (Figure 51B and C). Importantly, we observe an extreme reduction in the number of osteoprogenitors $Runx2^{+}Osx^{-}$ in the Mtz+BMPRi+ condition (Figure 51B and D).

Overall, we have demonstrated that not only Bmp signalling is active in $Runx2^{+}$ osteoprogenitors, but also that there is a reduction in this cell population number when Bmp signalling is suppressed, in both normal and in osteoblast depleted regenerating caudal fins. This supports the hypothesis that Bmp signalling could be required for the formation and commitment of newly formed osteoblasts progenitors during regeneration.

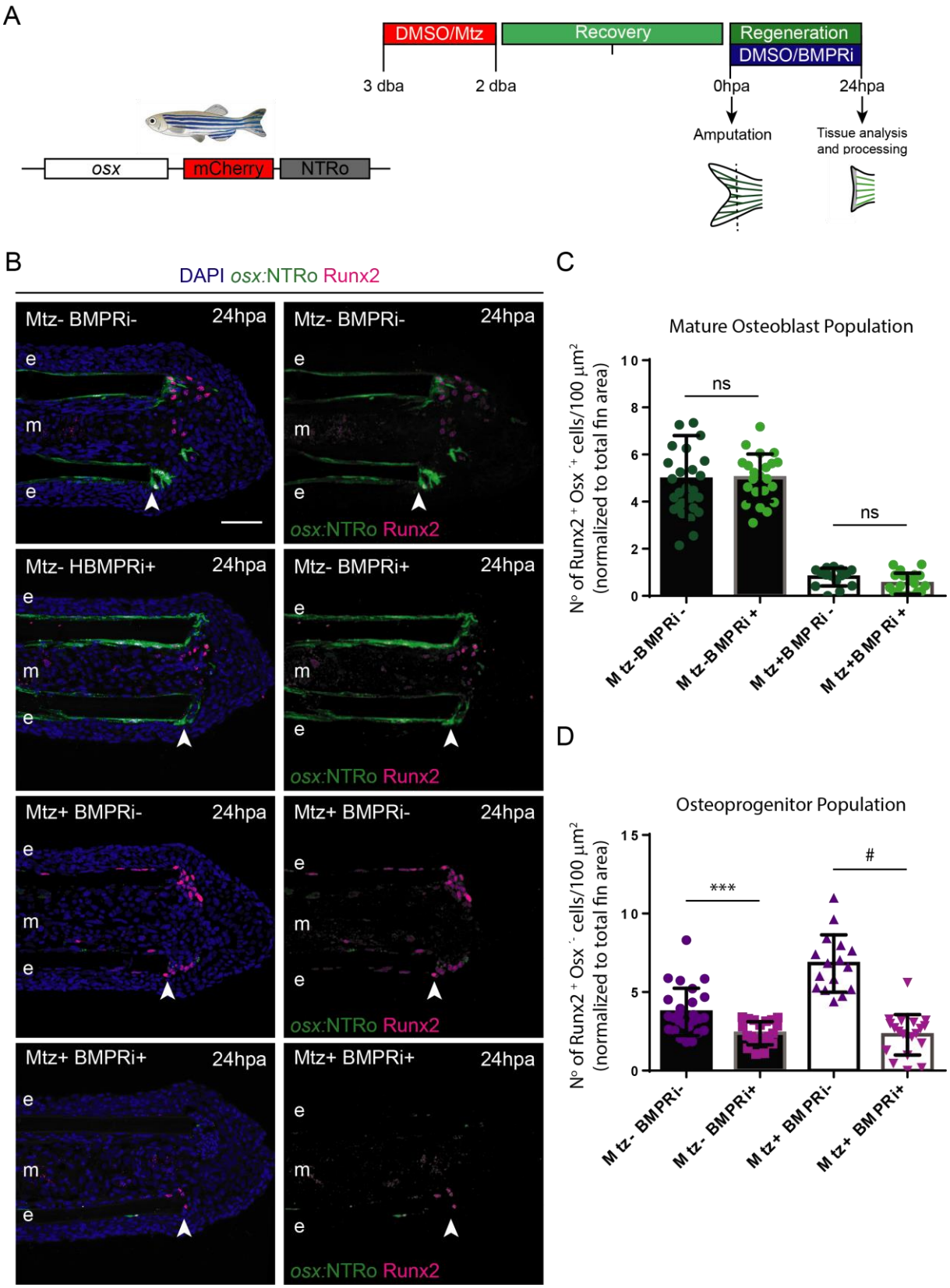

Figure 51: Requirement of Bmp signalling for *de novo* osteoblast formation in osteoblast depleted fins during caudal fin regeneration. (A) Schematic representation of the experimental setup used to perform functional manipulation of Bmp signalling and address the function of this pathway for *de novo* osteoblast formation. For that, we subjected *osx:*NTRo animals to the osteoblast ablation protocol shown in Figure 40A. After recovery caudal fins were amputated and animals were incubated for 24 hours either with a DMSO (Control, BMPRi-) or

with a BMP signalling inhibitor (BMPRi+) and divided in four main groups: controls (DMSO) without Mtz and without BMPRi (Mtz- BMPRi-); controls (DMSO) without Mtz and with BMPRi (Mtz- BMPRi+); treated with Mtz and without BMPRi (Mtz+ BMPRi-); and treated with Mtz and with BMPRi (Mtz+ BMPRi+). Fins were collected at 24 hpa for tissue imaging and subsequent processing. (B) Representative images of 24 hpa caudal fin longitudinal cryosections of *osx:*NTRo divided into the groups described above. Cryosections were immunostained for mCherry (to visualize *osx* expression and confirm correct osteoblast ablation, green), Runx2 (preosteoblast/ osteoprogenitor marker, magenta) and counterstained for DAPI (nucleus, blue). (C) Graph showing the quantification of mature osteoblast ($Runx2^{+}Osx^{+}$) at 24 hpa for all the four animal groups; bars on graph correspond to total number of $Runx2^{+}Osx^{+}$ cells normalized to total fin area and statistical analysis corresponds to Mann-Whitney test with Mean ± SD displayed (Mtz- BMPRi- : n= 27 bony-rays compiled from 8 fish; Mtz- BMPRi+ : n= 22 bony-rays compiled from 6 fish; Mtz+ BMPRi- : n= 16 bony-rays compiled from 5 fish; Mtz+ BMPRi+ : n= 21 bony-rays compiled from 6 fish). (D) Graph showing the quantification of osteoprogenitors ($Runx2^{+}Osx^{-}$) at 24 hpa for all the four animal groups; bars on graph correspond to total number of $Runx2^{+}Osx^{+}$ cells normalized to total fin area and statistical analysis corresponds to Mann-Whitney test with Mean ± SD (Mtz- BMPRi- : n= 27 bony-rays compiled from 8 fish; Mtz- BMPRi+ : n= 22 bony-rays compiled from 6 fish; Mtz+ BMPRi- : n= 16 bony-rays compiled from 5 fish; Mtz+ BMPRi+ : n= 21 bony-rays compiled from 6 fish). This shows that BMP signalling manipulation does not affect the mature osteoblast population, but it might be required for proper formation of $Runx2^{+}$ osteoprogenitors in normal regenerating fins and in fins subjected to osteoblast ablation. hpa: hours post-amputation, e: epidermis, m: mesenchyme; arrowheads define the amputation plane; scale bars represent 50 µm; ***p<0.001, # p< 0.0001, ns: non-significant.

Chapter VI

GENERAL DISCUSSION

1 OVERVIEW

Regenerative medicine is an emerging field that promises to have a relevant impact on human health and life quality by repairing and replacing injured tissues. The success of regenerative therapies depends on the identification of biological circuits that regulate wound closure, cell recruitment, survival, proliferation and cell fate determination. The study of natural regenerative properties of model organisms, such as zebrafish (Poss et al. 2003; Evans 2011; Goldsmith and Jobin 2012; Gemberling et al. 2013; Tavares and Lopes 2013; Shi et al. 2015; Antos et al. 2016), provides new insights into the mechanisms regulating the regenerative programs (Muneoka et al. 2008; Forbes and Rosenthal 2014; Godwin 2014). In this PhD thesis, we used the zebrafish caudal fin regeneration system to investigate the cellular and molecular strategies underlying bone formation. Upon injury, the formation of new bone relies on a tight and controlled regulation of the following sequence of events: generation of osteoprogenitors from resident osteoblasts and from intersegment progenitors (Knopf et al. 2011; Sousa et al. 2011; Ando et al. 2017); osteoprogenitor pool maintenance and proliferation; and redifferentiation and maturation of the osteoprogenitors, leading to bone matrix deposition (Stewart et al. 2014; Pfefferli and Jaźwińska 2015; Antos et al. 2016). In this project, we unravelled new findings on bone regeneration by uncovering new signalling pathways required for mature osteoblast dedifferentiation and osteoprogenitor redifferentiation. In addition, we identified alternative cellular sources for mature osteoblasts formation. In this section, we discuss the main results of this thesis and propose future directions and experiments.

2 OSTEOBLAST REPROGRAMMING AND DEDIFFERENTIATION DURING CAUDAL FIN REGENERATION

We and others have previously demonstrated that, after zebrafish caudal fin amputation, bone regeneration occurs via mature osteoblast dedifferentiation (Knopf et al. 2011; Sousa et al. 2011; Tu and Johnson 2011; Stewart and Stankunas 2012; Ando et al. 2017). However, since the molecular mechanisms that regulate this process are far from being understood, we proposed to identify new regulators of osteoblast dedifferentiation. Primarily, we uncovered the specific time-window when osteoblasts dedifferentiate during caudal fin regeneration. Subsequently, we performed an unbiased gene expression analysis of specifically isolated osteoblasts during multiple states of dedifferentiation, therefore revealing new key regulators of the process. In addition, we followed a targeted approach, where we examined the role of the Hippo/Yap signalling pathway in osteoblast dedifferentiation.

2.1 Dedifferentiation traits in osteoblasts

During dedifferentiation, osteoblasts lose their differentiated character. This process is characterized by downregulation of mature markers (such as *osc*) and upregulation of progenitor-like markers (such as *runx2*), cell shape-changes, and re-acquisition of proliferative capacity (Jopling et al. 2011; Tanaka and Reddien 2011; King and Newmark 2012; Maden 2013; Eguizabal et al. 2013; Kami and Gojo 2014). Therefore, the first part of this project consisted on characterizing the initial hours of the dedifferentiation process to clarify its time-window of occurrence. Previous studies addressed this process from 12 hpa to 24 hpa, showing that mature osteoblasts downregulate the mature marker *osc* at 12 hpa and undergo an EMT-like event, begin to migrate, start to express progenitor markers, and proliferate at around 18-24 hpa (Knopf et al. 2011; Sousa et al. 2011; Stewart et al. 2014). Since we increased the temporal resolution of these events, we were able to observe that osteoblast dedifferentiation is triggered during the first stages of wound healing (0 – 18 hpa). Differences in expression of mature and progenitor markers start as early as 3 to 6 hpa and the acquisition of motility and cell cycle re-entry are observed at 6 to 9 hpa, suggesting that osteoblast dedifferentiation is initiated in a time-window between 3 to 6 hpa. Additionally, these results show that in the first few hours after amputation, important transcriptional and phenotypic alterations occur within mature osteoblasts. At this stage, the more relevant events that had been described so far were wound closure, apoptosis and ROS production induced by amputation (Poss et al. 2003; Gauron et al. 2013; Niethammer 2016; Owlarn et al. 2017). Thus, we have shown for the first time that mature osteoblast dedifferentiation is an early response to injury and happens concomitantly with wound closure. We can thus speculate that early wound response signals are important to trigger osteoblast dedifferentiation. Importantly, this characterization served as a basis to design the subsequent experiments that aimed to identify novel regulators of this process.

2.2 Genome-wide expression of dedifferentiating osteoblasts: unravelling new regulators of osteoblast dedifferentiation during fin regeneration

After identifying the time-window at which osteoblast dedifferentiation is triggered, we carried out an unbiased approach to reveal novel regulators of this process. We performed a microarray approach that encompasses up-to-date content with high coverage of the zebrafish transcriptome. Previous works performing wide-genome transcriptional analysis addressed stages later than 12 hpa (Schebesta et al. 2006; Kang et al. 2016; Rabinowitz et al. 2017), thus potentially missing initial regulators of the dedifferentiation process. Additionally, these gene expression studies have used the whole tissue, which can result in the dilution of important factors. In our approach we introduced two main novelties: transcriptional analysis of early time-points of the regenerative process (3 to 9 hpa); and characterization of a specifically isolated cell population, therefore uncoupling osteoblast response from surrounding tissues.

2.2.1 Transcription profiling of osteoblast dedifferentiation: general appreciations

The analysis of the expression profile of osteoblasts was performed by comparing homeostasis with three time-points during regeneration, resulting in 3 different data sets: 3 hpa versus uncut, 6 hpa versus uncut, and 9 hpa versus uncut. These comparisons have shown that there is a considerable amount of differentially expressed genes in all time-points in comparisons to control samples. Data from HCA, PCA and from the three genome comparisons obtained, suggest that all the time-points analysed are similar between each other and that the 3 hpa time-point was the most similar to uncut samples. These time-points share many differentially expressed genes, with only 15% from 3 and 9 hpa and 30% from 6 hpa being exclusive of each time-point, and around 304 were differentially expressed in all time-points analysed (see Chord Diagram in Figure 22 from Chapter III). This analysis reinforces our observation that significant differences in gene expression happen very early upon amputation (as early as 3 hpa). Gene enrichment and GSA analysis revealed relevant functional categories altered upon osteoblast dedifferentiation related to cell cycle control, cytoskeletal dynamics, migration regulation and ECM remodelling, cellular junction assembly, metabolic regulation, signal transduction pathways and chromatin organization and remodelling. Most of these categories are known to be important in several aspects of the regenerative process.

2.2.2 Cell cycle control during osteoblast dedifferentiation

One of the most important aspects following dedifferentiation is the acquisition of proliferative capacity (Poss et al. 2003; Stoick-Cooper et al. 2007; Poss 2010; Tanaka 2016). Interestingly, our transcriptomic analysis showed what might be two different cell cycle responses triggered by amputation: an anti-proliferative response, in which osteoblasts seem to activate cell cycle arrest and possibly DNA repair, as shown by the upregulation of *tumour protein 53* (*tp53*); and a pro-proliferative response, with upregulation of *cyclinD1,* among others that drive the G1/S transition. This suggests the presence of two different osteoblast populations, of which we can only speculate about: one that is deleteriously affected by the injury, which arrests the cell cycle to evaluate the damage, and another that initiates proliferation. While it is unclear if the first has a role in regeneration, the latter is potentially contributing to the pool of osteoprogenitors to ensure correct bone formation during regeneration. Focusing on Tp53, its specific role in this context is not obvious. Contrasting with our results, where it is highly upregulated during the osteoblast dedifferentiation process, during salamander limb regeneration downregulation of Tp53 is necessary for cell cycle re-entry of differentiated cells during blastema formation, with its activation being required at later stages for redifferentiation (Yun et al. 2013; Charni et al. 2017). Tp53 is a major tumour suppressor protein (Aubrey et al. 2016) known to mediate cell cycle arrest of cells that have undergone DNA damage. Interestingly, although tumorigenesis and regeneration share common signalling pathways, the outcome of these processes is quite different. While regeneration comprises a well-coordinated and restrained sequence of events, cancer cell

transformation is achieved via unrestrained activation or inactivation of pathways that culminate in uncontrolled proliferation (Charni et al. 2017). Therefore, we hypothesize that during osteoblast dedifferentiation some are exposed to severe environmental changes, such as differences in osmotic pressure and ROS release, in particular, those next to the amputation plane. These cells may require activation of Tp53 to promote cell cycle arrest and DNA repair or to trigger apoptosis if they are damaged beyond possible recovery, avoiding continuous proliferation of damaged osteoblasts and potential tumour initiation. We suggest that Tp53 activity might not only be necessary at late stages of regeneration but also at early stages, functioning as a surveillance mechanism to dispose the tissue of deleterious cells before regeneration is fully launched. This implies a tight regulation of the cell cycle re-entry and proliferation during regeneration and might be one important feature that distinguishes it from tumorigenesis. Nonetheless, a role for Tp53 during osteoblast reprogramming can also be proposed. In mice, Tp53 has been shown to be a negative regulator of osteoblast differentiation: p53-null mice display accelerated differentiation and augmented *osterix* expression (Wang et al. 2006). Thus, another hypothesis is that in zebrafish, tp53 is required to inhibit osteoblasts differentiation markers and promote the progenitor-like phenotype. Further testing will be required to address these hypotheses.

2.2.3 Migratory behaviour during osteoblast dedifferentiation

Regarding genes associated with cell migration we detected regulation of actin, myosin and microtubule dynamics, downregulation of Adherens and Tight junction components, upregulation of focal adhesion components, and upregulation of ECM remodelling regulators, all important traits of migrating cells (Wozniak et al. 2004; Baum et al. 2008; Huttenlocher and Horwitz 2011). In homeostasis, osteoblasts are organized in an epithelial-like sheet, connecting with each other via junction components (Stewart et al. 2014). As shown in Chapter III, upon amputation, osteoblasts start migrating very early, around 5-10 hpa (Figure 18) and undergo an EMT-like event (Stewart et al. 2014). Thus, in this context, downregulation of Adherens and Tight junction should be essential to disassemble their epithelial organization and promote EMT and migration. Focal adhesion assembly is also required in osteoblasts that undergone EMT, in order to reach the amputation plane and contribute to blastema formation. Therefore, our results suggest that dedifferentiating osteoblasts will undergo great cytoskeletal adaptations with disassembly of their cell-cell adhesions and promotion of pro-migratory focal-adhesions. Furthermore, we noticed the upregulation of pro-migratory ECM components (Godwin et al. 2014), such as TenC.

2.2.4 Chromatin remodelling and signal transduction

Chromatin remodelling modulators and signal transduction pathways are considered the best candidates to play a direct role in cell fate plasticity and cell fate decisions, as they can directly regulate specific transcription factors that specify or maintain cell identity (Onder et al. 2012;

Moris et al. 2016; Guo and Morris 2017). In fact, our microarray analysis revealed that some chromatin modifying enzymes are differentially expressed during dedifferentiation. These enzymes activate or suppress gene expression by modifying nucleosome histones or by mobilizing the DNA-histone structure (Kouzarides 2007; Onder et al. 2012; Zhang et al. 2016). In general terms, HATs and HDMs enzymes are associated with chromatin opening and activation of gene expression, whereas HTMs and HDACs enzymes are associated with closed chromatin and lower gene transcription. With our analysis, we found that enzymes promoting both gene transcription and gene silencing are upregulated during the early stages of regeneration. This is not surprising, given that a hallmark of the regenerative process is the re-activation of silenced development-related genes (Stewart et al. 2009; Katsuyama and Paro 2011; Percharde et al. 2017). Therefore, chromatin remodelling may be required during osteoblast dedifferentiation to allow these cells to adopt new features, such as: expression of progenitor traits, including genes required for proliferation; and shutdown of functions related to their function in homeostasis, such as mature markers and genes associated with bone matrix secretion (Knopf et al. 2011; Sousa et al. 2011; Blum and Begemann 2015b). In fact, chromatin decondensation has already been demonstrated to happen during cell dedifferentiation in plants (Zhao et al. 2001; Williams et al. 2003) and in newt lens regeneration (Maki et al. 2010). Moreover, initiation of caudal fin regeneration was shown to be dependent on the conversion of bivalent chromatin (with both repressing and activating histone modification) into an active state, by a histone demethylase (Stewart et al. 2009). Thus, histone modifications at discrete genomic positions may be important to regulate osteoblast dedifferentiation.

Signal transduction cascades leading to activation of transcription factors, are the most direct causes of transcription alterations and encompass the most well-studied mechanism underlying the cell fate decisions, inclusively when talking about pluripotency reprogramming events (e. g.: iPCs) (Takahashi and Yamanaka 2006; Sánchez Alvarado and Yamanaka 2014). Our transcriptome analysis detected several signal transduction pathways that are differentially expressed such as Wnt, Insulin, leptin, and Jak/Stat signalling pathways.

Some Wnt signalling components are upregulated in our data set, suggesting that this pathway is activated during osteoblast dedifferentiation. One of these components is the Wnt ligand *wnt10a*, which specifically activates β-catenin-dependent Wnt signalling. Corroborating our data, *wnt10a* has already been demonstrated to be upregulated at 6 hpa in whole caudal fins (Stoick-Cooper et al. 2006), but not specifically in osteoblasts. In addition, besides being important for later aspects of the regenerative outgrowth (from 72 hpa onwards) (Stewart et al. 2014; Wehner et al. 2014), Wnt signalling was shown to be required in the first 24 hpa to initiate osteoblast EMT-like process, necessary for their recruitment and integration into the blastema (Stewart et al. 2014). Therefore, we propose that Wnt signalling is promoted by osteoblasts (a source of Wnt ligands) during regeneration while regulating their dedifferentiation state. Nevertheless, future experiments are required to understand whether

Wnt signalling is necessary and sufficient to trigger osteoblast dedifferentiation during caudal fin regeneration.

Our analysis also showed that the insulin signalling pathway is regulated in osteoblasts, with the expression of ligands being generally increased and the expression of receptors being decreased. This may indicate that osteoblasts act as a source of insulin ligands but do not activate the signalling pathway in a cell autonomous manner. Besides being an important regulator of glucose metabolism in the body (Lizcano and Alessi 2002), insulin signalling also has specific roles in osteoblasts (Ferron et al. 2010; Pramojanee et al. 2014). In mammalian systems, insulin signalling promotes glucose uptake, homeostasis and metabolic regulation during osteoblast growth and differentiation. In addition, it has been shown to induce the expression of differentiation markers, such as Osteocalcin (Ferron et al. 2010; Pramojanee et al. 2014). This fits with our data, which shows that insulin receptors are downregulated in osteoblasts, leading us to hypothesise that, during osteoblast dedifferentiation, insulin signalling needs to be downregulated in order to shut down the expression of mature markers such as Osteocalcin. Therefore, although metabolic regulation is important in osteoblast dedifferentiation, the role of insulin signalling in this context seems to be independent of its role in metabolism. Nevertheless, functional experiments will be necessary to address the requirement of this pathway in osteoblasts dedifferentiation.

Another interesting finding in our data sets was the upregulation of *leptin b* in all the three time-points. Leptin b is a conserved secreted hormone that activates the leptin signalling pathway which, similarly to insulin signalling, is known to control energy homeostasis and glucose metabolism (Dalman et al. 2013; Park and Ahima 2014; Michel et al. 2016). Leptin b has already been shown to be upregulated (130 folds) at later time-points, during the outgrowth phase in the amputation region (Kang et al. 2016). Here, we show for the first time that *leptin b* is upregulated much earlier than what has been described (from 3 hpa onwards), leading us to identify osteoblasts as the source of *Leptin b* during dedifferentiation. Unfortunately, we were not able to identify other differentially expressed components of the leptin pathway, in order to elucidate whether it is also active in osteoblasts. Leptin signalling can act in parallel and/or interact with the insulin pathway in other contexts to regulate energy consumption and glucose metabolism (Amitani et al. 2013; Thon et al. 2016) and, like insulin signalling, Leptin can regulate mammalian bone homeostasis through Osteocalcin (Ferron and Lacombe 2014; Upadhyay et al. 2015). Taking this into account, further studies are required to clarify if insulin and leptin signalling pathways have overlapping roles during osteoblast dedifferentiation through the regulation of *osteocalcin*, as well as the relevance of the insulin/leptin-glucose axis for this process and its implications for osteoblast metabolic adaptation.

Another pathway potentially regulated in our data set was the Jak/Stat signalling pathway, known to regulate proliferation, cell fate and cell migration (Rawlings 2004; Murray 2007). Upon ligand binding to the receptors, Janus kinases (Jak) are activated, which then

phosphorylate signal transducers and activators of transcription (Stat) members to trigger target gene expression (Rawlings 2004). Some of the components of this pathway, such as *jak1*, *jak2a* and *stat1a*, are upregulated in all time-points, suggesting that this pathway is activated and plays a role in osteoblast dedifferentiation during caudal fin regeneration. In fact, during regeneration of the zebrafish retina, Jak/Stat signalling is activated in injury responsive Müller glia and induces their dedifferentiation into progenitors that will compensate for photoreceptor loss (Zhao et al. 2014). Interestingly, in this context, leptins have also been shown to be important activators of Jak/Stat signalling (Zhao et al. 2014). Nonetheless, further experiments are required to investigate whether Jak/Stat signalling is indeed a regulator of osteoblast dedifferentiation and whether its activation is mediated by leptin signalling.

The above-mentioned signal transduction pathways Wnt, Insulin and Jak/Stat, have already been shown to be required for the regeneration of several zebrafish organs, including the caudal fin, by controlling cell proliferation, cell-shape changes and rearrangements, cell fate determination (Stoick-Cooper et al. 2006; Chablais and Jazwinska 2010; Fang et al. 2013; Stewart et al. 2014). Accordingly, we found, for the first time, that these signalling pathways are also regulated in osteoblasts during dedifferentiation.

2.2.5 Metabolic reprogramming during osteoblast dedifferentiation

One of the most differentially regulated gene categories in our microarray is related to the cellular metabolism. Several enzymes from the glycolytic pathway, genes related to mitochondrial dynamics and components of the electron transport chain were upregulated during all three time-points after amputation. This suggests that, during osteoblast dedifferentiation, metabolic adaptation, namely the balance between glycolysis and OxPhos, plays an important role.

Cellular metabolism encompasses highly coordinated mechanisms through which energy is used to produce and breakdown cell molecular constituents, in order to maintain its integrity. It can be generally categorized as catabolic (oxidative), completed in the mitochondria where metabolites are transformed to produce energy (oxidative phosphorylation), or as anabolic (non-oxidative), completed in the cytoplasm where macromolecules (e.g. lipids and nucleotides) are generated from precursor molecules (glycolysis). (Prigione et al. 2015; Ryall et al. 2015; Chandel et al. 2016). The metabolic state of a cell results of a wide array of inputs: energetic and biomass demands, availability of resources (e.g. oxygen and glucose), environmental cues and cell differentiation status. Beyond providing energetic supply, metabolic networks can also trigger genetic programs and control cell behaviour and cell fate specification. It is known that cellular identity and functional state reflects specific metabolic pathways used (Tatapudy et al. 2017; Wei et al. 2018). A switch in the type of metabolism is thus seen as a key mode of regulating cell fate transitions and is often collectively designated as “metabolic reprogramming” or “metabolic adaptation”. In homeostatic conditions,

differentiated, non-dividing somatic cells use OxPhos as their primary source of energy, allowing them to catabolize substrates in a more energy efficient manner to perform their specialized housekeeping functions. In contrast, a common metabolic trait of ESCs (and iPSCs), quiescent stem cells (e.g. hematopoietic stem cells or mesenchymal stem cells) and progenitor cells is their preference in performing glycolysis (with lactate production) and in decreasing mitochondrial OxPhos (Folmes et al. 2012; Ryall et al. 2015; Chandel et al. 2016; Wei et al. 2018). Interestingly, this switch in the metabolic signature observed in of some stem cells and progenitor cells, in which they prefer glycolysis with lactate generation over OxPhos, even in the presence of oxygen, is reminiscent of the "Warburg effect", also termed aerobic glycolysis, which occurs in cancer cells. (Warburg 1925; Prigione et al. 2015; Shyh-Chang and Daley 2015; Liberti and Locasale 2016; Potter et al. 2016). Prioritizing glycolysis enables the generation of essential intermediaries or building blocks required for the synthesis of macromolecules, such as amino acids, lipids, and nucleotides, which are required for biomass assembly, cell growth and division. In addition, although glycolysis is inefficient in terms of total ATP production when compared to OxPhos (2 ATP versus 36 ATP, respectively), the rate of ATP generation of glycolysis is faster (Lunt and Vander Heiden 2011). Also, another important aspect of using glycolysis over OxPhos is the reduction of ROS production by mitochondrial respiration (Chandel et al. 2016). This is particularly an advantage for quiescent stem cells, as they are often more sensitive to oxidative damage that can lead to genomic instability. However, recent data also suggest that actively growing and highly proliferative cells (either progenitors cells or cell that have to undergo stage dependent proliferative events, such as enterocytes or lymphocytes) have bivalent metabolism and use both glycolysis (with lactate production) and OxPhos (Prigione et al. 2015; Tatapudy et al. 2017).

Another important feature during metabolic reprogramming is mitochondrial dynamics. OxPhos is maximised by mitochondrial fusion, which stabilises the respiratory network and minimized by mitochondrial fission, needed to generate new mitochondria. Thus, mitochondrial dynamics can also have a great impact in regulating cell identity (van der Bliek et al. 2013; Xu et al. 2013; Khacho et al. 2016).

Given the fundamental roles of metabolism in mediating cell fate decisions upon demand, it is therefore plausible that during major cellular reconstruction events, such as the ones observed during regeneration, would involve significant changes in cell metabolism. Despite the considerable amount of information on the role of metabolism in health and disease, the link between metabolic reprogramming, regeneration and repair remains poorly understood and controversial. A recent study showed that, during planarian regeneration, there is an increase in glycolysis and that most of the glucose catabolized is fated for aerobic glycolysis (Osuma et al. 2018). In mice models of ear and digit injuries, *Lin28a* induces the expression of different metabolic enzymes that lead to an increase in both glycolysis and oxidative phosphorylation, promoting the enhancement of tissue repair. In addition, tissue repair was

abrogated by OxPhos inhibition, suggesting that in this context OxPhos is required for tissue repair (Shyh-Chang et al. 2013).

In our data sets, we observed that several important glycolytic enzymes, such as *pfkpa*, *aldoaa*, *pgam1a*, *hk1* and *pdhb* were consistently upregulated in osteoblasts from 3 to 9 hpa and that the expression of the enzyme *ldha*, responsible for the interconversion of pyruvate and lactate, is upregulated. These results suggest that, during osteoblast dedifferentiation, glycolytic influx and lactate production is increased (Figure 52) and that at least part of the pyruvate is being converted into lactate and shunt away from OxPhos. We have also detected the upregulation of genes that control mitochondria dynamics and function, particularly mitochondrial fission, such as *fis1*. Moreover, at 3 hpa we noticed a downregulation of genes related to the electron transport chain, such as *cox5b*, *ndufb3* and *ndufb5*, suggesting a decrease in OxPhos. However, from 6-9 hpa we observed an upregulation of several components of the electron transport chain, such as cytochrome c subunits or assembly factors, NADH and succinate dehydrogenase components, following the initial upregulation of glycolytic enzymes, suggesting that OxPhos is also increased.

Taking all into account, our results show that during osteoblast dedifferentiation, osteoblasts may change their metabolic profile to better adapt to the new energetic demands of the regenerative process. Therefore, we speculate that dedifferentiating osteoblasts suffer a metabolic reprogramming event in the form of a glycolytic switch triggered very early during this process (starting at 3 hpa). In particular, our results suggest that glycolytic enzymes might be required to trigger dedifferentiation, but that the dedifferentiation process might rely on a bivalent metabolic profile that requires both glycolysis and OxPhos, as described for other types of progenitor cells. It would be interesting to evaluate whether changes in metabolism are required prior to osteoblast dedifferentiation during regeneration, as shown during reprogramming of iPSC (Prigione et al. 2015; Tatapudy et al. 2017). We have also shown that changes in the expression of glycolytic enzymes and electron transport chain components are not exclusive to osteoblasts but also occurred at the level of the whole caudal fin tissue (Figure 24). However, in the whole fins, the upregulation of glycolytic enzymes was more evident than upregulation of OxPhos-related genes.

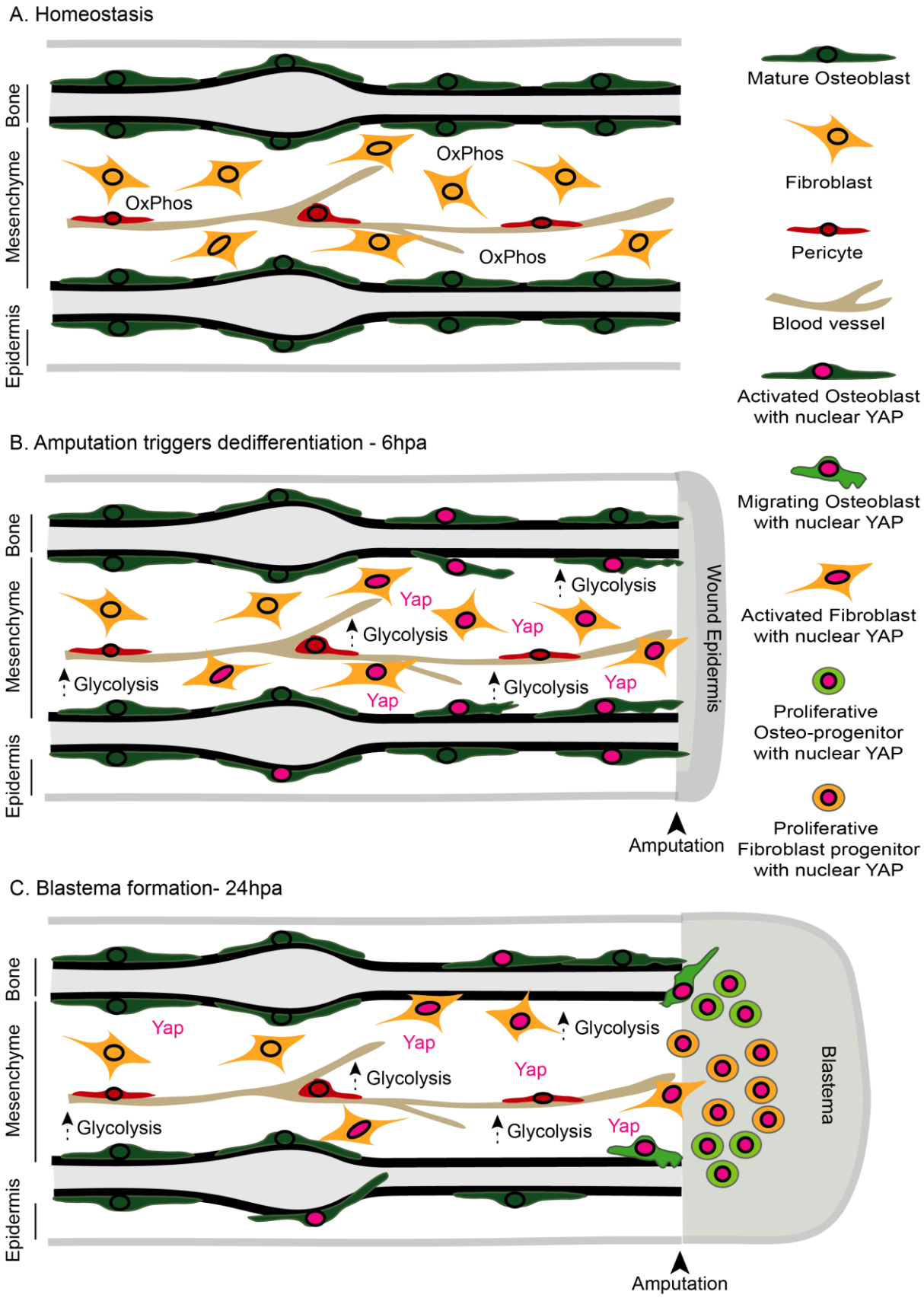

Figure 52: Model of zebrafish caudal fin dedifferentiation regulation during regeneration. Schematic representation of the bilateral organization of the caudal fin bony-ray through longitudinal sections. The caudal fin is composed of two concave bones or hemirays surrounded by a multilayered epidermis. The space between the hemirays is filled with connective tissue (mesenchyme) that contains densely interconnected fibroblasts,

enclosing also other cell types and tissues such as blood vessels. (A) During homeostasis, the caudal fin skeletal elements are produced and maintained by osteoblasts that deposit a collagenous bone matrix, on which the robustness of the caudal fin depends. In this homeostatic condition, osteoblasts and other cell types rely mainly on oxidative phosphorylation (OxPhos) to produce the required energy for performing their normal functions. (B) After caudal fin amputation, the regenerative process is triggered, and new cellular demands arise. The osteoblasts that are below the amputation plane dedifferentiate and, although lineage committed, divide and produce new cells that reconstitute the missing structure. Our findings suggest that osteoblast dedifferentiation is triggered very early during regeneration, at 3-6 hpa, coinciding with the upregulation of the major glycolic enzymes. This increase is also observed at the whole-tissue level near the amputation region. We hypothesize that, during osteogenic dedifferentiation and during regeneration, metabolic reprogramming/glycolytic switch occurs to enable cells to produce the biomass required to divide later in the regenerative process. Concomitantly, the Hippo pathway effector Yap translocates to the nucleus in osteoblasts and fibroblasts within the mesenchymal compartment, suggesting a role for Yap in dedifferentiation during fin regeneration. (C) Both pathways are important in later stages of blastema formation since their inhibition leads to several defects including in cell cycle re-entry, a major requirement during tissue regeneration.

In the course of this work, we have also demonstrated that inhibition of glycolysis during early stages of regeneration leads to impairment of proliferation, not only in osteoblasts but also in other cell types (Figure 53). In addition, it also leads to a decrease in the expression of osteoblast markers and in the number of proliferative $Runx2^{+}Osx^{+}$ immature osteoblasts, while the progenitor pool $Runx2^{+}Osx^{-}$ subtype remains unchanged within the blastema. This suggests that glycolysis may not be required to maintain the self-renewing pool of immature osteoprogenitors but to maintain the proliferative $Runx2^{+}Osx^{+}$ osteoblast population (Figure 53). Moreover, we found that the formation of the wound epidermis is defective upon glycolysis inhibition. Since this tissue provides signals that induce differentiation from $Runx2^{+}Osx^{-}$ to $Runx2^{+}Osx^{+}$ immature osteoblasts (Wehner and Weidinger 2015), these defects could also explain the decrease and disorganised $Runx2^{+}Osx^{+}$ osteoblast subtype. These data provide evidence that glycolysis is required during caudal fin regeneration, in particular for bone repair (Figure 53). However, more experiments are required to understand what exactly the role of glycolysis. The metabolic changes in dedifferentiating osteoblasts occur concomitantly with significant transcriptional changes, alterations in morphology, EMT and acquisition of motility, and cell cycle re-entry and proliferation. Future experiments should thus address how glycolysis influences the expression of osteoblast maturation markers, acquisition of EMT and cell migration. In addition, monitorization of cellular metabolites, such as glucose, glutamate, lactate and ATP/ADP ratios, should help us clarify and dissociate the roles of glycolysis and OxPhos during osteoblast dedifferentiation in regenerating caudal fins.

Taken together, our data provides the first evidence that metabolism is regulated during osteoblast dedifferentiation and suggest that both glycolysis and OxPhos play important roles in this process.

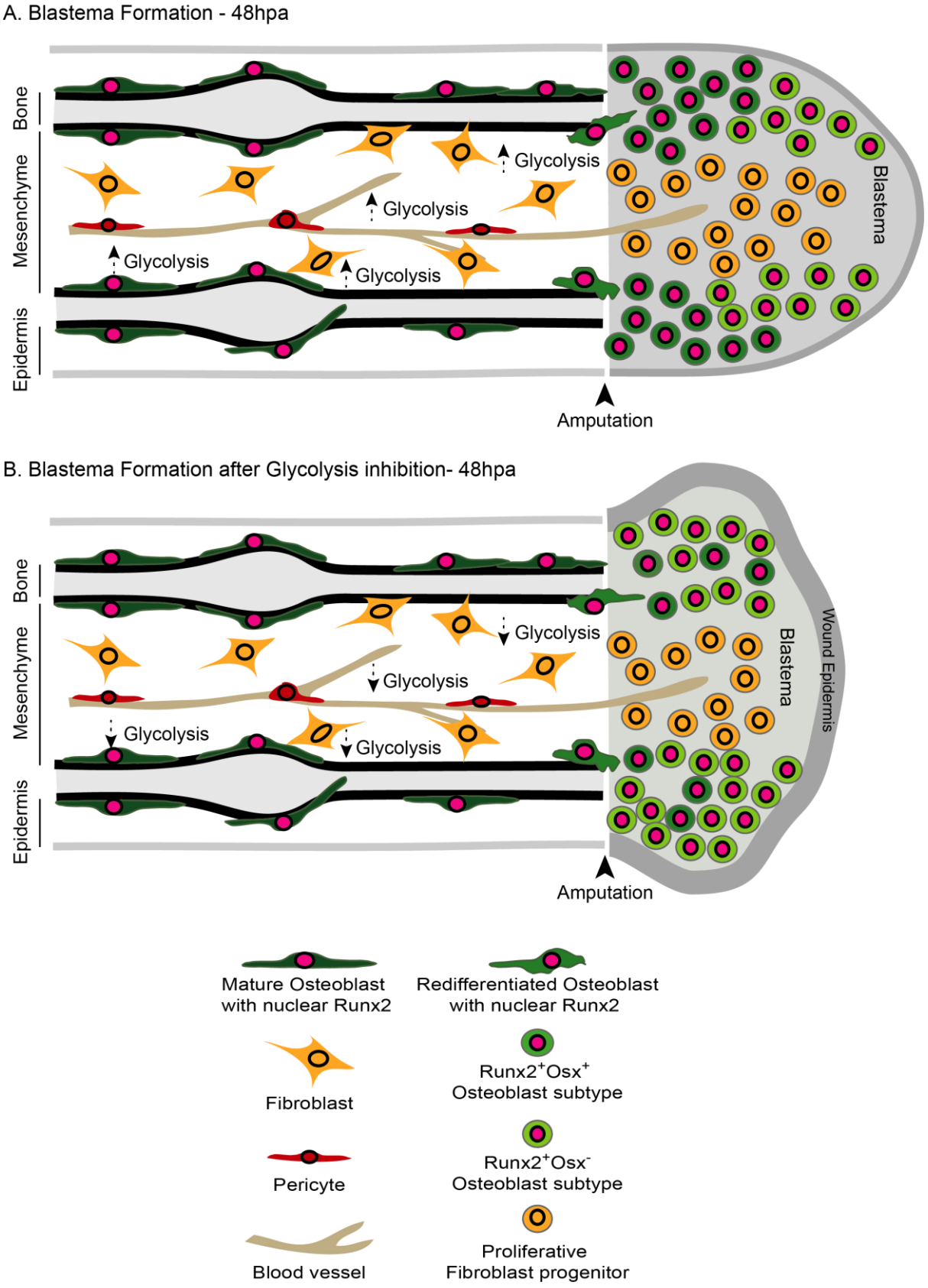

Figure 53: Model for the role of glycolysis during bone repair after caudal fin amputation. (A) During normal bone regeneration, at the end of the blastema formation phase (48 hpa), osteoprogenitors have already formed and started to redifferentiate to form fully differentiated osteoblasts that will produce the newly caudal fin skeletal tissue. Within the blastema, bone maturation occurs in overlapping proximal-distal compartments, such that it increases in a distal-proximal manner: while near the amputation plane, in the proximal blastema region,

proliferative Runx2+Osx+ differentiating osteoblasts predominate; the distal blastema contains more self-renewing Runx2+Osx- progenitor/precursors. During this phase, the cell cycle accelerates, and the formation of cellular biomass increases. (B) Besides a general impairment of the regenerative process, inhibition of glycolysis during blastema formation leads to an accentuated decrease in the proliferative Runx2+Osx+ differentiating osteoblast population, whereas the self-renewing Runx2+Osx- progenitor population remains unchanged. In addition, the few emerging Runx2+Osx+ osteoblasts appear more scattered along the proximal-distal axis of the blastema than in the control condition. Importantly, inhibition of the glycolytic influx also leads to cell cycle re-entry impairment and to the disorganization of the wound epidermis, which functions as a signalling centre for the underlying cells.

2.3 Hippo/Yap pathway in osteoblast dedifferentiation during caudal fin regeneration

After our transcriptomic- wide approach, we performed a targeted gene approach, where we explore the contribution of the Hippo/YAP signalling pathway for osteoblast dedifferentiation, as it has been involved in cell dedifferentiation in other contexts (Nicolay et al. 2010; Yu and Guan 2013; Zhao 2014; de Sousa et al. 2018).

We showed that during osteoblast dedifferentiation (6 hpa), Yap translocates to the nucleus in resident mature osteoblasts and in mesenchymal cells (Figure 52), suggesting that Yap is activated in these cells around this time-point. The nuclear localization persists until latter time-points (24 hpa) inclusively in the osteoprogenitor pool. We found that Yap loss of function leads to a decrease in the number of proliferating osteoblasts (and also mesenchymal cells) and to impaired osteoblast migration towards the amputation region (Figure 54). In addition, Yap loss of function lead to a significant reduction in the number of osteoprogenitors formed during regeneration (Figure 54). On the other hand, a gain of function tool, with expression of a constitutively active form of Yap, induced an increase in the number of osteoprogenitors. Overall, these data suggest that the Hippo pathway effector Yap regulates osteoblast proliferation, and migration during dedifferentiation upon amputation. As mentioned for glycolysis, future experiments should evaluate osteoblast maturation markers and other dedifferentiation features that are still missing, in order to conclude if indeed Yap is required for osteoblast dedifferentiation.

We also checked whether known Yap target genes were differentially expressed in our genome-wide expression microarray. Unfortunately, many Yap targets are also common to other signalling pathways that, depending on the cellular context, are known to act synergistically and to interact with Yap (Attisano and Wrana 2013; Kim and Jho 2014; Park et al. 2015). Therefore, no clear evidence for regulation of specific Yap targets during osteoblast dedifferentiation was observed in our array. Given that Yap is required for osteoblast proliferation and motility, it would be interesting to evaluate whether Yap regulates genes related to those categories identified in our transcriptome profile analysis.

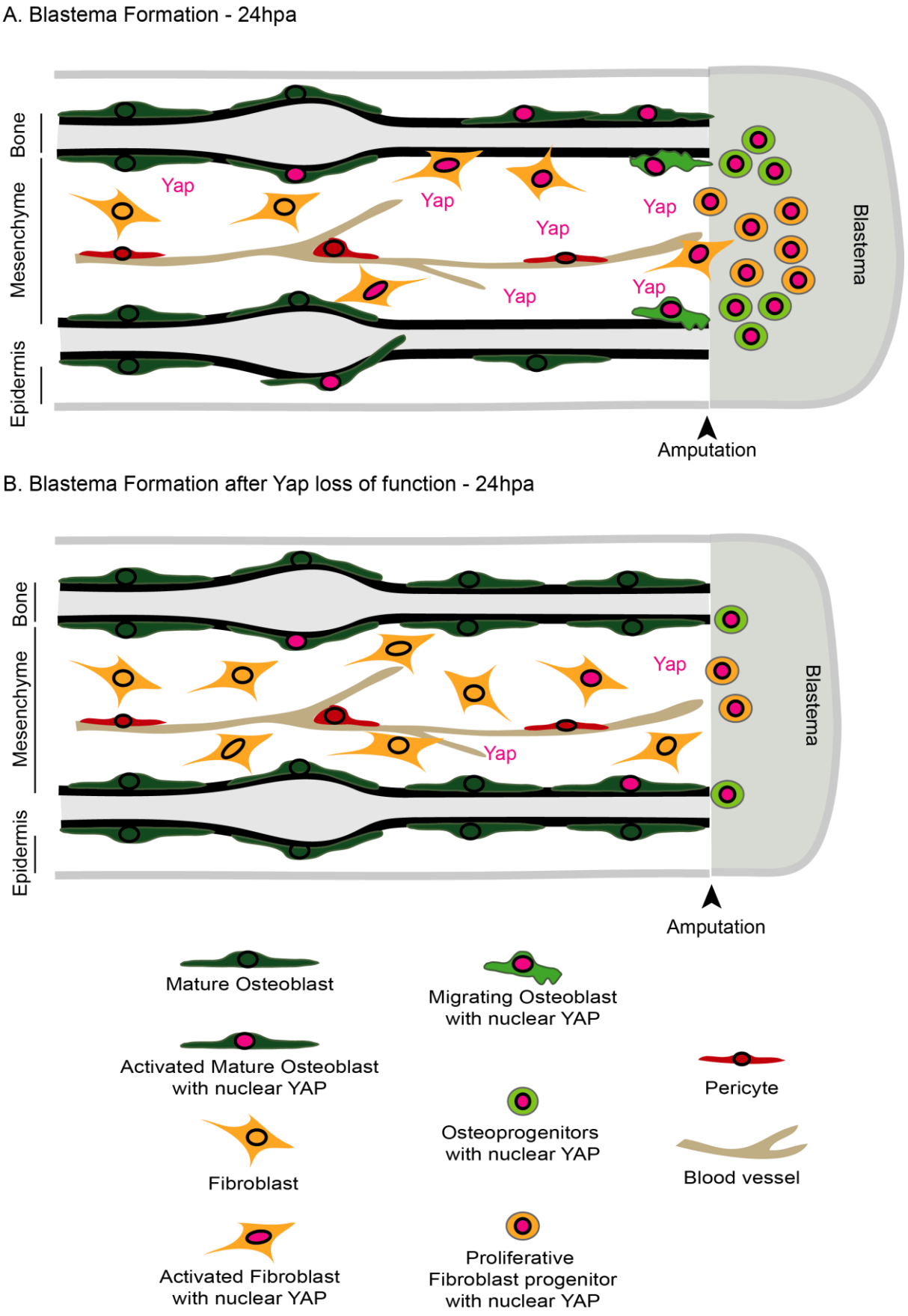

Figure 54: Model for the role of Yap during osteoblast dedifferentiation after caudal fin amputation. (A) In the first 24 hpa, in a normal regenerating condition, mature osteoblasts undergo dedifferentiation, detach from the

bony-ray surface and migrate distally to incorporate the blastema. There, these osteoprogenitors proliferate to generate more progenitors that are crucial for bone repair. During the dedifferentiation time-window, the Hippo pathway co-activator Yap translocates from the cytoplasm to the nucleus in mesenchymal fibroblasts and in mature osteoblasts in close contact with the bone surface. This suggests that Yap may promote mature osteoblast reprogramming and consequently osteoprogenitor formation. (B) After manipulating Yap function, using a loss of function transgenic line, mature osteoblasts remain in close proximity with the bone surface and their migration towards the blastema is impaired. Moreover, their proliferative capacity is decreased, leading to an impaired generation of new osteoprogenitors. These features are considered important hallmarks of the dedifferentiation process. Thus, the Hippo/Yap signalling pathway may be an important regulator of osteoblast dedifferentiation during zebrafish caudal fin regeneration.

Importantly, the defects observed regarding osteoblast recruitment to the amputation region in the context of Yap loss of function can be due to impairment in osteoblast migration itself or in EMT. Wnt signalling is known to be required to mediate EMT in osteoblasts and allow their recruitment to the stump ((Stewart et al. 2014)). Interestingly, we show that both pathways seem to be activated in dedifferentiating osteoblasts from early time-points during regeneration (6 hpa). In the future, it would be important to understand whether Yap also mediates osteoblast EMT and whether it acts together with Wnt signalling to promote this process. This hypothesis is plausible since cell culture and mammalian mouse models showed that these pathways interact, mediating a wide range of responses (Tsai et al. 2012; Kim and Jho 2014; Park et al. 2015). For example, during mouse intestine crypt growth and regeneration, Yap can be sequestered and incorporated in the Axin/β-catenin destruction complex and, when Wnt signalling is activated, YAP is physically dislodged from the destruction complex, allowing nuclear accumulation and activation of Wnt/YAP/TAZ-dependent biological responses (Tsai et al. 2012; Azzolin et al. 2014).

So far, only the RA signalling pathway has been shown to be required for osteoblast dedifferentiation. Retinoic acid levels need to be decreased in osteoblasts by the RA degrading enzyme Cyp26b1 to allow their dedifferentiation (Blum and Begemann 2015b). Thus, it would be interesting to address a connection and regulation between Yap and the RA signalling.

Surprisingly, a recent and unexpected link between Yap and metabolic adaptation was observed in a breast cancer cell line and in the *Drosophila* wing imaginal disc. In this context, Pfk1 (Phosphofructokinase), the enzyme regulating the first step of glycolysis, binds to TEAD transcription factors and regulates their interaction with Yap/Taz, promoting Yap/Taz transcriptional activity. Supporting this, when cells actively incorporate glucose that is shunt into glycolysis, Yap/Taz are fully active, while when glucose metabolism is impaired, Yap/Taz transcriptional activity decreases (Enzo et al. 2015; Santinon et al. 2015; Koo and Guan 2018). This implies that metabolism does not only regulate cell fate by adapting to metabolic demands or by regulating epigenetic modification, but also by directly influencing signal transduction pathways. It would be interesting to investigate whether in our system the same kind of correlation between Yap and metabolism is involved during osteoblast dedifferentiation.

3 YAP REGULATES THE SIGNALLING CENTRES THAT GOVERN OSTEOBLAST REDIFFERENTIATION DURING CAUDAL FIN REGENERATION

The Hippo signalling pathway emerged as an evolutionarily conserved signal transduction pathway that plays an important function in tissue growth and organ size control during development, tissue homeostasis and regeneration (Zhang et al. 2008; Xin et al. 2013; Hayashi et al. 2014; Zhao 2014; Moya and Halder 2016). This pathway acts predominantly via regulation of proliferation, cell survival and cell fate determination (Udan et al. 2003; Huang et al. 2005; Azzolin et al. 2014; Fu et al. 2017). To this date, there is a great amount of data implicating the Hippo pathway transcriptional co-activators Yap and Taz as either regulators of stem cell properties (Lian et al. 2010; Shaw et al. 2010; Hiemer and Varelas 2013; Santucci et al. 2015), but also in actively mediating cell differentiation (Lin et al. 2012; Yimlamai et al. 2014; de Sousa et al. 2018).

More recently, the Hippo pathway transcriptional co-activator Yap and Taz have been shown to be important regulators of the osteoblast lineage determination *in vitro* (Hong et al. 2005; Dupont et al. 2011b; Seo et al. 2013) and of bone development (Kegelman et al. 2017; Tang and Weiss 2017; Xiong et al. 2018), remodelling (Tang et al. 2013; Pan et al. 2018) and repair (Deng et al. 2016) in mice models. Nevertheless, these studies have failed to provide a clear consensus on the role of the Hippo pathway effectors Yap and Taz in regulating the osteoblast cell fate. Both co-activators have been implicated in promoting or inhibiting osteoblast differentiation and bone formation, depending on the cellular context. Some studies show that they inhibit terminal differentiation and thus are required to maintain the osteoblast precursor niche (Zaidi et al. 2004; Seo et al. 2013; Xiong et al. 2018), while others demonstrate their requirement for osteoblast commitment, differentiation and bone matrix formation (Tang et al. 2013; Tang and Weiss 2017; Kegelman et al. 2018; Pan et al. 2018). More thorough analysis indicates that they may play different roles depending on the stage of osteoblast differentiation: deletion of Yap and Taz from osteoprogenitor cells increased osteoblast differentiation and deletion from mature osteoblasts lead to reduced osteoblast number and bone formation in mice (Xiong et al. 2018).

We should emphasize that the previously mentioned studies were mainly performed in cell culture, during embryonic development and in fracture repair mammalian models, which possess some limitations. Therefore, in order to enlighten these divergences, in this Chapter IV we investigated the role of the Hippo pathway effector Yap during osteoblast lineage specification using as model system the zebrafish caudal fin regenerative process. We took advantage of a previously established transgenic line that expresses a dominant-negative form of *yap1* (DN-Yap) upon heat-shock (Mateus et al. 2015). Although there are currently homozygous viable mutant lines for *yap1* (Astone et al. 2018), this strategy enables to address the role of Yap in the adult animal, in a context of *de novo* bone formation, at a specific regeneration phase. Thus, we decided to not to interfere with the early regenerative events,

such as with osteoblast dedifferentiation and blastema formation (Knopf et al. 2011; Sousa et al. 2011; Stewart and Stankunas 2012), and manipulated Yap function exclusively during the outgrowth phase. This gives us the unique opportunity to study, in a Yap loss of function context, its requirement for either progenitor cell maintenance or for osteoblast differentiation in a regenerative context. At the onset of the regenerative outgrowth phase, the bone formation process is tightly controlled, and different osteoblast subsets are arranged in a proximal-distal organization that reflects their maturation state (Brown et al. 2009; Marí-Beffa and Murciano 2010; Stewart et al. 2014). The distal blastema region is populated by a self-renewing osteoprogenitor pool ($Runx2^{+}Osx^{-}$ osteoblast subset). As this pool is maintained, some osteoprogenitors start to differentiate in immature osteoblasts ($Runx2^{+}Osx^{+}$ osteoblast subset) that will continue the differentiation program until full maturation.

Here we show that continuous manipulation of Yap during three consecutive days after blastema formation lead to reduced bone formation and thinning of the of the bony-ray width even when normalized to the total regenerated area. Previous work from our lab shown that Yap manipulation during blastema formation and outgrowth leads to decrease in cell division and to a general impairment of the regenerative process (Mateus et al. 2015). Although we cannot exclude that the phenotypes described in Chapter IV may be explained also by defects in cell proliferation mediated by Yap, several lines of evidence described here point to a clear role of Yap in controlling osteoblast differentiation. We suggest that, in addition to controlling proliferation, Yap may be fundamental for correct bone formation. We demonstrate that Yap manipulation during outgrowth lead to major changes in specific osteoblast subtypes within the regenerating fin: a clear reduction in the number of the differentiating osteoblast subset ($Runx2^{+}Osx^{+}$) is observed, while the osteoprogenitor pool ($Runx2^{+}Osx^{-}$) remains unchanged and which ultimately becomes more proximal. In accordance, through gene expression analysis, we discriminated additional osteoblast markers and observed that immature and mature markers were also downregulated in contrast to the progenitor markers. These findings point to a clear function of Yap in controlling osteoblast differentiation during outgrowth and further indicate that this phenotype is independent, at least to a certain extent, of a general impairment of regeneration mediated by decreased proliferation. Nonetheless, given the conserved roles of the Hippo/Yap signalling pathway in regulating cell proliferation, apoptosis and survival (Udan et al. 2003; Huang et al. 2005; Azzolin et al. 2014; Wehner et al. 2017), future work should include a through characterization of these parameters and their contribution to the phenotypes described in Chapter IV.

Since Yap transcriptional activation can be monitored through its translocation to the nucleus (Cherrett et al. 2012; Piccolo et al. 2014; Varelas 2014) our characterization of Yap subcellular localization during outgrowth revealed that it is not accumulated in the nucleus of differentiating $Runx2^{+}Osx^{+}$ osteoblasts nor in the distal $Runx2^{+}$ Osx^{-} osteoprogenitors. This indicates that Yap is not promoting Yap-dependent target gene expression in these osteoblast subsets and argues in favour of a non-cell autonomous role of Yap in promoting osteoblast

differentiation. In the most recent model of bone regeneration in the caudal fin, a complex signalling network is required to control distal progenitor pool maintenance and correct differentiation (Wehner and Weidinger 2015; Antos et al. 2016). In this model Bmp and Wnt signalling pathways have leading and opposing roles. Distal Wnt signalling sustains the self-renewing capacities of the $Runx2^{+}$ Osx^{-} osteoprogenitor pool. As the pool expands, some progenitors became out of the influence of Wnt signalling and initiate a Bmp-dependent differentiation. Bmp signalling is required in a cell-autonomous manner to induce osteoprogenitor differentiation into $Runx2^{+}Osx^{+}$ osteoblasts in the proximal blastema compartment (Stewart et al. 2014). Our analysis demonstrates that active (nuclear) Yap is observed in the mesenchymal cells from the proximal blastema region and patterning zone and does not colocalize with the active Wnt signalling distal domain, suggesting antagonist activities. Moreover, we observed that some of these mesenchymal cells with active Yap have also activated Bmp signalling, monitored by pSmad 1/5/8 immunofluorescence, and are localized in close proximity to pSmad 1/5/8-positive differentiating osteoblasts. Gene expression analysis of key components of signalling pathways implicated in the maintenance of the osteoprogenitor pool, such as Wnt signalling (Stewart et al. 2014), and osteoblast differentiation, such as Bmp (Quint et al. 2002; Smith et al. 2006; Stewart et al. 2014), Ra (Blum and Begemann 2015b) and Shh (Laforest et al. 1998) was also monitored and revealed that in the Yap loss of function context only *dkk1a,* Wnt signalling inhibitor (MacDonald et al. 2010), and *bmp2a*, a bmp ligand (Rosen 2009; Wang et al. 2014), were differentially expressed. Downregulation of *dkk1a* after Yap manipulation may indicate that Yap activity in proximal mesenchymal cells counteracts the expansion of Wnt signalling to the proximal mesenchymal compartment via Dkk1a (Figure 55). Most importantly, given the proximity of mesenchymal cells with nuclear Yap to differentiating osteoblasts and the decrease of *bmp2a* expression in the Yap loss of function context, we hypothesized that a Yap-dependent *bmp2a* expression in mesenchymal cells may promote activation of Bmp signalling in neighbouring osteoprogenitors and trigger their differentiation (Figure 55).

Interestingly, previous studies shown that a population of basal epidermal cells that resides close to the amputation site, where the new bone will deposit, express both *shh* and *bmp2b* (Laforest et al. 1998; Lee et al. 2009). In these studies, inhibition both Shh and Bmp signalling lead to abnormal bone formation (Quint et al. 2002; Smith et al. 2006) whereas overexpression of *shh* and *bmp2* lead to ectopic bone formation (Quint et al. 2002). The later phenotype was rescued using an Bmp inhibitor, indicating that Shh might act upstream of Bmp signalling in mediating osteoblast differentiation and maturation during caudal fin regeneration (Quint et al. 2002). Yet, in this study, we were not able to notice differences of expression in *shh* or *bmp2b* transcripts in the Yap loss of function context, indicating that Yap is mediating osteoblast differentiation through an alternative mechanism. Therefore, in this context, we propose that together with the epidermis, the mesenchyme could also be an important signalling centre to promote osteoblast differentiation and maturation via Yap. To

further evaluate this hypothesis, we are planning to monitor Bmp pathway activation in the Yap loss of function situation and evaluate whether there is any impairment of Bmp signalling activity in the differentiating osteoblast population.

Herein, by investigating the role of the Hippo/Yap pathway in regulating osteoblast fate determination during fin regeneration, we were able not only to support previous studies showing that Yap is necessary for osteoblast differentiation and maturation (Tang et al. 2013; Tang and Weiss 2017; Kegelman et al. 2018; Pan et al. 2018), but also to place Yap in the signalling network that regulates bone regeneration. Importantly, we shown that Yap activity in mesenchymal cells in proximal blastema regions is able to influence via a paracrine signalling Bmp and Wnt pathway activity and promote osteoblast differentiation. Taken together, we hope the findings described here aid to provide a deeper understanding of the mechanism regulating bone regeneration and to clarify the role of the Hippo/Yap signalling pathway during osteoblast lineage specification.

.

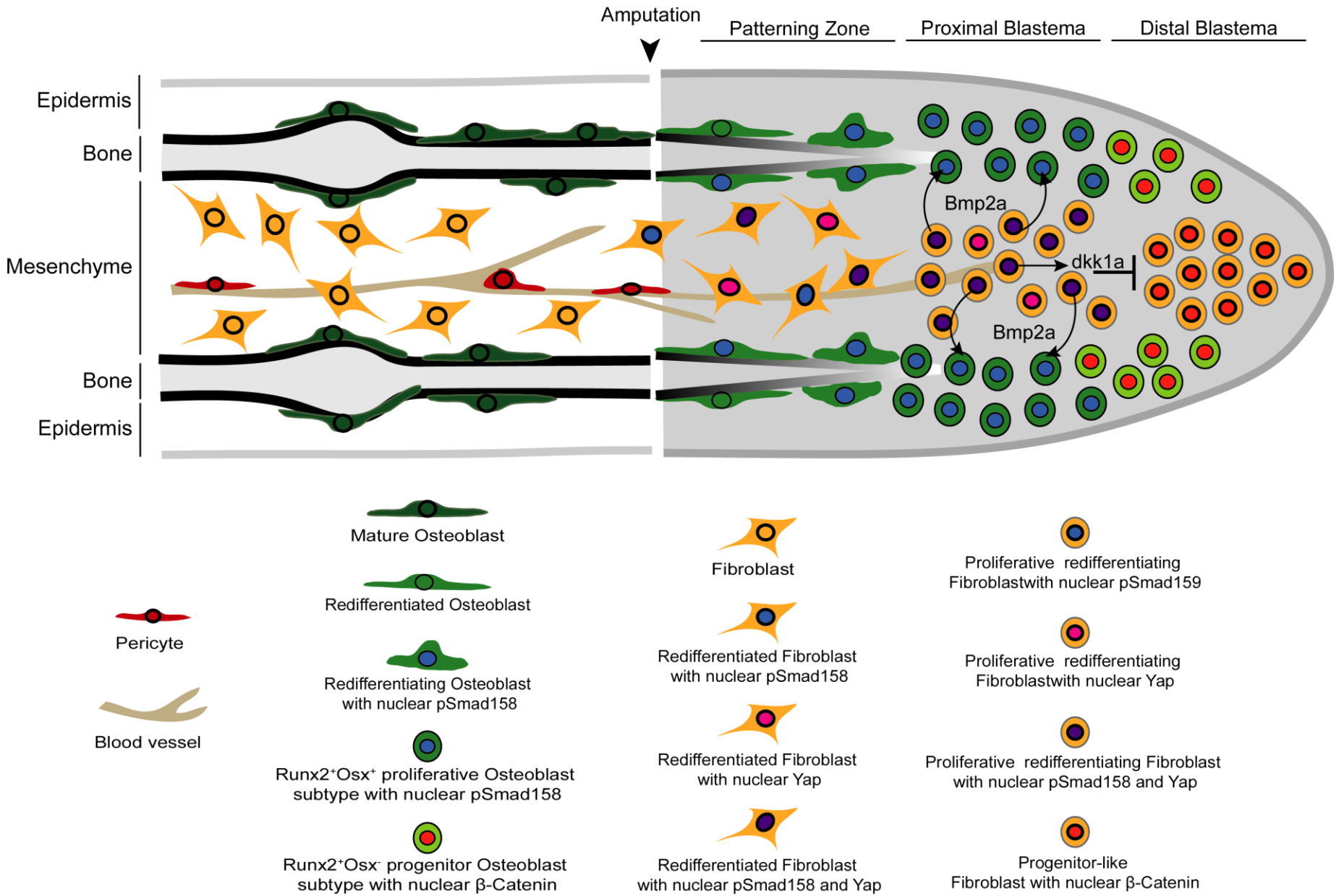
Amputation
Patterning Zone
Proximal Blastema
Distal Blastema
Epidermis
Bone
Mesenchyme
Bone
Epidermis
Bmp2a
dkk1a
Bmp2a
Pericyte
Blood vessel
Mature Osteoblast
Redifferentiated Osteoblast
Redifferentiating Osteoblast with nuclear pSmad158
Runx2+Osx+ proliferative Osteoblast subtype with nuclear pSmad158
Runx2+Osx- progenitor Osteoblast subtype with nuclear β-Catenin
Fibroblast
Redifferentiated Fibroblast with nuclear pSmad158
Redifferentiated Fibroblast with nuclear Yap
Redifferentiated Fibroblast with nuclear pSmad158 and Yap
Proliferative redifferentiating Fibroblastwith nuclear pSmad159
Proliferative redifferentiating Fibroblastwith nuclear Yap
Proliferative redifferentiating Fibroblast with nuclear pSmad158 and Yap
Progenitor-like Fibroblast with nuclear β-Catenin

Figure 55: Model for the role of Hippo/Yap signalling pathway during osteoblast redifferentiation after caudal fin amputation. Schematic representation of the bilateral organization of the caudal fin bony-rays through a longitudinal section, during the regenerative outgrowth phase (72 hpa), which starts after blastema formation (48 hpa onwards). A fine-tuned balance between progenitor expansion ($Runx2^{+}Osx^{-}$ cells) and terminal differentiation ($Runx2^{+}Osx^{+}$) must be maintained to sustain bone regeneration after caudal fin amputation. In this context, both Wnt and Bmp signalling play key and opposing roles: Wnt/β-catenin maintains a pool of distal $Runx2^{+}$ osteoprogenitors, while Bmp restricts Wnt activity to promote osteoblast differentiation in the proximal blastema region. In addition, Wnt signalling regulates important secondary signals that are required for proper bone regeneration. Based on our findings, another key player, the Hippo/Yap signalling pathway, may be added to this signalling network. Yap is accumulated inside the nucleus together with pSmad1/5/8 in the mesenchymal compartment, just adjacent to proliferative $Runx2^{+}Osx^{+}$ differentiating osteoblasts. In this region, Yap regulates the expression of *bmp2a* (Bmp ligand), which through a paracrine signalling activates Bmp signalling in this osteoblast population. In addition, in the proximal region, Yap restrains, together with Bmp signalling, Wnt activity to the distal blastema region by inducing dkk1a (Wnt inhibitor).

4 OSTEOGENIC PLASTICITY CHALLENGED: UNRAVELLING OSTEOBLAST SOURCES DURING CAUDAL FIN REGENERATION

Until recently, zebrafish caudal fin bone regeneration was believed to be totally dependent on the dedifferentiation of mature osteoblasts that reside near the amputated region (Knopf et al. 2011; Sousa et al. 2011). However, a study has demonstrated that genetically induced ablation of mature osteoblast does not impair the bony-ray regenerative capacity. These findings suggested that restoration of the lost osteoblast population is accomplished via *de novo* osteoblast formation from an unknown source (Singh et al. 2012). Interestingly, more recent data have demonstrated that, in addition to the mature osteoblast population, there is a niche of osteoprogenitor cells associated with the intersegment/joint regions of the caudal fin. These osteoprogenitors contribute to bone formation and, together with mature osteoblast dedifferentiation, supply to the osteoprogenitor pool during regeneration (Ando et al. 2017). Since joint-associated osteoprogenitors are not targeted in the mature osteoblast ablation context, the authors hypothesize that they provide an alternative source for *de novo* osteoblast formation in osteoblast-depleted fins. However, this is yet to be demonstrated (Ando et al. 2017). In fact, the osteoblast ablation system could be used as a model to investigate the contribution of joint-associated osteoblast progenitors in this context, and whether alternative cellular sources, that do not normally contribute to regeneration, emerge to compensate for osteoblast dedifferentiation. This kind of response has also been shown to happen after osteoblast ablation in adult mice, where bone-lining cells, which are quiescent in normal conditions, are activated and function as major contributors of bone formation during homeostasis and fracture healing (Matic et al. 2016). Another study in mice has demonstrated that, after airway epithelial stem cell ablation, differentiated and fully committed epithelial secretory cells dedifferentiate and revert to a stable stem cell population indistinguishable from the ablated one. This new stem cell population operates as well as their endogenous counterparts in repairing the epithelia after injury (Tata et al. 2013). With this in mind, when osteoblasts are ablated, the molecular mechanisms that regulate *de novo* formation might be different from those leading to progenitor assembly derived from

dedifferentiation of mature cells. Therefore, the main aims of Chapter V were to identify other cellular sources of new osteoblasts and the molecular mechanisms behind *de novo* osteoblast formation.

4.1 Cell sources for *de novo* osteoblast formation in osteoblast-depleted fins

To address alternative cell sources of new osteoblasts during regeneration, we performed a detailed characterization of cell proliferation, osteoprogenitor recruitment and lineage tracing experiments in the context of osteoblast-depleted fins. We observed that during regeneration, the epidermis surrounding the bony-ray and the mesenchymal intraray compartment are the first tissues to respond to osteoblast ablation, by initiating a proliferative response. Proliferating cells are preferentially located at the interface between these tissues and the bone matrix. Upon amputation, Runx2$^+$ osteoprogenitors emerge at the outer and inner bone surfaces in close contact with the surrounding epidermis and mesenchyme, respectively. These Runx2$^+$ osteoprogenitors seem to be sufficient to compensate for the lack of mature osteoblasts since the total number of osteoblasts (Runx2$^+$Osx$^+$ together with Runx2$^+$Osx$^-$, in a non-ablation context, and Runx2$^+$Osx$^-$, in an ablation context) in the regenerating fin remains the same or is even higher in the ablation context. This suggests that bone surrounding tissues function as a source of newly formed osteoblasts during fin regeneration after osteoblast ablation (Figure 56). Interestingly, these Runx2$^+$ osteoprogenitors seem to comprise two independent populations that may derive from different sources with distinct properties, reflecting different requirements given their location. While osteoprogenitors that arise at the inner bone surface express the mesenchymal marker *ctgfa*, Runx2$^+$ osteoprogenitors that arise at the outer bone surface are negative for this marker. This is important, since in a non-ablation context both outer and inner osteoblasts express *ctgfa* upon amputation, reflecting their mesenchymal origin (Lee et al. 2013).

4.1.1 Possible origin for outer bony-ray Runx2$^+$ osteoprogenitors

To assess the contribution of the epidermis as a source of osteoprogenitors that arise at the outer bone matrix, we set up a series of lineage tracing experiments. Our results demonstrated that either basal or differentiated epidermal cells do not contribute to other tissues but epidermis after amputation. This is in accordance with lineage restriction notion observed during regeneration (Tu and Johnson 2011; Stewart and Stankunas 2012) and highlights that, even in osteoblast ablation context, epidermal cells do not transdifferentiate to give rise to new osteoblasts. Additionally, there are two other possible sources contributing to the Runx2$^+$ osteoprogenitors that arise adjacently to the epidermis: the recently discovered joint-associated osteoprogenitors (Ando et al. 2017) or cells from the interray mesenchyme. In fact, we observed that the mesenchymal marker *ctgfa* is expressed in the interray mesenchymal tissue at lower levels when compared to the intraray mesenchyme after

amputation (Mateus et al. 2015; Pfefferli and Jaźwińska 2017). This would be in line with the lower, or lack of, *ctgfa* expression in the Runx2^{+} osteoprogenitors present at the outer bone surface observed in our study. Nevertheless, these two sources were not tested and future studies should investigate their contribution in osteoblast depleted caudal fins.

4.1.2 Possible origin for inner bony-ray Runx2^{+} osteoprogenitors

Regarding the inner bone osteoblasts, we hypothesized that they were derived from intraray mesenchyme. To test that, we used the *careg*:CreERT2 transgenic line that has been described to label all mesenchymal cells that contribute to regeneration, in their majority fibroblast-like cells (Pfefferli and Jaźwińska 2017). However, we were not successful with our labelling protocol when compared to what was previously demonstrated (Pfefferli and Jaźwińska 2017). Inefficient lineage tracing analysis could have three main reasons: inefficient tamoxifen treatment, a drug that is quite unstable and difficult to reach maximum activity; reduced levels of Cre transcription in the cells of interest, due to poor activity of the promoter or regulatory element driving Cre expression; and low activity of the promoter used in the switch line that reports Cre activation (Hans et al. 2009; Felker et al. 2016; Carney and Mosimann 2018). We believe that in our experiments the last factor is the most relevant, as our tamoxifen protocol was performed as described to allow for efficient Cre activation (Felker et al. 2016) and the previous report showing strong labelling using the *careg*:CreERT2 (Pfefferli and Jaźwińska 2017). Therefore, defective labelling could be explained by differences in the loxP reporter transgenic used to detect Cre-mediated recombination in *careg* expressing cells. Nevertheless, our experiments revealed that intraray mesenchymal cells contribute to mature osteoblasts in osteoblast-depleted fins but not in a non-ablation context (Figure 56). This contribution of intraray fibroblast-like mesenchymal cells for *de novo* osteoblast, after ablation, has already been proposed (Singh et al. 2012), as fibroblasts and osteoblasts are closely related by origin and share multiple features (Alberts et al. 2002). In fact, these two types of cells have been shown to be interconvertible in cell culture experiments (Yamamoto et al. 2015). However, we were the first to show evidence that osteoprogenitors derive from intraray mesenchymal cells. In the future, more experiments will be performed to increase the sample number and improve quantitative analysis. Nevertheless, we cannot exclude the possibility that this population of outer Runx2^{+} osteoprogenitors can also be derived from joint-associated osteoprogenitors.

4.1.3 Development of new tools to address the contribution of joint-associated osteoprogenitors

While looking for new progenitor markers, we generated a *col10a1* transgenic reporter line. Previous works have shown that *col10a1* labels putative osteoblast precursors in medaka (Renn et al. 2013). In fact, we show that *col10a1* expression was observed in some Runx2^{+} osteoprogenitors that emerge between the bone matrix and the basal epidermal layer during

regeneration of osteoblast depleted caudal fins. In addition, we showed that the *col10a1* reporter line labels the osteoprogenitors population that resides in the joint region. Moreover, upon ablation, prior to amputation, joint-associated *col10a1*-positive osteoprogenitors expand in number, indicating that these cells are responsive to osteoblast ablation. In parallel, we generated a *col10a1* ablation line (*col10a1*:EGFP-NTRo) (Supplementary Figure 8) that will be very useful to address important questions: 1) whether joint-associated osteoprogenitors are essential for osteoblast formation, in osteoblast depleted fins during regeneration, and are they able to compensate the lack of mature osteoblasts; and (2) if joint-associated osteoprogenitors originate the Runx2^{+} osteoprogenitors that we have identified in the outer and inner bone surfaces, in the osteoblast ablation context during caudal fin regeneration. In the future, we plan to perform double ablations of mature osteoblast and joint-associated *col10a1*-positive osteoprogenitors, thus evaluating whether in this condition bone regeneration still occurs. These experiments should clarify the contribution of joint-associated osteoprogenitors for *de novo* osteoblast formation during regeneration in caudal fins lacking mature osteoblast.

4.2 Molecular mechanisms regulating *de novo* osteoblast formation: RA and Bmp signalling

In parallel to finding new cellular sources for osteoblasts, I proposed to identify the molecular mechanisms that regulate osteoblast emergence during regeneration when the mature population is absent. Here we report unique roles for RA and Bmp signalling pathways in regulating *de novo* osteoblast formation during caudal fin regeneration (Figure 56). Not only we demonstrate that both pathways are activated in Runx2^{+} osteoprogenitors, but also that their separate inhibition leads to a severe decrease in the number of Runx2^{+} osteoprogenitors in caudal fins lacking mature osteoblasts during regeneration. Despite the fact that in both mammals and zebrafish fin regeneration RA (Renn and Winkler 2012; Blum and Begemann 2015b; Green et al. 2017) and Bmp signalling (Laforest et al. 1998; Kamiya and Mishina 2011; Beederman et al. 2013; Stewart et al. 2014; Wu et al. 2016) are potent regulators of osteoblast formation, this work shows that they are indispensable for the recruitment of additional sources for new osteoprogenitor generation. In the future, we would like to investigate if RA and Bmp pathways act synergistically to promote *de novo* Runx2^{+} osteoprogenitors formation during regeneration.

It is noteworthy to mention that during the course of this work we noticed, in the osteoblast ablation context, several molecular similarities between the basal epidermal layer and the osteoprogenitors that arise in at outer bone matrix surface. Both cell types express *col10a1* (Figure 47B, Bi and B' from Chapter V) and activate Bmp signalling (Figure 50B and B' from Chapter V). In fact, basal epidermal cells are known to function as a signalling centre during regeneration of the zebrafish caudal fin skeleton and scales, and to interact with osteoblasts to promote bone regeneration and patterning (Wehner et al. 2014; Thorimbert et al. 2015;

Antos et al. 2016; Armstrong et al. 2017; Iwasaki et al. 2018). Importantly, a study has demonstrated that during regeneration the basal epidermal layer can be a source of *bmp2* (Laforest et al. 1998). Altogether, this leads us to hypothesize that in the early phases of regeneration, prior to blastema formation, and especially in osteoblast-depleted fins, the basal epidermis also functions as a signalling centre for the adjacent cells, such as the newly formed osteoprogenitors, aiding in their formation and commitment. To specifically test the requirement of the basal epidermis for *de novo* osteoblast formation, we have generated a basal epidermis ablation line, using the *krt19* specific basal epidermis promoter and the NTR/Mtz system (Supplementary Figure 9). We have performed functional assays confirming proper basal epidermal layer ablation (Supplementary Figure 9) and in the future, this line will be used to address the requirement of the basal epidermis for *de novo* osteoblast formation. In addition, it could also be a valuable tool to understand the cellular and molecular mechanisms behind basal epidermal formation after ablation.

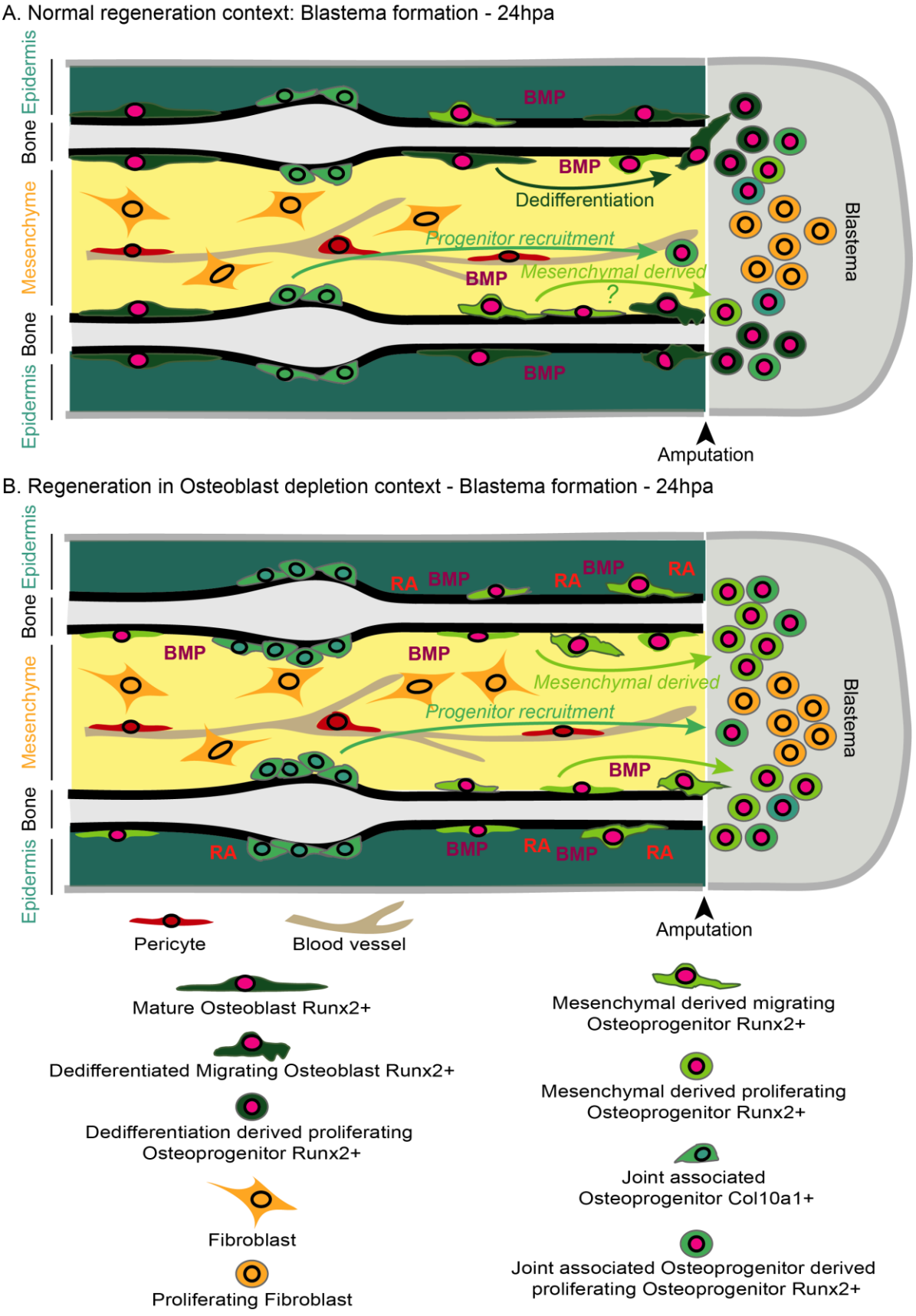

Figure 56: Model for the cellular and molecular mechanisms that regulate osteoblast plasticity, independently of osteoblast dedifferentiation, during caudal fin regeneration. (A) During regeneration, osteoblasts that contribute to blastema formation arise from dedifferentiation of mature resident osteoblasts, just below the amputation plane, and from osteogenic precursors localized in the intersegment/joint regions of the caudal fin.

Our data also suggest that other osteoprogenitors may emerge near the bone surface and in a process dependent on Bmp signalling. (B) When the mature osteoblast population is compromised, such as in osteoblast-depleted caudal fins, *de novo* osteoblasts may arise from the precursors localized in the intersegment region. In addition, we propose that other osteoprogenitor sources contribute to *de novo* osteoblast formation. These osteoprogenitors arise in the region close to the bone matrix surface at the interface with the surrounding tissues, namely mesenchyme and epidermis. Lineage tracing experiments suggest that mesenchymal cells, but not epidermal cells, can give rise to newly formed osteoblasts. We also propose that both RA and Bmp signalling are important regulators of *de novo* osteoblast formation during zebrafish caudal fin regeneration.

5 IMPLICATIONS OF ZEBRAFISH BONE REGENERATION STUDIES TO THE FIELD OF REGENERATIVE MEDICINE

Regenerative medicine aims at replacing lost/damaged tissues or cells in the human body through a new source of healthy transplanted cells or by stimulating endogenous repair. Bone is considered to be an exception to the limited capacity found in mammals, as it is capable of replacing itself and to regenerate after fracture, without excessive scar formation (Dimitriou et al. 2011; Loeffler et al. 2018). However, many skeletal dysplasias can affect bone formation and the efficacy of repair mechanisms, causing functional disabilities. Osteodegenerative disorders, like osteoporosis or osteoarthritis, affect significantly the elderly population. Also, congenital disorders, such as skeletal malformations and massive bone loss, represent frequent clinical situations. Thus, bone regenerative therapies are in high demand (Illich et al. 2011).

Tissue-replacement therapies are the most widely used to promote bone repair, including implantation of biomaterials (to substitute bone) and autologous bone graft implants. Autologous bone grafting is considered to be the "gold standard" for bone reconstructive procedures. In fact, demand for bone grafts is very significant, with approximately 2.2 million bone grafts being performed annually worldwide in orthopedics and dentistry (Illich et al. 2011; Chaparro 2016). Nevertheless, it also possesses limitations, such as restriction to the patient's bone tissue, risk of morbidity in the donor site, high cost and long surgical procedure (Chaparro 2016). Cell-based therapies have also been extensively investigated. Various cell types, such as osteoblasts, MSCs and iPSCs, have been proposed and used as alternatives for bone reconstruction (Patel et al. 2013; Sheyn et al. 2016; Csobonyeiova et al. 2017). However, a consistent obstacle when using cell-based therapies is that they often present inefficient osteogenic capacity, probably because they lack the correct signalling cues or environmental stimulation when implanted back into the host.

Consequently, evidences point to the necessity of performing combined approaches using a wide range of available treatments to increase the efficiency of bone regeneration. Given that the current therapies are still far from ideal, there is an urgent necessity to further understand the processes that drive the biology of bone regeneration. Unfortunately, many processes remain largely unknown.

Mammalian bone regeneration and fracture healing involve numerous and highly complex interactions, between a multitude of cell types and molecules that have not been sufficiently

characterized. It is of major importance to improve our understanding of how fracture healing and bone regeneration processes occur, by identifying not only the potential cell types but also the molecular mechanisms that contribute to these processes.

Multiple animal models with enhanced regenerative ability have been extensively used in biomedical research. Zebrafish is a non-mammalian model system of excellence for the study of the mechanisms behind tissue regeneration. Although other systems allow the study of bone regeneration, the zebrafish caudal fin provides unique advantages to elucidate the molecular and cellular strategies underlying the intrinsic bone regenerative capacity (Spoorendonk et al. 2010; Bruneel and Witten 2015; Cardeira et al. 2016). In this PhD thesis, we used zebrafish to shed light into some key aspects of caudal fin bone regeneration that were not understood. In the next two sections, we propose possible implication of our findings for the field of regenerative medicine.

5.1 The potential of osteoblast dedifferentiation and osteogenic plasticity for bone regenerative medicine and skeletal dysplasias

In Chapter III, we have discovered new regulators of the osteoblast dedifferentiation process, namely metabolic reprogramming and the Hippo/ Yap signalling pathway. It would be interesting if, in mammalian systems, we could stimulate regenerative mechanisms by activating other endogenous sources for osteoblasts precursors through limited and controlled dedifferentiation. Instead of relying solely on MSCs to provide new osteoblasts, we could propel other cells within the skeletal tissue to undergo dedifferentiation into a committed progenitor-like stage. For this, the more obvious candidates are the bone lining cells (Matic et al. 2016). These are quiescent under normal conditions and cover non-remodelling bone surfaces, however, they have the intrinsic capacity to respond by proliferating and originating osteoblasts under special conditions (Matic et al. 2016).

Understanding the mechanisms that potentiate osteoblast dedifferentiation could also have implications for tumour biology, as both processes seem to rely on similar mechanisms. In fact, tumour cell plasticity is an event observed in various malignancies. This increased plasticity, which has been linked to metabolic reprogramming (Warburg 1925; Liberti and Locasale 2016; Potter et al. 2016), allows them to dedifferentiate, undergo EMT and acquire proliferative capacity (Friedmann-Morvinski and Verma 2014; Varga et al. 2014). These same characteristics have been described here as a hallmark of osteoblast dedifferentiation during caudal fin regeneration. This would be particularly meaningful for neoplasias that arise within bone cells, such as osteosarcoma. Importantly, dedifferentiation of mature osteoblasts has been observed in pediatric osteosarcomas (Pereira et al. 2009; Basu-Roy et al. 2013). Our genome-wide gene expression analysis, performed during osteoblast dedifferentiation in zebrafish, could also bring forward crucial information on the mechanisms that promote dedifferentiation of tumour cells. However, one important difference between tumour formation and bone regeneration seems to be the distinct regulation of the tumour

suppressor p53. In osteosarcoma cell lines, and in most cancer cells, p53 is mutated or has deficient activity (Pereira et al. 2009; Charni et al. 2017), while in our microarray p53 transcripts are upregulated, suggesting its activation. These differences in p53 activity might explain why during regeneration cell proliferation is tightly controlled but not in cancers cells.

5.2 Deepening into the mechanisms that control osteoblast commitment and differentiation

Osteoblast dysfunctions may affect the ability of the human body to perform correct bone remodelling and fracture healing, culminating in bone disorders. Both the quality and quantity of bone produced by osteoblasts are of major importance, as both can be related with incorrect osteoblast commitment or differentiation. Despite the identification of several essential transcriptional programs for bone development, the current understanding is not sufficient to entirely explain the heterogeneity found in human bone disorders (Feng and McDonald 2011; Marie 2015).

In this thesis, we sought to better understand the mechanisms involved in osteoblast differentiation, from progenitor cells to fully committed osteoblasts, during regeneration. We provide evidence for several signalling pathways that are required at specific stages of osteoblast lineage specification in a regenerative context. In Chapter IV, we demonstrate that the Hippo pathway transcriptional effector Yap regulates osteoprogenitor commitment and differentiation and that its loss of function leads to reduced bone matrix deposition and, consequently, to the thinning and fragility of caudal fin bony-rays. Similarly, combinatorial Yap/Taz deletion from mice osteoblasts causes an osteogenesis imperfecta-like phenotype, with defective bone matrix type I collagen formation and spontaneous fractures (Kegelman et al. 2018). This emphasises the role of the Hippo/Yap signalling pathway as a potent regulator of osteoblast maturation. Thus, it would be interesting to address whether Yap is also related to other disorders with ineffective bone matrix maturation and be used as an endogenous factor that could be manipulated to normalize bone formation in pathological conditions. In Chapter V, we revealed new functions for RA and Bmp signalling during *de novo* osteoblast formation, with both pathways being important to assemble an osteoprogenitor population in osteoblast depleted caudal fins. Pathologies like osteoporosis, which is characterized by an increase in bone resorbing activity (by osteoclasts) and the inability of osteoblasts to compensate for this loss of bone, lead to bone perforation, loss and increased risk of fracture (Feng and McDonald 2011; Marie 2015). Over time, osteoblasts also decrease in number, which intensifies the pathology of the disease. In this case, therapies that promote bone formation and osteoprogenitor formation and activation are of major importance. In this context, both RA and Bmp signalling pathways could be important targets to take into consideration and tackle this problem.

Although the work described here is very specific to the context of caudal fin regeneration, we hope that our data may contribute to further understand the mechanism that regulate

new osteoblast formation during zebrafish caudal fin regeneration and aids in the development of new and unconventional bone repair strategies for humans.

6 CONCLUDING REMARKS

During caudal fin regeneration, bone formation is achieved through a sequence of events that culminates in the complete renewal of the missing skeletal elements. Osteoblasts are the cells responsible for bone maintenance and regeneration of the new caudal fin skeletal system. Bone regeneration is achieved through a series of events: during blastema formation, by dedifferentiation of mature cells and commitment of joint associated progenitor cells that generate a pool of osteoprogenitors; and later on, during outgrowth, by the maintenance of a progenitor pool and redifferentiation in order to restore the lost tissue original shape, architecture and function. Although the overall mechanism through which zebrafish caudal fin bone regeneration is achieved is understood, multiple questions remain to be addressed. This system provides the unique opportunity to investigate the mechanisms that regulate osteoblast reprograming, plasticity and lineage specification during regeneration. During this PhD thesis, we enlighten different mechanism that regulate bone formation at different phases of the regenerative process: we uncover potential regulators of dedifferentiation; we determine important signalling pathways that regulate osteoblast redifferentiation; and we also unveil cellular and molecular mechanism behind *de novo* osteoblast formation in osteoblast depleted caudal fin during regeneration. Overall, we expect that the data generated in this PhD thesis aids to envision new therapeutic approaches that exploit the features of regenerative osteoblast biology

6.1 Regulators of osteoblast dedifferentiation

In Chapter III we aimed to bring new insights into the field of tissue regeneration by addressing one of the major questions regarding the regenerative capacity found in the animal kingdom: how can cells change their identity and reprogram themselves to ensure proper formation of a new tissue or organ, upon injury? During zebrafish caudal fin regeneration bone cells reprogramming occurs as a partial dedifferentiation process, with cells acquiring a progenitor-like phenotype (Knopf et al. 2011; Sousa et al. 2011; Tu and Johnson 2011; Stewart and Stankunas 2012). Our results show that, in order to do so, osteoblasts display significant changes at the level of gene transcription. In fact, we propose that osteoblast dedifferentiation can be regulated by activation of two processes: via metabolic adaptation, in which mature osteoblasts activate a bivalent metabolism to ensure the regeneration demands, and another through Yap-dependent activation in a cell autonomous manner (Figure 52). Inhibition of both mechanisms has a severe impact on regeneration, in particular on bone formation (Figure 53 and Figure 54). Importantly, to our knowledge, this is the first report suggesting the requirement of metabolic reprogramming for dedifferentiation in a

regenerative context and the implication the hippo pathways effector Yap for osteoblast dedifferentiation during caudal fin regeneration.

6.2 Osteoblast redifferentiation during outgrowth

In Chapter IV we intended to investigate if the Hippo/Yap signalling pathway is an important regulator of bone repair during the regenerative outgrowth phase. Despite several studies implicating Yap as a potent inducer of bone differentiation (Dupont et al. 2011a; Hiemer and Varelas 2013; Piccolo et al. 2014; Varelas 2014; Pan et al. 2018; Xiong et al. 2018), no link between Yap and bone regeneration in zebrafish has been proposed. Using a Yap loss of function transgenic line, we observed a robust and clear inhibition of bone regeneration during the outgrowth phase. Overall, these findings highlight a novel and important role for the transcriptional co-activator Yap during caudal fin bone regeneration, by specifically directing osteogenic differentiation via paracrine signalling from the adjacent mesenchyme (Figure 55). We hope that these findings help to clarify the roles of the Hippo/Yap signalling pathway during osteoblast lineage specification. Interestingly, we also brought into light an important duality of the Hippo/Yap pathway, considering the results from Chapters II and IV, where we show that Yap plays a broader and more significant role during caudal fin bone regeneration than previously thought. Depending on the regeneration phase, not only it regulates osteoblast dedifferentiation and osteoprogenitor assembly during blastema formation, but it is also a key regulator of osteoblast differentiation during outgrowth.

6.3 Mechanisms of *de novo* osteoblast formation

In Chapter V, we propose to bring light into the mechanisms that regulate cell plasticity during zebrafish caudal fin regeneration, in particular for bone repair. Mature osteoblast ablation, prior to amputation, deprives the system of osteoblast capable of dedifferentiating and contributing for new osteoblast formation during regeneration. Consequently, other cell sources may be activated to compensate for the lack of mature osteoblast. Here, we provide evidence for a heterogeneous population of osteoprogenitors that emerges at the outer and inner bone surface. In this context, the intraray mesenchymal tissue was discovered as a source of new osteoblast during regeneration. Thus, skeletal tissue regeneration in zebrafish seems to be accomplished by diverse cellular origins that together promote correct bone formation. These include: resident osteoblasts; joint associated osteoprogenitors; and mesenchymal fibroblasts that may arise only in special contexts when primary sources, such as mature osteoblast, are compromised. We also revealed that Bmp and RA signalling are required and may cooperate to ensure *de novo* osteoblast formation during regeneration in osteoblast depleted fins. In conclusion, our work elucidates the cellular and molecular mechanisms that regulate tissue plasticity in the context of fin ray regeneration, in particular, when the system is challenged, such as in osteoblast-depleted fins. It is possible that in this special context, dormant regenerative mechanisms emerge to ensure correct bone formation.

Chapter VII

BIBLIOGRAPHY

Agata K, Saito Y, Nakajima E (2007) Unifying principles of regeneration I: Epimorphosis versus morphallaxis. Dev Growth Differ 49:73–78. doi: 10.1111/j.1440-169X.2007.00919.x

Aghajanian P, Mohan S (2018) The art of building bone: emerging role of chondrocyte-to-osteoblast transdifferentiation in endochondral ossification. Bone Res 6:19. doi: 10.1038/s41413-018-0021-z

Ail D, Perron M (2017) Retinal Degeneration and Regeneration—Lessons From Fishes and Amphibians. Curr Pathobiol Rep 5:67–78. doi: 10.1007/s40139-017-0127-9

Akimenko M a, Johnson SL, Westerfield M, Ekker M (1995) Differential induction of four msx homeobox genes during fin development and regeneration in zebrafish. Development 121:347–357

Akimenko MA, Marí-Beffa M, Becerra J, Géraudie J (2003) Old questions, new tools, and some answers to the mystery of fin regeneration. Dev Dyn 226:190–201. doi: 10.1002/dvdy.10248

Akiyama H, Kim J-E, Nakashima K, et al (2005) Osteo-chondroprogenitor cells are derived from Sox9 expressing precursors. Proc Natl Acad Sci 102:14665–14670. doi: 10.1073/pnas.0504750102

Alberts B, Johnson A, Lewis J, et al (2002) Molecular Biology of the Cell, 4th editio. Garland Science, New York

Alford AI, Hankenson KD (2006) Matricellular proteins: Extracellular modulators of bone development, remodeling, and regeneration. Bone 38:749–757. doi: 10.1016/j.bone.2005.11.017

Alford AI, Kozloff KM, Hankenson KD (2015) Extracellular matrix networks in bone remodeling. Int J Biochem Cell Biol 65:20–31. doi: 10.1016/j.biocel.2015.05.008

Amitani M, Asakawa A, Amitani H, Inui A (2013) The role of leptin in the control of insulin-glucose axis. Front Neurosci 7:1–12. doi: 10.3389/fnins.2013.00051

Ando K, Shibata E, Hans S, et al (2017) Osteoblast Production by Reserved Progenitor Cells in Zebrafish Bone Regeneration and Maintenance. Dev Cell 43:643–650.e3. doi: 10.1016/j.devcel.2017.10.015

Anthoney N, Foldi I, Hidalgo A (2018) Toll and Toll-like receptor signalling in development. Development 145:dev156018. doi: 10.1242/dev.156018

Antos CL, Knopf F, Brand M (2016) Regeneration of Organs and Appendages in Zebrafish: A Window into Underlying Control Mechanisms. eLS 1–17. doi: 10.1002/9780470015902.a0022101.pub2

Apschner A, Schulte-Merker S, Witten PE (2011) Not All Bones are Created Equal - Using Zebrafish and Other Teleost Species in Osteogenesis Research, Third Edit. Elsevier Inc.

Armstrong BE, Henner A, Stewart S, Stankunas K (2017) Shh promotes direct interactions between epidermal cells and osteoblast progenitors to shape regenerated zebrafish bone. Development 144:1165–1176. doi: 10.1242/dev.143792

Astone M, Lai JKH, Dupont S, et al (2018) Zebrafish mutants and TEAD reporters reveal essential functions for Yap and Taz in posterior cardinal vein development. Sci Rep 8:1–15. doi: 10.1038/s41598-018-27657-x

Atala A, Irvine DJ, Moses M, Shaunak S (2010) Wound healing versus regeneration: Role of the tissue environment in regenerative medicine. MRS Bull 35:597–606. doi: 10.1557/mrs2010.528

Attisano L, Wrana JL (2013) Signal integration in TGF-β, WNT, and Hippo pathways. F1000Prime Rep 5:1–8. doi: 10.12703/P5-17

Aubrey BJ, Strasser A, Kelly GL (2016) Tumor-suppressor functions of the TP53 pathway. Cold Spring Harb Perspect Med 6:. doi: 10.1101/cshperspect.a026062

Azevedo AS, Grotek B, Jacinto A, et al (2011) The regenerative capacity of the zebrafish caudal fin is not affected by repeated amputations. PLoS One 6:1–8. doi: 10.1371/journal.pone.0022820

Azevedo AS, Sousa S, Jacinto A, Saúde L (2012) An amputation resets positional information to a proximal identity in the regenerating zebrafish caudal fin. BMC Dev Biol 12:. doi: 10.1186/1471-213X-12-24

Azzolin L, Panciera T, Soligo S, et al (2014) YAP/TAZ incorporation in the β-catenin destruction complex

orchestrates the Wnt response. Cell 158:157–170. doi: 10.1016/j.cell.2014.06.013

Basu-Roy U, Basilico C, Mansukhani1 A (2013) Perpectives on cancer stem cells in osteosarcoma. Cancer Lett 6:247–253. doi: 10.1111/j.1743-6109.2008.01122.x.Endothelial

Baum B, Settleman J, Quinlan MP (2008) Transitions between epithelial and mesenchymal states in development and disease. Semin Cell Dev Biol 19:294–308. doi: 10.1016/j.semcdb.2008.02.001

Becerra J, Montes GS, Bexiga SR, Junqueira LC (1983) Structure of the tail fin in teleosts. Cell Tissue Res 230:127–137. doi: 10.1007/BF00216033

Beederman M, Lamplot JD, Nan G, et al (2013) BMP signaling in mesenchymal stem cell differentiation and bone formation. J Biomed Sci Eng 06:32–52. doi: 10.4236/jbise.2013.68A1004

Beer RL, Parsons MJ, Rovira M (2016) Centroacinar cells: At the center of pancreas regeneration. Dev Biol 413:8–15. doi: 10.1016/j.ydbio.2016.02.027

Bellayr I, Mu X, Li Y (2009) Biochemical insights into the role of matrix metalloproteinases in regeneration: Challenges and recent developments. Future Med Chem 1:1095–1111. doi: 10.4155/fmc.09.83

Bely AE, Nyberg KG (2010) Evolution of animal regeneration: re-emergence of a field. Trends Ecol Evol 25:161–170. doi: 10.1016/j.tree.2009.08.005

Bensimon-Brito A, Cardeira J, Dionísio G, et al (2016) Revisiting in vivo staining with alizarin red S - A valuable approach to analyse zebrafish skeletal mineralization during development and regeneration. BMC Dev Biol 16:. doi: 10.1186/s12861-016-0102-4

Berendsen AD, Olsen BR (2015) Bone development. Bone 80:14–18. doi: 10.1016/j.bone.2015.04.035

Bergers G (2005) The role of pericytes in blood-vessel formation and maintenance. Neuro Oncol 7:452–464. doi: 10.1215/S1152851705000232

Beyret E, Martinez Redondo P, Platero Luengo A, Izpisua Belmonte JC (2018) Elixir of Life: Thwarting Aging with Regenerative Reprogramming. Circ Res 122:128–141. doi: 10.1161/CIRCRESAHA.117.311866

Bielby R, Jones E, McGonagle D (2007) The role of mesenchymal stem cells in maintenance and repair of bone. Injury 38:. doi: 10.1016/j.injury.2007.02.007

Blum N, Begemann G (2012) Retinoic acid signaling controls the formation, proliferation and survival of the blastema during adult zebrafish fin regeneration. Development 139:107–116. doi: 10.1242/dev.065391

Blum N, Begemann G (2015a) Retinoic acid signaling spatially restricts osteoblasts and controls ray-interray organization during zebrafish fin regeneration. Development 142:2888–2893. doi: 10.1242/dev.120212

Blum N, Begemann G (2015b) Osteoblast de- and redifferentiation are controlled by a dynamic response to retinoic acid during zebrafish fin regeneration. Development 142:2894–2903. doi: 10.1242/dev.120204

Boland K, Flanagan L, Prehn JHM (2013) Paracrine control of tissue regeneration and cell proliferation by Caspase-3. Cell Death Dis 4:e725-6. doi: 10.1038/cddis.2013.250

Bolstad BM, Irizarry RA, Astrand M, Speed TP (2003) A comparison of normalization methods for high density oligonucleotide array data based on variance and bias. Bioinformatics 19:185–193. doi: 10.1093/bioinformatics/19.2.185

Borday V, Tharon C, Avaron F, et al (2001) evx1 Transcription in bony fin rays segment boundaries leads to a reiterated pattern during zebrafish fin development and regeneration. Dev Dyn 220:91–98. doi: 10.1002/1097-0177(2000)9999:9999<::AID-DVDY1091>3.0.CO;2-J

Boulevard H (2010) Apoptosis, Stem cells, and Tissue Regeneration. Sci Signal 3:1–16. doi: 10.1126/scisignal.3145re8.Apoptosis

Bouzaffour M, Dufourcq P, Lecaudey V, et al (2009) Fgf and Sdf-1 pathways interact during Zebrafish fin regeneration. PLoS One 4:1–8. doi: 10.1371/journal.pone.0005824

Brittijn SA, Duivesteijn SJ, Belmamoune M, et al (2009) Zebrafish development and regeneration: new tools for biomedical research. Int J Dev Biol 53:835–850. doi: 10.1387/ijdb.082615sb

Brockes JF, Kumar A (2005) Appendage regeneration in adult vertebrates and implications for regenerative medicine. Science (80-) 310:1919–1923. doi: 10.1126/science.1115200

Brockes JP, Kumar A (2008) Comparative Aspects of Animal Regeneration. Annu Rev Cell Dev Biol 24:525–549. doi: 10.1146/annurev.cellbio.24.110707.175336

Brockes JP, Kumar A, Velloso CP (2001) Regeneration as an evolutionary variable. J Anat 199:3–11. doi: 10.1017/S0021878201008299

Broussonet M (1786) Observations sur la régénération de quelques parties du corps des poissons. Hist l'Academie R des Sci 684–688

Brown AM, Fisher S, Iovine MK (2009) Osteoblast maturation occurs in overlapping proximal-distal compartments during fin regeneration in zebrafish. 6:247–253. doi: 10.1111/j.1743-6109.2008.01122.x.Endothelial

Bruneel B, Witten PE (2015) Power and challenges of using zebrafish as a model for skeletal tissue imaging. Connect Tissue Res 56:161–173. doi: 10.3109/03008207.2015.1013193

Cai J, Zhang N, Zheng Y (2010) The Hippo signaling pathway restricts the oncogenic potential of an intestinal regeneration program. 2383–2388. doi: 10.1101/gad.1978810

Cai S, Fu X, Sheng Z (2007) Dedifferentiation: A New Approach in Stem Cell Research. Bioscience 57:655. doi: 10.1641/B570805

Campbell LJ, Suárez-Castillo EC, Ortiz-Zuazaga H, et al (2011) Gene expression profile of the regeneration epithelium during axolotl limb regeneration. Dev Dyn 240:1826–1840. doi: 10.1002/dvdy.22669

Cardeira J, Gavaia PJ, Fernández I, et al (2016) Quantitative assessment of the regenerative and mineralogenic performances of the zebrafish caudal fin. Sci Rep 6:1–16. doi: 10.1038/srep39191

Carlson BM (2007) Principles of Regenerative Biology. Elsevier Inc.

Carney TJ, Mosimann C (2018) Switch and Trace: Recombinase Genetics in Zebrafish. Trends Genet 34:362–378. doi: 10.1016/j.tig.2018.01.004

Cavalli G (2006) Chromatin and epigenetics in development: blending cellular memory with cell fate plasticity. Development 133:2089–2094. doi: 10.1242/dev.02402

Chablais F, Jazwinska A (2010) IGF signaling between blastema and wound epidermis is required for fin regeneration. Development 137:871–879. doi: 10.1242/dev.043885

Chandel NS, Jasper H, Ho TT, Passegué E (2016) Metabolic regulation of stem cell function in tissue homeostasis and organismal ageing. Nat Cell Biol 18:823–832. doi: 10.1038/ncb3385

Chaparro O (2016) Regenerative Medicine : A New Paradigm in Bone Regeneration. doi: 10.5772/62523

Charni M, Aloni-Grinstein R, Molchadsky A, Rotter V (2017) P53 on the crossroad between regeneration and cancer. Cell Death Differ 24:8–14. doi: 10.1038/cdd.2016.117

Chassot B, Pury D, Jaźwińska A (2016) Zebrafish fin regeneration after cryoinjury-induced tissue damage. Biol Open 5:819–828. doi: 10.1242/bio.016865

Chen C-H, Poss KD (2017) Regeneration Genetics. Annu Rev Genet 51:63–82. doi: 10.1146/annurev-genet-120116-024554

Chen CH, Merriman AF, Savage J, et al (2015) Transient laminin beta 1a Induction Defines the Wound Epidermis during Zebrafish Fin Regeneration. PLoS Genet 11:1–21. doi: 10.1371/journal.pgen.1005437

Chen CH, Puliafito A, Cox BD, et al (2016a) Multicolor Cell Barcoding Technology for Long-Term Surveillance of Epithelial Regeneration in Zebrafish. Dev Cell 36:668–680. doi: 10.1016/j.devcel.2016.02.017

Chen G, Deng C, Li YP (2012) TGF-β and BMP signaling in osteoblast differentiation and bone formation. Int J Biol Sci 8:272–288. doi: 10.7150/ijbs.2929

Chen Q, Shou P, Zheng C, et al (2016b) Fate decision of mesenchymal stem cells: Adipocytes or osteoblasts? Cell Death Differ 23:1128–1139. doi: 10.1038/cdd.2015.168

Chen T, Dent S (2014) Chromatin modifiers: regulators of cellular differentiation. Nat Rev Genet 15:93–106. doi: 10.1038/nrg3607.Chromatin

Cherrett C, Furutani-Seiki M, Bagby S (2012) The Hippo pathway: key interaction and catalytic domains in organ growth control, stem cell self-renewal and tissue regeneration. Essays Biochem 53:111–127. doi: 10.1042/bse0530111

Christensen RN, Tassava RA (2000) Apical epithelial cap morphology and fibronectin gene expression in regenerating axolotl limbs. Dev Dyn 217:216–224. doi: 10.1002/(SICI)1097-0177(200002)217:2<216::AID-DVDY8>3.0.CO;2-8

Cirio MC, de Caestecker MP, Hukriede NA (2015) Zebrafish Models of Kidney Damage and Repair. Curr Pathobiol Rep 3:163–170. doi: 10.1007/s40139-015-0080-4

Colnot C (2009) Skeletal cell fate decisions within periosteum and bone marrow during bone regeneration. J Bone Miner Res 24:274–282. doi: 10.1359/jbmr.081003

Cordeiro J V., Jacinto A (2013) The role of transcription-independent damage signals in the initiation of epithelial wound healing. Nat Rev Mol Cell Biol 14:249–262. doi: 10.1038/nrm3541

Crisan M, Yap S, Casteilla L, et al (2008) A Perivascular Origin for Mesenchymal Stem Cells in Multiple Human Organs. Cell Stem Cell 3:301–313. doi: 10.1016/j.stem.2008.07.003

Csobonyeiova M, Polak S, Zamborsky R, Danisovic L (2017) iPS cell technologies and their prospect for bone regeneration and disease modeling: A mini review. J Adv Res 8:321–327. doi: 10.1016/j.jare.2017.02.004

Curado S, Anderson RM, Jungblut B, et al (2007) Conditional targeted cell ablation in zebrafish: A new tool for regeneration studies. Dev Dyn 236:1025–1035. doi: 10.1002/dvdy.21100

Curado S, Stainier DYR, Anderson RM (2009) Nitroreductase-mediated cell/tissue ablation in zebrafish: a spatially and temporally controlled ablation method withApplications in Developmental and Regeneration Studies. Nat Protoc 3:948–954. doi: 10.1038/nprot.2008.58.Nitroreductase-mediated

Dalman MR, Liu Q, King MD, et al (2013) Leptin expression affects metabolic rate in zebrafish embryos (D. Rerio). Front Physiol 4 JUL:1–7. doi: 10.3389/fphys.2013.00160

Das BC, Thapa P, Karki R, et al (2014) Retinoic Acid Signaling Pathways in Development and Diseases. Bioorg Med Chem 22:673–683. doi: 10.1016/j.bmc.2013.11.025.Retinoic

de Sousa N, Rodríguez-Esteban G, Rojo-Laguna JI, et al (2018) Hippo signaling controls cell cycle and restricts cell plasticity in planarians. PLoS Biol 16:1–28. doi: 10.1371/journal.pbio.2002399

Demaria M, Ohtani N, Youssef SA, et al (2014) An essential role for senescent cells in optimal wound healing through secretion of PDGF-AA. Dev Cell 31:722–733. doi: 10.1016/j.devcel.2014.11.012

Deng Y, Wu A, Li P, et al (2016) Yap1 Regulates Multiple Steps of Chondrocyte Differentiation during Skeletal Development and Bone Repair. Cell Rep 14:2224–2237. doi: 10.1016/j.celrep.2016.02.021

Deng Z, Sharff KA, Tang N, et al (2008) Regulation of osteogenic differentiation during skeletal development. 2001–2021

Devreotes P, Horwitz AR (2015) Signaling networks that regulate cell migration. Cold Spring Harb Perspect Biol 7:a005959. doi: 10.1101/cshperspect.a005959

Dimitriou R, Jones E, McGonagle D, Giannoudis P V. (2011) Bone regeneration: Current concepts and future directions. BMC Med 9:66. doi: 10.1186/1741-7015-9-66

Dingwall M, Marchildon F, Gunanayagam A, et al (2011) Retinoic acid-induced Smad3 expression is required for

the induction of osteoblastogenesis of mesenchymal stem cells. Differentiation 82:57–65. doi: 10.1016/j.diff.2011.05.003

Doherty MJ, Ashton BA, Walsh S, et al (1998) Vascular pericytes express osteogenic potential in vitro and in vivo. J Bone Min Res 13:828–838

Ducy P, Zhang R, Geoffroy V, et al (1997) Osf2/Cbfa1: A transcriptional activator of osteoblast differentiation. Cell 89:747–754. doi: 10.1016/S0092-8674(00)80257-3

Dufourcq P, Vriz S (2006) The chemokine SDF-1 regulates blastema formation during zebrafish fin regeneration. Dev Genes Evol 216:635–639. doi: 10.1007/s00427-006-0066-7

Dupont S, Morsut L, Aragona M, et al (2011a) Role of YAP/TAZ in mechanotransduction. Nature 474:179–184. doi: 10.1038/nature10137

Dupont S, Morsut L, Aragona M, et al (2011b) Role of YAP/TAZ in mechanotransduction. Nature 474:179–184. doi: 10.1038/nature10137

Durán I, Marí-Beffa M, Santamaría JA, et al (2011) Actinotrichia collagens and their role in fin formation. Dev Biol 354:160–172. doi: 10.1016/j.ydbio.2011.03.014

Echeverri K, Clarke JDW, Tanaka EM (2001) In vivo imaging indicates muscle fiber dedifferentiation is a major contributor to the regenerating tail blastema. Dev Biol 236:151–164. doi: 10.1006/dbio.2001.0312

Echeverri K, Tanaka EM (2002) Ectoderm to mesoderm lineage switching during axolotl tail regeneration. Science (80-) 298:1993–1996. doi: 10.1126/science.1077804

Echeverri K, Tanaka EM (2005) Proximodistal patterning during limb regeneration. Dev Biol 279:391–401. doi: 10.1016/j.ydbio.2004.12.029

Eguizabal C, Montserrat N, Veiga A, et al (2013) Dedifferentiation, Transdifferentiation, and Reprogramming: Future Directions in Regenerative Medicine. Semin Reprod Med 31:82–94. doi: 10.1055/s-0032-1331802

Elliott SA, Sánchez Alvarado A (2013) The history and enduring contributions of planarians to the study of animal regeneration. Wiley Interdiscip Rev Dev Biol 2:301–326. doi: 10.1002/wdev.82

Enyedi B, Kala S, Nikolich-Zugich T, Niethammer P (2013) Tissue damage detection by osmotic surveillance. Nat Cell Biol 15:1123–1130. doi: 10.1038/ncb2818

Enzo E, Santinon G, Pocaterra A, et al (2015) Aerobic glycolysis tunes YAP/TAZ transcriptional activity. EMBO J 34:1349–1370. doi: 10.15252/embj.201490379

Etienne-Manneville S (2013) Microtubules in Cell Migration. Annu Rev Cell Dev Biol 29:471–499. doi: 10.1146/annurev-cellbio-101011-155711

Evans C (2011) Gene therapy for the regeneration of bone. Injury 42:599–604. doi: 10.1016/j.injury.2011.03.032

Fan Y, Bergmann A (2008) Apoptosis-induced compensatory proliferation. The Cell is dead. Long live the Cell! Trends Cell Biol 18:467–473. doi: 10.1016/j.tcb.2008.08.001

Fang Y, Gupta V, Karra R, et al (2013) Translational profiling of cardiomyocytes identifies an early Jak1/Stat3 injury response required for zebrafish heart regeneration. Proc Natl Acad Sci 110:13416–13421. doi: 10.1073/pnas.1309810110

Fazio M, Zon LI (2017) Fishing for answers in precision cancer medicine. Proc Natl Acad Sci 114:10306–10308. doi: 10.1073/pnas.1713769114

Felker A, Nieuwenhuize S, Dolbois A, et al (2016) In vivo performance and properties of Tamoxifen metabolites for CreERT2 control. PLoS One 11:1–17. doi: 10.1371/journal.pone.0152989

Feng X, McDonald JM (2011) Disorders of Bone Remodeling. Annu Rev Pathol Mech Dis 6:121–145. doi: 10.1146/annurev-pathol-011110-130203

Ferron M, Lacombe J (2014) Regulation of energy metabolism by the skeleton: Osteocalcin and beyond. Arch

Biochem Biophys 561:137–146. doi: 10.1016/j.abb.2014.05.022

Ferron M, Wei J, Yoshizawa T, et al (2010) Insulin Signaling in Osteoblasts Integrates Bone Remodeling and Energy Metabolism. Cell 142:296–308. doi: 10.1016/j.cell.2010.06.003

Fischer B, Metzger M, Richardson R, et al (2014) p53 and TAp63 Promote Keratinocyte Proliferation and Differentiation in Breeding Tubercles of the Zebrafish. PLoS Genet 10:. doi: 10.1371/journal.pgen.1004048

Folmes CDL, Dzeja PP, Nelson TJ, Terzic A (2012) Metabolic plasticity in stem cell homeostasis and differentiation. Cell Stem Cell 11:596–606. doi: 10.1016/j.stem.2012.10.002

Forbes SJ, Rosenthal N (2014) Preparing the ground for tissue regeneration: From mechanism to therapy. Nat Med 20:857–869. doi: 10.1038/nm.3653

Friedmann-Morvinski D, Verma IM (2014) Dedifferentiation and reprogramming: Origins of cancer stem cells. EMBO Rep 15:244–253. doi: 10.1002/embr.201338254

Fu V, Plouffe SW, Guan KL (2017) The Hippo pathway in organ development, homeostasis, and regeneration. Curr Opin Cell Biol 49:99–107. doi: 10.1016/j.ceb.2017.12.012

Galliot B, Crescenzi M, Jacinto A, Tajbakhsh S (2017) Trends in tissue repair and regeneration. Development 144:357–364. doi: 10.1242/dev.144279

Galliot B, Ghila L (2010) Cell plasticity in homeostasis and regeneration. Mol Reprod Dev 77:837–855. doi: 10.1002/mrd.21206

Garza-Garcia AA, Driscoll PC, Brockes JP (2010) Evidence for the local evolution of mechanisms underlying limb regeneration in salamanders. Integr Comp Biol 50:528–535. doi: 10.1093/icb/icq022

Gault WJ, Enyedi B, Niethammer P (2014) Osmotic surveillance mediates rapid wound closure through nucleotide release. J Cell Biol 207:767–782. doi: 10.1083/jcb.201408049

Gauron C, Rampon C, Bouzaffour M, et al (2013) Sustained production of ROS triggers compensatory proliferation and is required for regeneration to proceed. Sci Rep 3:1–9. doi: 10.1038/srep02084

Gemberling M, Bailey TJ, Hyde DR, Poss KD (2013) The zebrafish as a model for complex tissue regeneration. Trends Genet 29:611–620. doi: 10.1016/j.tig.2013.07.003

Géraudie J, Ferretti P (1997) Correlation between RA-induced apoptosis and patterning defects in regenerating fins and limbs. Int J Dev Biol 41:529–532

Geurtzen K, Knopf F, Wehner D, et al (2014) Mature osteoblasts dedifferentiate in response to traumatic bone injury in the zebrafish fin and skull. Development 141:2225–2234. doi: 10.1242/dev.105817

Ghosh S, Hui SP (2016) Regeneration of zebrafish CNS: Adult neurogenesis. Neural Plast 2016:. doi: 10.1155/2016/5815439

Godwin J (2014) The promise of perfect adult tissue repair and regeneration in mammals: Learning from regenerative amphibians and fish. BioEssays 36:861–871. doi: 10.1002/bies.201300144

Godwin J, Kuraitis D, Rosenthal N (2014) Extracellular matrix considerations for scar-free repair and regeneration: Insights from regenerative diversity among vertebrates. Int J Biochem Cell Biol 56:47–55. doi: 10.1016/j.biocel.2014.10.011

Godwin JW, Pinto AR, Rosenthal NA (2013) Macrophages are required for adult salamander limb regeneration. Proc Natl Acad Sci 110:9415–9420. doi: 10.1073/pnas.1300290110

Goessling W, North TE (2014) Repairing quite swimmingly: advances in regenerative medicine using zebrafish. Dis Model Mech 7:769–776. doi: 10.1242/dmm.016352

Goldman D (2014) Müller glial cell reprogramming and retina regeneration. Nat Rev Neurosci 15:431–442. doi: 10.1038/nrn3723

Goldman JA, Kuzu G, Lee N, et al (2017) Resolving Heart Regeneration by Replacement Histone Profiling. Dev Cell

40:392–404.e5. doi: 10.1016/j.devcel.2017.01.013

Goldsmith JR, Jobin C (2012) Think small: Zebrafish as a model system of human pathology. J Biomed Biotechnol 2012:. doi: 10.1155/2012/817341

Gorsuch RA, Lahne M, Yarka CE, et al (2017) Sox2 regulates Müller glia reprogramming and proliferation in the regenerating zebrafish retina via Lin28 and Ascl1a. Exp Eye Res 161:174–192. doi: 10.1016/j.exer.2017.05.012

Govindan J, Iovine MK (2015) Dynamic remodeling of the extra cellular matrix during zebrafish fin regeneration. Gene Expr Patterns 19:21–29. doi: 10.1016/j.gep.2015.06.001

Grafi G (2009) The complexity of cellular dedifferentiation: implications for regenerative medicine. Trends Biotechnol 27:329–332. doi: 10.1016/j.tibtech.2009.02.007

Grafi G, Barak S (2015) Stress induces cell dedifferentiation in plants. Biochim Biophys Acta - Gene Regul Mech 1849:378–384. doi: 10.1016/j.bbagrm.2014.07.015

Green AC, Kocovski P, Jovic T, et al (2017) Retinoic acid receptor signalling directly regulates osteoblast and adipocyte differentiation from mesenchymal progenitor cells. Exp Cell Res 350:284–297. doi: 10.1016/j.yexcr.2016.12.007

Grillo M, Konstantinides N, Averof M (2016) Old questions, new models: Unraveling complex organ regeneration with new experimental approaches. Curr Opin Genet Dev 40:23–31. doi: 10.1016/j.gde.2016.05.006

Grohmann M, Paulmann N, Fleischhauer S, et al (2009) A mammalianized synthetic nitroreductase gene for high-level expression. BMC Cancer 9:1–12. doi: 10.1186/1471-2407-9-301

Grotek B, Wehner D, Weidinger G (2013) Notch signaling coordinates cellular proliferation with differentiation during zebrafish fin regeneration. Development 140:1412–1423. doi: 10.1242/dev.087452

Grunwald DJ, Eisen JS (2002) Headwaters of the zebrafish — emergence of a new model vertebrate. Nat Rev Genet 3:711–717. doi: 10.1038/nrg891

Guo C, Morris SA (2017) Engineering cell identity: establishing new gene regulatory and chromatin landscapes. Curr Opin Genet Dev 46:50–57. doi: 10.1016/j.gde.2017.06.011

Gurtner GC, Werner S, Barrandon Y, Longaker MT (2008) Wound repair and regeneration. Nature 453:314–321. doi: 10.1038/nature07039

Halder G, Johnson RL (2011) Hippo signaling: growth control and beyond. Development 138:9–22. doi: 10.1242/dev.045500

Hans S, Kaslin J, Freudenreich D, Brand M (2009) Temporally-controlled site-specific recombination in zebrafish. PLoS One 4:. doi: 10.1371/journal.pone.0004640

Hansen CG, Moroishi T, Guan KL (2015) YAP and TAZ: A nexus for Hippo signaling and beyond. Trends Cell Biol 25:499–513. doi: 10.1016/j.tcb.2015.05.002

Harikumar A, Meshorer E (2015) Chromatin remodeling and bivalent histone modifications in embryonic stem cells. EMBO Rep 16:1609–1619. doi: 10.15252/embr.201541011

Hawkins RD, Hon GC, Lee LK, et al (2011) Distinct Epigenomic Landscapes of Pluripotent and Lineage- committed Human Cells. 6:479–491. doi: 10.1016/j.stem.2010.03.018.Distinct

Hayashi S, Kawaguchi A, Uchiyama I, et al (2015) Epigenetic modification maintains intrinsic limb-cell identity in Xenopus limb bud regeneration. Dev Biol 406:271–282. doi: 10.1016/j.ydbio.2015.08.013

Hayashi S, Tamura K, Yokoyama H (2014) Yap1, transcription regulator in the Hippo signaling pathway, is required for Xenopus limb bud regeneration. Dev Biol 388:57–67. doi: 10.1016/j.ydbio.2014.01.018

Heallen T, Zhang M, Wang J, et al (2012) Hippo Pathway Inhibits Wnt Signaling to Restrain Cardiomyocyte Proliferation and Heart Size. Science (80-) 332:458–461. doi: 10.1126/science.1199010.Hippo

Heiden MG Vander, Cantley LC, Thompson CB (2009) Understanding the warburg effect: The metabolic requirements of cell proliferation. Science (80-) 324:1029–1033. doi: 10.1126/science.1160809

Herschel Conaway H, Henning P, Lerner UH (2013) Vitamin a metabolism, action, and role in skeletal homeostasis. Endocr Rev 34:766–797. doi: 10.1210/er.2012-1071

Hiemer SE, Varelas X (2013) Stem cell regulation by the Hippo pathway. Biochim Biophys Acta - Gen Subj 1830:2323–2334. doi: 10.1016/j.bbagen.2012.07.005

Hirose K, Shiomi T, Hozumi S, Kikuchi Y (2014) Mechanistic target of rapamycin complex 1 signaling regulates cell proliferation, cell survival, and differentiation in regenerating zebrafish fins. BMC Dev Biol 14:1–15. doi: 10.1186/s12861-014-0042-9

Holman EC, Campbell LJ, Hines J, Crews CM (2012) Microarray Analysis of microRNA Expression during Axolotl Limb Regeneration. PLoS One 7:1–10. doi: 10.1371/journal.pone.0041804

Hong J, Hong J, Hwang ES, et al (2005) Taz, a Transcriptional Modulator of Mesenchymal Stem Cell Differentiation. Science 1074:1074–1078. doi: 10.1126/science.1110955

Hong YJ, Choi YW, Myung KB, Choi HY (2011) The immunohistochemical patterns of calcification-related molecules in the epidermis and dermis of the zebrafish (Danio rerio). Ann Dermatol 23:299–303. doi: 10.5021/ad.2011.23.3.299

Howe K, Clark M, Torroja C, et al (2013) The zebrafish reference genome sequence and its relationship to the human genome. Nature 496:498–503. doi: 10.1038/nature12111.The

Huang J, Wu S, Barrera J, et al (2005) The Hippo signaling pathway coordinately regulates cell proliferation and apoptosis by inactivating Yorkie, the Drosophila homolog of YAP. Cell 122:421–434. doi: 10.1016/j.cell.2005.06.007

Hui SP, Sheng DZ, Sugimoto K, et al (2017) Zebrafish Regulatory T Cells Mediate Organ-Specific Regenerative Programs. Dev Cell 43:659–672.e5. doi: 10.1016/j.devcel.2017.11.010

Huttenlocher A, Horwitz AR (2011) Integrins in cell migration. Cold Spring Harb Perspect Biol 3 VN-re:1–16. doi: 10.1101/cshperspect.a005074

Iismaa SE, Kaidonis X, Nicks AM, et al (2018) Comparative regenerative mechanisms across different mammalian tissues. npj Regen Med 3:6. doi: 10.1038/s41536-018-0044-5

Illich DJ, Demir N, Stojković M, et al (2011) Concise review: Induced pluripotent stem cells and lineage reprogramming: Prospects for bone regeneration. Stem Cells 29:555–563. doi: 10.1002/stem.611

Iovine MK (2007) Conserved mechanisms regulate outgrowth in zebrafish fins. Nat Chem Biol 3:613–618. doi: 10.1038/nchembio.2007.36

Iovine MK, Higgins EP, Hindes A, et al (2005) Mutations in connexin43 (GJA1) perturb bone growth in zebrafish fins. Dev Biol 278:208–219. doi: 10.1016/j.ydbio.2004.11.005

Irvine KD (2012) Integration of intercellular signaling through the Hippo pathway. Semin Cell Dev Biol 23:812–817. doi: 10.1016/j.semcdb.2012.04.006

Irvine KD, Harvey KF (2015) Control of organ growth by patterning and hippo signaling in drosophila. Cold Spring Harb Perspect Biol 7:1–16. doi: 10.1101/cshperspect.a019224

Itou J, Kawakami H, Burgoyne T, Kawakami Y (2012) Life-long preservation of the regenerative capacity in the fin and heart in zebrafish. Biol Open 1:739–746. doi: 10.1242/bio.20121057

Iwasaki M, Kuroda J, Kawakami K, Wada H (2018) Epidermal regulation of bone morphogenesis through the development and regeneration of osteoblasts in the zebrafish scale. Dev Biol 437:105–119. doi: 10.1016/j.ydbio.2018.03.005

Jahn C, Weidinger G (2017) Regulatory T Cells Know What Is Needed to Regenerate. Dev Cell 43:651–652. doi: 10.1016/j.devcel.2017.12.010

Jaźwińska A, Badakov R, Keating MT (2007) Activin-βA Signaling Is Required for Zebrafish Fin Regeneration. Curr Biol 17:1390–1395. doi: 10.1016/j.cub.2007.07.019

Jaźwińska A, Sallin P (2016) Regeneration versus scarring in vertebrate appendages and heart. J Pathol 238:233–246. doi: 10.1002/path.4644

Jessen JR (2015) Recent advances in the study of zebrafish extracellular matrix proteins. Dev Biol 401:110–121. doi: 10.1016/j.ydbio.2014.12.022

Jessen KR, Mirsky R, Arthur-Farraj P (2015) The Role of Cell Plasticity in Tissue Repair: Adaptive Cellular Reprogramming. Dev Cell 34:613–620. doi: 10.1016/j.devcel.2015.09.005

Johnson SL, Weston JA (1995) Temperature-sensitive mutations that cause stage-specific defects in zebrafish fin regeneration. Genetics 141:1583–1595

Jopling C, Boue S, Belmonte JCI (2011) Dedifferentiation, transdifferentiation and reprogramming: Three routes to regeneration. Nat Rev Mol Cell Biol 12:79–89. doi: 10.1038/nrm3043

Jopling C, Sleep E, Raya M, et al (2010) Zebrafish heart regeneration occurs by cardiomyocyte dedifferentiation and proliferation. Nature 464:606–609. doi: 10.1038/nature08899

Jun Du S, Frenkel V, Zohar Y, Kindschi G (2001) Visualizing normal and defective bone development in zebrafish embryos using the fluorescent chromophore calcein. Dev Biol 238:239–246. doi: 10.1006/dbio.2001.0390

Kami D, Gojo S (2014) Tuning cell fate: From insights to vertebrate regeneration. Organogenesis 10:231–240. doi: 10.4161/org.28816

Kamiya N, Mishina Y (2011) New insights on the roles of BMP signaling in bone-A review of recent mouse genetic studies. BioFactors 37:75–82. doi: 10.1002/biof.139

Kang J, Hu J, Karra R, et al (2016) Modulation of tissue repair by regeneration enhancer elements. Nature 532:201–206. doi: 10.1038/nature17644

Karin M, Clevers H (2016) Reparative inflammation takes charge of tissue regeneration. Nature 529:307–315. doi: 10.1038/nature17039

Karsenty G (2008) Transcriptional Control of Skeletogenesis. Annu Rev Genomics Hum Genet 9:183–196. doi: 10.1146/annurev.genom.9.081307.164437

Katsuyama T, Paro R (2011) Epigenetic reprogramming during tissue regeneration. FEBS Lett 585:1617–1624. doi: 10.1016/j.febslet.2011.05.010

Kaverina I, Straube A (2011) Regulation of cell migration by dynamic microtubules. Semin Cell Dev Biol 22:968–974. doi: 10.1016/j.semcdb.2011.09.017

Kawakami A (2009) Stem cell system in tissue regeneration in fish. Dev Growth Differ 52:77–87. doi: 10.1111/j.1440-169X.2009.01138.x

Kawakami A, Fukazawa T, Takeda H (2004) Early fin primordia of zebrafish larvae regenerate by a similar growth control mechanism with adult regeneration. Dev Dyn 231:693–699. doi: 10.1002/dvdy.20181

Kawakami K, Asakawa K, Muto A, Wada H (2016) Tol2-mediated transgenesis, gene trapping, enhancer trapping, and Gal4-UAS system. Elsevier Ltd

Kegelman CD, Mason DE, Dawahare JH, et al (2018) Skeletal cell YAP and TAZ combinatorially promote bone development. FASEB J 32:2706–2721. doi: 10.1096/fj.201700872R

Kegelman CD, Mason DE, Dawahare JH, et al (2017) Skeletal cell YAP and TAZ redundantly promote bone development by regulation of collagen I expression and organization. 1–40

Khacho M, Clark A, Svoboda DS, et al (2016) Mitochondrial Dynamics Impacts Stem Cell Identity and Fate Decisions by Regulating a Nuclear Transcriptional Program. Cell Stem Cell 19:232–247. doi: 10.1016/j.stem.2016.04.015

Kikuchi K (2014) Advances in understanding the mechanism of zebrafish heart regeneration. Stem Cell Res 13:542–555. doi: 10.1016/j.scr.2014.07.003

Kikuchi K, Holdway JE, Werdich AA, et al (2010) Primary contribution to zebrafish heart regeneration by gata4+ cardiomyocytes. Nature 464:601–605. doi: 10.1038/nature08804

Kikuchi K, Poss KD (2012) Cardiac Regenerative Capacity and Mechanisms. Annu Rev Cell Dev Biol 28:719–741. doi: 10.1146/annurev-cellbio-101011-155739

Kim M, Jho EH (2014) Cross-talk between Wnt/b-catenin and Hippo signaling pathways: A brief review. BMB Rep 47:540–545. doi: 10.5483/BMBRep.2014.47.10.177

King BL, Yin VP (2016) A conserved microRNA regulatory circuit is differentially controlled during limb/appendage regeneration. PLoS One 11:1–25. doi: 10.1371/journal.pone.0157106

King RS, Newmark PA (2012) The cell biology of regeneration. J Cell Biol 196:553–562. doi: 10.1083/jcb.201105099

Kizil C, Kaslin J, Kroehne V, Brand M (2012) Adult neurogenesis and brain regeneration in zebrafish. Dev Neurobiol 72:429–461. doi: 10.1002/dneu.20918

Kizil C, Kyritsis N, Brand M (2015) Effects of inflammation on stem cells: together they strive? EMBO Rep 16:416–426. doi: 10.15252/embr.201439702

Knopf F, Hammond C, Chekuru A, et al (2011) Bone regenerates via dedifferentiation of osteoblasts in the zebrafish fin. Dev Cell 20:713–724. doi: 10.1016/j.devcel.2011.04.014

Komori T (2006) Regulation of osteoblast differentiation by transcription factors. J Cell Biochem 99:1233–1239. doi: 10.1002/jcb.20958

Komori T, Yagi H, Nomura S, et al (2017) Targeted Disruption of Cbfa1 Results in a Complete Lack of Bone Formation owing to Maturational Arrest of Osteoblasts. Cell 89:755–764. doi: 10.1016/S0092-8674(00)80258-5

König D, Page L, Chassot B, Jaźwińska A (2018) Dynamics of actinotrichia regeneration in the adult zebrafish fin. Dev Biol 433:416–432. doi: 10.1016/j.ydbio.2017.07.024

Koo JH, Guan KL (2018) Interplay between YAP/TAZ and Metabolism. Cell Metab 28:196–206. doi: 10.1016/j.cmet.2018.07.010

Kouzarides T (2007) Chromatin Modifications and Their Function. Cell 128:693–705. doi: 10.1016/j.cell.2007.02.005

Kragl M, Knapp D, Nacu E, et al (2009) Cells keep a memory of their tissue origin during axolotl limb regeneration. Nature 460:60–65. doi: 10.1038/nature08152

Kretzschmar K, Watt FM (2012) Lineage tracing. Cell 148:33–45. doi: 10.1016/j.cell.2012.01.002

Kujawski S, Lin W, Kitte F, et al (2014) Calcineurin Regulates Coordinated Outgrowth of Zebrafish Regenerating Fins. Dev Cell 28:573–587. doi: 10.1016/j.devcel.2014.01.019

Kumar A, Brockes JP (2012) Nerve dependence in tissue, organ, and appendage regeneration. Trends Neurosci 35:691–699. doi: 10.1016/j.tins.2012.08.003

Kumar A, Godwin JW, Gates PB, et al (2009) Molecular Basis for the Nerve Dependence of Limb Regeneration in an Adult Vertebrate. 318:772–777. doi: 10.1126/science.1147710.Molecular

Laforest L, Brown CW, Poleo G, et al (1998) Involvement of the sonic hedgehog, patched 1 and bmp2 genes in patterning of the zebrafish dermal fin rays. Development 125:4175–4184

Lai SL, Marín-Juez R, Moura PL, et al (2017) Reciprocal analyses in zebrafish and medaka reveal that harnessing the immune response promotes cardiac regeneration. Elife 6:1–20. doi: 10.7554/eLife.25605

Laizé V, Gavaia PJ, Cancela ML (2014) Fish: A suitable system to model human bone disorders and discover drugs

with osteogenic or osteotoxic activities. Drug Discov Today Dis Model 13:29–37. doi: 10.1016/j.ddmod.2014.08.001

Le Guellec D, Morvan-Dubois G, Sire JY (2004) Skin development in bony fish with particular emphasis on collagen deposition in the dermis of the zebrafish (Danio rerio). Int J Dev Biol 48:217–231. doi: 10.1387/ijdb.15272388

LeBert D, Squirrell JM, Freisinger C, et al (2018) Damage-induced reactive oxygen species regulate vimentin and dynamic collagen- based projections to mediate wound repair. Elife 7:1–26. doi: 10.7554/eLife.30703

LeBert DC, Squirrell JM, Rindy J, et al (2015) Matrix metalloproteinase 9 modulates collagen matrices and wound repair. Development 142:2136–2146. doi: 10.1242/dev.121160

LeClair EE, Topczewski J (2010) Development and regeneration of the zebrafish maxillary barbel: A novel study system for vertebrate tissue growth and repair. PLoS One 5:. doi: 10.1371/journal.pone.0008737

Lee HRT, Thiery JP, Carney TJ (2013) Dermal fin rays and scales derive from mesoderm, not neural crest. Curr Biol 23:R336–R337. doi: 10.1016/j.cub.2013.02.055

Lee RTH, Asharani P V., Carney TJ (2014) Basal keratinocytes contribute to all strata of the adult zebrafish epidermis. PLoS One 9:. doi: 10.1371/journal.pone.0084858

Lee SH, Dominguez R (2010) Regulation of actin cytoskeleton dynamics in cells. Mol Cells 29:311–325. doi: 10.1007/s10059-010-0053-8

Lee Y (2005) Fgf signaling instructs position-dependent growth rate during zebrafish fin regeneration. Development 132:5173–5183. doi: 10.1242/dev.02101

Lee Y, Hami D, De Val S, et al (2009) Maintenance of blastemal proliferation by functionally diverse epidermis in regenerating zebrafish fins. Dev Biol 331:270–280. doi: 10.1016/j.ydbio.2009.05.545

Lenkowski JR, Raymond PA (2014) Müller glia: Stem cells for generation and regeneration of retinal neurons in teleost fish. Prog Retin Eye Res 40:94–123. doi: 10.1016/j.preteyeres.2013.12.007

Levy JR, Holzbaur ELF, Parsons JT, et al (2010) Cell adhesion: integrating cytoskeletal dynamics and cellular tension. Mol Cell 11:633–643. doi: 10.1038/nrm2957.Cell

Li L, Yan B, Shi YQ, et al (2012) Live imaging reveals differing roles of macrophages and neutrophils during zebrafish tail fin regeneration. J Biol Chem 287:25353–25360. doi: 10.1074/jbc.M112.349126

Li N, Felber K, Elks P, et al (2009) Tracking gene expression during zebrafish osteoblast differentiation. Dev Dyn 238:459–466. doi: 10.1002/dvdy.21838

Li N, Kelsh RN, Croucher P, Roehl HH (2010) Regulation of neural crest cell fate by the retinoic acid and Pparg signalling pathways. Development 137:389–394. doi: 10.1242/dev.044164

Li Q, Yang H, Zhong TP (2015) Regeneration across metazoan phylogeny: Lessons from model organisms. J Genet Genomics 42:57–70. doi: 10.1016/j.jgg.2014.12.002

Lian I, Kim J, Okazawa H, et al (2010) The role of YAP transcription coactivator in regulating stem cell self-renewal and differentiation. Genes Dev 24:1106–1118. doi: 10.1101/gad.1903310

Liberti M V., Locasale JW (2016) The Warburg Effect: How Does it Benefit Cancer Cells? Trends Biochem Sci 41:211–218. doi: 10.1016/j.tibs.2015.12.001

Lieschke GJ, Currie PD (2007) Animal models of human disease: Zebrafish swim into view. Nat Rev Genet 8:353–367. doi: 10.1038/nrg2091

Lieschke GJ, Oates AC, Kawakami K (2009) Methods in Molecular Biology Zebrafish Methods and Protocols. Humana Press, Springer Science, Hatfield, Hertfordshire

Lin YT, Ding JY, Li MY, et al (2012) YAP regulates neuronal differentiation through Sonic hedgehog signaling pathway. Exp Cell Res 318:1877–1888. doi: 10.1016/j.yexcr.2012.05.005

Ling L, Nurcombe V, Cool SM (2009) Wnt signaling controls the fate of mesenchymal stem cells. Gene 433:1–7. doi: 10.1016/j.gene.2008.12.008

Liu FY, Hsu TC, Choong P, et al (2018a) Uncovering the regeneration strategies of zebrafish organs: A comprehensive systems biology study on heart, cerebellum, fin, and retina regeneration. BMC Syst Biol 12:. doi: 10.1186/s12918-018-0544-3

Liu H, Li D, Zhang Y, Li M (2018b) Inflammation, mesenchymal stem cells and bone regeneration. Histochem Cell Biol 149:393–404. doi: 10.1007/s00418-018-1643-3

Livak KJ, Schmittgen TD (2001) Analysis of relative gene expression data using real-time quantitative PCR and the 2-ΔΔCT method. Methods 25:402–408. doi: 10.1006/meth.2001.1262

Lizcano JM, Alessi DR (2002) The insulin signalling pathway. Curr Biol 12:236–238. doi: 10.1016/S0960-9822(02)00777-7

Loeffler J, Duda GN, Sass FA, Dienelt A (2018) The Metabolic Microenvironment Steers Bone Tissue Regeneration. Trends Endocrinol Metab 29:99–110. doi: 10.1016/j.tem.2017.11.008

Long F (2012) Building strong bones: Molecular regulation of the osteoblast lineage. Nat Rev Mol Cell Biol 13:27–38. doi: 10.1038/nrm3254

Louie KW, Saera-Vila A, Kish PE, et al (2017) Temporally distinct transcriptional regulation of myocyte dedifferentiation and Myofiber growth during muscle regeneration. BMC Genomics 18:1–17. doi: 10.1186/s12864-017-4236-y

Love NR, Chen Y, Ishibashi S, et al (2013) Amputation-induced reactive oxygen species (ROS) are required for successful *Xenopus* tadpole tail regeneration. Nat Cell Biol 15:222–228. doi: 10.1038/ncb2659

Lund TC, Patrinostro X, Krame AC, et al (2014) sdf1 Expression Reveals a Source of Perivascular-Derived Mesenchymal Stem Cells in Zebrafish. Stem Cells 6:247–253. doi: 10.1111/j.1743-6109.2008.01122.x.Endothelial

Lunt SY, Vander Heiden MG (2011) Aerobic Glycolysis: Meeting the Metabolic Requirements of Cell Proliferation. Annu Rev Cell Dev Biol 27:441–464. doi: 10.1146/annurev-cellbio-092910-154237

Luo W, Friedman MS, Shedden K, et al (2009) GAGE: Generally applicable gene set enrichment for pathway analysis. BMC Bioinformatics 10:1–17. doi: 10.1186/1471-2105-10-161

Lush ME, Piotrowski T (2014) Sensory hair cell regeneration in the zebrafish lateral line. Dev Dyn 243:1187–1202. doi: 10.1002/dvdy.24167

Luu HH, Wagner ER, Luther G, et al (2011) Defective osteogenic differentiation in the development of osteosarcoma. Sarcoma 2011:5–7. doi: 10.1155/2011/325238

MacDonald BT, Tamai K, He X (2010) Wnt/β-catenin signaling: components, mechanisms, and diseases. Dev Cell 17:9–26. doi: 10.1016/j.devcel.2009.06.016.Wnt/

Mackie EJ, Tucker RP (1992) Tenascin in bone morphogenesis: expression by osteoblasts and cell type-specific expression of splice variants. J Cell Sci 103 (Pt 3:765–71

Maden M (1978) Neurotrophic control of the cell cycle during amphibian limb regeneration. J Embryol Exp Morphol 48:169–175

Maden M (2013) Who needs stem cells if you can dedifferentiate? Cell Stem Cell 13:640–641. doi: 10.1016/j.stem.2013.11.020

Maes C, Kobayashi T, Selig MK, et al (2010) Osteoblast precursors, but not mature osteoblasts, move into developing and fractured bones along with invading blood vessels. Dev Cell 19:329–344. doi: 10.1016/j.devcel.2010.07.010

Maki N, Tsonis P a, Agata K (2010) Changes in global histone modifications during dedifferentiation in newt lens regeneration. Mol Vis 16:1893–7. doi: 205 [pii]

Marí-Beffa M, Murciano C (2010) Dermoskeleton morphogenesis in zebrafish fins. Dev Dyn 239:2779–2794. doi: 10.1002/dvdy.22444

Marí-Beffa M, Santamaría JA, Fernández-Llebrez P, Becerra J (1996) Histochemically defined cell states during tail fin regeneration in teleost fishes. Differentiation 60:139–149. doi: 10.1007/s002580050144

Marí-Beffa M, Santamaría JA, Murciano C, et al (2007) Zebrafish fins as a model system for skeletal human studies. ScientificWorldJournal 7:1114–1127. doi: 10.1100/tsw.2007.190

Mariani F V. (2010) Proximal to distal patterning during limb development and regeneration: A review of converging disciplines. Regen Med 5:451–462. doi: 10.2217/rme.10.27

Marie PJ (2008) Transcription factors controlling osteoblastogenesis. Arch Biochem Biophys 473:98–105. doi: 10.1016/j.abb.2008.02.030

Marie PJ (2015) Osteoblast dysfunctions in bone diseases: From cellular and molecular mechanisms to therapeutic strategies. Cell Mol Life Sci 72:1347–1361. doi: 10.1007/s00018-014-1801-2

Marsell R, Einhorn TA (2011) The biology of fracture healing. Injury 42:551–555. doi: 10.1016/j.injury.2011.03.031

Massagué J (2012) TGFβ signalling in context. Nat Rev Mol Cell Biol 13:616–630. doi: 10.1038/nrm3434

Mateus R, Lourenco R, Fang Y, et al (2015) Control of tissue growth by Yap relies on cell density and F-actin in zebrafish fin regeneration. Development 142:2752–2763. doi: 10.1242/dev.119701

Mateus R, Pereira T, Sousa S, et al (2012) In Vivo Cell and Tissue Dynamics Underlying Zebrafish Fin Fold Regeneration. PLoS One 7:. doi: 10.1371/journal.pone.0051766

Mathew LK, Sengupta S, Kawakami A, et al (2007) Unraveling tissue regeneration pathways using chemical genetics. J Biol Chem 282:35202–35210. doi: 10.1074/jbc.M706640200

Mathieu J, Ruohola-Baker H (2017) Metabolic remodeling during the loss and acquisition of pluripotency. Development 144:541–551. doi: 10.1242/dev.128389

Matic I, Matthews BG, Wang X, et al (2016) Quiescent Bone Lining Cells Are a Major Source of Osteoblasts During Adulthood. Stem Cells 34:2930–2942. doi: 10.1002/stem.2474

Meda F, Rampon C, Dupont E, et al (2017) Nerves, H2O2and Shh: Three players in the game of regeneration. Semin Cell Dev Biol. doi: 10.1016/j.semcdb.2017.08.015

Mescher AL (2017) Macrophages and fibroblasts during inflammation and tissue repair in models of organ regeneration. Regeneration 4:39–53. doi: 10.1002/reg2.77

Mescher AL, Neff AW, King MW (2017) Inflammation and immunity in organ regeneration. Dev Comp Immunol 66:98–110. doi: 10.1016/j.dci.2016.02.015

Michel M, Page-McCaw PS, Chen W, Cone RD (2016) Leptin signaling regulates glucose homeostasis, but not adipostasis, in the zebrafish. Proc Natl Acad Sci 113:3084–3089. doi: 10.1073/pnas.1513212113

Mills AA, Zheng B, Wang XJ, et al (1999) P63 Is a P53 Homologue Required for Limb and Epidermal Morphogenesis. Nature 398:708–713. doi: 10.1038/19531

Mohamed FF, Franceschi RT (2017) Skeletal Stem Cells : Origins , Functions , and Uncertainties

Monteiro J, Aires R, Becker JD, et al (2014) V-ATPase proton pumping activity is required for adult zebrafish appendage regeneration. PLoS One 9:. doi: 10.1371/journal.pone.0092594

Morgan TH (1902) Further experiments on the regeneration of the tail of fishes. Arch f??r Entwicklungsmechanik der Org 14:539–561. doi: 10.1007/BF02188503

Morgan TH (1901) Regeneration. Columbia Univ Biol Ser VII 342

Moris N, Pina C, Arias AM (2016) Transition states and cell fate decisions in epigenetic landscapes. Nat Rev Genet

17:693–703. doi: 10.1038/nrg.2016.98

Morrison JI, Lööf S, He P, Simon A (2006) Salamander limb regeneration involves the activation of a multipotent skeletal muscle satellite cell population. J Cell Biol 172:433–440. doi: 10.1083/jcb.200509011

Mosimann C, Kaufman CK, Li P, et al (2011) Ubiquitous transgene expression and Cre-based recombination driven by the ubiquitin promoter in zebrafish. Development 138:169–177. doi: 10.1242/dev.059345

Mosteiro L, Pantoja C, Alcazar N, et al (2016) Tissue damage and senescence provide critical signals for cellular reprogramming in vivo. Science (80-) 354:. doi: 10.1126/science.aaf4445

Moussaieff A, Rouleau M, Kitsberg D, et al (2015) Glycolysis-mediated changes in acetyl-CoA and histone acetylation control the early differentiation of embryonic stem cells. Cell Metab 21:392–402. doi: 10.1016/j.cmet.2015.02.002

Moya IM, Halder G (2016) The Hippo pathway in cellular reprogramming and regeneration of different organs. Curr Opin Cell Biol 43:62–68. doi: 10.1016/j.ceb.2016.08.004

Munch J, Gonzalez-Rajal A, de la Pompa JL (2013) Notch regulates blastema proliferation and prevents differentiation during adult zebrafish fin regeneration. Development 140:1402–1411. doi: 10.1242/dev.087346

Muneoka K, Allan CH, Yang X, et al (2008) Mammalian regeneration and regenerative medicine. Birth Defects Res Part C - Embryo Today Rev 84:265–280. doi: 10.1002/bdrc.20137

Murawala P, Tanaka EM, Currie JD (2012) Regeneration: The ultimate example of wound healing. Semin Cell Dev Biol 23:954–962. doi: 10.1016/j.semcdb.2012.09.013

Murciano C, Fernández TD, Durán I, et al (2002) Ray-interray interactions during fin regeneration of Danio rerio. Dev Biol 252:214–224. doi: 10.1006/dbio.2002.0848

Murray PJ (2007) The JAK-STAT Signaling Pathway: Input and Output Integration. J Immunol 178:2623–2629. doi: 10.4049/jimmunol.178.5.2623

Murrell M, Oakes PW, Lenz M, Gardel ML (2015) Forcing cells into shape: The mechanics of actomyosin contractility. Nat Rev Mol Cell Biol 16:486–498. doi: 10.1038/nrm4012

Nachtrab G, Czerwinski M, Poss KD (2011) Sexually dimorphic fin regeneration in Zebrafish controlled by androgen/GSK3 signaling. Curr Biol 21:1912–1917. doi: 10.1016/j.cub.2011.09.050

Nachtrab G, Kikuchi K, Tornini VA, Poss KD (2013) Transcriptional components of anteroposterior positional information during zebrafish fin regeneration. Development 140:3754–3764. doi: 10.1242/dev.098798

Nacu E, Tanaka EM (2011) Limb Regeneration: A New Development? Annu Rev Cell Dev Biol 27:409–440. doi: 10.1146/annurev-cellbio-092910-154115

Nakashima K, Zhou X, Al. GKE (2002) The novel zinc fingercontaining transcription factor Osterix is required for osteoblast differentiation and bone formation. Cell 108:17–29

Nauroy P, Guiraud A, Chlasta J, et al (2018) Gene profile of zebrafish fin regeneration offers clues to kinetics, organization and biomechanics of basement membrane. Matrix Biol #pagerange#. doi: 10.1016/j.matbio.2018.07.005

Nechiporuk A, Keating MT (2002) A proliferation gradient between proximal and msxb-expressing distal blastema directs zebrafish fin regeneration. Development 129:2607–2617

Nicolay BN, Bayarmagnai B, Moon NS, et al (2010) Combined inactivation of pRB and Hippo pathways induces dedifferentiation in the Drosophila retina. PLoS Genet 6:. doi: 10.1371/journal.pgen.1000918

Niethammer P (2016) The early wound signals. Curr Opin Genet Dev 40:17–22. doi: 10.1016/j.gde.2016.05.001

Niethammer P, Grabher C, Look AT, Mitchison TJ (2009) A tissue-scale gradient of hydrogen peroxide mediates rapid wound detection in zebrafish. Nature 459:996–999. doi: 10.1038/nature08119

Nolte H, Hölper S, Housley MP, et al (2014) Dynamics of Zebrafish Fin Regeneration Using a Pulsed SILAC Approach Abstract The zebrafish owns remarkable regenerative capacities allowing regeneration of several. 1–27. doi: 10.1002/pmic.201400316.This

Noorimotlagh Z, Babaie M, Safdarian M, et al (2017) Mechanisms of spinal cord injury regeneration in zebrafish: A systematic review. Iran J Basic Med Sci 20:1287–1296. doi: 10.22038/ijbms.2017.9620

Odelberg SJ (2005) Cellular plasticity in vertebrate regeneration. Anat Rec - Part B New Anat 287:25–35. doi: 10.1002/ar.b.20080

Onder TT, Kara N, Cherry A, et al (2012) Chromatin-modifying enzymes as modulators of reprogramming. Nature 483:598–602. doi: 10.1038/nature10953

Ono N, Kronenberg HM (2016) Bone repair and stem cells. Curr Opin Genet Dev 25:368–379. doi: 10.1016/j.cogdev.2010.08.003.Personal

Oppedal D, Goldsmith MI (2010) A chemical screen to identify novel inhibitors of fin regeneration in zebrafish. Zebrafish 7:53–60. doi: 10.1089/zeb.2009.0633

Orkin SH, Hochedlinger K (2011) Chromatin connections to pluripotency and cellular reprogramming. Cell 145:835–850. doi: 10.1016/j.cell.2011.05.019

Osuma EA, Riggs DW, Gibb AA, Hill BG (2018) High throughput measurement of metabolism in planarians reveals activation of glycolysis during regeneration. Regeneration 78–86. doi: 10.1002/reg2.95

Owlarn S, Klenner F, Schmidt D, et al (2017) Generic wound signals initiate regeneration in missing-tissue contexts. Nat Commun 8:1–13. doi: 10.1038/s41467-017-02338-x

Padhi BK, Joly L, Tellis P, et al (2004) Screen for genes differentially expressed during regeneration of the zebrafish caudal fin. Dev Dyn 231:527–541. doi: 10.1002/dvdy.20153

Pan J-X, Xiong L, Zhao K, et al (2018) YAP promotes osteogenesis and suppresses adipogenic differentiation by regulating β-catenin signaling. Bone Res 6:18. doi: 10.1038/s41413-018-0018-7

Park D, Spencer JA, Koh BI, et al (2012) Endogenous bone marrow MSCs are dynamic, fate-restricted participants in bone maintenance and regeneration. Cell Stem Cell 10:259–272. doi: 10.1016/j.stem.2012.02.003

Park H-K, Ahima RS (2014) Leptin signaling. F1000Prime Rep 6:. doi: 10.12703/P6-73

Park HW, Kim YC, Yu B, et al (2015) Alternative Wnt Signaling Activates YAP/TAZ. Cell 162:780–794. doi: 10.1016/j.cell.2015.07.013

Patel DM, Shah J, Srivastava AS (2013) Therapeutic potential of mesenchymal stem cells in regenerative medicine. Stem Cells Int 2013:496218. doi: 10.1155/2013/496218

Pearson G, Robinson F, Gibson TB, et al (2001) Mitogen-activated protein(MAP) Kinase pathways: Regulation and Physiological Functions. Endocr Rev 22:153–183. doi: 10.1210/edrv.22.2.0428

Perathoner S, Daane JM, Henrion U, et al (2014) Bioelectric Signaling Regulates Size in Zebrafish Fins. PLoS Genet 10:. doi: 10.1371/journal.pgen.1004080

Percharde M, Bulut-Karslioglu A, Ramalho-Santos M (2017) Hypertranscription in Development, Stem Cells, and Regeneration. Dev Cell 40:9–21. doi: 10.1016/j.devcel.2016.11.010

Pereira BP, Zhou Y, Gupta A, et al (2009) Runx2, p53, and pRB status as diagnostic parameters for deregulation of osteoblast growth and differentiation in a new pre-chemotherapeutic osteosarcoma cell line (OS1). J Cell Physiol 221:778–788. doi: 10.1002/jcp.21921

Perez-Garijo A, Steller H (2015) Spreading the word: non-autonomous effects of apoptosis during development, regeneration and disease. Development 142:3253–3262. doi: 10.1242/dev.127878

Pescitelli MJ, Stocum DL (1980) The origin of skeletal structures during intercalary regeneration of larval Ambystoma limbs. Dev Biol 79:255–275. doi: 10.1016/0012-1606(80)90115-3

Petrie TA, Strand NS, Yang C-T, et al (2015) Macrophages modulate adult zebrafish tail fin regeneration. Development 142:406–406. doi: 10.1242/dev.120642

Pfefferli C, Jaźwińska A (2017) The careg element reveals a common regulation of regeneration in the zebrafish myocardium and fin. Nat Commun 8:. doi: 10.1038/ncomms15151

Pfefferli C, Jaźwińska A (2015) The art of fin regeneration in zebrafish. Regeneration 2:72–83. doi: 10.1002/reg2.33

Pfefferli C, Müller F, Jaźwińska A, Wicky C (2014) Specific NuRD components are required for fin regeneration in zebrafish. BMC Biol 12:1–17. doi: 10.1186/1741-7007-12-30

Phimphilai M, Zhao Z, Boules H, et al (2006) BMP signaling is required for RUNX2-dependent induction of the osteoblast phenotype. J Bone Miner Res 21:637–646. doi: 10.1359/jbmr.060109

Piccirillo R, Demontis F, Perrimon N, Goldberg A (2013) Cx43 suppresses evx1 expression to regulate joint initiation in the regenerating fin. Dev Dyn 080507:1–47. doi: 10.1002/dvdy.

Piccolo S, Dupont S, Cordenonsi M (2014) The Biology of YAP/TAZ: Hippo Signaling and Beyond. Physiol Rev 94:1287–1312. doi: 10.1152/physrev.00005.2014

Pirotte N, Leynen N, Artois T, Smeets K (2016) Do you have the nerves to regenerate? The importance of neural signalling in the regeneration process. Dev Biol 409:4–15. doi: 10.1016/j.ydbio.2015.09.025

Pittlik S, Begemann G (2012) New sources of retinoic acid synthesis revealed by live imaging of an Aldh1a2-GFP reporter fusion protein throughout zebrafish development. Dev Dyn 241:1205–1216. doi: 10.1002/dvdy.23805

Poleo G, Brown CW, Laforest L, Akimenko MA (2001) Cell proliferation and movement during early fin regeneration in zebrafish. Dev Dyn 221:380–390. doi: 10.1002/dvdy.1152

Poss KD (2010) Advances in understanding tissue regenerative capacity and mechanisms in animals. Nat Rev Genet 11:710–722. doi: 10.1038/nrg2879

Poss KD, Keating MT, Nechiporuk A (2003) Tales of regeneration in zebrafish. Dev Dyn 226:202–210. doi: 10.1002/dvdy.10220

Poss KD, Nechiporuk A, Hillam AM, et al (2002) Mps1 defines a proximal blastemal proliferative compartment essential for zebrafish fin regeneration. Development 129:5141–5149

Poss KD, Shen J, Keating MT (2000a) Induction of lef1 during zebrafish fin regeneration. Dev Dyn 219:282–286. doi: 10.1002/1097-0177(2000)9999:9999<::AID-DVDY1045>3.3.CO;2-3

Poss KD, Shen J, Nechiporuk A, et al (2000b) Roles for Fgf signaling during zebrafish fin regeneration. Dev Biol 222:347–358. doi: 10.1006/dbio.2000.9722

Potter M, Newport E, Morten KJ (2016) The Warburg effect: 80 years on. Biochem Soc Trans 44:1499–1505. doi: 10.1042/BST20160094

Pramojanee SN, Phimphilai M, Chattipakorn N, Chattipakorn SC (2014) Possible roles of insulin signaling in osteoblasts. Endocr Res 39:144–151. doi: 10.3109/07435800.2013.879168

Prigione A, Ruiz-Pérez MV, Bukowiecki R, Adjaye J (2015) Metabolic restructuring and cell fate conversion. Cell Mol Life Sci 72:1759–1777. doi: 10.1007/s00018-015-1834-1

Puri S, Aegerter-Wilmsen T, Jaźwińska A, Aegerter CM (2017) *In-vivo* quantification of mechanical properties of caudal fins in adult zebrafish. J Exp Biol jeb.171777. doi: 10.1242/jeb.171777

Qin Z, Barthel LK, Raymond PA (2009) Genetic evidence for shared mechanisms of epimorphic regeneration in zebrafish. Proc Natl Acad Sci U S A 106:9310–9315. doi: 10.1073/pnas.0811186106

Quaranta V (2000) Cell migration through extracellular matrix: Membrane-type metalloproteinases make the way. J Cell Biol 149:1167–1169. doi: 10.1083/jcb.149.6.1167

Quint E, Smith A, Avaron F, et al (2002) Bone patterning is altered in the regenerating zebrafish caudal fin after ectopic expression of sonic hedgehog and bmp2b or exposure to cyclopamine. Proc Natl Acad Sci U S A 99:8713–8718. doi: 10.1073/pnas.122571799

Rabinowitz JS, Robitaille AM, Wang Y, et al (2017) Transcriptomic, proteomic, and metabolomic landscape of positional memory in the caudal fin of zebrafish. Proc Natl Acad Sci 114:E717–E726. doi: 10.1073/pnas.1620755114

Raftopoulou M, Hall A (2004) Cell migration: Rho GTPases lead the way. Dev Biol 265:23–32. doi: 10.1016/j.ydbio.2003.06.003

Raggatt LJ, Partridge NC (2010) Cellular and molecular mechanisms of bone remodeling. J Biol Chem 285:25103–25108. doi: 10.1074/jbc.R109.041087

Rahman MS, Akhtar N, Jamil HM, et al (2015) TGF-β/BMP signaling and other molecular events: Regulation of osteoblastogenesis and bone formation. Bone Res 3:. doi: 10.1038/boneres.2015.5

Ramachandran R, Fausett B V., Goldman D (2010) Ascl1a regulates Müller glia dedifferentiation and retinal regeneration through a Lin-28-dependent, let-7 microRNA signalling pathway. Nat Cell Biol 12:1101–1107. doi: 10.1038/ncb2115

Ratnayake D, Currie PD (2017) Stem cell dynamics in muscle regeneration: Insights from live imaging in different animal models. BioEssays 39:1–9. doi: 10.1002/bies.201700011

Rawlings JS (2004) The JAK/STAT signaling pathway. J Cell Sci 117:1281–1283. doi: 10.1242/jcs.00963

Renn J, Büttner A, To TT, et al (2013) A col10a1: NlGFP transgenic line displays putative osteoblast precursors at the medaka notochordal sheath prior to mineralization. Dev Biol 381:134–143. doi: 10.1016/j.ydbio.2013.05.030

Renn J, Winkler C (2012) Osterix: NlGFP transgenic medaka identify regulatory roles for retinoic acid signaling during osteoblast differentiation in vivo. J Appl Ichthyol 28:360–363. doi: 10.1111/j.1439-0426.2012.01983.x

Ribeiro A, Monteiro JF, Certal AC, et al (2017) Foxj1a is expressed in ependymal precursors, controls central canal position and is activated in new ependymal cells during regeneration in zebrafish. Open Biol 7:. doi: 10.1098/rsob.170139

Rink JC (2011) Planarian Regeneration. Humana Press, New York

Ritschka B, Storer M, Mas A, et al (2017) The senescence-associated secretory phenotype induces cellular plasticity and tissue regeneration. Genes Dev 31:172–183. doi: 10.1101/gad.290635.116

Rolland-Lagan A-G, Paquette M, Tweedle V, Akimenko M-A (2012) Morphogen-based simulation model of ray growth and joint patterning during fin development and regeneration. Development 139:1188–1197. doi: 10.1242/dev.073452

Rosen V (2009) BMP2 signaling in bone development and repair. Cytokine Growth Factor Rev 20:475–480. doi: 10.1016/j.cytogfr.2009.10.018

Rutkovskiy A, Stensløkken K-O, Vaage IJ (2016) Osteoblast Differentiation at a Glance. Med Sci Monit Basic Res 22:95–106. doi: 10.12659/MSMBR.901142

Ryall JG, Cliff T, Dalton S, Sartorelli V (2015) Metabolic Reprogramming of Stem Cell Epigenetics. Cell Stem Cell 17:651–662. doi: 10.1016/j.stem.2015.11.012

Sacchetti B, Funari A, Michienzi S, et al (2007) Self-Renewing Osteoprogenitors in Bone Marrow Sinusoids Can Organize a Hematopoietic Microenvironment. Cell 131:324–336. doi: 10.1016/j.cell.2007.08.025

Saera-Vila A, Kish PE, Kahana A (2016) Fgf regulates dedifferentiation during skeletal muscle regeneration in adult zebrafish. Cell Signal 28:1196–1204. doi: 10.1016/j.cellsig.2016.06.001

Sánchez Alvarado A (2000) Regeneration in the metazoans: Why does it happen? BioEssays 22:578–590. doi:

10.1002/(SICI)1521-1878(200006)22:6<578::AID-BIES11>3.0.CO;2-#

Sánchez Alvarado A (2008) Stem cells in animal models of regeneration. StemBook 1–24. doi: 10.3824/stembook.1.32.1

Sánchez Alvarado A, Yamanaka S (2014) Rethinking differentiation: Stem cells, regeneration, and plasticity. Cell 157:110–119. doi: 10.1016/j.cell.2014.02.041

Sander V, Davidson AJ (2014) Kidney injury and regeneration in zebrafish. Semin Nephrol 34:437–444. doi: 10.1016/j.semnephrol.2014.06.010

Sandoval-Guzmán T, Currie JD (2018) The journey of cells through regeneration. Curr Opin Cell Biol 55:36–41. doi: 10.1016/j.ceb.2018.05.008

Sandoval-Guzmán T, Wang H, Khattak S, et al (2014) Fundamental differences in dedifferentiation and stem cell recruitment during skeletal muscle regeneration in two salamander species. Cell Stem Cell 14:174–187. doi: 10.1016/j.stem.2013.11.007

Santamaría J a, Becerra J (1991) Tail fin regeneration in teleosts: cell-extracellular matrix interaction in blastemal differentiation. J Anat 176:9–21

Santamaría JA, Marí-Beffa M, Becerra J (1992) Interactions of the lepidotrichial matrix components during tail fin regeneration in teleosts. Differentiation 49:143–150. doi: 10.1111/j.1432-0436.1992.tb00662.x

Santinon G, Enzo E, Dupont S (2015) The sweet side of YAP / TAZ. 34:2543–2544

Santoro MM (2014) Zebrafish as a model to explore cell metabolism. Trends Endocrinol Metab 25:546–554. doi: 10.1016/j.tem.2014.06.003

Santos-Ruiz L, Santamaría JA, Becerra J (2005) Cytoskeletal dynamics of the teleostean fin ray during fin epimorphic regeneration. Differentiation 73:175–187. doi: 10.1111/j.1432-0436.2005.00016.x

Santos-Ruiz L, Santamaría JA, Ruiz-Sánchez J, Becerra J (2002) Cell proliferation during blastema formation in the regenerating teleost fin. Dev Dyn 223:262–272. doi: 10.1002/dvdy.10055

Santucci M, Vignudelli T, Ferrari S, et al (2015) The Hippo Pathway and YAP/TAZ-TEAD Protein-Protein Interaction as Targets for Regenerative Medicine and Cancer Treatment. J Med Chem 58:4857–4873. doi: 10.1021/jm501615v

Satoh A, Bryant S V., Gardiner DM (2008) Regulation of dermal fibroblast dedifferentiation and redifferentiation during wound healing and limb regeneration in the Axolotl. Dev Growth Differ 50:743–754. doi: 10.1111/j.1440-169X.2008.01072.x

Schall KA, Holoyda KA, Grant CN, et al (2015) Adult zebrafish intestine resection: a novel model of short bowel syndrome, adaptation, and intestinal stem cell regeneration. Am J Physiol - Gastrointest Liver Physiol 309:G135–G145. doi: 10.1152/ajpgi.00311.2014

Schebesta M, Lien CL, Engel FB, Keating MT (2006) Transcriptional profiling of caudal fin regeneration in zebrafish. ScientificWorldJournal 6:38–54. doi: 10.1100/tsw.2006.326

Schindeler A, McDonald MM, Bokko P, Little DG (2008) Bone remodeling during fracture repair: The cellular picture. Semin Cell Dev Biol 19:459–466. doi: 10.1016/j.semcdb.2008.07.004

Schindelin J, Arganda-Carreras I, Frise E, et al (2012) Fiji: An open-source platform for biological-image analysis. Nat Methods 9:676–682. doi: 10.1038/nmeth.2019

Schoors S, De Bock K, Cantelmo AR, et al (2014) Partial and transient reduction of glycolysis by PFKFB3 blockade reduces pathological angiogenesis. Cell Metab 19:37–48. doi: 10.1016/j.cmet.2013.11.008

Schulte CJ, Allen C, England SJ, et al (2011) Evx1 is required for joint formation in zebrafish fin dermoskeleton. Dev Dyn 240:1240–1248. doi: 10.1002/dvdy.22534

Sehring IM, Jahn C, Weidinger G (2016) Zebrafish fin and heart: what's special about regeneration? Curr Opin Genet Dev 40:48–56. doi: 10.1016/j.gde.2016.05.011

Seifert AW, Muneoka K (2018) The blastema and epimorphic regeneration in mammals. Dev Biol 433:190–199. doi: 10.1016/j.ydbio.2017.08.007

Seo E, Basu-Roy U, Gunaratne PH, et al (2013) SOX2 Regulates YAP1 to Maintain Stemness and Determine Cell Fate in the Osteo-Adipo Lineage. Cell Rep 3:2075–2087. doi: 10.1016/j.celrep.2013.05.029

Serrano M (2014) Senescence helps regeneration. Dev Cell 31:671–672. doi: 10.1016/j.devcel.2014.12.007

Shao J, Chen D, Ye Q, et al (2011) Tissue regeneration after injury in adult zebrafish: The regenerative potential of the caudal fin. Dev Dyn 240:1271–1277. doi: 10.1002/dvdy.22603

Shaul YD, Seger R (2007) The MEK/ERK cascade: From signaling specificity to diverse functions. Biochim Biophys Acta - Mol Cell Res 1773:1213–1226. doi: 10.1016/j.bbamcr.2006.10.005

Shaw RL, Kohlmaier A, Polesello C, et al (2010) The Hippo pathway regulates intestinal stem cell proliferation during Drosophila adult midgut regeneration. Development 137:4147–4158. doi: 10.1242/dev.052506

Sheyn D, Ben-David S, Shapiro G, et al (2016) Human induced pluripotent stem cells differentiate into functional mesenchymal stem cells and repair bone defects. Stem Cells Transl Med 5:1447–1460. doi: 10.5966/sctm.2015-0311

Shi WC, Fang ZB, Li L, Luo LF (2015) Using zebrafish as the model organism to understand organ regeneration. Sci China Life Sci 58:343–351. doi: 10.1007/s11427-015-4838-z

Shibata E, Ando K, Murase E, Kawakami A (2018) Heterogeneous fates and dynamic rearrangement of regenerative epidermis-derived cells during zebrafish fin regeneration. Development dev.162016. doi: 10.1242/dev.162016

Shibata E, Yokota Y, Horita N, et al (2016) Fgf signalling controls diverse aspects of fin regeneration. Development 143:2920–2929. doi: 10.1242/dev.140699

Shimizu N, Kawakami K, Ishitani T (2012) Visualization and exploration of Tcf/Lef function using a highly responsive Wnt/B-catenin signaling-reporter transgenic zebrafish. Dev Biol 370:71–85. doi: 10.1016/j.ydbio.2012.07.016

Shyh-Chang N, Daley GQ (2015) Metabolic switches linked to pluripotency and embryonic stem cell differentiation. Cell Metab 21:349–350. doi: 10.1016/j.cmet.2015.02.011

Shyh-Chang N, Zhu H, Yvanka De Soysa T, et al (2013) Lin28 enhances tissue repair by reprogramming cellular metabolism. Cell 155:778–792. doi: 10.1016/j.cell.2013.09.059

Simões MG, Bensimon-Brito A, Fonseca M, et al (2014) Denervation impairs regeneration of amputated zebrafish fins. BMC Dev Biol 14:10–12. doi: 10.1186/s12861-014-0049-2

Sims NA, Martin TJ (2014) Coupling the activities of bone formation and resorption: a multitude of signals within the basic multicellular unit. Bonekey Rep 3:1–10. doi: 10.1038/bonekey.2013.215

Singh SP, Holdway JE, Poss KD (2012) Regeneration of amputated zebrafish fin rays from de novo osteoblasts. Dev Cell 22:879–86. doi: 10.1016/j.devcel.2012.03.006

Slack JM (2017) Animal regeneration: ancestral character or evolutionary novelty? EMBO Rep e201643795. doi: 10.15252/embr.201643795

Smith A, Avaron F, Guay D, et al (2006) Inhibition of BMP signaling during zebrafish fin regeneration disrupts fin growth and scleroblast differentiation and function. Dev Biol 299:438–454. doi: 10.1016/j.ydbio.2006.08.016

Soroldoni D, Hogan BM, Oates AC (2009) Simple and Efficient Transgenesis with Meganuclease Constructs in Zebrafish. 546:117–130. doi: 10.1007/978-1-60327-977-2

Sousa S, Afonso N, Bensimon-Brito A, et al (2011) Differentiated skeletal cells contribute to blastema formation during zebrafish fin regeneration. Development 138:3897–3905. doi: 10.1242/dev.064717

Sousa S, Valerio F, Jacinto A (2012) A new zebrafish bone crush injury model. Biol Open 1:915–921. doi:

10.1242/bio.2012877

Spallanzani L (1769) An Essay On Animal Reproductions (1769). London

Spoorendonk KM, Hammond CL, Huitema LFA, et al (2010) Zebrafish as a unique model system in bone research: The power of genetics and in vivo imaging. J Appl Ichthyol 26:219–224. doi: 10.1111/j.1439-0426.2010.01409.x

Sriraman V, Eichenlaub-Ritter U, Bartsch JW, et al (2008) Regulated Expression of ADAM8 (a Disintegrin and Metalloprotease Domain 8) in the Mouse Ovary: Evidence for a Regulatory Role of Luteinizing Hormone, Progesterone Receptor, and Epidermal Growth Factor-Like Growth Factors1. Biol Reprod 78:1038–1048. doi: 10.1095/biolreprod.107.066340

Staley BK, Irvine KD (2010) Warts and yorkie mediate intestinal regeneration by influencing stem cell proliferation. Curr Biol 20:1580–1587. doi: 10.1016/j.cub.2010.07.041

Stanger BZ (2015) Cellular Homeostasis and Repair in the Mammalian Liver. Annu Rev Physiol 77:179–200. doi: 10.1146/annurev-physiol-021113-170255

Stewart S, Gomez WA, Armstrong BE, et al (2014) Sequential and Opposing Activities of Wnt and BMP Coordinate Zebrafish Bone Regeneration. 6:482–498. doi: 10.1111/j.1743-6109.2008.01122.x.Endothelial

Stewart S, Stankunas K (2012) Limited dedifferentiation provides replacement tissue during zebrafish fin regeneration. Dev Biol 365:339–349. doi: 10.1016/j.ydbio.2012.02.031

Stewart S, Tsun Z-Y, Belmonte JCI (2009) A histone demethylase is necessary for regeneration in zebrafish. Proc Natl Acad Sci 106:19889–19894. doi: 10.1073/pnas.0904132106

Stocum DL (2017) Mechanisms of urodele limb regeneration. Regeneration 159–200. doi: 10.1002/reg2.92

Stoick-Cooper CL, Moon RT, Weidinger G (2007) Advances in signaling in vertebrate regeneration as a prelude to regenerative medicine. Genes Dev 21:1292–1315. doi: 10.1101/gad.1540507

Stoick-Cooper CL, Weidinger G, Riehle KJ, et al (2006) Distinct Wnt signaling pathways have opposing roles in appendage regeneration. Development 134:479–489. doi: 10.1242/dev.001123

Straube WL, Tanaka EM (2006) Reversibility of the differentiated state: Regeneration in amphibians. Artif Organs 30:743–755. doi: 10.1111/j.1525-1594.2006.00296.x

Streisinger G, Walker C, Dower N, et al (1981) Production of clones of homozygous diploid zebra fish (Brachydanio rerio). Nature 291:293–296. doi: 10.1038/291293a0

Takahashi K, Yamanaka S (2006) Induction of Pluripotent Stem Cells from Mouse Embryonic and Adult Fibroblast Cultures by Defined Factors. Cell 126:663–676. doi: 10.1016/j.cell.2006.07.024

Tal TL, Franzosa JA, Tanguay RL (2010) Molecular signaling networks that choreograph epimorphic fin regeneration in Zebrafish - A mini-review. Gerontology 56:231–240. doi: 10.1159/000259327

Tamura K, Ohgo S, Yokoyama H (2010) Limb blastema cell: A stem cell for morphological regeneration. Dev Growth Differ 52:89–99. doi: 10.1111/j.1440-169X.2009.01144.x

Tanaka EM (2016) The Molecular and Cellular Choreography of Appendage Regeneration. Cell 165:1598–1608. doi: 10.1016/j.cell.2016.05.038

Tanaka EM (2003) Cell differentiation and cell fate during urodele tail and limb regeneration. Curr Opin Genet Dev 13:497–501. doi: 10.1016/j.gde.2003.08.003

Tanaka EM, Reddien PW (2011) The Cellular Basis for Animal Regeneration. Dev Cell 21:172–185. doi: 10.1016/j.devcel.2011.06.016

Tang Y, Rowe RG, Botvinick EL, et al (2013) MT1-MMP-Dependent Control of Skeletal Stem Cell Commitment via a β1-Integrin/YAP/TAZ Signaling Axis. Dev Cell 25:402–416. doi: 10.1016/j.devcel.2013.04.011

Tang Y, Weiss SJ (2017) Snail/Slug-YAP/TAZ complexes cooperatively regulate mesenchymal stem cell function

and bone formation. Cell Cycle 16:399–405. doi: 10.1080/15384101.2017.1280643

Tata PR, Mou H, Pardo-Saganta A, et al (2013) Dedifferentiation of committed epithelial cells into stem cells in vivo. Nature 503:218–223. doi: 10.1038/nature12777

Tata PR, Rajagopal J (2016) Cellular plasticity: 1712 to the present day. Curr Opin Cell Biol 43:46–54. doi: 10.1016/j.ceb.2016.07.005

Tatapudy S, Aloisio F, Barber D, Nystul T (2017) Cell fate decisions: emerging roles for metabolic signals and cell morphology. EMBO Rep 18:e201744816. doi: 10.15252/embr.201744816

Tauzin S, Starnes TW, Becker FB, et al (2014) Redox and Src family kinase signaling control leukocyte wound attraction and neutrophil reverse migration. J Cell Biol 207:589–598. doi: 10.1083/jcb.201408090

Tavares B, Lopes SS (2013) The Importance of Zebrafish in Biomedical Research. 26:583–592

Thatcher EJ, Paydar I, Anderson KK, Patton JG (2008) Regulation of zebrafish fin regeneration by microRNAs. Proc Natl Acad Sci U S A 105:18384–9. doi: 10.1073/pnas.0803713105

Thon M, Hosoi T, Ozawa K (2016) Insulin enhanced leptin-induced STAT3 signaling by inducing GRP78. Sci Rep 6:1–8. doi: 10.1038/srep34312

Thorimbert V, König D, Marro J, et al (2015) Bone morphogenetic protein signaling promotes morphogenesis of blood vessels, wound epidermis, and actinotrichia during fin regeneration in zebrafish. FASEB J 29:4299–4312. doi: 10.1096/fj.15-272955

Ton Q V., Iovine MK (2013) Identification of an evx1-dependent joint-formation pathway during fin regeneration. PLoS One 8:1–10. doi: 10.1371/journal.pone.0081240

Tornini VA, Poss KD (2014) Keeping at arm's length during regeneration. Dev Cell 29:139–145. doi: 10.1016/j.devcel.2014.04.007

Tornini VA, Puliafito A, Slota LA, et al (2016) Live Monitoring of Blastemal Cell Contributions during Appendage Regeneration. Curr Biol 26:2981–2991. doi: 10.1016/j.cub.2016.08.072

Tornini VA, Thompson JD, Allen RL, Poss KD (2017) Live fate-mapping of joint-associated fibroblasts visualizes expansion of cell contributions during zebrafish fin regeneration. Development 144:2889–2895. doi: 10.1242/dev.155655

Tsai BP, Hoverter NP, Waterman ML (2012) Blending hippo and WNT: Sharing messengers and regulation. Cell 151:1401–1403. doi: 10.1016/j.cell.2012.12.007

Tsonis PA (2002) Regenerative biology: The emerging field of tissue repair and restoration. Differentiation 70:397–409. doi: 10.1046/j.1432-0436.2002.700802.x

Tu S, Johnson SL (2010) Clonal analyses reveal roles of organ founding stem cells, melanocyte stem cells and melanoblasts in establishment, growth and regeneration of the adult zebrafish fin. Development 137:3931–3939. doi: 10.1242/dev.057075

Tu S, Johnson SL (2011) Fate restriction in the growing and regenerating zebrafish fin. Dev Cell 20:725–732. doi: 10.1016/j.devcel.2011.04.013

Turing A (1952) The chemical basis of morphogenesis. Univ Manchester

Udan RS, Kango-Singh M, Nolo R, et al (2003) Hippo promotes proliferation arrest and apoptosis in the Salvador/Warts pathway. Nat Cell Biol 5:914–920. doi: 10.1038/ncb1050

Upadhyay J, Farr OM, Mantzoros CS (2015) The role of leptin in regulating bone metabolism. Metabolism 64:105–113. doi: 10.1016/j.metabol.2014.10.021

Valcourt U, Moustakas A (2005) BMP signaling in osteogenesis, bone remodeling and repair. Eur J Trauma 31:464–479. doi: 10.1007/s00068-005-2049-1

van der Bliek A, Shen Q, Kawajiri S (2013) Mechanisms of mitochondrial fission and fusion. Cold Spring Harb

Perspect Biol 5:1–16. doi: 10.1101/cshperspect.a011072

van Eeden JM., Granato M, Schach U, et al (1996) Genetic analysis of fin formation in the zebrafish, Danio rerio. Development 255–262

Varelas X (2014) The Hippo pathway effectors TAZ and YAP in development, homeostasis and disease. Development 141:1614–1626. doi: 10.1242/dev.102376

Varga J, De Oliveira T, Greten FR (2014) The architect who never sleeps: Tumor-induced plasticity. FEBS Lett 588:2422–2427. doi: 10.1016/j.febslet.2014.06.019

Varshney GK, Burgess SM (2014) Mutagenesis and phenotyping resources in zebrafish for studying development and human disease. Brief Funct Genomics 13:82–94. doi: 10.1093/bfgp/elt042

Vriz S, Reiter S, Galliot B (2014) Cell Death. A Program to Regenerate., 1st edn. Elsevier Inc.

Wan J, Goldman D (2016) Retina regeneration in zebrafish. Curr Opin Genet Dev 40:41–47. doi: 10.1016/j.gde.2016.05.009

Wang H, Simon A (2016) Skeletal muscle dedifferentiation during salamander limb regeneration. Curr Opin Genet Dev 40:108–112. doi: 10.1016/j.gde.2016.06.013

Wang RN, Green J, Wang Z, et al (2014) Bone Morphogenetic Protein (BMP) signaling in development and human diseases. Genes Dis 1:87–105. doi: 10.1016/j.gendis.2014.07.005

Wang S, Miller SR, Ober EA, Sadler KC (2017) Making It New Again: Insight Into Liver Development, Regeneration, and Disease From Zebrafish Research, 1st edn. Elsevier Inc.

Wang X, He H, Tang W, et al (2012) Two Origins of Blastemal Progenitors Define Blastemal Regeneration of Zebrafish Lower Jaw. PLoS One 7:. doi: 10.1371/journal.pone.0045380

Wang X, Kua HY, Hu Y, et al (2006) P53 Functions As a Negative Regulator of Osteoblastogenesis, Osteoblast-Dependent Osteoclastogenesis, and Bone Remodeling. J Cell Biol 172:115–125. doi: 10.1083/jcb.200507106

Warburg O (1925) The Metabolism of Carcinoma Cells. J Cancer Res 9:148–163. doi: 10.1158/jcr.1925.148

Watson CJ, Kwon RY (2015) Osteogenic programs during zebrafish fin regeneration. Bonekey Rep 4:745. doi: 10.1038/bonekey.2015.114

Wehner D, Cizelsky W, Vasudevaro M, et al (2014) Wnt/β-catenin signaling defines organizing centers that orchestrate growth and differentiation of the regenerating zebrafish caudal fin. Cell Rep 6:467–481. doi: 10.1016/j.celrep.2013.12.036

Wehner D, Tsarouchas TM, Michael A, et al (2017) Wnt signaling controls pro-regenerative Collagen XII in functional spinal cord regeneration in zebrafish. Nat Commun 8:1–16. doi: 10.1038/s41467-017-00143-0

Wehner D, Weidinger G (2015) Signaling networks organizing regenerative growth of the zebrafish fin. Trends Genet 31:336–343. doi: 10.1016/j.tig.2015.03.012

Wei P, Dove KK, Bensard C, et al (2018) The Force Is Strong with This One: Metabolism (Over)powers Stem Cell Fate. Trends Cell Biol 1–9. doi: 10.1016/j.tcb.2018.02.007

Weidinger G (2017) Regeneration: Recorded Live! Curr Biol 27:R30–R33. doi: 10.1016/j.cub.2016.11.022

Westerfield M (2000) The zebrafish book. A guide for the laboratory use of zebrafish (Danio rerio)., 4th editio. Univ. of Oregon Press, Eugene

White DT, Mumm JS (2013) The nitroreductase system of inducible targeted ablation facilitates cell-specific regenerative studies in zebrafish. Methods 62:232–240. doi: 10.1016/j.ymeth.2013.03.017

Whitehead GG, Makino S, Lien C-L, Keating MT (2005) fgf20 Is Essential for Initiating Zebrafish Fin Regeneration. Survival (Lond) 1957–1960. doi: 10.1126/science.1117637

Williams L, Zhao J, Morozova N, et al (2003) Chromatin reorganization accompanying cellular dedifferentiation is associated with modifications of histone H3, redistribution of HP1, and activation of E2F-target genes. Dev Dyn 228:113–120. doi: 10.1002/dvdy.10348

Wills AA, Kidd AR, Lepilina A, Poss KD (2008) Fgfs control homeostatic regeneration in adult zebrafish fins. Development 135:3063–3070. doi: 10.1242/dev.024588

Witkowska-Zimny M, Wrobel E, Przybylski J (2010) The most important transcriptional factors of osteoblastogenesis. Adv Cell Biol 2010:17–28. doi: 10.2478/v10052-010-0002-x

Witten PE, Harris MP, Huysseune A, Winkler C (2017) Small teleost fish provide new insights into human skeletal diseases. Elsevier Ltd

Wolpert L (1969) Positional information and the spatial pattern of cellular differentiation. J Theor Biol 25:1–47. doi: 10.1016/S0022-5193(69)80016-0

Wolpert L (2011) Positional information and patterning revisited. J Theor Biol 269:359–365. doi: 10.1016/j.jtbi.2010.10.034

Wood W, Jacinto A, Grose R, et al (2002) Wound healing recapitulates morphogenesis in Drosophila embryos. Nat Cell Biol 4:1–7. doi: 10.1038/ncb875

Wozniak MA, Modzelewska K, Kwong L, Keely PJ (2004) Focal adhesion regulation of cell behavior. Biochim Biophys Acta - Mol Cell Res 1692:103–119. doi: 10.1016/j.bbamcr.2004.04.007

Wu M, Chen G, Li YP (2016) TGF-β and BMP signaling in osteoblast, skeletal development, and bone formation, homeostasis and disease. Bone Res 4:. doi: 10.1038/boneres.2016.9

Wu S, Liu Y, Zheng Y, et al (2008) The TEAD/TEF family protein Scalloped mediates transcriptional output of the Hippo growth-regulatory pathway. Dev Cell 14:388–398. doi: 10.1016/j.devcel.2008.01.007

Xin M, Kim Y, Sutherland LB, et al (2013) Hippo pathway effector Yap promotes cardiac regeneration. Proc Natl Acad Sci 110:13839–13844. doi: 10.1073/pnas.1313192110

Xiong J, Almeida M, O'Brien CA (2018) The YAP/TAZ transcriptional co-activators have opposing effects at different stages of osteoblast differentiation. Bone 112:1–9. doi: 10.1016/j.bone.2018.04.001

Xu X, Duan S, Yi F, et al (2013) Mitochondrial regulation in pluripotent stem cells. Cell Metab 18:325–332. doi: 10.1016/j.cmet.2013.06.005

Yamamoto K, Kishida T, Sato Y, et al (2015) Direct conversion of human fibroblasts into functional osteoblasts by defined factors. Proc Natl Acad Sci 112:6152–6157. doi: 10.1073/pnas.1420713112

Yang A, Schweitzer R, Sun D, et al (1999a) P63 Is Essential for Regenerative Proliferation in Limb, Craniofacial and Epithelial Development. Nature 398:714–718. doi: 10.1038/19539

Yang E V., Gardiner DM, Carlson MRJ, et al (1999b) Expression of Mmp-9 and related matrix metalloproteinase genes during axolotl limb regeneration. Dev Dyn 216:2–9. doi: 10.1002/(SICI)1097-0177(199909)216:1<2::AID-DVDY2>3.0.CO;2-P

Yano T, Tamura K (2013) The making of differences between fins and limbs. J Anat 222:100–113. doi: 10.1111/j.1469-7580.2012.01491.x

Yao W, Guan M, Jia J, et al (2013) Reversing bone loss by directing mesenchymal stem cells to bone. Stem Cells 31:2003–2014. doi: 10.1002/stem.1461

Ye L, Robertson MA, Hesselson D, et al (2015) Glucagon Is Essential for Alpha Cell Transdifferentiation and Beta Cell Neogenesis. Development 142:1407–1417. doi: 10.1242/dev.117911

Yimlamai D, Christodoulou C, Galli GG, et al (2014) Hippo pathway activity influences liver cell fate. Cell 157:1324–1338. doi: 10.1016/j.cell.2014.03.060

Yin VP, Thomson JM, Thummel R, et al (2008) Fgf-dependent depletion of microRNA-133 promotes appendage regeneration in zebrafish. Genes Dev 22:728–733. doi: 10.1101/gad.1641808

Yokoyama H (2008) Initiation of limb regeneration: The critical steps for regenerative capacity. Dev Growth Differ 50:13–22. doi: 10.1111/j.1440-169X.2007.00973.x

Yoo SK, Freisinger CM, LeBert DC, Huttenlocher A (2012) Early redox, Src family kinase, and calcium signaling integrate wound responses and tissue regeneration in zebrafish. J Cell Biol 199:225–234. doi: 10.1083/jcb.201203154

Yu FX, Guan KL (2013) The Hippo pathway: Regulators and regulations. Genes Dev 27:355–371. doi: 10.1101/gad.210773.112

Yun MH (2015) Changes in regenerative capacity through lifespan. Int J Mol Sci 16:25392–25432. doi: 10.3390/ijms161025392

Yun MH, Davaapil H, Brockes JP (2015) Recurrent turnover of senescent cells during regeneration of a complex structure. Elife 4:1–16. doi: 10.7554/eLife.05505

Yun MH, Gates PB, Brockes JP (2013) Regulation of p53 is critical for vertebrate limb regeneration. Proc Natl Acad Sci 110:17392–17397. doi: 10.1073/pnas.1310519110

Zaidi SK, Sullivan AJ, Medina R, et al (2004) Tyrosine phosphorylation controls Runx2-mediated subnuclear targeting of YAP to repress transcription. EMBO J 23:790–799. doi: 10.1038/sj.emboj.7600073

Zhang J, Jeradi S, Strähle U, Akimenko MA (2012) Laser ablation of the sonic hedgehog-a-expressing cells during fin regeneration affects ray branching morphogenesis. Dev Biol 365:424–433. doi: 10.1016/j.ydbio.2012.03.008

Zhang L, Ren F, Zhang Q, et al (2008) The TEAD/TEF family of transcription factor Scalloped mediates Hippo signaling in organ size control. 14:377–387. doi: 10.1088/1367-2630/15/1/015008.Fluid

Zhang P, Torres K, Liu X, et al (2016) An Overview of Chromatin-Regulating Proteins in Cells. Curr Protein Pept Sci 17:401–10. doi: 10.1016/j.molmed.2014.11.008.Mitochondria

Zhang R, Han P, Yang H, et al (2013) In vivo cardiac reprogramming contributes to zebrafish hearTregeneration. Nature 498:497–501. doi: 10.1038/nature12322

Zhao A, Qin H, Fu X (2016) What determines the regenerative capacity in animals? Bioscience 66:735–746. doi: 10.1093/biosci/biw079

Zhao B (2014) The Hippo pathway in organ size control, tissue regeneration and stem cell self-renewal. Cell 13:877–883. doi: 10.1038/ncb2303.The

Zhao J, Morozova N, Williams L, et al (2001) Two phases of chromatin decondensation during dedifferentiation of plant cells. Distinction between competence for cell fate switch and a commitment for S phase. J Biol Chem 276:22772–22778. doi: 10.1074/jbc.M101756200

Zhao XF, Wan J, Powell C, et al (2014) Leptin and IL-6 family cytokines synergize to stimulate Müller Glia reprogramming and retina regeneration. Cell Rep 9:272–284. doi: 10.1016/j.celrep.2014.08.047

Zhou Q, Melton DA (2008) Extreme Makeover: Converting One Cell into Another. Cell Stem Cell 3:382–388. doi: 10.1016/j.stem.2008.09.015

Zhou X, von der Mark K, Henry S, et al (2014) Chondrocytes Transdifferentiate into Osteoblasts in Endochondral Bone during Development, Postnatal Growth and Fracture Healing in Mice. PLoS Genet 10:. doi: 10.1371/journal.pgen.1004820

Zielins ER, Ransom RC, Leavitt TE, et al (2016) The role of stem cells in limb regeneration. Organogenesis 12:16–27. doi: 10.1080/15476278.2016.1163463

APPENDIX A

Chapter III SUPPLEMENTARY TABLE AND FIGURES

Supplementary Table 1: GAGE analysis of all gene expression analysis (cut off free) corresponding to the 6 hpa versus uncut data set. Table shows the most significant pathways related to metabolism and canonical signalling pathways represented in our 6 hpa data set according to KEGG (dre represents the KEGG pathway identifier code). Only pathways with p-values less than 0,05 and FDR less than 0.1 were considered significantly different.

Pathways		p-value	q-value (FDR)
dre03040	**Spliceosome**	7.09E-11	1.03E-08
dre03013	**RNA transport**	4.19E-10	3.03E-08
dre03008	**Ribosome biogenesis**	5.16E-08	2.49E-06
dre01230	**Biosynthesis of amino acids**	3.57E-06	0.000121575
dre03015	**mRNA surveillance**	4.60E-06	0.000121575
dre01200	**Carbon metabolism**	5.03E-06	0.000121575
dre00240	**Pyrimidine metabolism**	1.70E-05	0.000342979
dre03050	**Proteasome**	1.89E-05	0.000342979
dre04141	**Protein processing in ER**	2.72E-05	0.000438333
dre04210	**Apoptosis**	0.000219483	0.003076139
dre00270	**Cysteine and methionine metabolism**	0.000233362	0.003076139
dre04140	**Autophagy**	0.000282262	0.00327104
dre00010	**Glycolysis / Gluconeogenesis**	0.000310485	0.00327104
dre03020	**RNA polymerase**	0.000330375	0.00327104

dre04120	**Ubiquitin mediated proteolysis**	0.000338383	0.00327104
dre00970	**Aminoacyl-tRNA biosynthesis**	0.000500443	0.004535262
dre04012	**ErbB signalling pathway**	0.000572645	0.004733329
dre00190	**Oxidative phosphorylation**	0.000587586	0.004733329
dre03018	**RNA degradation**	0.000682803	0.005210865
dre00230	**Purine metabolism**	0.000918095	0.006656189
dre00250	**Alanine, aspartate and glutamate metabolism**	0.000990202	0.006837112
dre04137	**Mitophagy**	0.002417843	0.015242923
dre03060	**Protein export**	0.003500105	0.021146469
dre04115	**p53 signalling pathway**	0.003662985	0.021245315
dre00280	**Valine, leucine and isoleucine degradation**	0.005466869	0.029845087
dre03022	**Basal transcription factors**	0.006218781	0.031249499
dre01212	**Fatty acid metabolism**	0.0062499	0.031249499
dre00071	**Fatty acid degradation**	0.007713348	0.037281184

dre04150	**mTOR signalling pathway**	0.008758609	0.040967689
dre04218	**Cellular senescence**	0.010333718	0.046824661
dre04623	**Cytosolic DNA-sensing pathway**	0.012218968	0.053689407
dre00310	**Lysine degradation**	0.014135981	0.060091192
dre00480	**Glutathione metabolism**	0.01450477	0.060091192
dre00051	**Fructose and mannose metabolism**	0.015511323	0.062476163
dre04910	**Insulin signalling pathway**	0.016787728	0.065789746
dre04621	**NOD-like receptor signalling pathway**	0.018083942	0.069004514
dre00520	**Amino sugar and nucleotide sugar metabolism**	0.019524559	0.072387671
dre04110	**Cell cycle**	0.019969013	0.072387671
dre00640	**Propanoate metabolism**	0.021729808	0.076849321
dre04144	**Endocytosis**	0.022752713	0.077773945
dre04068	**FoxO signalling pathway**	0.023063997	0.077773945
dre04142	**Lysosome**	0.028794476	0.093848057

dre01210 2-	**Oxocarboxylic acid metabolism**	0.029125259	0.093848057
dre04310	**Wnt signalling pathway**	0.031141071	0.096859013
dre03420	**Nucleotide excision repair**	0.03139568	0.096859013

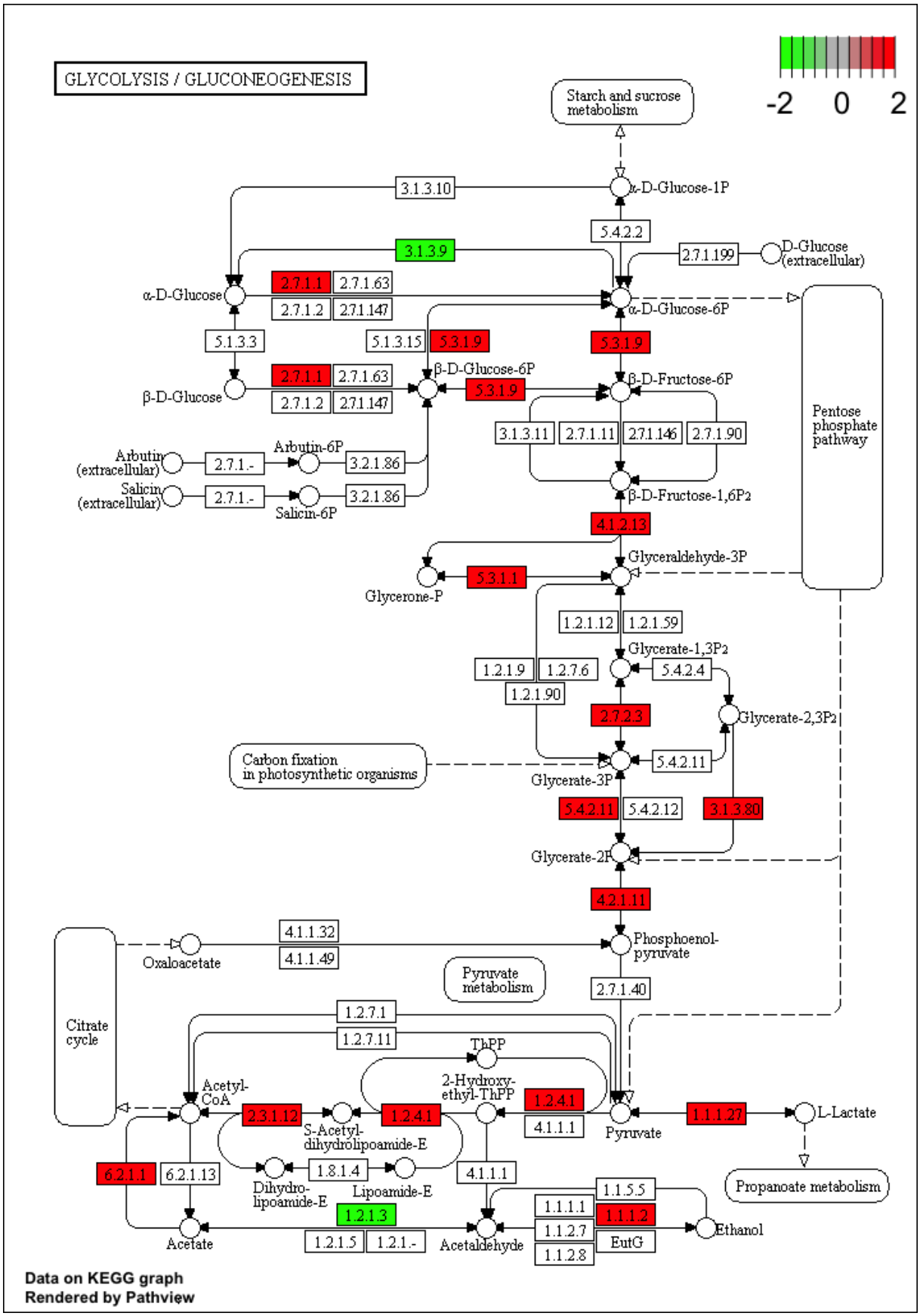

Supplementary Figure 1: Differentially expressed genes within the glycolytic pathway at 6 hpa. Schematic representation of the glycolysis pathway and the corresponding differentially expressed genes using the KeGG pathway database resource. Upregulated genes are shown in red and the downregulated genes in green.

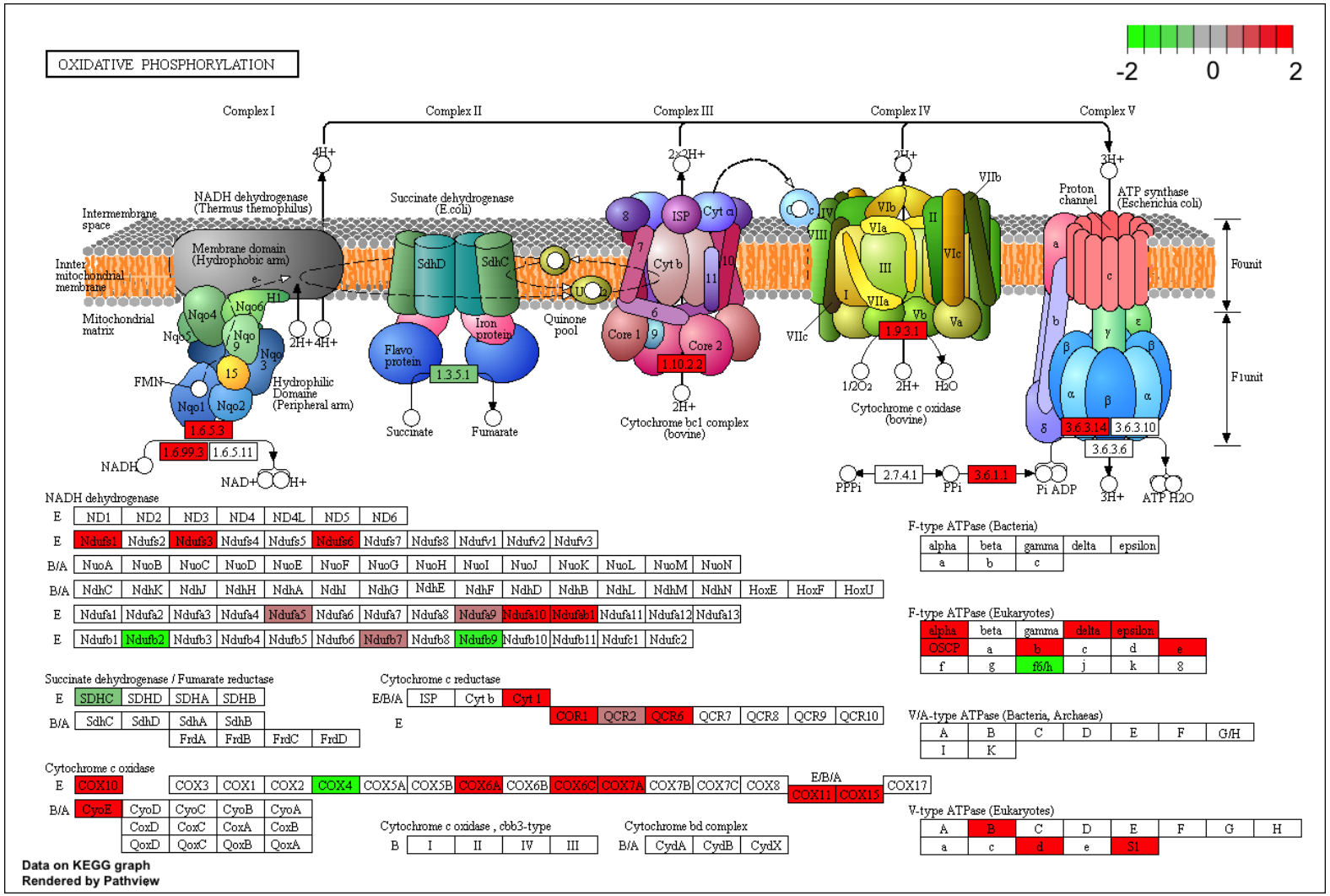

Supplementary Figure 2: Differentially expressed genes within the Oxidative phosphorylation pathway at 6 hpa. Schematic representation of the electron transport chain components and the corresponding differentially expressed genes using the KeGG pathway database resource. Upregulated genes are shown in red and the downregulated genes in green.

APPENDIX B

Manuscript submitted to *JCS* based on Chapter IV results

Yap induces osteoblast differentiation by modulating Bmp signalling during zebrafish caudal fin regeneration

Running title: Yap controls bone regeneration

Ana S. Brandão [1], Anabela Bensimon-Brito [2], Raquel Lourenço[1], Jorge Borbinha [1] and António Jacinto[1]

[1]CEDOC, NOVA Medical School, NOVA University of Lisbon, Campo Mártires da Pátria 130, Lisboa 1169-056, Portugal.

[2] Max Planck Institute for Heart and Lung Research, Department of Developmental Genetics, Bad Nauheim, Germany

Authors for correspondence:
Anabela Bensimon-Brito (anabela.bensimon-brito@mpi-bn.mpg.de)
António Jacinto (antonio.jacinto@nms.unl.pt)

Key Words: Zebrafish, Fin regeneration, osteoblasts, Hippo-Yap, Bmp

Summary statement

Yap regulates, in a cell non-autonomous manner, Bmp signalling activation in osteoprogenitors, therefore promoting osteoblast differentiation and proper bone formation during caudal fin regeneration.

Abstract

Osteoblast differentiation is a key process for bone homeostasis and repair. Multiple signalling pathways have been associated with osteoblast differentiation, yet much remains unknown on how this process is regulated in vivo. Previous studies have proposed that the Hippo pathway transcriptional co-activators YAP and TAZ maintain progenitor stemness and inhibit terminal differentiation of osteoblasts, whereas others suggest they potentiate osteoblast differentiation and bone formation. Here, we use zebrafish caudal fin regeneration as a model to address how Hippo pathway regulates de novo bone formation and osteoblast differentiation. We show that Yap is essential for this process by acting in a cell non-autonomous manner. Yap inhibition leads to an accumulation of the osteoprogenitor pool and to reduced osteoblast differentiation. This effect is correlated with a severe impairment of Bmp signalling in osteoblasts, possibly by suppressing the expression of the ligand bmp2a in the surrounding mesenchymal cells. Overall, our findings provide a new mechanism of bone formation through the Hippo-Yap pathway, placing Yap in the signalling cascade that governs osteoprogenitor maintenance and subsequent differentiation.

Introduction

Bone formation and repair are intrinsically associated with the balanced activity of the bone-forming cells, the osteoblasts (Eriksen, 2010; Long, 2012). A dysfunctional behaviour of osteoblasts leads to improper bone matrix deposition and mineralization, affecting the size, shape and integrity of the skeletal structures (Marie, 2015; Quiros-Gonzalez and Yadav, 2014; Valenti et al., 2017). Bone defects occur under pathological conditions, such as osteoporosis (Corrado et al., 2017; Feng and McDonald, 2006), or due to defective healing upon infection or trauma (Dimitriou et al., 2011; Schindeler et al., 2008). Current strategies to augment bone formation, such as autologous bone grafts, implementation of osteoconductive scaffolds (Collignon et al., 2017; Shrivats et al., 2014) or even the use of growth factors like BMP-2 (El Bialy et al., 2017; Garrison et al., 2010), show promising results. However, a better understanding of the osteoblast lineage specification, bone matrix deposition and bone regeneration would considerably improve these therapeutic strategies.

Osteoblasts derive from osteoprogenitors that differentiate by progressively expressing maturation markers (Håkelien et al., 2014; Rutkovskiy et al., 2016). More immature cells start expressing runt-related transcription factor 2 (runx2) (Ducy et al., 1997; Franceschi et al., 2003), followed by osterix (osx) (Nakashima et al., 2002) and lastly, the mature-osteoblast marker, osteocalcin (or bone gamma-carboxyglutamate (gla) protein, bglap) (Wei and Karsenty, 2016). The Hippo pathway has been recently suggested to mediate bone formation and repair by specifying the osteoblast lineage (Kegelman et al., 2018). The Hippo signal transduction pathway comprises a kinase core cascade which suppresses the transcriptional activity of its effectors, Yes-associates Protein 1(YAP) and Transcriptional co-activator with PDZ-binding motif (TAZ), through phosphorylation, leading to their sequestration in the cytoplasm and degradation. When Hippo

pathway is inactive, YAP and TAZ can be translocated to the nucleus and regulate target gene expression (Irvine, 2012; Piccolo et al., 2014). This pathway has been widely shown to play an important function in tissue growth, organ size and regeneration (Fu et al., 2017; Halder and Johnson, 2011; Moya and Halder, 2018; Zhao, 2014), by regulating cell proliferation, survival and fate determination (Hiemer and Varelas, 2013; Huang et al., 2005; Yimlamai et al., 2014). Recent works have showed that YAP and TAZ are required for proper osteoblast activity and bone formation in vitro (Halder et al., 2012; Hong et al., 2005), during mouse development and adult bone remodelling (Lucero et al., 2018; Pan et al., 2018; Tang and Weiss, 2017; Tang et al., 2013). However, their roles are often controversial and context-dependent, since their activity in osteoprogenitors maintains the progenitor state while in mature osteoblasts they promote osteoblast commitment and bone formation (Seo et al., 2013; Xiong et al., 2018).

While mammals show limited ability to regenerate (Godwin et al., 2014; Zhao et al., 2016), zebrafish can regrow multiple organs and tissues upon injury (Antos et al., 2016; Goessling and North, 2014). Bone is a major tissue in the zebrafish caudal fin, which virtually has an unlimited ability to regenerate upon amputation (Azevedo et al., 2011; Cardeira et al., 2016; Pfefferli and Jaźwińska, 2015). This process relies on the dedifferentiation of mature osteoblasts (Knopf et al., 2011; Sousa et al., 2011) and on the recruitment of resident progenitor cells (Ando et al., 2017), establishing a self-renewing progenitor pool that differentiates into mature osteoblasts to produce the new mineralized bone (Stewart et al., 2014; Wehner and Weidinger, 2015). It has been previously shown that the Hippo pathway, through its effector Yap, regulates the early stages of caudal fin regeneration by controlling key signalling pathways and cell proliferation (Mateus et al., 2015). Here we reveal a novel role for Yap in caudal fin regeneration by promoting osteoblast differentiation without compromising osteoprogenitor pool maintenance. Our results show that Yap activity in mesenchymal cells induces, via a paracrine signalling, the activation of Bmp signalling in osteoblasts, thereby leading to the initiation of osteoblast differentiation program.

Results and Discussion

Yap loss of function leads to major bone defects during caudal fin regenerative outgrowth

After amputation, the fin experiences a fast wound healing response (Chen et al., 2016), followed by the dedifferentiation of mature cells (Stewart and Stankunas, 2012; Tu and Johnson, 2011). These cells re-enter the cell cycle and form a less differentiated and proliferative pool of cells, called blastema, which is the driving force of the regenerative process (Kawakami, 2009; Poss et al., 2003). Once the blastema is fully formed and outgrowth is initiated, differentiation of new osteoblasts takes place, culminating in bone matrix deposition and patterning of new bony-rays (Marí-Beffa and Murciano, 2010). To determine whether Yap controls bone formation during caudal fin regeneration, we used an heat-shock transgenic line expressing a dominant-negative form of Yap, hsp70:RFP-DNyap (referred to as DN-Yap), that allows the inhibition of Yap function, as previously validated (Mateus et al., 2015).

Although homozygous viable mutants for yap1 are already available (Astone et al., 2018), the use of a heat-shock inducible strategy enables us to address the role of Yap in a time-specific manner. This time-controlled approach is particularly relevant since it has been previously shown that Yap regulates cell proliferation during blastema formation (Mateus et al., 2015), which could ultimately affect the number of new osteoblasts at later stages. Therefore, to determine the effect of Yap inhibition in the bone formation process, we heat-shocked daily DN-Yap (DN-Yap+) and sibling controls (DN-Yap-) from 48 to 96 hours post-amputation (hpa) and analysed the fins at 120 hpa (Fig. 1A). Analysis of the newly formed caudal fin bony-rays (Fig. 1B-E') showed that the DN-Yap+ animals had a significant reduction in mineralized area (Fig. 1F) and ray width (Fig. 1G). We confirmed that these defects are not due to a general delay in regeneration, as the measured bone regeneration was normalized to the total regenerated fin area in each animal. These results clearly demonstrate that Yap is required for bone formation during regeneration.

Yap regulates bone formation by inhibiting osteoprogenitor differentiation

Given the bone defects observed upon Yap inhibition, we hypothesized that Hippo pathway might be regulating osteoblast differentiation and their distribution during outgrowth. It has been previously described that, at the onset of outgrowth, osteoblasts start to differentiate, exhibiting a proximo-distal hierarchical organization that can be monitored using different osteoblast markers (Brown et al., 2009; Stewart et al., 2014) (Fig. S1A). The distal blastema (DB) is populated by osteoprogenitors positive for runx2 (defined as Runx2+; (Stewart et al., 2014)), a transcriptional regulator of mesenchymal cell commitment towards the osteoblast lineage (Ducy et al., 1997). The proximal blastema (PB) contains osteoblasts at the early stages of differentiation expressing both runx2 and osx (defined as Runx2+Osx+) (Brown et al., 2009; Stewart et al., 2014). The patterning zone (PZ), closer to the amputation plane, is populated by fully mature bone matrix-secreting osteoblasts expressing lower levels of runx2 and high levels of osx and bglap (Brown et al., 2009; Knopf et al., 2011). Taking advantage of two reporter lines for osx (Singh et al., 2012) and runx2 (Knopf et al., 2011) we characterized Yap subcellular localization at early stages of osteoblast differentiation (Fig. S1B-F'''). Yap subcellular localization reflects its activity status, since cytoplasmic Yap is often a read-out of inactivation, whereas its translocation to the nucleus promotes Yap-dependent transcriptional activity (Piccolo et al., 2014). Since Yap was mainly cytoplasmic in distal osteoprogenitors (DB, Fig. S1F, F'-F'''), in differentiating (PB, Fig. S1D, D'-D''') and mature osteoblasts (PZ, Fig. S1C, C'-C'''), we concluded that Yap is inactive in all osteoblast populations during outgrowth. However, we observed nuclear accumulation of Yap in multiple cells in proximity to the differentiating osteoblasts, mainly within the PZ and PB regions (Fig. S1C'-D'''). Surprisingly, when analysing the effect of Yap inhibition in the different osteoblast populations we could see a clear Yap-mediated regulation of osteoblast differentiation (Fig. 2A-H'''). By quantifying the relative number of osteoblast subsets, we noticed a significant increase in the number of osteoprogenitors (Runx2+), from 20% in DN-Yap- to 55% in the DN-Yap+ (Fig. 2I), and a reduction in the number of

differentiating osteoblasts (Runx2+Osx+), from 80% in DN-Yap- to 45% in DN-Yap+ (Fig. 2J). Additionally, the osteoprogenitor domain, usually confined to the DB compartment (Fig. 2A, D), had expanded and Runx2+ cells were also found in more proximal locations (Fig. 2E, F, G). This suggests that Yap inhibition does not disrupt the maintenance of the osteoprogenitor pool but instead prevents their differentiation into Runx2+Osx+ osteoblasts. Furthermore, gene expression analyses (Fig. 2K) showed that intermediate (immature) markers, such as osx and collagen 10a1 (col10a1), and mature markers (bone-forming osteoblasts), like bglap, bglapl, and osteonectin (osn), were significantly downregulated in DN-Yap+ regenerating caudal fins when compared to controls, while early progenitor markers, such as runx2a and runx2b, were unaltered.

Overall, these data suggest that Yap not only controls cell proliferation during blastema formation (Mateus et al., 2015), but it also regulates osteoblast differentiation. We propose that this regulation is via a paracrine signalling, pointing to an additional role for Yap during caudal fin regeneration.

Yap regulates osteoblast differentiation in a cell non-autonomous manner by compromising Bmp signalling

Osteoblast differentiation during caudal fin regeneration has been associated with the signalling activity of the newly formed basal epidermal layer (BEL) (Laforest et al., 1998; Quint et al., 2002; Smith et al., 2006). In this context, the BEL secretes Sonic hedgehog (Shh) to the PB compartment, leading to bmp2b expression, Bmp signalling activation, culminating in osteoblast differentiation (Laforest et al., 1998; Quint et al., 2002). Previous work has demonstrated that osteoblast differentiation and distal osteoprogenitor pool maintenance are regulated through antagonizing activities of Bmp and Wnt signalling pathways respectively. Therefore, in order to understand how Yap regulates osteoprogenitor differentiation, we analysed multiple components of key signalling pathways associated with osteoblast differentiation, such as Bmp (Smith et al., 2006; Stewart et al., 2014), Wnt (Stewart et al., 2014; Wehner et al., 2014), Shh (Laforest et al., 1998; Quint et al., 2002) and Retinoic acid (Ra) (Blum and Begemann, 2015) pathways in the Yap inhibition context. Upon Yap inhibition we did not detect differences of expression in shh or bmp2b transcripts, suggesting that Yap is not regulating osteoblast differentiation through the BEL. Furthermore, Yap is cytoplasmic (inactive) in the BEL cells (Fig. S2), indicating that Yap is mediating osteoblast differentiation through an alternative mechanism.

Interestingly, we observed a significant reduction of dkk1a (negative regulator of Wnt signalling; (MacDonald et al., 2010)) and bmp2a (ligand for Bmp signalling; (Rosen, 2009; Wang et al., 2014)) transcripts upon Yap inhibition (Fig. 3A), suggesting that Yap affects Wnt and Bmp signalling pathways during fin outgrowth. Since Yap was demonstrated to interact with both signalling pathways in other systems (Attisano and Wrana, 2013; Kim and Jho, 2014), we decided to investigate Yap subcellular localization in relation to activated Bmp and Wnt signalling at early stages of osteoblast differentiation (72 hpa). Regarding Bmp signalling, we measured the percentage of mesenchymal and osteoblast cells that contain active (nuclear) Yap and active/phosphorylated Smad 1/5/8 (pSmad), the Bmp signalling effector

(Wu et al., 2016) (Fig. 3B-F). We observed that Yap is nuclear in 50% of the mesenchymal cells within the PB whereas only 15% present pSmad (Fig. 3C,C'-C''',E). In the DB region, only a minority of cells (around 12%) presents nuclear Yap and/or pSmad (Fig. 3D,D'-D''',E). This Yap distribution along the proximal-distal axis had already been shown to correlate with differences of cell density within the blastema (Mateus et al., 2015). We also observed that, in accordance to what has been previously shown (Stewart et al., 2014), Bmp signalling is mainly active in differentiating osteoblasts that populate the PB compartment with almost 60% of osteoblasts showing nuclear pSmad (Fig. 3C,C'-C''',F), while this percentage decreases in the DB region (Fig. 3D,D'-D''',F). This shows that although Yap and pSmad are mostly active in different cells, mesenchyme and osteoblasts, respectively, they share a proximo-distal gradient of activation: more cytoplasmic (inactive) in distal-most regions and progressively more nuclear (active) towards proximal and patterning regions. Thus, we speculate that Yap may induce bmp2a expression in mesenchymal cells which then activates Bmp signalling in the adjacent osteoblasts, consequently promoting osteoblast differentiation. To test this hypothesis, we evaluated whether Yap inhibition perturbs Bmp signalling activation in differentiating osteoblasts. For that, we applied a single heat-shock at early stages of osteoblast differentiation (Fig. 4A) and evaluated the caudal fins at 72 hpa for Bmp signalling activation and ZNS5, which labels osteoblasts in all stages of differentiation (Ando et al., 2017; Brown et al., 2009) (Fig. 4B-G'). We observed that Yap inhibition led to a clear reduction in the number of pSmad-positive cells in the osteoblast populations (Fig. 4H), indicating that, indeed, Yap is required for Bmp signalling activation in osteoblasts.

Moreover, it has been reported that Bmp signalling activation promotes Dkk1b secretion, which restricts Wnt signalling to the DB compartment (Fig. S3A) (Stewart et al., 2014). Taking advantage of a transgenic line reporter for active Wnt signalling, we observed that while Wnt signalling is mainly active in the DB compartment, nuclear Yap is mostly excluded from this region, suggesting they have antagonist activities (Fig. S3B-E). Supporting this notion, we observed a tendency for the Wnt signalling activation domain to expand upon Yap inhibition (Fig. S4), which correlates with the lower expression of Wnt negative regulator dkk1a (Fig. 3A) and to the increase of the osteoprogenitor pool (Runx2+, Fig. 2I). Altogether this might imply that Yap and Bmp signalling act synergistically during fin regeneration to restrict Wnt signalling activity to distal-most regions. This is in agreement with previous studies where Yap has been shown to inhibit Wnt function in other regenerative contexts (Heallen et al., 2012).

Overall, our data shows that, in addition to controlling proliferation (Mateus et al., 2015), the Hippo-Yap pathway regulates osteoblast differentiation during zebrafish caudal fin regeneration, a link that has not been proposed so far. Our results indicate that Yap acts on bone regeneration mainly in a cell non-autonomous manner. On one hand, together with Bmp signalling, Yap may inhibit Wnt signalling expansion to the proximal blastema by regulating the expression of dkk1a in this region, consequently restricting osteoprogenitors to the distal blastema. On the other hand, and more

importantly, Yap seems to promote the secretion of Bmp2a by mesenchymal cells in the proximal blastema which then acts on adjacent osteoblasts to activate Bmp signalling and hence osteoblast differentiation. Taken together, these findings place Hippo-Yap pathway in the signalling events that direct osteoblast differentiation, mainly through regulation of Bmp signalling. We hope that the findings described here aid to provide a deeper understanding of the mechanisms regulating bone regeneration and to clarify the role of the Hippo-Yap signalling pathway during osteoblast lineage specification.

Acknowledgements

We are grateful to Lara Carvalho and Inês Cristo for advice and for reading the manuscript, to Duarte Mesquita and Rita Mateus for useful discussion and Telmo Pereira for data analysis. We thank the CEDOC Fish, Histology and Microscopy facilities for support and Kenneth Poss and Gilbert Weidinger for zebrafish transgenic line sharing.

Competing interests

The authors declare no competing or financial interests.

Author contributions

A. S. B. performed all experiments with the help of R.L. and. J.B.; A. S. B. and A. B.-B. conceived, and designed experiments; A.S.B performed data analysis; A.S.B, A. B.-B. and A. J. performed manuscript preparation.

Funding

This work was supported by funding from Fundação para a Ciência e Tecnologia [PTDC/BIM-MED/0659/2014; SFRH/BD/51990/2012].

Zebrafish used as animal model were reproduced and maintain in the CEDOC Fish Facility, with the support from Congento LISBOA-01-0145-FEDER-022170, co-financed by FCT (Portugal) and Lisboa2020, under the PORTUGAL2020 agreement (European Regional Development Fund).

Material and Methods

Ethics statement

All the people involved in animal handling and experimentation were properly trained and accredited by FELASA. All experimental procedures were approved by the Animal User and Ethical Committees at Centro de Estudos de Doenças Crónicas (CEDOC) and accredited by the Portuguese National Authority for Animal Health (DGAV) according to the directives from the European Directive (2010/63/UE) and Portuguese legislation (Decreto-Lei 113/2013) for animal experimentation and welfare.

Zebrafish lines

Wild-type AB, Tg(osterix:mCherryNTRo)pd46 (Singh et al., 2012), Tg(Has.RUNX2-Mmu.Fos:EGFP)zf259 (Knopf et al., 2011), Tg(6xTcf/Lef-miniP:d2GFP)isi01 (Shimizu et al., 2012) and Tg(hsp70l:RFP-dnyap1) (Mateus et al., 2015) zebrafish lines were maintained in a circulating system with 14 hour/day and 10 hour/night cycle periods at 28 °C. All experiments were performed in 4-18 months old

adult fish (Westerfield, 2000) and all transgenic animals were used as heterozygotes.

Caudal fin amputation and heat-shock experiments

Caudal fin amputations were performed in fish anaesthetized in buffered 160 mg/mL MS-222 (Sigma, E10521) using a sterile scalpel. Regeneration was allowed to proceed until defined time-points in an incubator at 33°C ± 1 °C, except for heat-shock experiments, and the water was renewed daily. Amputations were made 1 or 2 segments below the most proximal ray bifurcation, removing approximately one half of the fin. Regenerated fins from anaesthetized animals were collected at predefined time-points post-amputation, as previously described (Poss et al., 2000). For heat-shock experiments, Tg(hsp70l:RFP-dnyap1) and siblings were maintained and heat-shocked as previously described (Mateus et al., 2015). For Yap inhibition assays, animals were left to regenerate normally during the blastema formation phase (0-48 hpa), and heat-shocked afterwards. For short period manipulations, animals are heat-shocked once at 48 hpa and fins collected 24 hours after. For long period manipulations, animals are heat-shocked first at 48 hpa and in the next two consecutive days and fins collected at 120 hpa. Fins were then processed for cryosectioning or pooled for RNA extraction.

Total RNA isolation and quantitative PCR (qPCR)

For gene expression analysis, caudal fin regenerates were harvested, including one bony-ray segment proximal to the amputation plane. Pools from 4-5 caudal fins, were used per biological replicate and four biological replicates were used per time-point. Samples were homogenized in Trizol reagent (Invitrogen, 15596026) for cell disruption and RNA extraction. Chloroform was added, and the homogenate allowed to separate into a clear upper aqueous layer. RNA was precipitated and purified from the aqueous phase by adding an equal amount of 100% ethanol and loading the mixture into RNeasy Micro Spin columns (Qiagen, 74004). Remaining procedure was done following the RNeasy Micro kit (Qiagen, 74004) manufacturer's protocol. cDNA was synthesized from 1 µg total RNA for each sample using the Transcriptor High Fidelity cDNA Synthesis Kit (Roche, 05081963001), with a mixture of oligo dT and random primers. All qPCR primers are listed in Table S1. qPCR was performed using a FastStart Essential DNA Green Master Mix (Roche, 4385617) and a Roche LightCycler 480. Cycle conditions were: 15 min pre-incubation at 95°C and 3 step amplification cycles (50x), each cycle for 30 sec at 95°C, 15 sec at 65°C or 68°C (depending on primer melting temperature) and for 30 sec at 72°C.

Calcein staining, immunofluorescence and image acquisition

Calcein (Sigma-Aldrich, C0875-56) staining, used to label the regenerated bony-rays, was performed as previously described (Jun Du et al., 2001). Fins were imaged using a Zeiss Lumar V-12 fluorescence stereoscope equipped with a Zeiss digital camera using a 0.8X air objective and the Zen 2 PRO blue software.

Caudal fin fixation, preservation and embedding was done as previously described (Mateus et al., 2015). Longitudinal caudal fins sections were sectioned in 12 µm-thick slices using a Microm

cryostat (Cryostat Leica CM3050 S) and maintained at -20 °C until further use. For immunofluorescence on cryosections, sections were thawed for 15 min at room temperature, washed twice in 1x PBS at 37°C for 10 min, followed by a 0.1 M glycine (Sigma-Aldrich, in 1x PBS) incubation for 10 min. Sections were then permeabilized in acetone for 7 min at -20°C and incubated for 20 min in 0.2% PBST (1x PBS with 0.2% Triton X-100). Afterwards, they were incubated in a blocking solution of 10% non-fat dry milk in PBST for 2-4 h at room temperature. Samples incubated with primary antibodies, diluted in blocking solution, overnight at 4°C (for further antibody details see Table S2). On the following day, samples were washed with PBST (6x 10 min) and incubated with secondary antibodies, diluted in blocking solution, for 2 h at room temperature (for further antibody details see Table S2). Subsequently, slides were washed (3x 10 min) in PBST and then counterstained with 4',6- diamidino-2-phenylindole (DAPI; 0.001 mg/mL in 1x PBS, Sigma, D8417) for 5 min the dark for nuclei staining. Slides were washed (3x 10 min) in PBST and mounted in fluorescent Mounting Medium (DAKO, S3023). Slides were stored at 4°C protected from light until image acquisition.

For anti-Runx2 an antigen retrieval step was performed, which consisted of a 15-min incubation at 95°C with sodium citrate buffer (10mM Tri-sodium citrate with 0.05% Tween20, pH 6). For anti-pSmad 1/5/8 staining, slides were incubated in a blocking solution of 10% non-fat dry milk in PBST, containing 650 mM NaCl, and subsequently washed with PBST, containing 650 mM NaCl as previously described (Stewart et al., 2014). For anti-Yap staining, slides were washed in PBDX (1% BSA, 1% DMSO, 0,2% Triton-100, 50% PBS 1x in Milli-Q water) and blocked in PBDX containing 1,5% Goat Serum has previously described (Mateus et al., 2015). Incubation with anti-YAP was done overnight at room temperature.

Images were acquired in a confocal microscope Zeiss LSM 710 using the software ZEN 2010B SP1 and processed and analysed using the Fiji-ImageJ software (Schindelin et al., 2012). Caudal fin sections Z-stacks were acquired using a 40x water objective with 0.6x or 1x zoom and a step size of 1 µm. For image processing, composite maximum intensity z-stack projections were made, except when noted. Concatenation of several images along the proximal-distal axis of the same longitudinal section was performed using the Fiji plugin 3D Pairwise Stitching.

Quantifications and statistical analysis

For qPCR analysis all samples were analysed in 4-6 biological pools. For each biological pool, qPCR was performed for each target gene in 3 technical replicates. Gene expression values were normalized using the elongation factor 1α (ef1α, NM_131263) housekeeping gene and relative expression was calculated using the 2(-ΔΔC(T) method (Livak and Schmittgen, 2001). To determine differentially expressed genes, results were plotted using GraphPad Prism software and two-tailed Student's t-test with Welch's correction was used. Only p-values<0.05 were considered statistically significant.

The percentage of bony-ray formation was defined by the area stained by calcein labelling in relation to the total fin regenerated area. Briefly, the area of fluorescence intensity for each image was determined by empirically establishing a threshold to separate the signal fluorescence intensity from the background. The average

fluorescence area was then normalized to the total tissue regenerate area. Measurements of the total regenerated area were done using images of whole caudal fins and the regenerated fin area was delineated from the amputation plane to the distal end of the regenerate using the Area tool on Fiji, resulting in one measurement per animal. Six animals were used per condition.

Determination of bony-ray width, in calcein staining experiments, was performed automatically by thresholding the fluorescence signal, which was determined using the Otsu algorithm in Fiji. Subsequently, the width at the basis of each formed bony-ray was measured using the line tool on Fiji. Individual bony-ray widths from three different animals are plotted on graph (56 bony-rays from Sibling controls and 36 bony-rays from DN-Yap+ transgenics)

Yap subcellular localization and pSmad 1/5/8-positive cells in proximal and distal blastema regions of caudal fin cryosections were quantified using a custom-made FIJI macro. The macro automatically finds the nuclei in individual z-stack slices, searches for the signal surrounding the nuclei and compares the nuclear fluorescence intensity with the surrounding cytoplasmic fluorescence intensity. The nuclei images were pre-processed using a median filter with a kernel size of 2 pixels for noise removal. Local thresholding was performed using the Phansalkar method with a kernel size of 15 pixels. The resultant binary image was morphologically closed to fill holes. Finally, nuclei masks were created using the Analyse particles plugin. The signal surrounding the nuclei was found by enlarging each nuclear mask by 3 pixels and removing the correspondent nuclear region. Average signal intensity for both regions was obtained and a ratio was calculated (nuclear/cytoplasmic). A positive (nuclear) Yap signal was considered when this ratio was above 1.2. For quantification of the number of cells presenting nuclear pSmad 1/5/8 the same nuclei mask was used. Positive (nuclear) pSmad 1/5/8 signal was identified automatically using thresholding. Since the signal to noise ratio is high, the threshold value was selected manually using an average value between the background and the positive nuclei signals.

Percentage of osteoblasts subsets (Runx2+Osx- or Runx2+Osx+) and pSmad 1/5/8-positive cells in longitudinal cryosections was quantified by analysing the number of cells in the regenerated area in relation to the total number of osteoblast (Runx2+Osx- and Runx2+Osx+ or ZNS5-positive cells). Quantifications were done using the Cell-counter plugin on Fiji in individual cryosections representing at least 3 different blastemas per animal and 3-4 animals per condition. For osteoblast subset quantification, 15 cryosections from sibling controls and 15 from DN-Yap+ transgenics were used. For pSmad 1/5/8-positive cells quantification within the total osteoblast population (ZNS5+ population) we used 19 cryosections in DN-Yap+ and 20 cryosections in sibling controls.

Percentage of GFP area in Tg(6xTcf/Lef-miniP:d2GFP)isi01 was quantified by measuring the area occupied by GFP expressing cells in relation to the total regenerated area in fin cryosections representing at least three blastemas per animal and three animals were used per condition. Areas were delineated using the Area tool on Fiji.

Statistical significance between controls and manipulated animals was determined by non-paired, non-parametric comparison, using the

Mann-Whitney U test in the Prism Graphpad software. Means and standard deviations (SD) are displayed in the graphs. Only p-values less than 0,05 were considered statistically significant.

References

Ando, K., Shibata, E., Hans, S., Brand, M. and Kawakami, A. (2017). Osteoblast Production by Reserved Progenitor Cells in Zebrafish Bone Regeneration and Maintenance. Dev. Cell 43, 643–650.e3.

Antos, C. L., Knopf, F. and Brand, M. (2016). Regeneration of Organs and Appendages in Zebrafish: A Window into Underlying Control Mechanisms. eLS 1–17.

Astone, M., Lai, J. K. H., Dupont, S., Stainier, D. Y. R., Argenton, F. and Vettori, A. (2018). Zebrafish mutants and TEAD reporters reveal essential functions for Yap and Taz in posterior cardinal vein development. Sci. Rep. 8, 1–15.

Attisano, L. and Wrana, J. L. (2013). Signal integration in TGF-β, WNT, and Hippo pathways. F1000Prime Rep. 5, 1–8.

Azevedo, A. S., Grotek, B., Jacinto, A., Weidinger, G. and Saúde, L. (2011). The regenerative capacity of the zebrafish caudal fin is not affected by repeated amputations. PLoS One 6, 1–8.

Blum, N. and Begemann, G. (2015). Osteoblast de- and redifferentiation are controlled by a dynamic response to retinoic acid during zebrafish fin regeneration. Development 142, 2894–2903.

Brown, A. M., Fisher, S. and Iovine, M. K. (2009). Osteoblast maturation occurs in overlapping proximal-distal compartments during fin regeneration in zebrafish. 6, 247–253.

Cardeira, J., Gavaia, P. J., Fernández, I., Cengiz, I. F., Moreira-Silva, J., Oliveira, J. M., Reis, R. L., Cancela, M. L. and Laizé, V. (2016). Quantitative assessment of the regenerative and mineralogenic performances of the zebrafish caudal fin. Sci. Rep. 6, 1–16.

Chen, C. H., Puliafito, A., Cox, B. D., Primo, L., Fang, Y., Di Talia, S. and Poss, K. D. (2016). Multicolor Cell Barcoding Technology for Long-Term Surveillance of Epithelial Regeneration in Zebrafish. Dev. Cell 36, 668–680.

Collignon, A. M., Lesieur, J., Vacher, C., Chaussain, C. and Rochefort, G. Y. (2017). Strategies developed to induce, direct, and potentiate bone healing. Front. Physiol. 8, 1–8.

Corrado, A., Sanpaolo, E. R., Di Bello, S. and Cantatore, F. P. (2017). Osteoblast as a target of anti-osteoporotic treatment. Postgrad. Med. 129, 858–865.

Dimitriou, R., Jones, E., McGonagle, D. and Giannoudis, P. V. (2011). Bone regeneration: Current concepts and future directions. BMC Med. 9, 66.

Ducy, P., Zhang, R., Geoffroy, V., Ridall, A. L. and Karsenty, G. (1997). Osf2/Cbfa1: A transcriptional activator of osteoblast differentiation. Cell 89, 747–754.

El Bialy, I., Jiskoot, W. and Reza Nejadnik, M. (2017). Formulation, Delivery and Stability of Bone Morphogenetic Proteins for Effective Bone Regeneration. Pharm. Res. 34, 1152–1170.

Eriksen, E. F. (2010). Cellular mechanisms of bone remodeling. Rev. Endocr. Metab. Disord. 11, 219–227.

Feng, X. and McDonald, J. M. (2006). Disorders of Bone Remodeling. Sci. York 283, 345–356.

Franceschi, R. T., Xiao, G., Jiang, D., Gopalakrishnan, R., Yang, S. and Reith, E. (2003). Multiple Signaling Pathways Converge on the Cbfa1/Runx2 Transcription Factor to Regulate Osteoblast Differentiation. Connect. Tissue Res. 44, 109–116.

Fu, V., Plouffe, S. W. and Guan, K. L. (2017). The Hippo pathway in organ development, homeostasis, and regeneration. Curr. Opin. Cell Biol. 49, 99–107.

Garrison, R. K., Donell, S., Shemilt, I., Ryder, J. J., Mugford, M., Song, F., Harvey, I., Alt, V. and Song, F. (2010). Bone morphogenetic protein (BMP) for

fracture healing in adults. Cochrane Database Syst. Rev.

Godwin, J., Kuraitis, D. and Rosenthal, N. (2014). Extracellular matrix considerations for scar-free repair and regeneration: Insights from regenerative diversity among vertebrates. Int. J. Biochem. Cell Biol. 56, 47–55.

Goessling, W. and North, T. E. (2014). Repairing quite swimmingly: advances in regenerative medicine using zebrafish. Dis. Model. Mech. 7, 769–776.

Håkelien, A. M., Bryne, J. C., Harstad, K. G., Lorenz, S., Paulsen, J., Sun, J., Mikkelsen, T. S., Myklebost, O. and Meza-Zepeda, L. A. (2014). The regulatory landscape of osteogenic differentiation. Stem Cells 32, 2780–2793.

Halder, G. and Johnson, R. L. (2011). Hippo signaling: growth control and beyond. Development 138, 9–22.

Halder, G., Dupont, S. and Piccolo, S. (2012). Transduction of mechanical and cytoskeletal cues by YAP and TAZ. Nat. Rev. Mol. Cell Biol. 13, 591–600.

Heallen, T., Zhang, M., Wang, J., Bonilla-claudio, M., Klysik, E., Randy, L. and Martin, J. F. (2012). Hippo Pathway Inhibits Wnt Signaling to Restrain Cardiomyocyte Proliferation and Heart Size. Science (80-.). 332, 458–461.

Hiemer, S. E. and Varelas, X. (2013). Stem cell regulation by the Hippo pathway. Biochim. Biophys. Acta - Gen. Subj. 1830, 2323–2334.

Hong, J., Hong, J., Hwang, E. S., McManus, M. T., Amsterdam, A., Tian, Y., Kalmukova, R., Mueller, E., Benjamin, T., Spiegelman, B. M., et al. (2005). Taz, a Transcriptional Modulator of Mesenchymal Stem Cell Differentiation. Science 1074, 1074–1078.

Huang, J., Wu, S., Barrera, J., Matthews, K. and Pan, D. (2005). The Hippo signaling pathway coordinately regulates cell proliferation and apoptosis by inactivating Yorkie, the Drosophila homolog of YAP. Cell 122, 421–434.

Irvine, K. D. (2012). Integration of intercellular signaling through the Hippo pathway. Semin. Cell Dev. Biol. 23, 812–817.

Jun Du, S., Frenkel, V., Zohar, Y. and Kindschi, G. (2001). Visualizing normal and defective bone development in zebrafish embryos using the fluorescent chromophore calcein. Dev. Biol. 238, 239–246.

Kawakami, A. (2009). Stem cell system in tissue regeneration in fish. Dev. Growth Differ. 52, 77–87.

Kegelman, C. D., Mason, D. E., Dawahare, J. H., Horan, D. J., Vigil, G. D., Howard, S. S., Robling, A. G., Bellido, T. M. and Boerckel, J. D. (2018). Skeletal cell YAP and TAZ combinatorially promote bone development. FASEB J. 32, 2706–2721.

Kim, M. and Jho, E. H. (2014). Cross-talk between Wnt/b-catenin and Hippo signaling pathways: A brief review. BMB Rep. 47, 540–545.

Knopf, F., Hammond, C., Chekuru, A., Kurth, T., Hans, S., Weber, C. W., Mahatma, G., Fisher, S., Brand, M., Schulte-Merker, S., et al. (2011). Bone regenerates via dedifferentiation of osteoblasts in the zebrafish fin. Dev. Cell 20, 713–724.

Laforest, L., Brown, C. W., Poleo, G., Géraudie, J., Tada, M., Ekker, M. and Akimenko, M. a (1998). Involvement of the sonic hedgehog, patched 1 and bmp2 genes in patterning of the zebrafish dermal fin rays. Development 125, 4175–4184.

Livak, K. J. and Schmittgen, T. D. (2001). Analysis of relative gene expression data using real-time quantitative PCR and the 2-ΔΔCT method. Methods 25, 402–408.

Long, F. (2012). Building strong bones: Molecular regulation of the osteoblast lineage. Nat. Rev. Mol. Cell Biol. 13, 27–38.

Lucero, J., Castanon, R., Nery, J. R., Pinto-duarte, A., Davis, D. A., Mash, D. C., Behrens, M. M. and Ecker, J. R. (2018). Skeletal cell YAP and TAZ redundantly promote bone development by regulation of collagen I expression and organization. 1–40.

MacDonald, B. T., Tamai, K. and He, X. (2010). Wnt/β-catenin signaling: components, mechanisms, and diseases. Dev. Cell 17, 9–26.

Marí-Beffa, M. and Murciano, C. (2010). Dermoskeleton morphogenesis in zebrafish fins. Dev. Dyn. 239, 2779–2794.

Marie, P. J. (2015). Osteoblast dysfunctions in bone diseases: From cellular and molecular mechanisms to therapeutic strategies. Cell. Mol. Life Sci. 72, 1347–1361.

Mateus, R., Lourenco, R., Fang, Y., Brito, G., Farinho, A., Valerio, F. and Jacinto, A. (2015). Control of tissue growth by Yap relies on cell density and F-actin in zebrafish fin regeneration. Development 142, 2752–2763.

Moya, I. M. and Halder, G. (2018). Hippo–YAP/TAZ signalling in organ regeneration and regenerative medicine. Nat. Rev. Mol. Cell Biol.

Nakashima, K., Zhou, X. and Al., G. K. E. (2002). The novel zinc fingercontaining transcription factor Osterix is required for osteoblast differentiation and bone formation. Cell 108, 17–29.

Pan, J.-X., Xiong, L., Zhao, K., Zeng, P., Wang, B., Tang, F.-L., Sun, D., Guo, H., Yang, X., Cui, S., et al. (2018). YAP promotes osteogenesis and suppresses adipogenic differentiation by regulating β-catenin signaling. Bone Res. 6, 18.

Pfefferli, C. and Jaźwińska, A. (2015). The art of fin regeneration in zebrafish. Regeneration 2, 72–83.

Piccolo, S., Dupont, S. and Cordenonsi, M. (2014). The Biology of YAP/TAZ: Hippo Signaling and Beyond. Physiol. Rev. 94, 1287–1312.

Poss, K. D., Shen, J., Nechiporuk, A., McMahon, G., Thisse, B., Thisse, C. and Keating, M. T. (2000). Roles for Fgf signaling during zebrafish fin regeneration. Dev. Biol. 222, 347–358.

Poss, K. D., Keating, M. T. and Nechiporuk, A. (2003). Tales of regeneration in zebrafish. Dev. Dyn. 226, 202–210.

Quint, E., Smith, A., Avaron, F., Laforest, L., Miles, J., Gaffield, W. and Akimenko, M. A. (2002). Bone patterning is altered in the regenerating zebrafish caudal fin after ectopic expression of sonic hedgehog and bmp2b or exposure to cyclopamine. Proc Natl Acad Sci U S A 99, 8713–8718.

Quiros-Gonzalez, I. and Yadav, V. K. (2014). Central genes, pathways and modules that regulate bone mass. Arch. Biochem. Biophys. 561, 130–139.

Rosen, V. (2009). BMP2 signaling in bone development and repair. Cytokine Growth Factor Rev. 20, 475–480.

Rutkovskiy, A., Stensløkken, K.-O. and Vaage, I. J. (2016). Osteoblast Differentiation at a Glance. Med. Sci. Monit. Basic Res. 22, 95–106.

Schindeler, A., McDonald, M. M., Bokko, P. and Little, D. G. (2008). Bone remodeling during fracture repair: The cellular picture. Semin. Cell Dev. Biol. 19, 459–466.

Schindelin, J., Arganda-Carreras, I., Frise, E., Kaynig, V., Longair, M., Pietzsch, T., Preibisch, S., Rueden, C., Saalfeld, S., Schmid, B., et al. (2012). Fiji: An open-source platform for biological-image analysis. Nat. Methods 9, 676–682.

Seo, E., Basu-Roy, U., Gunaratne, P. H., Coarfa, C., Lim, D. S., Basilico, C. and Mansukhani, A. (2013). SOX2 Regulates YAP1 to Maintain Stemness and Determine Cell Fate in the Osteo-Adipo Lineage. Cell Rep. 3, 2075–2087.

Shimizu, N., Kawakami, K. and Ishitani, T. (2012). Visualization and exploration of Tcf/Lef function using a highly responsive Wnt/B-catenin signaling-reporter transgenic zebrafish. Dev. Biol. 370, 71–85.

Shrivats, A. R., McDermott, M. C. and Hollinger, J. O. (2014). Bone tissue engineering: State of the union. Drug Discov. Today 19, 781–786.

Singh, S. P., Holdway, J. E. and Poss, K. D. (2012). Regeneration of amputated zebrafish fin rays from de novo osteoblasts. Dev. Cell 22, 879–86.

Smith, A., Avaron, F., Guay, D., Padhi, B. K. and Akimenko, M. A. (2006). Inhibition of BMP signaling during zebrafish fin regeneration disrupts fin growth and scleroblast differentiation and function. Dev. Biol. 299, 438–454.

Sousa, S., Afonso, N., Bensimon-Brito, A., Fonseca, M., Simoes, M., Leon, J., Roehl, H., Cancela, M. L. and Jacinto, A. (2011). Differentiated skeletal cells contribute to blastema formation during zebrafish fin regeneration. Development 138, 3897–3905.

Stewart, S. and Stankunas, K. (2012). Limited dedifferentiation provides replacement tissue during zebrafish fin regeneration. Dev. Biol. 365, 339–349.

Stewart, S., Gomez, W. A., Armstrong, B. E., Henner, A. and Stankunas, K. (2014). Sequential and Opposing Activities of Wnt and BMP Coordinate Zebrafish Bone Regeneration. 6, 482–498.

Tang, Y. and Weiss, S. J. (2017). Snail/Slug-YAP/TAZ complexes cooperatively regulate mesenchymal stem cell function and bone formation. Cell Cycle 16, 399–405.

Tang, Y., Rowe, R. G., Botvinick, E. L., Kurup, A., Putnam, A. J., Seiki, M., Weaver, V. M., Keller, E. T., Goldstein, S., Dai, J., et al. (2013). MT1-MMP-Dependent Control of Skeletal Stem Cell Commitment via a β1-Integrin/YAP/TAZ Signaling Axis. Dev. Cell 25, 402–416.

Tu, S. and Johnson, S. L. (2011). Fate restriction in the growing and regenerating zebrafish fin. Dev. Cell 20, 725–732.

Valenti, M. T., Carbonare, L. D. and Mottes, M. (2017). Osteogenic differentiation in healthy and pathological conditions. Int. J. Mol. Sci. 18,.

Wang, R. N., Green, J., Wang, Z., Deng, Y., Qiao, M., Peabody, M., Zhang, Q., Ye, J., Yan, Z., Denduluri, S., et al. (2014). Bone Morphogenetic Protein (BMP) signaling in development and human diseases. Genes Dis. 1, 87–105.

Wehner, D. and Weidinger, G. (2015). Signaling networks organizing regenerative growth of the zebrafish fin. Trends Genet. 31, 336–343.

Wehner, D., Cizelsky, W., Vasudevaro, M., Özhan, G., Haase, C., Kagermeier-Schenk, B., Röder, A., Dorsky, R. I., Moro, E., Argenton, F., et al. (2014). Wnt/β-catenin signaling defines organizing centers that orchestrate growth and differentiation of the regenerating zebrafish caudal fin. Cell Rep. 6, 467–481.

Wei, J. and Karsenty, G. (2016). An overview of the metabolic functions of osteocalcin. 16, 93–98.

Westerfield, M. (2000). The zebrafish book. A guide for the laboratory use of zebrafish (Danio rerio). 4th editio. Eugene: Univ. of Oregon Press.

Wu, M., Chen, G. and Li, Y. P. (2016). TGF-β and BMP signaling in osteoblast, skeletal development, and bone formation, homeostasis and disease. Bone Res. 4.

Xiong, J., Almeida, M. and O'Brien, C. A. (2018). The YAP/TAZ transcriptional co-activators have opposing effects at different stages of osteoblast differentiation. Bone 112, 1–9.

Yimlamai, D., Christodoulou, C., Galli, G. G., Yanger, K., Pepe-Mooney, B., Gurung, B., Shrestha, K., Cahan, P., Stanger, B. Z. and Camargo, F. D. (2014). Hippo pathway activity influences liver cell fate. Cell 157, 1324–1338.

Zhao, B. (2014). The Hippo pathway in organ size control, tissue regeneration and stem cell self-renewal. Cell 13, 877–883.

Zhao, A., Qin, H. and Fu, X. (2016). What determines the regenerative capacity in animals? Bioscience 66, 735–746.

Manuscript figures

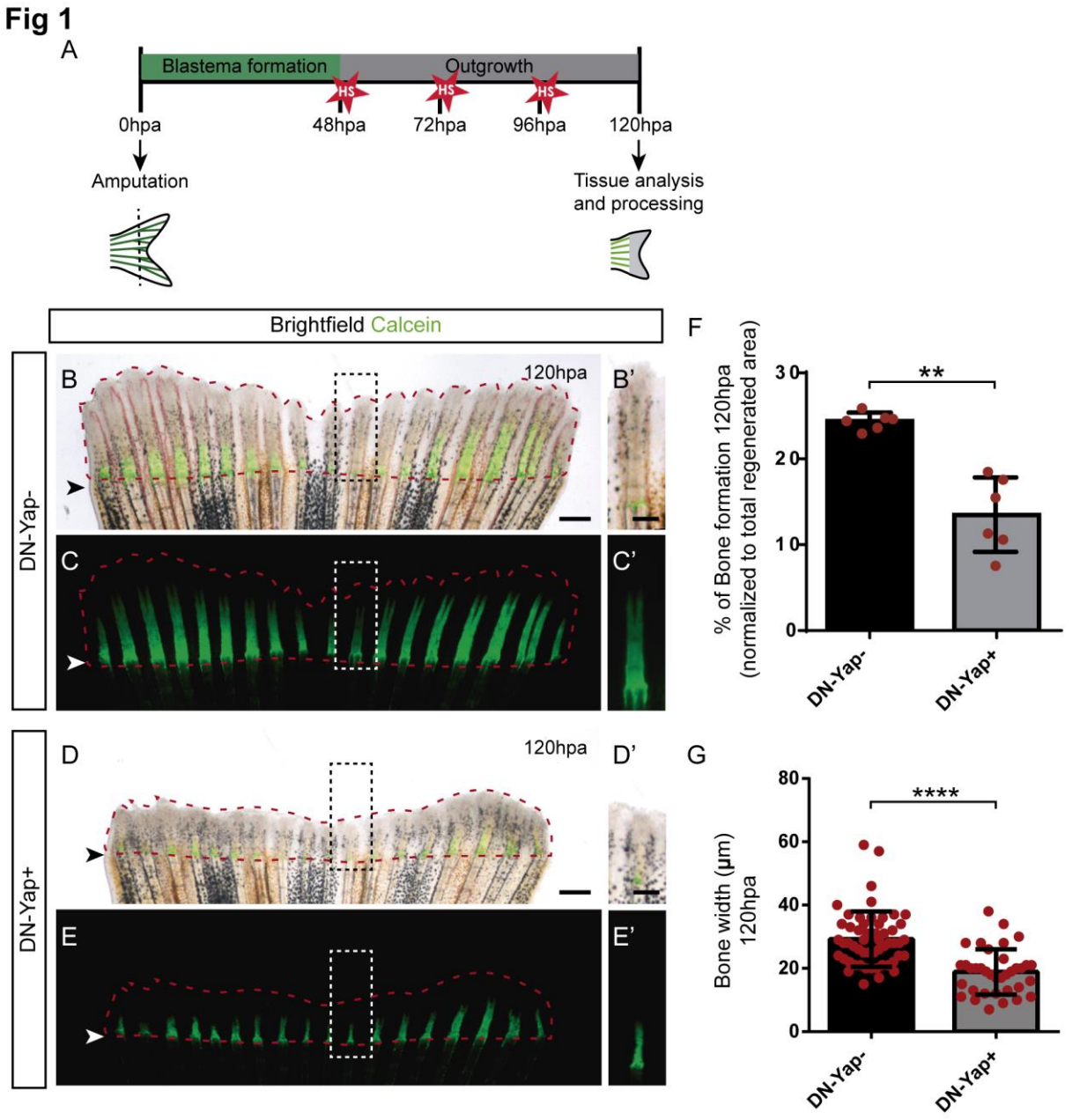

Figure 1- Inhibition of Yap activity during the regenerative outgrowth leads to bone formation defects. (A) Experimental setup used for prolonged Yap inhibition. (B-E') Representative images of caudal fins stained for calcein (green) in (B, B', C, C') DN-Yap- and (D, D', E, E') DN-Yap+ animals. Dashed rectangles correspond to magnified panels. (F) Percentage of bone formation (n=6 fish in DN-Yap and DN-Yap+). (G) Quantification of the bony-ray width (n=54 bony-rays in DN-Yap-; n=36 bony-rays in DN-Yap+). Dashed red line outlines regenerated area. Arrowheads define the amputation plane. Scale bars: (B, C, D, E) 1 mm and (B', C', D', E') 0,5 mm. Statistical analysis with Mann-Whitney test; **P<0.01, ****P<0.0001.

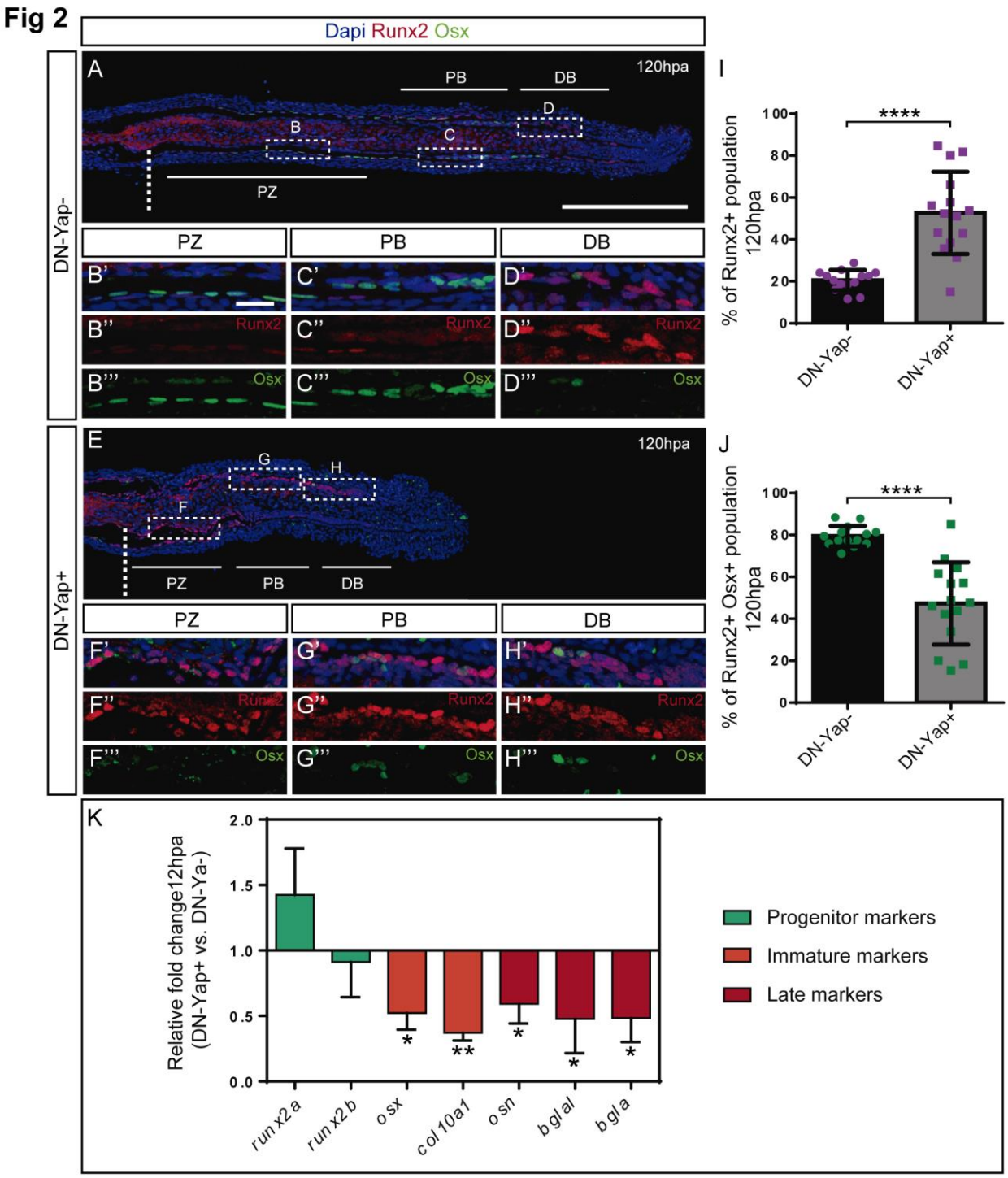

Figure 2- Inhibition of Yap activity leads to defects in osteoblast differentiation during regenerative outgrowth. (A, E) Representative z-stack image of longitudinal cryosections from (A-D''') DN-Yap- and (E-H''') DN-Yap+ caudal fins immunostained for Runx2 (red) and Osx (green). Dashed lines define the amputation plane. Regions bounded by dashed white boxes are magnifications of the (B, F) PZ, (C, G) PB and (D, H) DB regions. (I) Quantification of Runx2+ osteoprogenitors and (J) Runx2+ Osx+ osteoblasts in DN-Yap- and DN-Yap+ cryosections. Statistical analysis with Mann-Whitney test (n=15 cryosections in both DN-Yap- and DN-Yap+). (K) Relative gene expression of progenitor,

immature and late osteoblast markers. Statistical analysis with unpaired t test and Welch's correction (n=4 biological replicates). Scale bars: (A, E) 200 µm and (B'-D''', F'-H''') 20 µm. *P<0.05, **P<0.01, ****P<0.0001.

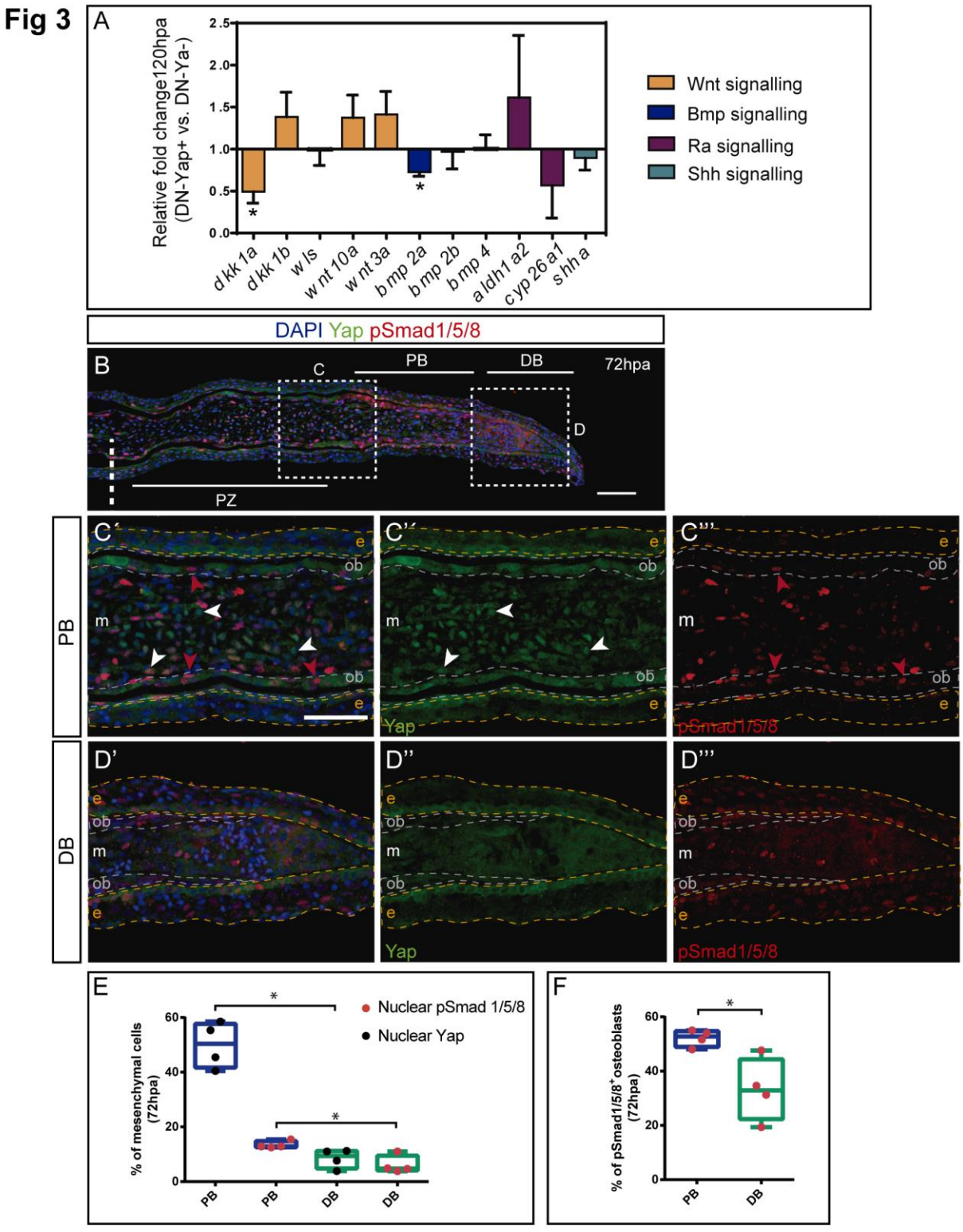

Figure 3– Yap and pSmad1/5/8 subcellular localization within the different blastema compartments during regenerative outgrowth. (A) Relative gene expression of components of multiple signalling pathways. Statistical analysis with unpaired t test and Welch's correction (n=4 biological replicates). (B) Representative z-stack image of a longitudinal fin cryosection immunostained for Yap (green) and pSmad1/5/8 (red). Dashed white line defines the amputation plane. Dashed boxes are magnifications of the (C'-C''') PB and (D'-D''') DB regions. White arrowheads indicate mesenchymal cells with nuclear Yap and red arrowheads point to osteoblasts with nuclear pSmad1/5/8. Dashed orange and grey lines define the epidermis and the osteoblast compartments, respectively. (E) Percentage of Yap- and pSmad1/5/8-positive mesenchymal cells and (F) pSmad1/5/8–positive osteoblasts. Statistical analysis with Mann-Whitney test (n=3 blastemas from 4 animals); *P <0.05. m: mesenchyme, ob: osteoblasts, e: epidermis. Scale bars: (B) 200 µm and (C'-D''') 50 µm.

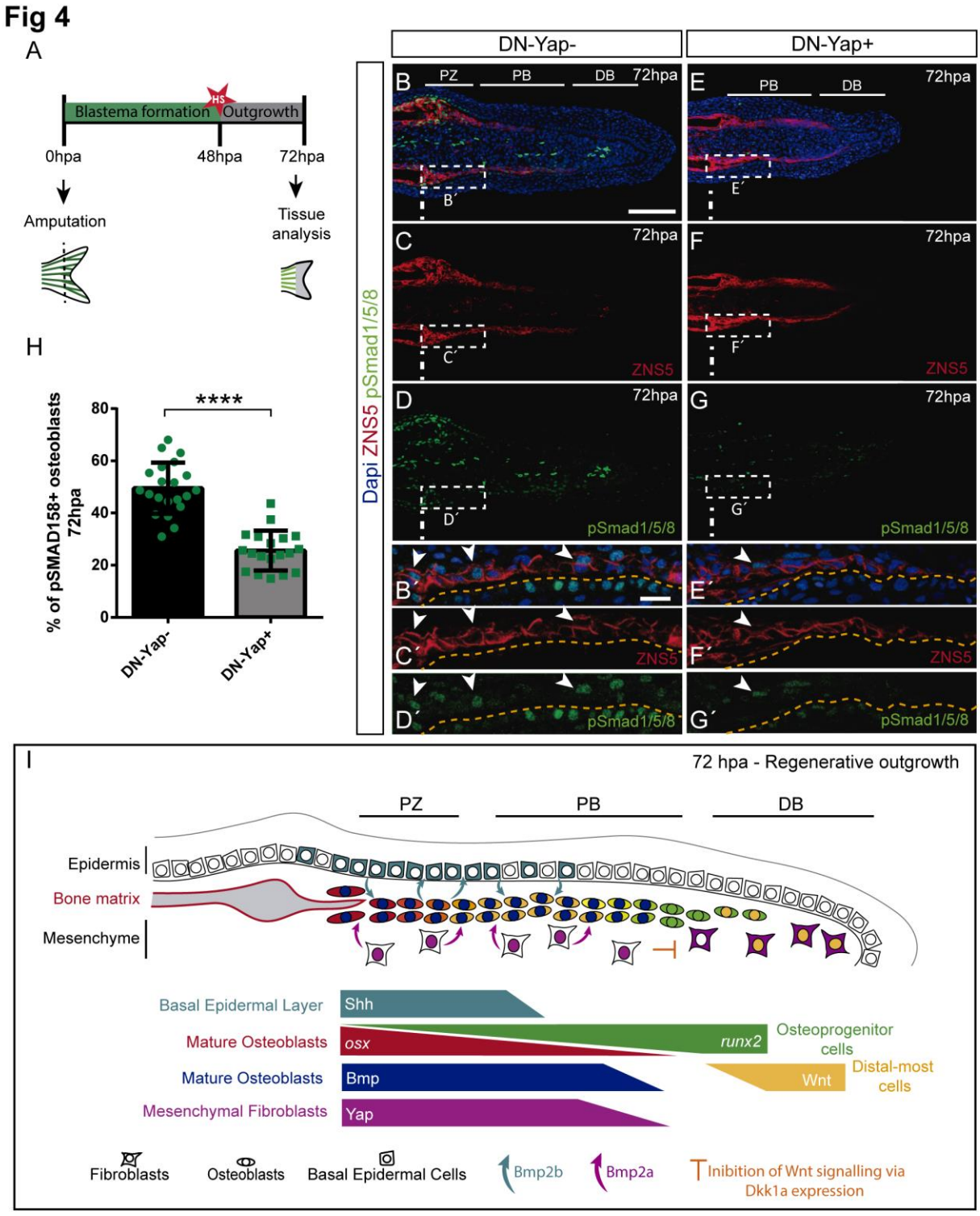

Figure 4– Manipulation of Yap activity inhibits Bmp signalling during regenerative outgrowth. (A) Experimental setup used for short Yap inhibition. (B-G) Representative z-stack images of longitudinal cryosections of (B-D') DN-Yap- and (E-G') DN-Yap+ caudal fins immunostained for ZNS5 (red) and pSmad1/5/8 (green). Dashed boxes are magnifications of the PZ regions. White and orange dashed lines define the amputation plane and the interface between osteoblast and BEL cells, respectively. Arrowheads point to osteoblasts (ZNS5+) with nuclear pSmad1/5/8. (H) Quantification of

pSmad1/5/8-positive osteoblasts (n=20 cryosections from DN-Yap-; n=18 cryosections from DN-Yap+). Statistical analysis with Mann-Whitney test. (I) Model based in our findings and others of a 72 hpa fin section highlighting the main players regulating osteoblast differentiation during caudal fin bone regeneration. Scale bars: (B-G) 200 µm and (B'-G') 20 µm. ****P<0.0001.

Manuscript supplementary figures

Fig S1

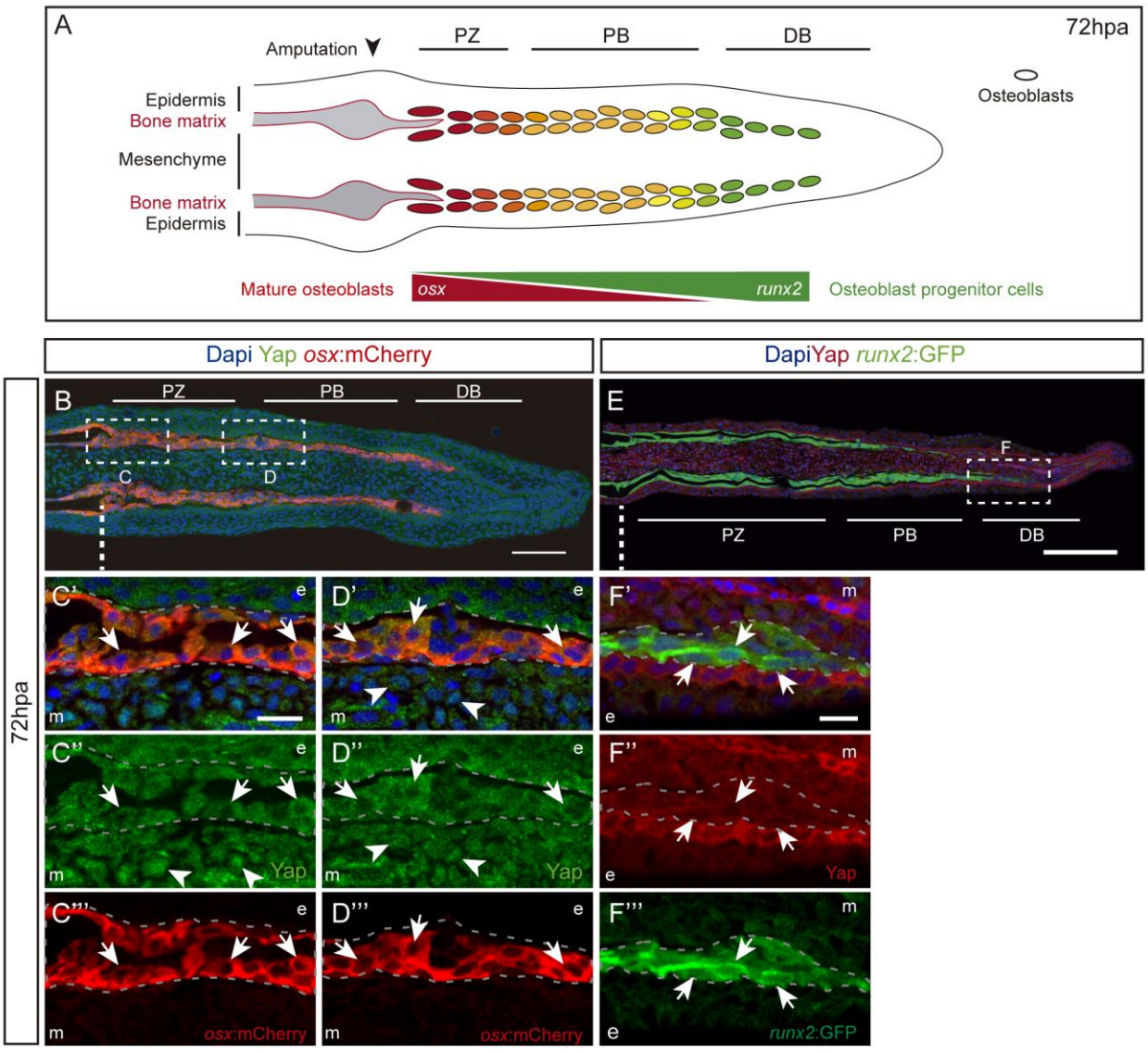

Figure S1 – Yap subcellular localization in different osteoblast subsets during the regenerative outgrowth. (A) Representation of the 72 hpa blastema osteoblast compartmentalization along the caudal fin proximo-distal axis, based on gradients of expression of osx and runx2. (B) Representative images of longitudinal cryosections of Yap immunodetection (green) in osx:mCherry (red) transgenic animal. (C'-D''') Magnifications of the (C'-C''') PZ and the

(D'-D''') PB regions. Arrows indicate osx+ osteoblasts where Yap is excluded from the nucleus and arrowheads indicate mesenchymal cells with nuclear Yap. (E) Representative image of longitudinal cryosection of Yap immunodetection (red) in runx2:EGFP (green) transgenic animals. (F'-F''') Magnification of the DB region. Arrows show runx2+ osteoblasts with Yap excluded from the nucleus. e: epidermis, m: mesenchyme. Dashed line defines the amputation plane. Scale bars: (B, E) 200 µm and (C'-F''') 20 µm

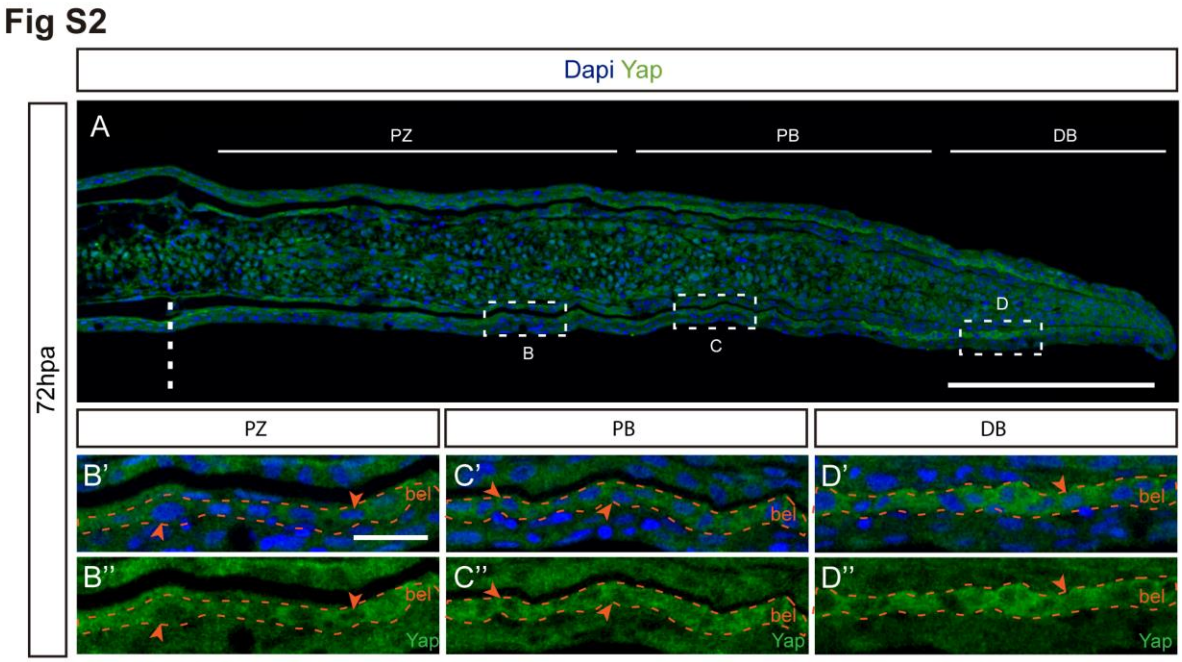

Figure S2 – Yap is excluded from the nucleus in the wound epidermis basal layer cells. (A) Representative z-stack image of longitudinal cryosection of wild-type animal immunostained for Yap (green). Dashed white line defines the amputation plane and dashed boxes are magnifications of the (B', B'') PZ, (C', C'') PB and (D', D'') DB regions. Dashed orange line delimitates the BEL. Arrowheads indicate BEL cells with Yap excluded from the nucleus. bel: basal epidermal layer. Scale bars: (A) 200 µm and (B'-D'') 20 µm.

Fig S3

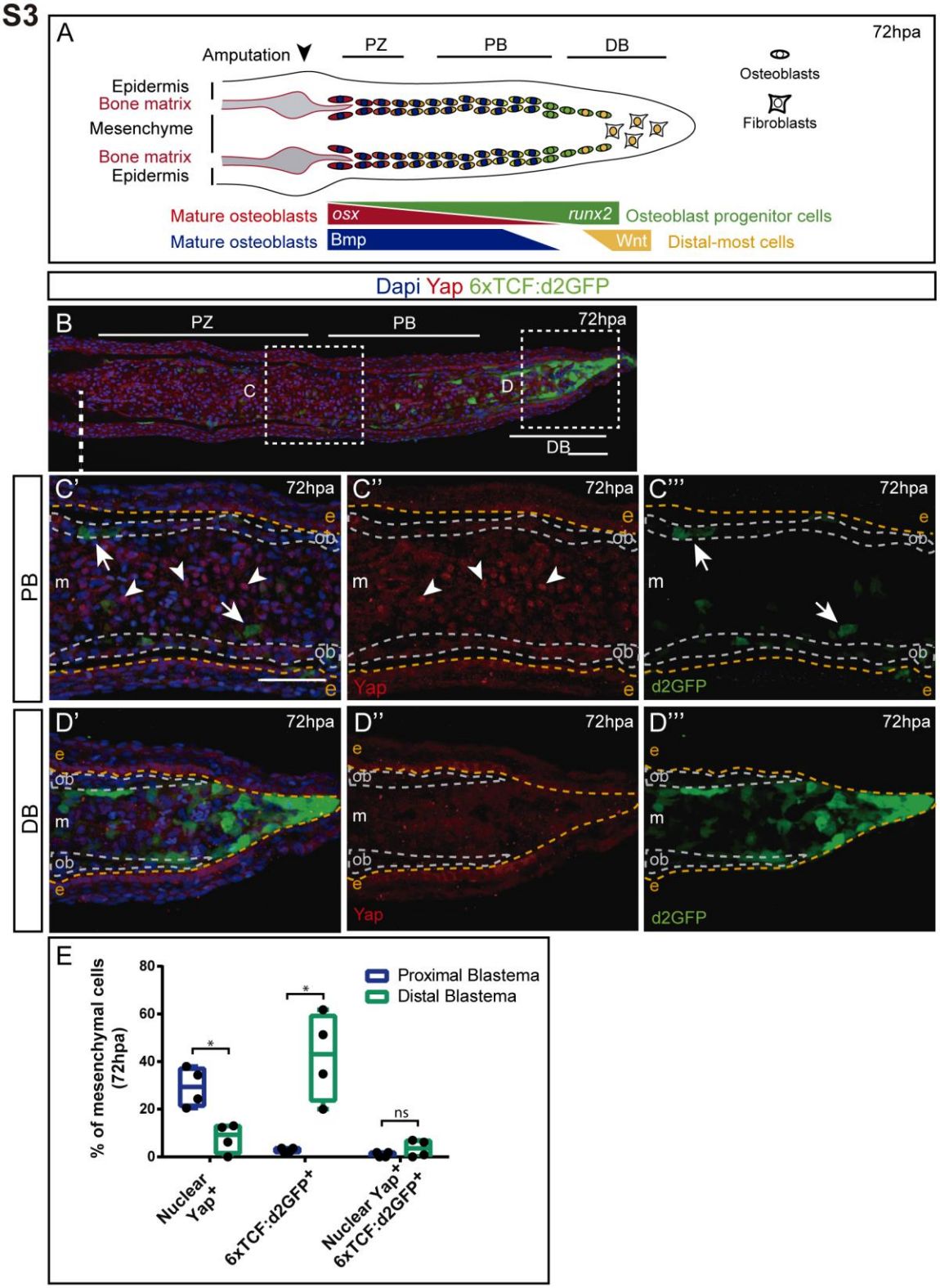

Figure S3 - Yap and Wnt signalling pathway activity compartmentalization within the blastema during regenerative outgrowth. (A) Representation of the 72 hpa blastema compartmentalization along the caudal fin proximo-distal axis, depicting the pathways responsible for osteoblast differentiation (Bmp) and progenitor

maintenance (Wnt). (B) Representative z-stack image of longitudinal cryosection of 6xTCF/Lef-mini:d2GFP animal immunostained for GFP (green) and Yap (red). White dashed lines define the amputation plane and dashed boxes are magnifications of the (C'-C''') PB and (D'-D''') DB regions. Arrows indicate cells with activated Wnt signalling and arrowheads show cells with nuclear Yap in the PB. Dashed orange and grey lines delimitate the epidermis and the osteoblast compartment respectively. (E) Percentage of mesenchymal cells with nuclear Yap and active Wnt signalling in both PB and DB regions. Statistical analysis with Mann-Whitney test (n = 3 average of blastemas from 4 animals). m: mesenchyme, e: epidermis, ob: osteoblasts. Scale bars: (B) 200 µm and (C'-D''') 50 µm. *: p<0.05. ns: not significant.

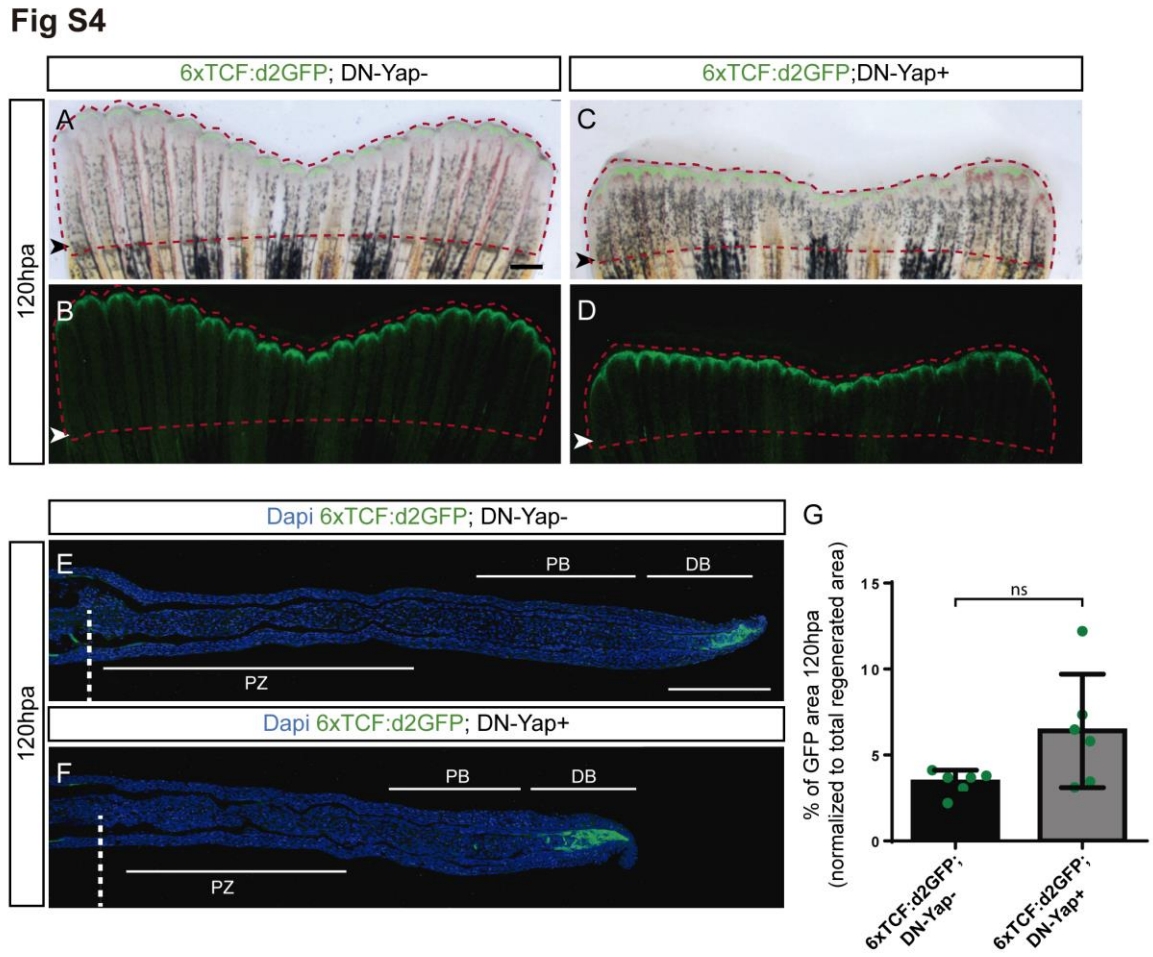

Figure S4 – Distal Wnt signalling activation domain upon Yap inhibition. (A-D) Caudal fins from 6xTCF:d2GFP; DN-Yap- sibling controls (A,B) and 6xTCF:d2GFP; DN-Yap+ double transgenics (C,D) heat-shocked from 48 to 96 hpa. Dashed red line delimitates the regenerated area. (E, F) Representative z-stack image of a longitudinal cryosection from (E) 6xTCF:d2GFP;DN-Yap- and (F) 6xTCF:d2GFP;DN-Yap+ animals, immunostained for GFP (green). (G) Percentage of 6xTCF:d2GFP-positive cells in the distal blastema region in relation to the total regenerated area. Statistical with Mann-Whitney test (n=6 cryosections from 3 animals from control 6xTCF:d2GFP;DN-Yap- and 6xTCF:d2GFP;DN-Yap+ animals). Arrowheads (A-D) and dashed lines (E-F) define the amputation plane. Scale bars: (A-D) 1 mm and (E, F) 200. ns: not significant.

APPENDIX C

Chapter V SUPPLEMENTARY FIGURES

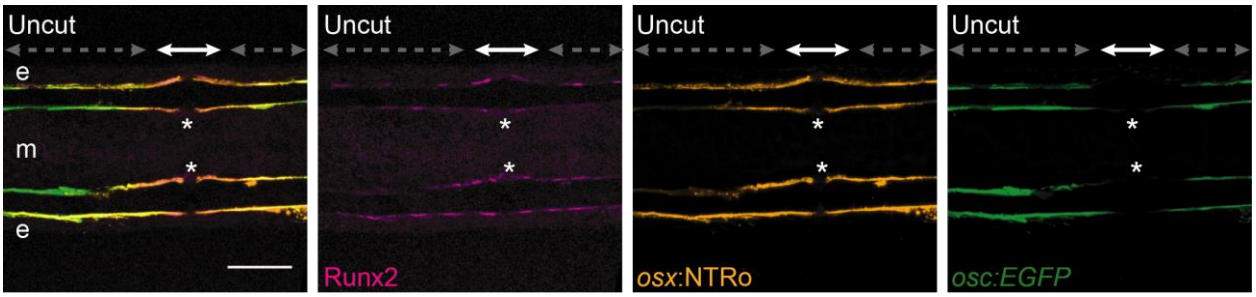

Supplementary Figure 3: Osteogenic markers in a homeostatic uncut situation. Panels show representative images of uncut caudal fin longitudinal cryosections of *osx:*NTRo; *osc*:EGFP double transgenic animals. Cryosections were immunostained for Runx2 (preosteoblast/osteoprogenitor marker, magenta), mCherry (to visualize *osx* expression, immature/intermediate osteoblast marker, orange) and for GFP (to visualize *osc* expression, mature/late osteoblast maker, green). Runx2 co-localizes with osc and osx expression in the segment region (green dashed arrows) and co-localizes with osx near the intersegment/joint region (grey arrows). The middle of the intersegment/joint region (asterisks) is not labelled for either osx or osc. This region might correspond to the pool where recently discovered osteoblast progenitor cells reside (Ando et al. 2017). Grey dashed arrows delineate the segment region; white arrows delineate the intersegment/joint region; asterisks point to the middle of the intersegment/joint region. Scale bar represents 50 µm.

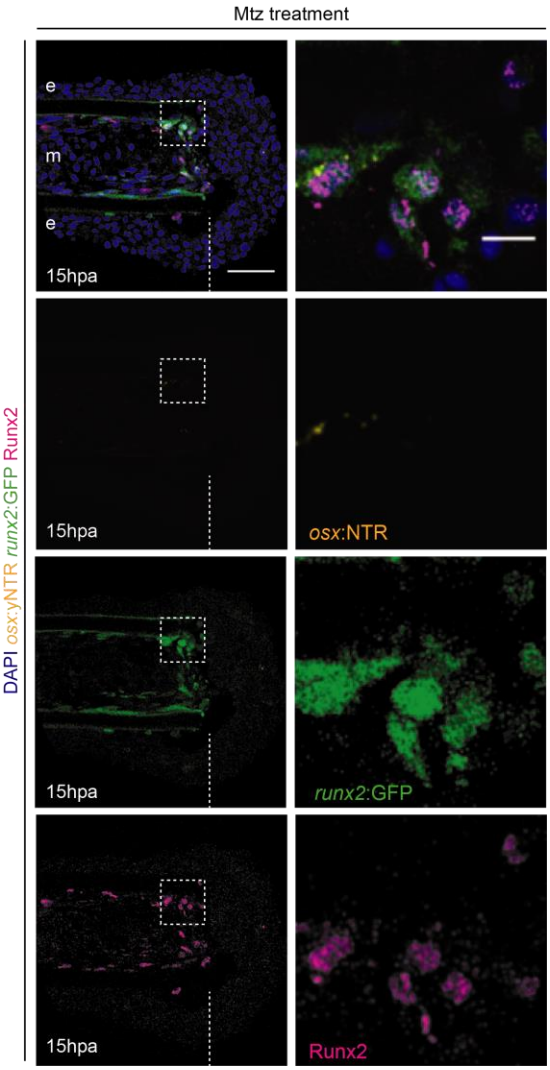

Supplementary Figure 4: Runx2 antibody co-localizes with runx2 reporter line. To confirm that the commercially available Runx2 antibody used in this study is labelling osteoprogenitors we used the *runx2* reporter line. We used double transgenic animals that also allowed to induce osteoblast ablation and also to monitor *runx2* expression, *osx*:NTRo; *runx2*:EGFP. Cryosections of 15 hpa caudal fins were immunostained for GFP (to monitor *runx2* expression, green), mCherry (to visualize osx expression and confirm correct osteoblast ablation, orange), Runx2 (pre-osteoblast/ osteoprogenitor marker, magenta) and counterstained for DAPI (nucleus, blue). We can observe that there is a clear co-localization between the runx2 reporter line and the commercial antibody in osteoblast depleted fins (see magnified panel), confirming that we are labelling osteoprogenitors. hpa: hours post-amputation, e: epidermis, m: mesenchyme; dashed white lines define the amputation plane; dashed boxes delimitate magnified panels; scale bars represent 50 µm and 10 µm in magnified panels.

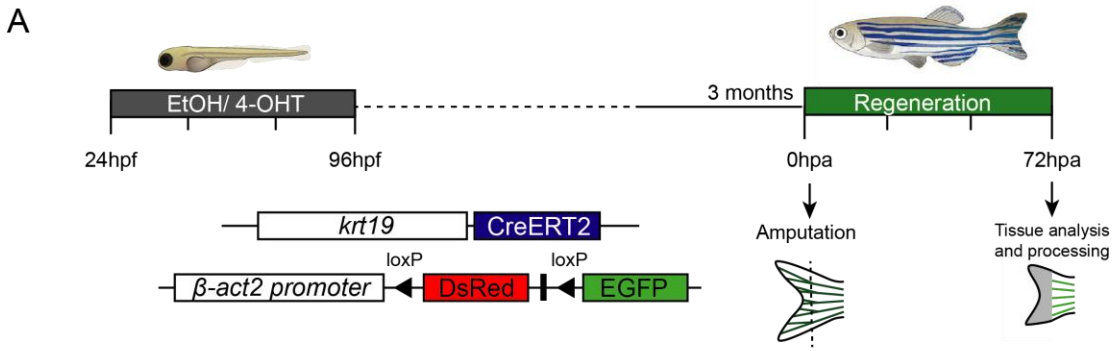
A
EtOH/ 4-OHT
3 months
Regeneration
24hpf
96hpf
0hpa
72hpa
krt19
CreERT2
loxP
loxP
β-act2 promoter
DsRed
EGFP
Amputation
Tissue analysis and processing

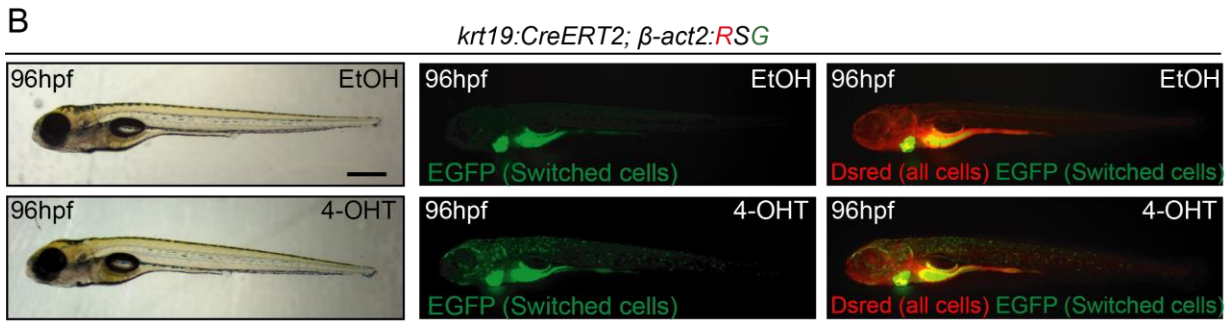
B
krt19:CreERT2; β-act2:RSG
96hpf EtOH
96hpf EtOH
EGFP (Switched cells)
96hpf EtOH
Dsred (all cells) EGFP (Switched cells)
96hpf 4-OHT
96hpf 4-OHT
EGFP (Switched cells)
96hpf 4-OHT
Dsred (all cells) EGFP (Switched cells)

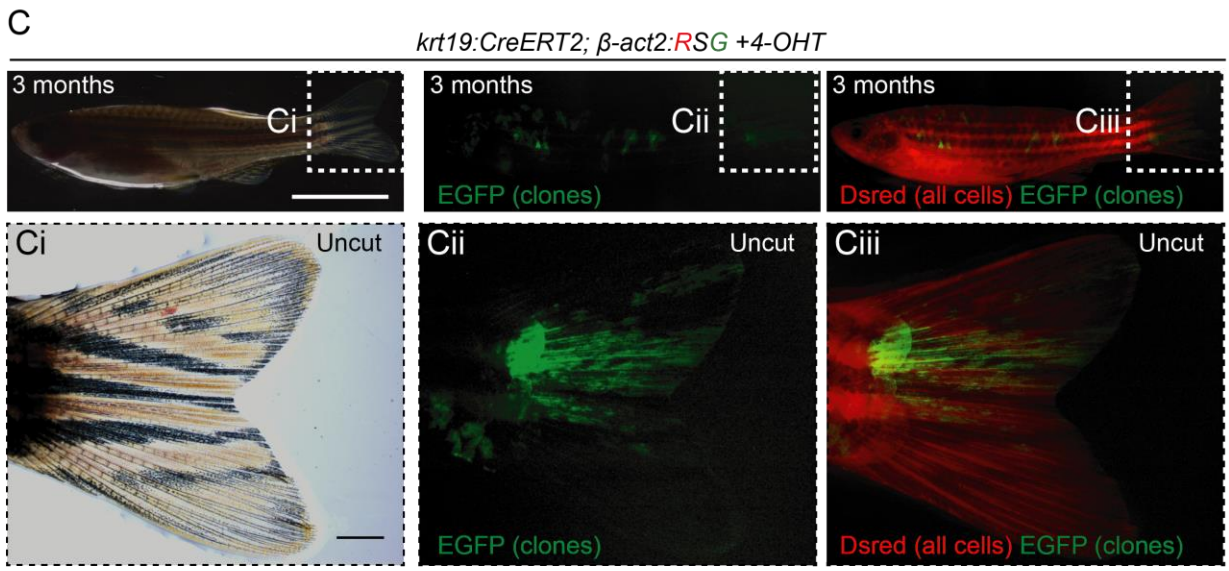
C
krt19:CreERT2; β-act2:RSG +4-OHT
3 months
Ci
3 months
Cii
EGFP (clones)
3 months
Ciii
Dsred (all cells) EGFP (clones)
Ci
Uncut
Cii
Uncut
EGFP (clones)
Ciii
Uncut
Dsred (all cells) EGFP (clones)

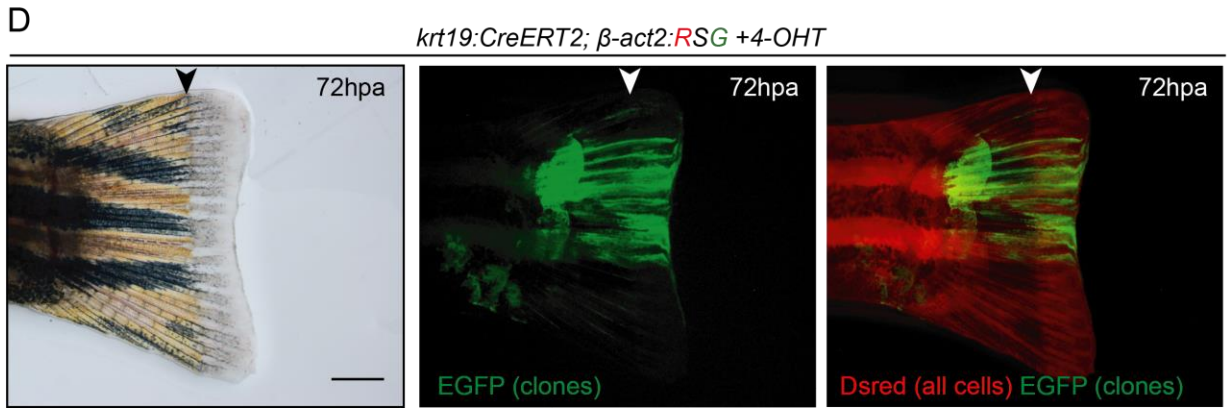
D
krt19:CreERT2; β-act2:RSG +4-OHT
72hpa
72hpa
EGFP (clones)
72hpa
Dsred (all cells) EGFP (clones)

Supplementary Figure 5: Lineage tracing experimental setup to monitor the contribution of the epidermis for de novo osteoblast formation during caudal fin regeneration. (A) Schematic representation of the experimental setup used to perform genetic fate mapping of the caudal fin epidermal tissue. For that, double transgenic animals, *krt19*:CreERT2;β-actin2:dsRed>EGFP (*krt19*:CreERT2; *β-actin2*:RSG) were used. Embryos with 24 hpf were incubated with 4-OHT or with the vehicle control (EtOH) for three consecutive days, to promote basal epidermal cells labelling. Afterwards, larvae were allowed to grow until adulthood. Basal epidermal cells that were permanently labelled formed EGFP+ clones in adult animals. Animals with strongest fin clones were then subjected to caudal fin amputation. Fins were collected at the desired time-point after amputation for imaging or latter processing to confirm correct epidermal labelling. (B) Representative images of 96 hpf *krt19*:CreERT2; β-actin2:RSG double transgenic larvae subjected to EtOH (control) or 4-OHT incubation. EtOH treated larvae did not show EGFP-positive cells, while larvae treated with 4-OHT present EGFP-positive cells throughout the body, indicative of a successful Cre-mediated recombination and allowing for proper cell-fate tracing of basal epidermal cells at later stages. (C) Representative images of *krt19*:CreERT2; β-actin2:RSG double transgenic adult zebrafish subjected to 4-OHT treatment during larval stages. We can observe regions/clones of $EGFP^+$ cells all over the zebrafish body, including in the caudal fin (see magnified panels in Ci-Ciii). (D) Representative images of *krt19*:CreERT2; β-actin2:RSG double transgenic adult zebrafish caudal fins shown in magnified panels Ci-Ciii and subjected to caudal fin amputation in the middle of the EGFP clone. At 72 hpa it is possible to observe $EGFP^+$ in the regenerated region, which demonstrates that through this protocol it is possible to follow the progeny and the contribution of epidermal cells during the regenerative process. hpa: hours post-amputation, hpf: hours post-fertilization; arrows define the amputation plane; dashed boxes delimitate magnified panels Ci-Ciii; scale bars represent 50 µm in B, 5 mm in C or 2 mm in magnified panels in Ci-Ciii.

A

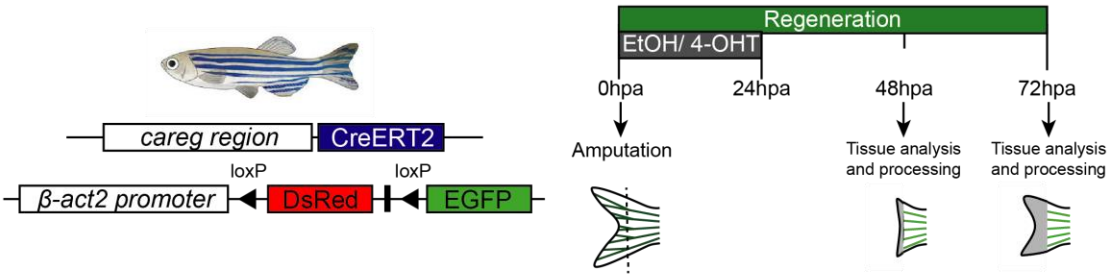
careg region
CreERT2
loxP
loxP
β-act2 promoter
DsRed
EGFP
Regeneration
EtOH/ 4-OHT
0hpa
24hpa
48hpa
72hpa
Amputation
Tissue analysis and processing
Tissue analysis and processing

B

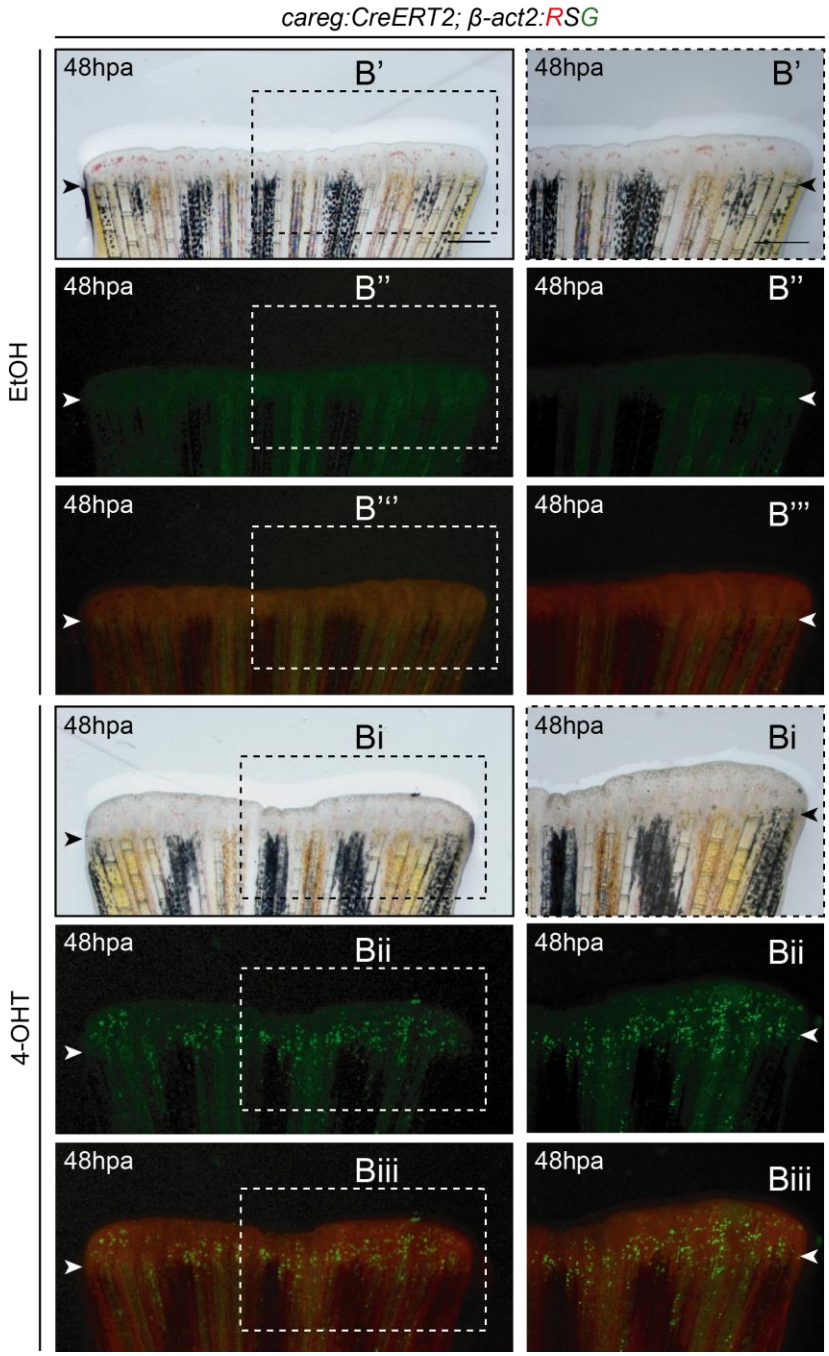
careg:CreERT2; β-act2:RSG
EtOH
4-OHT
48hpa
B'
B''
B'''
Bi
Bii
Biii

Supplementary Figure 6: Lineage tracing experimental setup to monitor the contribution of the mesenchyme for de novo osteoblast formation during the caudal fin regenerative process. (A) Schematic representation of the experimental setup used to perform genetic fate mapping of the caudal fin mesenchymal tissue. For that, transgenic animals based on the CreERT2/loxP system were obtained: careg:CreERT2; β-actin2:dsRed>EGFP, referred as careg:CreERT2; *β-actin2*:RSG. Double transgenic animals were subjected to caudal fin amputation and immediately incubated with 4-OHT or the vehicle (EtOH) for one day, to promote mesenchymal cell permanent labelling (from red to green). Fins were allowed to regenerate and collected at the desired time-point after amputation for imaging or later processing to confirm correct mesenchyme labelling. (B) Representative images of 48 hpa caudal fins from careg:CreERT2; β-actin2:RSG fish subjected to EtOH (control) or 4-OHT incubation. In contrast to EtOH treated animals (B and magnified panels in B'-B'''), EGFP positive cells are detected in the regenerated area of 4-OHT treated animals (B and magnified panels in Bi-Biii). hpa: hours post-amputation; arrowheads define the amputation plane; dashed boxes delimitate magnified panels B'-B''' and Bi-Biii; scale bars represent 2 mm.

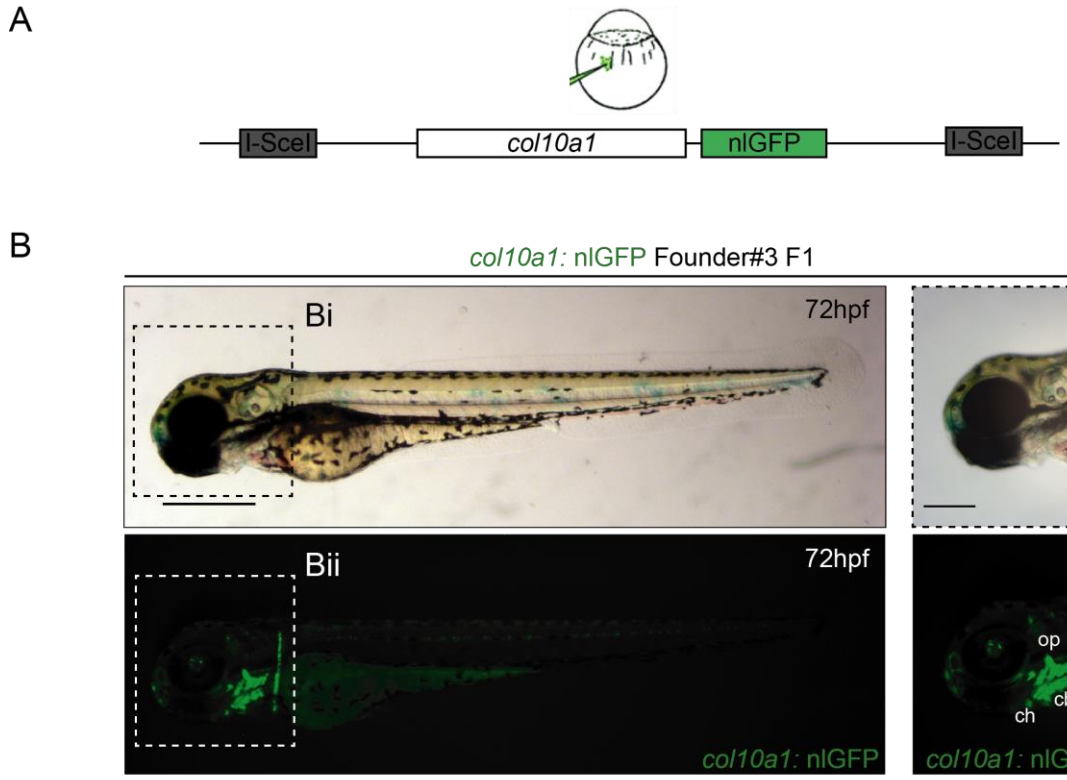
A
I-SceI
col10a1
nlGFP
I-SceI
B
col10a1: nlGFP Founder#3 F1
Bi
72hpf
Bi
Bii
72hpf
col10a1: nlGFP
Bii
op
cl
cb
ch
col10a1: nlGFP
C
col10a1: nlGFP Founder#3 F1
3-4 months
Ci
Ci
2
2
2
2
1
1
3-4 months
Cii
col10a1: nlGFP
Cii
col10a1: nlGFP

Supplementary Figure 7: Generation and expression pattern characterization of the *col10a1* reporter transgenic line. (A) Schematic representation of the construct injected in wild-type AB line to generate a promoter reporter line for *col10a1* to monitor the expression of this gene through GFP visualization. (B) Representative images of 72 hpf larvae from the F1 generation of the Tg(Ola.*col10a1*:nlGFP)reporter line, referred as *col10a1*:nlGFP. GFP is expressed in several craniofacial skeletal structures (B, Bi and Bii). (C) Caudal fin representative images of adult animals from the F1 generation of the *col10a1*:nlGFP reporter line. GFP is observed in the scales and in the segment (region 1 in Ci, asterisks) and intersegment (region 2 in Cii, arrowheads) regions of the fin. hpf: hours post-fertilization; dashed boxes delimitate magnified panels Bi and Bii in B and Ci and Cii in C; cb: ceratobranchial, ch: ceratohyal, cl: cleithrum and op: opercle; scale bars represent 50 µm in B and 2 mm in C and in magnified panels of C (Ci and Cii).

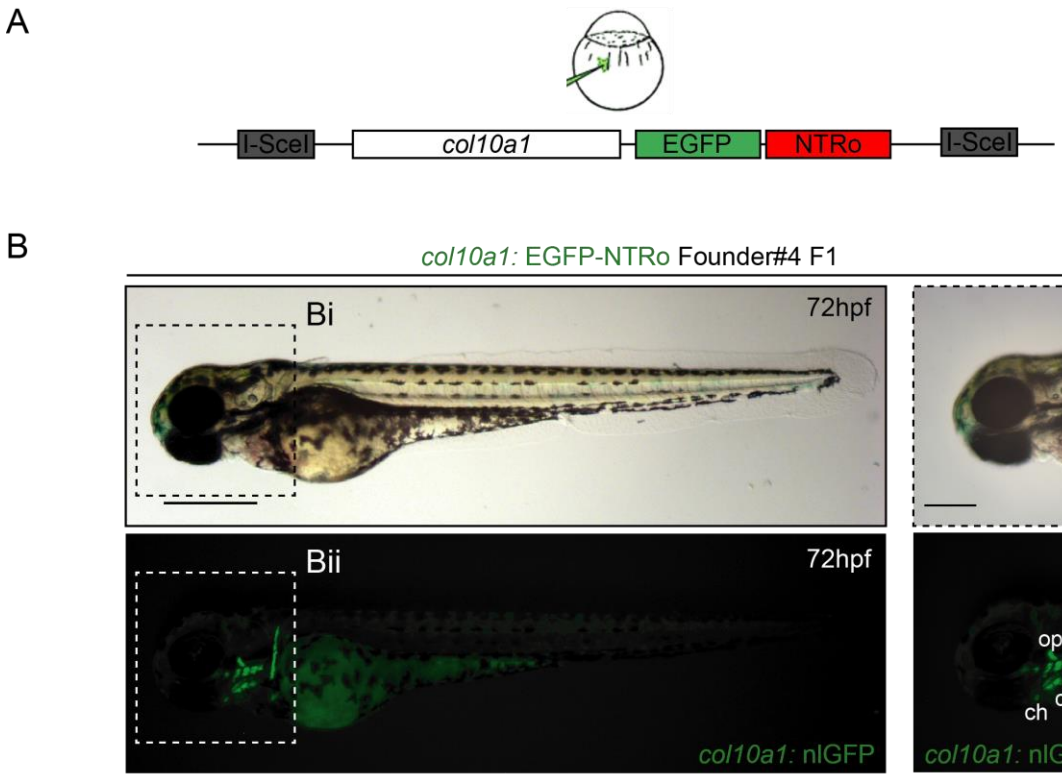
A
I-SceI
col10a1
EGFP
NTRo
I-SceI
B
col10a1: EGFP-NTRo Founder#4 F1
Bi
72hpf
Bi
Bii
72hpf
Bii
op
cl
ch
cb
col10a1: nlGFP
col10a1: nlGFP
C
col10a1: EGFP-NTRo Founder#4 F1
3-4 months
Ci
Ci
1
2
2
2
2
1
3-4 months
Cii
Cii
col10a1: nlGFP
col10a1: nlGFP

Supplementary Figure 8: Generation and expression pattern characterization of the *col10a1* ablation transgenic line. (A) Schematic representation of the construct injected in wild-type AB one-cell stage embryos to generate a *col10a1* ablation line based on the NTR/Mtz system. (B) Representative images of 72 hpf larvae from the F1 generation of the Tg(Ola.*col10a1*:EGFP-NTRo) ablation line, referred as *col10a1*:EGFP-NTRo. GFP is expressed in several craniofacial skeletal structures (B, Bi and Bii). (C) Caudal fin representative images of adult animals from the F1 generation of the *col10a1*:EGFP-NTRo ablation line. GFP is observed in the scales and in the segment (region 1 in Ci, asterisks in Cii) and intersegment (region 2 in Ci, arrowheads in Cii) regions of the fin. Hpf: hours post-fertilization; dashed boxes delimitate magnified panels Bi and Bii in B and Ci and Cii in C; cb: ceratobranchial, ch: ceratohyal, cl: cleithrum and op: opercle; scale bars represent 50 µm in B and 2 mm in C and in magnified panels of C (Ci and Cii).

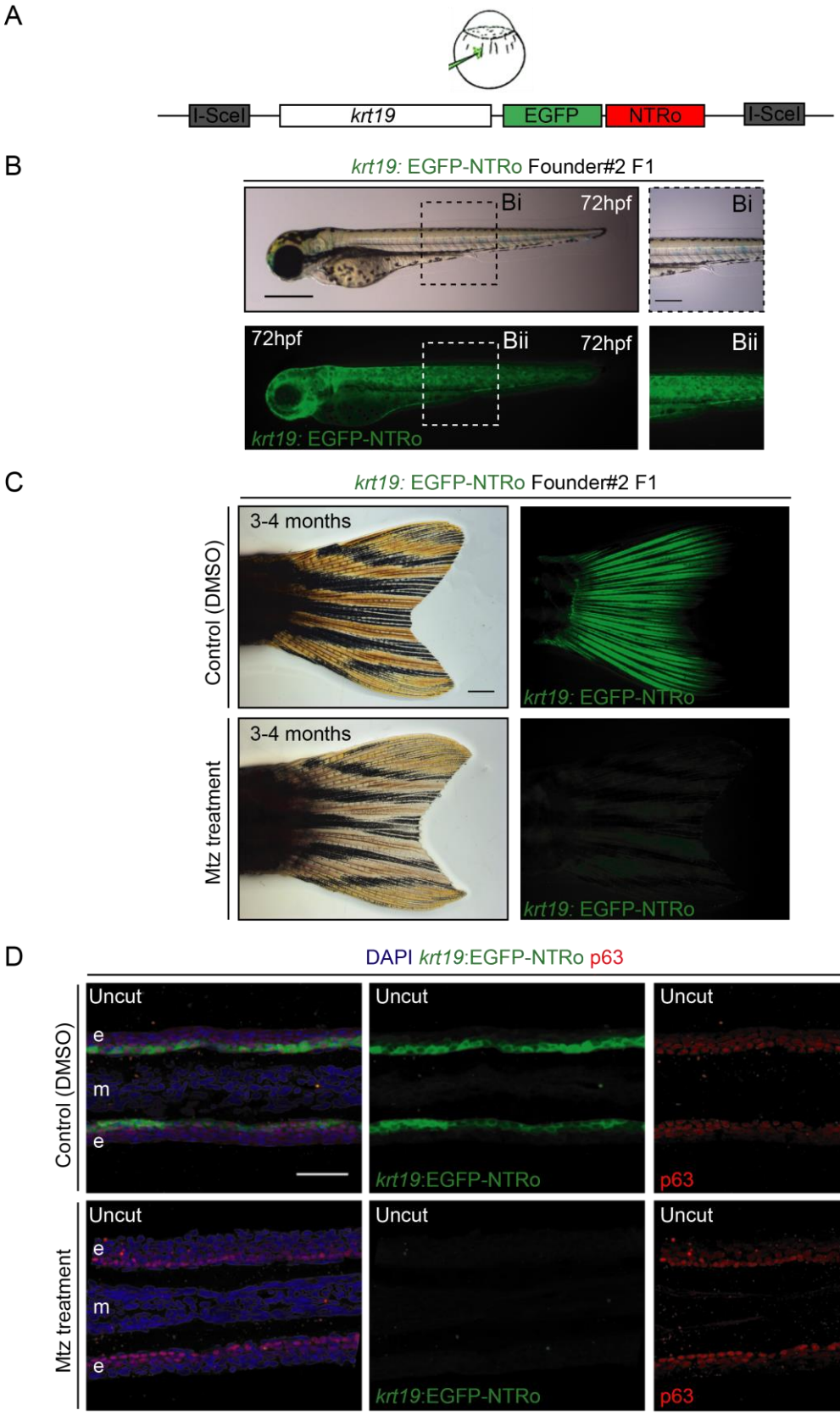
A
I-SceI
krt19
EGFP
NTRo
I-SceI
B
krt19: EGFP-NTRo Founder#2 F1
Bi
72hpf
Bi
72hpf
Bii
72hpf
Bii
krt19: EGFP-NTRo
C
krt19: EGFP-NTRo Founder#2 F1
Control (DMSO)
3-4 months
krt19: EGFP-NTRo
Mtz treatment
3-4 months
krt19: EGFP-NTRo
D
DAPI krt19:EGFP-NTRo p63
Control (DMSO)
Uncut
e
m
e
Uncut
krt19:EGFP-NTRo
Uncut
p63
Mtz treatment
Uncut
e
m
e
Uncut
krt19:EGFP-NTRo
Uncut
p63

Supplementary Figure 9: Generation and characterization of the *krt19* ablation transgenic line. (A) Schematic representation of the construct injected in wild-type AB 1-cell stage embryos to generate a *krt19* ablation line based on the NTR/Mtz system. This line will be used to specifically induce ablation of the basal epidermal layer. (B) Representative images of 72 hpf larvae from the F1 generation of the *krt19*:EGFP-NTRo ablation line. GFP seems to be expressed throughout the larval body (B, Bi and Bii). (C) Caudal fin representative images of adult animals from the F1 generation of the *krt19*:EGFP-NTRo ablation line subjected to vehicle DMSO (control) or to Mtz incubation for basal epidermal cell ablation. In control animals, GFP is observed all over the caudal fin, while in animals incubated with Mtz, GFP has strongly decreased. (D) Representative images of uncut caudal fin longitudinal cryosections of *krt19*:EGFP-NTRo animals shown in C. Cryosections were immunostained for GFP (to visualize *krt19* expression and confirm correct basal epidermis ablation, green), p63 (labels epidermal cells) and counterstained for DAPI (nucleus, blue). As observed in C, the ablation protocol was successful, since almost no GFP expression is observed in the Mtz treatment condition, in contrast to control (DMSO) caudal fins. hpf: hours post-fertilization; dashed boxes delimitate magnified panels Bi and Bii in B; e: epidermis, m: mesenchyme; scale bars represent 50 µm in B and D and 2 mm in C.